Lecture Notes in Civil Engineering

K. S. Satyanarayanan
Hyung-Joon Seo
N. Gopalakrishnan *Editors*

Sustainable Construction Materials

Select Proceedings of ACMM 2021

Springer

Lecture Notes in Civil Engineering

Volume 194

Lecture Notes in Civil Engineering (LNCE) publishes the latest developments in Civil Engineering—quickly, informally and in top quality. Though original research reported in proceedings and post-proceedings represents the core of LNCE, edited volumes of exceptionally high quality and interest may also be considered for publication. Volumes published in LNCE embrace all aspects and subfields of, as well as new challenges in, Civil Engineering. Topics in the series include:

- Construction and Structural Mechanics
- Building Materials
- Concrete, Steel and Timber Structures
- Geotechnical Engineering
- Earthquake Engineering
- Coastal Engineering
- Ocean and Offshore Engineering; Ships and Floating Structures
- Hydraulics, Hydrology and Water Resources Engineering
- Environmental Engineering and Sustainability
- Structural Health and Monitoring
- Surveying and Geographical Information Systems
- Indoor Environments
- Transportation and Traffic
- Risk Analysis
- Safety and Security

To submit a proposal or request further information, please contact the appropriate Springer Editor:

– Pierpaolo Riva at pierpaolo.riva@springer.com (Europe and Americas);
– Swati Meherishi at swati.meherishi@springer.com (Asia - except China, and Australia, New Zealand);
– Wayne Hu at wayne.hu@springer.com (China).

All books in the series now indexed by Scopus and EI Compendex database!

More information about this series at https://link.springer.com/bookseries/15087

K. S. Satyanarayanan · Hyung-Joon Seo ·
N. Gopalakrishnan
Editors

Sustainable Construction Materials

Select Proceedings of ACMM 2021

Springer

Editors
K. S. Satyanarayanan
Civil Engineering
SRM Institute of Science and Technology
Chennai, Tamil Nadu, India

N. Gopalakrishnan
Civil Engineering
CSIR- Central Building Research Institute
Roorkee, Uttarakhand, India

Hyung-Joon Seo
Civil Engineering and Industrial Design
University of Liverpool
Liverpool, UK

ISSN 2366-2557 ISSN 2366-2565 (electronic)
Lecture Notes in Civil Engineering
ISBN 978-981-16-6402-1 ISBN 978-981-16-6403-8 (eBook)
https://doi.org/10.1007/978-981-16-6403-8

Preface

This book, Sustainable Construction Materials: Select Proceedings of ACMM 2021 is devoted to the gamut of sustainable construction issues, from theoretical aspects to application-dependent studies and the validation of emerging sustainable construction materials.

This book was envisioned and founded to represent the growing needs of sustainable construction of buildings by using novel materials as an emerging and increasingly vital field. Its mission is to become a voice of the civil engineering community, addressing researchers, and practitioners presenting new construction materials, findings, and solutions.

This book comprises 44 contributions, connected by a unifying theme: sustainable construction materials. Specifically, the presented contributory articles can be categorized into the following parts:

- Material management
- Multi-functional materials
- Smart materials and civil engineering
- Polymers and functional materials
- Multi-disciplinary materials and composites
- Hydraulic engineering and amorphous materials

Many researchers and academicians have contributed to the creation and the success of this book compilation. We are very thankful to everybody who supported this book publication. This issue would not have been possible without the great support of the Editorial Board members, and we would like to express our sincere thanks to all of them. We would also like to express our gratitude to the editorial staff of Springer, in particular Sushmitha Shanmuga Sundaram and Ashok Kumar, who supported us at every stage of the work.

It is our hope that this fine collection of articles will be a valuable resource for Sustainable Construction Materials readers and will stimulate further research.

Chennai, India
July 2021

K. S. Satyanarayanan

Contents

Multi-functional Materials

Smart Materials and Civil Engineering

About the Editors

Dr. K. S. Satyanarayanan is currently working as Professor & Head of Department at SRM Institute of Science and Technology (formerly known as SRM University), Kattankulathur campus. He has obtained BE in Civil from College of Engineering, Guindy, 1984, ME in Structural Engineering from Coimbatore Institute of Technology, Coimbatore, 1987 and PhD in Civil Engineering-Structural Engineering from SRM Institute of Science and Technology. His major areas of research interest are Structural Systems, Sustainable Technology, Concrete Technology and Finite element Analysis. He has published 44 papers in peer reviewed international journals.

Dr. Hyung-Joon Seo received the bachelor's degree in civil engineering from Korea University, Seoul, South Korea, in 2007, and the Ph.D. degree in geotechnical engineering from Korea University in 2013. In 2013, he worked as a research professor in Korea University. He served as a visiting scholar at University of Cambridge, Cambridge, UK, and he worked for engineering department in University of Cambridge as a research associate from 2014 to 2016. In August 2016, he got a Lecturer position in the Department of Civil Engineering at the Xi'an Jiaotong Liverpool University (XJTLU), China. His research interests geotechnical engineering such as, SMART monitoring system for infrastructure, soil-structure interaction (tunneling, slope stability, pile), Antarctic survey and freezing ground.

Dr. N. Gopalakrishnan was a scientist at the Advanced Seismic Testing and Research Laboratory (ASTaR) of CSIR-SERC, before assuming charge as Director, CSIR-CBRI. He has done B.E at the college of Engineering, Guindy (CEG), 1984, followed by M.Tech at the Indian Institute of Technology, (IIT) Madras in Structural Engineering, 1986. He has obtained Ph.D. from the Indian Institute of Science (IISc), Bangalore during 2008. He was a design engineer at the Tata Consulting Engineers, Bangalore between 1986-1987. Later on, he joined CSIR-SERC at the then Structural Dynamics and Machine Foundation (SDL) division of CSIR-SERC as Scientist-B in 1987. He moved on to Earthquake Engineering division of CSIR-SERC called as the ASTaR lab in 2003 after the laboratory was commissioned. He was actively

involved in the planning, design and construction of this laboratory at CSIR-SERC. His field of interest include: (a) Structural Dynamics and Earthquake Engineering (b) Experimental methods in Structural Engineering (c) Machine supporting structure and soil-structure interaction (d) Reinforced concrete structures (e) Structural health monitoring (f) Smart materials and structures. He has co-authored 61 international and national journal publications and has been credited with the prestigious Ramaiah's prize for the best publication for five years. He has filed five Indian patents. He had been a UNDP visiting fellow at the University of Michigan, Ann Arbor, State University of New York, Buffalo (SUNY-B) and Cornell University, Ithaca during 1994–95. He has done many collaborative and sponsored industrial projects for industrial and strategic sectors, notable of them include those funded by National Programme of Micro and Smart Structures (NPMASS), ARDB, DST, Rubber Board, BRNS, IGCAR, BARC, NPCIL, DRDO, and VSSC.

Material Management

Comparative Study on Low-, Medium- and High-Rise RC Framed Buildings Using Force-Based Design Method and Direct Displacement-Based Design Method

Swetha Elizabeth Philip and M. Helen Santhi

1 Introduction

Earthquake is the most destructive of all hazards that kills people, destroys nature leaving behind a huge damage. In India, reinforced concrete moment frame structures have been developed and designed using seismic design and IS 13920: 1993, IS 1893 (Part 1): 2002 [6, 7] for several decades. These Indian standard codes are based on force-based design (FBD). Based on computations from elastic analysis of internal forces, every component of the structure is designed for strength so that the structure can survive low intensities without damage, can survive intermediate intensities without structural damage and can survive higher intensities without full collapse of the structure. In the recent years, studies have shown a progressive trend away from this stance, with researchers acknowledging that increase in strength may not enhance safety, or prevent damage. A four-storey RC structure was modelled and designed as per IS 456:2000 and analysed in SAP2000 v17 for life safety performance level, storey drift, pushover curve, capacity spectrum curve, performance point and plastic hinges as per FEMA 273 were discovered [4]. Base shear, storey drift, steel and concrete consumption at the performance point for 8-, 10-, 12-, 14- and 16-storey buildings were evaluated utilizing FBD and Direct displacement-based design (DDBD) approaches, with the DDBD technique proving to be the most cost-effective [9]. With hysteretic parameters and the high-mode effect, performance-based seismic design of self-centring steel frames with smart memory alloy bracing was investigated [3]. Seismic resistance design has undergone a major reassessment recently that focuses on shifting from 'strength' to 'performance' [1]. It was discovered that if plastic hinges are installed in beams rather than columns, the building

S. E. Philip (✉) · M. Helen Santhi
Vellore Institute of Technology, Chennai, Tamil Nadu, India
e-mail: swethaelizabeth.philip2019@vitstudent.ac.in

M. Helen Santhi
e-mail: helensanthi.m@vit.ac.in

K. S. Satyanarayanan et al. (eds.), *Sustainable Construction Materials*, Lecture Notes in Civil Engineering 194, https://doi.org/10.1007/978-981-16-6403-8_1

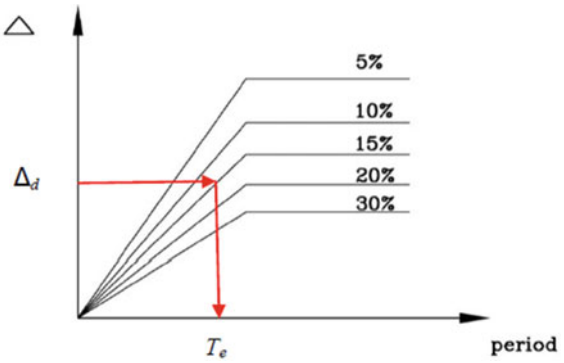

Fig. 1 Displacement response spectrums for various effective damping ratios [8]

frame would perform better during a seismic event. This can be seen as the beginning of performance-based seismic design, where the structure performance is used as a function of the design process [2].

In this investigation, the considered approaches to compare the building models are first the force-based approach, which is based on calculating the base shear force from the dynamic effect of earthquakes utilizing the acceleration response spectrum and the building's elastic period. Static lateral force actions, which are equivalent to most design symbols are used to model these effects by applying a force to each floor level, which is directly proportional to height [8] (Fig. 1). Second, the DDBD method which makes use of displacement response spectrum for computing the base shear force. It is the simplest design technique to analyse a structure with multiple degrees of freedom. The design technique is based on obtaining a specified displacement limit condition at the design level, which is established by either material strain limits or non-structural drift restrictions from design standards under seismic intensity [10, 11]. This procedure eliminates problems in strength-based design (FBD), in which it uses initial stiffness to define the elasticity period which is a fault seen in most of the building codes [5].

2 Modelling and Analysis

For comparing the considered approaches, a typical plan is considered which is shown in (Fig. 2). The number of storeys considered for low-, medium- and high-rise buildings is 4, 8 and 12, respectively, with a typical storey height of 3 m. There are three spans in the X direction and four spans in the Y-direction, each measuring 5 m in length. The detail of member sizes of the buildings under study is shown in (Table 1).

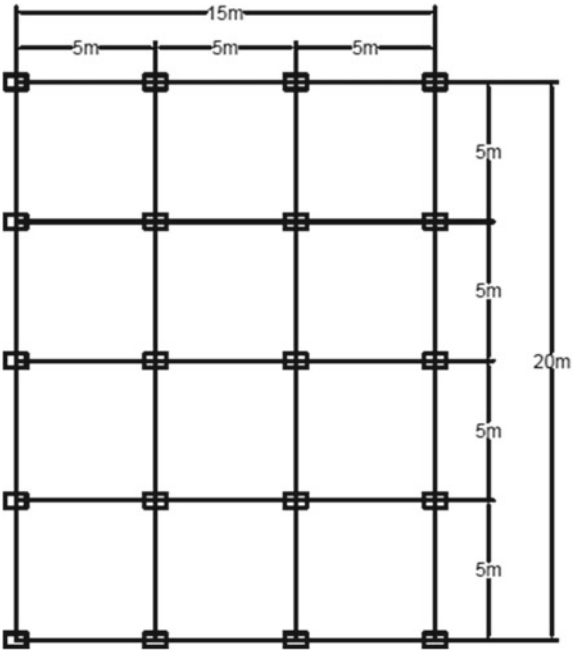

Fig. 2 Typical plan view

Table 1 Member sizes of all building models

Type of Building	Structural Elements		Width (mm)	Depth (mm)
4 storey	Beam		250	400
	Column		350	350
	Slab thickness		120 mm	
8 storey	Beam size in X-direction		300	500
	Beam size in Y-direction		300	600
	Column	4–8 storey	400	400
		1–3 storey	450	450
	Slab thickness		120 mm	
12 storey	Beam size in X-direction		300	500
	Beam size in Y-direction		300	600
	Column	6–12 storey	450	450
		1–5 storey	550	550
	Slab thickness		120 mm	

Table 2 Maximum storey drift values

Building model	Storey drift		
	FBD method	DDBD method	Difference in %
Low rise	0.001331	0.000917	18
Medium rise	0.000805	0.000484	25
High rise	0.000838	0.000457	29

3 Loading Data

The wall load on all beams and live load is taken to be as 13.8 kN/m and 3 kN/m^2, respectively. The three building models are considered to be at Zone V with a zone factor of 0.36. The soil is taken to be as medium soil. The importance factor and response reduction factor are 1 and 3, respectively, according to IS 1893: 2016.

4 Results and Discussion

In this section, the considered methods are used to analyse and create the three building models.

4.1 Comparison of Base Shear of All Building Models by Both Methods

The base shear calculated for all the three building models using FBD method as per IS 1893:2016 and base shear calculated by DDBD method is shown in (Fig. 3). It is observed that the total base shear shown by DDBD for 4, 8, and 12 storeys are 14%, 20% and 11%, respectively, lesser than that compared to FBD. The reduction in the base shear demand of the building models as per DDBD confirms the possibility of economical sizes of the members.

4.2 Comparison of Storey Displacement of All Building Models by FBD and DDBD Methods

The storey displacement for all the three structure models using FBD approach as per IS 1893:2016 compared with storey displacement by DDBD method is shown in (Fig. 4). It is observed that the maximum storey displacement shown by DDBD

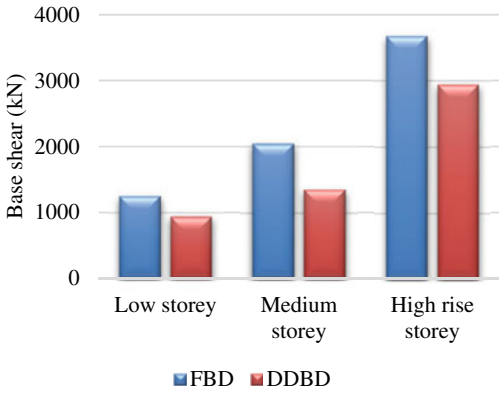

Fig. 3 Maximum base shear

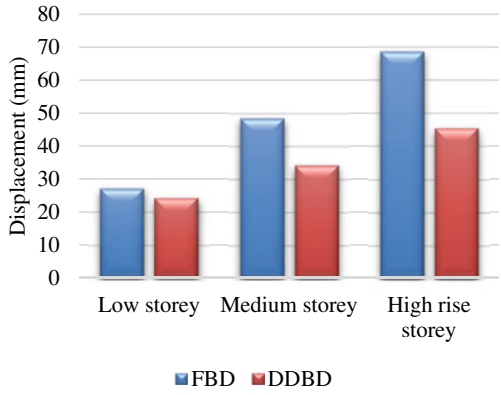

Fig. 4 Maximum storey displacement

for 8, 10, and 12 storeys are 13%, 17.2% and 20.3% less than when compared to FBD, respectively. The results showed significant reduction of displacement by using DDBD method which may be directly related to the reduced damage level in the framed buildings.

4.3 Comparison of Storey Drift of All Building Models by FBD and DDBD Methods

From (Fig. 5), it is observed that highest storey drift values for DDBD are less than the FBD approach in all the building models. The table infers that the drift of the building models are appreciably reduced when DDBD method is used (ref. Table 1). It is also observed that for all the building models, the maximum drift value did not exceed the drift limit (0.004) as given in IS 1893:2016, which means that the structure is within the permissible limit. From (Fig. 6a–c), the maximum storey drift

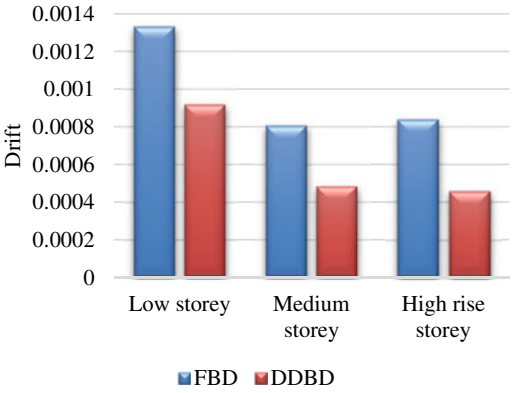

Fig. 5 Maximum storey drift

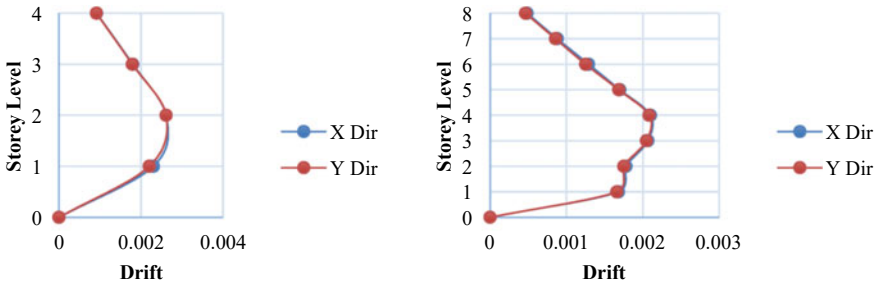

(a) 4 storey building **(b)** 8 storey building

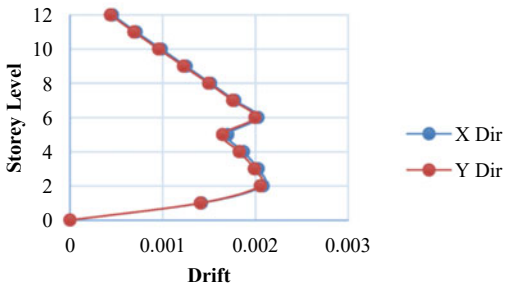

(c) 12 storey building

Fig. 6 Storey drift of building models

Table 3 Comparison between reinforcement requirements of all building models

Building type and design method	Beam Rebar %	Column Rebar %	Beam Req. area (mm^2)	Difference in %	Column Req. area (mm^2)	Difference in %
Low-rise FBD	1.5	3.75	1497	16.3	4600	22.84
Low-rise DDBD	1	2.11	1077		2889	
Medium-rise FBD	1.52	2.25	1744	22.47	4549	24.64
Medium-rise DDBD	1.1	1.36	1104		2750	
High-rise FBD	1.6	2.24	3093	35.95	6770	31.2
High-rise DDBD	1	1.17	1457		3545	

value for 4-storey building occurs at its second storey level, for 8-storey building the maximum drift value is at its fourth storey level and for 12-storey building the maximum drift value is at its sixth storey level. The maximum drift is found at the mid-height of the respective structure model (Table 2).

4.4 Comparison of Reinforcement Requirements

The reinforcement percentage and rebar area for all the three building models using FBD method and DDBD method is shown in (Table 3). It is observed that in buildings designed with direct displacement-based method requires reinforcement area for beam 16.3%, 22.47% and 35.95% less for 4, 8, and 12 storeys, respectively, than the building models designed with force-based method. The reinforcement area for column for building designed with DDBD requires 22.84%, 24.64% and 31.2% less for 4, 8, and 12 storeys, respectively, than the building models designed with FBD as per IS 1893:2016. It is found that as the floor level rises, the variation in percentage of reinforcement area also increases, from which is understood that at lower rise building models it is sufficient to follow FBD method.

4.5 Responses at Performance Point

The response of all the building models at performance point is shown in (Table 4). The load factor and material safety force in FBD building models are meant to provide actual steel for increased force. The building models are not designed using load

Table 4 Response of all the three structure models at performance point

Building model	Applied base shear V (kN)		Base shear at performance point (kN)		Displacement (mm)		Effective damping (%)		No. of hinges			
									IO		LS	
Direction	X	Y	X	Y	X	Y	X	Y	X	Y	X	Y
Low-rise FBD	1245	1261	5471	5631	27	26.4	0.051	0.052	71	34	–	–
Low-rise DDBD	1006	1032	1363	1429	24.24	24.6	0.06	0.068	156	133	–	–
Medium-rise FBD	2042	2087	7289	7311	44.4	43.5	0.05	0.05	97	81	62	67
Medium-rise DDBD	1851	1913	1402	1564	34.2	33.6	0.062	0.064	212	190	120	129
High-rise FBD	3675	3760	8752	8512	68.5	67.88	0.051	0.051	149	162	92	63
High-rise DDBD	2942	3006	2174	2263	45.4	44.7	0.064	0.066	282	276	146	135

factor and material factor because DDBD is a performance-based design. Therefore, base shear values at performance point are greater in FBD building model than in DDBD building model. The hinge formation in all the building models under study is shown in (Fig. 7). It is found that all the hinges remain at immediate occupancy state for low-rise building. There are hinges formed at immediate occupancy state and life safety state for medium-rise and high-rise building models.

5 Conclusion

From the comparison of parameters like base shear, storey drift, storey displacement, reinforcement requirement and hinges, the following conclusions are found:

- DDBD approach showed lower base shear value than FBD approach (as per IS 1893:2016). Base shear from DDBD is 14%, 20% and 11% for 4, 8 and 12 storeys, respectively, less than that of FBD. As medium-rise building has the higher difference, DDBD is more suitable for medium-rise building.
- It is found that the structures designed with DDBD approach are cost-effective than those by FBD approach. It is observed that as the storey level increases, the differences in percentage of reinforcement area also increases, from which it can be concluded that for low-rise building models, it is sufficient to follow FBD method.

Lots of improvements in the DDBD are being researched in terms of economy and seismic performance of buildings and other infrastructure. The current study can be extended to the existing buildings for the purpose of retrofitting or strengthening if required.

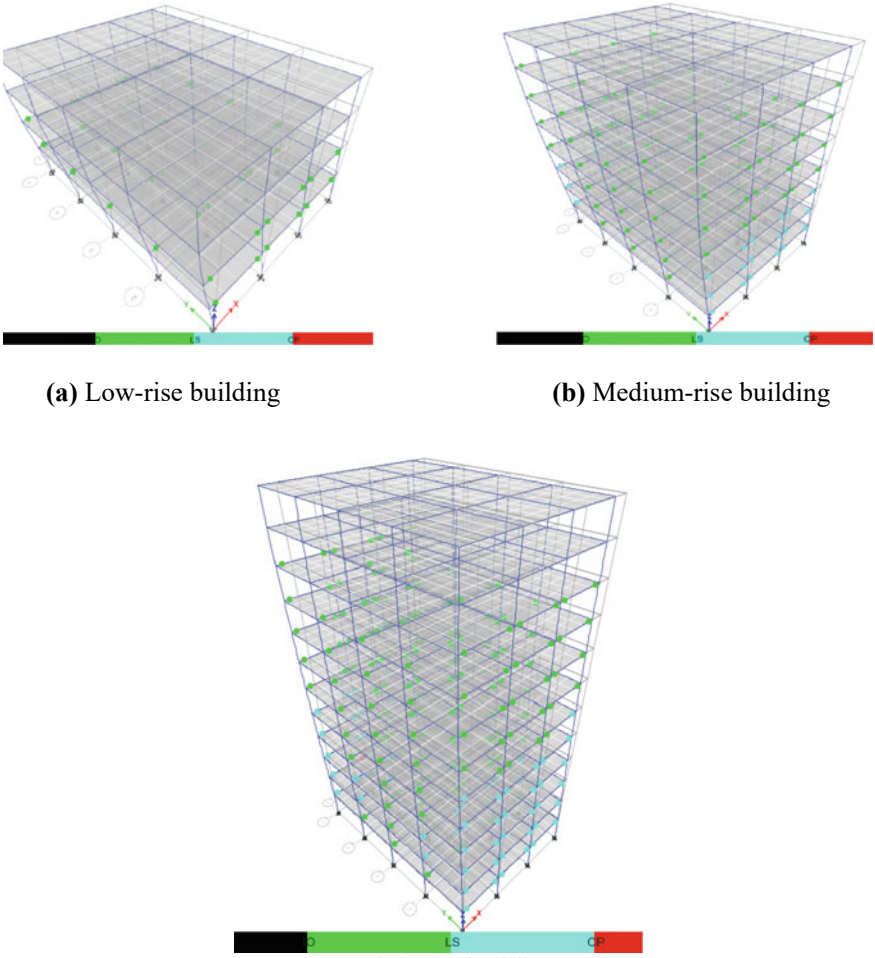

(a) Low-rise building

(b) Medium-rise building

(c) High-rise building

Fig. 7 Hinge formation of building models

References

1. Alphy M, Mathai A (2018) Comparison of force-based design and displacement-based design on regular buildings. Int Res J Eng Technol 5(5):1270–1275
2. Kahrizsangi AHS, Behnamfar F (2019) Comparison of nonlinear seismic behaviour of buildings designed using the force and displacement-based procedures. In: 8th Conference on seismology & earthquake engineering, Tehran, Iran, pp 22–25
3. Can-Xing Q, Zhu S (2017) Performance-based seismic design of self-centering steel frames with SMA-based braces. Eng Struct 130:67–82
4. Chaudhari DJ, Dhoot GO (2016) Performance based seismic design of reinforced concrete building. Open J Civil Eng 6:188–194

5. Calvi GM, Priestley MJN, Kowalsky MJ (2008) Displacement-based seismic design of structures. IUSS Press, Pavia, Italy, pp 184–189
6. IS 1893 (Part 1): 2016 Criteria for Earthquake Resistant Design of Structures, Part 1 General Provisions and Buildings
7. IS 13920: 2016 Ductile Design and Detailing of Reinforced Concrete Structures Subjected to Seismic Forces-Code of Practice
8. Pettinga JD, Priestley MJN (2005) Dynamic behaviour of reinforced concrete frames designed with direct displacement- based design. J Earthq Eng 9(2):309–330
9. Sutariya NK, Shah BA (2016) A comparative study of force-based design and direct displacement-based design for RC buildings. Int Res J Eng Technol 3(5):1–9
10. Sullivan TJ, Calvi GM et al (2003) The limitations and performances of different displacement-based design methods. J Earthq Eng 7(1):201–241
11. Sullivan TJ, Priestley MJN et al (2006) Direct displacement-based design of frame-wall structures. J Earthq Eng 10(1):91–124

A Comparative Study of FBD and DDBD of Two-Dimensional Steel Frames with Concentric Bracings

U. Sadhana and S. Karthiga

1 Introduction

Earthquake is one of the natural catastrophes that are random and uncertain. As these earthquake forces cause damage to the structures, the engineering tools needs to be enhanced for the analysis of structures constructed in seismically active regions. The Direct Displacement-Based Design (DDBD) is based on Force-Based Design (FBD), the ideal difference between both the methods are based on the displacement of the structure. In FBD, displacement of the structure is the final outcome to access the design performance level of the building, whereas the DDBD procedure applies designed target displacement. The main objective of DDBD procedure is to manage the structural deformations in order to control the structural damage [1]. The displacement profile is determined based on two criteria such as limit material strain and code specified drift limits [2, 3]. In this study, the drift limit of 0.020 was considered and the design procedure was carried out. Priestly methods were considered for the design procedure of DDBD.

2 Modelling and Analysis

The modelling and analysis of the concentrically braced steel frames were prepared using Structural Analysis Program SAP 2000 (version 14). Totally, 21 two-dimensional (2D) steel frames with concentric bracings [4] of height 15 m (5 storey), 30 m (10 storey), and 45 m (15 storey). The steel frames were modelled with 3 m constant storey height and 6 m bay width of 6 m. The gravity loads (dead load and

U. Sadhana · S. Karthiga (✉)
Department of Civil Engineering, College of Engineering and Technology, SRM Institute of Science and Technology, SRM Nagar, Kattankulathur 603203, Tamil Nadu, India
e-mail: karthigs@srmist.edu.in

K. S. Satyanarayanan et al. (eds.), *Sustainable Construction Materials*, Lecture Notes in Civil Engineering 194, https://doi.org/10.1007/978-981-16-6403-8_2

Table 1 Sectional properties of beams, columns and bracings

No. of storey	Beam elements (mm)	Column elements (mm)	Bracing elements (mm)
5	ISWB 300	ISWB 225	ISA 200 × 200X12
10	ISWB 350	ISHB 300	ISA 200 × 200X12
15	ISWB 300	ISHB 350	ISA 200 × 200X12

imposed load) on each storey were distributed as its own structure weight and the live load according to commercial buildings as per code [5]. ASTM A992Fy50 steel materials were used and the steel sections including the bracings were assigned as per code [6] after a series of iteration. The steel frames were sketched for the most actively seismic zone V [7] with a peak ground acceleration of 0.48 g and analysed for seven different ground movements [8]. The dimensions of beams, columns and bracings used in the study are shown in Table 1.

The elements of the steel frames were designed for flexural hinges as per code [9] and the ends are assigned with rigid support. The 2D steel frames modelled and designed by FBD were analysed by non-linear time history analysis. The concentrically braced steel frames at different levels are shown in Fig. 1. Further, design steps were carried out for DDBD procedure based on Priestly method.

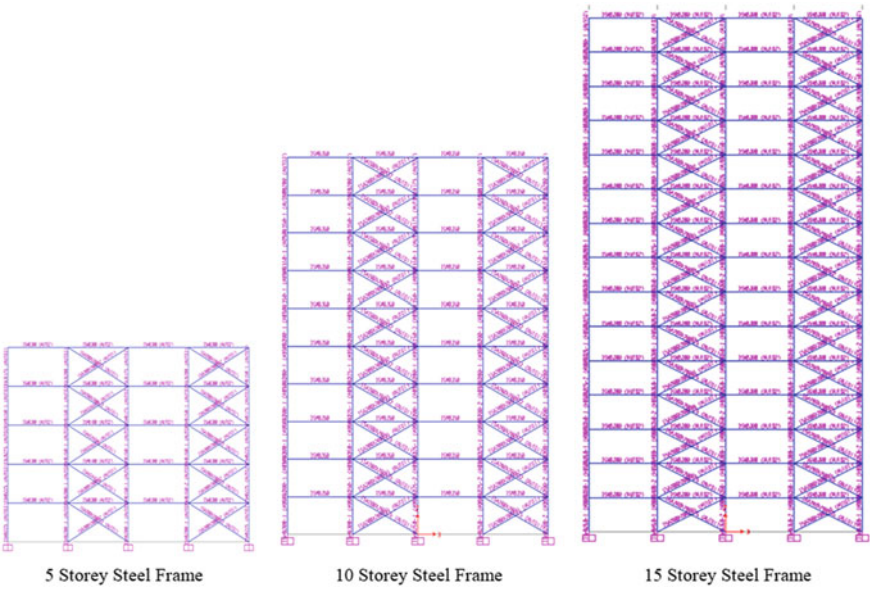

Fig. 1 Modelling of steel frames with concentric bracing

3 Results and Discussion

This paper elaborated the modelling, design and analysis of 2D concentrically braced steel frames (5S, 10S and 15S) of 5, 10 and 15 stories. The performances of the concentrically braced steel frames are evaluated by comparing their interstorey drift and base shear values. The results are shown below.

3.1 Interstorey Drift

Interstorey drift is defined has the relative displacement between one storey to the other storey, which is used as the parameter to examine the performance of the structure. The drift values are calculated from (Eq. 1) for FBDesign procedure.

$$\text{Interstorey drift} = \frac{(\Delta n + 1 - \Delta n)}{\text{h}} \tag{1}$$

Δ_{n+1} = Displacement at n+1th storey.
Δ_n = Displacement at nth storey.
h = height of storey.

The drift values of 5-, 10- and 15-storey 2D steel frames with concentric bracings for different ground motions by FBD and DDBD method are plotted below in Figs. 2, 4 and 6 and Figs. 3, 5 and 7, respectively.

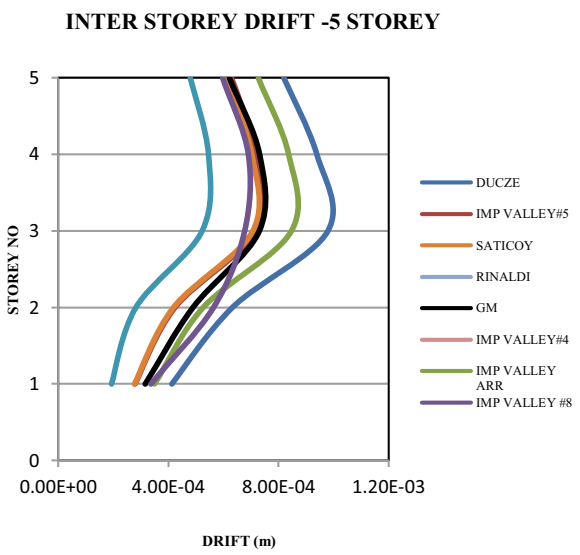

Fig. 2 Drift values by FBD (5S)

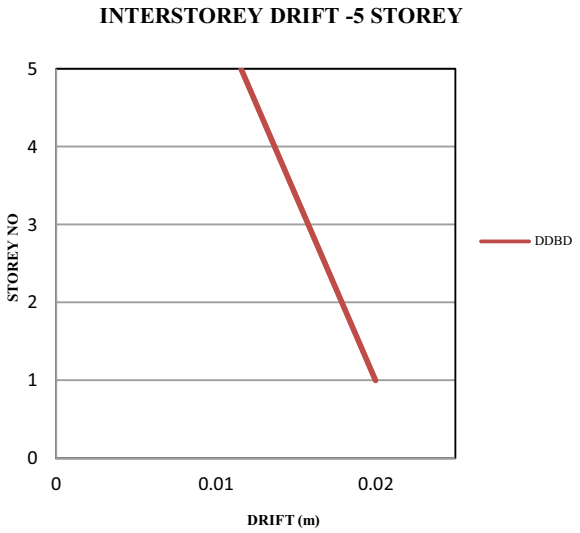

Fig. 3 Drift values by DDBD (5S)

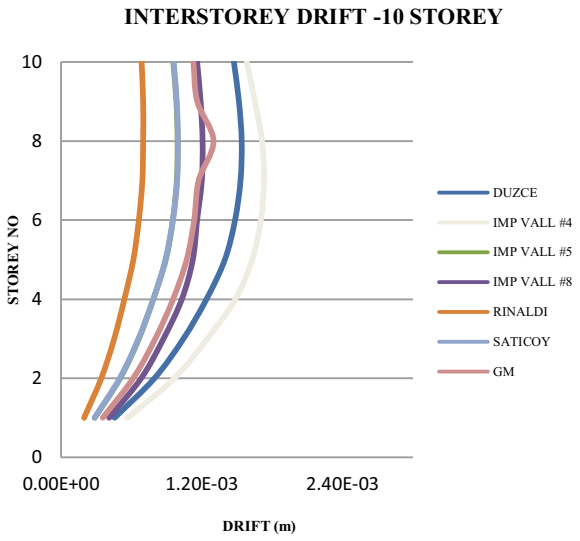

Fig. 4 Drift values by FBD (10S)

From the figures, it's clear that the interstorey drift value initially increases as the storey increases and then reduces as it reaches upper stories. The interstorey drift value gets increased by 56%, 66.8% and 79.5% at the intermediate stories for 5S, 10S and 15S frames, respectively, and then decreases by 15.1%, 5.15% and 6.83% for 5S, 10S and 15S frames, respectively, as the storey height increases. Generally, intermediate stories experiences higher interstorey drift values compared to lower and upper stories because of the elastic behaviour of lower and upper stories.

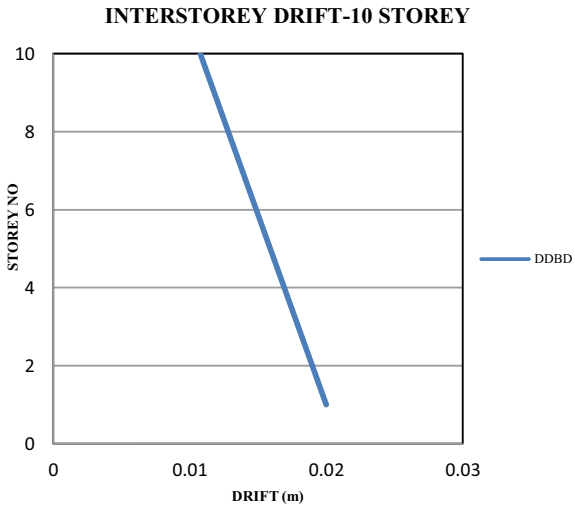

Fig. 5 Drift values by DDBD (10S)

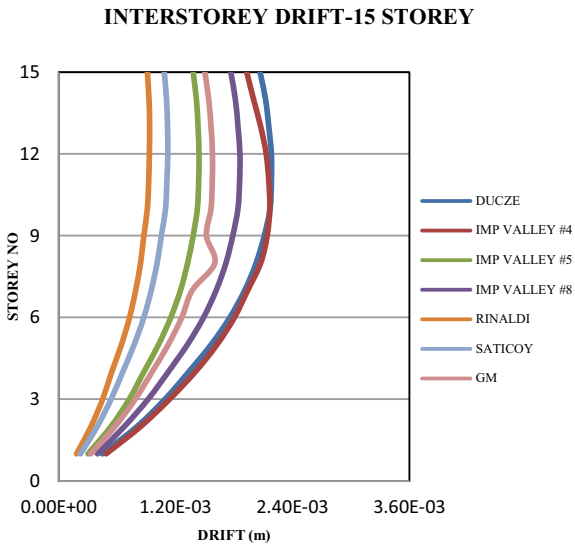

Fig. 6 Drift values by FBD (15S)

The design storey displacement (Δ_i) values for DDBD procedure was calculated manually by (Eq. 2) then the drift values are calculated from (Eq. 1), [10, 11].

$$\Delta_i = W_\Theta \Theta_c H_i \frac{4H - Hi}{4H - H1} \tag{2}$$

Hi = Storey Level at i Storey.
H = Total Height of the frame.

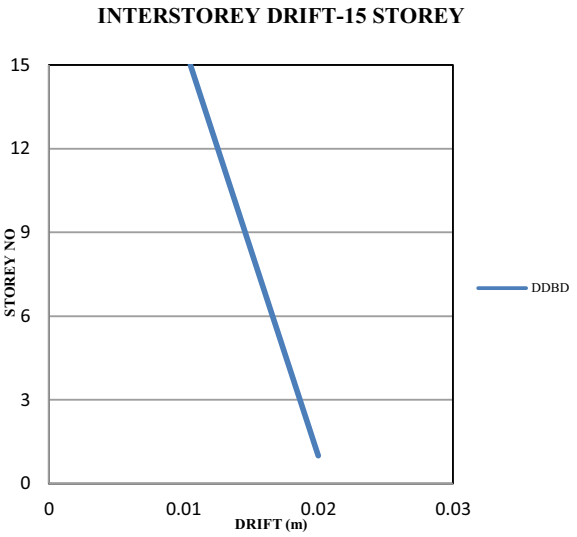

Fig. 7 Drift values by DDBD (15S)

Table 2 Comparison of interstorey drift values

No. of storey	FBD	DDBD
5	0.00073	0.015
10	0.0013	0.015
15	0.0016	0.015

H1 = Height of first storey.
$W_\theta = 1.15 - 0.0034\ H \leq 1.0$ is a reduction factor.
θ_c = Code drift limit.

The interstorey drift values are compared between FBD and DDBD of 2D steel concentrically braced frames are compared for their geomean values and are shown below in Table 2.

The interstorey drift values of DDBD is 95.4, 91.3 and 89.2% higher than the FBD for 5S, 10S and 15S frames, respectively, because of the rigid behaviour of the FBD, while the DDBD is more flexible in nature which helps in achieving higher drift values.

3.2 Base Shear

Base Shear is the measure of the expected lateral forces that occur at base of the structures during the earthquake. Typically, earthquake damage occurs at the base of the building and then the cracks develop due to the shear force. Hence, base shear is used as the parameter to define the performance of the structures. For FBD method,

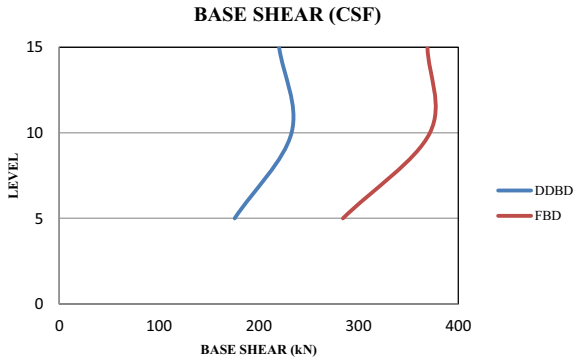

Fig. 8 Comparison of base shear values

Table 3 Base shear values of concentrically braced steel frames

No. of storey	FBD (kN)	DDBD (kN)
5	285	176
10	371	288
15	370	220

time history analysis of 5S, 10S and 15S steel frames were carried out and their geomean for base shear was calculated. In DDBD procedure, base shear (V_{base}) is calculated from (Eq. 3) [12]

$$V_{base} = K_e \Delta_d \tag{3}$$

K_e = Effective Stiffness (kN/m); Δ_d = Design Displacement (m).

The comparison of base shear values for 5, 10 and 15 stories of concentrically braced steel frames (CSF) is plotted in Fig. 8.

The base shear values of FBD and the DDBD are compared in Table 3.

On comparing the base shear of steel frames with concentric bracings shows that the values of FBD are greater than DDBD procedure. Table 3 indicates that the base shear values of FBD are greater than the DDBD by 61.7%, 29.3% and 67.43% for 5S, 10S and 15S, respectively, frames are indicated in Table 3.

4 Conclusion

This paper has explained the comparative study of DDBD and FBD, the methodology has been applied to 2D steel frames with concentric bracings.

(a) The above experiment shows that the interstorey drift values of DDBD is 95.4%, 91.3% and 89.2% higher than the FBD for 5S, 10S and 15S frames, respectively.

(b) The higher drift values explain the rigid behaviour of the FBD, while the DDBD is more flexible in nature which helps in achieving higher drift values.
(c) On comparing the base shear of steel frames with concentric bracings shows that the values of FBD are greater than the DDBD.
(d) The base shear values of FBD are 61.7%, 29.3% and 67.43% higher than the DDBD procedure for 5S, 10S and 15S frames, respectively, which explains better stability of the structure.
(e) From the results, it proves that the new methodology for the design and analysis of high-rise building gives better results, i.e. the DDBD is better when compared to FBD.

References

1. Priestly MJN, Calvi GM, Kowalsky MJ (2007) Displacement based seismic design of structures. IUSS PRESS, Pavia, Italy
2. Pirmoz A, (Max) Liu M (2017) Direct displacement based seismic design of semi-rigid steel frames. J Construct Steel Res 201–209
3. Priestly MJN, Kowalsky MJ (2000) Direct displacement based seismic design of concrete buildings. Bulletin New Zealand Soc Earthq Eng
4. Al Mashaykhi M, Rajeev P, Wijesundara KK (2019) Displacement profile for displacement based seismic design of concentric braced frames. J Constr Steel Res 155(2019):233–248
5. IS 1893 (Part-1)-2002 Indian standard code of practice for criteria for earthquake resistant design of structures. Bureau of Indian Standards, (New Delhi)
6. IS 800–2007 Indian standard code of practice for general construction in steel. Bureau of Indian Standards, (New Delhi)
7. Sil A, Das G, Hait P (2019) Characteristics of FBD and DDBD techniques for SMRF buildings designed for seismic zone-V in India. J Build Pathol Rehabilit 4:1
8. Moehle JP (1996) Displacement based seismic design criteria. Eleventh world conference on Earthquake Engineering
9. FEMA 356 (2000) (Federal Emergency and Management Agency)
10. Timothy John Sullivan (2013) Direct displacement based seismic design of steel eccentrically braced frame structures. Bull Earthq Eng 2013(11):2197–2231
11. Abhyuday T (2017) Fundamentals of direct displacement based design procedure-A brief introduction. Disaster Adv 10 (6)
12. Dohadwala AT, Sheth RK, Dr. Patel IN (2014) Comparison of base shear for forced based design method and direct displacement based design method. Int J Adv Eng

The Behaviour of Seven-Storey Infilled RC Frame with Opening in Infill—An Analytical Study

G. Prem Kumar, V. Thirumurugan, and K. S. Satyanarayanan

1 Introduction

The reinforced concrete member [1] and steel members [2] are used as a framed structure nowadays for all type of buildings. The precast members like beams and columns were also used as a framed structure [3]. In the recent research, the conventional reinforced concrete member and steel members were replaced with the glued—laminated timber fiber as a frame in structure [4]. The various frame members were practiced in the construction with infilled masonry as a combo model. The masonry infills are the un-reinforced members which is not having the specific codal provisions for designing. Various studied were made in analyzing the RC infilled frames under the lateral loading for measuring the stiffness, energy dissipation, drift factor, displacement and principal stresses [5, 6]. The masonry infills are the major portion of failure in all tall building structures. Many researchers have studied this effect of lateral loads in RC infilled framed structures and steel framed masonry infilled structures. The failure modes and crack propagation in different areas have been studied in detail by many authors. To overcome this issue, a diagonal strut model is designed at the loading end to the other beam column joint for resisting the lateral load transfer in the structure [6]. The strut models are not that much effective and it's not having the practical ability to implement in the construction fields. Introducing the infill in between the RC members creates damage in the infill when the load is applied acting it. This load transfer is due to reinforced concrete possesses the flexible range where the un-reinforced masonry failed that property. To overcome this flexibility issue, the shear walls are constructed by some researchers and analysed the stiffness and strength properties [7]. This technique possesses greater self-weight that cannot be used in

G. P. Kumar (✉) · V. Thirumurugan · K. S. Satyanarayanan
Department of Civil Engineering, SRM Institute of Science and Technology, SRM Nagar, Tamil Nadu, Kattankulathur 603 203, India
e-mail: pg2124@srmist.edu.in

K. S. Satyanarayanan et al. (eds.), *Sustainable Construction Materials*, Lecture Notes in Civil Engineering 194, https://doi.org/10.1007/978-981-16-6403-8_3

high-rise building. In recent days, an elastic medium like cork, lead, gaps, pneumatic and other elastic materials are used in the interface of the reinforced concrete member and masonry infilled panels [8]. These elastic mediums in between the members will resist the structure from damage and prevent the crack propagation and to avoid the structure from collapse. In the realistic models, the infilled walls possess openings for ventilations like door and windows. Some researchers have been made by incorporating the openings in the walls with varying size and location of the openings [4, 5, 7, 9–11]. The stiffness, displacement and stress were compared with the bare frame, RC infilled walls and RC infilled walls with openings. The members are tested by both static loading and cyclic loading [12]. Many researchers have tested the RC infilled frames with openings using up to three storey heights only. This study deals with the tall building effect of seven-storey RC infilled frames with openings in it.

2 Finite Element Model

The seven-storey RC infilled panel is tested using the Finite Element Analysis software (Abaqus). The panel is scaled down to 1/4 of prototype model and it is taken for testing. The dimensions of the specimens are described detail in Table 1.

The frame was cast using M20 grade of concrete for beams and columns, M40 grade of concrete for foundation. The steel used here was 16 mm main reinforcement for foundation, 10 mm main reinforcement for beams and columns and 6 mm bars for stirrups. The model was created using this material and the properties like modulus of elasticity and Poisson ratio were given to the model for respective materials. The openings in the infill are maintained as 50% from the masonry infill area.

Table 1 Dimension of single-bay seven-storey frame [13]

S. no	Specimen	Prototype model (mm)	Scale down model (mm)	Scale adopted
1	Ground floor storey height	2700	675	1/4
2	Other floors height	2400	600	1/4
3	Bay width	4000	1000	1/4
4	Beam dimension	400 × 600	100 × 150	1/4 × 1.5
5	Column dimension	400 × 800	100 × 200	1/4 × 1.5
6	Infill dimension (HxWxT)	3000 × 4720 x 2 30	600 × 1000 x 8 0	1/4 × 1.6x1.5

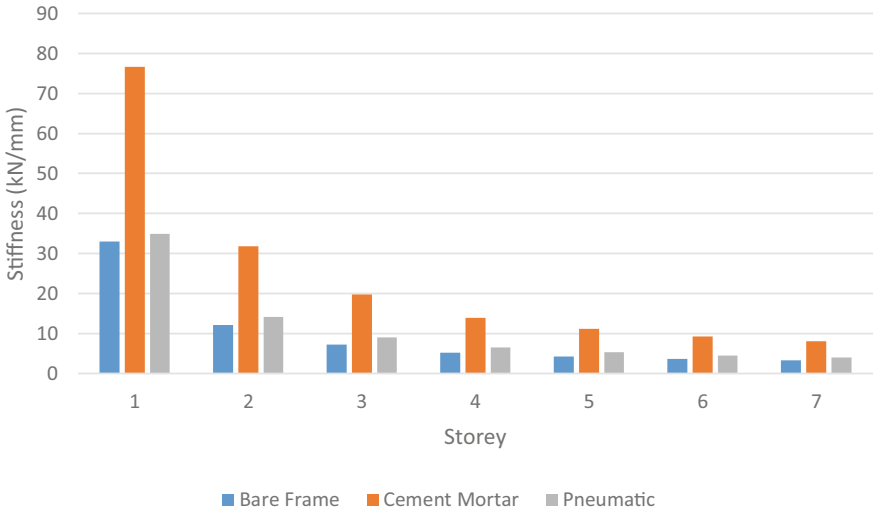

Fig. 1 Comparison of stiffness at various storeys with different interface materials

3 Results and Discussion

3.1 Lateral Stiffness

The stiffness value is calculated by the load applied in the seven-storey frame at three different points and to the displacement. The stiffness is compared to the three different specimens like RC bare frame, RC infilled frame with opening comprising the cement mortar as interface material and RC infilled frame with opening comprising the pneumatic interface material. The variation in stiffness for bare frame another infilled frame with different interface materials is shown in Fig. 1. The stiffness is more in cement mortar interface RC frame when compared to bare frame and pneumatic interface frame. There is only a slight difference in bare frame and pneumatic interface frame. The peak shows that there is high stiffness in cement mortar interface frame due to more rigidity in interface materials. The stiffness for IFCMO is 54.5% higher than the bare frame and IFPO frame due to the rigidity property of the cement mortar interface. When comparing the stiffness for bare frame and IFPO the stiffness is 5.5% more in IFPO than the bare frame.

3.2 Lateral Displacement

The displacement results shows that there is a peak in bare frame when comparing to other frames (Fig. 2). This peak is due to the flexibility in RC member with

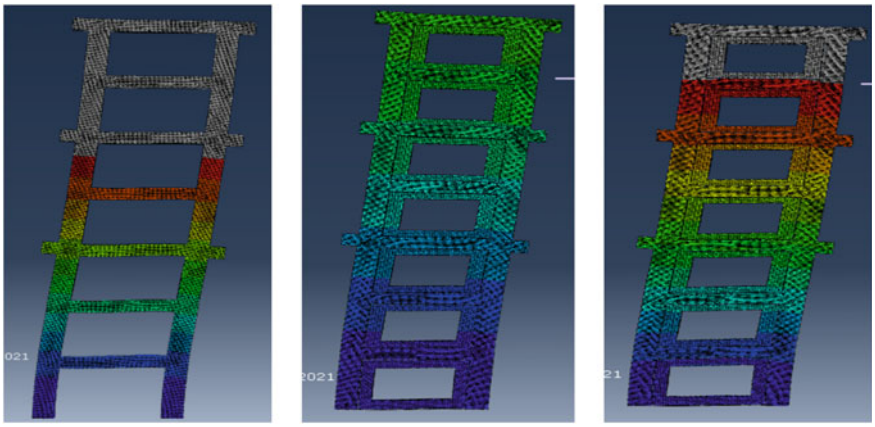

(a) Bare frame **(b)** IFCMO **(c)** IFPO

Fig. 2 Displacement in RC bare frame and infilled seven-storey frames

having infill in between the RC members. There is less displacement in RC infilled frame with opening in the masonry infill with cement mortar interface due to the high stiffness in the interface medium when comparing to pneumatic interface. The displacement for the IFCMO is 55.8% lesser when compared to bare frame and IFPO due to the higher stiffness by cement mortar having better bonding with the masonry infilled materials than the IFPO (Fig. 3).

3.3 Minimum Principal Stress

Figure 4 clearly shows the stress is initially at the opposite end to the loading point. The initial stress is starts at the point where the columns are supported. The minimum principal stress is compared with the infilled frame cement mortar interface with opening (IFCMO) and infilled frame pneumatic interface with opening (IFPO). Figure 5 represents that there is an increase in stress for IFCMO when compared to IFPO. This result is due to the increase in stiffness by cement mortar interface bonded with the masonry infill than the pneumatic interface.

3.4 Maximum Principal Stress

The stress is distributed along the masonry infills which is transferred from the reinforced concrete member (Fig. 6). The maximum principal stress is measured when the peak load is applied to it. The stress is high for the IFCMO than the IFPO

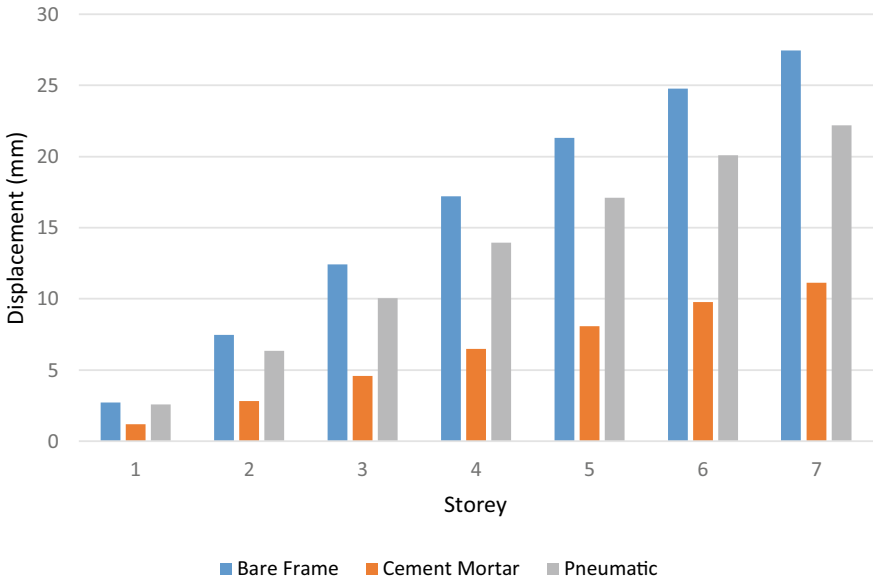

Fig. 3 Comparison of displacement at various storeys with different interface materials

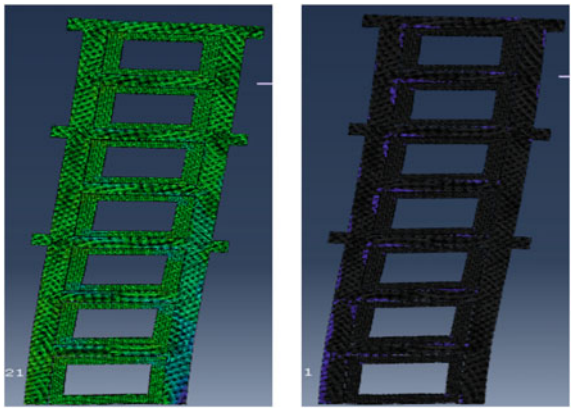

Fig. 4 Minimum principal stress in RC infilled seven-storey frame

due to the increase in rigidity of interface material comparatively (Fig. 7). The infilled frame have the poor resistance in lateral load due to its stress distribution through the masonry infills.

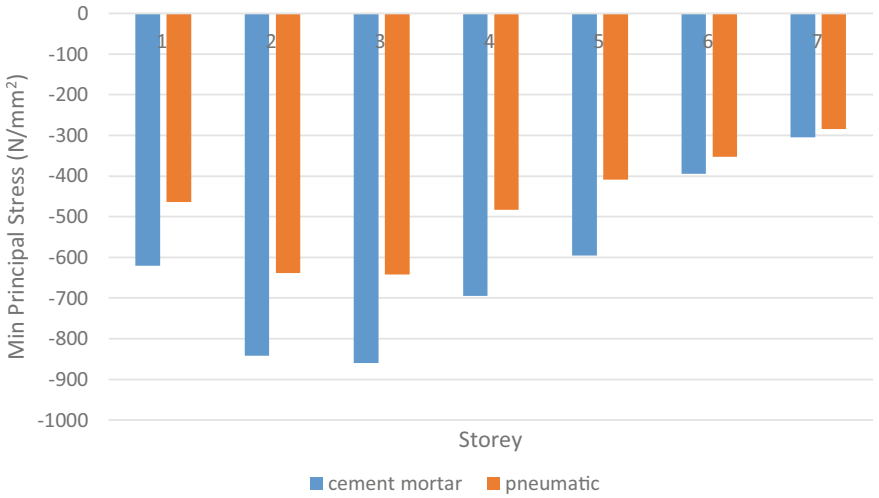

Fig. 5 Comparison of minimum principal stress at various storeys with different interface materials

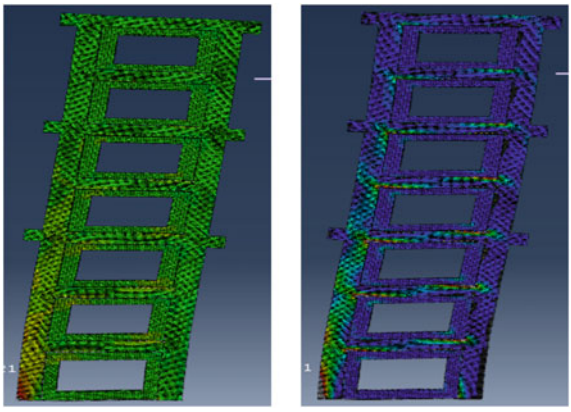

Fig. 6 Maximum principal stress in RC infilled seven-storey frame

4 Conclusion

The conclusions were made with the comparative results using different interface mediums:

1. The RC fully infilled frame increases the poor resistance in lateral loading which is clearly proved by many researchers. So, this study deals with the partial infill in the high-rise buildings and their characteristics were studied in detail.
2. The stiffness for IFCMO is 54.5% higher than the bare frame and IFPO frame due to the rigidity property of the cement mortar interface.

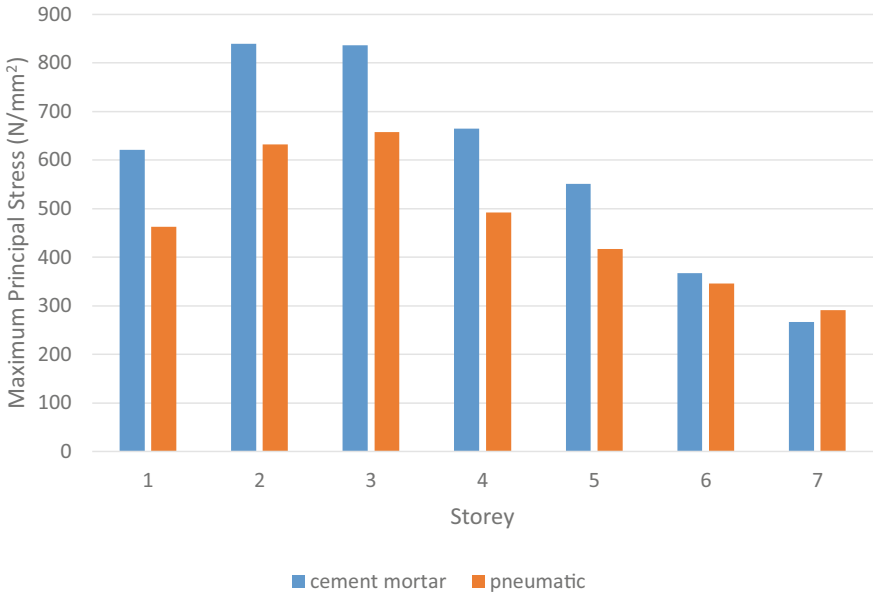

Fig. 7 Comparison of maximum principal stress at various storeys with different interface materials

3. When comparing the stiffness for bare frame and IFPO the stiffness is 5.5% more in IFPO than the bare frame.
4. The displacement for the IFCMO is 55.8% lesser when compared to bare frame and IFPO due to the higher stiffness by cement mortar having better bonding with the masonry infilled materials than the IFPO.
5. The IFPO frame is displaced more when comparing to IFCMO frame is due to the flexible interface material in between the masonry infill and RC member which transfers the load from RC member to the Pneumatic interface.
6. The displacement has slight difference by 19.06% lesser when comparing the bare frame due to absence of infill in the bare frame.
7. The maximum and minimum principal stresses show that the IFCMO has the maximum stress distribution due to its bonding and rigid property than IFPO.

References

1. Uva G, Porco F, Fiore A (2012) Appraisal of masonry infill walls effect in the seismic response of RC framed buildings: a case study. Eng Struct 34:514–526
2. Tasnimi AA, Mohebkhah A (2011) Investigation on the behavior of brick-infilled steel frames with openings, experimental and analytical approaches. Eng Struct 33:968–980
3. Wang L, Tang Z-Y, Li Y, Qian K (2019) Seismic behavior of masonry-infilled precast concrete frames considering effects of opening. Construct Build Mater 211:756–770

4. Xue J, Ren G, Qi L, Zhang X (2021) Lateral behavior of glued-laminated timber frame infilled with light-wooden-frame wall hybrid system: experimental and numerical analysis. Structures 30:352–367
5. Chen X, Liu Y (2015) Numerical study of in-plane behaviour and strength of concrete masonry infills with openings. Eng Struct 82:226–235
6. Mohamed H, Romão X (2020) Analysis of the performance of strut models to simulate the seismic behaviour of masonry infills in partially infilled RC frames. Eng Struct 222:111–124
7. Zhai X, Zhang X, Cao C, Hu W (2019) Study on seismic performance of precast fabricated RC shear wall with opening filling. Construct Build Mater 214:-539–556
8. Thirumurugan V, Muthu Kumar S, Husam Ahmed W, Ganesan TP, Satyanarayanan KS (2015) Behavior of infilled frames with different interface materials. RASCE
9. Liberatore L, AlShawa O, Marson C, Pasca M, Sorrentino L (2020) Out-of-plane capacity equations for masonry infill walls accounting for openings and boundary conditions. Eng Struct 207:110–198
10. Penavaa D, Sarhosis V, Kozar I, Guljas I (2018) Contribution of RC columns and masonry wall to the shear resistance of masonry infilled RC frames containing different in size window and door openings. Eng Struct 172:105–130
11. Yekrangnia M, Asteris PG (2020) Multi-strut macro-model for masonry infilled frames with openings. J Build Eng 32:101–683
12. Morandi P, Hak S, Magenes G (2018) Performance-based interpretation of in-plane cyclic tests on RC frames with strong masonry infills. Eng Struct 156:503–521
13. Thirumurugan V, Ganesan TP Studies on the use of pneumatic interface in reinforced concrete infilled frames. http://hdl.handle.net/10603/220960

Strength Enhancements in Tensile Properties of Steel by Press Brake Cold Forming

M. S. Deepak and G. Beulah Gnana Ananthi

1 Introduction

The cold-formed steel built-up Hybrid Double-I-Box Beams (HDIBBs) are made of different grades of steel sheets done by Deepak et al. [1, 2]. In this study, the steel sheets manufactured employing both hot-rolled and cold-rolled processes are used. The sections are formed by press braking operation. The amount of cold work varies for each segment in the different regions of the cross section. Ananthi et al. [3, 4] studied the behaviour of cold-formed structural steel in compression using medium strength steel. Knowing the exact material properties sheets (before forming) and sections (after forming) as essential to evaluate the tensile strength and stress–strain characteristics of each segment in a cold-formed steel member. Afshan et al. [5] conducted material testing programme on various grades of steel materials to evaluate the strength enhancements in cold-formed structural steel sections that arise during different methods of manufacturing processes. They proposed predictive models to estimate the increase in yield strength during manufacture of cold-formed steel sections. The method offers on an average of 19% and 36% strength enhancements comparative to the minimum codified strength as provided in the European standards. Chen and Young [6] assessed the feasibility of current design standards available for the design of stainless-steel structures. They reported that the tensile strength predictions by existing specifications are conservative and can be reliable. Ho et al. [7] reported that steels with same grades but made of different manufacturing processes possess deformation properties. Xiong and Liew [8] from their research reported that

M. S. Deepak (✉)
Department of Civil Engineering, BMS Institute of Technology and Management, Bengaluru, India

G. B. G. Ananthi
Department of Civil Engineering, Division of Structural Engineering, Anna University, Chennai, India
e-mail: beulah28@annauniv.edu

K. S. Satyanarayanan et al. (eds.), *Sustainable Construction Materials*, Lecture Notes in Civil Engineering 194, https://doi.org/10.1007/978-981-16-6403-8_4

high strength steel has smaller comparative thermal elongation and higher reductions of effective yield strength and elastic modulus at raised temperatures. In this study, the coupon specimens are prepared and tested according to the guidelines provided in European standards EN ISO 6892-1-2009 [9]. The stress–strain graphs are drawn for the tested coupon pieces and their properties are inferred from the plots. The results obtained are compared with the equivalent international standards and mill certificates provided by the manufacturer.

2 Research Significance

The material properties and engineering stress–strain characteristics obtained from these tensile tests are converted into true stress–strain values and can be provided as input in the modelling of finite element models, for performing the numerical analysis. The bending residual stresses are re-introduced due to forming. The paper gives a clear idea on the characteristics of commonly used steel materials for research and production purposes.

3 Steel Products

The sheet metal is manufactured by TATA steel (P) limited India and procured from Govindaraja Mudaliyar Sons, suppliers, Chennai. The supplier provided the mill certificates mentioning the grade of steel (G). The steel products and their equivalent European standards are as tabulated in (Table 1). In the present study, the prime interest is on European standards as the metallurgy and manufacturing technology of the products comply with EN 10,025 and EN 10,130.

4 Coupon Specimens' Preparation

Flat coupons in two groups are prepared and tested. The first group consists of are cut from the flat sheets before forming in three different regions, namely, longitudinal, transverse and diagonal directions. The second group consists of coupons which are extracted from different flat portions of the channels. At least two coupons are cut tested from each group of the sections to find out the average results; therefore, the error is minimised. The effect of cold work forming at the corners is not included in this study. All the tensile coupons specimens are prepared, sized and tested according to recommendations suggested in EN ISO 6892–1-2009 [9] standards. Coupons are sized using the available machining facilities. Accurate measurements of the cross sections, length, width and thickness are made using a digital Vernier calliper. Typical prepared coupon specimens are shown in (Fig. 1). Based on the gripped end width

Table 1 Product specifications and their equivalent European standards

Tata product name and size, L × B × t (mm)	Classification		Strength as per manufacturer		Elongation percentage	Nominal strength as per European code		Equivalent standards
	Product	Type	f_y (N/mm^2)	f_u (N/mm^2)	%	f_y (N/mm^2)	f_u (N/mm^2)	European
CRSHEET-ICF TATXXD AU03-2500 × 1250 × 2.5 mm	Cold Rolled (CR)	Low Tensile (LT)	140/ 220	280	35	140/180	270/330	EN 10,130: 2006 DC03 CR
HRC IS2062E250Fe410 WGrASME-2500 × 1250 × 2.5 mm	Hot Rolled (HR)	Medium Tensile (MT)	255	410	23	245	380	EN 10,025 Part 2:2004 S275 JO
HR COIL DIN17100ST52.3 SH-ECA-2500 × 1250 × 2.5 mm	Hot Rolled (HR)	High Tensile (HT)	355	490	22	310	450	EN 10,025 Part 2:2004 S355 JO

(a) Machined and sized coupons

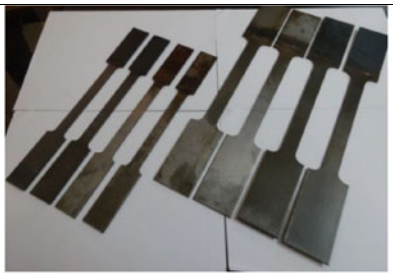

(b) Surface cleaned coupons

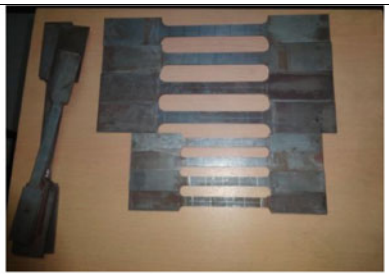

(c) Marked coupons

Fig. 1 Prepared coupon specimens

and the required parallel width of the specimen, the radius of the cutting is provided. The larger is the size of the coupons (parallel length and width), the greater is the precision. The coupon sizes are illustrated in (Fig. 2).

5 Test Set-Up and Instrumentation

The tests are performed using a Zwick/RoellZ100kN Electro-mechanical testing machine. The tensile test set-up for testing coupon specimens is shown in (Fig. 3). According to the procedure recommended in EN ISO 6982-1-2009 International standards, displacement control method of testing is adopted. The uniform crosshead displacement rate applied is 0.01 mm/s in the present investigation since the materials tested are having $E = 200{,}000\ N/mm^2$ or higher. Necking of coupons within the gauge length is observed due to the application of tensile load during testing, just before fracture. The testing of coupons and failure of a typical coupon specimen under tensile load is illustrated in (Fig. 4).

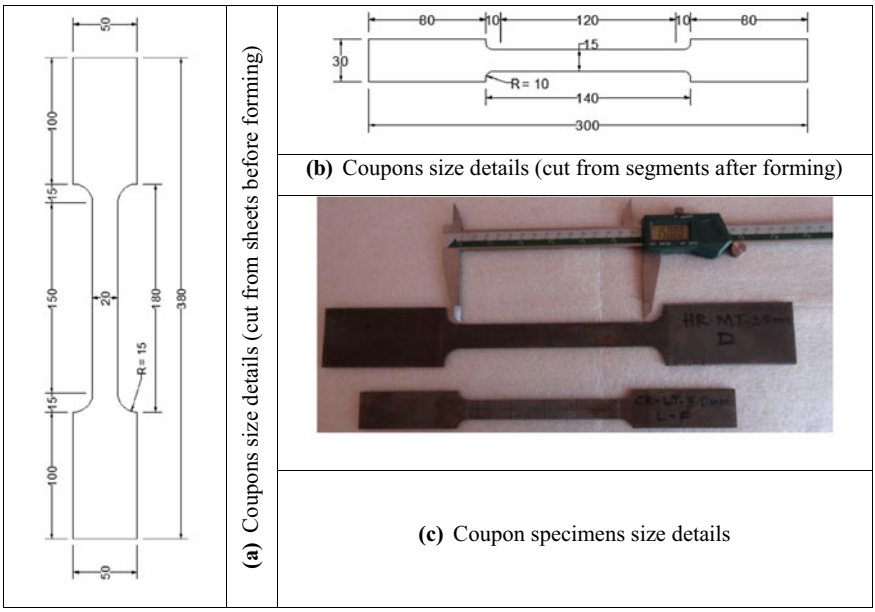

Fig. 2 Sizing of coupons

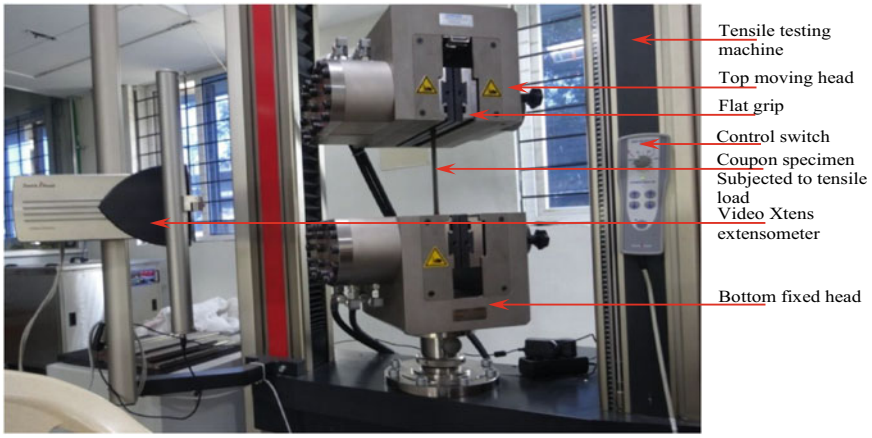

Fig. 3 Tensile test set-up

6 Results and Discussion on Tensile Properties of Materials

The static stress–strain plots are automatically generated and recorded for all the tests. Three key parameters are obtained they are the yield stress (f_y), the ultimate stress (f_u) and the best-fit modulus of elasticity (E). The comparison of stress–strain

Fig. 4 Failure of a coupon under tensile load

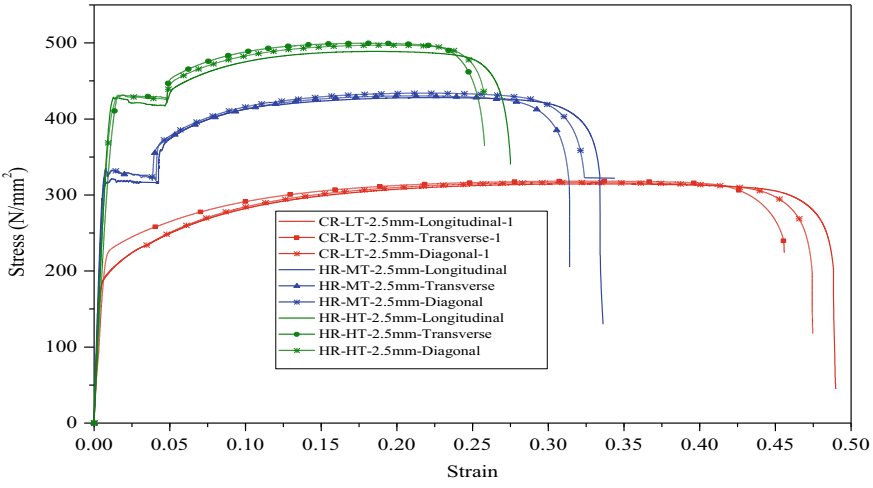

Fig. 5 Comparison of stress–strain characteristics of the sheet cut coupons

characteristics for 2.5 mm thick sheet cut coupons that are cut in all three directions from all three grades of steel are shown in (Fig. 5).

6.1 Material Properties of Coupons Extracted from Steel Sheets Before Forming

Large size coupons are cut in three directions, namely, longitudinal, transverse and diagonal directions from the steel sheets of size 2500 × 1250 mm and 2.5 mm think including all grades. The tensile test results for sheet cut coupons before forming is given in (Table 2). The cold-rolled-low tensile strength (CR-LT) steel material showed a gradual stress–strain response in which there a well-defined yield point is absent, hence 0.2% proof stress is taken as yield stress. The hot-rolled-medium tensile (HR-MT) and hot-rolled-high tensile (HR-HT) strength steel materials exhibited a sharp response; hence, their yield stresses are taken from a well-defined yield point.

6.1.1 Tensile Test Results of CR-LT Steel Sheets

The properties for nominal grade G140 cold-rolled steel sheets (DC03 CR) is confirming to Eurocode standards EN 10,130: 2006. The nominal basic yield strength (f_{yb}), of CR-LT sheets, is taken as 140 MPa according to (Table 3) of Eurocode EN

Table 2 Tensile test results of sheet cut coupons before forming

Classification as per eurocode standards	Location of strip cut	Thickness (mm)	Width B (mm)	Yield stress, f_y (N/mm^2)	Ultimate stress, f_u (N/mm^2)	Ratio, f_u/f_y	Elasticity modulus, E (GPa)
Group-1 (CR- LT)	Longitudinal	2.50	20.01	211.29	304.85	1.44	207
EN10130: 2006 DC03 CR	Transverse	2.49	20.01	226.37	308.08	1.36	206
Steel Grade: G 140	Diagonal	2.50	20.00	215.42	306.38	1.42	207
Group-2 (HR- MT)	Longitudinal	2.50	20.00	315.09	428.12	1.36	215
EN 10,025 Part 2:2004 S275 JO	Transverse	2.50	20.01	319.17	430.27	1.35	214
Steel Grade: G 245	Diagonal	2.50	20.02	318.83	421.49	1.32	215
Group-3 (HR- HT)	Longitudinal	2.50	20.01	417.10	494.08	1.18	221
EN 10,025 Part 2:2004 S355 JO	Transverse	2.49	20.02	420.80	499.52	1.21	221
Steel Grade: G 310	Diagonal	2.50	20.01	418.97	497.02	1.17	218

Table 3 Tensile test results of section cut coupons after forming

Classification as per Eurocode standards	Location of strip cut	Thickness (mm)	Width B (mm)	Yield stress, f_y (N/mm^2)	Ultimate stress, f_u (N/mm^2)	Ratio, f_u/f_y	Elasticity modulus, E (GPa)
Group-1 (CR- LT)	Flange –L-1	2.50	15.01	234.61	339.43	1.45	211
Steel grade: G 140	Flange –L-2	2.50	15.00	230.65	338.44	1.47	215
	Web –L-1	2.50	15.02	236.79	319.74	1.35	209
	Web –L-2	2.50	15.01	232.83	317.76	1.37	210
					Mean:	1.41	
Group-2 (HR- MT)	Flange –L-1	2.50	15.00	337.56	432.73	1.27	213
Steel grade: G 245	Flange –L-2	2.50	15.01	337.66	429.72	1.27	212
					Mean:	1.27	
Group-3 (HR- HT)	Flange –L-1	2.50	15.01	463.48	510.79	1.11	220
Steel Grade: G 310	Flange –L-2	2.50	15.00	459.52	503.86	1.11	221
*L—Long channel sections-2500 mm					Mean:	1.11	

3.1.3, that is given for materials used in forming structural sections that are not mentioned in the design standard. At first, for coupons cut in the longitudinal direction, the range of yield stress is between 211 and 222 MPa, and the range of ultimate stresses is between 305 and 320 MPa. The experimental yield stresses are on an average 50% higher than the nominal basic strength which is limited to 140Mpa. Secondly, for coupons cut in the transverse direction, the range of yield stresses is between 226 and 240 MPa, and the range of ultimate stresses is between 308 and 324 MPa. The experimental yield stresses are on an average 61% higher. Thirdly, for coupons cut in the diagonal direction, the range of yield stresses is between 215 and 234 MPa, and the range of ultimate stresses is between 306 and 321 MPa. The experimental yield stresses are at least 53% higher.

6.1.2 Tensile Test Results of HR-MT Steel Sheets

The properties for nominal grade G245 hot-rolled steel sheets (S275 JO-HR) are confirming to Eurocode standards EN 10,025 Part 2: 2004. The nominal basic yield strength of HR-MT sheets is taken as 275 MPa according to (Table 3) of EN 3.1.3. At first, for coupons cut in the longitudinal direction, the range of yield stresses is between 315 and 352 MPa, and the range of ultimate stresses is between 428 and

453 MPa. The experimental yield stresses are at least 15% higher than basic strength that is limited to 275 MPa; Secondly, for coupons cut in the transverse direction, the range of yield stresses is between 319Mpa and 357 MPa, and the range of ultimate stresses is between 430 and 468 MPa. The yield stresses are on average 16% higher. Thirdly, for coupons cut in the diagonal direction, the range of yield stresses is between 319 and 354 MPa, and the range of ultimate stresses is between 421 and 457 MPa. The measured yield stresses are at least 16% higher.

6.1.3 Tensile Test Results of HR-HT Steel Sheets

The properties for nominal grade G310 hot-rolled steel sheets (S355 JO-HR) are confirming to Eurocode standard EN 10,025 Part 2:2004 [10]. The nominal basic yield strength of HR-HT sheets is taken as 310 MPa according to (Table 3) of EN 3.1.3. At first, for coupons cut in the longitudinal direction, the range of yield stresses is between 417 and 429 MPa, and the range of ultimate stresses is between 494 and 505 MPa. The experimental yield stresses are at least 34% higher than basic strength that is limited to 310 MPa. Secondly, for coupons cut in the transverse direction, the range of yield stresses is between 421 and 423 MPa, and the range of ultimate stresses is between 500 and 513 MPa. The yield stresses are at least 35% higher. Thirdly, for coupons cut in diagonal the direction, the range of yield stresses is between 419 and 423 MPa, and the range of ultimate stresses is between 497 and 506 MPa. The yield stresses are at least 35% higher.

6.2 Material Properties of Coupons Extracted from Steel Sections After Forming

The CFS channels are 2500 mm long formed from the longitudinal direction of the steel sheet. The tensile tests result for section cut coupons after forming are given in (Table 3). Typical comparison plots showing stress–strain behaviour of sheet cut coupons (before forming) and section cut coupons (after forming) are illustrated in (Fig. 6).

6.2.1 Tensile Test Results of CR-LT Steel Sections

The properties of coupons for nominal grade G140 (i.e. CR-LT) cut from the flanges and web portions of the formed long channels, the yield stresses are in the range of 231 MPa and 235 MPa, and the range of ultimate stresses is 318 MPa and 340 MPa. The yield stresses are at least 10% higher than those obtained from testing longitudinal direction sheet cut coupons. This increase in stresses indicates that a substantial amount of cold work done. The elasticity modulus obtained from the tests is between

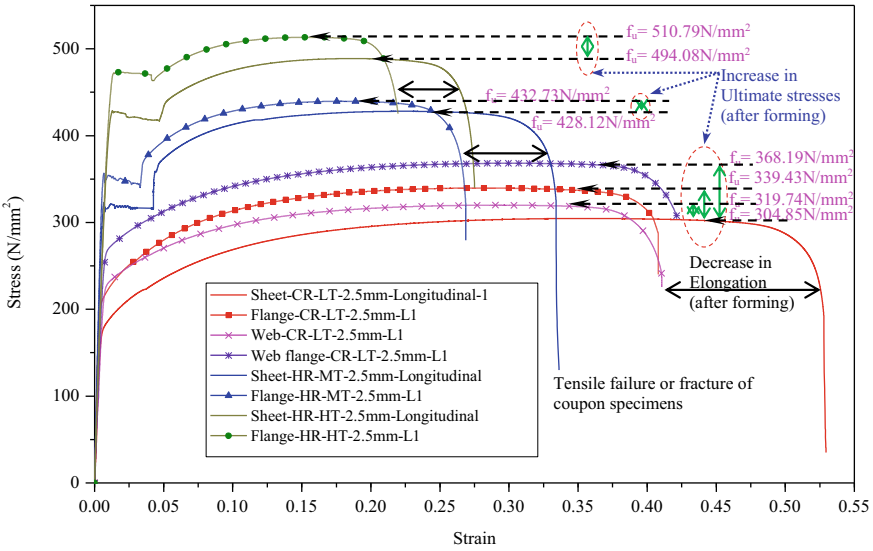

(a) Full stress-strain curves of longitudinal direction cut coupons- L1

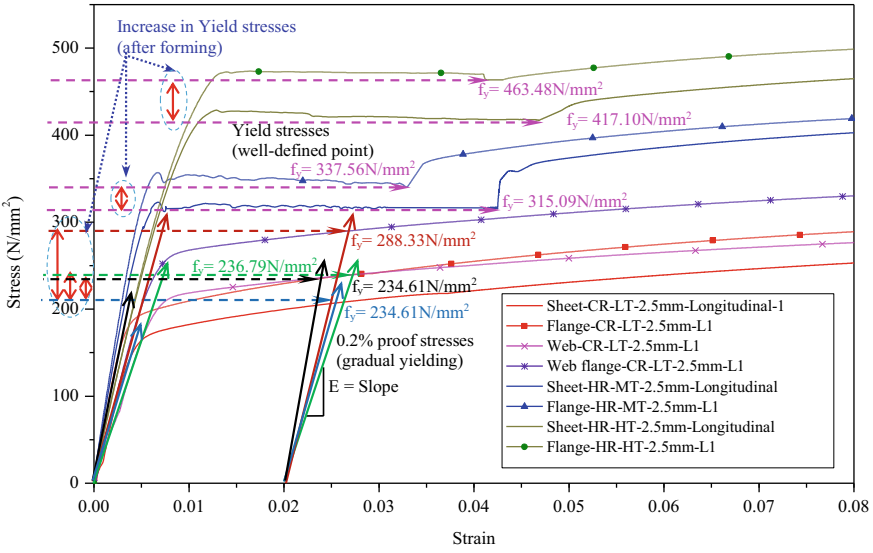

(b) Initial part of stress-strain curves- L1

Fig. 6 Comparison of stress–strain characteristics of 2.5 mm thick longitudinal direction cut coupons—L1 (before and after forming)

209 and 215GPa. The average ratio of ultimate strength to yield stress, $f_u/f_y = 1.41$ which is greater than 1.10 as recommended by EN 3.1.1 clause 3.2.2. This, shows that these cold-rolled sheets have good ductility behaviour. A large elongation and necking are observed before failure while testing of coupon specimens that exhibits CR-LT possesses high ductility behaviour.

6.2.2 Tensile Test Results of HR-MT Steel Sections

The properties of coupons for nominal grade G245 (i.e. HR-MT) cut from cut from the flange portions of the formed long channels, the yield stresses are in the range of 337 MPa and 338 MPa, and the range of ultimate stresses is 430 MPa and 433 MPa. The experimental yield stresses are 9% higher than those determined coupons tests from sheets. The modulus of elasticity obtained from the tests is between 212 and 213GPa. The average ratio of ultimate strength to yield stress, $f_u/f_y = 1.27$ which is greater than 1.10. This shows that these medium tensile-grade hot-rolled sheets have reasonable ductility behaviour. Average elongation and necking of coupon specimens occurred before failure while testing exhibiting normal ductility behaviour in HR-MT-grade steel sections.

6.2.3 Tensile Test Results of HR-HT Steel Sections

The properties of coupons for nominal grade G310 (i.e. HR-MT) cut from flange portions of the formed channels in longitudinal direction, the yield stresses are in the range of 460 MPa and 464 MPa, and the range of ultimate stresses is 504 MPa and 511 MPa. The experimental yield stresses are on at least 9% higher than those obtained by testing coupons cut from sheets in the longitudinal direction. The elasticity modulus obtained from the tests is between 220 and 221GPa. The average ratio of ultimate strength to yield stress, $f_u/f_y = 1.11$ which is greater than 1.10. This shows that this high strength-hot-rolled steel has less ductility behaviour. Low elongation and quick fracture of coupon specimens are observed while testing. These fracture characteristics display low ductility in HR-HT-grade steel sections. Fracture of coupon specimens both before and after forming is shown in (Fig. 7).

7 Conclusion

A series of experimental tests to determine the tensile properties of various grades of steel materials by testing their coupons extracted from the steel sheets before forming and from the various segments of the sections after forming have been conducted in this study. The following are the findings depicted based on the tensile test results of coupons and their characteristic stress–strain plots.

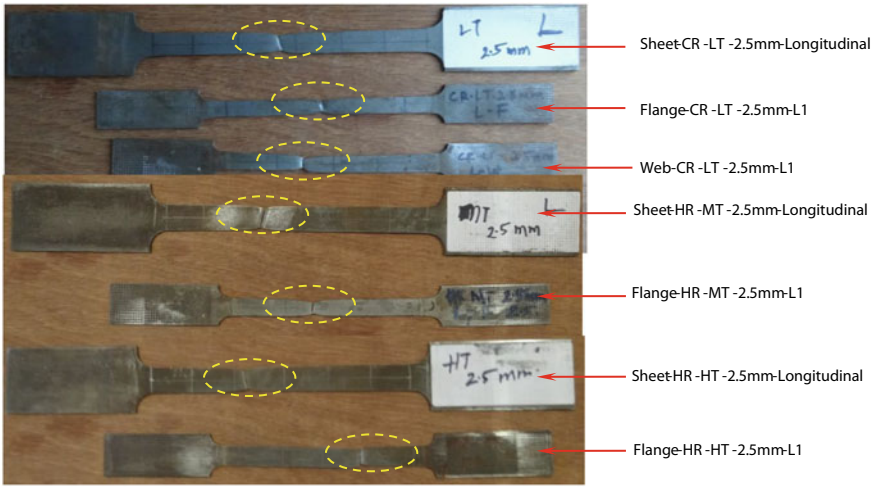

Fig. 7 Experimental fracture of 2.5 mm thick longitudinal direction cut coupons—L1 (before and after forming)

- In the sheet cut coupons testing from the results obtained, it is evident that there exists a marginal material anisotropy. The yield point strength and ultimate strength of tested coupons cut in transverse direction is slightly higher in comparison to those from longitudinal and diagonal directions. The coupons cut from longitudinal direction showed the minimum strength for all grades of steel.
- On comparison of the stress–strain plots cold-rolled process manufactured steel materials exhibited a gradual stress–strain response, whereas hot-rolled process manufactured products showed sharp definite yield point characteristics.
- The yield strengths and the ultimate strength of the plates are increased after press braking the sheets formed into sections. The higher the cold-forming at the segments the higher is the increase in their yield strength.
- The percentage increase in ultimate strength of the steel sheets formed into sections in longitudinal direction considered in this research are such that (i) for CR-LT steel grade, the increase is 10%, (ii) for HRMT steel grade, the increase is 9% and (iii) for HRHT steel grade, the increase is 9%
- The ductility is reduced after forming, whereas the elasticity modulus is enhanced.

References

1. Deepak MS, Shanthi VM (2018) Distortional buckling moment resistance capacity of hybrid-double-i-box beams. J Struct Eng 144(9)
2. Deepak MS, Shanthi VM (2018) Member distortional buckling behaviour of hybrid-double-i-box beams. Can J Civ Eng 45:605–622

3. Ananthi GBG, Roy K, Chen B, Lim JBP (2019) Testing, simulation and design of back-to-back built-up cold-formed steel unequal angle sections under axial compression, Steel and composite structures. Int J 33(4): 595–614
4. Ananthi GBG, Deepak MS, Roy K, Lim JBP (2021) Influence of intermediate stiffeners on the axial capacity of cold-formed steel back-to-back built-up unequal angle sections. Structures 32: 827–848
5. Afshan S (2013) Rossi, B and Gardner, L 'Strength enhancements in cold-formed structural sections - Part I: material testing.' J Constr Steel Res 83:177–188
6. Chen M-T, Young B (2020) Tensile tests of cold-formed stainless-steel tubes. J Struct Eng 146(9):04020165
7. Ho HC, Chung KF, Liu X, Xiao M, Nethercot DA (2019) Modelling tensile tests on high strength S690 steel materials undergoing large deformations. Eng Struct 192:305–322
8. Xiong M-X, Richard Liew JY (2016) Mechanical properties of heat-treated high tensile structural steel at elevated temperatures. Thin-Walled Struct 98:169–176
9. European Committee for Standardization (CEN) (2009) Metallic materials—Tensile testing—part 1: method of test at room temperature'. EN ISO 6892-1, Brussels. Belgium
10. European Committee for Standardization (CEN) (2005) 'Eurocode 3: Design of steel structures-part 1–1: general rules and rules for buildings, EN 1993-1-1. Belgium, Brussels

Seismic Performance Analysis of RC Bridge Subjected to Different Levels of Corrosion

Rosemary K. Thomas and M. Helen Santhi

1 Introduction

There are numerous bridges constructed across the world which play an important role in transportation. As time passes, all these structures exhibit wear and tear. We can observe signs of distress in many RC bridges constructed in the last three to four decades. Corrosion of rebar is one of the major causes of distress in RC bridges, especially in the coastal and industrial areas, which along with continuous loading can reduce the life of the bridge [1–3]. Chloride-induced and carbonation-induced corrosions are the major threats to the durability of any concrete structure. All around the world, a huge number of RC structures are located in close vicinity of the sea or subjected to frequent chemical attacks [4]. Since the mid-1970s, it has been identified that the corrosion of the rebar in concrete is induced by the presence of even small amounts of chlorides [5].

The structures show steel corrosion and deterioration of concrete only after a few years of construction. Reinforcement corrosion assessment is the main challenge in the maintenance policy of concrete bridges because it is influenced by a variety of bridges built in different localities, of different materials and in different years [6, 7]. The main causes of this structural deterioration are poor design, poor quality of materials used in construction, lack of skilled labour, continuous exposure to extreme environmental conditions and lack of timely maintenance [8, 9]. Combined structural deterioration due to steel corrosion and seismic damage is an important challenge in the field of structural engineering. It is a matter of concern when corrosion occurs in the plastic hinge regions of bridge columns, which are the regions requiring both strength and ductility and hence deterioration over there can increase the chances for the failure of the structure [10].

R. K. Thomas (✉) · M. Helen Santhi
Vellore Institute of Technology, Chennai, India

M. Helen Santhi
e-mail: helensanthi.m@vit.ac.in

K. S. Satyanarayanan et al. (eds.), *Sustainable Construction Materials*, Lecture Notes in Civil Engineering 194, https://doi.org/10.1007/978-981-16-6403-8_5

As per IRC: SP:60-2002, bridges in coastal regions have shown early distress because of corrosion in steel due to the high amount of salinity in the air. Corrosion in concrete girders can be faster than that in deck slab. Corrosion affects the load carrying capacity of the bridge. The code also mentions that corrosion on the bridge can lead to the following:

- loss of steel integrity,
- reduction in mechanical properties of steel like ductility and strength,
- spalling of concrete cover,
- loss of cross-sectional area of concrete,
- a drop in steel and concrete bond, if the cracks are in parallel direction of steel and
- loss of prestress in case of prestressed steel corrosion.

The need for a structural design concept for a target service life in view of the most familiar causes for structural degradation and by considering durability as one of the major parameters at the design stage is clearly stated in the code [11]. So, there is always a need to evaluate the performance of existing structures to ensure its stability and life [12].

2 Modelling of the Bridge

Geometry of the bridge considered for the work [13] is given in Table 1. Three-dimensional (3D) modelling and analysis of the bridge was done using the CSI Bridge software. The bridge model is shown in Fig. 1. Superstructure of the bridge was modelled in bridge modeller using the inbuilt T beam bridge section. Bent caps were modelled as beam column elements and bent columns were taken as circular columns. Foundations at base of bent columns were considered as fixed. Abutments were provided at the ends (rotations released). Elastomeric bearings between pier cap and girders were defined as link elements. Due to the bearings at the top of the column, the connection between the superstructure and the pier was assumed to be simply supported. P-M2-M3 (Axial–Moment–moment) hinges were assigned for columns and M3 hinges for beams. The bridge was designed as per IRC 6: 2016, class 70R loading [14]. Reinforcement details in T girder are shown in Fig. 2.

3 Analysis of Bridge Under Different Corrosion Levels

Corrosion was considered only in the reinforcement of the bridge deck girders. Reduction in diameter was done for the bottom reinforcement of the girders. All the girders were identical and the effect of corrosion was also assumed to be uniform in all the girders. Pushover analysis was done for 0, 5, 10 and 15% loss of steel in the bottom of the girder. The bridge was considered to be in seismic zone V as

Table 1 Geometry of bridge

Attributes	Specifications
Bridge type	RC T girder bridge
Number of spans	3
Number of lanes	2
Length of span	25 m each
Total width of deck	7.2 m
Thickness of deck slab	200 mm
Carriageway width	6.0 m
Number of longitudinal girders	3 (2000 mm × 350 mm)
Number of cross girders	5 per span (1500 mm × 250 mm)
Number of piers	3
Pier cap	2400 mm × 1400 mm
Pier diameter	2400 mm
Pier column length	5170 mm
Grade of concrete	M_{20} (for pier column) and M_{25} (for super structure and pier cap)
Grade of steel	Fe 415

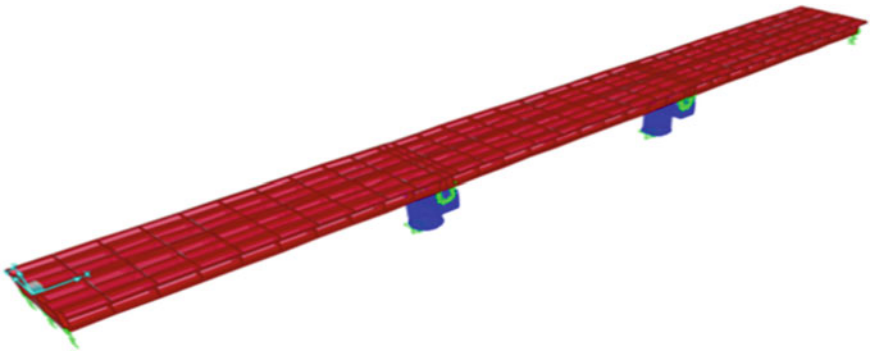

Fig. 1 Bridge model in CSI bridge

per IS 1893: 2016 [15] and IRC 6: 2016 with 5% damping and medium soil types. Importance factor was taken as 1.2 (river bridge [14]) and response reduction factor as 5. Threshold concentration of chloride was considered as 1 kg/m^3. Static nonlinear analysis or pushover analysis is a type of seismic analysis to predict the behaviour of a structure under earthquake loads to establish the pushover curve or capacity curve. The capacity curve is the plot of the total lateral force (base shear) on a structure against the displacement of the control node of the structure. The hinges formed after the analysis can be used to evaluate the performance of the bridge.

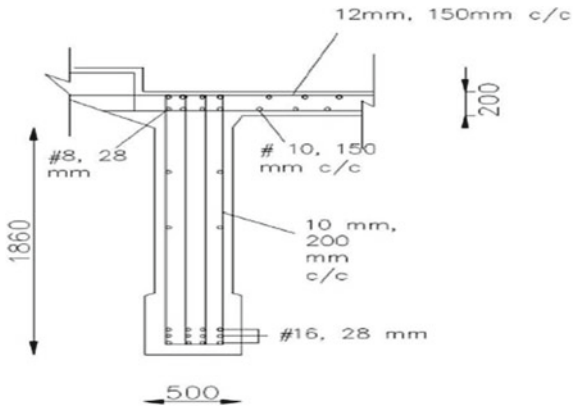

Fig. 2 Reinforcement details in the T girder

4 Results and Discussion

The base shear versus displacement curve (capacity curve), hinge formation and displacement ductility factor of the considered bridge are discussed below.

4.1 Capacity Curve

Capacity curves were obtained after pushover analysis for all the cases considered along the *X* and *Y* directions which are shown in Figs. 3 and 4, respectively. The longitudinal direction is denoted by the *X* direction and the transverse direction is denoted by the *Y* direction. The capacity curve along the *X* direction for 0, 5, 10 and 15% reduction in reinforcement steel due to corrosion are shown in Fig. 3. The capacity curve along the *Y* direction for all the corrosion cases are shown in Fig. 4.

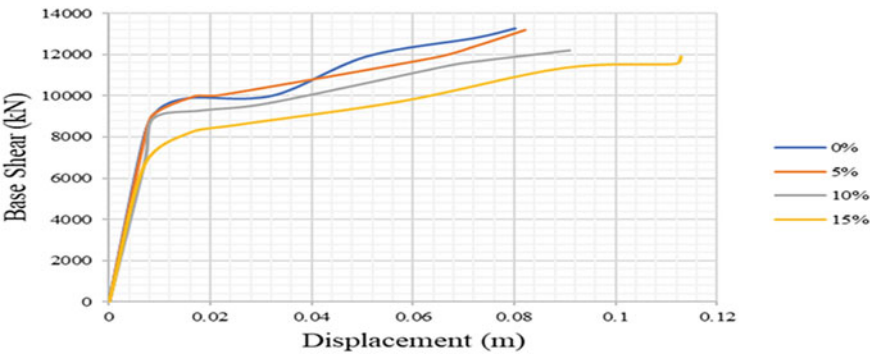

Fig. 3 Capacity curve along the *X* direction

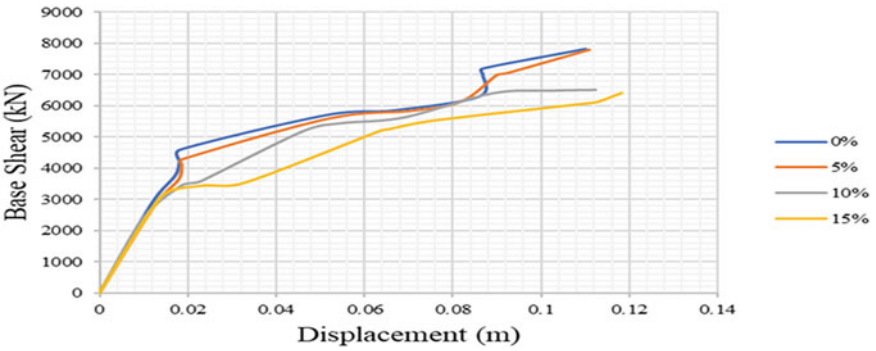

Fig. 4 Capacity curve along the *Y* direction

Table 2 Base shear and displacement for all cases

% steel loss	0%		5%		10%		15%	
Directions	*X*	*Y*	*X*	*Y*	*X*	*Y*	*X*	*Y*
Yield base shear (kN)	9895.21	3732.8	9992.21	3632.8	9292.65	3432.8	8592.86	3443.43
Yield displacement (mm)	15.4	17	17.2	17.89	18.7	18.4	25.7	24.1
Ultimate base shear (kN)	13,284.21	7811.98	13,182.21	7800.71	12,190.54	6511.9	11,880.54	6401.79
Ultimate displacement (mm)	80	110	82	111	91	112.4	112.9	118.2

The highest displacement was shown by the case of 15% loss of steel in both the directions. The displacement in the *X* and *Y* directions are discussed in Table 2.

4.2 Hinge Formation

Formation of hinges represents the performance levels of bridge. IO is the immediate occupancy level, LS is the life safety level, CP is the collapse prevention level and 'C' represents the behaviour between the ultimate strength and ultimate rotation, later which failure takes place [16]. All the hinges formed in the cases of 0–10% loss of steel, were within the collapse prevention limit. When the loss of steel was 15%, there were hinges at top of pier, which crossed the collapse prevention limit. In Fig. 5a, in the *X* direction, hinges were formed beyond collapse prevention level. Hence, the structure may experience failure for the given earthquake conditions, if

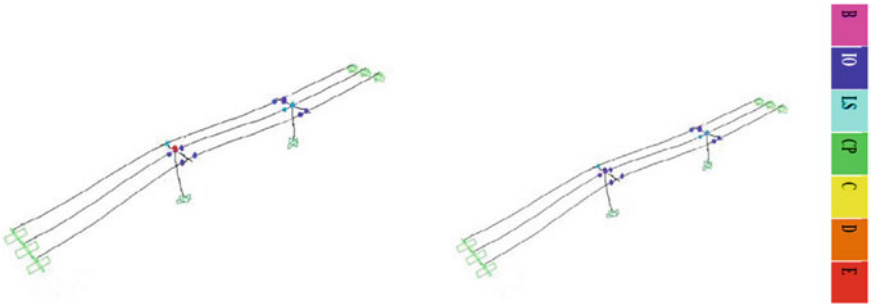

(a) (b)

Fig. 5 Hinges formed along the *X* (**a**) and *Y* (**b**) directions (15% loss of steel)

there is a loss of 15% loss in steel. But in *Y* direction, the hinges were formed within the safety limit (Fig. 5b).

4.3 Displacement Ductility Factor

Ductility is the ability of a structural component or a system to undergo both large deformations and several cycles of deformations, beyond its yield point. The ductility factor indicates the rate of delay caused by the structure between yield and damage state. The displacement ductility factor is the ratio between ultimate displacement and yield displacement of the structure. The high ductility factor denotes the high capacity of the bridge. The yield and ultimate displacements are given in Sect. 4.1. The highest factor for the considered bridge was 5.1 for 0% loss of steel, while the lowest was 3.7 for the highest loss of steel in the *X* direction. In the *Y* direction, 6.47 was the highest at 0% loss and 5.4, the lowest was for 15% loss of steel. So, the loss of capacity occurred due to increased corrosion. The delay between yield state and damage state was less in the case of 15% loss of steel due to corrosion. Also, the bridge showed more displacement ductility in the *Y* direction.

5 Conclusion

- From the study, it was found that there was a reduction in the capacity of the bridge, 10.56% in the *X* direction and 18% in the *Y* direction for 15% loss in steel reinforcement. The reduction in the capacity of the bridge when there was 5 and 10% loss in steel was less compared to that of 15%.
- Also, the hinges formed in cases of 0–10% reinforcement loss were within the life safety limit, that is damages may occur but there will not be a failure of structure.

But when there was a loss of 15% steel, the hinge formed at the top of the pier in *X* direction crossed the collapse prevention limit which makes that region a weak spot.

- The displacement ductility factor of the bridge was also reduced due to an increase in corrosion. The ductility factor was less in the case of 15% steel loss condition in both *X* and *Y* directions which was due to the less delay between yield state and damage state in that case. Also, the *Y* direction showed high ductility factor than the *X* direction.
- Even though the bridge when subjected to corrosion levels up to 10% hasn't shown much damage, there were certain hinges formed in LS to CP level. So, an overall examination of the bridge should be conducted to avoid the small damages from leading to big failures.
- Proper evaluation and retrofitting of the pier cap and pier are required to increase the seismic capacity of the considered bridge to withstand the effect of the highest level of corrosion considered in the study.

References

1. Andisheh K, Scott A, Palermo A (2016) Seismic behavior of corroded RC bridges: review and research gaps. Int J Corros 2016:1–22
2. Crespi P, Zucca M, Valente M (2020) On the collapse evaluation of existing RC bridges exposed to corrosion under horizontal loads. Eng Fail Anal 116:1047
3. Banerjee S, Sengupta AK (2012) A methodology to assess the degradation in the structural response of the deck of a reinforced concrete road bridge due to corrosion of reinforcing steel. J Inst Eng (India) Ser A 93:87–93
4. Kassir MK, Ghosn M (2002) Chloride-induced corrosion of reinforced concrete bridge decks. Cem Concr Res 32:139–143
5. Zhou Y, Gencturk B, ASCE A M, Willam K, ASCE F, Attar A (2014) Carbonation-induced and chloride-induced corrosion in reinforced concrete structures. J Mater Civ Eng 27(9):1–17
6. Amleh L, Lounis Z, Mirza MS (2002) Assessment of corrosion-damaged concrete bridge decks-a case study investigation. In: Proceedings of 6th international conference on short and medium span bridges, Vancouver, vol 2, pp 837–844
7. Li C, Hao H, Li H, Bi K (2015) Seismic fragility analysis of reinforced concrete bridges with chloride induced corrosion subjected to spatially varying ground motions. Int J Struct Stab Dyn 16:1–27
8. Chiu CK, Lyu YC, Jean WY (2014) Probability-based damage assessment for reinforced concrete bridge columns considering the corrosive and seismic hazards in Taiwan. Nat Hazards 71:2143–2164
9. Kamaitis Z (2002) Damage to concrete bridges due to reinforcement corrosion. Transport 17(4):137–142
10. Ou Y-C, Fan H-D, Nguyen ND (2013) Long-term seismic performance of reinforced concrete bridges under steel reinforcement corrosion due to chloride attack. Earthq Eng Struct Dyn 42:2113–2127
11. IRC: SP: 60 (2002) An approach document for assessment of remaining life of concrete bridges
12. Paraskeva TS, Kappos AJ, Sextos AG (2006) Extension of modal pushover analysis to seismic assessment of bridges. Earthq Eng Struct Dyn 35:1269–1293
13. Mahesh P (2013) Comparative Study of RCC T girder bridge design using different codes. M.Sc Thesis, Department of Civil Engineering, Lalitpur, Nepal

14. IRC 6 (2016) Standard specifications and code of practice for road bridges
15. IS 1893-part I (2016) Criteria for earthquake resistant design of structures
16. Firoj M, Ojha S, Poddar P, Singh SK (2020) Seismic hazard assessment of existing reinforced concrete bridge structure using pushover analysis. J Struct Eng Appl Mech 3:229–243

Demand Analysis on Natural River Sand Used in the Construction Project

S. Prakash Chandar and S. Loganathan

1 Introduction

The world continues to develop in the construction industry. Concrete is an binding material used in construction industry [1]. It consists of some chemically inert particulate substances like coarse aggregate and fine aggregate, which is binded with a cement and normal water [2]. As demand for fine aggregate increases in construction industry, some conflicts for the availability for the natural resources and environmental impacts become more intense [3, 4]. Aggregate is the major constitute of concrete, 60–75% of total volume of concrete is occupied by the fine and coarse aggregate [5]. Coarse aggregate gives the solidity to the concrete while fine aggregate fills the space between the particles. One of the major fine aggregate used in concrete is natural river sand [6, 7]. The construction industry is looking for an alternative material to natural river sand but a suitable alternative is not yet available. Hence the searching of alternate for natural river sand is continued by the construction industry in terms of standard quality and economy.

1.1 Demand on Natural River Sand

The use of natural river sand is increasing as the construction industry continues to grow. The construction sectors projects was halted in half due to unavailability of natural river sand. Using an alternative to natural river sand in concrete can provide

S. Prakash Chandar (✉) · S. Loganathan
Department of Civil Engineering, SRM Institute of Science and Technology, Kattankulathur, Tamil Nadu 603 203, India
e-mail: prakashs2@srmist.edu.in

S. Loganathan
e-mail: ls9208@srmist.edu.in

K. S. Satyanarayanan et al. (eds.), *Sustainable Construction Materials*, Lecture Notes in Civil Engineering 194, https://doi.org/10.1007/978-981-16-6403-8_6

solutions to problems of waste management, environmental degradation and reduction of natural resources [8]. According to the reports some of the projects gets delayed due to the unavailability of natural river sand in the market. Moreover production of natural river sand is not uniform across seasons with a shortage faced in many jurisdictions. The cost of the natural river sand is also rising due to many reasons like transportation from source of material to field. Due to uncertainties and insufficient in supply, they receive other low quality sand into river sand and sell it at a higher price. Cost and Quality of the material varies significantly leading to black marketing and illegal mining of the mineral.

1.2 Alternative Material

Using alternative material to a natural river sand in concrete can provide solutions to demand and sudden price hikes [5, 9]. Quarry dust is a rubbished substance formed after squashing the granite stone it has been proposed as a alternate material for the river sand. The hardness properties of quarry dust are similar to those of river sand [2, 10]. A comparatively good strength is expected when natural river sand is replaced partially or fully by quarry dust with the adding of some admixtures.

2 Methodology

From the detailed study some basic data were collected which co-related with the topic. Natural river sand demand in the market were analysed and studied. Hence, furthermore simple multiple choice questions for google questionnaires made and circulated. Both experimental study and analytical study are done. From the questionnaire results data should be analysed. The collected data were analysed statistically by statistical package for the social science (SPSS) analysis.

2.1 Primary Data Collection

Collected the last 10 years fine aggregate cost in some of cities in South India. Average price of fine aggregates in Hyderabad is shown in Table 1. Average price of fine aggregate in Bangalore is shown in Table 2. Average price of fine aggregate in Tiruvannamalai is shown in Table 3. This data are collected from construction companies.

Table 1 Average price of fine aggregate (Hyderabad, Telangana)

Year	River sand cost (per ton) without transportation charge and 20–30% cost increases when rain occurs	Manufactured sand cost (per ton) without transportation charge	Quarry dust cost (per ton) without transportation charge
2011	1300–1400	300–350	NA
2012	1400–1500	300–400	NA
2013	1400–1600	400–450	NA
2014	1500–1600	400–450	NA
2015	1600–1700	400–500	NA
2016	1700–1800	500–600	NA
2017	1700–1850	500–600	NA
2018	1800–1900	600–700	200–300
2019	1900–2000	600–700	300–400
2020	2000	700–800	400

Table 2 Average price of fine aggregate (Bangalore, Karnataka)

Year	River sand cost (per ton) without transportation charge	Manufactured sand cost (per ton) without transportation charge	Quarry dust cost (per ton) without transportation charge
2011	1000–1100	350–300	NA
2012	1100–1200	300–350	NA
2013	1200–1300	400–450	NA
2014	1300–1400	400–450	NA
2015	1400–1600	400–500	NA
2016	1500–1700	400–500	NA
2017	NA	550–600	100–250
2018	NA	550–600	200–300
2019	NA	550–600	200–400
2020	2100–2300	600–700	200–400

2.2 Collection of Secondary Information

The higher adoption is due to the shortage of natural river sand and the availability of raw material quarry dust. Quarry dust is getting some traction in other southern states due to the sand shortage, which pushing builders to move to another alterative material like quarry dust. Current natural river sand consumption in tones were collected from government mines report it was collected in state wise it was shown in Fig. 1.

From the ministry of mines report it can be clearly shown in the chart the top selling price of natural river sand in state wise. Karnataka, Maharashtra and Tamil Nadu the

Table 3 Average price of fine aggregate (Tiruvannamalai, Tamil Nadu)

Year	River sand cost (per ton) without transportation charge	Manufactured sand cost (per ton) without transportation charge	Quarry dust cost (per ton) without transportation charge
2011	1000–1100	350–300	NA
2012	1100–1200	300–350	NA
2013	1200–1300	400–450	NA
2014	1300–1400	400–450	NA
2015	1400–1600	400–500	NA
2016	1500–1700	400–500	NA
2017	NA	550–600	100–250
2018	NA	550–600	200–300
2019	NA	550–600	200–400
2020	2100–2300	600–700	200–400

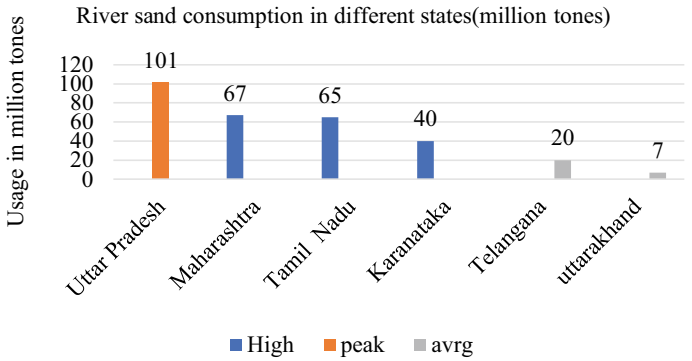

Fig. 1 River sand consumption

river sand price is extremely high compare to other states. From the government reports collected the sale price of sand was shown in Fig. 2.

From the analysis report of aggregate business international it has been clearly noted that, every year the demand for river sand increasing rapidly. They reported river sand demand in India till 2020; river sand demand chart was shown in Fig. 3.

3 Data Collection and Analysis Methods

Information has been gathered from the different developed organizations. The survey has been given to site engineers, Contractors and owners. After studying the records developed the Research questionnaires, the questionnaires will be based on

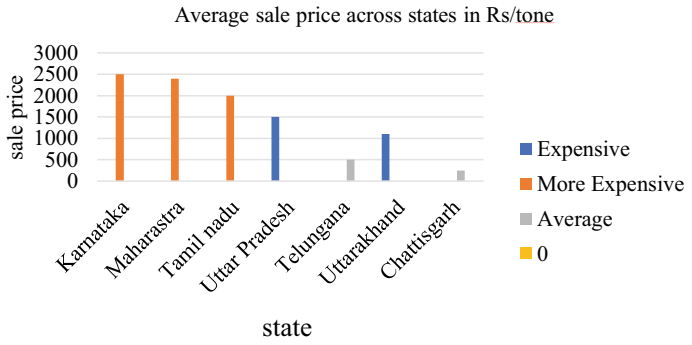

Fig. 2 Average sale price across state in Rs/ton

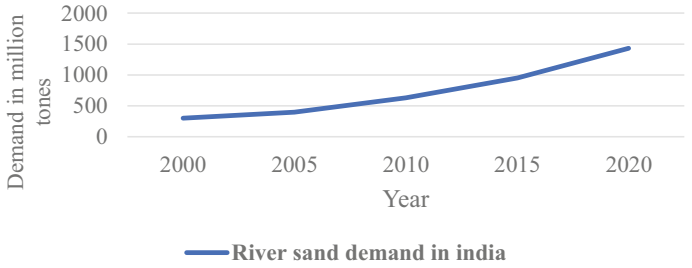

Fig. 3 River sand demand in India

river sand demand, shortages and alternative materials, 25 multiple choice questions for google questionnaires made and circulated then reactions have been submitted. The gathered information will be examined in SPSS programming. Two tests will be done the tests are ANOVA and Regression examination. ANOVA was utilized to contrast tests and also used to decide whether their disparities were measurably huge. Relapse investigation was utilized to distinguish potential connections between the venture contract cost and cost overwhelms.

3.1 Analysis of Statistical Significance

Investigation of difference (ANOVA) is one of the procedures with an evident level of exactness to evaluate the static reproachful of the limits with the responses. The ANOVA software is used to recognize the basic introduction of the limits are power, speed, and repeat to the laser exhausting cycle for the response. The s/n allocate is the base for the ANOVA to perform.

Fischer's test (F test) which relies upon the assessments of the s/n extent. The check of the f regard is by an ordinary measure of the square backslide to a typical measure of the square mix-up.

The ANOVA which is created for multi boundaries with multi responses the examination of ANOVA has been accomplished for each response independently and the ANOVA result has been introduced beneath. Sample question with ANOVA response are shown in Table 4.

The F estimation ought to be used in blend in with the p regard when you are picking if your overall results are basic. In case you have a tremendous result, it doesn't infer that all of your variables are basic. The estimation is basically taking the joint effect of the overall huge number of variables together. Where DF-No of Independent values, SS-Sum of Square and MS-Mean Square.

The ANOVA shows the f-esteem which show the significant responses which are given as a contribution of the nick time issue (Figs. 4 and 5). The ANOVA for the 25 responses has appeared in the f-esteem results.

The above chart shows the distinctions of every reaction f-esteem so the scope of every reactions f-esteem is around of 0.4–5.6 so the distinctions in the all-out f value is around 5 so the f value produced for every one of the reactions are in critical. The *y* axis represents 0 is neutral, 1 is agree, 2 is strongly agree, 3 is disagree and 4 is

Table 4 ANOVA for responses

Source	DF	Adj SS	Adj MS	F-value	P-value
Project gets delayed due to the unavailability of natural river sand	4	109.6	27.4	0.65	0.628
Error	42	1760.4	40.91		
Total	46	1870			

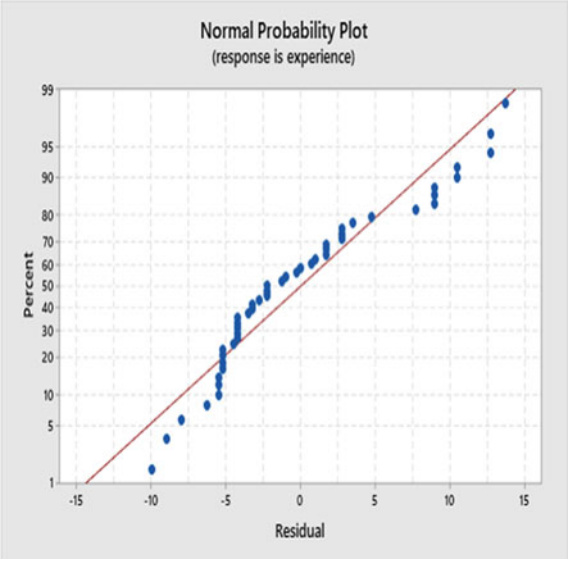

Fig. 4 Graphical representation of normal probability plot

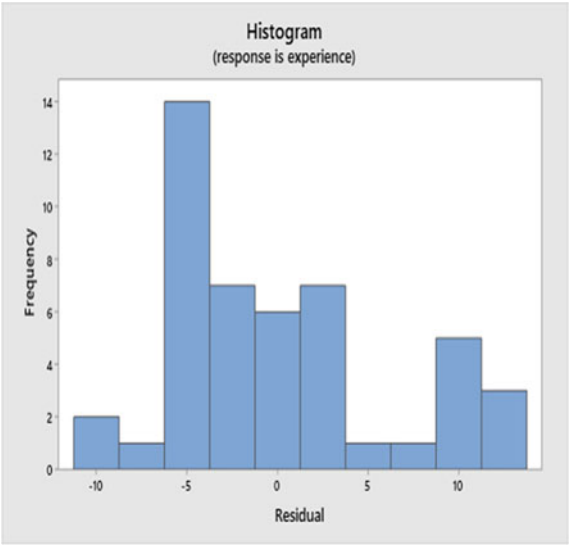

Fig. 5 ANOVA histogram chart

strongly disagree and the *x* axis represents number of questionnaires with responses shown in Fig. 6.

The ANOVA graph chooses of the hidden to indisputable steps of a single reactions which can show the distinctions of the reactions which has the effect of the decide the f-regard with the help of the four blueprints like histogram, interval plot and normal probability plot. People who have more than 10 years of experience agreed that the project delayed due to unavailability of natural river sand it is shown in Fig. 7.

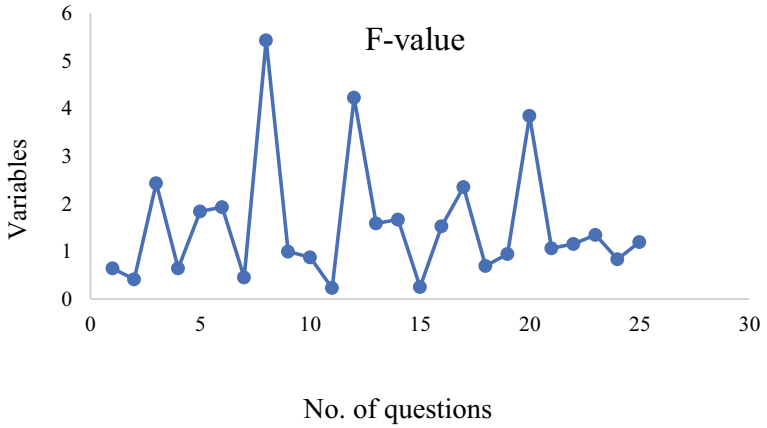

Fig. 6 F-value for each response

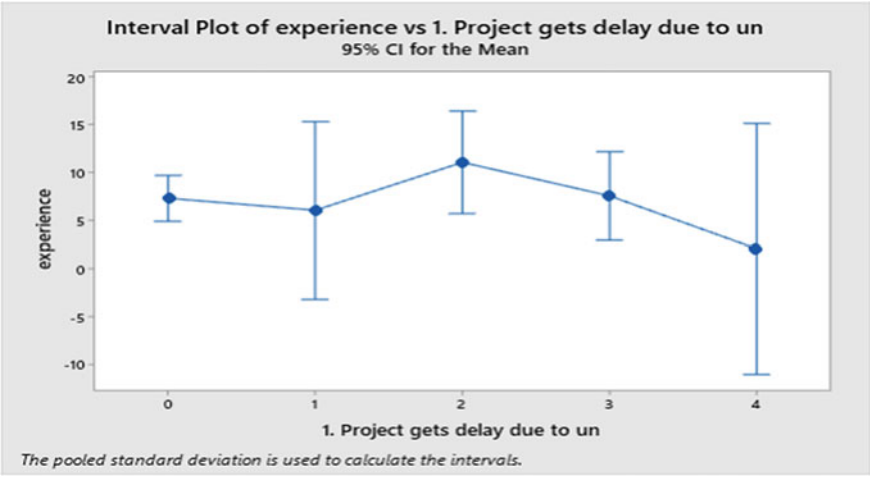

Fig. 7 Graph of the ANOVA (Project gets delayed due to unavailability of natural river sand)

3.2 Demand Forecasting

River sand demand in the recent years was high. So here, we performed trend analysis for forecast the future demand of Sand in India. By using aggregate business international report as primary data Fig. 3, we Forecasted for the year 2021–2025, the below graph shows the Demand of Sand in future. The actual value fits well with the linear graph shown in Fig. 8.

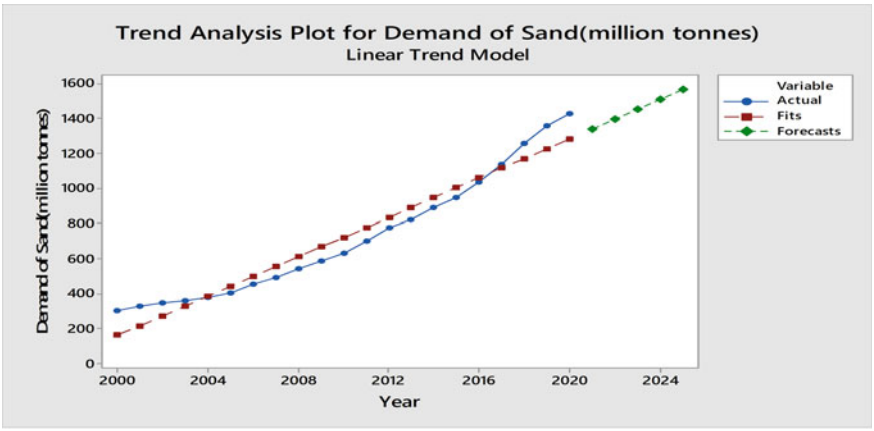

Fig. 8 Trend analysis for demand of sand

Table 5 Future demand of river sand

Years	Demand of Sand (in million tones)-India
2021	1342
2022	1398
2023	1455
2024	1511
2025	1567

The demand of sand (in million tone) in India for the year of 2021–2025 is shown in Table 5. From this table it has been clearly shown the next five years demand in India was sky high. So to overcome from this issue we have to choose the alternative material.

4 Results and Discussion

Based on the literature, articles and government regulations questions were developed. The cost of the fine aggregate for past 10 years has been collected from some of the construction sectors in South India, the average price of fine aggregate is clearly shows that the cost of natural river sand increasing rapidly and from the responses it is noted many of the constructions sectors claiming that project gets delay due to unavailability of natural river sand. Due to the widespread use of concrete natural river sand is in high demand around the world, forecasted results shows in future the river sand demand reaches 1567 million tones at the year of 2025. The ANOVA investigation which has been carried out shows that there is a huge reactions concurring with boundaries, so the trial of the ANOVA make the examination with more significance. As per the demand analyses carried out with the contractors/owners, engineers and the ANOVA results it is found that the demand for the natural river sand is high. From the gathered questionnaire survey data's several studies were conducted on a demand on natural river sand So, the overall Study Suggested that River Sand is in demand. The significant of the ANOVA is 0.05 and the f value is around 2. Since the natural river sand used in the construction is in demand it is found that quarry dust can be used as alternative material in concrete.

References

1. Gavriletea MD (2017) Environmental impacts of sand exploitation. Analysis of sand market. Sustainability (Switzerland) 9(7):1118
2. Prakash CS, Gunasekaran K et al (2018) Study on some durability properties of coconut shell concrete with quarry dust. Eur J Environ Civ Eng 24(6):709–723
3. Dung NM, Le NP (2015) An analysis of river sand mining management in Cau river of Vietnam. Asian J Res Bus Econ Manag 5(1):19–32

4. Sathiyapriya V, Venugopal V (2017) Spss based study and analysis on risk factors for effective construction management. Int J Mod Trends Eng Res 4(8):157–163
5. Srivastava M, Srivastava H et al (2017) Behaviour of concrete on the use of quarry dust and superplasticizer to replace sand. IOSR J Mech Civ Eng 14:06–11
6. Huang T et al (2013) Materials demand and environmental impacts of buildings construction and demolition in china based on dynamic material flow analysis. Resour conserve Recycl 72:91–101
7. Zolgadhar M, Zoomardian SMA (2021) Migration of sand mining pit in rivers: an experimental, numerical case study. Measurements 172:108944
8. Koirala MP**,** Joshi BR (2017) Construction sand, quality and supply management in infrastructure project. Int J Adv Eng Sci Res 4(4):01–15
9. de Leew J, Shankman D et al (2009) Strategic assessment of the magnitude and impacts of sand mining in Poyang lake, China. Reg Environ Change
10. Escavy JI, Herrero MJ et al (2020) Demographic vs economic variables in the modelling and forecasting of the demand of aggregates: the case of the Spanish market (1995–2016). Resour Polic 65:101537

A Partial Replacement of Cement Using Extract Powder Form of Silica Aerogel

Abiya Eldho K. Peter, M. Balasubramanian, A. Arul Jayakumar, P. Mukilan, and S. Aishwarya

1 Introduction

1.1 General

Concrete is mainly used to construct building structures. Thermal conductivity in cement replacement materials is created from agricultural waste [1]. In nanotechnology sector, aerogel became a trading material. In 1930, aerogels were discovered as a nanoporous lightweight material. Silica content is more in aerogel, so it is called silica aerogels [2]. In China, due to the rise in population, living space is becoming more excessive because of material insufficiency. The cost of materials is also rising. Introducing a new material in building construction can solve this problem. The wet chemical synthesis of aerogel is a complex process involving the extensive usage of chemical compounds [3]. To correct for those weaknesses, a new approach is required. Aerogel is good in energy saving and can be used as a cement-type insulation material [4]. Sustainable building materials are capable to rectify these defects also it helps in energy saving.

A. E. K. Peter · M. Balasubramanian (✉) · P. Mukilan · S. Aishwarya
Department of Civil Engineering, SRM Institute of Science and Technology, Chengalpattu District, Kattankulathur, Tamil Nadu 603203, India

S. Aishwarya
e-mail: as4136@srmist.edu.in

A. Arul Jayakumar
Department of Mechanical Engineering, SRM Institute of Science and Technology, Chengalpattu District, Kattankulathur, Tamil Nadu 603203, India

K. S. Satyanarayanan et al. (eds.), *Sustainable Construction Materials*, Lecture Notes in Civil Engineering 194, https://doi.org/10.1007/978-981-16-6403-8_7

1.2 Agricultural Waste

Agro-waste are either burnt into ashes or they are synthesized in order to create a new building product. Rice husk is one of agricultural waste materials which got attention in market [5]. It can be used as a replacement material for cement, fine and coarse aggregate.

1.3 Rice Husk and Aerogel

Rice husk can be used as a cement replacement product due to its richness in silica content. Silica aerogel is an advanced concrete material synthesized from rice husk. Aerogel is available in two different forms: semi-jelly solid and solid [6].

1.3.1 Synthesis Process

Sol–gel method is used to synthesis the aerogel, which is one of the most advanced and cheapest methods. To obtain rice husk ash (RHA), the rice husk needs to be calcined at 600 ℃ for 4 h and then from RHA amorphous silica is extracted. After 24 h of gelatinating, silica gel is obtained. With DI water wash, the gel is obtained after 12 h in room temperature. After that, the hydrogel is soaked in ethanol for 12 h at room temperature to create alcogel, which will be used to manufacture silica aerogels. The presence of silica Aerogel is hydrophobic, porous and has a low density (ref. Fig. 1) [7].

1.3.2 Chemical Composition

The chemical composition is tabulated in Table 1.

1.3.3 Impact of the Material

In nanotechnology sector, aerogel became a trading material. In 1930, aerogels were discovered as a nanoporous lightweight material. It is extremely light, has good density and strong compression strength [8]. It can be used in cement-based composite. It shows superlative performance in regeneration of indoor air and polluted water. It also has combined advantage of high surface area.

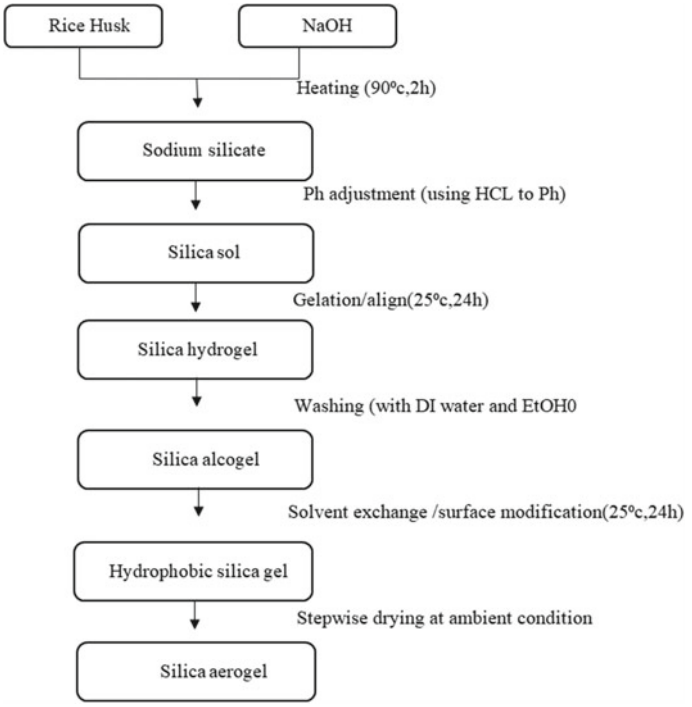

Fig. 1 Illustrative diagram of silica aerogel by using sol–gel method

Table 1 Chemical combination of cement and silica aerogel

Oxides	Cement %	Silica aerogel %
CaO	64.18	–
SiO_2	20.36	>95
Al_2O_3	4.59	–
SO_3	3.85	–
$CaCO_3$	3.7	–
Fe_2O_3	3.54	–
MgO	2.27	–
K_2O	0.48	–
Na_2O	0.41	–
P_2O_5	0.17	–
Cl^-	0.037	–
LOI	2.18	–

2 Literature Review

Hee Taik Kim et al. (2019), Aerogel is an encouraging nanostructural silica material which is highly porous, lightweight and holds good thermal conductivity. Comparing with other building materials, aerogel is more expensive than cement. Aerogel needs significant improvement in synthesis process.

Ólafur Haralds Wallevik et al. (2016), Solar photovoltaics and geothermal power method are used to measure the energy efficiency with less cost. The aerogel are asymmetrically shaped granules. The preliminary study stated that, with the increase in aerogel fraction, the thermal conductivity is reduced.

Stefan Jacobsen et al. (2014), Aerogel has numerous prime applications in contemporary construction. High strength ratio and good sound insulation characteristics are its advantages. The manufacturing cost of aerogel is high, therefore the cost is also high. The alkaline in environment can destroy aerogel due to the hydration of cementitious material.

Sughwan Kim et al. (2013), Providing extra plants and keeping a suitable interior environment improves thermal comfort. Aerogel has a high compressive strength of up to 3Mpa and a load-bearing capability.

3 Materials

3.1 Study of Cement Characterization

Cement is one of the unavoidable materials used in concrete. Cement plays an important role to give strength to the concrete. Manufacturing of cement is a complex process. It includes mixing and grinding of limestone and clay into powder form. Clinkers will be mixed with gypsum to obtain cement in a new product called clinkers [9].

3.2 Material Selection

After completing cement characterization study, the next step is to find out a material which has similar physical and chemical properties of cement. Aerogel obtained from rice husk is one of the materials which meets all this needs.

3.3 Characterization Study

Material analysis techniques such as XRD, SEM, TEM, BET and MIP can be used to study aerogels. The ratios of silica aerogel are determined by using X-ray florescence spectrometer (XRF). Mechanical properties are done according to DIN EN 196–1 standard in AIM. For AIC, the UNI-EN analysis method is used to analyse mechanical properties of AIC. For further detailed examination, transmission electron microscopy (TEM) is done. An amorphous carbon coating should be applied on the surface of material before SEM observation [10].

3.4 Laboratory Test

Density, compressive strength and thermal conductivity are the main laboratory test done to the aerogel. Density tests are done to study about the estimated composition of many kind of mixtures. Unit of density is kilogram per cubic meter and unit of compressive strength is N/mm^2.

3.5 Result Analysis

After each test, these results are recorded and a comparative study is performed to see whether it has similar chemical and physical characteristics to cement.

3.6 Material Used

In modern construction, aerogel has many important applications. It got much attention in cement-based composite. Aerogel can use in lightweight concrete. It is extremely light, and the density is 100 kg m^{-3}. Aerogels can also resist loads with high compression strengths of up to 3 M Pa. The main benefits are its high strength and superb sound insulation. It works well during the recovery of polluted indoor air and water. The source of silica aerogal is silicon alkoxide (ref. Eq. 1).

$$Si(OCH_3)_4 + nH_2O \leftrightarrow SiOn(OC_2H_5)_{4-2_n} + 2nC_2H_5OH \quad (1)$$

Fly Ash chemosphere and aerogels are used in lightweight aggregate (LWA) by using alkali-activated fly ash. The material shows a remarkable performance under high temperature comparing with ordinary Portland cement (OPC). OPC can even cause a fire hazard exist in a structural concrete. Aerogel cement may be created by combining powdered aerogel with methanol and cement paste [11]. It is good in

Fig. 2 The raw rice husk

energy saving and can be used as a cement-type insulation material. It reduces the thermal conductivity of OPC by up to 75% in certain conditions. It also has a better insulation property than OPC in case of absorbing overflow water or vapour [12].

4 Experimental Work

4.1 Collected Rice Husk

In India, rice husk is one of the cheapest and simplest ways to dispose agricultural wastes. It is gathered through an India market and receives around 2 kg (ref. Fig. 2).

4.2 Aerogel Prepared from Rice Husk

Aerogel is a type of rice husk that is collected and placed for the aerogel synthesis process. The sol–gel technique is used for the production. After a few days of drying, the resulting aerogel was crushed to get the production in powdered form Fig. 3.

4.3 Casting and Demoulding

- Total 9 cubes were casted
- Mortar ratio is 1:4 with 70 ml water
- 10, 20, and 30% of replacement are done (ref. Table 2).

Fig. 3 The extract aerogel powder

Table 2 The amount of cement, sand and water required for 10, 20 and 30% of aerogel replacement

Percentage of cement replaced (%)	Cement (g)	Sand (g)	Silica aerogel (g)	Water (ml)
10	156.6	690	17.4	70
20	139.2	690	34.8	70
30	121.8	690	52.2	70

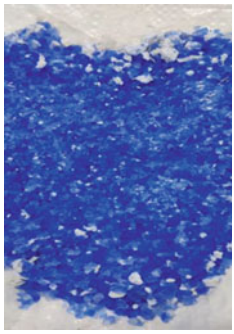

Fig. 4 The aerogel before grinding

Aft each weight batching the mortar is prepared by mixing everything in a Digi mortar mixer with 70 ml of water. The prepared specimen is placed in to steel Moulds of size 15 mm * 15 mm * 15 mm (ref. Figs. 4, 5, 6, 7, 8 and 9).

4.4 Curing Process

- Curing is the process which is done in order to protect the mortar cubes from losing moisture.
- Also it plays an important role to develop strength (ref. Fig. 10).

Fig. 5 The aerogel powder after grinding

Fig. 6 The mixing of mortar in Digital mortar mixer

Fig. 7 The casting of cube for 10 and 20% of aerogel replacement

Fig. 8 The casting of cube for 30% of aerogel

Fig. 9 The demould of 10, 20, and 30% cubes

Fig. 10 The curing of 10, 20 and 30% of aerogel replacement cubes

Table 3 Compressive testing values gained at 7th, 14th and 28th days for 10, 20 and 30% of aerogel replacement

Percentage of aerogel replaced (%)	7th day (N/mm^2)	14th day (N/mm^2)	28th day (N/mm^2)
10	11.2	20.4	38.7
20	13.6	21.8	41.3
30	14.3	23.4	44.2

5 Result and Discussion

5.1 Compressive Strength

This result and discussion cover the compressive strength, density and thermal conductivity of the cement mortar. Total nine cubes are casted for each percentage of replacement (ref. Table 3).

The compressive strength of aerogel for 30% of the material for cement replacement gained matching strength with 7th, 14th and 28th day strength of normal concrete mortar.

5.2 Density

Aerogel is a particle with low-level density and excessive porosity. The addition of silica aerogel up to 30% in cement-based mortar brought down the density to 1133 $kglm^3$ [13]. This is because of extreme hollow, air entrapping microstructure of aerogel (Fig. 11) [14].

5.3 Thermal Conductivity

The thermal conductivity of normal mortar is 1.76 W/mk and it is reduced to 1.16 W/MK when 30% of aerogel is replaced with cement [15]. The main advantage of thermal conductive material is that it limits the flow (Fig. 12).

6 Conclusion

(1) This research helps to find out an ultra-lightweight cement-based composite with good thermal conductivity from an agricultural waste material. The aerogels are considered as an extremely porous material with high surface area (760 m^2/g)

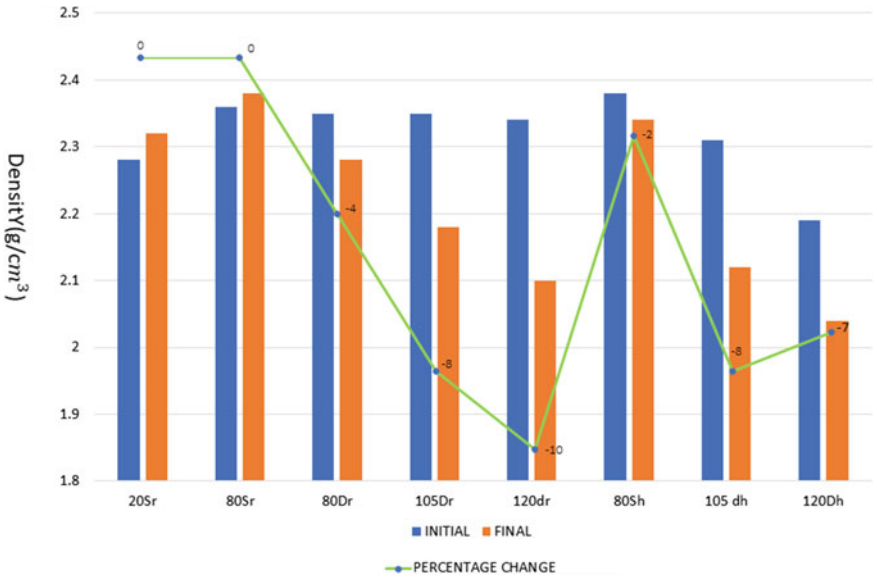

Fig. 11 Explanation about the variance of density according to temperature

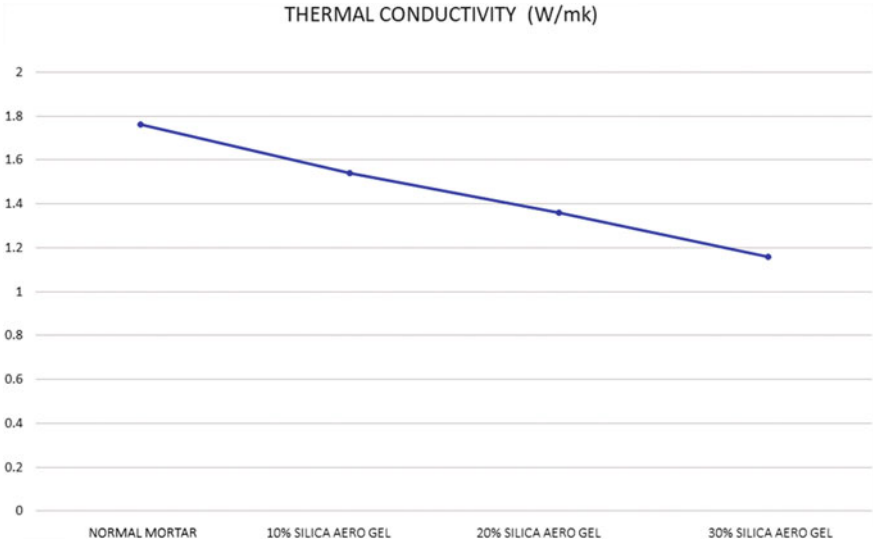

Fig. 12 Explanation about the volume of aerogel in AIM under different temperatures

(2) The microstructural properties of aerogel are competitive with commercially available, chemically synthesized aerogels
(3) Aerogel has a dominant mesoporous structure
(4) The thermal conductivity of aerogel is low, so they prevent heat transmission in and out of the building and reduce energy consumption
(5) The compressive strength of the aerogel mortar is similar to the normal mortar
(6) Density of the aerogel is low due to its air entrapping microstructure.

Future Scope

Aerogels are bit expensive material because of its synthesis process, so a better synthesis process needs to be found out in order to make the aerogel a cheap available material in market.

References

1. Abbas N, Khalid HR, Ban G, Kim HT, Lee HK (2019) Silica aerogel derived from rice husk: an aggregate replacer for lightweight and thermally insulating cement-based composites. Constr Build Mater 195:312–322
2. Ng S, Jelle BP, Zhen Y, Wallevik ÓH (2016) Effect of storage and curing conditions at elevated temperatures on aerogel-incorporated mortar samples based on UHPC recipe. Constr Build Mater 106:640–649
3. Gao T, Jelle BP, Gustavsen A, Jacobsen S (2014) Aerogel-incorporated concrete: an experimental study. Constr Build Mater 52:130–136
4. Kim YN, Shao GN, Jeon SJ, Imran SM, Sarawade PB, Kim HT (2013) Sol–gel synthesis of sodium silicate and titanium oxychloride based TiO_2–SiO_2 aerogels and their photocatalytic property under UV irradiation. Chem Eng J 231:502–511
5. Hanif A, Diao S, Lu Z, Fan T, Li Z (2016) Green lightweight cementitious composite incorporating aerogels and fly ash cenospheres–mechanical and thermal insulating properties. Constr Build Mater 116:422–430
6. Al-Homoud MS (2005) Performance characteristics and practical applications of common building thermal insulation materials. Build Environ 40:353–366
7. Park SM, Janga JG, Lee NK, Lee HK (2016) Physicochemical properties of binder gel in alkali-activated fly ash/slag exposed to high temperatures. Cem Concr Res 89:72–79
8. Rhee I, Kim YA, Shin G-O, Kim JH, Muramatsu H (2015) Compressive strength sensitivity of cement mortar using rice husk-derived graphene with a high specific surface area. Constr Build Mater 96:189–197
9. Kim S, Seo J, Cha J, Kim S (2013) Chemical retreating for gel-typed aerogel and insulation performance of cement containing aerogel. Constr Build Mater 40:501–505
10. ACI 213 (2003) Guide for structural lightweight-aggregate concrete
11. Huang X, Ranade R, Zhang Q, Ni W, Li VC (2013) Mechanical and thermal properties of green lightweight engineered cementitious composites. Constr. Build. Mater. 48:954–960. https://doi.org/10.1016/j.conbuildmat.2013.07.104
12. ACI 216.1 (1997) Standard method for determining fire resistance of concrete and masonry construction assemblies
13. Gurav JL, Jung I-K, Park H-H, Kang ES, Nadargi DY (2010) Silica aerogel: synthesis and applications. J Nanomater 2010:23.

14. Nilchi A, Janitabar-Darzi S, Mahjoub AR, Rasouli-Garmarodi S (2010) New TiO_2/SiO_2 nanocomposites—phase transformations and photocatalytic studies. Colloids Surf A 361:25–30
15. Tsioulou O, Erpelding J, Lampropoulos A (2016) Development of novel low thermal conductivity concrete using aerogel powder

Behaviour of Seven-Storey Reinforced Concrete Frames with Infill and Interfaces Under Static Load

A. Selvakumar, V. Thirumurugan, and K. S. Satyanarayanan

1 Introduction

Modern construction techniques and advanced equipment are simplifying the construction practise. Reinforced concrete (RC) is primarily used in the construction industry for building the structures. The development of high-rise buildings is becoming a symbol of urbanization in an area. In these urbanizing and urbanized areas, high-rise buildings are more to manage the space. The problems associated with these buildings are also common. In small structures, the effects of imposed loads are ignored because of their null impact or slight impact in the structures. But, in tall buildings, the impacts due to imposed loads are unavoidable, since they are giving drastic damage to the structures based on the intensity of imposed loads. Bricks are most commonly used as non-structural infill material which increase the strength and stiffness of the frame. Understanding the behaviour of infill in such structures is essential for the structural engineers to nullify or minimize the drastic damages due to impact loads. Masonry work in a structure is mainly for partitioning the space. But they absorb and dissipate the energy due to loading actions. This case changed the structurally determined failure modes and it is due to the interactions between the infill and RC elements.

The effects of masonry infill in an RC frame are positive in some cases and cause drastic damage to the structure in many cases. Kaplan and Sarah say the effects of non-structural infill elements are considered in earthquake regulations of many

A. Selvakumar (✉) · V. Thirumurugan · K. S. Satyanarayanan
Department of Civil Engineering, SRM Institute of Science and Technology, SRM Nagar, Kattankulathur 603 203, Tamil Nadu, India
e-mail: sa1108@srmist.edu.in

V. Thirumurugan
e-mail: assocdirector.cl@srmist.edu.in

K. S. Satyanarayanan
e-mail: satyanak@srmist.edu.in

K. S. Satyanarayanan et al. (eds.), *Sustainable Construction Materials*, Lecture Notes in Civil Engineering 194, https://doi.org/10.1007/978-981-16-6403-8_8

countries (Algeria, Colombia, Costa Rica, the European Union, France, Israel, the Philippines, etc.) [1]. A vast research has been done to study the frame and infill interaction effects in recent decades used tie bars as a connector for rigid frame–infill interaction [2–7]. From the study, it is suggested that frame–infill interaction due to uneven arrangement of infill walls may create torsional damage or soft storey effect which is harmful in seismic response [8–10].

It is mentioned that static monotonic and reverse cyclic loading tests are conducted by many authors on un-reinforced masonry models [11–15]. It is proposed to avoid the brittle failure of masonry infill in a structure with masonry work 'strong frame-weak infill' method [16, 17]. The isolators or the flexible element between infill and frame is found to be effective to reduce the frame–infill interaction and leaving gap between frame and infill is also found to be effective. The failures in infill are reduced considerably by different interface materials or providing frame–infill gap was reported in the study [1, 18–23]. The effective stiffness of the model is slightly greater for reverse cyclic loading than monotonic loading. The test results obtained vary with the loading mechanism, material properties, size of the specimen, scale of the model, aspect ratio of the frame, etc. [24]. The loading arrangement differs based on the application of model and with the above-mentioned parameters [25]. Authors have done different types of loading arrangements and tests in which loads are applied in laboratory tests rather different for real-time seismic loads [15, 26, 27]. An adoptive interface investigation study revealed that the RC frame with masonry infill and pneumatic interface is found better for energy absorption and dissipation. Experimental and analytical study of single-bay seven-storey RC frames are studied for different interfaces and varying interface pressures in pneumatic interface [28–30].

2 Finite Element Modelling of the Frame

A seven-storey finite element model is designed for the proposed design specifications using finite element modelling software Abaqus. Three different types of RC frames are modelled and analysed to study the performance. The frames modelled and analysed are RC bare frame (BF), infill frame with cement mortar interface (IFCMI) and infill frame with pneumatic interface (IFPI). BF, infill frame with interface and reinforcement in frames are shown in Figs. 1, 2 and 3, respectively. The dimensions and the reinforcement details of the model are given in Tables 1 and 2. Each element in the models is meshed into finite elements based on optimization study. For the interaction between interface with infill and RC frame, tie connection is provided. Embedded interaction is assumed between concrete and reinforcement. The cover of 10 mm is provided in the model. Boundary condition is considered as fixed boundary and 150 mm of projection of the beam is designed at the loading floors for the convenience of loading in experimental investigations. The conventional (cement mortar) interface and non-conventional interface (pneumatic interface) are designed as solid element and pressure elements.

Fig. 1 BF in ABAQUS

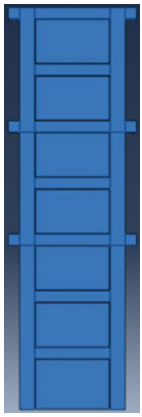

Fig. 2 Infill frame with interface

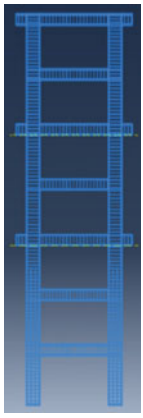

Fig. 3 Reinforcement in models

Table 1 Details of elements

S. no.	Element	Dimensions in (mm)	Specifications (mm)
1	Beam	1000 (clear span)	150 × 100 (cross section)
2	Column (ground storey)	675 (clear height)	200 × 100 (cross section)
	Column (all other storeys)	600 (clear height)	
3	Infill (ground storey)	980 × 655	100 (depth)
	Infill (all other storeys)	980 × 580	
4	Interface (ground storey)	1000 × 675	10 (thickness)
	Interface (all other storeys)	1000 × 600	

Table 2 Reinforcement details

S. no.	Element		Description
1	Beam	Main bar	4 Nos of 10 mm dia. bars
		Stirrups	6 mm dia. 2-legged stirrups @ 50 mm c/c
2	Column	Main bar	12 Nos of 10 mm dia. bars
		Stirrups	6 mm dia. 2-legged stirrups @ 50 mm c/c

3 Analysis Procedure

The seven-storey models are analysed in finite element modelling software Abaqus 6.14. Elements of the frame models are created as different parts. Material properties are assigned to each part. The complete frame model is done by assembling the parts together. Elements are meshed based on their size and optimization study (Figs. 4 and 5). The single-bay seven-storey model is fixed at the base of the two columns.

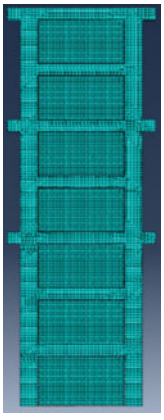

Fig. 4 Elements meshed for analysis

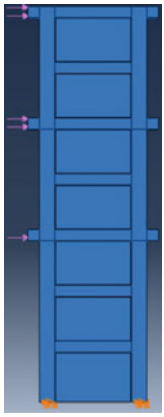

Fig. 5 Boundary condition and loads

Total lateral load of 90 kN (each 30 kN load at 3rd, 5th and 7th storeys) is applied to the frame model. Load is applied as equivalent pressure force of 2 N/mm^2 (for the cross section of beam 100 mm × 150 mm).

4 Results and Discussions

Three models are analysed in this study. From the analysis, output parameters of BF, IFCMI and IFPI are compared. Parameters like von Mises stress, maximum and minimum principal stress and displacements are compared.

4.1 Principal Stress

Principal stress is the maximum normal stress acts on the structure from which the performance of the material can be examined based on the allowable criteria. The maximum and minimum principal stress values of each storey are compared for IFCMI and IFPI. Distribution of the maximum and minimum principal stresses of the RC frame with infill and interface are shown in Figs. 6, 7, 8 and 9. Comparison of the stresses shown in Figs. 10 and 11. It is clear from the images that maximum principal stress is higher till the third storey for IFCMI than IFPI and, from there on, it is almost equal for both. Similarly, the minimum principal stress is lower till the fifth storey for IFCMI than IFPI and, from there on, it is almost equal for both.

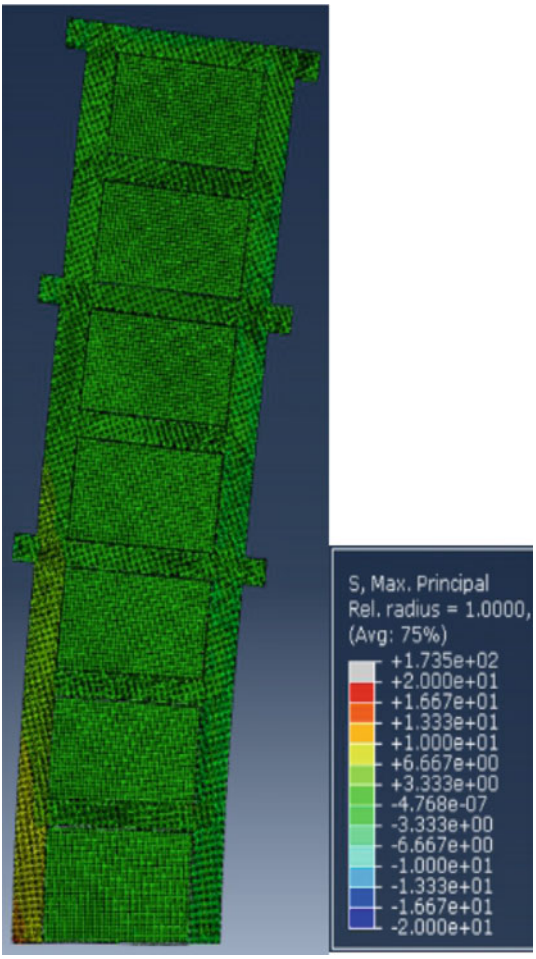

Fig. 6 Maximum principal stress—IFCMI

4.2 Displacement

The maximum displacements at each storey for all the three frames are taken from the analytical results. Comparisons of the displacements of all the three frames are shown in Fig. 15. In this, BF is displaced to the maximum of 27.44 mm, IFPI is displaced to 11.31 mm and IFCMI and displaced to 6.07 mm at top storey. Displacements of the different storeys of all the three frame models are shown in Figs. 12, 13 and 14. The minimum deflections at the first storey of the frames found as 2.73 mm for BF, 0.44 mm for IFCMI and 1.08 mm for IFPI.

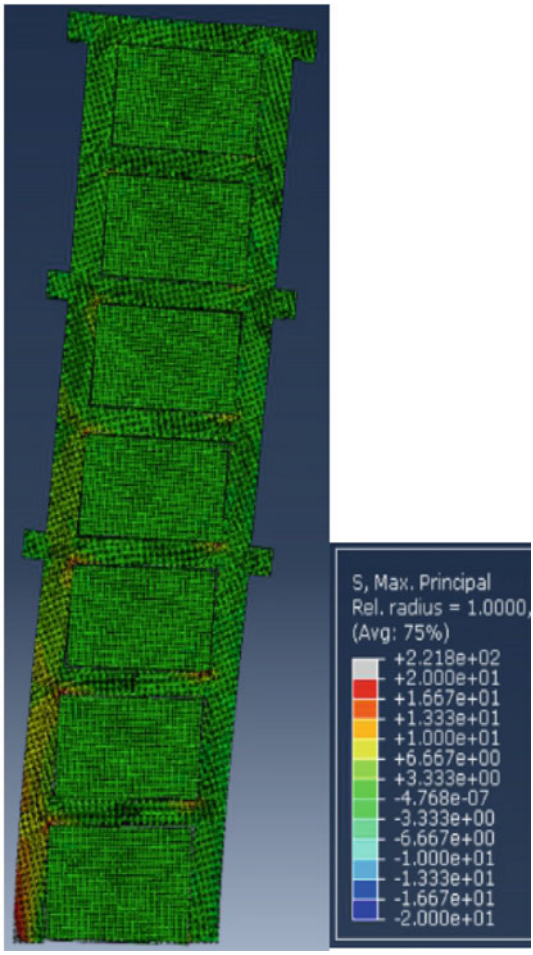

Fig. 7 Maximum principal stress—IFPI

4.3 Von Mises Stress

The yield of a material can be predicted under different loading conditions using von Mises stresses. Von Mises stress distributions of the BF, IFCMI and IFPI are shown in Figs. 16, 17 and 18. From the figure, it is clear that von mises stress is higher for BF and lower for IFCMI than the others.

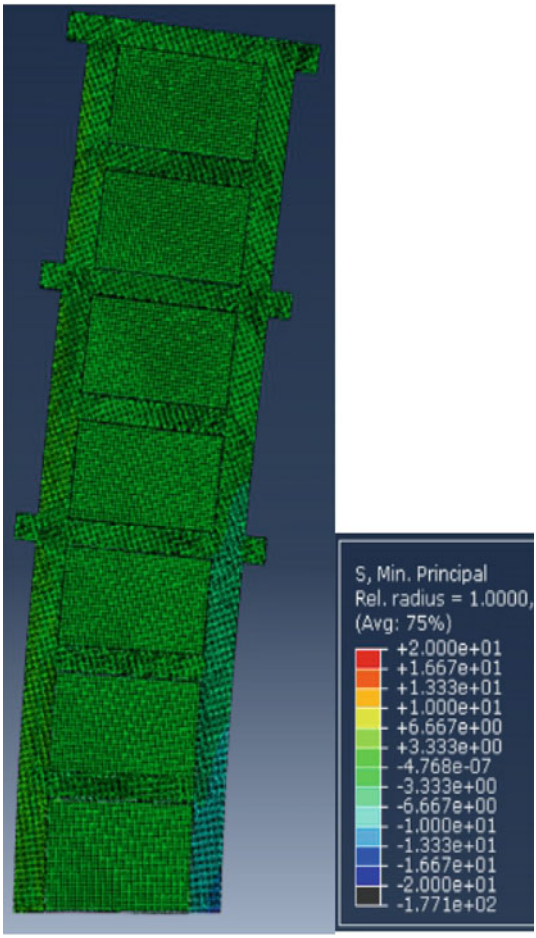

Fig. 8 Minimum principal stress—IFCMI

5 Conclusion

The following conclusions are given based on the analysis of the single-bay seven-storey RC frame.

1. The presence of interface and the types of interface are altering the principal stresses.
2. Maximum principal stress of IFCMI is more than that of IFPI up to third storey, and after that, it is comparatively equal for rest of the stories.
3. Minimum principal stress is more for IFPI than IFCMI up to fifth storey, and after that, it is approximately equal.

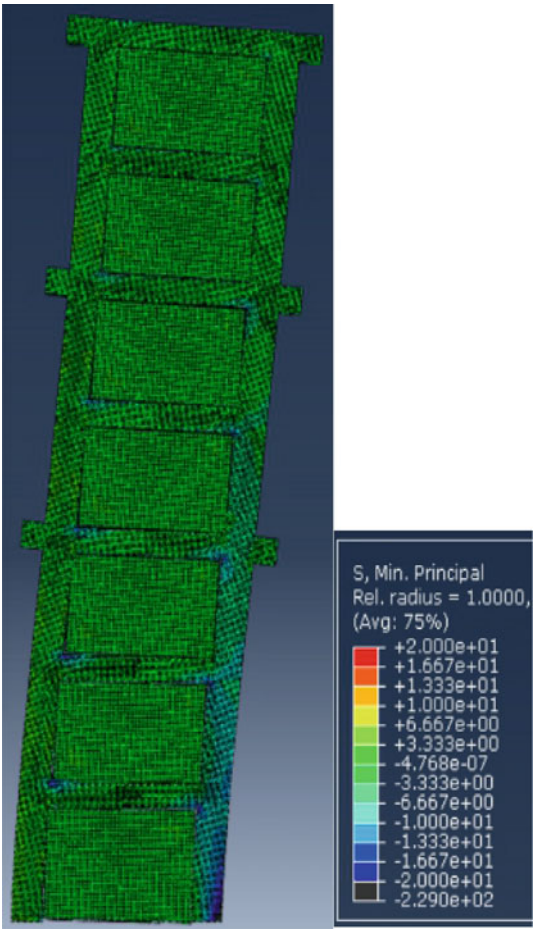

Fig. 9 Minimum principal stress—IFPI

4. BF is displaced to larger extent than IFCMI and IFPI.
5. The maximum displacement of BF is 27.44 mm. IFPI and IFCMI are displaced 0.41 times and 0.22 times of BF.
6. Von Mises stress is more at beam column joints of BF than IFCMI and IFPI.

From the results of the analysis, it is clear that infill frames are good in strength and load-carrying capacity. The infills and interfaces are playing vital role in the stability of structure, load-carrying and load distribution mechanisms as well as changes in structural parameters.

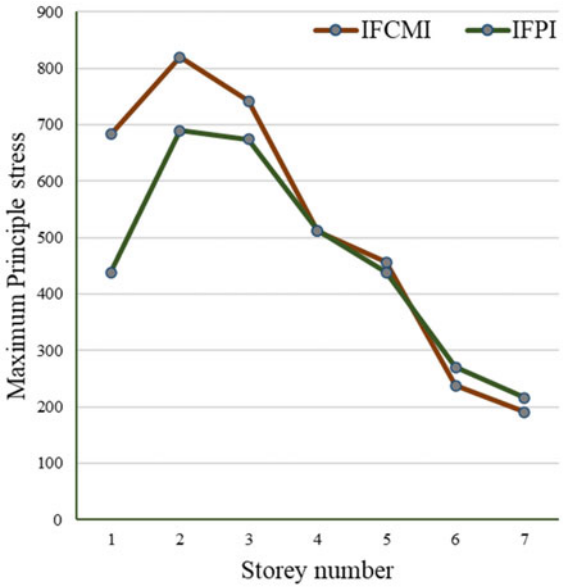

Fig. 10 Comparison of maximum principal stresses

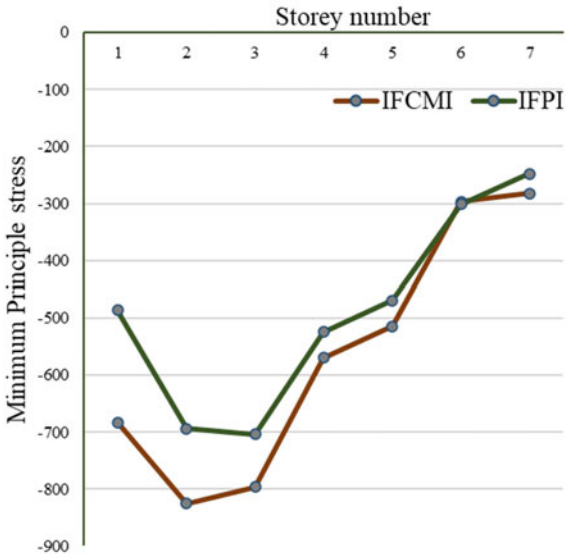

Fig. 11 Comparison of minimum principal stresses

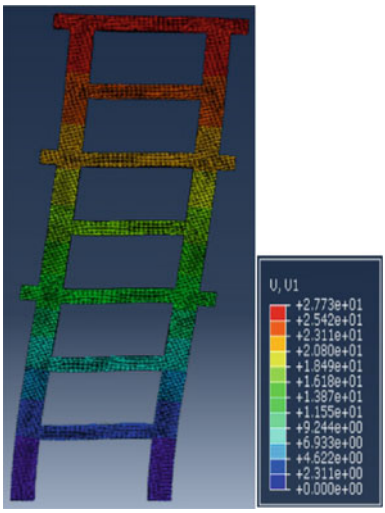

Fig. 12 Deflection of BF

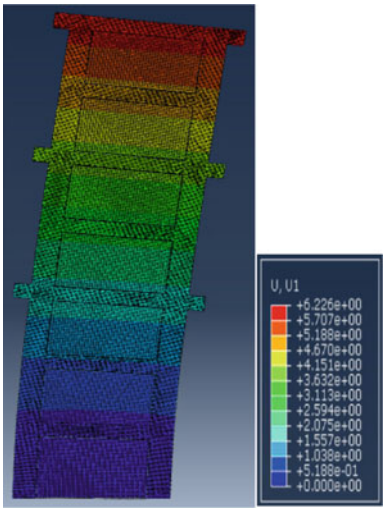

Fig. 13 Deflection of IFCMI

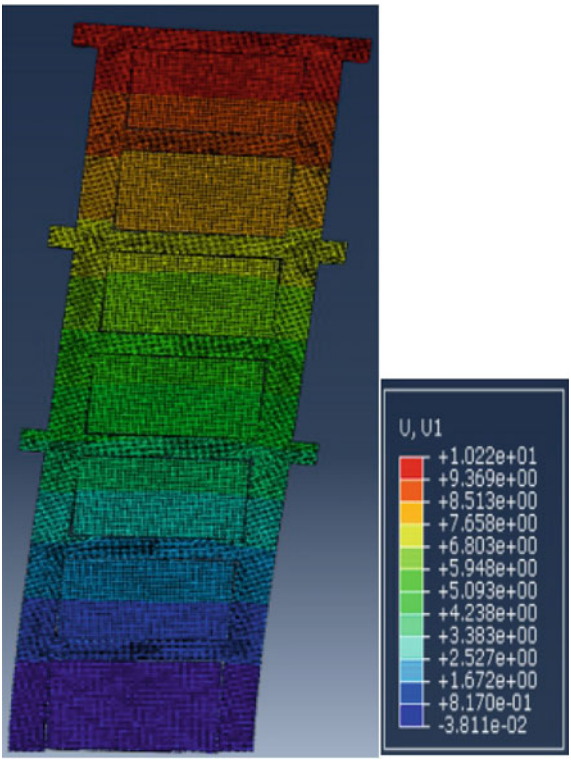

Fig. 14 Deflection of IFPI

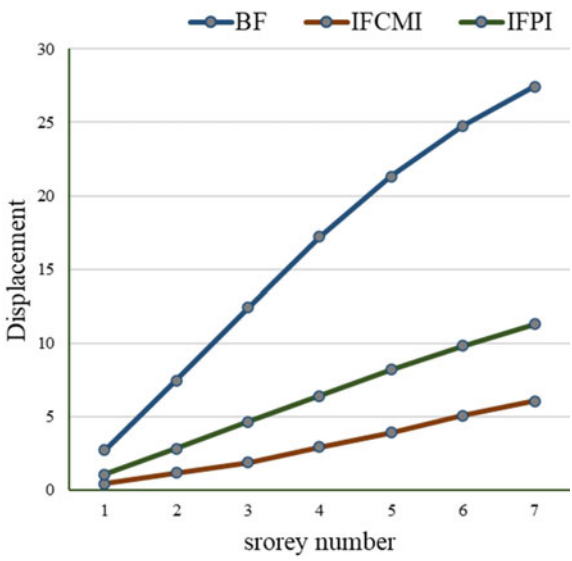

Fig. 15 Deflections of BF, IFCMI and IFPI

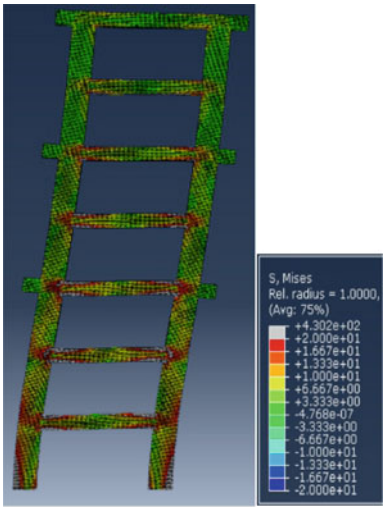

Fig. 16 Von Mises stress in BF

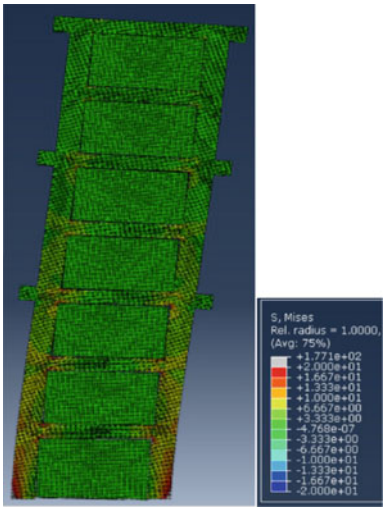

Fig. 17 Von Mises stress in IFCMI

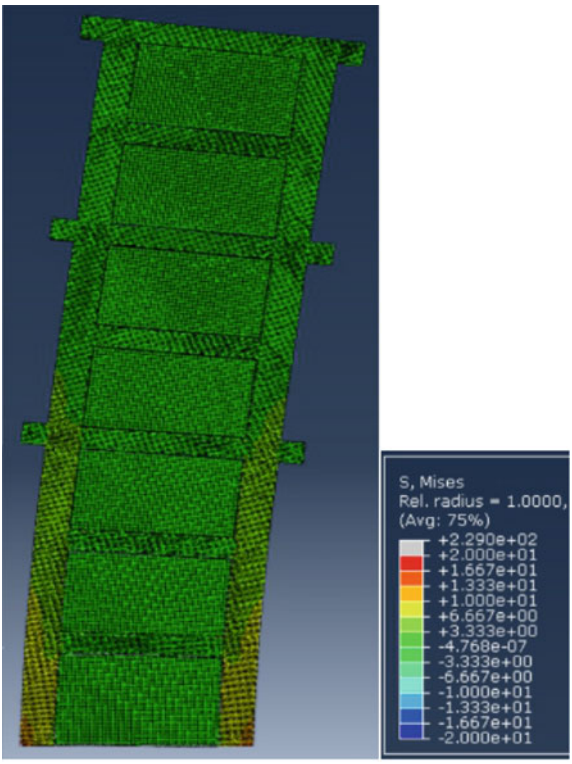

Fig. 18 Von Mises stress in IFPI

References

1. Kaplan S (2008) Framing contests: strategy making under uncertainty. Organ Sci 19(5):729–752
2. Asteris PG et al (2011) Mathematical macromodeling of infilled frames: state of the art. J Struct Eng 137(12):1508–1517
3. Bahreini V, Mahdi T, Najafizadeh MM (2017) Numerical study on the in-plane and out-of-plane resistance of brick masonry infill panels in steel frames. Shock Vib
4. Filippou, Christiana A., Nicholas C. Kyriakides, and Christis Z. Chrysostomou. "Numerical modeling of masonry-infilled RC frame." *The Open Construction & Building Technology Journal* 13.1 (2019).
5. Cavaleri L, Di Trapani F (2015) Prediction of the additional shear action on frame members due to infills. Bull Earthq Eng 13(5):1425–1454
6. Di Trapani F et al (2015) Masonry infills and RC frames interaction: literature overview and state of the art of macromodeling approach. Eur J Environ Civ Eng 19(9):1059–1095
7. Aliaari M, Memari AM (2005) Analysis of masonry infilled steel frames with seismic isolator subframes. Eng Struct 27(4):487–500
8. Chiou Y-J, Tzeng J-C, Liou Y-W (1999) Experimental and analytical study of masonry infilled frames. J Struct Eng 125(10):1109–1117
9. Dolatshahi KM, Aref AJ (2011) Two-dimensional computational framework of meso-scale rigid and line interface elements for masonry structures. Eng Struct 33(12):3657–3667
10. Moaveni B et al (2013) Finite-element model updating for assessment of progressive damage in a 3-story infilled RC frame. J Struct Eng 139(10):1665–1674

11. Beyer K et al (2014) Towards displacement-based seismic design of modern unreinforced masonry structures. In: Perspectives on European earthquake engineering and seismology. Springer, Cham, pp 401–428
12. Salmanpour AH, Mojsilović N, Schwartz J (2015) Displacement capacity of contemporary unreinforced masonry walls: an experimental study. Eng Struct 89:1–16
13. Wilding BV, Dolatshahi KM, Beyer K (2017) Influence of load history on the force-displacement response of in-plane loaded unreinforced masonry walls. Eng Struct 152:671–682
14. Zhou X et al (2018) Influence of infill wall configuration on failure modes of RC frames. Shock Vib 2018
15. Thirumurugan V et al (2021) Influence of pneumatic interface pressure in reinforced concrete infilled frames. Mater Today Proc 34:395–403
16. Manfredi G et al (2014) 2012 Emilia earthquake, Italy: reinforced concrete buildings response. Bull Earthq Eng 12(5):2275–2298
17. Tomaževič M (2007) Damage as a measure for earthquake-resistant design of masonry structures: Slovenian experience. Can J Civ Eng 34(11):1403–1412
18. Varum H et al (2017) Seismic performance of the infill masonry walls and ambient vibration tests after the Ghorka 2015, Nepal earthquake. Bull Earthq Eng 15(3):1185–1212
19. Yuen YP, Kuang JS (2015) Nonlinear seismic responses and lateral force transfer mechanisms of RC frames with different infill configurations. Eng Struct 91:125–140
20. Kuang JS, Wang Z (2014) Cyclic load tests of RC frame with column-isolated masonry infills. In: Second European conference on earthquake engineering and seismology, Istanbul
21. Ming L, Cheng Y, Liu X (2011) Shaking table test on out-of-plane stability of infill masonry wall. Trans Tianjin Univ 17(2):125–131
22. Palios X et al (2017) Unbonded brickwork for the protection of infills from seismic damage. Eng Struct 131:614–624
23. Thirumurugan V et al (2021) Experimental behaviour on seven storeyed infilled frame with pneumatic interface pressure. Mater Today Proc 40:S45–S51
24. Huang Q, Guo Z, Kuang JS (2016) Designing infilled reinforced concrete frames with the 'strong frame-weak infill' principle. Eng Struct 123:341–353
25. Preti M et al (2016) Analysis of the in-plane response of earthen masonry infill panels partitioned by sliding joints. Earthq Eng Struct Dyn 45(8):1209–1232
26. Zhao B, Taucer F, Rossetto T (2009) Field investigation on the performance of building structures during the 12 May 2008 Wenchuan earthquake in China. Eng Struct 31(8):1707–1723
27. Thirumurugan V et al (2019) Feasibility studies on adaptive interface for square infilled frame. Mater Today Proc 14:602–617
28. Preti M, Bolis V (2017) Masonry infill construction and retrofit technique for the infill-frame interaction mitigation: test results. Eng Struct 132:597–608
29. Zhang H, Kuang JS, Yuen TYP (2017) Low-seismic damage strategies for infilled RC frames: shake-table tests. Earthq Eng Struct Dyn 46(14):2419–2438
30. Mergos PE, Beyer K (2014) Loading protocols for European regions of low to moderate seismicity. Bull Earthq Eng 12(6):2507–2530

Multi-functional Materials

A Study on Strength Behaviour of Seasonal Frozen Soils Stabilized with Cement and Wood Ash

Yamem Tamut, Ajanta Kalita, and S. K. Singh

1 Introduction

Road construction in high-altitude areas where the subgrade soil is affected by seasonal frozen area is a herculean task. Owing to the frequent freezing–thawing cycles during cold seasons, it is quite challenging to maintain a durable and good quality road throughout the year. During freezing–thawing cycle, temperature in the pavement fluctuates from below freezing to above freezing; this cycle is frequently encountered during winter season in seasonally frozen areas. When the temperature rises, the accumulated snow or rainwater penetrates into the pavement subgrades through small cracks or fissures. And, when the temperature drops down below freezing point, the water trapped inside the pavement layers freezes and causes the cracks to widen. With the rise in the number of freezing–thawing cycles, volumetric contraction and expansion and the resulting cracks multiply leading to loss of strength and permanent failure of the pavement. The structure of soil changes after cycles of freezing and thawing [1] along with changes in its geotechnical properties including the physical and mechanical properties of soil [2–4]. Pavement constructed over in situ subgrades soil which suffered freeze–thaw cycles without proper treatment may undergo significant pavement distress because of the expansions during freezing and contraction due to melting of the accumulated snow during thawing periods. The incessant restructuring of water, ice and displacement accompanying with freezing and thawing causes significant alterations in the microstructure of soil fabric [5]. The modification techniques of the in situ soil by calcium-based stabilizer [6] to improve their engineering properties responsible for strong and durable subgrade are found to be highly effective.

The modification of weak subgrade soil with waste or low-cost materials is widely recognized and practised worldwide. The most commonly recognized stabilizing

Y. Tamut (✉) · A. Kalita · S. K. Singh
North Eastern Regional Institute of Science and Technology, Nirjuli, Arunachal Pradesh, India
e-mail: ymt@nerist.ac.in

K. S. Satyanarayanan et al. (eds.), *Sustainable Construction Materials*, Lecture Notes in Civil Engineering 194, https://doi.org/10.1007/978-981-16-6403-8_9

agents is lime followed by ordinary Portland cement. Although both cement and lime are capable of providing calcium, they differ in their chemical nature, their mode of reaction in the presence of water and their resulting reaction products [7]. Several researchers have worked on the effectiveness of lime [8, 9], cement [10–12] and industrial waste materials such as silica fume, fly ash and red mud in the modification of granular soils in order to remove the effects of freezing–thawing cycles [13].

Though the study on wood ash as concrete blocks have been previously carried out [14, 15], the study on wood ash as stabilizing agent in road construction materials has not been sufficiently explored, especially under freezing–thawing conditions. The strength properties of subgrade treated with wood ash, which is abundantly available as a waste product, needs to be explored to study its effectiveness in mitigating the damage caused to the pavement due to freezing–thawing cycles. The study area is located at Sela Pass Tawang, Arunachal Pradesh (India), with an average altitude of 13,700 feet (4170 m) above the mean sea level. This highway is of national importance as it is the lifeline for strategically important Tawang district which shares borders with China in the north and Bhutan in the west. Every year, it encounters long winter which generally begins in November and extends up to May. During winter, temperature in the Sela Pass area drops below −20 °C and a thick layer of snow covers the road for a long period which ultimately leads to considerable damage to the road subgrade after melting down of snow. The harsh winter is followed by a seasonal monsoon with a minimum recovery period of bearing capacity due to which this vital road remains in dilapidate condition throughout the year.

In the current study, the parent soil was stabilized with, cement, wood ash and combination of cement and wood ash to nullify the barbarous effects of freezing–thawing cycles. The prime objective of this work is to evaluate the effectiveness of soil stabilized with cement and wood ash to be used as alternate subgrade course, where similar weather conditions prevail with high cycles of freeze–thaw in road construction.

2 Materials and Methodology

2.1 Materials

The subgrade soil was taken from Tawang District, Arunachal Pradesh (India). Samples were collected after removing the top soil and excavating an open pit of 1.5 m depth below the ground level. The soil was oven dried for 24 h and index and engineering properties were determined in the laboratory. The physical properties of the parent soil are shown in Table 1.

The wood ash was collected from a household in Tawang Township, Arunachal Pradesh. It is a residue left after the burning of firewood in a closed hollow compartment locally called Bukhari generally meant for room-warming or water-heating

Table 1 Physical properties of the parent soil

Sl. no.		Properties	Value
1		Sieve analysis	
	i	Gravel size (>4.75 mm)	00.00%
	ii	Sand size (0.075–4.75 mm)	86.99%
	iii	Silt (0.075–0.002 mm)	11.01%
	iv	Clay (<0.002 mm	2.00%
2		IS soil classification	Silty sand (SM)
3		Specific gravity	2.67
4		Liquid limit	27.55%
5		Plastic limit	NP (non-plastic)
6		Maximum dry density (MDD)	19.05 kN/m^3
7		Optimum water content (OMC)	11.42%

system. The collected samples were oven dried for 24 h and per cent passing through 75 microns IS sieve size was taken for the analysis.

The cement used is fly ash-based Portland Pozzolana Cement conforming to Indian Standard BIS 1489, Part-1, 2015 of 53 grades. The chemical constituents of the parent soil, wood ash and the cement obtained from EDX results are provided in Table 2. Cement is selected for the study as it is readily available in the local market. In the present study, higher cement percentage was chosen to alleviate the effect of extreme weather conditions, but it has been restricted to 6% while considering the economical constraints in developing countries like India. This conforms to the recommendations of [11, 16].

2.2 Details of the Experimental Program

2.2.1 Sample Preparation

In the present study, cement was mixed with soil at 2, 4 and 6% and wood ash was mixed at 5, 10, 15 and 20% by weight of dry soil. To investigate the efficiency of the stabilizers, samples of various combinations such as Soil+Cement, Soil+Wood ash and Soil+Cement+Wood ash were prepared. The representative dry masses of the samples were prepared as per the compositions shown in Table 3 and uniform mixing of the samples were done manually using stainless steel spatula in dry state. Wet mixing was done by slowly adding potable water into the mixture. Standard proctor compaction tests as per IS 2720 (Part VII)-1980 were carried out on the

Table 2 Chemical composition of the parent soil, wood ash and cement

Standard	Parent soil			Wood Ash			Cement		
	Elements	Wt.%	Atomic wt.%	Elements	Wt.%	Atomic wt.%	Elements	Wt.%	Atomic wt.%
O SiO_2	O K	51.57	67.77	Ca K	22.42	34.28	O K	46.83	68.16
Na Albite	Na K	1.27	1.16	O K	42.02	48.24	Mg K	0.68	0.65
Mg MgO	Mg K	1.58	1.37	Na K	0.41	0.33	Al K	2.99	2.58
Al Al_2O_3	Al K	9.46	7.37	Mg K	1.25	0.94	Si K	8.05	6.67
Si SiO_2	Si K	21.40	16.02	Al K	0.97	0.66	S K	0.96	0.70
K MAD-10 Feldspar	K K	4.60	2.48	Si K	1.71	1.12	K K	0.68	0.41
Ca Wollastonite	Ca K	0.73	0.38	P K	0.59	0.35	Ca K	32.03	18.61
Fe Fe	Fe K	7.61	2.87	S K	0.38	0.22	Fe K	3.25	1.36
Cu Cu	Cu	1.78	0.59	K K	7.65	3.59	Sb L	4.52	0.86
		–	–	Ca K	21.86	10.02		–	–
		–	–	Fe K	0.75	0.25		–	–

Table 3 Details of the experimental programme for UCS tests

Mix proportion	Cement content (%)	Curing period (days)	F-T cycle (Nos)
S	0, 2, 4, 6	0, 3, 7, 14, 28	0, 3, 7, 14, 28
S+5%WA	-do-	-do-	-do-
S+10%WA	-do-	-do-	-do-
S+15%WA	-do-	-do-	-do-
S+20%WA	-do-	-do-	-do-

S: soil sample, C: cement, WA: wood ash, Normal: without curing and freezing–thawing, F–T: freezing–thawing cycles tests

untreated, cement-treated and cement- and wood ash-treated samples to obtain the MDD and OMC of all the combinations.

2.2.2 Unconfined Compressive Strength Test

Once the OMC and MDD of the various combinations were obtained, the UCS was determined for the untreated and treated samples as per IS 2720 (Part 10): 1991 to evaluate the performance of the various dosages of cement and wood ash in improving the strength of frost affected subgrade soil. Three replicas of samples were prepared at its OMC and MDD and average of three samples were taken as the UCS value. The prepared samples were cured in a desiccator at room temperature and their UCS were found out after 0, 3, 7, 14 and 28 days of curing periods.

2.2.3 Freeze–Thaw Cycles

Since the freezing of soil samples can be undertaken either in closed or open systems [4] in the present study, it was done in a closed environment to assess the effect of freeze–thaw cycles on the subgrade soil by preparing separate sets of samples with various combinations exposing them to freezing in a closed system without allowing water from any external source. For freezing, a commercial deep freezer was used and samples were kept in it for 12 h at $-18°$ centigrade with its lid closed; upon completion of 12 h, the samples were taken out from the deep freezer and let to thaw for 12 h at room temperature of about 20° in a desiccator. One cycle of freezing–thawing comprised of freezing for 12 h and thawing for 12 h. The samples were tested for UCS after 0, 3, 7, 14 and 28 freeze–thaw cycles.

3 Results and Discussions

3.1 Unconfined Compressive Strength (UCS) Performances of Frost-Affected Soil Stabilized with Cement and Wood Ash

The UCS value of the parent soil after 28 days curing period was found to be 258 kPa and the samples undergone for 28 freeze–thaw cycles was 237 kPa, which shows that the compressive strength of the parent soil without treatment was significantly reduced when subjected to freeze–thaw cycles.

3.1.1 Effect of Cement on Unconfined Compressive Strength Behaviour of Soil

After treating the parent soil with different percentages of cement, samples were tested for their UCS values. The variation of experimental result of UCS treated with varying percentages of cement at different curing periods and freezing–thawing cycles are shown in Fig. 1. Increased in UCS is noticed for soil treated with higher amount of cement, which is in line with the earlier reported findings [10, 17]. This increase is consistent with the increase in curing periods and freezing–thawing cycles for all the samples. The strength of soil not only depends on cement content but also depends on the curing period of soil [17]. However, the samples subjected to freeze–thaw cycles show lower UCS value than the samples in normal and cured states.

The mechanism of cement stabilization may be attributed to restructuring of soil/aggregate particles due to presence of cement [18]. The two basic reactions occurring in cement stabilization are hydration reactions and pozzolanic reactions

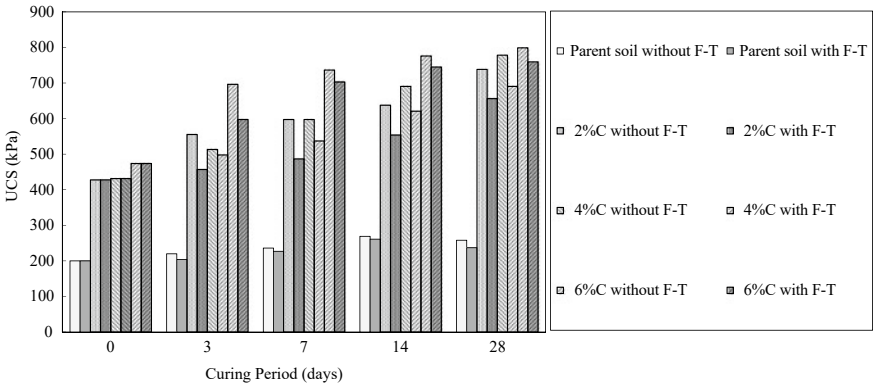

Fig. 1 UCS variation of cement percentage with curing periods

[19]. With the addition of water, hydration reactions take place and involvement of calcium, silica and water resulted into formation of C–S–H and extra CH. Then, steadily pozzolanic reactions take place which leads to formation of additional C–S–H or C–A–H, respectively, and ultimately contribute to the gain in strength of soil treated with cement. The increase in UCS may thus be attributed to the hydration and pozzolanic processes between the soil and cement content.

3.1.2 Effect of Wood Ash on Unconfined Compressive Strength Behaviour of Soil

Samples were also treated with varying percentages of wood ash and their UCS values found. The variation of UCS with different percentages of wood ash with curing periods and freezing–thawing cycles are shown in Figs. 2, 3, 4 and 5. It is clear from Fig. 5 that the UCS of the soil is noticeably improved after treating the soil

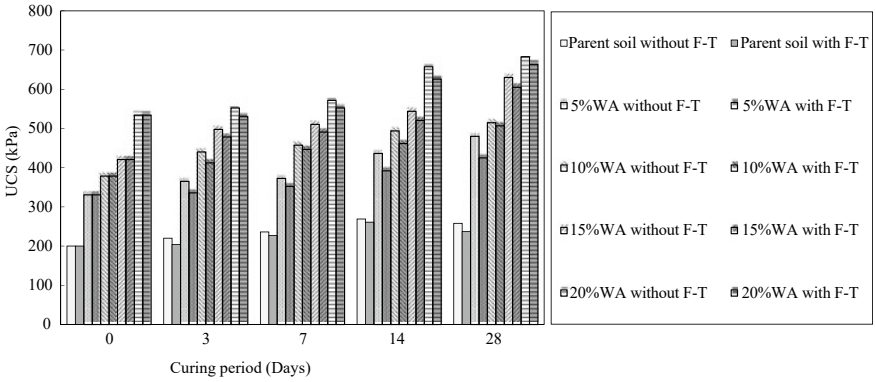

Fig. 2 UCS variation of wood ash percentage with curing periods

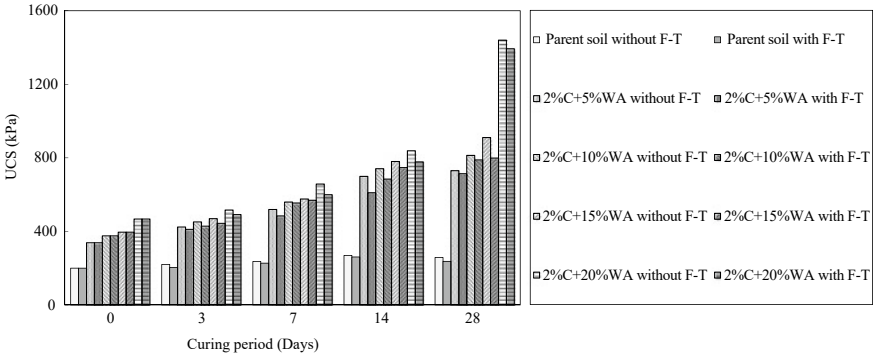

Fig. 3 UCS variation of 2%C+%wood ash with curing periods

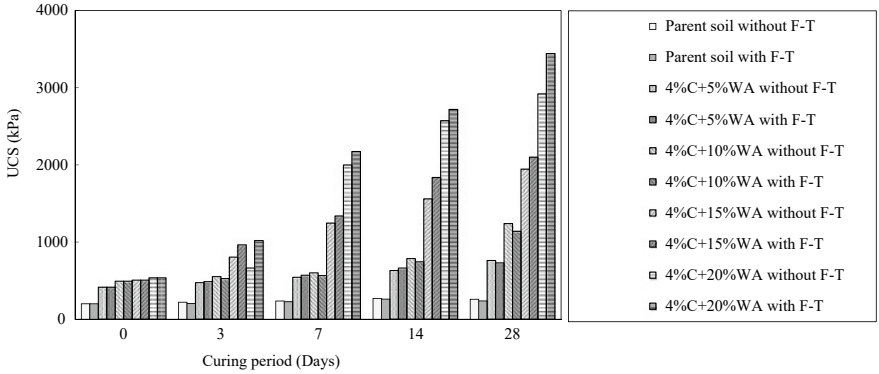

Fig. 4 UCS variation of 4%C+%Wood ash with curing periods

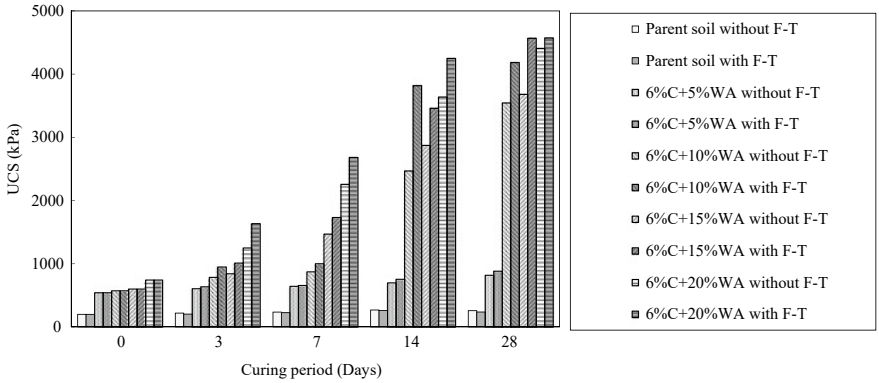

Fig. 5 UCS variation of 6%C+%wood ash with curing periods

with wood ash. The increase in UCS with wood ash content shows a similar trend as the cement contents, which means that the mechanism responsible for strength gain in both cases are the same. However, the increase in UCS of soil treated with wood ash is significantly less compared to the strength gain of cement treated soil. This could be attributed by lower concentration of Ca in wood ash compared to that in cement.

3.1.3 Effect of Cement and Wood Ash on Unconfined Compressive Strength Behaviour of Soil

Figures 3, 4 and 5 show the variation of UCS with 2%C+%WA, 4%C+%WA and 6%C+%WA, with the percentages of wood ash being varied from 5 to 20%, under different curing periods and freezing–thawing cycles. The figures show that the

combined mixture of cement and wood ash enormously improves the UCS of the soil as compared to the cement and wood ash alone. The increase in UCS is exponential with increase in curing periods and freezing–thawing cycles. The optimum UCS value was found with the dosage of 20%WA. The UCS values of 2%C+20%WA, 4%C+20%WA and 6%C+20%WA at 28th day of curing period were 1393 kPa, 2920 kPa and 4405 kPa, respectively, and after exposing to 28 freezing–thawing cycles were 1440 kPa, 3444 kPa and 4572 kPa. Additionally, it was noticed that the UCS of 4%C+20%WA, 6%C+15%WA and 6%C+20%WA exposed to 28 freezing–thawing cycles shows higher UCS value than the 28 days curing periods. The increase in strength can be attributed to the formations of C–S–H and C–A–H, which are cementitious products, with higher cement and wood ash contents. Although for the untreated soil, freeze–thaw cycles tend to weaken it, when cement is added to the soil, the samples show some improvement in strength. On freezing–thawing, the mobility of entrapped moisture seems to be high because of successive contraction and expansions, which is resulting in a better pozzolanic action of cementitious materials.

3.2 Microstructural Analysis

To explore the microstructural mechanism behind the strength gain and formation of compounds with and without stabilizers, a series of Scanning Electron Microscopic (SEM) and Energy-Dispersive X-ray (EDX) tests were conducted by JEOL JSM-6390LV and Oxford Instruments model 7582 EDX at Tezpur University, Tezpur, Assam, India. The SEM images of the untreated soil, wood ash and cement are shown in Fig. 6. The optimum combination, i.e. S+6%WA+20%WA-treated soil under 28 days of curing and 28 days of freeze–thaw cycles is shown in Fig. 7. It can be clearly confirmed from Figs. 6 and 7 that larger pores are observed in Fig. 6 as

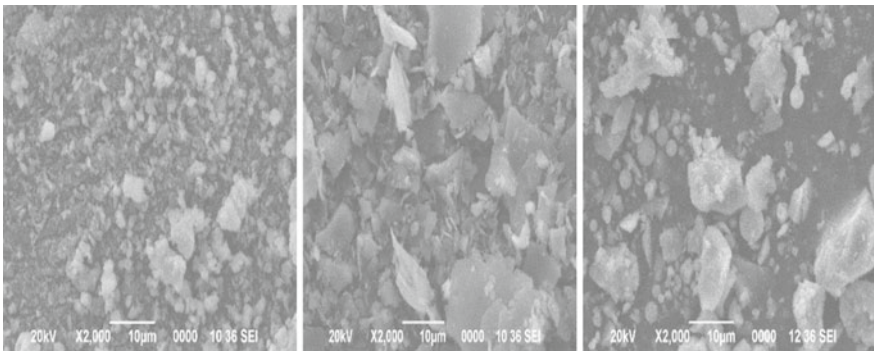

Fig. 6 SEM image of untreated soil, wood ash and cement

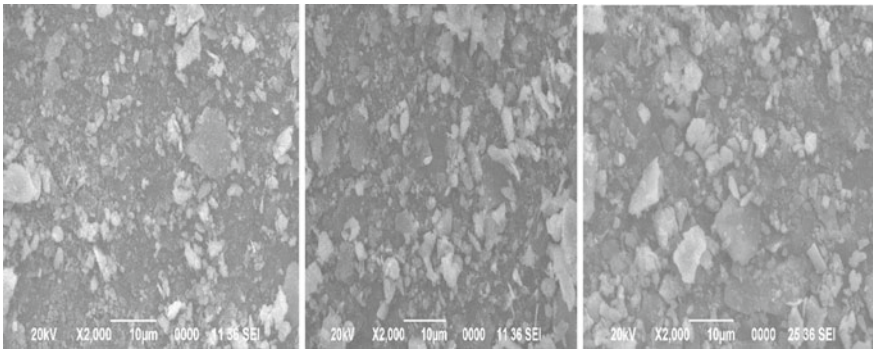

Fig. 7 SEM image of S+6%C+20%WA at normal condition, 28 days curing period and 28 freeze–thaw cycles

compared to Fig. 7. In Fig. 7, the large pores are filled by finer cementitious products to form a stable and denser structure which lead to pozzolanic reactions.

To compare the chemical composition of untreated and treated soil as well as the effect of curing and freezing–thawing with cement and wood ash treatment. As shown in Table 4, EDX analysis was performed after curing periods of 28 days and 28 freezing–thawing cycles. Changes in composition of elements and inclusion of new elements due to curing and freezing–thawing are also confirmed.

4 Conclusion

The study examined the effectiveness of cement and wood ash in improving the strength properties of seasonal frozen soil further to recommend for road constructions if found appropriate. Based on the investigational findings following inferences are drawn:

- UCS of the parent soil decreases on curing and after subjected to freeze–thaw cycles.
- UCS of soil stabilized with cement increases with increase in amount of cement in the soil mixture.
- UCS of soil mixture increases with the increase in period of curing and freeze–thaw cycles; however, samples exposed to freeze–thaw cycles show lower UCS compared to those after curing, when treated separately with cement and wood ash. Further, UCS value of cement treated soil is found to be higher than the one treated with wood ash.
- The mixture of Soil+Cement+Wood ash shows remarkable increase in the UCS value. The optimum UCS was obtained with S+6%C+20%WA both in curing and freeze–thaw conditions.

Table 4 Composition of elements under normal condition, 28 days curing and 28 days freeze–thaw cycles

	S+6%C+20%WA normal condition			S+6%C+20%WA 28 days curing			S+6%C+20%WA 28 freeze–thaw cycles		
Standard	Elements	Wt.%	Atomic wt.%	Elements	Wt.%	Atomic wt.%	Elements	Wt.%	Atomic wt.%
O SiO_2	C K	3.46	5.94	O K	56.61	73.86	O K	47.12	68.85
Na Albite	O K	52.96	68.25	Mg K	1.35	1.16	Na K	0.90	0.91
Mg MgO	Mg K	1.37	1.16	Al K	5.14	3.97	Mg K	1.03	0.99
Al Al_2O_3	Al K	4.50	3.44	Si K	11.78	8.76	Si K	13.23	11.01
Si SiO_2	Si K	10.56	7.75	K K	5.46	2.91	K K	5.73	3.43
K MAD-10 Feldspar	P K	0.55	0.36	Ca K	13.72	7.14	Ca K	17.30	10.09
Ca Wollastonite	K K	6.26	3.30	Ti K	0.54	0.24	Fe K	3.74	1.56
Fe Fe	Ca K	15.47	7.96	Fe K	4.03	1.51	Br L	8.75	2.56
Cu Cu	Ti K	0.48	0.20	Cu K	1.36	0.45	Sr L	2.20	0.59
	Fe K	4.39	1.62		–	–		–	–

- The highest UCS is for sample treated with S+6%C+20%WA, where the UCS value increases from 258 kPa of untreated soil to 4405 kPa of treated soil without freeze–thawing, and 237–4572 kPa for 28 days freeze–thaw cycles.
- The UCS of the mixture S+4%C+20%WA also performed well and UCS of 28 days curing period was found to be 2921 kPa and 28 days freezing–thawing cycles was found to be 3444 kPa.
- SEM analysis shows that macro pores in soils are filled by finer cementitious products. The formations of cementitious materials are accountable for the gain of strength.
- EDX analysis confirms the change in elements formation after treatment and with curing and freezing–thawing cycles.
- The combination of Soil+4% Cement+20% Wood Ash is recommended for stabilizing the subgrade below pavements in colder regions to overcome the problems associated with freeze–thaw cycles, as a cost-effective stabilization technique. Higher cement content, though marginally improves the strength, may lead to higher construction cost.

References

1. Zhen-Dong C, Peng-Peng He, Wei-Hao Y (2013) Mechanical properties of silty clay subjected to freezing-thawing. Cold Reg Sci Technol 98:26–34
2. Jiankun L, Chang D, Qianmi Yu (2016) Influence of freeze-thaw cycles on mechanical properties of a silty sand. Eng Geol 210:23–32
3. Jilin Qi, Vermeer PA, Cheng G (2006) A review of the influence of freeze-thaw cycles on soil geotechnical properties. Permafr Periglac Process 17:245–252
4. Da-Yan W, Ma W et al (2007) Effects of cyclic freezing and thawing on mechanical properties of Qinghai–Tibet clay. Cold Reg Sci Technol 48:34–43
5. Hohmann-Porebska M (2002) Microfabric effects in frozen clays in relation to geotechnical parameters. Appl Clay Sci 21:77–87
6. Prusinski JR, Bhattacharja S (1999) Effectiveness of portland cement and lime in stabilizing clay soils. J Trans Res Board 1652:215–227
7. Sankar B, Bhatty JI, Alan Todres H (2003) Stabilization of clay soils by Portland cement or lime-a critical review of literature. In: Portland cement association, Skokie, Illinois USA, PCA R&D Serial No 2066, 60 pages
8. Pavan A, Little DN (2020) Analytical tests to evaluate pozzolanic reaction in lime stabilized soils. Methods X 7:100928
9. Subhradeep D, Hussain M (2019) The strength and microstructural behavior of lime stabilized subgrade soil in road construction. Int Jo Geotechn Eng
10. Abhinaba P, Hussain M (2020) Cement Stabilization of Indian Peat: an experimental investigation. J Mater Civ Eng @ ASCE 32(11). 04020350-1-04020350-16
11. Portland Cement Association (2003) Properties and uses of cement-modified soil. Soil-Cement Inf
12. Hao W, Suo C et al (2020) Effect of freezing-thawing cycle on the mechanical properties and micromechanism of red mud-calcium-based composite cemented soil. Hindawi Adv Civ Eng 2020:14
13. Necmi Y, Kalkan E, Akbulut S (2007) Modification of the geotechnical properties, as influenced by freeze–thaw, of granular soils with waste additives. Cold Reg Sci Technol 48:44–54

14. Subramaniam P, Subasinghe K, Fonseka Keerthi WR (2015) Wood ash as an effective raw material for concrete blocks. Int J Res Eng Technol 4:228–233
15. Tarun RN, Rudolph NK, Rafat S (2003) Use of wood ash in cement-based materials. A CBU Report, CBU-2003–19 (REP-513)
16. Portland Cement Association (1992) Soil-cement laboratory handbook. Publication EB052.07S, Skokie, Illinois, USA
17. Anil P, Rabbani A (2017) Soil stabilisation using cement. Int J Civ Eng Technol 8(6):316–322
18. Halsted GE, Adaska WS, McConnell WT (2008) Guide to cement-modified soil (CMS). In: Portland cement association
19. Spencer GW, Parker JW et al (2011) Evaluation of laboratory durability tests for stabilized subgrade soils. In: Portland cement association, Skokie, Illinois, USA, SN3045a, 88 p

Evaluation of Failure Mode Analysis and Strength Behavior of Fly Ash Brick Masonry Prisms

S. T. Devi Suganya, L. Krishnaraj, and G. Nakkeeran

1 Introduction

Brickwork is an assembly of brick units bonded together with mortar. The property of brick masonry is highly influenced by two major factors, compressive strength and bonding properties at the brick–mortar interface, and it also depends on several other factors like the thickness of mortar joints, moisture content present in the brick material at the time of casting, positioning of bricks and its quality [1]. The bond strength at the interface of brick and mortar is exhibited through the penetration of mortar paste and hydration products like calcium silicates hydrates, into the voids and pores of the brick surface [2, 3]. A wrench test for testing the bond strength was developed in Australia, which is being used for laboratory research and as a tool for quality control in the brick masonry walls and for the in-situ measurements of bonding on the existing structure. Adopting advanced construction methods using new materials and technologies can improve the strength and stability of structures [4–7]. Until now, the use of masonry units has not been reduced as it still is followed in many parts of the world. But, the cause of failure of many ancient Masonry structures may be due to the poor design on the aspects of durability and strength. These facilities are very essential to understand and study brick masonry and helps in the prediction of their behavior and properties [8–10].

The previous researcher indicated that the GGBS and silica fume were found to be increasing the performance while considering the compressive strength of the cement mortars. During hydration, because of the substitution of the fly ash and silica fume, the calcium hydrate formation is reduced in the cement mortars. Due to that reason, the development of compressive strength in its initial stages was lesser when

S. T. Devi Suganya · L. Krishnaraj (✉) · G. Nakkeeran
Department of Civil Engineering, SRM Institute of Science and Technology, Kattankulathur 603 203, Tamil Nadu, India

G. Nakkeeran
e-mail: ng2683@srmist.edu.in

K. S. Satyanarayanan et al. (eds.), *Sustainable Construction Materials*, Lecture Notes in Civil Engineering 194, https://doi.org/10.1007/978-981-16-6403-8_10

compared with the Portland cement [11]. To full fill the requirements of the engineers, there are no appropriate results published according to the standard specifications. This leaves a space for further research in the field, which requires an understanding of the heterogeneous property of materials and knowledge about their behavior.

In the present study, an attempt was made for optimum replacement of OPC mortar by secondary cementitious materials like GGBS and SF with different water to binder ratio. This experimental research work attempted to study the investigating the properties of fly ash brick masonry prism under uniaxial compression test using wire cut bricks with mix combination and different types of mortar specimens. The physical properties, compressive, tensile and shear strength tests of various mix proportions of fly ash brick masonry have been reported. The failure mechanisms of brick masonry for different combinations of brick and mortar have also been reported.

2 Experimental Investigations

2.1 Materials Involved

In this exploration, Ordinary Portland Cement (OPC)—43 evaluations—is utilized for projecting mortar shapes and stonework crystals. The standard encore sand comprises of three grades will be quartz, light gray, or whitish variety and free from silt, which is confirming with IS 650. In this study, the sand that passes through a 2 mm IS sieve and retained on 90 microns IS sieve was used for tests. The conplast SP430 (SP) is a superplasticizer that is employed for investigating the improvement in workability with minimum water to cement ratio of 0.4. The first-class fly ash bricks, size 230 × 70 × 70 mm, were used. The locally available Ground Granulated Blast Furnace Slag (GGBS) confirming IS12089 (1987) and silica fume conforming to ASTM C1240 were used to prepare the mortar specimens [12, 13].

2.2 Proportioning of Mix and Parameters Studied

According to IS: 4031 (Part-6), the mix ratio of 1: 2.75 (Binder: Sand) was taken in this study. The binder consists of only OPC as a control mortar and the OPC replaced by GGBS and SF with 15, 30, and 45% separately by weight at the age 7, 14, 28 days was tested. For the preparation of mortar cubes, two different water binder ratios of 0.485 and 0.4 + 1% superplasticizer were taken for this study. The mix ratio is 30% replacement of OPC by GGBS and SF used to prepare the Fly ash brick prism and tested at the age of 28 days for both 0.485 and 0.4 + 1% SP w/b ratio [14]. In this study, the basic properties of materials, compressive strength of blended mortar cubes, compressive, tensile, and shear strength parameters of fly ash brick prism were studied.

2.3 Preparation of Test Specimens

For quantifying the compressive strength for the mortar sample, the cube was cast using 70 mm cube mold. The placing of mortar is done in two layers and is well compacted as directed in IS: 1727:1967. The OPC with GGBS and SF modified mortar cubes were prepared, and saturated limewater is employed for curing with various curing periods. To identify the compressive strength of brick–mortar prism specimens, first-class fly ash bricks were used to make the stack bonded type of masonry prism. The prism size is height × width × thickness (230 × 230 × 70 mm) with six mix proportions of mortar have been prepared as shown in Fig. 1. For testing the shear strength of the prism, the long faces of three bricks were joined by mortar.

The brick in the middle was kept 9 cm above the other two bricks as shown in Fig. 2. For testing the tensile strength of the prism, two bricks were kept in the opposite direction, and the third brick is kept above the two bricks with a 2.5 cm distance from the center point of the third brick as shown in Fig. 3. The mortar thickness is 10 mm provided in all brick joints. Three specimens for each combination of mortar are prepared for testing of compression, tension, and shear strength. The samples were prepared on a leveled platform, and for preventing direct contact with the ground, polythene sheets are used. The specimens were allowed to set for 48 h and cure under the gunny bags wet condition for 28 days up to testing of specimens [15–17]. The entire test conducted was the stress-controlled test. For investigating the performance of fly ash brick masonry, 18 prism specimens were examined in uni-axial compressive

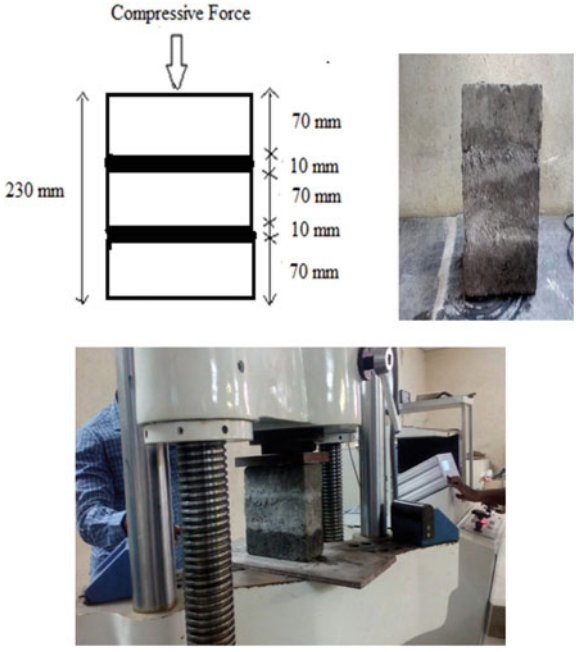

Fig. 1 Compressive strength test setup

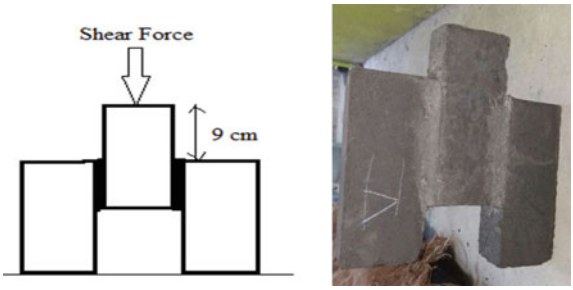

Fig. 2 Shear strength test setup

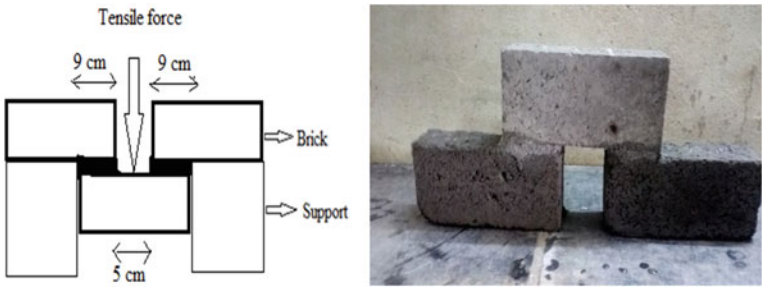

Fig. 3 Tensile strength test setup

loading. The experimental program for this study has been divided into three various types of tests, which were conducted in this testing program.

2.3.1 Compressive Strength Test on Prism

To quantify the compressive strength of prism, masonry prism of H/T ratio 3.28 was tested under uniaxial compressive loading according to the IS1905:1987 [18]. For obtaining the ultimate strength of the specimens, the axial load test was conducted with a gradual increase in load. Three specimens were carried out for each type of mix proportions of mortar specimens (Eq. 1).

$$\text{Compressive strength of masonry prism } \left(\text{N/mm}^2\right) = 0.25 \times \text{f}'\text{m} \tag{1}$$

where, f'm represents the compressive strength of masonry prism.

2.3.2 Shear Strength Test of Prism

Lateral loads like wind and earthquakes cause shear, which has been identified as a chief mode of failure in masonry constructions. Thus, for testing purposes, the pure shear is converted into shear compression mode. Certain issues must be considered while during testing, where direct shear loading is applied to the joints by normal loading. The direct shear test is a very demanding experiment, as it is very difficult to create a steady state of pressure at the joints. There are several different test methods available to promote uniform stress distribution on the prism; among them, the most standard test configuration is found to be the triplet test (three units and two joints). For testing of shear strength of the prism, the shearing load was given over the top surface of the center layer of brick as shown in Fig. 3. The uniform loading rate of 0.5 tons was sustained according to ACI specifications until failure occurs in this specimen.

2.3.3 Tensile Strength Test of a Prism

The tensile strength of the mortar unit interface is a critical mechanical property of masonry prism testing. In view that most of the time, the nonlinear behavior is through cracks in the mortar joints. It should be stated that the mortar unit interface controls the nonlinear behavior of the joints. Distinct varieties of tests had been used to assess the tensile strength; however, no clear consensus has been acquired from the test setup for use. Tensile bond strength test may be divided into two principal classes that are direct bond strength test and flexural bond strength, which is shown in the figure. For the tensile property test, in accordance with standard testing techniques, the test samples have been positioned as shown in Fig. 4. The standard loading rate became maintained till the specimens were failed. Correct fixing of the specimens inside the loading platter of the apparatus used for testing was achieved to evade compound strain consequences.

3 Results and Discussion

3.1 Physical and Chemical Properties

The specific gravity of the OPC, GGBS, and SF is 3.12, 2.85, and 2.2, respectively. The SF is having a less specific gravity value compared with the OPC and GGBS due to their high fineness. The chemical properties of OPC, GGBS, and SF are shown in Table 1. From the obtained values, it is observed that the silica content present is high in silica fume when compared with OPC and GGBS. It leads to improving the strength gaining of mortar.

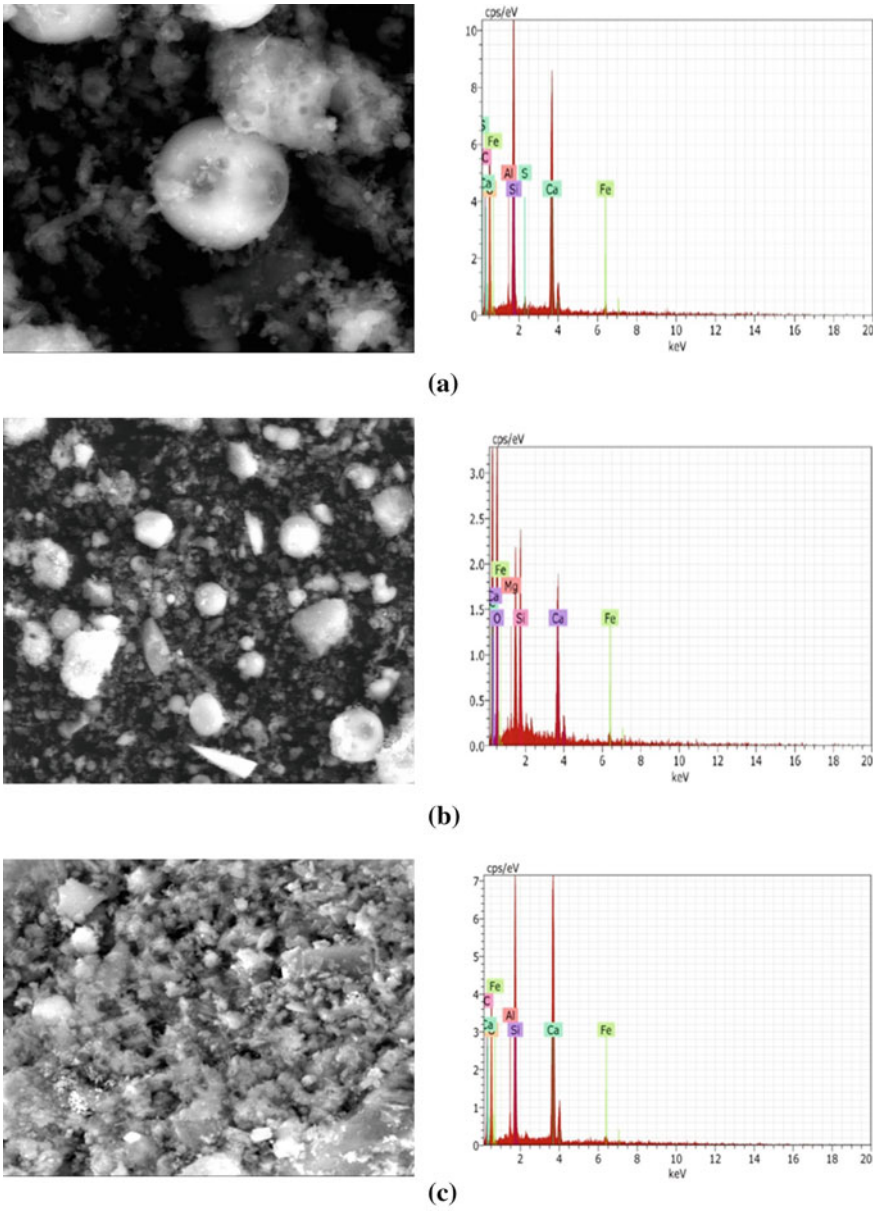

Fig. 4 **a** SEM imaging and EDX structure of OPC mortar at 28 days. **b** SEM imaging and EDX structure of 30% GGBS with SPL blended mortar sample at 28 days. **c** SEM imaging and EDX structure of 30% SF with SPL blended mortar at 28 days

Table 1 Chemical properties

Composition in %	OPC	GGBS	SF
Silicon dioxide	19.64	22	92
Aluminum oxide	5.65	19	0.7
Ferric oxide	5.4	1.2	0.6
Calcium oxide	62.5	36	0.3
Magnesium oxide	0.91	11.5	0.7

3.2 Masonry Brick Test

In this study, the fly ash bricks were exposed to the subsequent tests to discover their aptness for the building works. The efflorescence, water absorption, shape, size, hardness, and compressive strength tests have been performed on the fly ash bricks [19, 20], and test outcomes are shown in Table 2.

From the test values; the water absorption test is completed to decide the quantity of water captivated by the brick at 24 h immersion in water. The test result figures out the water captivated rate is less (8.48%) only, which proves the suitability of bricks. Based on the results, it is visible that there is no impression created at the surface of the brick. The soluble salts present in the brick are moderate; the compound of the brick is identical, condensed without any lumps. After striking the brick, there is a clear ringing sound heard. Based on results, the study established that the brick that was taken is possessed a satisfactory good in nature and appropriate to the building works.

Table 2 Brick suitability of construction work

Tests	IS code specification	Test result
Water absorption test	It should not exceed 20% of the weight of a dry brick	8.48%
Hardness	No impression should be found after scratching the brick with nail	An impression is not found
Compressive strength	7–14 N/mm^2 are classified as A and above 14 N/mm^2 are graded as AA	11.86 N/mm^2 (A-Grade)
Efflorescence test	If there is any white deposits are formed around 10%—slight; 50%—moderate; More than 50%—heavy efflorescence	Slight
Shape and size	Nonmodular bricks of size (230 × 110 × 70 mm)	230 × 100 × 70 mm
Soundness	Ringing sound should be produced in the brick	Ringing sound is heard
Structure	Homogeneous in nature and it should be free from lumps	Homogeneous compound

3.3 Microstructural Analysis

The Scanning Electron Microscope (SEM) analysis and Energy-dispersive X-ray spectroscopy (EDX) were conducted to analyze the microstructure of the various blended mortar samples at the age of 28 days as shown in Fig. 4a, b, c. The shape of the particles was analyzed by using SEM analysis, and elemental composition was analyzed using EDX. SEM analysis results revealed that the shape of silica fume samples was regular and spherical. GGBS blended samples showed a nonspherical shape that was the reason GGBS mortar specimens show better results than control mortar [20, 21].

3.4 Compressive Strength of Mortar Cubes

To estimate the influence of GGBS and SF addition on mechanical strength increase of pozzolanic materials, the test mixes should be 15, 30, and 45% will accordingly replace the OPC with two different water to binder ratio of 0.485 and 0.4 + 1% SPL were adopted, and test results are shown in Figs. 5 and 6.

According to the experimental findings, from Fig. 5, the GGBS of 15 and 30% with 0.485 w/ b ratio coded OPC mortar samples exhibit 4 and 16% increases in strength at the end of 28 days compared with the mortar samples produced by OPC. Similarly, the mortar mix prepared using 0.4 + 1% spl gives 20, 37% increases in strength at the end of 28 days compared with OPC mortar. Contrary to the previous findings, 45% replacement of OPC samples by GGBS using 0.485 and 0.4 + 1% spl w/c ratio decreases the strength 34 and 8%, respectively. From Fig. 6, the OPC replaced by SF with 0.485, 0.4 + 1% spl w/c ratio of 15 and 30% replacement exhibits 3, 10% and 11, 21%, respectively. From the test results clear that the optimum replacement of OPC by GGBS and SF is 30% based on the compressive strength test results. There

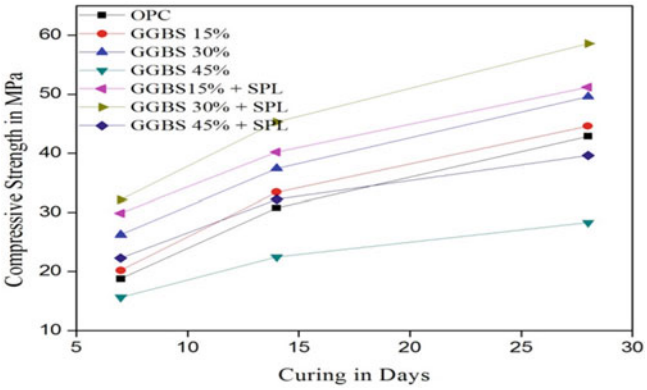

Fig. 5 Compressive strength of mortar cube using GGBS modified mortar

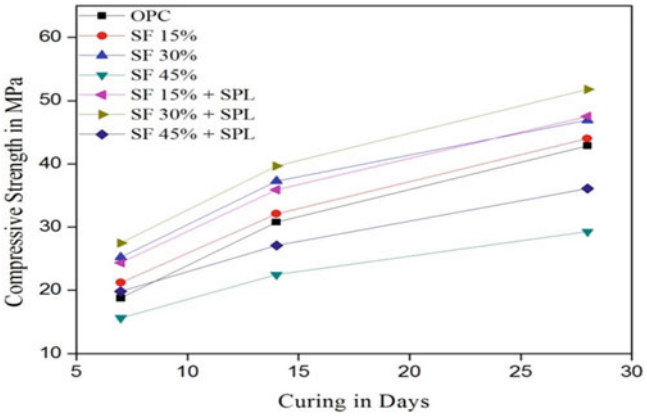

Fig. 6 Compressive strength of mortar cube using SF modified mortar

is a difference in the strength of GGBS and SF substituted OPC modified mortar used in the study with OPC mortar because of the difference in pozzolanic activity, fineness of particle size.

Besides, in all substituted OPC mortars, the presence of pozzolanas in the environment causes a decrease in C3A and decrease CH formation. however, GGBS and SF having the pozzolanic property that turns CH into a new Calcium silicate hydrate gel by means of binding CH in time and specifically fine SF particles block the pores, cause an increase in strength. The usage of GGBS in mortar reduces CO_2 emission. It is highly resistant to sulfate and chloride attack. The mortar failure will be prevented, and therefore, the life of the building will be increased [3, 16, 17, 22, 23].

3.5 Compressive Strength on Masonry Prism

The strength of the masonry prism has been shown in Table 3 and Fig. 7 given the various mix combinations of the brick prism. The superficial compressive strength values acquired from the test and in addition to that the normalized compressive strength is observed as according to the recommendations of IS: 1905-1987 making use of correction elements for the parallel height to thickness (h/t) ratio for the masonry prism. The compressive strength consequences were characterized concerning the efficiency of masonry that is described as the normalized compressive strength to that of brick.

Commencing the test outcomes, the brick prism was made with OPC, which is substituted by 30% GGBS with and without the addition of 1% superplasticizer gives 23 and 39% more compressive strength compared with OPC mortar prism. Similarly, the masonry prism was made with OPC with 30% replacement by SF with and without the addition of 1% superplasticizer gives 9 and 29% more compressive

Table 3 Compressive strength of masonry prism

Mix combination	Mortar strength in Mpa	Specimen size (b × h × t) mm	Compressive strength (Mpa)		Normalized compressive strength (Mpa)	Normalized masonry efficiency in %	Mode of failure
			Range	Average			
OPC 43	42.88	230 × 230 × 70	5.3–6.1	5.6	4.984	42.02	Bond
GGBS 30%	49.6		6.29–7.63	6.89	6.132	51.7	Bond and splitting
SF 30%	46.9		5.54–6.73	6.04	5.375	45.32	Splitting and crushing
GGBS 30 + 1% SPL	58.6		7.41–8.67	7.78	6.924	58.38	Splitting
SF 30 + 1% SPL	51.8		6.11–8.14	7.19	6.399	53.95	Splitting

Mean compressive strength of bricks = 11.86 MPa

[a] Each mortar mix is tested with three samples

[b] Compressive strength of the prism after smearing the correction factors for h/t ratio of specimens according to IS 1905–1987

[c] Normalized masonry efficiency = Normalized compressive strength/brick strength

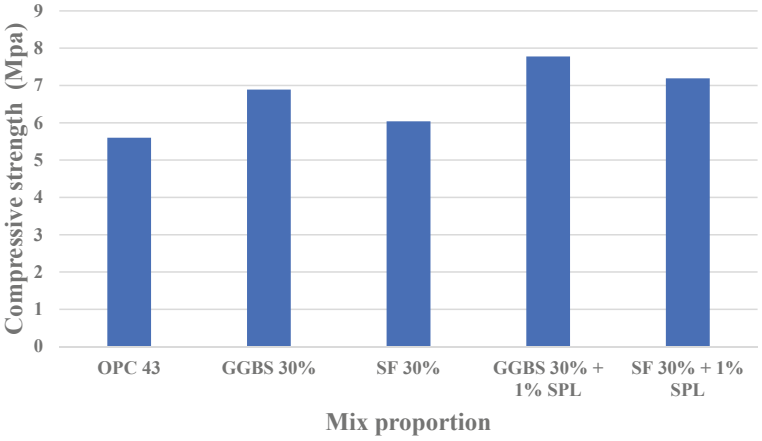

Fig. 7 Compressive strength of masonry prisms

strength compared with OPC mortar prism. The outcomes give positive capabilities in the strength variations with numerous parameters. It's noted that a hike in mortar strength ends in increased strength of brick–mortar prism. This may be qualified to two traits inside the samples experienced. Primarily, the difference in the brick strength is so substantial that the crack is originated mostly on the weakest brick because of its low compressive strength. Then, some sample failures are originated

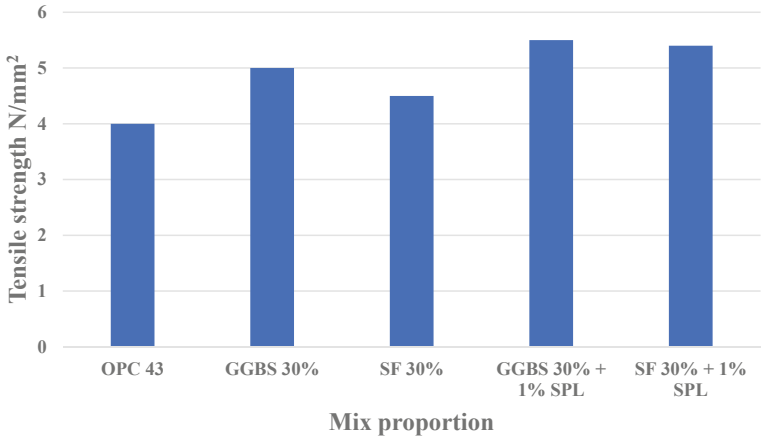

Fig. 8 Tensile strength of masonry prism with different mix proportions

with the aid of loss of bonding among brick–mortar mainly when the mortar may be every week [3, 24, 25].

3.6 Tensile Strength of Prism

The fly ash brick prism specimen was cast using OPC mortar, and 30% replacement of OPC by GGBS and SF mortar sample with and without the addition of water binder ratio outcomes are shown in Fig. 8. From the test outcomes, 30% replacement of GGBS with 0.485 and 0.4 + 1% spl gives 38 and 64% higher tensile strength compared with OPC mortar prism. Similarly, SF mortar prism provides 19 and 29% higher tensile strength compared with OPC mortar prism [26, 27].

3.7 Shear Strength of Masonry Prism

The amalgamation of brick and cement is masonry where the homogeneity property of the material is vital. The bond strength of mortar has an impact on the homogeneity. But due to the contrast in the material properties, homogeneity is practically difficult to achieve. The bond strength mainly depends on the characteristics of mortar and the properties of bricks. There is no codal provision for testing the shear bond strength. Therefore, to study the shear bond strength, a setup was made as shown in Fig. 9. The masonry prism specimen was prepared using OPC as a control specimen and the replacement of OPC with 30% of GGBS and SF with different water to binder ratio test outcomes shown in Fig. 6. From the outcomes, the replacement of OPC by

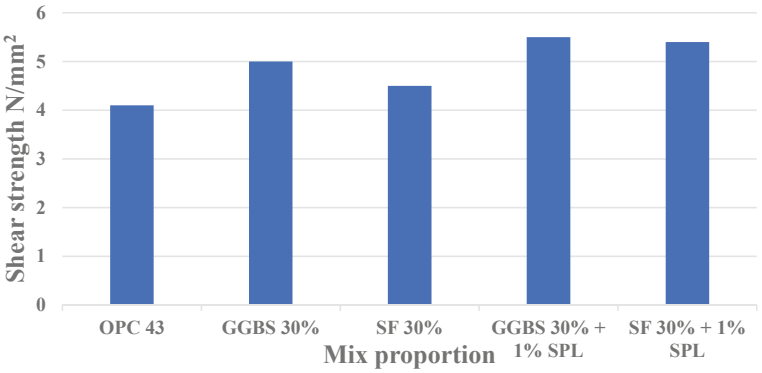

Fig. 9 Shear strength of masonry prism with different mix proportions

30% of GGBS with and without the addition of superplasticizer gives 33 and 43% of higher shear strength while comparing the OPC mortar specimen. Similarly, OPC replaced by 30% of SF with and without the addition of superplasticizer gives 7 and 25% of higher shear strength while comparing the OPC mortar specimen [28–30].

3.8 Failure Mechanisms Analysis

Earlier research has developed some failure mechanisms, which were based on uniaxial compression for masonry prism. It's been aware that when axial compression test is done for masonry, vertical cracks form and fail laterally in tension. This paper has also observed this failure pattern. But unlike the conventional bricks, these bricks were wrecked into pieces during failure. No crushing of brick happens but a dissimilar plane is formed by a straight-up crack. Two more processes have been spotted from this study [30–32]:

(a) If there is a loss of bonding, the interface between the brick and mortar fails due to shear, vanishing the lateral compression in bricks leading to failure by tension splitting.
(b) Failure by crushing in advance of splitting failure of bricks occurs if one of the bricks is comparably weak.

3.9 Cost Analysis of Masonry Prism

A cost analysis is a comprehensive breakdown of all expenditures related to the construction process. This breakdown includes material, labor, equipment, overhead, and profit cost. The quantity of the materials is estimated for preparing 54 masonry prisms. Based on the unit price of each material, the estimation for one cubic meter

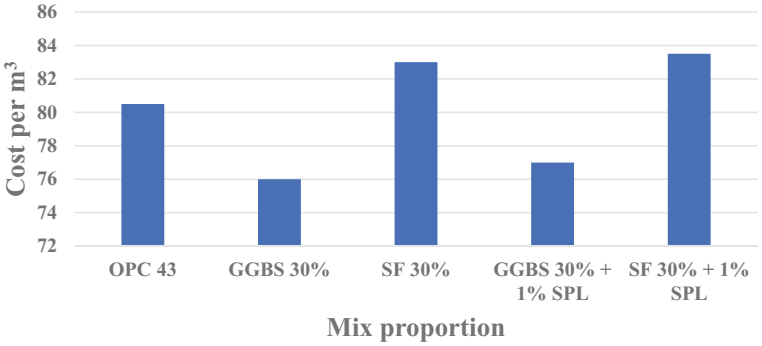

Fig. 10 Cost analysis between different mix proportions

is drawn up and cost analysis is done, and results are shown in Fig. 10. It is observed that when 30% of GGBS replaces OPC, the cost is minimized with and without the addition of superplasticizer. From the results, the cost of construction reduced by 30% of the total cost can be observed.

4 Conclusion

Through the experimental studies on fly ash masonry prism were prepared with various mortar to have been summarized below:

- The study has found that the fly ash bricks are adequately firm and rigid, are soundable, and also have good structure and homogeneity. The pulverizing strength of bricks was found to be 11.84 N/mm^2. Based on the test results of brick suitability, it has been evident that the brick has superior quality and satisfactory for construction works.
- The mortar cube is made with OPC and it is replaced with 30% GGBS and SF by 0.485 w/b ratios gives 16 and 10% higher compressive strength when related to the conventional mortar. Similarly, it gives 37 and 21% superior strength related to the conventional mortar with a 0.4 + 1% SPL w/b ratio. The optimum replacement of OPC by GGBS and SF is 30% by weight.
- The masonry prism test results of mechanical strength proved that the 30% of GGBS with 0.4 + 1% spl w/b ratio has proved that it has enhanced compressive strength, tensile and shear strength than the conventional and SF modified mortar prism.
- The failure of brick prism in compressive loading is due to the failure of the bond. Hence, if the bond strength is improved by mixing some adhesive material in a mortar then the strength can be increased.
- When compared with conventional cement mortar, the cost of GGBS mortar is minimized by 5–7% with and without superplasticizer.

Acknowledgements We acknowledge Nano Technology Research Centre and Department of Physics and Nano Technology, SRM University, Kattankulathur for help in microstructural studies.

References

1. Tiwari V, Choudry UB (2014) Experimental study of fly-ash brick masonry under subjected to cyclic loading. Int J Sci Technol Eng 1:1–9
2. Gumaste KS, Nanjunda Rao KS, Venkatarama Reddy BV, Jagadish KS (2007) Strength and elasticity of brick masonry prisms and wallets under compression. Mater Struct 40:241
3. Oliveira DV, Lourenço PB, Roca P (2000) Experimental characterization of the behavior of brick masonry subjected to cyclic loading. In: Proceedings of the 12th international brick/block masonry conference, Madrid, Spain, p 2119
4. Axely JW, Bertero V (1979) Infill panels: their influence on seismic response of buildings, Earthquake Engineering. Research Center, University of California at Berkele, Report No. EERC, pp 79–28
5. Benjamin JR, Williams HA (1958) The behavior of one story shear walls. In: Proceedings of the ASCE, vol 4, pp 1723–1730
6. Brokken ST, Bertero VV (1981) Studies on effects of infills in seismic resistance R/C construction. In: Earthquake engineering research center, the University of California at Berkeley, Report No. Conference, Melbourne, Australia, pp 81–12
7. Chrysostomou C, Gergely P, Abel JF (1988) Preliminary studies of the effect of Degrading infill walls on the nonlinear seismic response of steel frames. National Center for Earthquake Engineering Research, Technical Report NCEER, 88–0046
8. Krishnaraj L, Ravichandiran PT, Annadurai R, Kannan Rajkumar PR (2015) Study on micro structural behavior and strength characteristics of ultra-fine fly ash as a secondary cementitious material with portland cement. Int J Chem Tech Res 7:555–563
9. Mauren Brecher AHP (1980) Effect of test procedures on compressive strength of masonry prisms. In: Proceedings of the second canadian masonry symposium, held in Ottawa 9–11, p 119
10. Mohamad G, Lourenço PB, Roman HR (2005) Mechanical behavior assessment of concrete block masonry prisms under compression. In: Proceedings of international conference on concrete for structures (INCOS 05), Coimbra, p 261
11. Mojsilovic N (2005) A discussion of masonry characteristics derived from compression tests. In: 10th Canadian masonry symposium, Banff, Alberta
12. Mosalam K, Glascoe L, Bernier J (2009) Mechanical properties of unreinforced brick masonry section-1. Documented to U.S. Department of Energy by Lawrence Livermore National Laboratory
13. Krishnaraj L, Ravichandran PT, Kannan Rajkumar PR (2016) Investigation on effectiveness of the top down nanotechnology in mechanical activation of high calcium fly ash in mortar. Indian J Sci Technol 9(23):1–8
14. Zhao J, Wang D, Wang X, Liao S, Lin H (2015) Ultrafine grinding of fly ash with grinding aids: Impact on particle characteristics of ultrafine fly ash and properties of blended cement containing ultrafine fly ash. Constr Build Mater 78:250–259
15. Shrive NG, Reda Taha MM (2004) Bond strength of clay masonry prisms constructed with normal and fly ash substituted mortars. In: 13th international brick and block masonry conference, Amsterdam, July 2004
16. Tiwari V, Choubey UB (2014) An experimental study of fly ash brick masonry wall panels under cyclic loading. Int J Res Innov Sci Technol 1(1)
17. Pereira J, Campos J, Lourenço PB (2014) Experimental study on masonry infill walls under blast loading. In: 9th international masonry conference, Guimarães

18. Sigmund V, Penava D (2012) Experimental study of masonry infilled R/C frames with opening. In: 15th WCEE, LISBOA
19. Chuang S, Zhuge Y, Mcbean PC (2004) Seismic retrofitting of unreinforced masonry walls by cable system. In: 13th world conference on earthquake engineering, Vancouver, B.C., Canada, Paper No. 3228, August 1–6, 2004
20. Chuang SW, Zhuge Y, Wong TY, Peters L (2003) Seismic retrofitting of unreinforced masonry walls by FRP strips. In: Pacific conference on earthquake engineering
21. Ullah MA, Haque S, Ahsan R, Ikraz H (2013) Shear and tensile test of brick masonry unit for earthquake safety. Institute of Research Engineers and Doctors
22. Mistry S, Patel S, Bhavsar JJ, Zala LB, Umrigar FS (2011) Fly ash bricks masonry: an experimental study. In: National conference on recent trends in engineering &technology, May 2011
23. Remayanti C, Susanti L (2012) Experiment and numeric analysis of brick masonry wall with bracing under cyclic loading. Int J Emerg Technol Adv Eng 12:33–41
24. Rafat S (2003) Effect of fine aggregate replacement with class F fly ash on the mechanical properties of concrete. Cem Concr Res 33:539
25. Reda TMM, Shrive NG (2002) The use of pozzolans to improve bond and bond strength. In: 9th Canadian masonry symposium
26. Vintzileou EN, Toumbakari E-EE (2001) The effect of deep rejoining on the compressive strength of brick masonry historical constructions. Historical Constructions, Lourenço PB, Roca P (eds) Guimarães, pp 995–1002
27. Krishnaraj L, Ravichandiran PT, Rajkumar PRK (2016) Investigation on effectiveness of the top down nanotechnology in mechanical activation of high calcium fly ash in mortar. Ind J Sci Tech 9:23
28. Katsioti M, Tsakiridis PE, Giannatos P, Tsibouki Z, Marinos J (2009) Characterization of various cement grinding aids and their impact on grindability and cement performance Const. Build Mat 23:1954–1959
29. Seetharaman S, Subramanian J, Tun KS, Hamouda AS (2013) Synthesis and characterization of nano boron nitridereinforced magnesium composites produced by the microwave sintering method. Materials 6:1940–1955
30. Supit WMS, Shaikh UAF, Sarker PK (2014) Effect of ultrafine fly ash on mechanical properties of high volume fly ash mortar. Const Build Mat 51:1121–1127
31. Sankaranarayanan S, Jayalakshmi SS, Gupta M (2011) Effect of ball milling the hybrid reinforcements on the microstructure and mechanical properties of Mg^{-}(Ti+n-Al_2O_3) composites. J Alloys Comp 509:7229–7237
32. Papadakis VG, Tsimas S (2002) Supplementary cementing materials in concrete Part-I: efficiency and design. Cement Concr Res 32:1525–1532
33. Shrive NG, Reda Taha MM (2004) Bond strength of clay masonry prisms constructed with normal and fly ash substituted mortars. In: 13th international brick and block masonry conference (Amsterdam)

Experimental Study on Properties of Fresh and Hardened Concrete with Treated Waste Domestic Water

Prerna Sharma, S. Sathvik, V. R. Prasath Kumar, and L. Krishnaraj

1 Introduction

The groundwork of existence is water, but still very less importance is given toward conservation of potable water. Of the total global water, world's freshwater accounts for only 2.5%, and larger portion of it is frosted in glaciers and ice caps [1]. Rest of the thawed freshwater is primarily presented as groundwater, with less amount present in air. The accessibility of freshwater is depicted in the following pie chart. Population has been increasing in a burdensome manner. From 1959 to 1999, the world's population has been doubled [1], from 3 to 6 billion. By 2043, the world's population is envisaged to reach 9 billion (USCB, 2009) [1]. Increasing population leads to increasing water demand. Growing water demand means growing water scarcity. Bengaluru is located on the Deccan plateau, in Southern India. Bengaluru is also known as Garden City. The natural growth of urban population and migration of rural masses has made Bengaluru one of the most populated metropolitan cities in India. In recent decades, encroachment and destruction of lakes and canals have minimized the potential of groundwater recharge. Due to various economic activities and population growth, there is an increasing demand for enormous quantity of water.

P. Sharma · S. Sathvik · V. R. Prasath Kumar · L. Krishnaraj (✉)
Department of Civil Engineering, SRM Institute of Science and Technology, Kattankulathur, Tamil Nadu 603203, India
e-mail: krishnal@srmist.edu.in

P. Sharma
e-mail: ps9977@srmist.edu.in

S. Sathvik
e-mail: ss6118@srmist.edu.in

V. R. Prasath Kumar
e-mail: prasathv@srmist.edu.in

K. S. Satyanarayanan et al. (eds.), *Sustainable Construction Materials*, Lecture Notes in Civil Engineering 194, https://doi.org/10.1007/978-981-16-6403-8_11

Now, Bengaluru is at the peak of water crisis. As water is becoming insufficient, thus there is a need to control the usage of freshwater and reduce the pressure on potable water resources.

Bengaluru (in 2019) generates around 1600 million liters per day (MLD) of sewage, but only 1060 MLD is treated by about 25 treatment plants set up by BWSSB. Of this 1060 MLD, not more than 10th, i.e. only around 310 MLD is reused [2]. Government enterprises and multinational companies reuse this treated wastewater for agriculture, environmental rejuvenation, flushing of toilets, and industrial uses. As stated by NITI Aayog's Composite Water Management Index Report, 21 cities in India will run short of water by 2020 and Bengaluru is one among them. Thus, the measures have been taken by BWSSB to install many numbers of STPs in various areas of Bengaluru [3]. The utilization of treated wastewater minimizes the consumption of freshwater and thus, cutting down the burden on potable water resources, which also establishes the balance between serviceable resources and requirements. But the problem arises in the effective utilization of treated wastewater. In a complementing world, every year, construction industry expends around one trillion gallons of water universally, excluding cleansing water and curing water [4]. It appears that the construction industry consumes a huge amount of water (next to agriculture). According to the study conducted by Jadhavpur University, Kolkata, construction industry expends between 3000 and 8000 L of water for every square meter of built-up area [5, 6]. In India, population is rapidly increasing; also with an increase in developments of construction industry. In construction field, there is no substitute for concrete. Concrete is a crucial part of structure. Concrete is the most greatly employed unnatural heterogeneous mixture in the world [7, 8]. Concrete is a batter achieved by blending cementitious materials, fine and coarse aggregates and water in congruous proportions. These blends while poured into forms and avowed to cure, it coagulates to form hard rock, which is referred as concrete [9]. The characteristics of the constituents, proportions, technique of compaction and curing influence the strength, durability, and other features of the hardened concrete.

2 Materials

In concrete, OPC-53 grade is used, and it is conforming to Bureau of Indian Standards (BIS) be normally used in India. Fine aggregates used are the particle that entirely ravines through 4.75 mm IS sieve. Coarse aggregates are those gravels, crushed rocks, or a mixture of these, which are always larger than 4.75 mm and up to 150 mm. The main role of water stands for uniform mixing of materials; which also affects the hydration process of Portland cement [10, 11]. Water should be free from vegetation and impurities, which may influence the properties of the concrete. Potable water and treated wastewater are utilized in this study to test the variation in the properties of the concrete developed using both potable water and treated wastewater.

Acceptable mixing water

The crowning considerations for the acceptance of quality of mixing water are of two kinds: performance requirements and physical and chemical requirements, according to Neville [7]. The Permissible Limit for Solids as per IS 456:2000 is shown in Table 1 [12].

The study intends to utilize potable water and treated wastewater for making concrete. Potable water was obtained from bore well. Treated wastewater was procured from the domestic Sewage Treatment Plant (STP) of Volvo Group India Pvt. Ltd. Both the samples were collected and chemically tested for various parameters (that are required as per IS requirements). The tests were conducted in accordance with IS: 3025, and the test results show that the chemical structure of treated wastewater is much beyond potable water but is well within the limits as per IS 456:2000 [14, 15]. Both the samples will be employed in the study as mixing water and curing water. Table 2 describes the test results of chemical analysis of potable water and treated wastewater.

Table 1 Permissible limit for solids as per IS 456:2000 [13]

Sl. no.	Parameters	Tested as per	Permissible limits
1	Organic solids	IS 3025 (Part 18)	200 mg/l
2	Inorganic solids	IS 3025 (Part 18)	3000 mg/l
3	Sulphates (as SO_4)	IS 3025 (Part 24)	400 mg/l
4	Chlorides (as Cl)	IS 3025 (Part 32)	2000 mg/l for concrete not containing embedded steel and 500 mg/l for reinforced concrete work
5	Suspended matter	IS 3025 (Part 17)	2000 mg/l
6	pH	IS 3025 (Part 24)	≥6

Table 2 Parameters of water samples

Sl. no.	Parameters	Result of PW	Result of TWW	Requirement as per IS 456: 2000	Test method
1	Organic solids	73	91	200 mg/l	IS:3025/Part 16
2	Inorganic solids	603	1059	3000 mg/l	IS:3025/Part 16
3	Sulphates (as SO_4)	18.6	34.7	400 mg/l	IS:3025/Part 24
4	Chlorides (as Cl)	160	310	500 mg/l	IS:3025/Part 32
5	Suspended matter	<1.0	18	2000 mg/l	IS:3025/Part 17
6	pH	7.7	7.1	≥6	IS:3025/Part 24

Note PW = Potable water, TWW = Treated Wastewater

3 Methodology

Mix design of concrete was developed in accordance with IS 10262: 2019 [16, 17]. Concrete mix proportioning was developed with water–cement ratio of 0.45. Totally, five mixes were developed with varying % of treated wastewater 0, 25, 50, 75 and 100%. All the five mixes follow the same mix design procedure. The details of each mix are tabulated in Table 3.

3.1 Testing the Fresh Properties and Hardened Properties of Concrete

(a) **Fresh properties**

Workability of concrete was evaluated by performing slump test and was performed according to IS 1199: 1959 [18, 19]. The slump test helps to assess the uniformity of concrete. Quality of concrete is observed depending on changes in slump values; lower w/c ratio gives greater slump values, and increased w/c ratio gives lower values of slump hence water–cement ratio must be controlled to get prerequisite slump values.

(b) **Compression test**

Compression test is performed in accordance with IS 516-1959 [20, 21]. Three cubes of 150 × 150 × 150 mm are casted and tested. Tests are performed at specific ages of specimen, i.e. 7 and 28 days. The cubes are then positioned in the compression machine in such a way that the load shall be uniformly distributed over the entire surface of cube, and the rate of 140 kg/cm^2/min is applied without shock (ref. Eq. 1).

$$\text{Compressive strength} = [\text{Load}/\text{Area}]\,\text{N}/\text{mm}^2 \tag{1}$$

Table 3 Details of mix proportions (by mass)

Mixes	% of treated wastewater	Water content (ltr/m^3)		w/c ratio	Cement content (Kg/m^3)	Fine aggregate (Kg/m^3)	Coarse aggregate (Kg/m^3)
		PW	TW				
Mix 1	0	149	0	0.45	329	722	1307
Mix 2	25	111.75	37.25	0.45	329	722	1307
Mix 3	50	74.5	74.5	0.45	329	722	1307
Mix 4	75	37.25	111.75	0.45	329	722	1307
Mix 5	100	0	149	0.45	329	722	1307

Legend PW = Potable water, TW = Treated Wastewater

(c) **Split tensile test**

Split tensile test is effectuated in accordance with IS 5816: 1999 (ref. Eq. 2) [22]. Three cylinders of 150 mm × 300 mm are casted, cured and then tested. Tests shall be conducted at definite intervals of 28 days. Marking is done on the opposite faces of cylinder prior to testing. Metal splices are placed over the specimen, which converts compressive load to tensile load. The load is applied at the rate of 1.2–2.4 N/(mm^2/min).

$$\text{Split tensile strength} = 2 \times [P/\pi\, DL]\, N/mm^2 \tag{2}$$

where P = failure load at which the specimen fails,

D = diameter of cylinder specimen,

L = length of cylinder specimen.

(d) **Flexural test**

Flexural strength of concrete is evaluated by flexural test. The test is performed as per IS 516-1959 [23, 24]. Three beams of 100 × 100x500 mm are casted, cured and then tested. Tests are conducted at recognized ages of test specimen, i.e. at 28 days [25]. Concrete specimen is stationed in the machine and the load is applied at a pace of 7 kg/cm^2/min, finally, the load wherein specimen fails and the distance of breakdown from the nearest support at tension surface is noted. Flexural strength of concrete is calculated by Eqs. 3 and 4:

$$\text{Flexural strength} = Pl/bd^2 \left[\text{when a is greater than } 13.3\text{ cm}\right] N/mm^2 \tag{3}$$

$$\text{Flexural strength} = 3\,Pa/bd^2\ [\text{when a is lower than } 13.3\text{ cm}]\, N/mm^2 \tag{4}$$

where P = ultimate applied load wherein the specimen fails,

l = span length,

b = width of specimen, d = depth of specimen,

a = distance of breakdown from the nearest support.

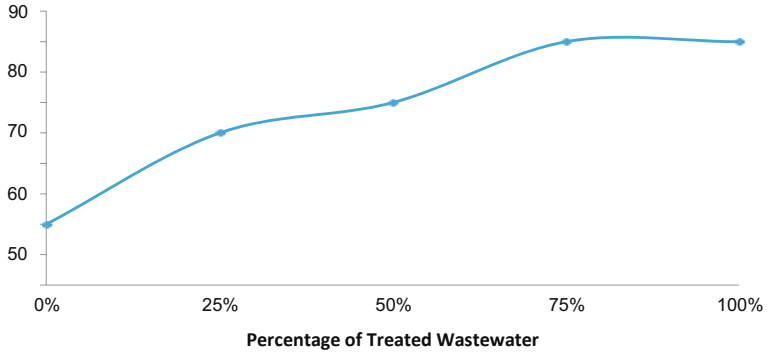

Fig. 1 Comparison of slump against percentage of treated wastewater

4 Results and Discussions

4.1 Slump Test

From Fig. 1, it can be noticed that the slump value (in mm) increases as the percentage of treated wastewater increases, which also explains that the workability has improved when the proportion of treated wastewater has increased.

4.2 Compression Test

(a) **Curing in potable water**

Table 4 represents the values of compression test of concrete cubes, which were cured in potable water, and Fig. 2 illustrates the variation of cube compressive strength with differing proportions of treated wastewater.

4.3 Curing in Treated Wastewater

Table 5 shows the values of compression test of concrete cubes when they were cured in treated wastewater, and Fig. 3 displays the variation of cube compressive strength with varying proportions of treated wastewater.

Table 4 Compressive strength test (curing in potable water)

Mixes	% of treated wastewater	Water content (kg/m^3)		w/c ratio	Cement content (Kg/m^3)	Fine aggregate (Kg/m^3)	Coarse aggregate (Kg/m^3)	C S (MPa)	
		PW	TW					7 days	28 days
Mix 1	0	149	0	0.45	329	722	1307	**14**	**18**
Mix 2	25	111.75	37.25	0.45	329	722	1307	**16**	**22**
Mix 3	50	74.5	74.5	0.45	329	722	1307	**19**	**26**
Mix 4	75	37.25	111.75	0.45	329	722	1307	**21**	**27**
Mix 5	100	0	149	0.45	329	722	1307	**23**	**27**

Note C S = Compressive Strength

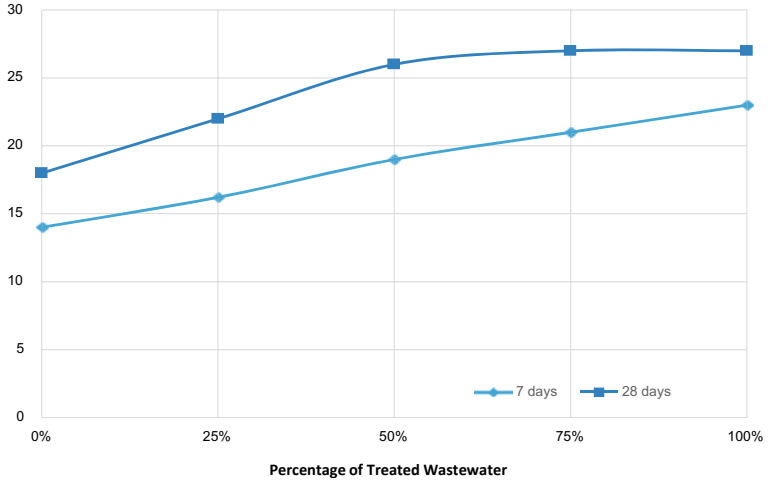

Fig. 2 Cube compressive strength with varying proportions of treated wastewater

4.4 Split Tensile Strength

The results of split. Tensile strength test results are provided. It is evident that the 28 days split tensile strength improves with addition in treated wastewater content when curing water is potable water. When treated water is curing water, split tensile strength increases till 50% of treated water and then decreases. Cylinder with 100% substitution of treated sewage water over potable water cured in potable water shows the maximum value of 2.92 MPa.

4.5 Flexural Strength

Figure 4 depicts the trend in flexural strength against treated wastewater.

The topmost flexural strength of 3.65 MPa can be noticed in beam specimen made with 100% treated water and cured in potable water. 18.35% increase in flexural strength can be observed when beam specimens are produced using treated wastewater and cured in potable water. Maximum decrease of 3.8% in flexural strength can be noticed between different mixes and different curing options.

5 Conclusion

The chemical structure of treated sewage water is more than potable water, however, they are not beyond the IS limits. The health risk of its utilization is minimal because of limits of impurities and pH is as same as normal water. The compressive strength

Table 5 Compressive strength tests (cubes were cured in treated waste water)

Mixes	% of treated wastewater	Water content (kg/m^3)		w/c ratio	Cement content (Kg/m^3)	Fine aggregate (Kg/m^3)	Coarse aggregate (Kg/m^3)	C S (MPa)	
		PW	TW					7 days	28 days
Mix 1	0	149	0	0.45	329	722	1307	**20**	**24**
Mix 2	25	111.75	37.25	0.45	329	722	1307	**21**	**25**
Mix 3	50	74.5	74.5	0.45	329	722	1307	**22**	**26**
Mix 4	75	37.25	111.75	0.45	329	722	1307	**21**	**25**
Mix 5	100	0	149	0.45	329	722	1307	**19**	**22**

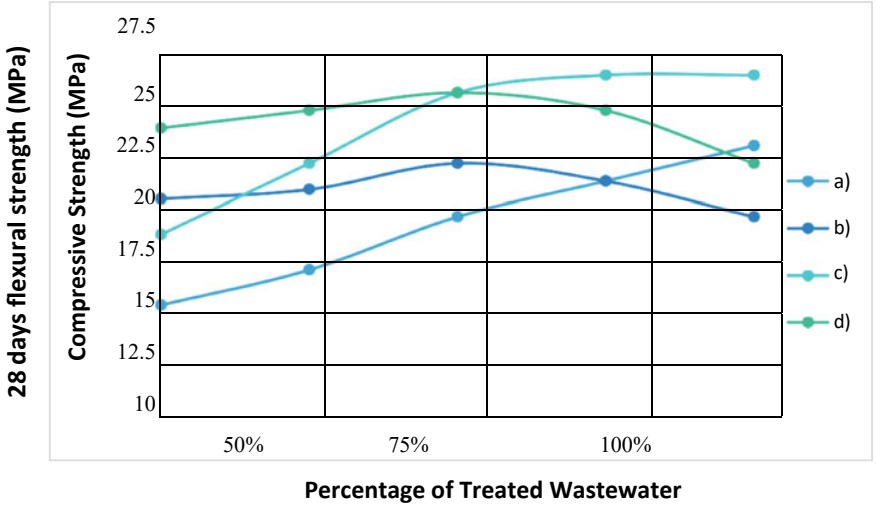

Fig. 3 Cube compressive strength with varying proportions of treated wastewater. *Note* (a) 7 days strength—potable water as curing water, (b) 28 days strength—potable water as curing water. (c) 7 days strength—treated wastewater as curing water, (d) 28 days strength—treated wastewater as curing water

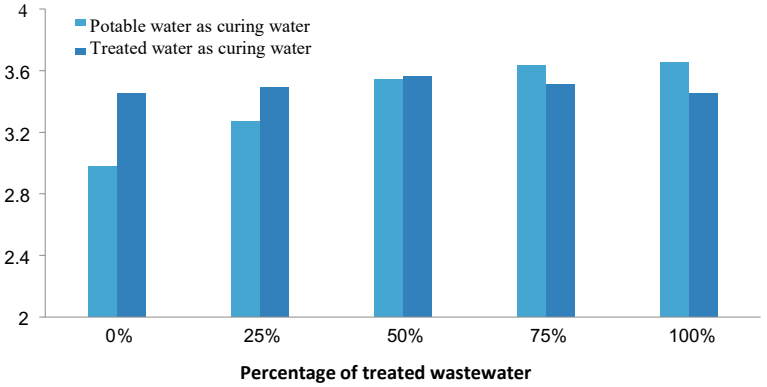

Fig. 4 Graph showing flexural strength against treated wastewater

increases till 50% of replacement and then declines down when treated wastewater is employed as curing water. The average compressive strength decreases by 10.7% when treated wastewater is utilized as curing water. The split tensile strength rose with addition of treated wastewater. 18.35% raise in split tensile strength can be identified while treated wastewater is employed as mixing water. The graph follows a hill trend with maximum value at 50% replacement when curing water is treated wastewater. 5.5% decrease in split tensile strength can be recognized when cured in treated water.

As the quantity of treated wastewater increases, the flexural strength increases. 18.5% increase in flexural strength can be observed when blended using treated sewage. When treated wastewater is employed as curing water, flexural strength increases till 50% replacement and then declines down. 3.8% decrease in flexural strength can be observed when curing water is treated wastewater.

References

1. https://www.census.gov/
2. https://www.thehindubusinessline.com/specials
3. https://niti.gov.in/
4. Meyer C (2004) Sustainable development and the concrete industry. CIB Bulletin, Sep 2009
5. https://www.downtoearth.org.in/
6. Kosmatka SH, Panarese WC (1995) Mixing water for concrete. Design and control of concrete mixtures, 6th Canadian edn, Portland Cement Association, pp 32–35
7. ASTM C 94-98 (1916) Standard specification for ready-mixed concrete. AST Minternational
8. IS 456: 2000 (2000) Plain and reinforced concrete-code of practice. Bureau of Indian Standards, New Delhi
9. Cebeci OZ, Saatci AM (1989) Domestic sewage as mixing water in concrete. ACI Mater J 86(5):503–506
10. Swami D, Sarkar K, Bhattacharjee B (2015) Use of treated domestic effluent as mixing water for concrete: effect on strength and water penetration at 28 days. Indian Concr J 89
11. Al-Jabri KS, Al-Saidy AH, Taha R, Al-Kemyani AJ (2011) Effect of using wastewater on the properties of high strength concrete. Procedia Eng 14:370–376
12. IS 12269: 2013 (2013) Ordinary Portland cement, 53 grade-specifications. Bureau of Indian Standards, New Delhi
13. IS 383: 2016 (2016) Coarse and fine aggregate for concrete-specification. Bureau of Indian Standards, New Delhi
14. IS 2386 (Part 1): 1963 (1963) Methods of test for aggregate for concrete, Part 1-particle size and shape. Bureau of Indian Standards, New Delhi
15. IS 2386 (Part 3): 1963 (1963) Methods of test for aggregate for concrete, Part 3-specific gravity, voids, absorption and bulking. Bureau of Indian Standards, New Delhi.
16. IS 10262: 2019 (2019) Concrete mix proportioning–guidelines. Bureau of Indian Standards, New Delhi
17. IS 1199: 1959 (1959) Methods of sampling and analysis of concrete. Bureau of Indian Standards, New Delhi
18. IS 516: 1959 (1959) Methods of tests for strength of concrete. Bureau of Indian Standards, New Delhi
19. IS 5816: 1999 (1999) Splitting tensile strength of concrete: method of test. Bureau of Indian Standards, New Delhi
20. Gómez Aguilar DL, Rodríguez Miranda JP, Esteban Muñoz JA, Betancur PJF (2019) Coffee pulp: a sustainable alternative removal of Cr (VI) in wastewaters. Processes 7:403
21. Khan R, Inam MA, Park DR, ZamZam S, Shin S, Khan S, Akram M, Yeom IT (2018) Influence of organic ligands on the colloidal stability and removal of ZnO nanoparticles from synthetic waters by coagulation. Processes 6:170
22. Liao L, Zhang P (2018) Preparation and characterization of polyaluminum titanium silicate and its performance in the treatment of low-turbidity water. Processes 6:125
23. Le TM, Vo PT, Do TA, Tran LT, Truong HT, Le Xuan TT, Chen Y-H, Chang C-C, Chang C-Y, Tran QT et al (2019) Effect of assisted ultrasonication and ozone pretreatments on sludge characteristics and yield of biogas production. Processes 7:743

24. Kyzas GZ, Christodoulou E, Bikiaris DN (2018) Basic dye removal with sorption onto low-cost natural textile fibers. Processes 6:166
25. Saroyan H, Kyzas GZ, Deliyanni EA (2019) effective dye degradation by graphene oxide supported manganese oxide. Processes 7:40

Case Study on Effective Utilization of Wastes by Implementing Lean Principles in the Auditorium Building

Sruthi Chandran, Ahmad Alothman, and L. Krishnaraj

1 Introduction

Construction project management is the process of managing resources such as men, materials, and labours over the total life cycle of the project using various tools, techniques, and methodologies [1]. In the construction industry, project management is a significant process to control the scope, time, manpower, and quality of the project throughout the lifetime of the project [2]. There will be a variety of constraints that arise between the design and execution of the construction projects. Construction project management will create an opportunity to interact with the various discipline of the project from architectural design to the execution of the project [3].

Construction project management is processed by the construction project manager [4]. This person deals with the planning, coordination, design, budgeting, and supervision of construction projects [5]. The project manager will deal with the total process involved in the execution of the project such as approval and planning of the project, deciding the schedule of the project completion and ensuring the project execution is ongoing on the proposed schedule, preparing the budget of the project costs and negotiating the costs with the contractors who were appointed for execution of the project, communicating with the client and stakeholders in the project, and other professionals on technical and contract details [6].

S. Chandran · A. Alothman · L. Krishnaraj (✉)
Department of Civil Engineering, College of Engineering and Technology, SRM Institute of Science and Technology, Kattankulathur 603203, Tamil Nadu, India
e-mail: krishnal@srmist.edu.in

A. Alothman
e-mail: aa1192@srmist.edu.in

K. S. Satyanarayanan et al. (eds.), *Sustainable Construction Materials*, Lecture Notes in Civil Engineering 194, https://doi.org/10.1007/978-981-16-6403-8_12

Fig. 1 Sequence of the construction project

1.1 Conventional Construction Projects

The conventional method of construction projects indicates a particular sequential method of construction such as planning, executing, monitoring, controlling, and closing [3]. Conventional construction methods are best for the projects completed in the above sequence. It is most suitable for remote projects [5]. Since the conventional method of construction involves less complexity, it meets the requirements of the client easily. In a conventional method, the project initiates with a simple design that is processed by the development cycles that permit the general project design [4].

In the conventional method, construction project management involves various skills and project managers can ability to interfere with different types of agencies and people to lead the project from planning to execution [7]. The construction project manager should follow the principles of management in every phase of construction. The construction management process helps to smooth the flow of work progress [8]. The following Fig. 1 is the conventional sequence for the construction projects.

1.2 Lean Principles

Since there are a lack of coordination, time mismanagement, lack of client involvement, slow development process if the requirements are not clear, lack of dynamic teamwork and leadership as a central authority which leads to lack of coordination and optimization of work, increase in the number of wastes, there is no space for new ideas in a conventional method of handling the construction projects [9]. To overcome all the above issues, much modern construction management is adopted [10]. One of the significant methods is the lean construction management method that helps in eliminating the wastes in construction projects or optimizing the resources of the project for creating value for the customer's requirements [11]. In lean management, the client involvement will be high because all the process of execution is an open process that leads to complete satisfaction of the client or customer [12]. The lean management startup movement is always based on the five core principles they are, Identity value, Map the value stream, Create workflow, Establish pull, and Continuous improvement [13].

The major objectives of using lean management are to improve the traditional management work progress, involving master scheduling, phase scheduling, look ahead scheduling, and weekly work scheduling can help to optimize the resources of

the construction projects. Identifying the value-added activities and non-value added activities that are to be eliminated for successful future projects, and Enhancing the ability of the product in the estimated time and budget as possible.

2 Methodology

In this study, the analysis of the problems is prepared from the literature review, and lean scheduling will be done based on the analysis of the problem for a completed IIT auditorium project at the IIT Madras campus, which was a delay in the cost and time of the project, comparing two schedules pre-project schedule of the project, and lean planning schedule of the project.

2.1 Lean Management

Lean management is the process of project management that approaches to manage an organization that enhances the concept of continuous improvement, the systematic achievement of small and incremental changes by the long-term approach of work to improve efficiency and quality [14]. The lean methodology involves three simple steps:

1. Delivers value from the customer emotions.
2. Elimination of wastes.
3. Continuous improvement of the work process.

The lean methodology is adopted for continuous improvement of work processes, purposes, and people, lean management provokes shared responsibility and leadership [15]. The following Fig. 2 is the Toyota production system invention of lean management; the two main pillars of the lean methodology are respect for people and continuous improvement. Lean is a concept widely adopted in various industries [16,

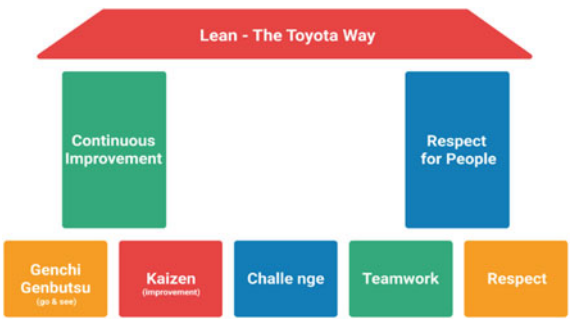

Fig. 2 Toyota production system

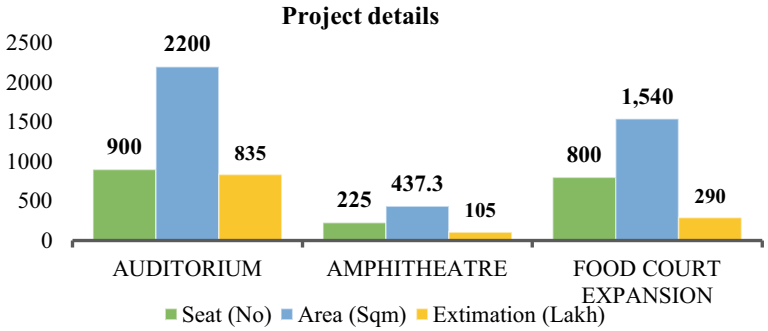

Fig. 3 Project details

17]. In the 1940s, Toyota found lean manufacturing, which reduces the non-valued processes in production. Their achievements are:

Improvements in productivity, efficiency, cycle time, and cost-efficiency. The term "Lean" was made up by John Krafcik (currently CEO of Google's self-driving car project Waymo) in his 1988 article "Triumph of the Lean Production System" [9].

2.2 Project Details

IIT Madras Research Park, Taramani, Chennai attempts to enable companies with a research focus to set up a base in the Park to hold the expertise of IIT Madras. It is modelled in the lines of successful Research Parks such as Stanford, MIT, and Harvard. IIT Madras Research Park, Chennai constructed an Auditorium with approximate area of 2500 Sqm, time limit of 4 months, tender issuing date 10 December 2018, and project budget (Rs. 8,50,00,000), an Amphitheatre on the seventh and eighth floors of Block-D of Phase-II Building. The following Fig. 3 represents the project (Auditorium, Amphitheatre, Food court expansion) brief details; includes the seat number for each project, the area (Sqm), and the estimation cost (Lakh) for each project.

2.3 Data Collection and Analysis

Lean management techniques encourage the approach of expects' unexpected things by prior visualization and planning. If the work is tracked and handled in a scheduled way by proper scheduling then the unexpected problems are easy to handle for the project manager. All the data related to the project like project principle details project tender, contract conditions, overall project schedule, and parameter analysis collected to analyze using the lean principle method.

2.4 Overall Project Schedule

In project management, the schedule creates a lifecycle of the project. The life-cycle begins when an owner identified market needs and ends when the project is completed. A well-executed construction project schedule outlines each activity step by step and provides dates for completion of each activity. The schedule may be crucial to keep the project on time and budget. The following Table 1 is the detailed schedule of the project.

2.5 Parameter Analysis

The project is scheduled properly and the budget is given for the client requirements, but still the project is delayed by 2 months and the estimated budget becomes under budget. Many problems arise during the execution that are listed below:

(a) Problems in the planning phase.
(b) Problems in the design phase.
(c) Problems in the execution phase.
(d) General problems.

I. **On planning phase**:
   (a) In the conventional method of scheduling, only the execution of work is included no paperwork process is included, but the schedule begins when the client asks their requirements for execution.
   (b) The drawings were delayed from the architect's side and the project start date itself was extended for 1 month.
   (c) The architect proposed the curved shape staircase but the schedule is done for general shape buildings without any ahead practical execution knowledge.
   (d) Proper planning is not done priory for material procurement and storage at the site.

II. **Problems on design phase**:
   (a) The structural consultant was designed the structure only based on the drawings given by the architect, they did not even visit the site.
   (b) The structural consultant who designed the structure has suddenly dropped the project during execution after procuring the designed material.
   (c) Due to the pinned connection, the steel section was very high which we cannot get readymade in the market, so the section has to be cut and fabricate, but this concept is not included in the planning stage before itself.

Table 1 Detailed schedule of the project

No.	Description of works	Start date	Number of days	End date
1	Existing brick wall demolishing work including cleaning	06-02-19	3	08-02-19
2	Marking of steel column and Aerocon block wall at a lower level	06-02-19	4	09-02-19
3	Aerocon block, M-sand lifting work	07-02-19	3	09-02-19
4	Structural material procurement unloading, lifting, etc.	09-02-19	7	15-02-19
5	200 mm Aerocon block work lower level at north side, stage's east side, west and south side	08-02-19	11	18-02-19
6	Base plate anchoring and column erection work	10-02-19	4	13-02-19
7	Purlin and decking sheet fixing work	13-02-19	3	15-02-19
8	Steel reinforcement including cutting, bending, placing, and binding for steps	14-02-19	4	17-02-19
9	Concreting the lower level steps	18-02-19	1	18-02-19
10	Toilet partition brick work	10-02-19	3	12-02-19
11	Tiles laying work at toilet and floor	20-02-19	6	25-02-19
12	Gypsum partition work at green room	26-02-19	3	28-02-19
13	Wall panelling work at north and south side	26-02-19	3	28-02-19
14	Marking of steel column at upper level	10-02-19	13	22-02-19
15	Steel column base plate anchoring and erection	23-02-19	6	28-02-19
16	Purlin and decking sheet fixing work	01-03-19	8	08-03-19
17	Bar bending and placing for upper level steps	08-03-19	3	10-03-19
18	Concreting the upper level steps and corridor etc.	11-03-19		10-03-19

(continued)

Table 1 (continued)

No.	Description of works	Start date	Number of days	End date
19	200 mm thick Aerocon block work at upper level up to roof including lifting	12-03-19	11	22-03-19
20	Plastering work at inside and outside of the upper and lower level	22-03-19	10	31-03-19
21	Plumbing work (EWC, Washbasin fixing work)	26-03-19	3	28-03-19
22	Joineries Fixing work	25-03-19	4	28-03-19
23	False ceiling work	26-03-19	6	31-03-19
24	Painting work inside and outside	31-03-19	6	05-04-19
25	Site cleaning work (balance material removing etc.…)	06-04-19	1	06-04-19
26	Snag list attending work	07-04-19	2	08-04-19
27	Handing over	09-04-19	1	09-04-19
Duration of project		**06-02-19**	**62**	**09-04-19**

(d) The cutting and fabricating location is different for a steel section. So the delay occurs because the section has to take from one place to another for fabrication after cutting, it is been a long process.

III. **Problems on execution phase**:

(a) The main contractor appointed for work is only strong in the interior not much in structural steel works.
(b) The auditorium design was done by a previous structural consultant, and the amphitheatre design was done by a new structural consultant who creates confusion in the structural design.
(c) The tendon on the existing PT slab is getting punctured when the drilling is done for new construction.
(d) The Jacketing process is also very complicated in execution.

IV. **General problems**

These are the problems that arise generally almost in all the projects such as labour hours including, break time, contractual disputes occurred among the contractors and consultancy about the wastage time of labours and materials, lack of planning, lack of controlled schedule, lack of work progress tracking, lack of risk management, poor communication, unrealistic expectations scope changing.

This study is to ensure that lean management techniques are the solution for all the above problems that arise in the above-said project. The following Fig. 4 indicates the difference between the planned and actual cost of an IIT auditorium project.

Fig. 4 Difference between the planned and actual cost

3 Result in Analysis

In the conventional method, the project manager tries to PUSH some unrealistic and overly complex concepts of work execution. This method is not committed to the estimated schedule. Lean scheduling is part of the lean technique approach, which aimed to shift the responsibility of planning "what is done" and "when" to the people who should execute their work and encourage flexibility. Lean scheduling is fully based on the PULL effort. In practice, lean scheduling needs four phases of scheduling which correlated they are,

(1) Master planning.
(2) Phase planning.
(3) Look ahead planning.
(4) Weekly work planning.

The forms of wastes in the construction industry are time, transport, staff down-time, rework and corrections, overproduction, inventory, to reduce these forms of wastes, lean schedule approach was adopted. Tracking the project keeps the project delivery on time but it cannot reduce the wastes generated, if we try to minimize the wastes in each form of the project, then the project will be delayed. Therefore, for performing both processes simultaneously, we are adopting a new approach of lean techniques.

3.1 Lean Project Schedule

In the above case study, some forms of wastes occur and the project is delayed, so this study is to recommend an idea about how can change the mistakes that happen

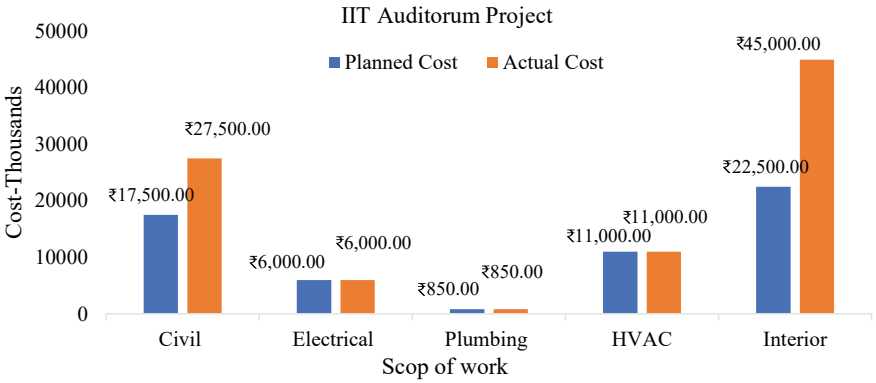

Fig. 5 Difference in time and project budget as per execution

in conventional scheduling. Figure 5 shows the difference in time and project budget as per execution.

3.1.1 Master Planning

The project team provides the Master planning, in this the project milestones, the timeline of the project is decided based on the phases of the project. This sets boundaries for all others to move within. This will be as same as the conventional method, it would not change, and it should not change. The following Table 2 is the master planning schedule of the project.

The master planning involves the scope of the project but in the previous schedule, only the execution stage is scheduled in the project. However, according to the lean schedule planning and design stage is scheduled is included. On Table 2, the first 1–12 items is included extra in the project schedule. The items involved are defined below.

3.1.2 Phase Planning

In this phase planning, each phase of the project is calculated such as men, materials, and equipment schedule. This is based on backward planning. In the planning, the constraints that arise can be analyzed priory so that we can solve the problem at the planning stage itself. The following Table 3 is the detailed phase schedule of materials. The above phase schedule input.

Will be obtained from the look ahead and weekly work schedule that is generally indicated as reverse phase scheduling. By this phase, scheduling the number of men and materials can obtain. Planning for storage of materials and equipment is analyzed.

Table 2 Master schedule of an IIT auditorium project

Project: IIT Madras Research Park—Block D—7th floor auditorium				
No.	Description of works	Starting date	Number of days	Completion date
Planning and Design Stage Schedule				
1	User requirements	01-12-18	5	05-12-18
2	Project site visit	07-12-18	2	09-12-18
3	Project kick off meeting	10-12-18	1	10-12-18
4	Finalize the stakeholder's	11-12-18	10	21-12-18
5	Problem and risk analysis	22-12-18	7	28-12-18
6	Inventory control	29-12-18	5	03-01-19
7	Design schedule	04-01-19	2	06-01-19
8	Feasibility layout	07-01-19	3	09-01-19
9	Quality analysis	09-01-19	5	14-01-19
9	Client's approval	15-01-19	3	18-01-19
10	Legal approval	19-01-19	10	29-01-19
11	Design and documentation	30-01-19	3	03-02-19
12	Site cleaning (mechanically)	04-02-19	3	05-02-19
	Duration of project	**01-12-18**	**69**	**05-02-19**
Execution Stage Schedule				
1	Existing brick wall demolishing work including cleaning	06-02-19	3	08-02-19
2	Marking steel column, Aerocon block wall at lower level	06-02-19	4	09-02-19
3	Aerocon block, M-sand lifting work	07-02-19	3	09-02-19
4	Structural material procurement unloading, lifting etc.	09-02-19	7	15-02-19
5	200 mm Aerocon block work lower level at north side, stage's east side, west and south side	08-02-19	11	18-02-19
6	Base plate anchoring and column erection work	10-02-19	4	13-02-19
7	Purlin and decking sheet fixing work	13-02-19	3	15-02-19
8	Steel reinforcement including cutting, bending, placing and binding for steps	14-02-19	4	17-02-19
9	Concreting the lower level steps	18-02-19	1	18-02-19
10	Toilet partition brick work	10-02-19	3	12-02-19
11	Tiles laying work at toilet and floor	20-02-19	6	25-02-19

(continued)

Table 2 (continued)

Project: IIT Madras Research Park—Block D—7th floor auditorium				
No.	Description of works	Starting date	Number of days	Completion date
12	Gypsum partition work at green room	26-02-19	3	28-02-19
13	Wall panelling work at north and south side	26-02-19	3	28-02-19
14	Marking of steel column at upper level	10-02-19	13	22-02-19
15	Steel column base plate anchoring and erection	23-02-19	6	28-02-19
16	Purlin and decking sheet fixing work	01-03-19	8	08-03-19
17	Bar bending and placing for upper level steps	08-03-19	3	10-03-19
18	Concreting the upper level steps and corridor etc.	11-03-19		10-03-19
19	200 mm thick Aerocon block work at upper level up to roof including lifting	12-03-19	11	22-03-19
20	Plastering work inside and outside of upper and lower level	22-03-19	10	31-03-19
21	Plumbing work (EWC, Wash basin fixing work)	26-03-19	3	28-03-19
22	Joineries fixing work	25-03-19	4	28-03-19
23	False ceiling work	26-03-19	6	31-03-19
24	Painting work inside and outside	31-03-19	6	05-04-19
25	Site cleaning work (balance material removing etc.)	06-04-19	1	06-04-19
26	Snag list attending work	07-04-19	2	08-04-19
27	Handing over	09-04-19	1	09-04-19
	Duration of project	**06-02-19**	**62**	**09-04-19**

3.1.3 Look Ahead Planning

Look ahead schedules provide prioritize work planning. Usually, 5–6 weeks look ahead schedule of the current phase. A special focus is to eliminate the constraints that are currently influencing the work. The objective of this is to maximize the flexibility for the execution of work. The following Table 4 is the look ahead scheduling abstract.

Table 3 Phase schedule abstract

Description	Day	Start date				End date			
		Plan	Actual	Delay	Reason	Plan	Actual	Delay	Reason
Marking of steel column and Aerocon block wall at lower level	4	06-02-19	06-02-19	0		09-02-19	09-02-19	0	
200 mm Aerocon block work lower level at north side, stage's east side, west and south side	11	08-02-19	09-02-19	−1	Material transportation get delayed	18-02-19	19-02-19	−1	Start date delayed
Base plate anchoring and column erection work	4	10-02-19	11-02-19	−1	Previous activity delayed	13-02-19	14-02-19	−1	Start date delayed

Table 4 Look ahead schedule abstract

Description	Start date	Day	End date	Weeks ahead	Look ahead planning date	Remarks
Marking of steel column and Aerocon block wall at a lower level	6-02-19	4	10-02-19	2 weeks	23-Jan-2019	Based on the inventory management
200 mm Aerocon block work lower level at north side, stage's east side, and west and south side	8-02-19	11	19-02-19	2 weeks	25-Jan-2019	
Base plate anchoring and column erection work	10-02-19	4	14-02-19	3 weeks	20-Jan-2019	

3.1.4 Weekly Work Planning

All activities planned by the project manager in the look ahead schedule are to be committed in a certain week. Every week the Planned Percent Complete is calculated and analyzed, after which variances are identified and resolved. The following Table 5 indicates the weekly working schedule.

The following Fig. 6 indicates the comparison of time and cost for traditional and lean planning schedule of an IIT project, and Fig. 7 indicates the savings of time and cost in percentage by lean planning schedule.

4 Conclusion

In the above case study, the project experienced 2 months delay, and an increase in costs occurs in the small scale project such as the proposed construction of a steel structure on an existing six floors building, then in case of large-scale projects, these planning, and scheduling inefficient creates a large scale of loss and wastage to the project. The above study represents that there is no problem in the traditional method of scheduling, but the work is not executed as per the schedule during execution. For these constraints, a new approach is integrated in a way of lean thinking that encourages forward-thinking planning with the following benefits.

1. An IIT auditorium project should complete in May 2019 but it got completed in September 2019 due to improper planning and coordination, and the budget

Table 5 Weekly work schedule

No.	Date	Activity	Status
1	23-01-19		
(a)		Marking of steel column and Aerocon block wall at a lower level	
		Enquire about vendor	Completed
(b)		Base plate anchoring and column erection work	
		Receive quotation from vendor	Completed
2	24-01-19		
(a)		Marking of steel column and Aerocon block wall at lower level	
		Receive quotation from vendor	Completed
(b)		Base plate anchoring and column erection work	
		Receive quotation from vendor	Completed
3	25-01-19		
(a)		Marking of steel column and Aerocon block wall at a lower level	
		Receive quotation from vendor	Completed
(b)		200 mm Aerocon block work lower level at north side, stage's east side, west and south side	
		Enquire about vendor	Completed
(c)		Base plate anchoring and column erection work	
		Negotiation meeting with a vendor	Yet to done
4	26-01-19		
(a)		Marking of steel column and Aerocon block wall at a lower level	
		Compare the amount quoted by various vendor	Completed
(b)		200 mm Aerocon block work lower level at north side, stage's east side, west and south side	
		Receive quotation from vendor	Completed
(c)		Base plate anchoring and column erection work	
		A section is sent for cutting	Yet to done
5	27-01-19		
(a)		Marking of steel column and Aerocon block wall at a lower level	
		Receive quotation from vendor	Completed
(b)		200 mm Aerocon block work lower level at north side, stage's east side, west and south side	
		Enquire about vendor	Completed
(c)		Base plate anchoring and column erection work	

(continued)

Table 5 (continued)

No.	Date	Activity	Status
		Negotiation meeting with a vendor	Yet to done
6	28-01-19		
(a)		Marking of steel column and Aerocon block wall at lower level	
		Receive quotation from vendor	Completed
(b)		200 mm Aerocon block work lower level at north side, stage's east side, west and south side	
		Enquire about vendor	Completed
(c)		Base plate anchoring and column erection work	
		Negotiation meeting with a vendor	Yet to done
7	29-01-19		
(a)		Marking of steel column and Aerocon block wall at a lower level	
		Receive quotation from vendor	Completed
(b)		200 mm Aerocon block work lower level at north side, stage's east side, west and south side	
		Enquire about vendor	Completed
(c)		Base plate anchoring and column erection work	
		Negotiation meeting with vendor	Yet to done

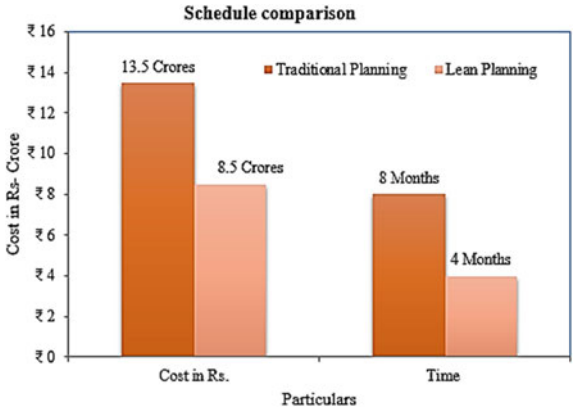

Fig. 6 Comparison of time and cost for traditional and lean planning schedule

increased by Rs. 3.25 Crores results in a total project cost of Rs. 13.5 Crores instead of actual budget Rs. 8.50 Crores.

2. The wastes that occur in the planning and design stage by the traditional method are affected by 50% of the total project time because the planning is done only during execution.

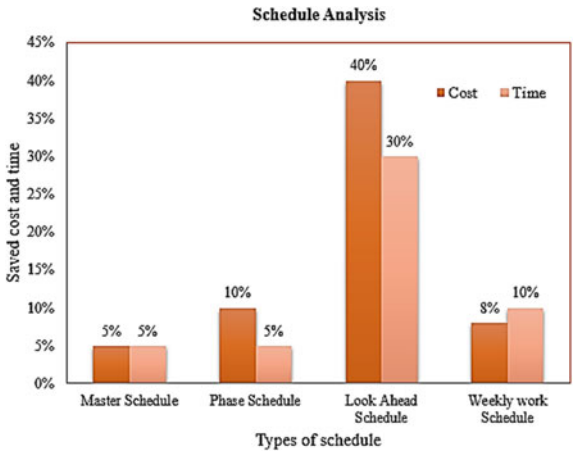

Fig. 7 Savings of time and cost by lean planning schedule

3. Look ahead planning schedule is prepared for prior planning of the work to be done, so it can sort out the problems earlier or it can track the project schedule for any activity completed earlier and balancing the risk activity.
4. The traditional schedule of the above said project was delayed by a 63% increase in the project budget and a 50% increase in the project duration.
5. By the four stages of schedule, such as Master schedule saves 5% of the time and 5% of the budget, phase schedule saves 10% of the time and 5% of the budget, look ahead schedule saves 40% of the time and 30% of the budget, weekly work planning schedule saves 8% of the time and 30% of the budget. Also, help to complete the project in 4 months as estimated and within the Rs. 8.50 Crores.

5 Recommendations and Suggestions

By this research and templates of schedule used in the above study that can proceed with the new construction to complete the project on time and budget, were sometimes on ahead of the schedule that improves the customer's satisfaction and relationship. Therefore, the study suggests implementing the lean management techniques from the initial stage that represents the client requirements to the final stage indicates the handover.

References

1. Mali ML, Warudkar MAA (2016) Causes of delay in the construction industry in Pune region of India. Int J Appl or Innov Eng Manag 5(5):177–187. https://doi.org/10.1016/0145-2134(92)90045-S
2. Gebrehiwet T, Luo H (2017) Analysis of delay impact on construction project based on RII and correlation coefficient: empirical study. Procedia Eng 196:366–374. https://doi.org/10.1016/j.proeng.2017.07.212
3. AlNasseri H, Aulin R (2015) Assessing understanding of planning and scheduling theory and practice on construction projects. EMJ Eng Manag J 27(2):58–72. https://doi.org/10.1080/10429247.2015.1035963
4. Alajeeli HKB, Alkaabi SAM (2016) A study of waste management reality in construction projects in Iraq. Wasit J Eng Sci 4(1):75-92. https://www.iasj.net/iasj?func=fulltext&aId=116401.
5. Sharanyasreenivas J, Gajalakshmi G, Theja R (2017) Project planning, scheduling and preparation of quality assurance control documents. Int Res J Eng Technol, 1862–1869
6. Singh S (2018) Comparative study of planning and scheduling of a construction project using microsoft project. Int J Res Eng Technol 07(06):32–40. https://doi.org/10.15623/ijret.2018.0706006
7. Samari M, Godrati N, Esmaeilifar R, Olfat P, Shafiei MWM (2013) The investigation of the barriers in developing green building in Malaysia. Mod Appl Sci 7(2):1–10. https://doi.org/10.5539/mas.v7n2p1
8. Kauskale L, Geipele I, Zeltins N, Vanags J (2018) Sustainable construction industry development and green buildings: a case of Latvia. Latv J Phys Tech Sci 55(1):44–52. https://doi.org/10.2478/lpts-2018-0005
9. Ballard G, Howell GA (2003) Competing construction management paradigms. In: Construction research congress: wind of change: integration and innovation, vol 1, pp 321–328
10. Salem OM et al (2015) Lean construction: from theory to implementation lean construction: from theory to implementation 4:61–67. https://doi.org/10.1061/(ASCE)0742-597X(2006)22
11. Puvanasvaran P, Megat H, Sai Hong T, Mohd Razali M, Abdel Magid SH (2010) Lean process management implementation through enhanced problem solving capabilities. J Ind Eng Manag 3(3):447–493. https://doi.org/10.3926/jiem.2010.v3n3.p447-493
12. Wojtys EM, Schley L, Overgaard KA, Agbabian J (2009) Applying lean techniques to improve the patient scheduling process. J Healthc Qual 31(3):10–16. https://doi.org/10.1111/j.1945-1474.2009.00025.x
13. Pearce A, Pons D (2013) Implementing lean practices: managing the transformation risks. J Ind Eng
14. Binninger M, Dlouhy J, Haghsheno S (2017) Technical takt planning and takt control. In: Proceedings of the 25th anniversary conference of the international group for lean construction, vol II, pp 605–612
15. Dinesh S, Sethuraman R, Shivaprakasam S (2017) The review on lean construction an effective approach in construction. Int J Eng Res Mod Educ, 119–123. https://doi.org/10.5281/zenodo.570523
16. Ansah RH, Sorooshian S, Bin Mustafa S (2016) Lean construction: an effective approach for project management. ARPN J Eng Appl Sci 11(3):1607–1612
17. Dinesh RS, Sivaprakasam S (2017) The review on lean construction an effective approach in construction industry. Special issue, April 2017

Analysis and Design of Shear Capacity of Sisal Fibre-Reinforced Concrete Member in Rectangular Cross-Section

T. L. Abinaya, M. Balasubramanian, and G. Surendar

1 Introduction

Natural fibre materials have sparked a lot of attention in recent decades from fundamental research to industrial applications. Concrete is characterised by compression strength and tension weakness [1]. The use of lightweight aggregate concrete frequently saves 10–20% of the overall cost of comparable standard. The lighter weight concrete allows for smaller structural element sections, while the lower density allows for smaller structural element sections. The most pressing concern in today's society is environmental deterioration. Many scientists focused their efforts on developing environmentally friendly materials and products based on ecologically sustainable concepts [2]. As a result, natural fibres have replaced mainly synthetic fibres due to their lower cost, ease of availability, minor waste collection challenges, equivalent strength, non-toxicity, and environmentally favourable surroundings.

Sisal fibre is a substantial natural fibre derived from a Sisal tree and is widely accessible in Andhra Pradesh. Bio fibres appear to be recyclable materials that might be pushed in the building industry [3]. There is a global trend towards using both treated and untreated industrial by-products, household wastes, and other wastes as cement and concrete raw materials. Sisal fibre helps not only with garbage repurposing but also with the production of a cleaner, greener environment [4]. The fibre utilised for reinforcement is called sisal fibre, and it is considered an alternate material in mount. This sisal fibre is thought to be the most cost-effective in terms of production while also providing social and economic benefits [5]. If sisal fibre is utilised for structural purposes, it will be helpful not only to the environment but also to low-income families, particularly in the vicinity of sisal farms. SF beams flexure

T. L. Abinaya
School of Architecture and Interior Design, SRM Institute of Science and technology, Kattankulathur, Chennai, India

M. Balasubramanian (✉) · G. Surendar
Department of Civil Engineering, SRM Institute of Science and technology, Chennai, India

K. S. Satyanarayanan et al. (eds.), *Sustainable Construction Materials*, Lecture Notes in Civil Engineering 194, https://doi.org/10.1007/978-981-16-6403-8_13

and shear behaviour are crucial parameters for structural applications and must be thoroughly studied and established [6]. As a necessary consequence, the results of an experimental investigation of the shear behaviour of reinforced SF beams are presented in this paper [7].

2 Sisal

The Agave fibre is monocotyledonous, with roots that emerge from the base of the pseudostem. Sisal plants have sharp-edged leaves that grow to be 1.5–2 metres tall. Budding immature leaves feature small teeth along the margins of the leaves, as do adult leaves. Sisal plants have a life span of 7–10 years and yield 200–250 good leaves. Each bud comprises thousands of fibres [8]. The fibres account for 4% of the plant's bulk. Agave sisalana Perrine (Agavaceae), sometimes known as the sisal plant, is a monocotyledonous plant native to Mexico. Sisal fibre is the first natural fibre employed in corporate applications, accounting for more than half of all fibres used, which grows under 25 °C, and sunshine, which is considered to be a plant of the tropics and subtropics [9].

2.1 Process of Sisal Fibre Extraction

A retting process and a mechanical process are the two types of extraction processes for natural fibre. Decortication is the process of removing fibre from the plant. After crushing new leaves, the leaves are pounded in a revolving wheel with the point of confinement edges, and only the fibres remain at the end of the operation. The natural sisal fibre and property of sisal fibre are shown in Fig. 1 and Table 1. The leftover fibres are rinsed in water to remove any lingering leaves. The fibres were then dried, brushed, and bagged for use in concrete [10]. The yield of fibre in the retting process

Fig. 1 Natural sisal fibre

Table 1 Property of sisal fibre

Diameter	Density	Tensile strength	Elastic modulus	Elongation break
50–200 mm (micro-m)	1450 kg/m^3	68 MPa	3.77 GPa	5–14%

is around 5.5%, whereas the product in the mechanical function is approximately 3–4% based on the weight of green leaves. Hand extraction equipment, such as serrated or non-serrated blades, is used to extract the fibre.

2.2 Materials

The materials, which used for experimental verification of this study, are ordinary portland cement (OPC)—53 grade, natural fine aggregate—sand (IS 383:1970), natural coarse aggregate—crushed 12 mm and 20 mm maximum size (IS 383:1970), natural fibre—sisal fibre, steel—Fe500, Ye—500 N/mm^2, and ultimate tensile strength—545–600 N/mm^2.

3 Test Program

3.1 Details of Beam

A cube specimen and beams were built and tested as part of this experimental effort. The beams were made of sisal fibre. This beam is developed using the Park and Pauly technique, which includes inclined stirrups that resist the principal tensile force acting in an inclined direction, causing stress reversal through reinforcement. Beams were examined for standard shear reinforcements (NS) and Park and Pauly method shear reinforcements in each case (PS). In each pair, two parts of 10 mm (NS1 and PS1) and two parts of 12 mm (NS2 and PS2) diameters were used as reinforcements. Three sets of cubes and cylinders were tested on the same day as the beams to determine the concrete's properties. According to several publications, the size of the beam for shear testing must be 2600 m; if it exceeds the restrictions, the result will be inaccurate. For the reasons stated above, the following beam size is intended for the experimental specimen [11]. The beams' breadth (b), depth (d), and length (l) remained constant at 150 × 100 × 2600 mm, respectively. The size and length of the beam were designed to assure shear failure. PS beam reinforcement was developed in accordance with IS 456:2000, with minimum shear reinforcement standards also taken into account, guaranteeing that at least one web reinforcement intercepted a diagonal fracture. As a consequence, mild steel two-legged shear reinforcements with a diameter of 6 mm were put across the beams at 150 mm centre to centre [12]. Four-point load testing with a constant effective span was performed on the beam

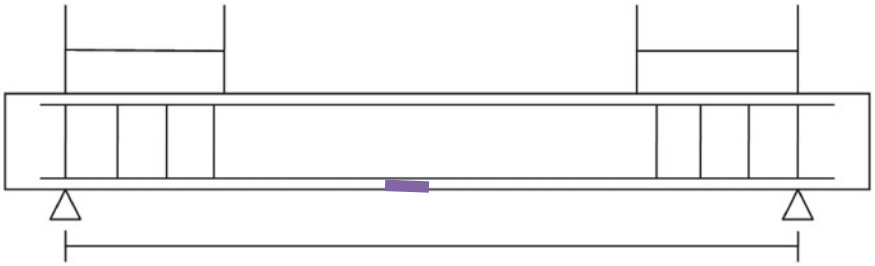

Fig. 2 Normal shear reinforcement

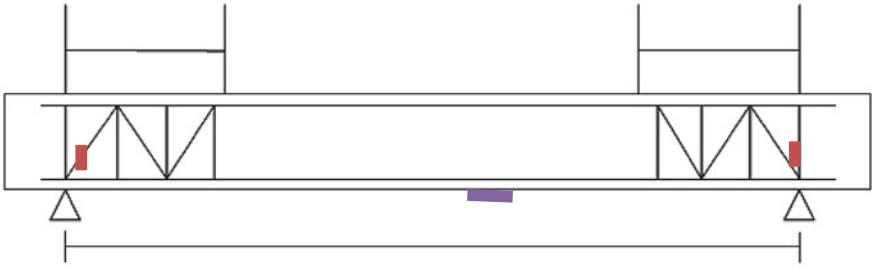

Fig. 3 Park and Pauly method shear reinforcement

Fig. 4 Cross-sectional rod details

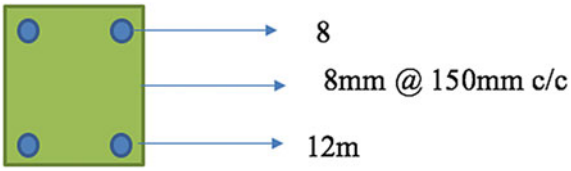

specimens. Figures 2, 3, 4, and 5 illustrate a beam and its reinforcing configurations in longitudinal and cross-sectional views using the Park and Pauly technique.

3.2 Beam Preparation and Instrumentation

For the beam size, formwork made of plywood was created. A 20-mm section of tension bar at the mid-span was ground smooth to permit the attachment of strain gauges. To remove rust, dust, and grease, the surfaces were smoothed with sandpaper and cleaned with acetone. The strain gauge was verified for 120 ± 1 X after it was

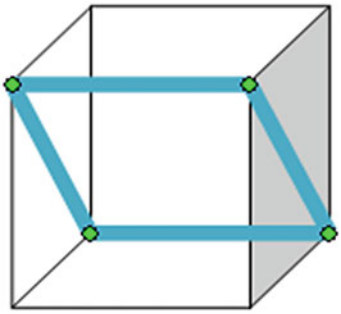

Fig. 5 Cross-sectional view of park pauly method shear reinforcement

attached with steel reinforcement. The beams were immediately covered with a plastic sheet following the beam casting to reduce water evaporation from the beam specimen's surface. The formwork sides were removed after 24 h and treated with a damp gunny bag on a regular basis for 28 days, following which the beams were set alone until testing.

Beams were painted and the area on the beam's surface where strain gauges were mounted was treated, prior to testing. The strain gauges on the outside, the effective spans, the neutral axes, and the centre lines were all measured and recorded. To smooth out the treated surface, fine sandpaper was scraped over it. The strain gauge lead wires were linked to a 10-channel strain bridge, which was then partially to the data logger. A linear variable displacement transducer (LVDT) was inserted in the beam's centre, and one dial gauge was set at the (1/4)th distance on either side of the span to measure deflection. The strain gauge diagram of the test is shown in Fig. 6. The load was applied in 1 kN increments at first, increasing to 6 kN in the end. Manual tension and deflection measurements were also taken. During testing, the beams were preloaded with a force of around 0.5 kN to activate the LVDT and strain gauges.

Fig. 6 Strain gauge

4 Results and Discussion

4.1 Structural Behaviour

All of the beams had typical structural shear behaviour. Since there were no horizontal fractures at the reinforcement level, there were no instances of bond separating the concrete from the reinforcement Table 2 shows the experimental data for the first shear fracture, ultimate shear loads, and shear force at yield, whereas Table 3 shows as a result of displacement ductility (Fig. 7).

For simplicity, the structural shear behaviour of all of the beams was conventional. There were no instances of bond separating the concrete from the reinforcement since there were no horizontal fractures at the reinforcement level.

The ductility ratio, defined as the displacement ratio at the yield to displacement at ultimate values, was 2.50–3.70 for SFRC beams and 1.80–2.67 for CC beams.

Table 2 Shear fracture, shear force, and ultimate beam shear

Type of beam	Shear fracture (kN)		Shear force (kN)		Ultimate shear (kN)	
	CC	SFRC	CC	SFRC	CC	SFRC
Normal shear reinforcement NS1	12.23	15.67	18.45	22.98	23.78	25.45
Normal shear reinforcement NS2	13.65	16.87	19.87	24.78	28.89	30.67
Park and Pauly method shear reinforcement PS1	15.44	17.82	40.42	41.67	51.34	55.78
Park and Pauly method shear reinforcement PS2	16.67	18.98	39.33	45.89	50.11	58.22

NS, Normal shear reinforcement; PS, Park and Pauly reinforcement; SFRC, Sisal fibre reinforcement; CC, Control concrete

Table 3 Displacement ductility experiment data

Beam design	Upper yield displacement (mm)		Ultimate displacement (mm)		Ductility ratio	
	CC	SFRC	CC	SFRC	CC	SFRC
Normal shear reinforcement NS1	15	16	30	65	2.67	3.50
Normal shear reinforcement NS2	22	24	31	70	2.11	3.90
Park and Pauly method shear reinforcement PS1	13	14	20	50	2.89	2.68
Park and Pauly method shear reinforcement PS2	15	20	23	61	1.87	2.98

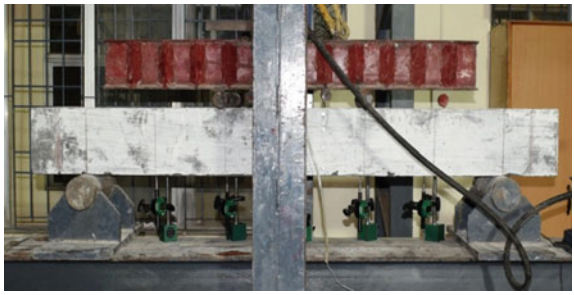

Fig. 7 Shear test setup

This suggests that ductile failure modes were present in all SFRC beams. In the flexure mode, all of the beams with shear reinforcement were failed. Following the emergence of diagonal stress fractures, all beams lacking shear reinforcing broke in shear failure modes.

4.2 Behaviour of Cracking

The decreased flexural strength of SFRC beams may explain the early flexural fractures. They were all found at the flexural zone, there is initial flexural cracking. The flexural and shear cracks in the SFRC beams with normal shear reinforcement and Park and Pauly method reinforcement were larger and closer together than in the similar CC beams. These findings imply that the connection between the tension reinforcement and the SRRC is as strong as that between the tension reinforcement and the CC. Additionally, the higher frequency of fractures in SFRC beams resulted in smaller crack widths when compared to CC beams with larger crack widths. Without shear reinforcement at the support, diagonal tension fractures appeared in all SFRC and CC beams, and these cracks advanced towards load regions. Cracks in SFRC beams propagated more zigzag than smooth fractures in CC beams [13]. A strong aggregate interlock in SFRC is the most plausible explanation for this phenomenon.

4.3 Behaviour of Deflection

Figures 8 and 9 demonstrate the experimental mid-span deflections for beams reinforced with the Park and Pauly PS1 and PS2 shear reinforcing systems. Figures 10 and 11 depict the experimental mid-span deflections of beams reinforced with average shear (NS1 and NS2). The early linear part of all curves demonstrates that beam stiffness remains constant prior to flexural cracking. The performance of the SFRC beams was comparable to that of the CC beams at this level. When flexural fractures appeared, the stiffness of both the SFRC and CC beams was dramatically reduced. The deflections of the SFRC beams with average shear and Park and Pauly method

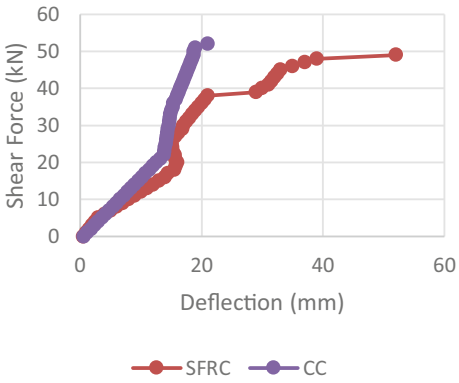

Fig. 8 Force versus deflection of beams PS1

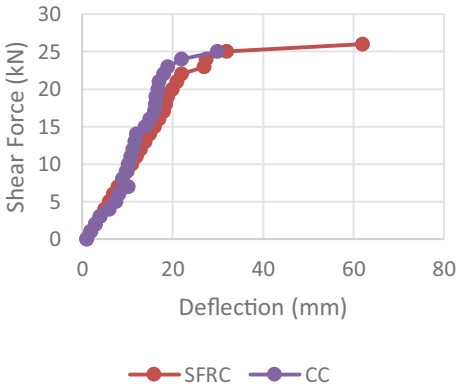

Fig. 9 Force versus deflection of beams PS2

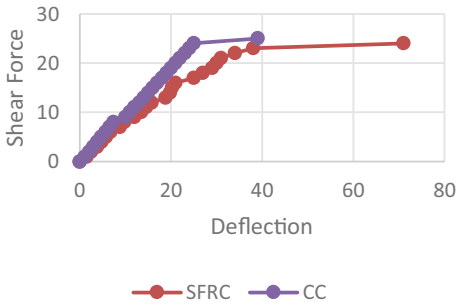

Fig. 10 Force versus beam deflection PS1

Shear reinforcement was greater than in CC beams. This might be because, despite deflections under service loads, SFRC has a lower elasticity modulus than CC [14]. Both types of concrete met acceptable standards. The ultimate deflection of SFRC shear reinforcement beams was greater than that of CC shear reinforcement beams.

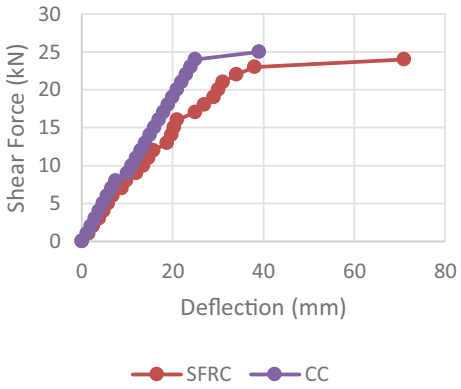

Fig. 11 Force versus beam deflection PS2

Table 4 Experimental result of beam

Beam type	Shear force (kN)	
	CC	SFRC
PS1	27.88	25.78
PS2	50.34	48.67
NS1	21.56	20.87
NS2	24.89	22.54

4.4 Comparison of Experimental

The beams' shear resistance was obtained and in comparison to the experimental results provided in Table 4. At the reinforcing level, no horizontal cracks have been seen, indicating that no bond failures occurred [15]. SFRC beams had around double the number of shears and flexural fractures as CC beams. Fracture spacing was determined to be closer in SFRC beams than in CC beams. The shear strength of the SFRC normal shear reinforcement beam was the same as that of the corresponding CC beams. Beams showed significant bending, providing enough notice of the impending failure.

5 Conclusion

Shear-reinforced beams frequently failed in flexure mode, but ordinary shear-reinforced beams failed in diagonal shear modes. The ductility ratios of SFRC beams with normal shear reinforcements and Park and Pauly technique shear reinforcements are more than the values for CC beams. There were no horizontal fractures seen at the reinforcing level, indicating no instances of bond failure. SFRC beams had approximately doubled as many shears and flexural fractures as CC beams. Fracture spacing

in SFRC beams was found to be closer than in CC beams. Shorter, narrower deformation with rough surfaces in SFRC normal shear reinforcement beams revealed excellent aggregate interlock, boosting the SFRC beams' shear strength. The SFRC shear reinforcement beam's shear strength was equivalent to that of comparable CC beams. Beams displayed substantial bending, indicating that it was on the verge of collapsing. Under shear loadings, the concrete compression strain and steel tension strain findings show that SFRC can attain its maximum strain capacity. In SFRC beams, slightly higher steel and concrete stresses suggested a strong SFRC steel connection.

References

1. Kadarningsih R, Satyarno I, Muslikh, Triwiyono A (2017) analysis and design of reinforced concrete beam-column joint using king cross steel profile. Procedia Eng 171:948–56
2. Wu Y, Li Y, Niu B (2014) Assessment of the mechanical properties of sisal fiber-reinforced silty clay using triaxial shear tests. Sci World J
3. Sarkar P, Agrawal R, Menon D (2007) Design of RC beam-column joints under seismic loading—a review. J Struct Eng 33:449–57
4. Almusallam TH , Al-Salloum YA (2007) Seismic response of interior RC beam-column joints upgraded with FRP sheets. II: analysis and parametric study J Compos Constr 11:590–600
5. Kumar N, Grewal J S, Kumar S, Kumar N, Kashyap K (2021) Mechanical and thermal properties of NaOH treated sisal natural fiber reinforced polymer composites: Barium sulphate used as filler Mater. Today Proc 45:5575–8
6. Ren G, Yao B, Huang H, Gao X (2021) Influence of sisal fibers on the mechanical performance of ultra-high performance concretes. Constr Build Mater 286:122958
7. Codispoti R, Oliveira DV, Olivito RS, Lourenço PB, Fangueiro R (2015) Mechanical performance of natural fiber-reinforced composites for the strengthening of masonry Compos. Part B Eng 77:74–83
8. Batista dos Santos GZ, Passos de Oliveira D, de Almeida Melo Filho J, Marques da Silva N (2021) Sustainable geopolymer composite reinforced with sisal fiber: durability to wetting and drying cycles. J Build Eng 43
9. Sen T, Reddy HNJ (2011) A numerical study of strengthening of RCC beam using natural bamboo fibre. Int J Comput Theory Eng 3:707–13
10. Gunasekaran K, Annadurai R, Kumar PS (2013) Study on reinforced lightweight coconut shell concrete beam behavior under shear Mater. Des 50:293–301
11. Sahoo G, Kamalakannan R, Pradeep GM, Manivelmuralidaran V, Girimurugan R (2021) A process of analyzing the performance evaluation of sisal fiber in fiber reinforced composites Mater. Today Proc
12. Solai Mathi S, Karthikeyan S, Johnpaul V, Riyas PR, Chidambaram N, Vegumathi M (2021) Experimental investigation on self compacting concrete with sisal fibre Mater. Today Proc
13. Yu W, Yi Y, Wang H, Yang Y, Zeng L, Tan Z (2021) Light-colored cellulose nanofibrils produced from raw sisal fibers without costly bleaching Ind. Crops Prod 172:114009
14. Singh G, Singh S, Kumar R, Chohan JS (2021) Exploration of sisal fibre for modification of bituminous mix Mater. Today Proc
15. Thomas BC, Jose YS (2021) A study on characteristics of sisal fiber and its performance in fiber reinforced concrete Mater. Today Proc

Experimental Investigation of Cement Mortar to Improve the Strength by Adding Sisal Fiber

M. Balasubramanian, S. SenthilSelvan, S. Aishwarya, and M. Ram Kumar

1 Introduction

Mortar is one of the mandatory components in construction industry, which is used as the binding agent in masonry works. Mortar is a combination of fine aggregate, cement and water. In general, the fine aggregate and water are the most available materials in India at very low cost among all components. Since cement is relatively expensive, it would also be appropriate to partially replace the cement with other locally available industrial and agricultural waste materials. Ground Granulated Blast-furnace Slag (GGBFS), Iron Industry's non-hazardous and non-metallic waste materials can be used in the mortar I order to achieve the mortar properties such as: (1) Increase in compressive strength (2) Reduction in drying shrinkage & hydration heat (3) Delayed cement setting time, etc. With the new increased interest in low-cost biodegradable material manufactured with improved properties, natural fiber has acquired more prominence [1].

Nowadays, a lot of research works are being centralized towards the capability of sisal fiber, the reason is sisal fiber is a natural fiber that can be incorporated to achieve sustainability and better quality mortar, the sisal fiber is chosen to improve the mortars' strength properties [2]. Sisal fiber is obtained from cactus, which is a member of the cetacean plant family [3]. It is a biodegradable fiber, which is produced with gelatin-modified soy protein resin. It is locally available, renewable

M. Balasubramanian (✉) · S. SenthilSelvan · S. Aishwarya · M. R. Kumar
Department of Civil Engineering, SRM Institute of Science and Technology, Tamil Nadu, Kattankulathur 603 203, India
e-mail: balasubm1@srmist.edu.in

S. SenthilSelvan
e-mail: senthils10@srmist.edu.in

S. Aishwarya
e-mail: as4136@srmist.edu.in

K. S. Satyanarayanan et al. (eds.), *Sustainable Construction Materials*, Lecture Notes in Civil Engineering 194, https://doi.org/10.1007/978-981-16-6403-8_14

and biodegradable material at low cost [4]. The methods for extraction of sisal fiber are (1) retting followed by scraping and (2) mechanical means using decorticators [3]. After the extraction fiber is washed and dried in plate, to these plates, 10% NaOH arrangement was added, and the sisal is absorbed the answer for 10 h. At that point, the sisal is again washed altogether with water to eliminate the overabundance of NaOH adhering to the strands [5].

Moreover, sisal fiber is one of the most grounded, stable and adaptable materials and it has been perceived as a significant source of fiber for composites [6]. The manufacturing of a sisal plant will be around 200–250 leaves and each leaf contains 1000–1200 fiber groups, which is made out of 4% fiber, 0.75% fingernail skin, 8% dry matter and 87.25% water [3]. The expansion of sisal strands in the solid expanded the tractable and flexural modulus of the solid arranged with 10 wt.% of acetylated sisal fiber [7]. In addition to the above advantages of sisal fibers, it has the ability to bridge the cracks and restrict them [8]. In spite of the advantages, some of the negative aspects of natural fibers (Sisal fibers) are that they can undergo degradation at elevated temperatures comparing to the polymer [9] and will decompose in alkaline environments or in biological attack [10].

In order to overcome the above disputes, the GGBFS is added with the sisal fiber. Ground Granulated Blast Furnace Slag (GGBFS) is widely used in mortar with combination of Portland cement. It has several advantages, including enhancing strength, durability, economic and environmental aspects. The combination of sisal fiber with the addition of GGBS in mortar reduces cost of cement and achieves strength [11]. This paper deals with adding sisal fiber and ggbs in mortar with the into bond super plasticizer.

Micro-structural analysis will analyze weather the sisal fibers were able to achieve higher mechanical performance and higher energy absorption [12]. The basic micro-structural study is SEM, EDS and XRD. In this study, crushed powder of mortar mixes was used to study their micro-structural properties. Scanning Electron Microscopy (SEM) was conducted using powder crushed after 28 days of curing. EDS (Energy Dispersive Spectroscopy) was conducted for the raw materials of Cement & GGBS and also for the mortar-powered specimen after 28 days of curing to study the micro-structural characterization.

2 Methodology

The initial step is to study and gather the information from all the past works of literature based on sisal fibers, GGBS and super plasticizer used in mortar. All the basic properties should be tested properly and the water–cement ratio should be determined using flow table test. High-quality materials should be procured and should be mixed properly according to the mix design. Sisal fiber is added to an Ordinary Portland Cement with a percentage of 0.25, 0.5, 0.75, 1 and 30% of GGBS. For all these mixes, the super plasticizer adds 2%. All the specimens like cubes, cylinders and beams should be cured and tested for the compression on 7th, 14th and

Table 1 Physical properties of cement

S. no	Specifications	Results
1	Type	Open
2	Specific gravity	3.10
3	Initial setting time	28 min
4	Final setting time	596 min
5	Fineness	2%

28th days. From the results, the optimum value will obtain and the masonry prism should be made for that optimum value and the shear mortar should be found. That optimum mix design is also used for micro-structural study (SEM & EDS).

3 Experimental Study

3.1 Cement

The cement taken for the experiments is M53 grade (Ordinary Portland Cement). The physical properties of the cement such as specific gravity, initial and final setting time and fineness are shown in Table 1. As per the IS code 8112–1989, the experiments were conducted.

3.2 Fine Aggregates

The locally available sieved river sand is used as fine aggregates for the experiments. Table 2 describes the physical parameters of fine aggregates such as specific gravity, water absorption and fineness. As per the IS code 383–1970, the experiments were conducted.

Table 2 Properties of fine aggregate

S. no	Specifications	Results
1	Type	River sand
2	Specific gravity	2.58
3	Grading	Zone III
4	Fineness module	2.65%
5	Water absorption	1.25%

Table 3 Identification of sisal fiber

Properties	Sisal fiber
Cellulose (%)	65
Hemicelluloses (%)	12
Lignin (%)	9.9
Moisture content (%)	10
Others (%)	3.10
Density (Kg *I* m3)	1450
Flexural modulus (GPa)	12.50–17.50
Lumen size (mm)	11
Tensile strength (MPa)	68
Young's modulus *(GP* a)	3.77

3.3 Sisal Fiber

The physical parameters of sisal strands are generally described by the chemical and physical parameters such as the structure of fibers, cellulose content and angle of fibrils, cross-section and by the degree of polymerization [13]. The chemical properties of sisal fiber are discussed in Table 3. The sisal fiber physical properties such as tensile strength configuration are 348 to 375 N I mm^2, l.35 specific gravity and 1.25 g I cm^3 density [14, 15].

3.4 GGBS

The physical properties of the GGBS are also investigated; Table 4 shows the results of bulk density, specific gravity, fineness and moisture content of the ground-granulated ballast furnace slag.

Table 4 Physical properties of GGBS

Color	Off-white
Specific gravity	2.95
Bulk density	1090 kg/m^3 (loose) 1272 kg/m^3 (vibrated)
Fineness	340 m^2/kg
Moisture content	0.1%

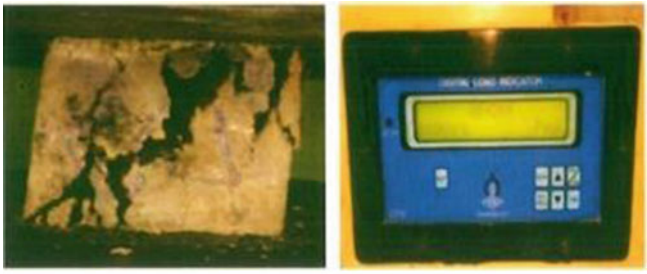

(a) (b)

Fig. 1 **a** Testing of cubes, **b** Testing in digital values

3.5 Nitro Bond

Nitro bond is a super plasticizer of high-range weather resistance used in mortar to enhance durability. It provides screeds, plasters and slurries that are waterproof. This super plasticizer provides enhanced tensile strength and flexural strength. This is compatible with and cost-effective with all common hydraulic cements.

4 Experimental Investigation and Results

4.1 Compression Strength Test

The casting and testing of 50 mm × 50 mm × 50 mm cubes are done using compressive testing machine to determine compressive mortar strength in accordance with IS456. On the 7th, 14th, 28th day, nine cubes of each mix proportion were casted, and the compressive strength was found by taking three cubes on average as shown in Fig. 1 and Table 5.

Figure 2 reveals the compressive strength test results of the mortar added with GGBFS and sisal fiber at different percentages and tested after 7 days, 14 days and 28 days of proper curing. The highest value is obtained for the mix proportion of mortar added with 30% of GGBFS, 0.75% of Sisal Fiber and 2% Super Plasticizer.

4.2 Split Tensile Strength Test

The rigidity of mortar is one of the essential and significant properties that incredibly influence the degree and size of splitting in structures. The cylinder size of 75 mn × 50 mm × 50 mm was casted (Fig. 3; Table 6).

Table 5 Compression strength test values of different percentages

Mix proportions	7th day	14th day	28th day	Mix proportions	7th day	14th day	28th day
OPC + 2%SP	10.20	12.53	12.93	OPC + 30%GGBS + 2% SP	12.86	13.37	17.54
OPC + 0 0.25SF + 2%SP	11.20	12.66	15.33	OPC + 30%GGBS + 0.25% SF + 2% SP	14.80	17.04	19.60
OPC + 0.5% SF + 2%SP	15.06	17.60	18.60	OPC + 30%GGBS + 0.5% SF + 2%SP	17.06	20.06	28.26
OPC + 0.75SF + 2%SP	15.30	18.30	18.69	OPC + 30%GGBS + 0.75% SF + 2%SP	19.46	21.5	31.33
OPC + 1% SF + 2%SP	14.53	14.80	15.60	OPC + 30%GGBS + 1 % SF + 2%SP	15.20	19.20	23.47

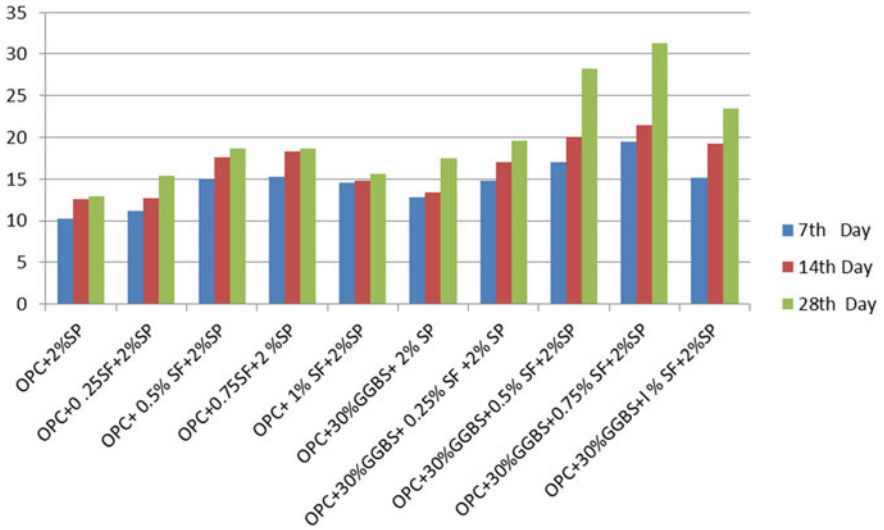

Fig. 2 Compression strength test values of mortar added with sisal fiber and GGBFS (Different percentages)

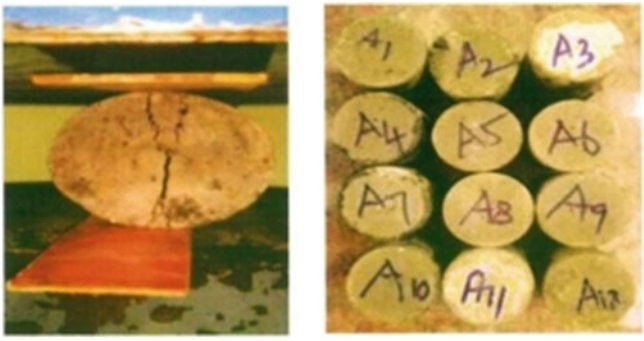

(a) (b)

Fig. 3 **a** Casting of cylinders, **b** Testing of cylinders

Table 6 Flexural strength test values of different percentages

Mix proportions	7th day	14th day	28th day	Mix proportions	7th day	14th day	28th day
OPC + 2%SP	1.125	1.592	1.615	OPC + 30%GGBS + 2%SP	1.65	2.04	2.269
OPC + 0.25SF + 2%SP	1.242	1.648	1.745	OPC + 30%GGBS + 0.25% SF + 2%SP	2.07	2.125	2.294
OPC + 0.5 SF + 2%SP	1.357	1.823	1.854	OPC + 30%GGBS + 0.5% SF + 2%SP	2.346	2.396	2.548
OPC + 0.75SF + 2%SP	**1.612**	**2.117**	**2.585**	**OPC + 30%GGBS + O. 75% SF + 2%SP**	**2.588**	**2.622**	**2.723**
OPC + 1 SF + 2%SP	1.272	1.686	1.755	OPC + 30%GGBS + 1% SF + 2%SP	2.137	2.291	2.321

Figure 4 reveals the split tensile strength test results of the mortar added with GGBFS and sisal fiber at different percentages and tested after 7 days, 14 days and 28 days of proper curing. The highest value is obtained for the mix proportion of mortar added with 30% of GGBFS, 0.75% of Sisal Fiber and 2% Super Plasticizer.

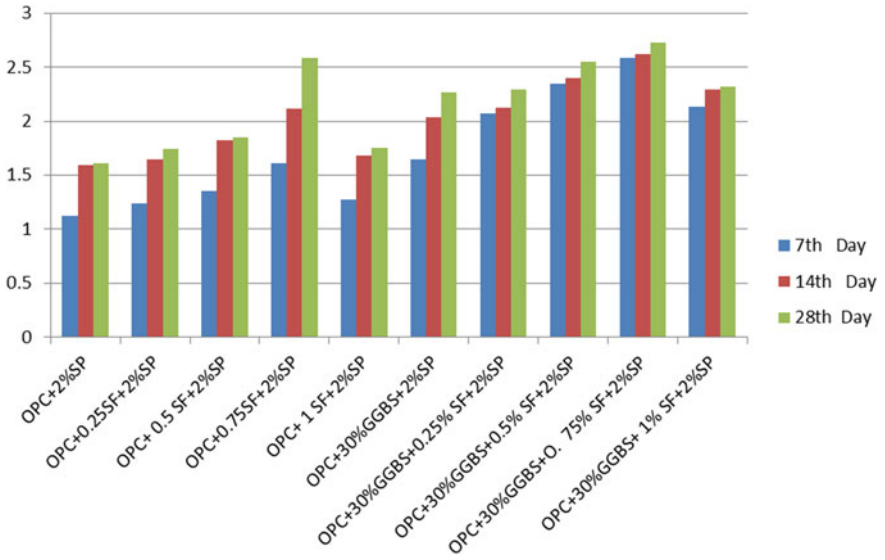

Fig. 4 **a** Casting of beams, **b** Testing of beams

4.3 Flexural Strength Test

The size of the beam should be 160 mm x 40 mm × 40 mm. For the casting of beam, the wooden molds were used (Fig. 5). Components such as mixtures of cement, sand, water super plasticizer and GGBS should be prepared (Table 7).

Figure 6 reveals the flexural strength test results of the mortar added with GGBFS and sisal fiber at different percentages and tested after 7 days, 14 days and 28 days of proper curing. The highest value is obtained for the mix proportion of mortar added with 30% of GGBFS, 0.75% of Sisal Fiber and 2% Super Plasticizer.

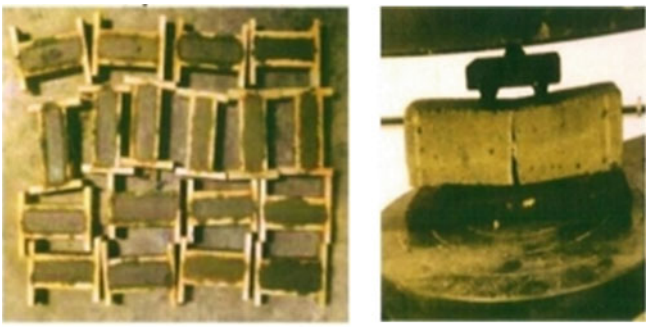

Fig. 5 **a** Casting of beams, **b** Testing of beams

Table 7 Flexural strength test values of different percentages

Mix proportions	7th day	14th day	28th day	Mix proportions	7th day	14th day	28th day
OPC + 2%SP	4.5	7.12	9.31	OPC + 30%GGBS + 2%SP	5.6	6.94	9.82
OPC + 0 0.25SF + 2%SP	5.6	7.81	9.79	OPC + 30%GGBS + 0.25% SF + 2%SP	5.95	7.98	9.85
OPC + 0.5 SF + 2%SP	7.69	8.12	10.56	OPC + 30%GGBS + 0.5% SF + 2%SP	7.56	8.34	10.61
OPC + 0.75SF + 2%SP	**8.21**	**9.56**	**11.53**	**OPC + 30%GGBS + O.75% SF + 2%SP**	**8.59**	**9.67**	**11.56**
OPC + 1 SF + 2%SP	7.89	8.78	10.67	OPC + 30%GGBS + **1**% SF + 2%SP	8.1	8.76	10.89

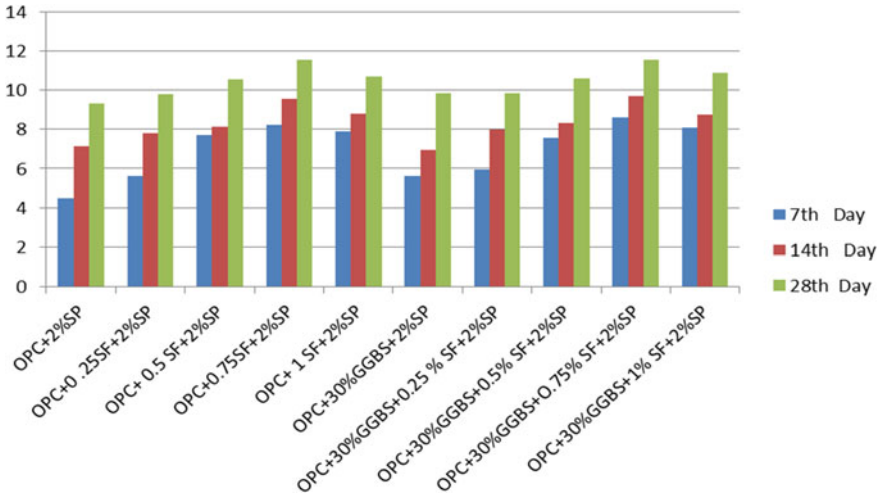

Fig. 6 Flexural Strength Test Values of Mortar added with Sisal Fiber and GGBFS (Different Percentages)

(a) (b)

Fig. 7 Testing of shear mortar specimen

Table 8 Shear mortar test values for optimum strength

Mix proportions	OPC + 30%GGBS + 0.75SF + 2SP
7th day	7.55
14th day	10.03
28th day	15.36

4.4 Shear Mortar

Bricks with 19 mm (length) × 9 mm (width) × 9 mm (height) average size have been selected. In conjunction with IS 3495, these bricks compressive strength were determined. Determined OPC + 0.75SF + 30% GBS + 2% SP are the mix design of mortar collected from optimum value in previous trials and mix ratio. Content attributes are used in both Portland pozzolana cement and in local river sand. A total of three masonry prisms are prepared to determine compression strength of mortar as shown in Fig. 7. Table 8 shows the shear test for that optimum strength at 7th day, 14th day and 28th day.

5 Micro-Structural Study

5.1 SEM (Scanning Electron Microscope)

See Fig. 8.

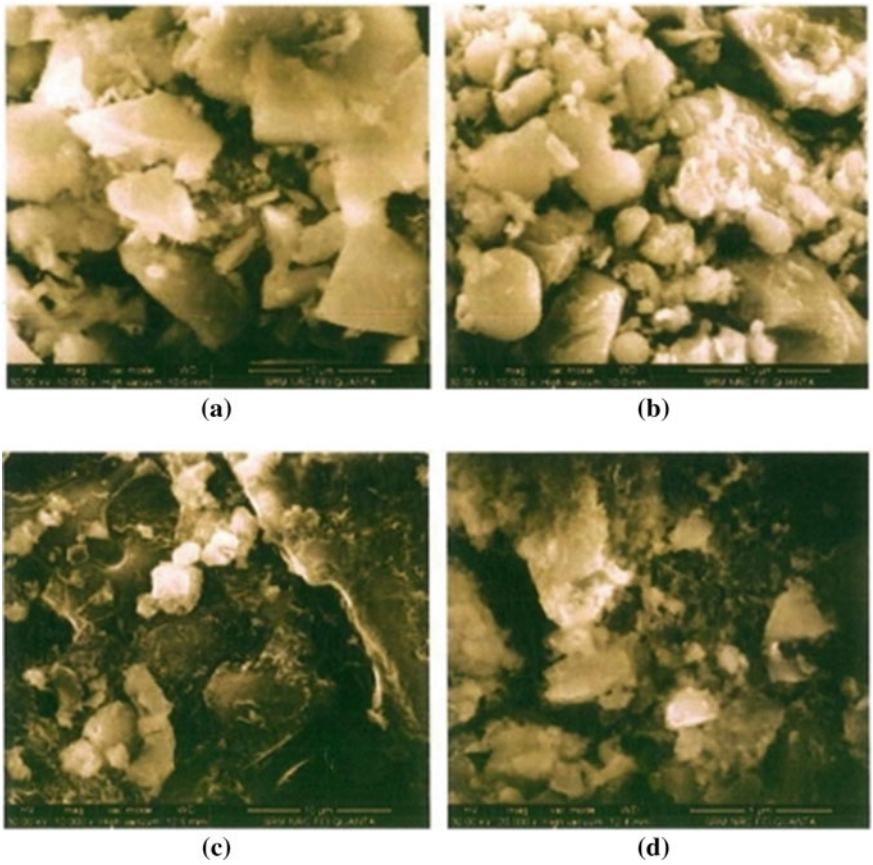

Fig. 8 **a** Raw material of cement 10 μm, **b** Raw material of GGBS l0μm, **c** OPC + 30% GGBS + 2% SP of l0 10μm, **d** OPC + 30% GGBS + 0.75S.F + 2% SP of l0 μm

5.2 EDS (Energy Dispersive Spectroscopy)

The chemical contents of the mortar mix from the EDS for the mortar without the addition of sisal fiber are shown in Table 9.

The chemical contents of the mortar mix from the EDS for the mortar with the addition of 0.75% of sisal fiber (optimal percentage) are shown in Table 10.

6 Conclusion

As to conclude, the incorporation of GGBS has increased the water–cement ratio required for the mortar due to its fineness property. Adding GGBS to the mortar also

Table 9 OPC + 30% GGBS + 2% SP

Element	Atom number	Mass %	Mass norm %	Atom %	Absolute error %(1sigma)	Relative error% (1 sigma)
Ca	20	50.44	41.06	24.07	1.56	3.08
0	8	48.46	39.44	57.92	10.58	21.83
Si	14	9.77	7.95	6.65	0.52	5.28
C	6	4.19	3.41	6.67	223	53.35
Fe	26	3.66	2.98	1.25	0. 17	4.65
Al	13	2.90	2.36	2.03	0.23	7.80
Cu	29	1.04	0.85	0.31	0.10	9.36
S	16	0.96	0.78	0.57	0.09	9.38
Zn	30	0.78	0.64	0.23	0.09	11.06
Ti	22	0.66	0.54	0.26	0.08	11.68
		122.85	100.00	100.00		

Table 10 OPC + 30% GGBS + 0.75 SF + 2% SP

Element	Atom number	Mass %	Mass norm %	Atom %	Absolute error % (O'sigma)	Relative error % (1 sigma)
0	8	48.58	44.89	53.25	16.11	33.17
Si	14	29.43	27.19	18.38	1.62	5.52
C	6	15.12	13.97	22.08	11.58	76.58
Ca	20	8.58	7.93	3.75	0.48	5.57
Fe	26	5.05	4.67	1.59	0.39	7.75
Al	13	1.46	1.35	0.95	0.23	16.07
		108.22	100.00	100.00		

increases the mechanical properties like compressive, tensile and flexural strength around 5%–30%.

- From the mechanical study of the mortar, it is clearly seen that the optimum addition of sisal fiber is found to be 0.75%. Further increase has reduced the strength properties.
- The micro structural characterization study has revealed that the silicon oxide content for the mix OPC + 30%GGBS + 0 0.75SF + 2%SP is high thus it has improved hydration process in the mortar by more formation of C-S–H and C-A-S–H products.
- The images from SEM analysis have proved to form a dense mix when GGBS is incorporated and improved hydration products when 0.75% SF is added to the mortar.

Thus, from the overall study, the addition of GGBS and sisal fiber has improved the quality properties of mortar and, thus, it can be used as a superior-partial replacement for cement. And, thus, the GGBS addition will reduce the environmental impact during the hydration process and also the natural depletion.

References

1. Bakare IO, Okieimen FE, Pavithran C, Abdul Khalil HPS, Brahmakumar M (2010) Mechanical and thermal properties of sisal fiber-reinforced rubber seed oil-based polyurethane composites. Mater Des 31(9):4274–4280. https://doi.org/10.1016/j.matdes.2010.04.013
2. Xin X, Xu CG, Qing LF (2007) Friction properties of sisal fibre reinforced resin brake composites. Wear 262(5–6):736–741. https://doi.org/10.1016/j.wear.2006.08.010
3. Li Y, Mai Y, Ye L (2000) Sisal fibre and its composites : a review of recent developments IM PA US AS DO ME US EX ON AS. Compos Sci Technol 60(2000):2037–2055
4. Joseph PV, Joseph K, Thomas S (1999) Effect of processing variables on the mechanical properties of sisal-fiber-reinforced polypropylene composites. Compos Sci Technol 59(11):1625–1640. https://doi.org/10.1016/S0266-3538(99)00024-X
5. Girisha C, Sanjeevamurthy, Srinivas GR (2012) Sisal/coconut coir natural fibers-epoxy composites: Water absorption and mechanical properties. Int J Eng Innov Technol 2(3):166–170
6. Zhong JB, Lv J, Wei C (2007) Mechanical properties of sisal fibre reinforced ureaformaldehyde resin composites. Express Polym Lett 1(10):681–687. https://doi.org/10.3144/expresspolymlett.2007.93
7. Fávaro SL, Ganzerli TA, de Carvalho Neto AGV, da Silva ORRF, Radovanovic E (2010). Chemical, morphological and mechanical analysis of sisal fiber-reinforced recycled high-density polyethylene composites. Express Polym Lett 4(8):465–473. https://doi.org/10.3144/expresspolymlett.2010.59
8. Raut LL (2014) Torsional strengthening of under reinforced concrete beams using crimped steel fiber. Int J Res Eng Technol 03(06):466–471. https://doi.org/10.15623/ijret.2014.0306087
9. Martin AR, Martins MA, Da Silva ORRF, Mattoso LHC (2010) Studies on the thermal properties of sisal fiber and its constituents. Thermochim Acta 506(1–2):14–19. https://doi.org/10.1016/j.tca.2010.04.008
10. Sen T, Reddy HNJ (2011) Application of Sisal, Bamboo, Coir and Jute natural composites in structural upgradation. Int J Innov Management Technol 2(3):186–191
11. Ramakrishna G, Sundararajan T, Kothandaraman S (2010) Evaluation of durability of natural fibre reinforced cement mortar composite-a new approach. J Eng Appl Sci 5(6):44–51
12. de Silva FA, Mobasher B, Filho RDT (2009) Cracking mechanisms in durable sisal fiber reinforced cement composites. Cem Concr Compos 31(10):721–730. https://doi.org/10.1016/j.cemconcomp.2009.07.004
13. Girisha C, Sanjeevamurthy, Srinivas G (2012) Effect of alkali treatment, fiber loading and hybridization on tensile properties of sisal fiber , banana empty fruit bunch fiber and bamboo fiber reinforced thermoset composites. Int J Eng Sci Adv Technol 2(3):706–711
14. Li Y, Mai YW, Ye L (2000) Sisal fibre and its composites: a review of recent developments. Compos Sci Technol 60(11):2037–2055. https://doi.org/10.1016/S0266-3538(00)00101-9
15. de Silva FA, Filho RDT, de Filho JAM, de Fairbairn EMR (2010) Physical and mechanical properties of durable sisal fiber-cement composites. Constr Build Mater 24(5):777–785. https://doi.org/10.1016/j.conbuildmat.2009.10.030

Investigation on Micromechanical Behavior of High-Performance Fiber Concrete

N. Arivusudar and S. Sureshbabu

1 Introduction

Concrete is perceived as a delicate material when presented to standard burdens and effect loads. Its elasticity is only one-tenth of its compressive strength under such conditions [1]. The concrete flexural members also cannot perform under such loads during their life period [2–5]. The presentation of filaments is acquired as an answer to provide concrete with improved ductility and flexibility [6–9]. Plastics are regularly utilized substances that assume a significant job in each part of human lives [10–12].

The usage of plastics across ages needs legitimate reusing as well as the reuse of its executives [13]. The most noteworthy sum utilization of plastics has been found in holders and bundling of products since it is long lasting and removal merchandise. Removing different residues is not a kidding issue in the cutting-edge days. So, it ought to be settled possibly to stay away from such circumstances [14–16].

Concrete is the most flexible man-made material used in different constructional occasions. As a material, its usage in the world is second to water these days [17]. This is an immediate aftereffect of its mouldability, of which its quality and strength are viewed as the brand name when set. Strong development has made impressive strides in the previous decade [18]. Concrete is, as of now not, now, a material containing solid, aggregates, water, and admixtures; notwithstanding, it is an assembled material with a couple of new constituents [19].

There are no united definitions for High-Performance Concretes (HPC), while different institutions and experts out of the blue describe High-Performance Concrete [20]. The American Concrete Institute demonstrates High-Performance Concrete as "Strong that meets outstanding execution and consistency necessities that can't happen by and large be obtained by using customary trimmings, conventional mixing

N. Arivusudar (✉) · S. Sureshbabu
Department of Civil Engineering, Adhiyamaan College of Engineering, Hosur, Krishnagiri 635109, India

K. S. Satyanarayanan et al. (eds.), *Sustainable Construction Materials*, Lecture Notes in Civil Engineering 194, https://doi.org/10.1007/978-981-16-6403-8_15

technique, and normal calming practices." In less muddled words, HPC is a firm that has one exceptional property, viz regardless. Compressive strength, high workability, enhanced resistances to chemical or mechanical stresses, lower permeability, durability, etc., when appeared differently about conventional concrete [21]. For example, self-compacting concrete is a specific piece of high-performance concrete that isolates itself with self-association properties joined with high stream capacity.

2 Materials and Method

This part manages different solid materials' physical and compound properties, like concrete, good total, coarse total, flying debris, silica rage, GGBS, PVA fiber, PP fiber, and steel fiber and water. A conventional Portland concrete of 53 evaluations, adjusting to IS 8112–1989, was utilized. The industrially accessible stream sand, which has been removed from the waterway Cauvery, is being used as the fine total for this exploration. The Fine total is tested as per IS: 2386–1963 [22–24]. This fine aggregate is clean, with no clay and no chemical constituents in it. The other name of concrete is artificial stone since its volume around 75 to 85% is occupied by the crushed stone, i.e., coarse aggregate. These coarse aggregates are derived from the rock quarry. The maximum size of coarse aggregate that has been taken for this research is 20 mm. Fly ash is the environmental pollutant produced by the coal-based thermal power station, and it has the potential to be used as a resource material due to its properties. So this fine waste material is used in cement, concrete, and other cement-based applications. The chemical properties of GGBS are shown in Fig. 1.

Silica fume is the environmental pollutant produced by the coal-based thermal power station, and it has the potential to use as a resource material due to its properties. So this fine waste material is used in cement, concrete, and other cement-based applications. GGBS (Ground Granulated Blast heater Slag) is a cementitious material predominantly utilized in cement, and it is a result of the impact heaters used to make iron. Impact heaters work at about 1500 °C and are taken care of with a deliberately controlled combination of iron mineral, coke, and limestone. The iron mineral is decreased to press, and the excess materials structure a slag that coasts on top of the iron. Water is an essential ingredient in concrete to strengthen strength from cement gel enhancing through the hydration process. So, it is necessary to check its quality. The water used in concrete is to satisfy the standard of IS 456–2000.

2.1 Mix Proportions

A blend is planned according to IS 10262–2009 to accomplish the solid evaluation of M40. The created and embraced blend extent is 1:1.711: 2.867: 0.40. A steady water–concrete proportion of 0.40 has been utilized for all the blends. This concrete mix design gives the high-performance concrete, the silica fume is added with cement

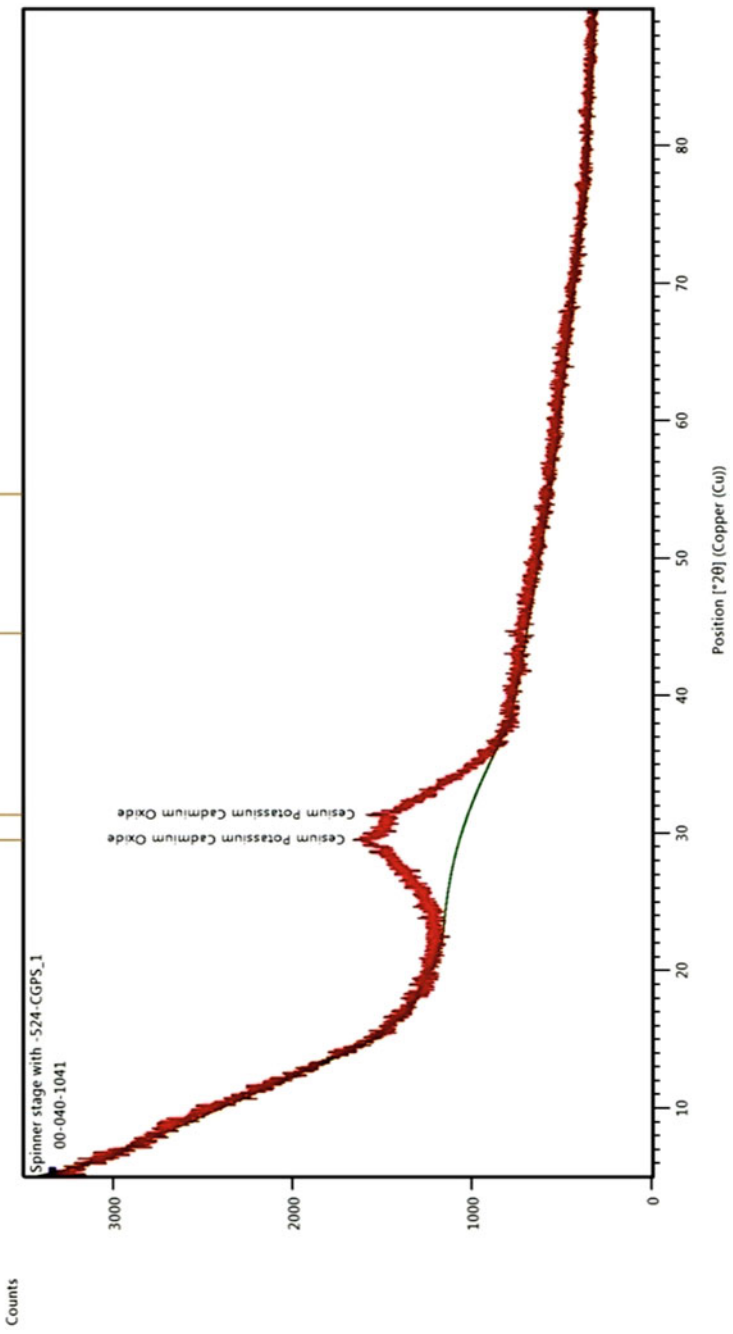

Fig. 1 XRD test on GGBS

by 40% and fly ash, GGBS replaced with cement by 10, 20, 30, 40, and 50%. By using these combinations, around 12 mixes were prepared and which is displayed in Table 1.

To prepare the fiber-reinforced concrete and cement, the silica fume by 40% and fly ash by 30% have been added together with cement to get the fly ash-based high-performance concrete. Along with that, PVA, PP, and glass have been added by 0.5, 1, 1.5, 2, and 2.5% concerning the cement weight. Similarly, instead of fly ash, GGBS has been used by 30% for the above category, so that a total of 30 different mixes were prepared for the above M40 grade mix and displayed in Table 2.

2.2 Casting and Testing

For the standard M40 concrete, a laboratory base mixer machine is used to mix the concrete ingredients (Figs. 2, 3, 4 and 5). Fibers are added with cement mortar paste slowly to get mixed and scattered in the concrete eventually. All the specimens are well compacted using a table vibrator. The illustrations are demoulded after 24 h, then after those specimens have undergone 28 days of water curing.

2.3 Compressive Strength Test

The compression test over the cube specimens has been performed according to IS: 516–1959 specifications. The cube specimens of size 150 mm x 150 mm x 150 mm were used for this test after 28 days of curing. The test specimens were removed from their mold after 24 h from casting and submerged immediately in water under room temperature and kept there until taken out just before the test. A Compression Testing Machine (CTM) of capacity 2000 KN was used to carry out this test. The specimen was placed in the CTM, and the sample is tested until it fails. The concrete cube specimen under a compression load in CTM is shown in Fig. 6.

$$\text{Compressive strength of the cube} = \text{Applied Load/Surface Area (MPa)}$$

2.4 Split Tensile Strength Test

One of the roundabout techniques is to discover the rigidity of cement that is the part malleable test. The split rigidity test is done on the pressure testing machine (CTM) over the chamber (Fig. 7) example as per IS: 516 – 1959 specifications. The cylinder of 150 mm diameter and 300 mm height specimens are used. Split tensile strength formula used is given below in (Eq. 1)

Table 1 Different concrete mixes for the grade of M40

S.No	Specimen ID	Cement	Fly ash	Silica Fume	GGBS	Fine aggregate	Coarse aggregate		Water to cement ratio	Water	SP
							10 mm	20 mm			
High-performance concrete											
1	CC	415	–	–	–	710	540	650	0.4	166	1.2
2	HPC	415	–	166	–	710	540	650	0.4	166	1.2
Fly ash-based high-performance concrete											
1	FHPC1	373.5	41.5	166	–	710	540	650	0.4	149.4	1.2
2	FHPC2	332	83	166	–	710	540	650	0.4	132.8	1.2
3	FHPC3	290.5	124.5	166	–	710	540	650	0.4	116.2	1.2
4	FHPC4	249	166	166	–	710	540	650	0.4	99.6	1.2
5	FHPC5	207.5	207.5	166	–	710	540	650	0.4	83	1.2
GGBS-based high-performance concrete											
1	GHPC1	373.5	–	166	41.5	710	540	650	0.4	149.4	1.2
2	GHPC2	332	–	166	83	710	540	650	0.4	132.8	1.2
3	GHPC3	290.5	–	166	124.5	710	540	650	0.4	116.2	1.2
4	GHPC4	249	–	166	166	710	540	650	0.4	99.6	1.2
5	GHPC5	207.5	–	166	207.5	710	540	650	0.4	83	1.2

Table 2 Fly ash and GGBS-based mixes for the grade of M40 with fibers

S. No	Specimen ID	Cement	Fly ash	Silica Fume	GGBS	Fine aggregate	Coarse Aggregate		Water to cement ratio	Water	SP	PVA fiber	PP fiber	Glass fiber
							10 mm	20 mm						
Fly ash-based high-performance fiber reinforced concrete														
1	$FHPC3_{PVA0.5}$	415	124.5	166	–	710	540	650	0.4	166	1.2	0.5		
2	$FHPC3_{PVA1.0}$	415	124.5	166	–	710	540	650	0.4	166	1.2	1		
3	$FHPC3_{PVA1.5}$	415	124.5	166	–	710	540	650	0.4	166	1.2	1.5		
4	$FHPC3_{PVA2.0}$	415	124.5	166	–	710	540	650	0.4	166	1.2	2		
5	$FHPC3_{PVA2.5}$	415	124.5	166	–	710	540	650	0.4	166	1.2	2.5		
6	$FHPC3_{PP0.5}$	415	124.5	166	–	710	540	650	0.4	166	1.2		0.5	
7	$FHPC3_{PP1.0}$	415	124.5	166	–	710	540	650	0.4	166	1.2		1	
8	$FHPC3_{PP1.5}$	415	124.5	166	–	710	540	650	0.4	166	1.2		1.5	
9	$FHPC3_{PP2.0}$	415	124.5	166	–	710	540	650	0.4	166	1.2		2	
10	$FHPC3_{PP2.5}$	415	124.5	166	–	710	540	650	0.4	166	1.2		2.5	
11	$FHPC3_{G0.5}$	415	124.5	166	–	710	540	650	0.4	166	1.2			0.5

Fig. 2 Conventional concrete cube specimens

Fig. 3 Conventional concrete cylinder specimens

$$\text{Split tensile strength} = \frac{2P}{\pi dl} \tag{1}$$

where

P = compressive load in kN.
l = length of the cylinder = 300 mm.
d = diameter of the cylinder = 150 mm.

Fig. 4 Specimen for pull out test

Fig. 5 Cube specimens in curing

Fig. 6 Compression test—cube specimen

Fig. 7 Split tensile test—cylinder specimen

2.5 Modulus of Rupture Test

The crystal example of size 100 mm × 100 mm × 500 mm is utilized to discover the modulus of a break on solidified cement following 28 days of restoring according to IS: 516–1959. The example is set in the flexure testing machine, and the burden is applied to the crystal's highest surface as a two-point stacking framework. The heap is used without stun and constantly expanded until the example fizzles. Figure 8 shows the flexural test arrangement on the solid crystal. The modulus of break is determined by utilizing the accompanying condition. The modulus of rupture formula used is given in Eq. 2.

$$\text{Modulus of rupture, fb} = \left(\text{x d}^2\right)/\left(\text{P x l}\right) \tag{2}$$

where P = maximum load applied to the specimen in kN
L = supported length = 500 mm
d = depth of the specimen = 100 mm
b = breath of the specimen = 100 mm.

Fig. 8 Modulus of rupture test—prism specimen

3 Result and Discussion

3.1 Compressive Strength Test

The test outcomes tracked down that the compressive strength of traditional solid (CC) and superior cement (HPC) were 42.3 MPa and 45.1 MPa, separately. The concrete is substituted by fly debris for 10%, 20%, 30%, 40%, and half, individually, and their particular compressive strength for fly debris-based superior cement, to be specific FHPC1, FHPC2, FHPC3, FHPC4, and FHPC5, are tried to be 43.5 MPa, 44.1 MPa, 45.5 MPa, 44.3 MPa, and 43.5 MPa, separately. On examining these outcomes, it is tracked down that 30% fly debris substitution (FHPC3) has the most extreme compressive strength contrasted with another level of fly debris substitution. The compressive strength of FHPC3 is 7.29% and 0.88% higher than CC and HPC concrete, separately. The test outcomes have appeared in Fig. 9.

Now, cement is replaced by GGBS for 10%, 20%, 30%, 40%, and 50%, respectively, and their compressive strength for GGBS high-performance concrete, namely, GHPC1, GHPC2, GHPC3, GHPC4, and GHPC5 are found to be 42.2 MPa, 44.1 MPa, 45.2 MPa, 44 MPa, and 43.2 MPa, respectively. On analyzing these results, it is found that 30% GGBS replacement (GHPC3) has maximum compressive strength compared with another percentage of GGBS replacement. The compressive strength of GHPC3 is 6.63% and 0.22% higher than CC and HPC concrete, respectively. The test results are shown in Fig. 10.

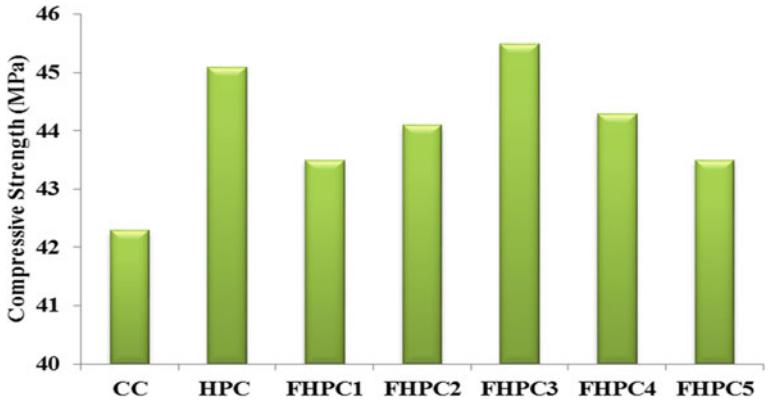

Fig. 9 Compressive strength of fly ash-based high-performance concrete

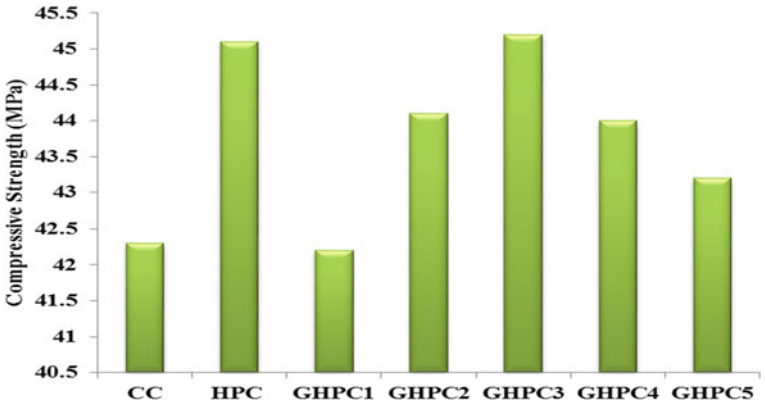

Fig. 10 Compressive strength of GGBS-based high-performance concrete

3.2 Split Tensile Strength Test

The test results found that the split tensile strength of conventional concrete (CC) and high-performance concrete (HPC) was 3.34 MPa and 3.56 MPa, respectively. The cement is replaced by fly ash for 10%, 20%, 30%, 40%, and 50%, respectively, and their respective split tensile strength for fly ash-based high-performance concrete, namely FHPC1, FHPC2, FHPC3, FHPC4, and FHPC5, was tested to be 3.44 MPa, 3.48 MPa, 3.59 MPa, 3.50 MPa, and 3.44 MPa, respectively. On analyzing these results, it is found that 30% fly ash replacement (FHPC3) has maximum split tensile strength compared with other percentages of fly ash replacement. The split tensile strength of FHPC3 is 7.22% and 0.84% higher than CC and HPC concrete, respectively. The test results are shown in Fig. 11.

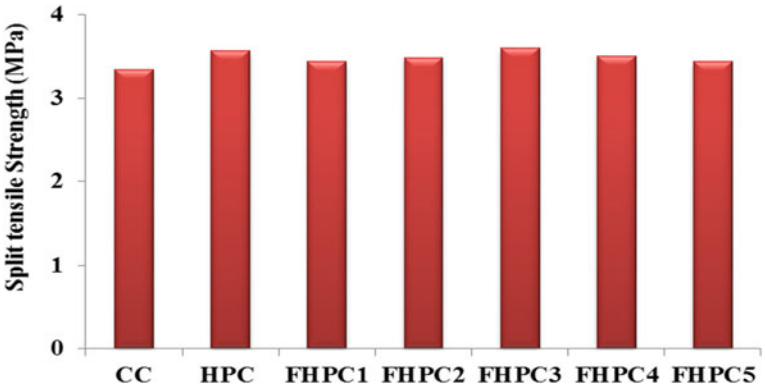

Fig. 11 Split tensile strength of fly ash-based high-performance concrete

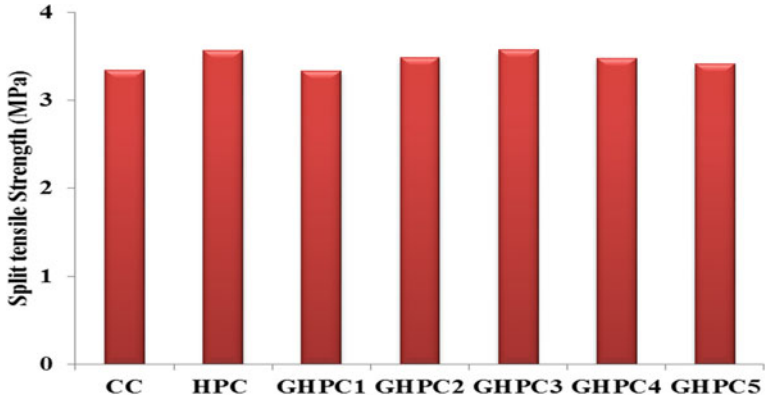

Fig. 12 Split tensile strength of GGBS-based high-performance concrete

Now, cement is replaced by GGBS for 10%, 20%, 30%, 40%, and 50%, respectively, and their split tensile strength for GGBS high-performance concrete, namely, GHPC1, GHPC2, GHPC3, GHPC4, and GHPC5 is found to be 3.33 MPa, 3.48 MPa, 3.57 MPa, 3.48 MPa, and 3.57 MPa, respectively. On analyzing these results, it is found that 30% GGBS replacement (GHPC3) has maximum split tensile strength compared with another percentage of GGBS replacement. The split tensile strength of GHPC3 is 6.66% and 0.28% higher than CC and HPC concrete, respectively. The test results are shown in Fig. 12.

3.3 Modulus of Rupture Test

The test outcomes tracked down that the modulus of the crack of customary solid (CC) and special cement (HPC) was 4.35 MPa and 4.63 MPa. The concrete is substituted by fly debris for 10%, 20%, 30%, 40%, and half, individually, and their different modulus of burst for fly debris-based superior cement, in particular, FHPC1, FHPC2, FHPC3, FHPC4, and FHPC5 are tried to be 4.62 MPa, 4.65 MPa, 4.72 MPa, 4.66 MPa, and 4.62 MPa, individually. It is tracked down that 30% fly debris substitution (FHPC3) has the greatest modulus of burst contrasted with another level of fly debris substitution on examining these outcomes. The modulus of FHPC3 is 8.16% and 1.93% higher than CC and HPC concrete, individually. The test outcomes have appeared in Fig. 13.

Now, cement is replaced by GGBS for 10%, 20%, 30%, 40%, and 50%, respectively, and their modulus of rupture for GGBS high-performance concrete, namely GHPC1, GHPC2, GHPC3, GHPC4, and GHPC5 is found to be 4.55 MPa, 4.65 MPa, 4.71 MPa, 4.64 MPa, and 4.60 MPa, respectively. On analyzing these results, it is found that 30% GGBS replacement (GHPC3) has a maximum modulus of rupture

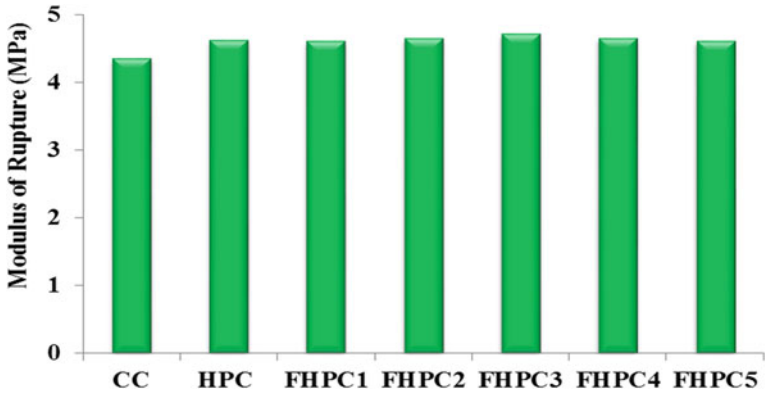

Fig. 13 Modulus of rupture of fly ash based high-performance concrete

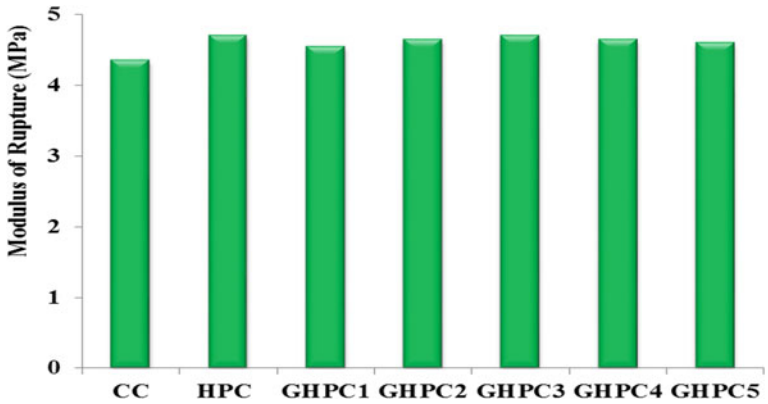

Fig. 14 Modulus of rupture of GGBS-based high-performance concrete

compared with another percentage of GGBS replacement. The modulus of rupture of GHPC3 is 7.95% and 1.71% higher than CC and HPC concrete, respectively. The test results are shown in Fig. 14.

4 Conclusion

Various tests have been conducted throughout the research work. In this research work, high-performance concrete, fly ash-based high-performance concrete, GGBS-based high-performance concrete, fly ash-based high-performance fiber-reinforced concrete and GGBS-based high-performance fiber-reinforced concrete in different proportions to study the mechanical properties, durability properties and structural performance of concrete.

The compressive strength of fly debris-based special cement (FHPC3) and fly debris-based elite fiber supported cement with mono fiber FHPC3G2.0, with mixture fiber (FHPC3) PVA0.5+G1.5 are discovered to be 7.29%, 10.1%, 8.16% higher than customary solid CC.

The split rigidity of fly debris-based special cement (FHPC3) and fly debris-based elite fiber-supported cement with monofiber FHPC3G2.0, with mixture fiber (FHPC3) PVA0.5+G1.5 are discovered to be 7.21%, 18.48%, 8.32% higher than traditional solid CC.

The modulus of a burst of fly debris-based superior cement (FHPC3) and fly residue-based elite fiber built up concrete with monofiber FHPC3G2.0, with half breed fiber (FHPC3) PVA0.5+G1.5, are discovered to be 8.16%, 13.01%, 14.7% higher than regular solidCC.

References

1. Ali M, Nehdi M (2017) Innovative crack-healing hybrid fiber reinforced engineered cementitious composite. Constr Build Mater 150:689–702
2. Ali M, Soliman A, Nehdi M (2017) Hybrid-fiber reinforced engineered cementitious composite under tensile and impact loading. Mater Des 117:139–149
3. Al-Oraimi SK, Seibi AC (1995) Mechanical characterization and impact behaviour of concrete reinforced with natural fibres. Compos Struct 32:165–171
4. Anbuvelan K, Khadar MM, Lakshmipathy M, Sathyanarayanan KS (2007) Studies on concretes' properties containing polypropylene, steel and re-engineered plastic shred fiber. Indian Concr J 81(4):38–44
5. Asha, P, Sundararajan, R, Rozario JM, Moorthy V (2006) Cyclic response of reinforced concrete exterior beam-column joint. In: Proceedings of international conference in innovative technologies in civil engineering, Coimbatore, India, pp 203–213
6. Atiş CD, Karahan O (2009) Properties of steel fiber reinforced fly ash concrete. Constr Build Mater 23(1):392–399
7. Bairagi NK, Modhera CD (2001) Shear strength of fibre reinforced concrete. ICI J 1(4):47–52
8. Ezeldin AS, Balaguru PN (1992) Normal-and high-strength fiber-reinforced concrete under compression. J Mater Civ Eng 4(4):415–429
9. Baruah P, Talukdar S (2007) A comparative study of compressive, flexural, tensile and shear strength of concrete with fibres of different origins. Indian Concr J 81(7):17–24
10. Batayneh M, Marie I, Asi I (2007) Use of selected waste materials in concrete mixes. Waste Manage 27(12):1870–1876
11. Bayasi MZ, Soroushian P (1992) Effect of steel fiber reinforcement on fresh mix properties of concrete. Mater J 89(4):369–374
12. CAN/CSA S806–02 (2002) Design and construction of building components with fiber-reinforced polymer. Canadian Standard Association, Rexdale, Ontario, Canada
13. Chanvillard G, Banthia N, Aitcin PC (1990) Normalized load-deflection curves for fibre reinforced concrete under flexure. Cement Concr Compos 12(1):41–45
14. Committe, ACI 1996 State of the art report on FRP for concrete structures
15. Douglas KS, Billington SL (2011) Strain rate dependence of HPFRCC cylinders in monotonic tension. Mater Struct 44(1): 391–404
16. Ganesan N, Indira PV (2000) Latex modified SFRC beam-column joints subjected to cyclic loading. Indian Concr J 416–420
17. Ganesan N, Murthy R (1990) Strength and behaviour of confined steel fiber reinforced concrete columns. ACI Mater J 87(3):221–227

18. Ganesan K, Rajagopal K, Thangavel K (2007) Evaluation of bagasse ash as supplementary cementitious material. Cement Concr Compos 29(6):515–524
19. Ganesan N, Indira PV (2000) Latex modified SFRC beam-column joints subjected to cyclic loading. Indian Concr J 74(7):416–420
20. Vondran GL (1991) Applications of steel fiber reinforced concrete. Am Concr Inst 13(11):44–49
21. Ghosh S, Bhattacharya, Ray SP (1989) Tensile strength of steel fibre reinforced concrete. IE (I) Journal-CI 69:222–227
22. Fischer G, Li VC (2003) Intrinsic response control of moment-resisting frames utilizing advanced composite materials and structural elements. ACI Struct J 100(2):166–176
23. Parra-Montesinos GJ, Peterfreund SW, Shih-Ho-Chao, (2005) Highly damage-tolerant beam-column joints through use of high-performance fibre-reinforced cement composites. ACI Struct J 102(3):487–495
24. Toutanji HA, El-Korchi T, Nathan Katz R (1994) Strength and reliability of carbon-fiber-reinforced cement composites. Cement Concr Compos 16(1):15–21

Concocting Nanostructured Plant Molecules for Inhibiting the Corrosion Activity in HYSD Bars

G. K. Monica Nandini, N. Gokul, Bipin Chandra, and Khalid

1 Introduction

Many heavy metals are being slowly prohibited with the help of enormous by-laws due to their poisonous behaviour along with their disposal hurdles especially in the marine environment [1]. In order to replace inorganic compounds, nowadays extracts of plants are considered the vital source of naturally concocted one that involves simple low-cost extraction procedure [2–6]. These extracts have the tendency to replace synthetic organic and inorganic inhibitors with many successive literatures. Active ingredients present in the natural extract help in the treatment of many wastes and helped many researchers to formulate related theories [7–10].

Most of the industries such as cleaning industries, petrochemical related works, pickling processes and others, using corrosion inhibitors are the most critical thing in the current trends of research [12–14]. Inhibitors with oxygen, nitrogen and sulphur proved to be effective in the majority areas. Among various synthetic compounds showing good anticorrosive properties, they emerge as toxic to human beings and their surrounding environment. Characteristics such as natural, low cost, availability and renewable nature make the extracts of plants suitable in all scenarios. In this regard, one of the perennial trees like Musa paradisiaca (Banana) is used in many research-related activities [15]. Researches to find more compounds as corrosion inhibitors in various acidic and alkaline media are yet to be done. More works are

G. K. M. Nandini (✉) · N. Gokul · B. Chandra · Khalid
Department of Civil Engineering, Sona College of Technology, Salem, Tamil Nadu, India
e-mail: monicanandhini.civil@sonatech.ac.in

N. Gokul
e-mail: gokul.17civil@sonatech.ac.in

B. Chandra
e-mail: bipinchandarraj.17civil@sonatech.ac.in

Khalid
e-mail: khalid.17civil@sonatech.ac.in

K. S. Satyanarayanan et al. (eds.), *Sustainable Construction Materials*, Lecture Notes in Civil Engineering 194, https://doi.org/10.1007/978-981-16-6403-8_16

done to find active plant compounds from various natural substances [11, 16]. Thus, in this work, the suitability of Musa extract under varying time and concentration to act as a green corrosion inhibitor over HYSD bar specimen is planned to be tested [17].

2 Experimental Work

2.1 Concoction of Leaves Powder

Musa were dried naturally and used to make the fine powder. Initially, leaves were collected from local farmers and washed thoroughly and soaked in deionized water for 5 h followed by air drying using natural sunlight. This extract of leaf powder was used as an inhibitor for HYSD bars [18].

2.2 Making of Trial Compound

Acidic compound of 0.25 molarity H_2SO_4 was prepared by the dilution of Analytical Grade 98% H_2SO_4 with deionized water to a volume of 100 ml in the existence or non-existence of various concentrations of leaves extract varying from 3 to 10 g/l.

2.3 Arrangement of Specimen

Initially, the HYSD specimen of 16 mm diameter was cleaned with various emery paper up to 300 grade and cut into 2.5 cm length and used for further process. Each specimen was thoroughly cleaned with deionized water then air dried with acetone and preserved in an air tight container.

2.4 Weight Loss Technique

Weight loss technique (WLT) is one of the common corrosive action observing methods. It includes exposure of specimen to a specific duration, then removed for measurement of the same. It is a basic measurement where the W_L happening over a particular period of exposure is given in terms of rate of corrosive action. In this work, HYSD bars in three trials were submerged in 100 ml of the trial compound of acidic nature (0.25 molarity H_2SO_4) in the existence or non-existence of the inhibitor at varying temperatures.

The metal samples were taken out from the trial compounds after 5 h at temperatures of 27 and 40 °C. After cleaning the specimen with Dimethyl ketone, the W_L was found as the difference in weight of the samples before and after immersion using analytical balance with an accuracy of ± 0.1 mg. For the authenticity of the outcome and to report the average value of the W_L, observations were performed triple time. Using this technique, the average rate of corrosive action was expressed in mg per sq cm per hr. Assuming, that uniform corrosion taking place over the sample, corrosiveness is calculated. Using the W_L measurements, the rate of corrosion will be found using the following Eq. 1:

$$\text{Rate of Corrosion (MMPY)} = (87.6 \times W_L)/(\text{d.a.t}) \quad (1)$$

where MMPY = Milli metre per year, W_L = Weight Loss (mg), d = Density (g per cubic metre), A = Area of sample (square cm), t = time (hours).

The Inhibition Efficiency (% I.E.) and Surface Coverage (θ_s) were found using the below Eqs. (2) and (3),

$$\text{Inhibition Efficiency (\%I.E.)} = [(Wt_1 - Wt_2)/(Wt_1)] \times 100 \quad (2)$$

$$\text{Surface Coverage } (\theta_s) = [(Wt_1 - Wt_2)/(Wt_1)] \quad (3)$$

where Wt_1 = Rate of Corrosion with the extract and Wt_2 = Rate of Corrosion without the extract.

3 Results and Discussion

As per Fig. 1, the SEM image of Banana leaf powder represents the formation of shielding coat around the HYSD bar. Because of 5 h contact period, for a sample length of 2.5 cm, most of the surface has been covered with the particles of Musa.

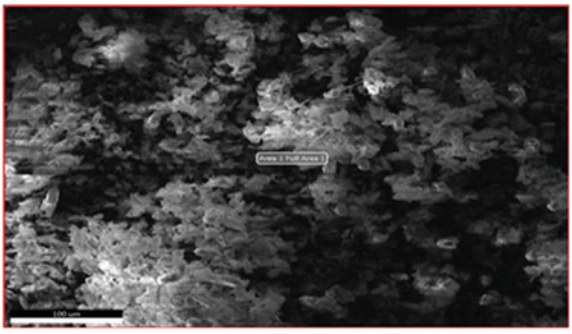

Fig. 1 Area 1 SEM result banana leaf powder

This shielding coat will play an important role in inhibiting the corrosion in HYSD bar specimen used in this work.

Figures 2 and 3 substantiate the effective role of Banana leaf powder as a protective sheath over the HYSD bar. Various elements present in the leaf powder help to analyze the inhibiting property of Musa extract.

Figure 4 shows the composition of various elements in the duplicate sample of Musa powder. Elements such as C, O are present in enormous amount, whereas minor elements such as Mg, Si, Mo, Cl are present in minimal amount. Carbon and Oxygen play an important role as protective cover for the high-yield strength deformed bars.

From Fig. 5, it is found that the percentage transmittance of the peaks obtained in FTIR has around a value of 100. High peaks were obtained around 455.20 per cm. Between 3956.65 and 2000 per cm, the peaks followed an uniform pattern layer

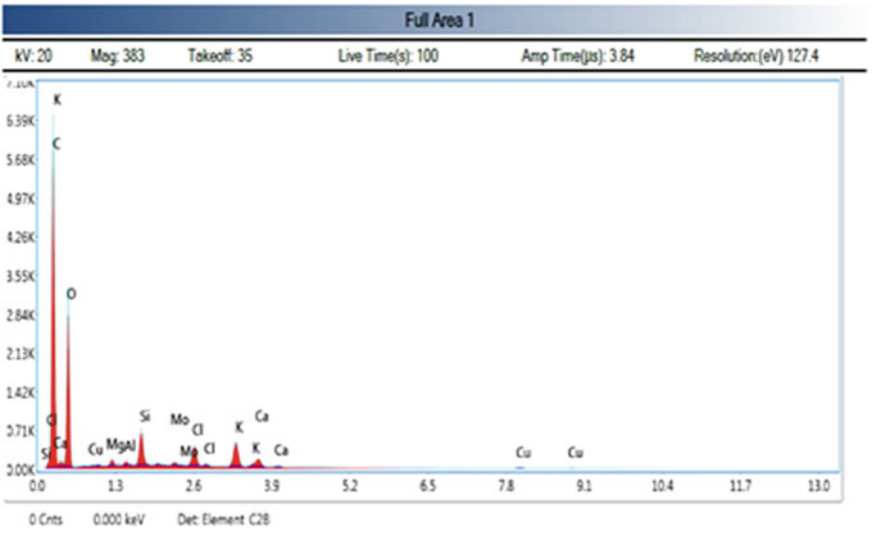

Fig. 2 Elemental analysis 1 SEM result

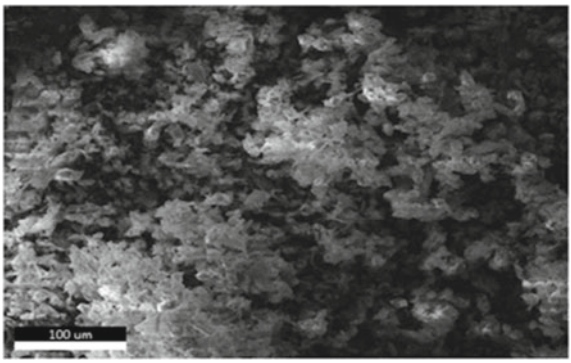

Fig. 3 Area 2 banana leaf powder SEM result

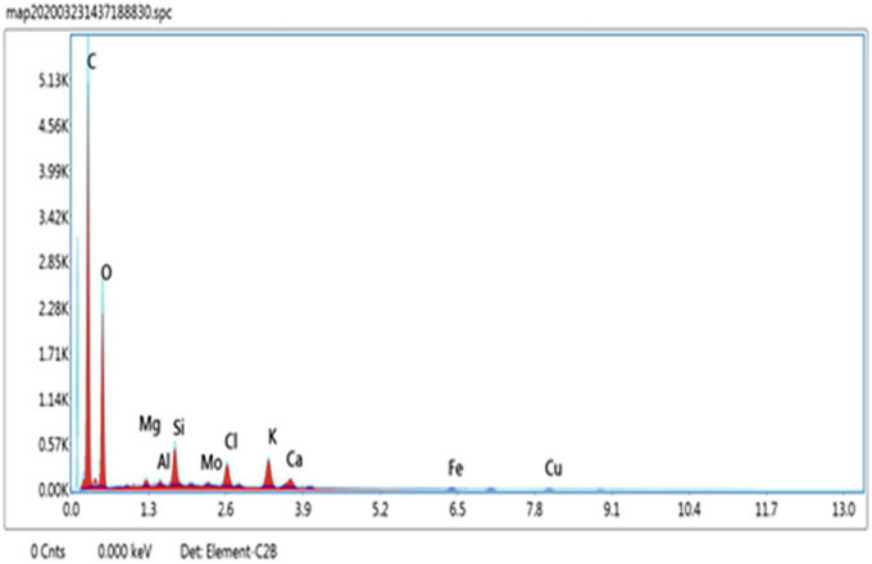

Fig. 4 Elemental analysis 2 SEM result

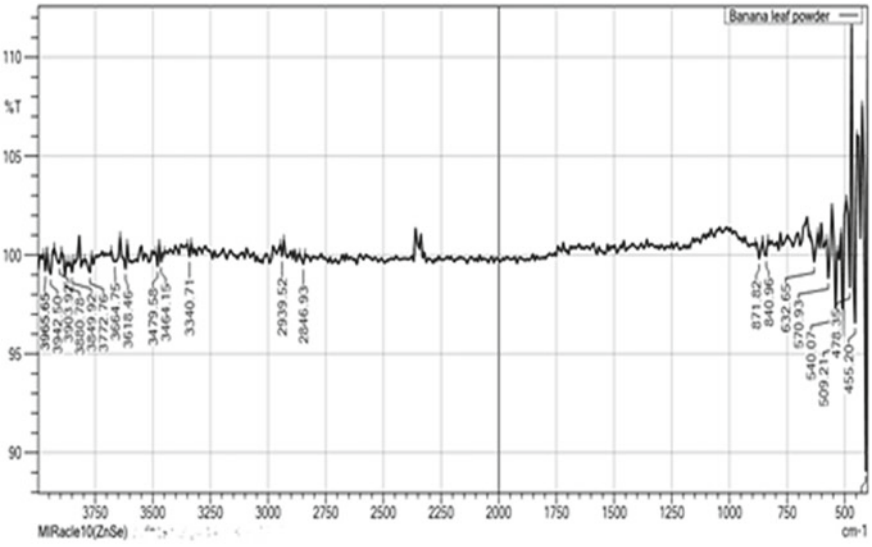

Fig. 5 FTIR result

of single bond, which varies from 2500 to 4000 per cm; the layer of triple bond varies from 2000 to 2500 per cm; the layer of double bond varies from 1500 to 2000 per cm; and the layer of fingerprint region varies from 600 to 1500 per cm. It contains methyl as band regions between 3650 and 3250 per cm exist, along with the presence of hydrogen bond. At above 3000 per cm, aromatic C–H stretch exists along with functional groups such as acetylenic (2140–2100), alcohol hydroxy compound (3570–3200 per cm), ether and oxy compound (2820–2810 per cm), tertiary amino(1210–1150 per cm), carbonyl compound (2100–1800 per cm) and others.

4 Conclusion

With the help of the above points, it is proved that Musa plant extract plays a vital role in effective green inhibition against high-yield strength deformed bar specimen. It is justified that with the help of WLT, corrosion inhibition of HYSD in acidic environment can be verified. Scanning the specimen treated with or without Musa extract using SEM and FTIR equipments, shows the increment in the activation energy values of the corrosion process; and also indicates this plant extract creates a hurdle to charge and mass transfer thereby producing decrement in the rate of corrosive action over HYSD bar specimen when 0.25 molarity Sulphuric acid medium used. With the above data, it is confirmed that both physical adsorption and chemical sorption are involved while treating the specimen with Musa. Thus, the study done confirms that the corrosion inhibition due to Musa extract over HYSD specimen using 0.25 molarity sulphuric acid is due to the adsorption mechanism of the extract.

References

1. Nandiyanto ABD (2019) How to read and interpret FTIR spectroscope of organic material, pp 97–118
2. Al-Asadi AA, Abdullah AS, Khaled NI, Alkhafaja RJM (2015) Effect of an Aloe Vera as a natural inhibitor on the corrosion of mild steel in 1 wt% NaCl. Int J Eng Technol 02(06)
3. Singh A, Ahamad I, Quraishi MA (2016) Piper longum extract as green corrosion inhibitor for aluminium in NaOH solution. Arab J Chem 9:S1584–S1589
4. Khadom AA, Abd AN, Ahmed NA (2017) Xanthium strumarium leaves extracts as a friendly corrosion inhibitor of low carbon steel in HCl: Kinetics and mathematical studies. S Afr J Chem Eng 25:13–21
5. Yaro AS, Khadom AA, Wael RK (2013) Apricot Juice as green corrosion inhibitor of mild steel in phosphoric acid. Alex Eng J 52:129–135
6. Nahe A, Abu-Abdoun I, Abdel- Rahman I (2010) UAE Neem Extract as a corrosion inhibitor for carbon steel in HCl solution. Int J Corros 2010. (de Souza ECCA, de Andrade Ripper B, Perrone D, D'Elia E (2016) Roasted coffee extracts as corrosion inhibitors for mild steel in HCl solution. Mater Res 19(6):1276–1285)
7. Jeetendra Bhaswar PK, Jain PJ (2015) Experimental and computational studies of Nicotiana tabacum leaves extract as green corrosion inhibitor for mild steel in acidic medium. Alex Eng J 54:769–775

8. Loto CA, Loto RT, Popoola API (2011) Effect of neem leaf (Azadiratcha indica) extract on the corrosion inhibition of mild steel in dilute acids. Int J Phys Sci 6(9):2249–2257
9. Chigondo M, Chigondo F (2016) Recent natural corrosion inhibitors for mild steel: an overview, J Chem
10. Muthukrishnan P, Jeyaprabha B, Prakash P (2017) Adsorption and corrosion inhibiting behavior of Lannea coromandelica leaf extract on mild steel corrosion. Arab J Chem S2343–S2354
11. Chaubey N, Singh VK, Quarishi MA (2016) Papaya peel extract as potential corrosion inhibitor for Aluminium alloy in 1M HCl: electrochemical and quantum chemical study. Ain Shams Eng J
12. Michael NC, Olubunmi JA (2014) The corrosion inhibition of mild steel in sulphuric acid solution by flavonoid (catechin) separated from Nypa fruticans Wurmb leaves extract. Sci J Chem 2(4):27–32
13. Odewunmi NA, Umoren SA, Gasem ZM (2015) Watermelon waste products as green corrosion inhihbitors for mild steel in HCl solution. J Environ Chem Eng 285–296
14. Mayangalambam RS, Sharma V, Singh G (2011) Musa paradisiacal extract as a green inhibitor for corrosion of mild steel in 0.5 M sulphuric acid solution. Portugaliae Elecrochimica Acta 29(6):405–417
15. Ramananda Singh M, Gupta P, Gupta K (2015) The litchi (Litchi Chinesis) peels extract as a potential green inhibitor in prevention of corrosion of mild steel in 0.5 M H2SO4 solution. Arab J Chem
16. Sangeetha M, Rajendran S, Sathiyabama J, Prabhakar P (2012) Eco friendly extract of Banana Peel as corrosion inhibitor for carbon steel in sea water. Sch Res Libr 2(5):601–610
17. Sharma SK, Peter A, Obot IB (2015) Potential of Azadiratcha indica as a green corrosion inhibitor against mild steel, aluminium, and tin: a review. J Anal Sci Technol 6:26
18. Sastri VS (2011) Green Corrosion inhibitors: theory and Practice. Wiley Publications

Smart Materials and Civil Engineering

Experimental Investigation of Cold-Formed Steel Castellated Beams

S. T. Dhaarini, C. Manoj Kumar, and D. Vinoth Raj

1 Introduction

In this scientific world with many modern construction methodologies, many researchers are analyzing all the structural components for their increased load capacity rate, whereas cold-formed steel is a newly developing material for past years [1–5]. Castellated beam is one of the innovations in the construction field [4, 6, 7]. These beams can be used as a secondary beam in industrial building, parking garages [5, 8–10]. The uniqueness of the castellated beam is without increasing the self-weight if the for the beam the depth of the beam is increased. Manufacturing of castellated beams is done by cutting the beam along with the web in a "zig-zag" pattern, and then offsetting the two halves, and then welding the two halves together [1, 5, 6, 8, 11]. Through this physical alteration of the material, the stiffness of the beam is increased, without any changes to the material's weight [5, 7, 8, 12]. Compared with the original beam, the newly cut castellated beam can withstand more vibration resistance due to its increased depth of the beam. In this paper, castellated beams are fabricated with cold-rolled sheet and are analyzed [13–15]. Totally four beams are fabricated and analyzed, one normal I section beam and three Castellated beams manufactured from that I section beam with variation in the number of holes.

S. T. Dhaarini (✉) · C. M. Kumar
Sathyabama Institute of Science and Technology, Chennai, India

D. V. Raj
Mount Zion College of Engineering and Technology, Pudukkotai, India

K. S. Satyanarayanan et al. (eds.), *Sustainable Construction Materials*, Lecture Notes in Civil Engineering 194, https://doi.org/10.1007/978-981-16-6403-8_17

2 Material Property and Test Specimen

2.1 Material Property

Cold-rolled steel sheet of Grade IS 513CR2 of 3 mm thickness having yield stress, ultimate tensile strength, and elongation percentage as 220, 280 MPa and 35% respectively. According to the dimensions of flange and web, machine cutting, i.e., straight cutting is done on the cold-rolled sheet are Laser cutting is done on web for the zig-zag pattern for castellated beam.

2.2 Test Specimen

A total of four beams made of cold-rolled sheet CR2 is fabricated and tested. For Castellated beam, initially, I section is fabricated for 1500 mm span and 200 mm depth, and then by the method of castellation, the span of all three castellated beams is 1300 mm and depth is 250 mm. The opening details are shown in Fig. 1. The end distance for the beam is altered to attain 1300 mm span. These castellated beams are compared with Buildup I section (CRB) of span 1300 and depth 200 mm as shown in Fig. 2. The dimension of the specimens, CRB (Cold-Rolled Beam), CRCB-1 (Cold-Rolled Castellated Beam-1), CRCB-2 (Cold-Rolled Castellated Beam-2), CRCB-3 (Cold-Rolled Castellated Beam-3) are given in Table 1. The method of castellation for CRCB-1, CRCB-2, CRCB-3, and their dimensions are shown in Figs. 3, 4 and 5, respectively.

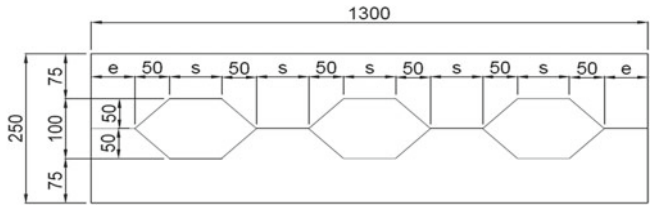

Fig. 1 Opening details of castellated beam

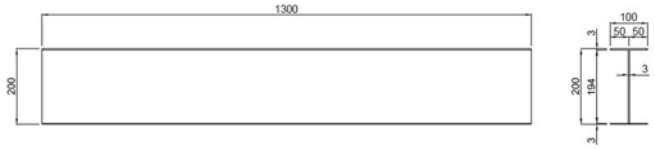

Fig. 2 CRB

Table 1 Specimen dimensions

Specimen		Build up I section beam	Castellated built up I section Beam		
	Units	CRB	CRCB-1	CRCB-2	CRCB-3
Depth	mm	200	250	250	250
Breadth	mm	100	100	100	100
Span	mm	1300	1300	1300	1300
Web and flange thickness	mm	3	3	3	3
Spacing (s)	mm	–	150	100	75
End pitch (e)	mm	–	125	100	62.5
Number of openings		–	3	4	5

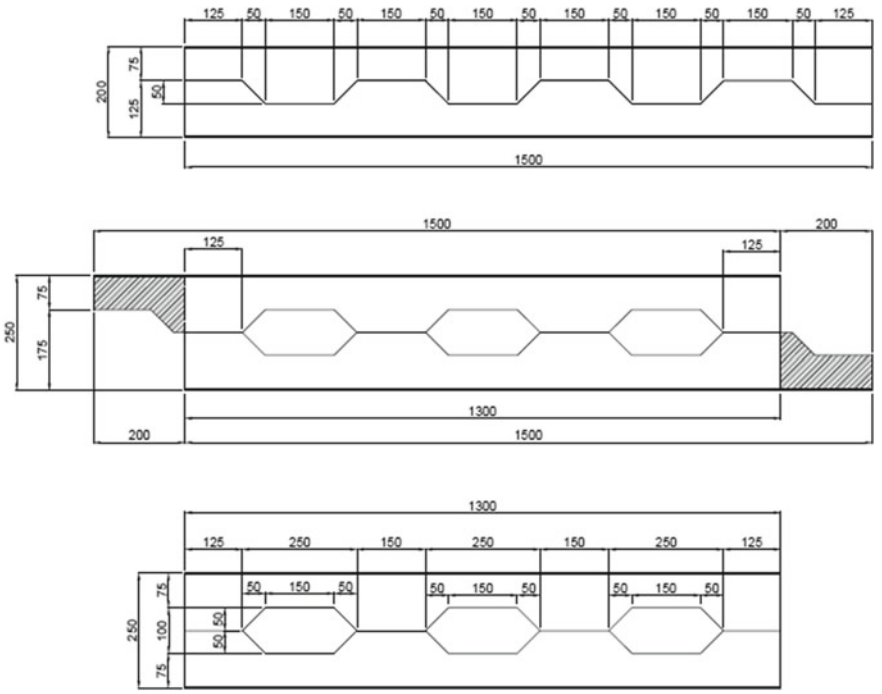

Fig. 3 Method of castellation for CRCB-1

3 Analytical Procedure

The finite element analysis is done using ANSYS software. Fine meshing was applied to all the beams to avail the accuracy in result. The beams were analyzed by four-point loading condition. The load is applied gradually, and corresponding stress, strain and total deformation are analyzed.

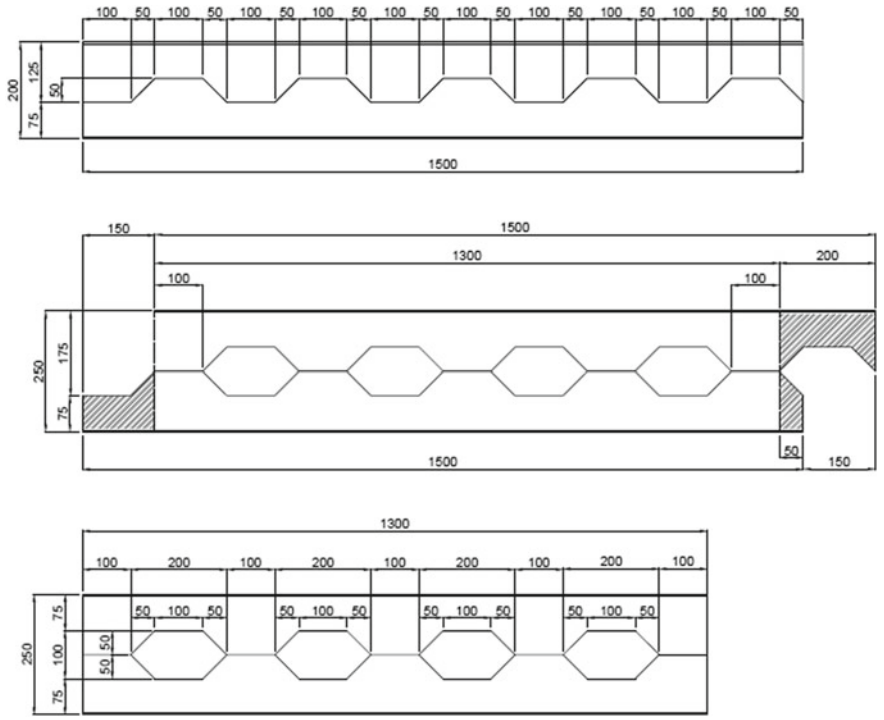

Fig. 4 Method of castellation for CRCB-2

The total deformation for CRB, CRCB-1, CRCB-2, CRCB-3 is given in Figs. 6, 7, 8 and 9 respectively.

4 Experimental Procedure

4.1 Fabricated Beam

The CR sheet is brought for 2500 mm and 1200 mm and cut into required sizes. The cutting was done in machine cutting (Fig. 10) and for the zig-zag pattern laser cutting (Fig. 11). Finally, all the flange and web were welded. Continuous weld has been applied on the flanges and web as shown in Fig. 12, and final fabricated beams are shown in Fig. 13.

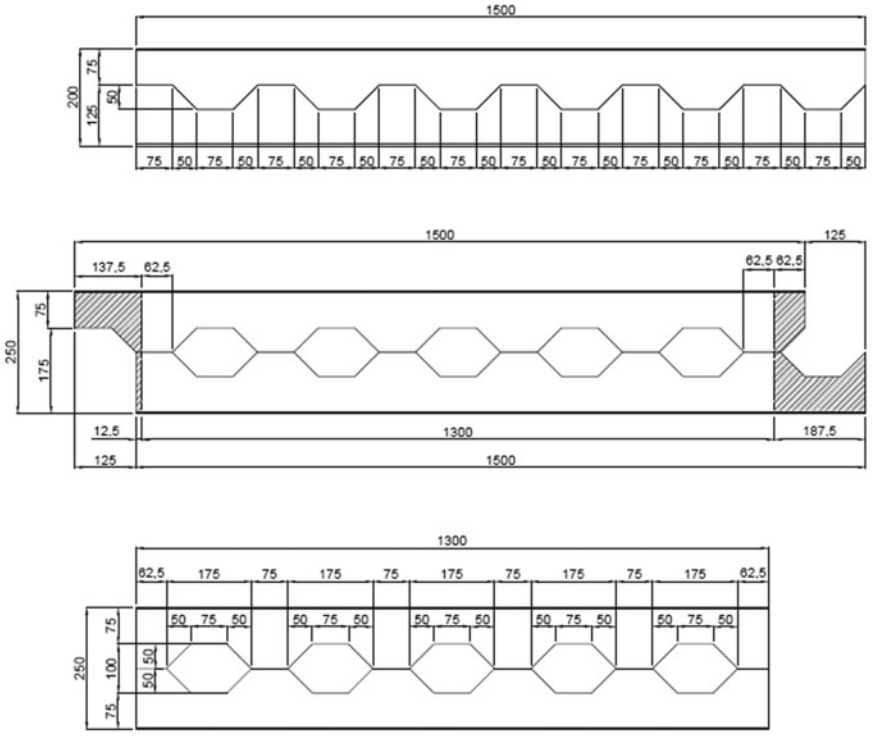

Fig. 5 Method of castellation for CRCB-3

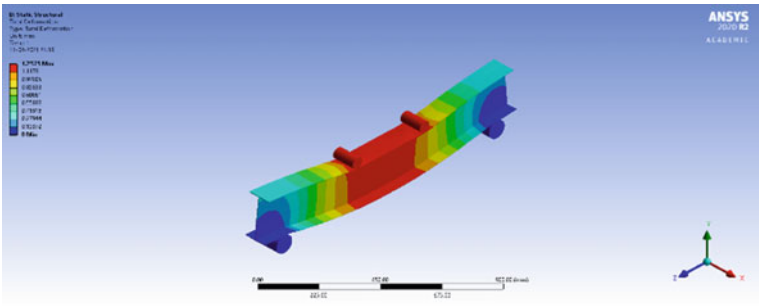

Fig. 6 Total deformation for CRB

4.2 Experimental Setup

The experimental setup of beam with four-point loading condition was arranged with three dial gauges to measure the deflection, hydraulic jack and pivot ring as shown in Figs. 14, 15, 16 and 17 for CRB, CRCB-1, CRCB-2, CRCB-3, respectively. Gradually

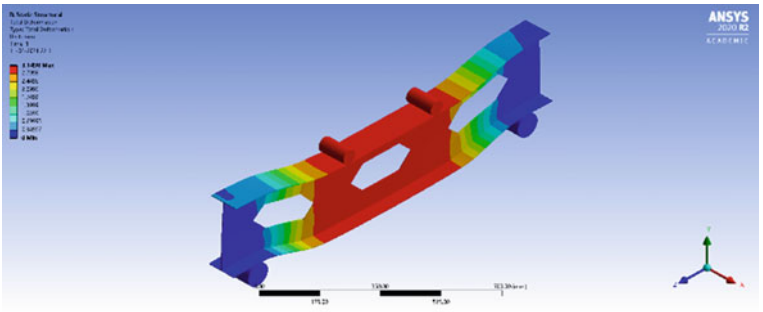

Fig. 7 Total deformation for CRCB-1

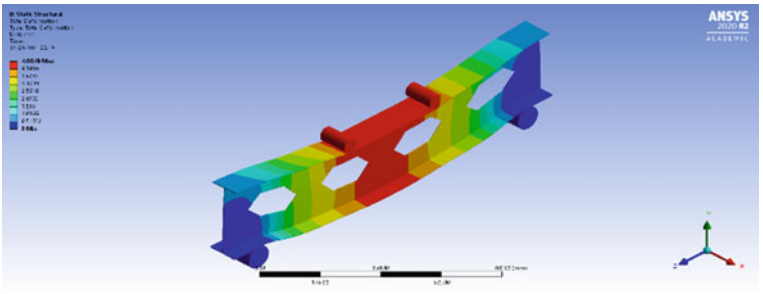

Fig. 8 Total deformation for CRCB-2

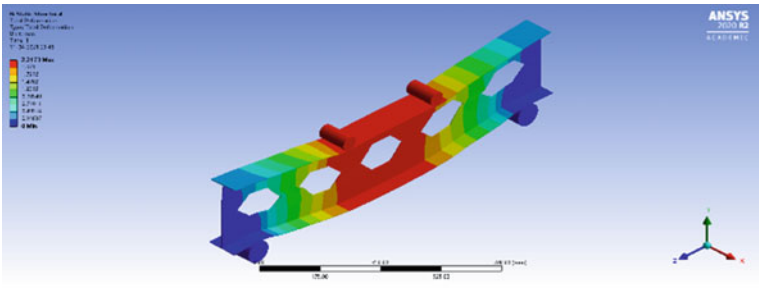

Fig. 9 Total deformation for CRCB-3

increasing load of 2 kN load was applied, and the corresponding deflection was noted from dial gauge.

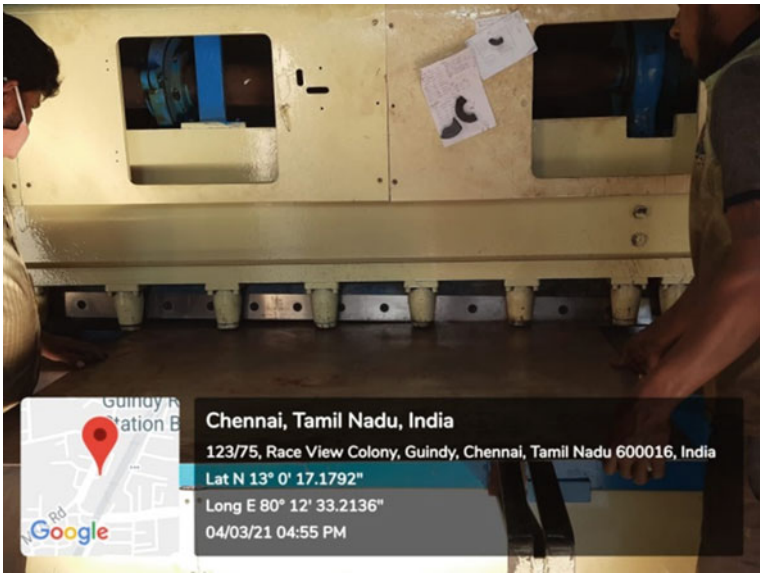

Fig. 10 Machine cutting

Fig. 11 Laser cutting

Fig. 12 Arc welding

Fig. 13 Fabricated beams

5 Results and Discussions

5.1 Results

5.1.1 ANSYS Results

The yield point is obtained to be 14 kN, 16 kN, 18 kN, 16 kN for CRB, CRCB-1, CRCB-2, CRCB-3, respectively. The load–deflection curve for all the specimens by ANSYS is obtained as per Fig. 18. The maximum deflection is seen in CRCB-2.

Fig. 14 4-Point loading setup for CRB

Fig. 15 4-Point loading setup for CRCB-1

5.1.2 Experimental Results

The yield point is obtained to be 14 kN, 16 kN, 18 kN, 16 kN for CRB, CRCB-1, CRCB-2, CRCB-3, respectively. The load–deflection curve for all the specimens by experiment analysis is obtained as per Fig. 19. The maximum deflection is seen in CRCB-2.

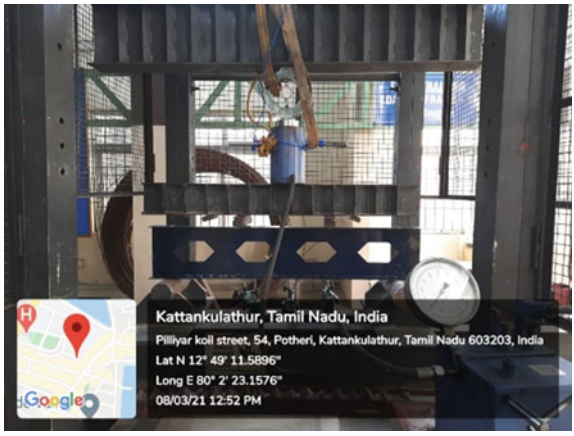

Fig. 16 4-Point loading setup for CRCB-2

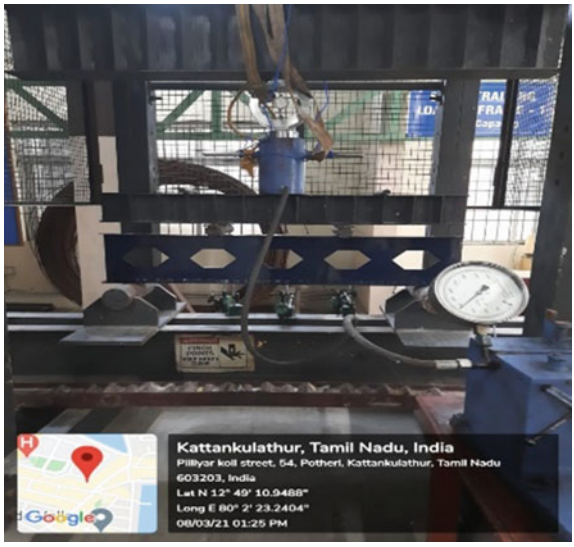

Fig. 17 4-Point loading setup for CRCB-3

5.1.3 Comparison of ANSYS and Experimental Results

The yield point is determined to be 14 kN, 16 kN, 18 kN, 16 kN for CRB, CRCB-1, CRCB-2, CRCB-3, respectively from both experimental and ANSYS results. The load–deflection curve for all the specimens by experiment and ANSYS analysis is shown in Fig. 20. The total deformation comparison between ANSYS and experiment at its yield point is shown in Fig. 21. The local buckling of compression flanges in each specimen is shown in Figs. 22, 23, 24 and 25 for CRB, CRCB-1, CRCB-2, CRCB-3, respectively.

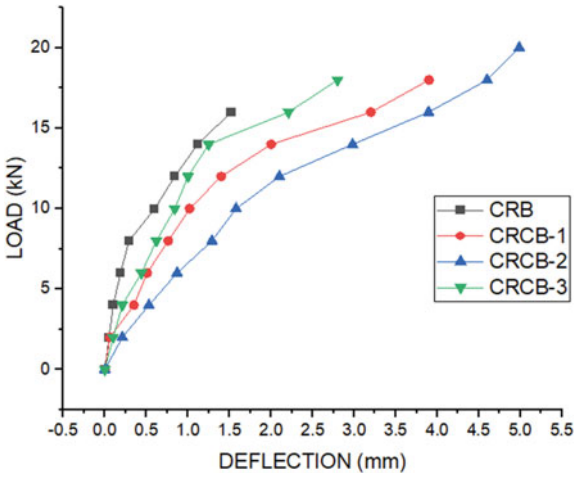

Fig. 18 Comparison of load–deflection curve for CRB, CRCB-1, CRCB-2, CRCB-3 from ANSYS results

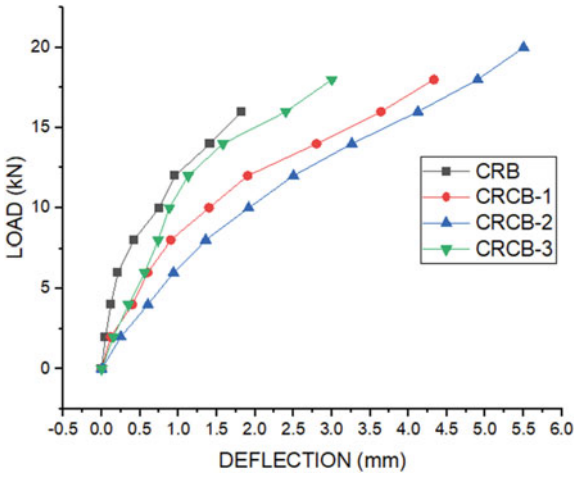

Fig. 19 Comparison of load–deflection curve for CRB, CRCB-1, CRCB-2, CRCB-3 from experimental results

5.1.4 Discussion

In experimental and ANSYS results, the yield state for CRB, CRCB-1, CRCB-2, CRCB-3 is obtained at 14 kN, 16 kN, 18 kN, 16 kN, respectively. Local bucking for CRB, CRCB-1, CRCB-2, CRCB-3 beams is obtained at 16 kN, 18 kN, 20 kN, 18 kN, respectively.

- The total deformation for CBCR-2 is maximum among all specimens. The local buckling was seen in top flange during the plastic state for all specimens, and CBCR-1 had more local buckling since load was applied above the holes.
- Local buckling at bottom flange was seen only during elastic state.

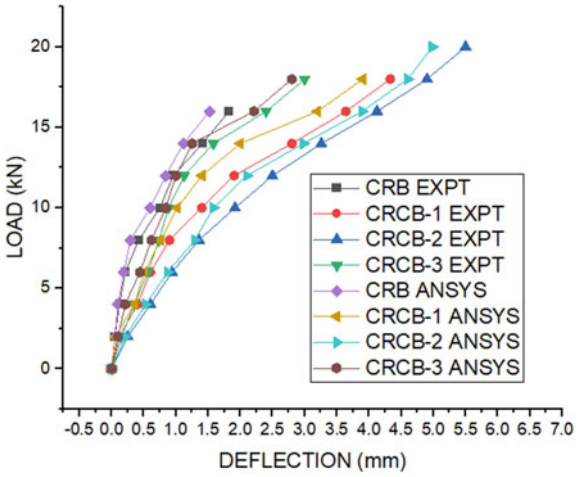

Fig. 20 Comparison of load–deflection for CRB, CRCB-1, CRCB-2, CRCB-3 between ANSYS and experiment

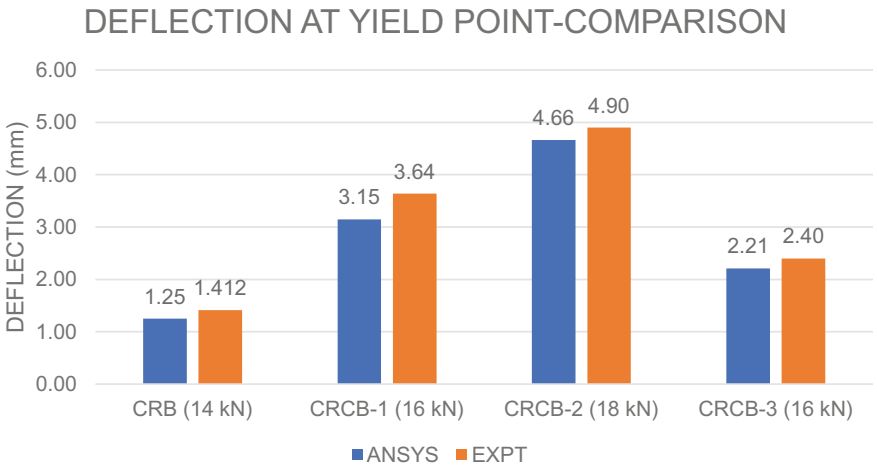

Fig. 21 Comparison of deformation values for CRB, CRCB-1, CRCB-2, CRCB-3 between ANSYS and experiment

- Web crippling in all specimens was observed near the mid-span during elastic state. All the three castellated beam (CRCB) behavior is better than CRB.
- Among the castellated beams, CBCB-2 withstands higher load because of equal spacing and end pitch distance throughout the span. CRCB-1 and CRCB-3 have different end pitches hence they withstand load smaller than beam with CBCB-2.
- End pitch in castellated beam depends upon the required span.

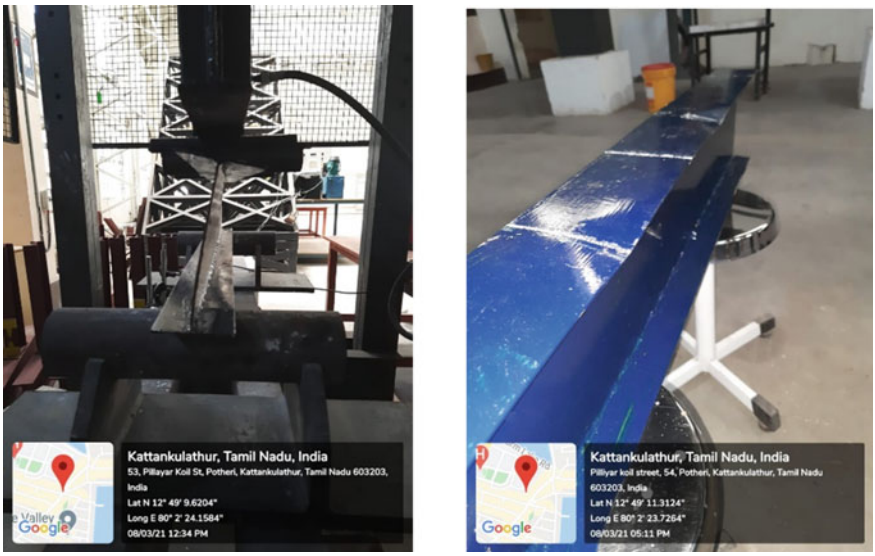

Fig. 22 Local buckling of CRB

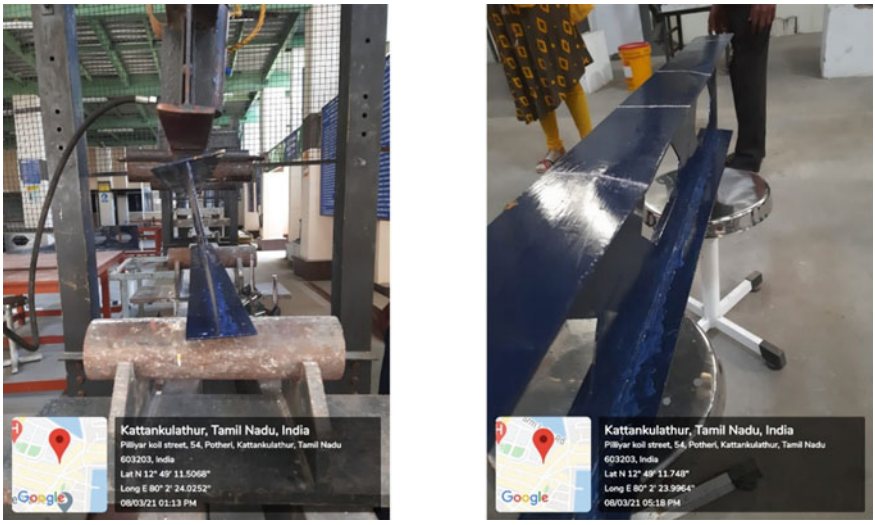

Fig. 23 Local buckling of CRCB-1

- Comparing the ANSYS and experimental results, the total deformation is 2% higher in experimental results.
- The maximum stress concentration is seen near the hexagonal perforations formed due to castellation in CRCB-1, CRCB-2, CRCB-3.

Fig. 24 Local buckling of CRCB-2

Fig. 25 Local buckling of CRCB-3

- Increase in depth of section increases the load-bearing capacity and deformation as obtained in built-up I section and built-up castellated beams.
- To reduce the self-weight of the structure, castellated beams can be used as secondary beams in buildings.

6 Conclusion

The structural performance of castellated beam is studied, and it is more evident that without an increase in self-weight of the structure, the depth is increased. This castellated beams can be even more effectively designed considering the factors like span, loading and depth required. From this analysis, it was observed that as the depth of opening increases, stress concentrations increase at the hole corners and at load application point. The results also confirm that the flexural stiffness of the castellated beams decreases as the depth of opening increases. Finally, the performance and benefits of castellated beam are understood, and this can be used in general construction practice as secondary beams to reduce the self-weight for structure.

References

1. Kerdal D, Netercot DA (1984) Failure modes for castellated beams. J Constr Steel Res 4:295–315
2. Jamadar AM, Kumbhar PD (2015) Parametric study of castellated beam with circular and diamond shaped openings. Int J Eng Innov Technol (IJEIT) 2(2):715–722
3. Morkhade SG, Shaikh S, Kumbhar A, Shaikh A, Tiwari R (2018) Comparative study of ultimate load for castellated and plain-webbed beams. Int J Civil Eng Technol (IJCIET) 9(8):1466–1476
4. Wakchaure MR, Sagade AV, Auti VA (2012) Parametric study of castellated beam with varying depth of web opening. Int J Sci Res Publ 2(8):287–292
5. Pachpor PD, Dr Mittal ND, Dr Gupta LN, Dr Deshpande NV (2011) Finite element analysis and comparison of castellated & cellular beam. Adv Mater Res 264–265:694–699.
6. Wakchaure MR, Sagade AV (2012) Finite element analysis of castellated steel beam. Int J Eng Innov Technol (IJEIT) 2(1):365–371
7. Morkhade SG, Lokhande RS, Gund UD, Divate AB, Deosarkar SS, Chavan MU (2020) Structural behaviour of castellated steel beams with reinforced web openings. Asian J Civil Eng
8. Shaikh AS, Aher HR (2015) Structural analysis of castellated beam. Int J Recent Technol Mech Electric Eng (IJRMEE) 2(6):081–084
9. Aglan AA, Redwood RG (1974) Web buckling in castellated beams, pp 307–320
10. Boyer JP (1964) Castellated beam–new developments. AISC Natl Eng Conf, AISC Eng J 3:106–108
11. Gandomi AH, Tabatabaei SM, Moradian MH, Radfar A, Alavi AH (2011) A new prediction model for the load capacity of castellated steel beams. J Constr Steel Res 67:1096–1105
12. Soltani MR, Bouchair A, Mimoune M (2012) Nonlinear FE analysis of the ultimate behavior of steel castellated beams. J Constr Steel Res 70:101–114
13. Ellobody E (2011) Interaction of buckling modes in castellated steel beams. J Constr Steel Res 67:814–825
14. Zirakian T, Showkati H (2006) Distortional buckling of castellated beams. J Constr Steel Res 62:863–871
15. Redwood R, Demirdjian S (1998) Castellated beam web buckling in shear. J Struct Eng 124:1202–1207

Effect of Elevated Temperature on Flexural Behaviour of Prestressed Concrete Beam

Bandari Shanmukha Teja and T. M. Jeyashree

1 Introduction

Prestressed concrete is a structural member that allows for predetermined engineering stresses to be placed in members to counteract the stresses due to applied loading. It combines the high-strength compressive properties of concrete with the high tensile strength of steel. The steel includes tendons and strands that are most commonly made of high tensile steel. Prestressed concrete members are widely used as they allow longer spans and reduced structural thickness when compared with simple reinforced concrete. Typical applications include high-rise buildings, foundation systems, residential slabs, bridge and dam structures. The present study deals with the analytical investigation of prestressed members subjected to elevated temperatures [1, 2]. Exposure of prestressed members to fire results in crack development and concrete spalling, which further results in strength degradation [3, 4]. Beam components have good fire resistance for 20–30 min, and then the members are damaged resulting in failure of members. The present study deals with the analysis of posttensioned beam subjected to elevated temperature using the software ABAQUS. The aim of the study is to understand the effect of parameters such as clear cover, fire exposure length and position of fire on the behaviour of prestressed beams.

B. Shanmukha Teja · T. M. Jeyashree (✉)
Department of Civil Engineering, SRM Institute of Science and Technology, Tamil Nadu, Kattankulathur 603203, India

K. S. Satyanarayanan et al. (eds.), *Sustainable Construction Materials*, Lecture Notes in Civil Engineering 194, https://doi.org/10.1007/978-981-16-6403-8_18

2 Analytical Investigation

The model considered for the study is developed using the software ABAQUS. The software helps in a detailed investigation of the flexural behaviour of the selected prestressed beam for analysis [5]. The beam considered is subjected to posttensioning. Coupled temperature analysis is performed with beam subjected to the transient state of temperature. The prestressed beam considered is exposed to an elevated temperature of 600° with nominal live load, and the behaviour of the members is studied.

2.1 Validation of the Model

The model is selected for validation as per the selected literature [6]. The model is a prestressed beam with a single tendon included in it. The work carried in the literature was to determine the flexural behaviour of the posttensioned beam. The dimensions of the beam were 400 × 300 mm with a length of 2000 mm. The diameter of the tendon was 15.4 mm provided at the centre of the beam. Four bars with a diameter of 12 mm were used for main steel reinforcement; bars of 10 mm were used for distribution with a spacing of 200 mm c/c. The ends of the beam were simply supported. The concentrated force of 1000 kN was applied at the selected points of the member. Static, general analysis was performed on the model. The maximum displacement obtained from the analysis is 0.58 mm, and a maximum displacement of 0.6 mm was obtained in the selected literature [7]. The percentage of error is 3% and the parametric study is carried out further. Figure 1 shows the displacement obtained from analysing the model.

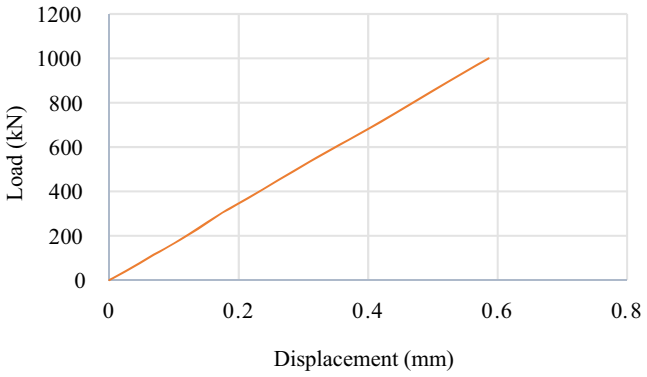

Fig. 1 Load (vs) displacement curve

Table 1 Properties of the material

Description	Concrete	Steel
Modulus of elasticity	31,000 N/mm^2 [a]	205,000 N/mm^2
Poisson's ratio	0.16	0.33
Density	2400 kg/m^3	8050 kg/m^3
Specific heat	1100 J/kg°C	767.55 J/kg°C
Conductivity	0.9152 W/mK	31.3 W/mK

[a] Value varies with temperature

2.2 Finite Element Analysis

An analytical investigation is carried out on prestressed beams of size 400 mm × 250 mm with a length of 2500 mm. Three tendons are provided in the beam. The beam is simply supported at both ends. The temperature-dependent properties of steel and concrete are assigned according to the codal provisions suggested in the Eurocode [8]. Specific heat and thermal conductivity of concrete and steel play a key role in the analysis. The assembly of the individual components is done and the interaction is provided for steel tendons with concrete as a host material. The beam is subjected to a nominal live load of 3 kN/m^2. Coupled temperature analysis is performed with a temperature of 600 °C for 4 h and the behaviour of the member is studied. The properties used for modelling the prestressed beam are shown in Table 1.

3 Parametric Study

The effect of clear cover, fire exposure length and position on the flexural behaviour of prestressed beams is studied by conducting a parametric study.

3.1 Clear Cover

Clear cover is the minimum distance which is provided between the concrete surface and the reinforcement. When concrete is exposed to high temperature it results in spalling, which will eventually result in loss of strength. So, it is observed that the clear cover plays a key role in the behaviour of the beam. The cover of the beam is varied and the displacement of the beam is investigated. The cover of the beam is increased and decreased by 10 mm with respect to the conventional beam. Coupled temperature analysis is performed on the three beams with a temperature of 600 °C for 4 h and the behaviour of the member is studied.

The variation of displacement with load for the analysed beams is shown in Fig. 2. Table 2 shows the summary of results obtained from the analysis.

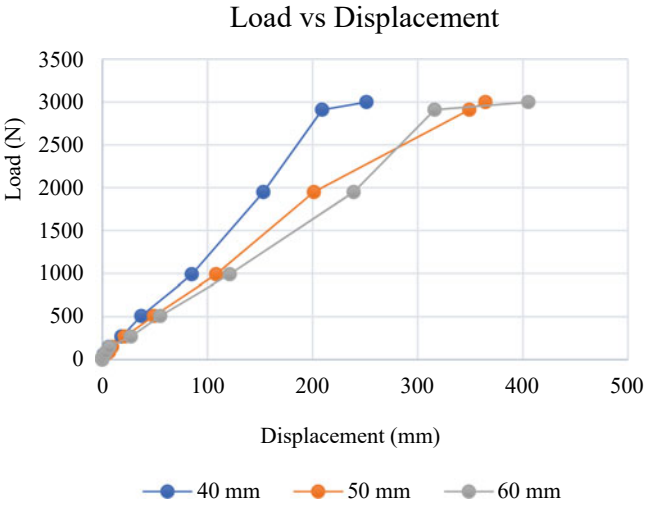

Fig. 2 Load versus displacement graph for varying concrete cover

Table 2 Summary of results by varying the cover

S. no	Clear cover (mm)	Maximum displacement (mm)	Maximum absolute stress (N/mm^2)	Maximum absolute strain
1	40	251	402,161	4.81
2	50	364	384,242	4.3
3	60	405	330,132	3.9

The variation in stress induced into the beam during the analysis and the corresponding strain obtained are shown in Fig. 3. The deformed shape of the beam with a 40 mm cover is shown in Fig. 4.

After performing the coupled temperature analysis, the deformed shapes of the beams are obtained. Figure 5 shows the deformed shape of the beam with a 50 mm cover, and Fig. 6 shows the deformed shape of the beam with a 60 mm cover.

From Figs. 4, 5 and 6, it is observed that the beams are subjected to lateral-torsional buckling due to a combined effect of temperature loading and nominal live load.

3.2 Fire Acting Length and Position

Fire exposure is a key parameter, which affects the displacement and load-carrying capacity of the beam. The higher temperature will result in concrete deterioration and hence results in the formation of creep and eventually results in affecting the reinforcement within the concrete members. It is also observed that the length and

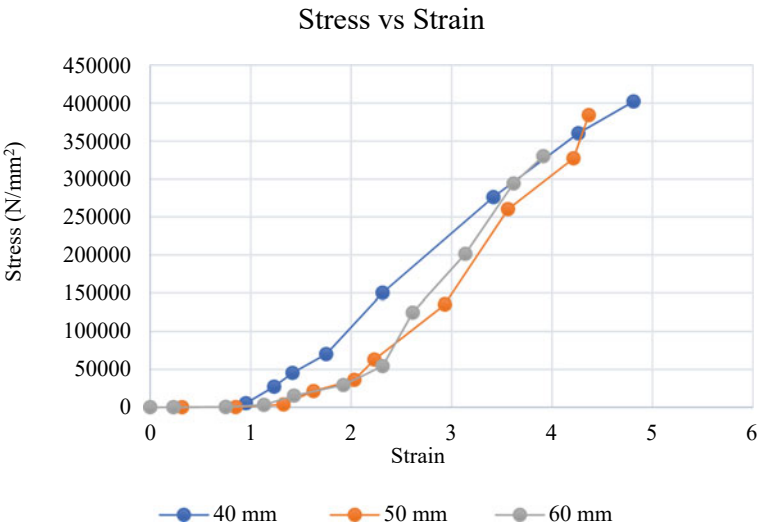

Fig. 3 Stress versus strain graph

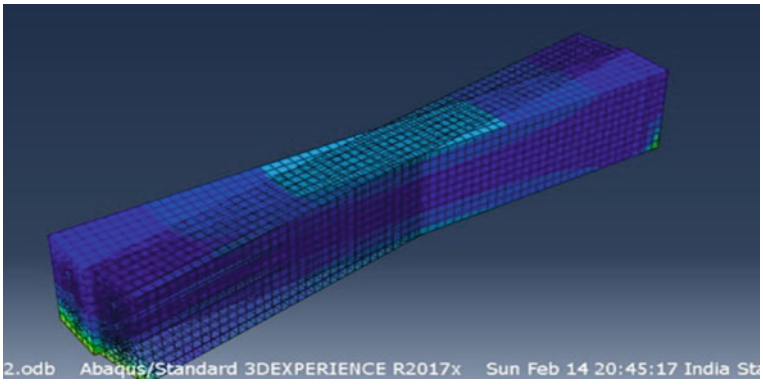

Fig. 4 Deformed shape of the beam with 40 mm cover

Fig. 5 Deformed shape of the beam with 50 mm cover

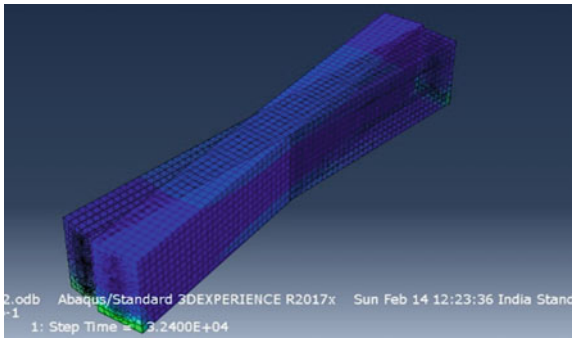

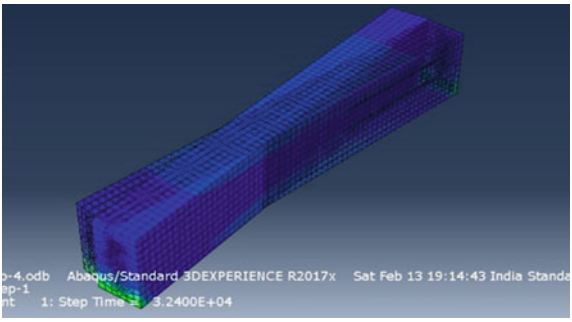

Fig. 6 Deformed shape of the beam with 60 mm cover

Table 3 Summary of results by varying the fire acting length and position

S. no	Type of fire exposure	Maximum displacement (mm)	Maximum absolute stress (N/mm^2)	Maximum absolute strain
1	Total bottom region	364	384,242	4.3
2	Half of the bottom region	149	314,235	3.7
3	One side of the beam	195	360,132	1.9
4	Two sides of the beam	88	416,131	5.14

portion of the beam exposed to fire will also affect the displacement of the beam. The beam considered for the study is exposed to four variations of fire based on length and position of acting. The summaries of results obtained from the analysis are shown in Table 3.

The variation of displacement with load for the analysed beams is shown in Fig. 7. The stress induced into the beam during the analysis and the corresponding strains obtained are shown in Figs. 8, 9 and 10, which show the deformed shapes of the beams with fire acting in the total bottom region and half of the bottom region, respectively.

Figures 11 and 12 show the deformed shapes of the beams with fire acting on one side and fire acting on two sides, respectively. Beams are subjected to various types of buckling due to the change in fire exposure length and position.

4 Results and Discussion

The prestressed beam is subjected to elevated temperature, and coupled temperature analysis is performed on it. The main parameters like clear cover, fire exposure length and position are studied. It is observed that the maximum displacement is varying with cover; a beam with 60 mm has higher displacement. The maximum

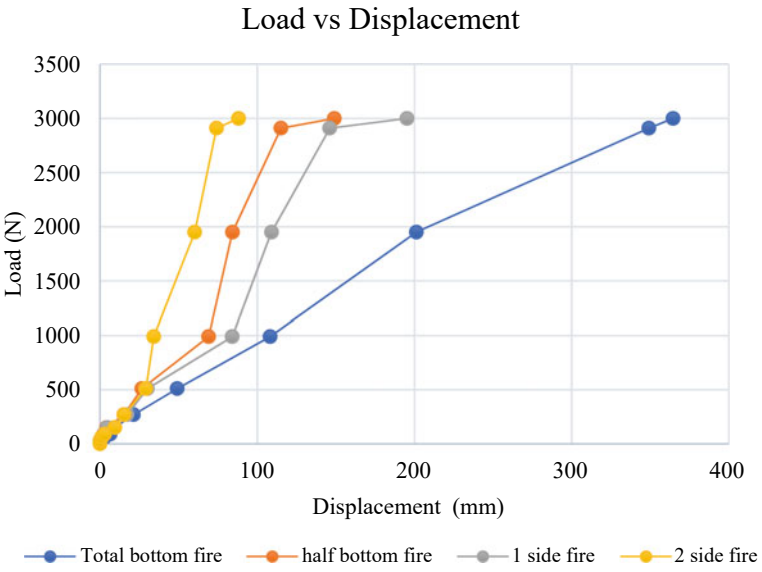

Fig. 7 Load versus displacement graph

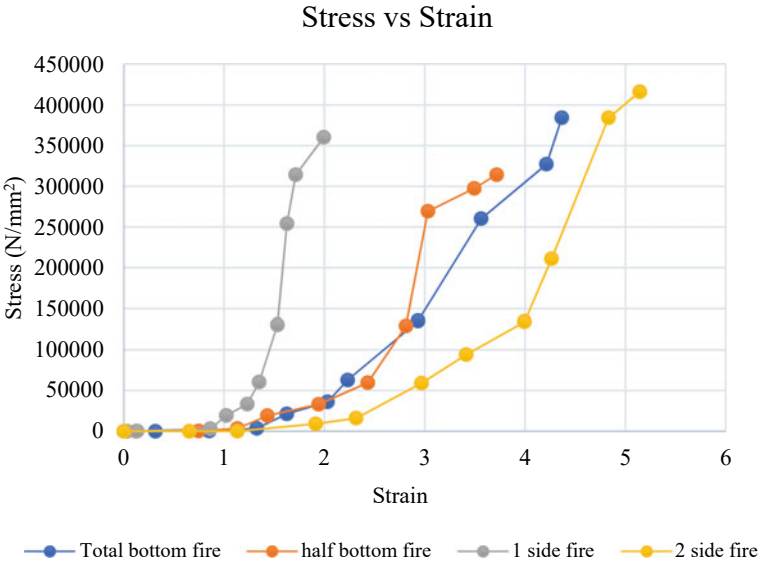

Fig. 8 Stress versus strain graph

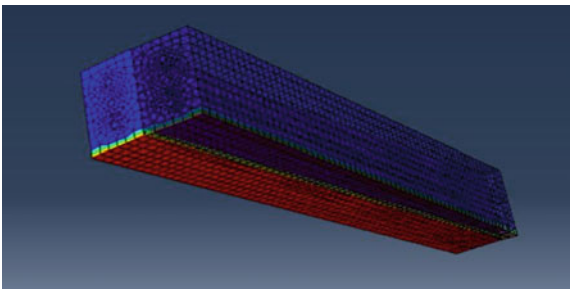

Fig. 9 Beam with total bottom fire

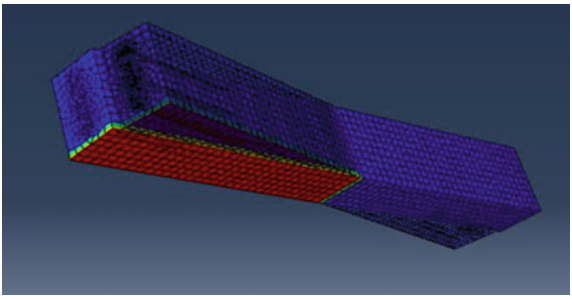

Fig. 10 Beam with half of the bottom fire

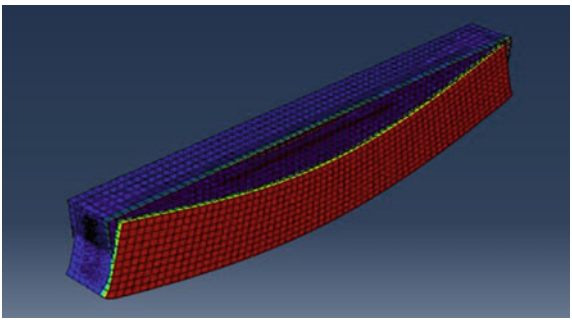

Fig. 11 Beam with fire on one side

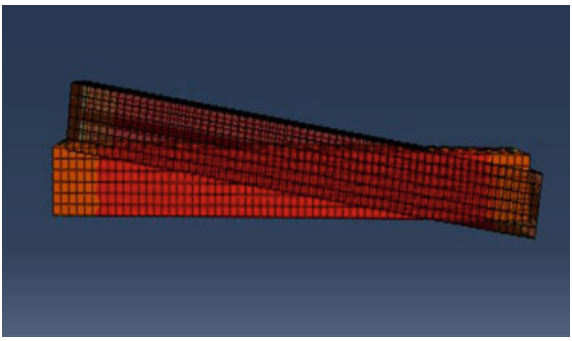

Fig. 12 Beam with fire on two sides

absolute stress is higher for 40 mm and lesser for 60 mm. The beam with 50 mm cover carries 4% less and 14% more maximum absolute stress than the beams with 40 mm and 60 mm cover, respectively. The beam with a 40 mm cover has a higher strain than the beams with a 50 mm or 60 mm cover. The beam with 50 mm cover carries 10% less and 9% more maximum absolute strain than the beams with 40 mm and 60 mm cover, respectively. By varying the fire to half of the bottom length, the maximum displacement was 149 mm. The beam with fire exposure on the one side has 195 mm maximum displacement and the beam with fire on two sides has a very less maximum displacement of 88 mm. The conventional beam with a 50 mm cover has higher displacement, i.e., 364 mm than beams with different fire exposure patterns. The beams with half of the bottom fire exposure, one side of fire exposure and two sides of fire exposure have 59%, 46% and 75% less maximum displacement, respectively, than the beam with the full bottom exposed to fire. The conventional beam selected for the study has less maximum stress of 384,242 N/mm^2. The beam with the full bottom exposed to fire carries 18% and 6% more, 8% less maximum absolute stress than the beams with half of the bottom fire exposure, one side of fire exposure and two sides of fire exposure, respectively. The values of strain are higher for the beam which is exposed to fire on two sides than the beam exposed to fire with other patterns. These parameters have a significant impact on the behaviour of the beam when they are exposed to high temperature.

5 Conclusion

- The beam with a 40 mm cover has a maximum displacement of 40% less and a 60 mm cover has 10% more, respectively, than the beam with a 50 mm cover. Hence it is inferred that with the decrease in clear cover the maximum displacement of the prestressed beam decreases.
- The beam with the full bottom exposed to fire carries 13 and 55% more maximum absolute strain than the beams with half of the bottom fire exposure and one side of fire exposure and 16% less than the beam with two sides of fire exposure, respectively. It can be noticed that the beam exposed to fire on two sides has minimum displacement and maximum strain. From this, it is inferred that the beam has reached its plastic stage and failure can occur as the fire exposure time increases.

References

1. Bamonte P, Kalaba N, Felicetti R (2018) Computational study on prestressed concrete members exposed to natural fires. Fire Saf J 97:54–65
2. Rozsypalova I, Schmida P, Danek P (2016) Determining the condition of reinforced and prestressed concrete structures damaged by elevated temperatures. In: 18th international conference on rehabilitation and reconstruction of buildings, pp 120–126

3. Gao WY, Dai JG, Teng JG, Chen GM (2013) Finite element modelling of reinforced concrete beams exposed to fire. Eng Struct 488–501
4. Albero V, Saura H, Hospitaler A, Montalva JM, Romero ML (2018) Optimal design of prestressed concrete hollow core slabs taking into account its fire resistance. Adv Eng Soft 122:81–92
5. Liua X, Yua C, Quan W, Chen L (2019) Inspection, materials testing and field testing of a prestressed concrete box bridge after fire exposure. Fire Saf J 108
6. Ankith MK, Jayaramappa N, Kiran T (2018) Flexural behaviour of post tensioned beam. Int J Sci Eng 9
7. Choi I-R, Chung K-S, Kim D-H (2014) Thermal and mechanical properties of high-strength structural steel HSA800 at elevated temperatures. Mater Des 63:544–551
8. EN 1992–1–2 (2004) (English): Eurocode1, 2: Design of concrete structures-Part 1–2: General rules-Structural fire design

Effect of Strength Parameters Upon Partial Replacement of Moderately Burnt and Completely Burnt Sugarcane Bagasse Ash

P. J. R. L. P. Susmitha and M. Kanta Rao

1 Introduction

Manufacturing of ordinary portland cement leads to the greenhouse effect due to the emission of CO_2 gas. Production of one tonne OPC resulted in 1.1 tonne emission of CO_2, and due to the increase of greenhouse gases, the mean global surface temperature had inclined by 0.7 °C [1]. Sugarcane is a commercial crop that abundantly grows in a tropical climate. Bagasse is a waste product that can be obtained after extracting sugar. After the controlled burning of this waste product, the particulate matter obtained was termed as bagasse ash and studied that the increase of compressive strength by 12% was observed at 5% replacement of bagasse ash when compared to the normal concrete [2]. In the production of sugarcane, India owns second place which resulted in the production of a large quantity of bagasse ash which needs area to large extent for its disposal [3]. The industrial revolution resulted in rapid and continuous production of sugar which resulted in the formation of bagasse in huge amounts. The ash precipitated after the burning of bagasse may induce ecological imbalances [4]. Bagasse ash comprises non-combustible matter, oxides of silica, alumina and calcium. The ash obtained directly from the mill will be inert due to the burning process involved with temperatures that are not controllable [5]. Free lime present in the concrete result in the formation of CSH gel which is responsible for the enhancement of mechanical properties of the blended concrete and sound resistance of chloride diffusion and the suitability of using this ash as a viscosity altering agent in the blended concrete was investigated [6, 7]. Controlled combustion of bagasse resulted in bagasse ash and made as a pozzolanic material. The suitability of using this ash as a viscosity altering agent in the blended concrete was investigated and

P. J. R. L. P. Susmitha (✉) · M. K. Rao
Department of Civil Engineering, V. R. Siddhartha Engineering College, Vijayawada, AP 520007, India

M. K. Rao
e-mail: mkrao99ce@vrsiddhartha.ac.in

K. S. Satyanarayanan et al. (eds.), *Sustainable Construction Materials*, Lecture Notes in Civil Engineering 194, https://doi.org/10.1007/978-981-16-6403-8_19

noticed that the compressive strength was inclined by 13% by replacing 20% finely ground ash in the concrete [8].

Because of the finer particle size, pore solution and total porosity of the blended concrete was lowered compared to normal concrete and the later strength was induced by the reaction of silica with the portlandite which is a pozzolanic activity [9, 10]. The mechanical properties of concrete can be influenced by the type and quantity, quality of secondary cementitious material and the curing age adopted [11]. Hydrates of silica are responsible for the enhancement of mechanical properties in the concrete and observed that optimum replacement of 15% in conventional concrete and 5% in lightweight concrete and 10% in self-compacting concrete proportionally enhanced the concrete performance [12, 13]. The SCBA samples were collected at different temperatures 600 and 900 °C. As per the standards of ASTM C 618, the loss of ignition of supplementary particle should be less than 6% [14, 15]. The ash from sugarcane has the ability to utilize the CH gel which may increase with the fineness of ash and the reactivity of ash can be enhanced using grinding [16]. As mentioned above there is confinement for the utilization of bagasse ash in order to meet the strength and durability requirements. The main aim of this research is to represent the experimental results and the effect on strength and durability parameters by the incorporation of bagasse ash in concrete and its microstructural changes that lead to change in the mechanical properties.

2 Experimental Program

2.1 Materials

Ordinary portland cement of 53 grade confirming to the codal specifications of IS: 12,269–1987 and coarse aggregate of 12, 20 mm size were considered. Locally available river sand was used as fine aggregate which confirms the codal specifications of IS 383 (1970) along with the potable water were utilized in the concrete production. The source of SCBA was K.C.P. Sugar and Industries Corporation LTD, Vuyyuru, Vijayawada. SCBA comprises 50% cellulose, 25% hemi-cellulose and 25% lignin. By producing one tone sugarcane, 26% of bagasse was obtained with 0.62% residual ash at 50% moisture content. Bagasse ash was combusted at a controlled temperature of 1000 °C in a muffle furnace at A.P.H.M.E.L at Autonagar, Vijayawada. Bagasse ash that was moderately burnt was designated as (SCBA1) and the ash that completely burnt was termed as (SCBA2). The chemical composition of cement and bagasse ash was tabulated in Table 1. The specific gravity of cement was 3.15. The fineness of cement considered was 2240 cm^2/g and of SCBA using Blane's apparatus was 1167.7 cm^2/g. The physical properties of fine and coarse aggregate were tabulated in Table 2. The mix proportions and quantities of cement, fine and coarse aggregate, bagasse ash for the water/binder ratio (W/B) of 0.42 were tabulated in Table 3.

Table 1 Chemical composition of OPC and SCBA1, SCBA2

Composition (%)	SiO_2	Al_2O_3	CaO	Fe_2O_3	MgO	SO_3	Na_2O	K_2O	Cl^-	LOI
OPC	21.23	6.45	62.5	3.2	1.45	1.57	0.23	0.25	0.12	2.32
SCBA1	61.2	6.1	13.3	5.7	2.1	….	4.3	3.4	…	2.5
SCBA2	72.4	6.5	4.2	3.6	2.4	….	1.4	3.9	…	4.0

Table 2 Physical properties of aggregates

Property	Fineness	Specific gravity
Coarse aggregate	2.85	2.73
Fine aggregate	7.12	2.65

Table 3 Mix proportions

% of replacement	Bagasse ash (kg)	Cement (kg)	Coarse aggregate (kg)	Fine aggregate (kg)	Water (kg)
0	0	380	1244.16	638	160
5	19	361	1155.2	577.6	160
10	38	342	1094.4	547.2	160
15	57	323	1036.8	516.8	160
20	76	304	972.8	486.4	160
25	95	285	912	456	160
30	114	266	851.2	425.6	160
35	133	247	790.4	395.2	160
40	152	228	729.6	364.8	160

Note Same mix proportions were used for both SCBA1 and SCBA2

The mineral composition of SCBA was studied through the X-ray diffraction technique. X'pert pro diffractometer was used in this test with X-ray tubes comprising Cu anode. The scanning speed was 5°/min with a minimal step of 0.5°. The scan range was 3–90° with voltage being 40 kV and a current of 15 mA was used to perform the test. Quartz which comprises a high amount of silica was identified majorly. The highest peak was obtained between 20° and 30° (2θ) which indicates the existence of unstructured content in the SCBA1 which induces the pozzolanic activity. The existence of crystalline structure was also confirmed between the range of 10° and 30° (2θ) for SCBA2. During the combustion process, the reactive unstructured silica present in the SCBA1 induced pozzolanic action. Due to the presence of high amounts of silica and alumina which react with portlandite (CH) and consume it considerably, this also coexisted in the preceding findings. The chemical composition and the peak presence of SCBA1 and SCBA2 were plotted in Fig. 1, respectively. Due to the combustion of bagasse ash, a crystalline structure was induced during the pozzolanic reaction which occurs at the hydration stage. The chemical composition and the peak

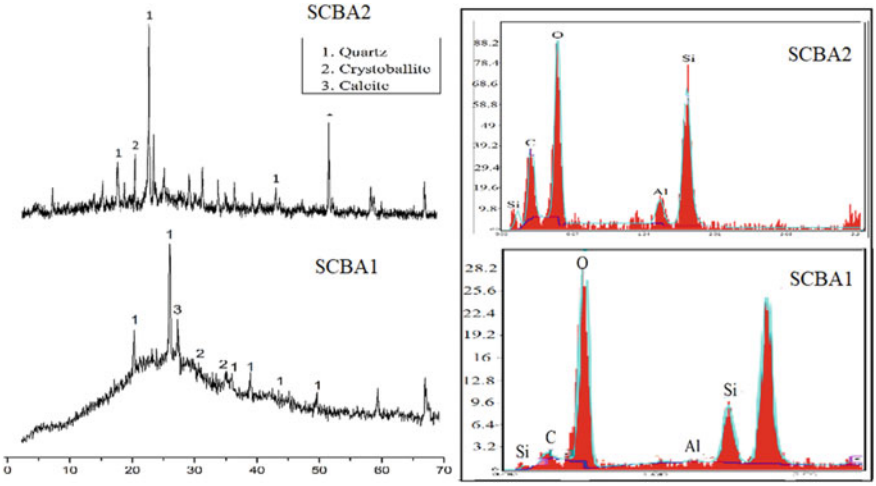

Fig. 1 XRD and EDS analysis of SCBA1 and SCBA2

presence of SCBA1 and SCBA2 were plotted in Fig. 1. It was evident that the presence of quartz (SiO_2) was 12.8% in SCBA1 which increased to 68.6% in SCBA2.

2.2 Methods

In order to determine the hardened properties of blended concrete, the specimens of 100 × 100 × 100 mm size were cast to determine the compressive strength as per the IS: 516:1959 code, cylinders of 150 × 300 mm as per the IS 5816 (1999) code along with prisms of 100 × 100 × 150 mm were cast for flexural strength test as per the codal provisions of IS: 516:2002 code in order to perform the following strength and durability tests after the curing age of 28 days.

3 Results and Discussion

3.1 Compressive Strength

The compressive strength of specimens was performed as per the codal provisions of IS: 516:1959. The loading capacity of the compression testing machine was 300 kN per minute. The resistance offered by the specimen divided by the cross-sectional area of the specimen at the failure load was considered to be the strength of the specimen and the compression test results for SCBA1 and SCBA2 replacement were plotted in Fig. 2. At all replacement proportions, the compressive strength

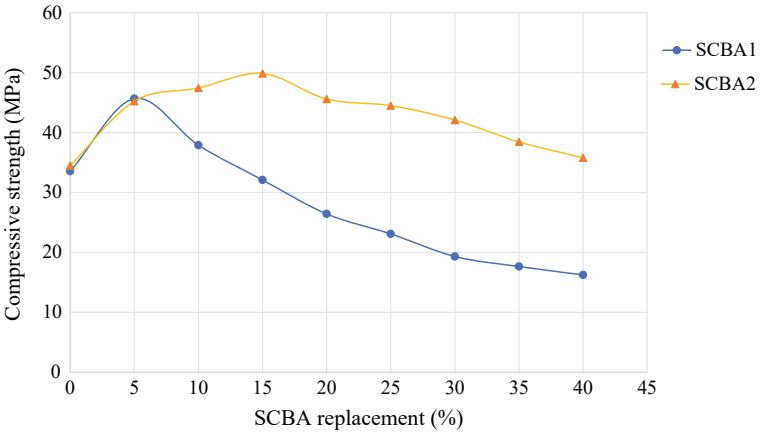

Fig. 2 Compressive strength

of completely burnt ash resulted in the maximum compressive strength was noticed at 15% replacement for the completely burnt bagasse ash (SCBA2), and for partially burnt bagasse ash (SCBA1) the maximum strength was noticed at 5% replacement. Due to the combustion of bagasse at high temperature, pozzolanic properties were induced predominantly which resulted in higher compression strength because of the dense bond between the binder and the aggregates. The use of sections to divide the text of the paper is optional and left the decision to the author. When the author wishes to divide the paper into sections, the formatting shown in Table 2 should be used.

3.2 Split Tensile Strength

In order to determine the tensile strength of concrete indirectly, this test was performed which is also termed as diametric compression test. According to the codal provisions of IS: 5816 (1999) in which 150 mm × 300 mm height cylinders were used. The test results were plotted in Fig. 3. For completely burnt ash, the strength obtained at all replacement proportions was relatively higher than the strength of the control specimen. Upon replacing the SCBA1, the maximum strength attained was 3.43 MPa and the strength increment for SCBA2 was continued up to the replacement of 40%.

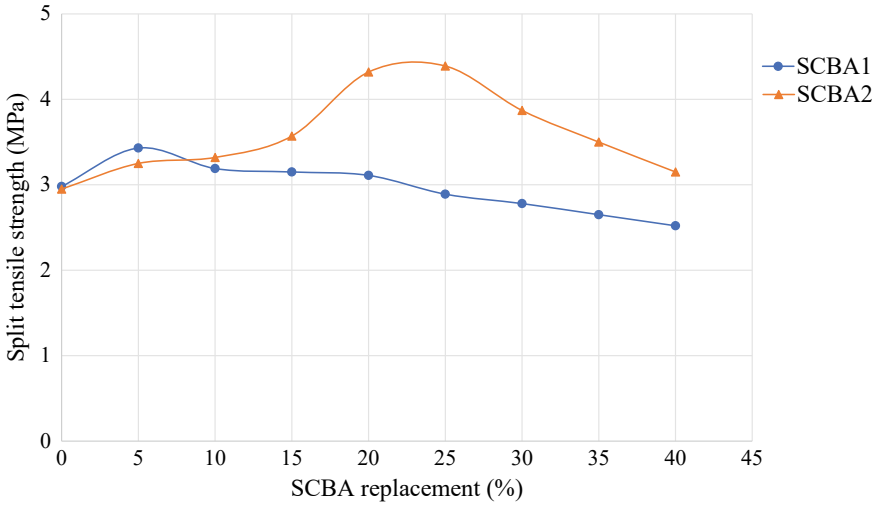

Fig. 3 Split tensile strength

3.3 Flexural Strength

This test is also termed as standard beam test as per the codal specifications of IS: 516:2002 which was performed on prisms of 100 × 100 × 500 mm size. The span of the beam to be placed while testing was 400 mm and the loading is applied on the specimen. The rate of loading was 1.8 kN per minute and continued up to the failure of the specimen. The test results were plotted in Fig. 4. The maximum flexural strength was noticed at 5% for moderately burnt ash (SCBA1), and for SCBA2 the strength increment was continued up to the replacement of 30%.

3.4 Durability

3.4.1 Acid Attack

After the completion of curing, the completely burnt ash blended specimens were immersed in water with 2% concentrated sulphuric acid for a period of 60 days according to the codal provisions of ASTM C1898-20. After the immersion period, the specimens were weighed and a compressive strength test for the specimens was performed in order to determine the loss of strength due to the acid attack. The test results were plotted in Fig. 5. For the control specimen, the maximum percentage of strength loss was observed for both mixes. The loss of strength was minimum for SCBA2 when compared to SCBA1 at all replacement proportions. Minimum loss

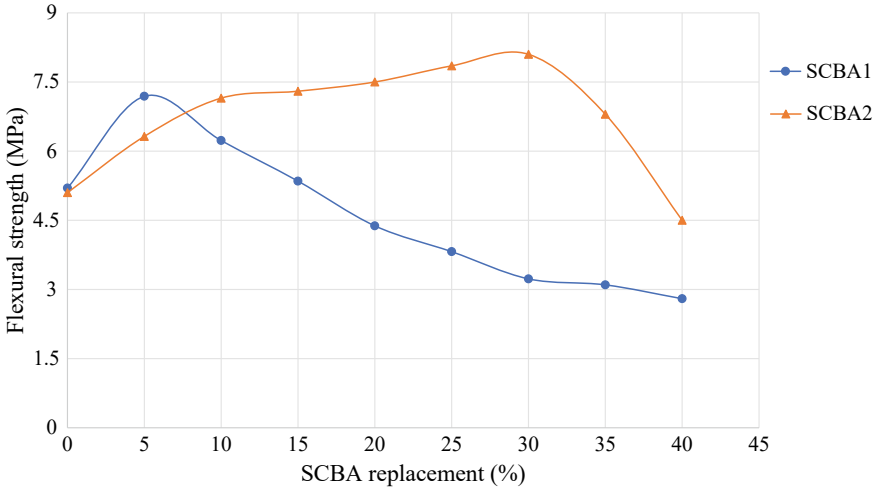

Fig. 4 Flexural strength

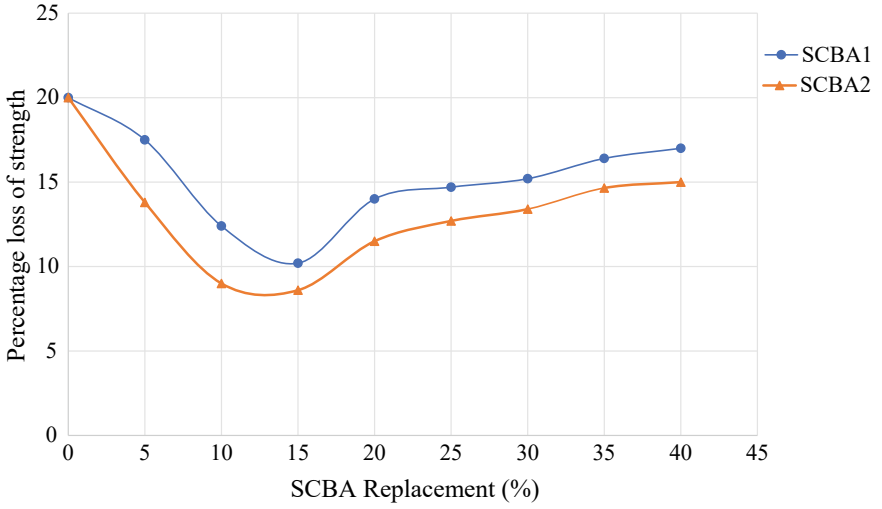

Fig. 5 Acid attack

percentage was observed for 15% replacement in case of SCBA2 due to the precipitation of sulphate ions on the cementitious matrix was declined with the replacement of bagasse ash because of the absence of CH gel which gets consumed by the pozzolanic action. With the continuous increase of SCBA2, the percentage loss of strength was further increased because of the excessive presence of CSH gel but it was less compared to SCBA1.

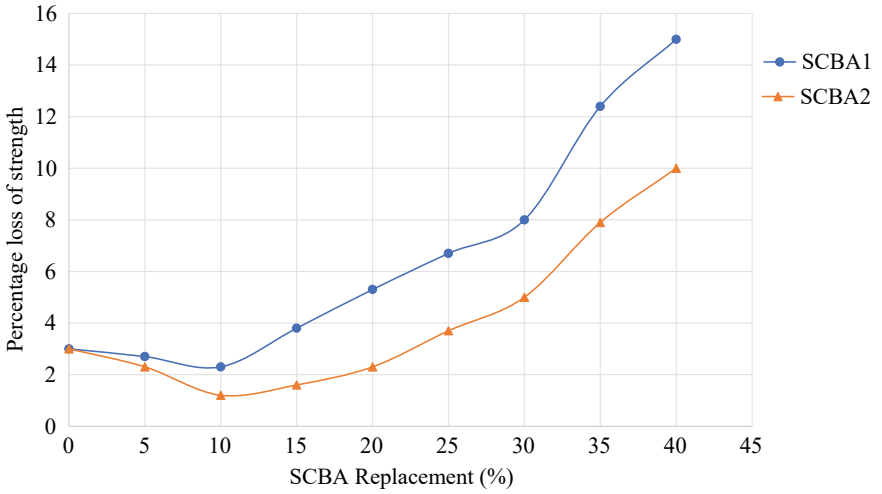

Fig. 6 Alkaline attack

3.4.2 Alkaline Attack

After the completion of curing, the completely burnt ash-blended specimens were immersed in 2% sodium sulphate for 60 days as per the codal provisions of IS: 9103 (1999). The specimens were subjected to a compressive strength test and weighed after the completion of the immersion period and the test results were plotted in Fig. 6. Percentage loss of strength was more in the case of SCBA1 when compared to SCBA2. The percentage of strength loss for SCBA2 continued to decrease up to 20% replacement because of the presence of silica in abundant quantity. Beyond that replacement, the percentage of strength loss was increasing because of the excessive presence of CSH gels which access the diffusion of ions through it and enhance the impact of an alkaline attack.

3.4.3 RCPT Test

This test involves assessing the migration of chloride ions through the bagasse blended concrete specimen at 28 days. The test cell consists of two chambers in which one of the chambers was filled with sodium hydroxide of 0.3 M and the other chamber was filled with 3% NaCl solution. The chloride concentration was thoroughly checked by titration analysis using $AgNO_3$ solution. From the test result (Fig. 7), it was found that the chloride diffusion was declined by the incorporation of SCBA2 when compared to the control specimen and SCBA1. The chloride diffusion was minimum at 20% replacement proportion because of the reduced pore size

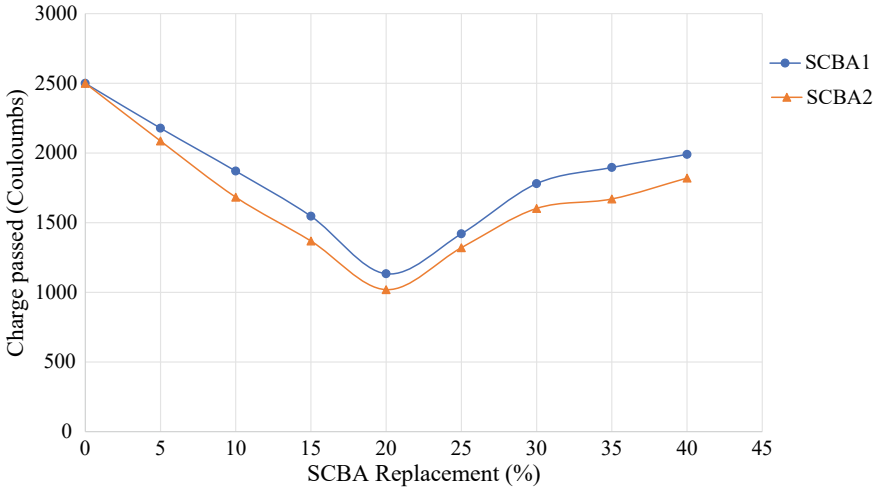

Fig. 7 RCPT results

by the active binding action induced from SCBA2. From the microstructural view, an increase in silica content thoroughly reduced the portlandite formation and thus cause the migration of chloride ions as well.

4 Conclusion

- Combustion of bagasse ash at high temperature resulted in crystalline silica which reacts with the CH gel present in cement.
- Incorporation of SCBA1 resulted in maximum compressive strength of 45.67 MPa, while the percentage of incorporation can be enhanced up to 15% in the case of SCBA2 which yielded 49.87 MPa. The filler effect was increased in the blended concrete which reduced the capillary pores and the diffusion of particles resulted in resistance against acid attack.
- The percentage loss of strength was almost negligible for SCBA2 at 10% replacement due to the resistance against diffusion of particles.
- The replacement percentage of SCBA1 was confined to 5%, whereas the SCBA2 can be replaced up to 20% in the binder content.
- The presence of crystalline silica in huge amounts access the incorporation of SCBA2 in the concrete as supplementary material to OPC.

References

1. Magudeswaran PN, George S, John J (2007) Reduction of global warming gas emissions from the manufacture of Portland cement using high volume fly ash concrete. Nat Environ Pollut Technol 6(3):495
2. Mangi SA, Jamaluddin N, Wan Ibrahim MH, Abdul Awal ASM, Sohu S, Ali N (2017) Utilization of sugarcane bagasse ash in concrete as partial replacement of cement. In: IOP conference series: materials science and engineering, vol 271, no 1, p 012001. IOP Publishing
3. Bahurudeen A, Kanraj D, Gokul Dev V, Santhanam M (2015) Performance evaluation of sugarcane bagasse ash blended cement in concrete. Cement Concr Compos 59:77–88
4. Shafiq N, Hussein AAE, Nuruddin MF, Mattarneh HA (2016) Effects of sugarcane bagasse ash on the properties of concrete. In: Proceedings of the institution of civil engineers-engineering sustainability, vol 171, no 3, pp 123–132. Thomas Telford Ltd
5. Amin N-U (2011) Use of bagasse ash in concrete and its impact on the strength and chloride resistivity. J Mater Civ Eng 23(5):717–720
6. Rukzon S, Chindaprasirt P (2012) Utilization of bagasse ash in high-strength concrete. Mater Des 34: 45–50
7. Chindaprasirt P, Kroehong W, Damrongwiriyanupap N, Suriyo W, Jaturapitakkul C (2020) Mechanical properties, chloride resistance and microstructure of Portland fly ash cement concrete containing high volume bagasse ash. J Build Eng 31:101415
8. Javed MF, Amin MN, Shah MI, Khan K, Iftikhar B, Farooq F, Aslam F, Alyousef R, Alabduljabbar H (2020) Applications of gene expression programming and regression techniques for estimating compressive strength of bagasse ash-based concrete. Crystals 10(9):737
9. Xu Q, Ji T, Gao S-J, Yang Z, Wu N (2019) Characteristics and applications of sugar cane bagasse ash waste in cementitious materials. Materials 12(1):39
10. Chusilp N, Jaturapitakkul C, Kiattikomol K (2009) Utilization of bagasse ash as a pozzolanic material in concrete. Constr Build Mater 23(11):3352–3358
11. Zareei SA, Ameri F, Bahrami N (2018) Microstructure, strength, and durability of eco-friendly concretes containing sugarcane bagasse ash. Constr Build Mater 184:258–268
12. Sireesha G, Kanta Rao M, Kanta Rao P (2013) An experimental study on strength properties of concrete when cement is partially replaced with sugar-cane bagasse ash. IOSR J Mech Civil Eng 35–38
13. Torres Agredo J, Mejía de Gutiérrez R, EscandónGiraldo CE, González Salcedo LO (2014) Characterization of sugar cane bagasse ash as supplementary material for Portland cement. Ingeniería e Investigación 34(1): 5–10
14. Pourkhorshidi AR, Najimi M, Parhizkar T, Jafarpour F, Hillemeier B (2010) Applicability of the standard specifications of ASTM C618 for evaluation of natural pozzolans. Cement Concr Compos 32(10):794–800
15. Berenguer RA, Capraro APB, de Medeiros MHF, Carneiro AMP, De Oliveira RA (2020) Sugar cane bagasse ash as a partial substitute of Portland cement: effect on mechanical properties and emission of carbon dioxide. J Environ Chem Eng 8(2):103655
16. Cordeiro GC, Kurtis KE (2017) Effect of mechanical processing on sugar cane bagasse ash pozzolanicity. Cem Concr Res 97:41–49

Comparison of Energy Analysis in a Residential Building Using Building Information Modeling

Injarapu Chaarvika, Ayush Bhatnagar, Rohit Sammeta, M. Balasubramanian, and R. Monisha

1 Introduction

In this research, the analysis of energy efficiency and its advantages in residential buildings using different materials as a substitute of cement which are more economical and eco-friendlier are mentioned. The energy analysis for a G+2 residential building taking different wall infill materials that satisfy the required standards [1] proposed an energy analysis for a G+2 building using the BIM tool. They did the energy analysis for different zones in India. They found different operational parameters like set point, heating, cooling by providing different design parameters like glazing type, wall type, roof type, and building orientation. They optimized the building for energy efficiency [2] and examined the impacts of the shape of the building and its orientations for the thermal efficiency of the two-story buildings. They have analyzed three different shaped buildings with 24 orientations for each building to check the thermal comfort of the building [3]. It also needs a large amount of spreading awareness of the advantages of BIM [4] that mainly focuses on using the ancient method to utilize the natural resources and lower the increasing energy usage requirement of a building. The paper fails to talk about optimizing the structure based on the economic factors and availability of the material in the particular area that is selected [5]. It talks on how to enhance the structure's energy by using the authors' in-house software. Various equations simulate the different layers of the walls and the change in the properties depends on the inner wall or external wall. The results are attained where the energy is preserved based on the various changes that include and are not limited to the changes in the window sizes, the ventilation openings, and the material composition of the walls [6]. The paper described the trends of increasing demand for electrical energy and the potential of increasing

I. Chaarvika · A. Bhatnagar · R. Sammeta · M. Balasubramanian (✉) · R. Monisha
Department of Civil Engineering, SRM Institute of Science and Technology, Tamil Nadu, Kattankulathur, India
e-mail: balasubm1@srmist.edu.in

K. S. Satyanarayanan et al. (eds.), *Sustainable Construction Materials*, Lecture Notes in Civil Engineering 194, https://doi.org/10.1007/978-981-16-6403-8_20

the energy efficiency of buildings by using different wall materials. The author also described how BIM had provided a platform for architects and engineers to visualize and analyze the energy efficiency of buildings. The research work was conducted for three different mortar mixes, which included the first mix in which the basalt fiber was not present, the second mix contains basalt fiber of length 5 mm, and the third mix contains basalt fiber of length 12 mm. The flexural strength and compressive strength were tested on the 3rd, 7th, and 28th day using suitable cubes and cylinders containing fiber and without fibers. From this research, the author concluded that the flexural strength of the mortar mixes increased by adding fiber of greater length, but at the same time, the compressive strength got decreased. Basalt fiber with lengths 5 mm and 12 mm decreased the compressive strength by about 5% or 10–15%. The research work in this paper is restricted to up to two tests only, such as flexural and compressive strength tests. Some other tests can also be conducted to find out properties such as porosity, permeability, electrical conductivity, and emissivity to get a broader idea about adding basalt fiber in a mortar [7]. After a 28-day curing period, the effect of the water/binder ratio on the hardened state characteristics of cement mortar was examined. The study is limited to cement mortar testing and mixtures. A comparable research may be conducted to determine the appropriate water/binder ratio for concrete using a similar procedure [8]. The paper discusses how the use of high-quality construction materials with strong thermal characteristics may enhance the energy efficiency of the buildings. The research is being conducted on a sample of energy-efficient buildings in the Czech and Slovak Republics. The sample comprises a variety of new energy-efficient buildings, including single and multi-story structures with or without basements and a variety of building materials. Buildings are powered by a variety of energy sources, including heating, hot water heating, controlled ventilation, cooling, and lighting. The author came to the conclusion that new and contemporary construction materials might help to decrease buildings' energy and environmental consequences. Building materials designed for use in a building outside cladding must have a strong resistance to heat transmission in thin layers. To improve energy performance and minimize greenhouse gas emissions, the amount of natural, recycled, and renewable construction materials must be increased. Building supplies should be acquired and made close to the building site. The reason for this is a reduction in transportation energy [9]. A study was conducted to identify building materials that may optimize a building's energy requirements over its entire life cycle by analyzing both embodied and operational actual material composition and energy usage in a climatically sensitive construction in southern Israel's Negev desert region. It was revealed that the incarnated energy of the building accounted for around 60% of total life cycle energy consumption, which may be considerably decreased by using "alternative" wall infill materials. This material replacement saves approximately 20% of total energy during a 50-year-life lifetime. While the investigated wall systems (mass, insulation, and finish materials) account for a substantial percentage of the building's initial EE, the concrete structure (columns, beams, floor, and ceiling slabs) accounts for approximately half of the building's preuse phase energy. The real building used as the foundation case for this research was constructed using reinforced concrete, cast in situ for external walls and floor and

ceiling slabs. Extruded polystyrene (XPS) is used to cover the concrete walls (and roof), which is a hard foam with closed cells manufactured in a continuous extrusion process and sold locally as Rondopan. The findings of the research also show the significance of a number of additional methodological problems. Because LCA software techniques are currently restricted in their use owing to the size of accessible databases, site-dependence, and so on, identifying significant correlations required a comprehensive local study of material energy characteristics for each building phase investigated [10]. The author discusses how energy retrofitting of existing buildings decreases energy usage during the operating phase, while the usage of extra materials impacts energy usage throughout later life cycle phases of retrofitted structures. The purpose of this study was to examine the life cycle primary energy implications of several material options while upgrading an existing structure to reach high-energy performance requirements. For passive home requirements available in Sweden, the author created retrofitting alternatives assuming the greatest and lowest values of ultimate energy usage, respectively. Thermal enhancement of the building exterior is one of the retrofitting possibilities. The author computed the primary energy used in the operation phase as well as the manufacturing, maintenance, and end-of-life phases (operation primary energy and non-operation primary energy). The findings indicate that the non-operational main energy usage varies substantially based on the materials used for thermal insulation, cladding systems, and windows. Although the operation energy use decreases by 50–62%, they find that the non-operation energy for building retrofitting accounts for up to 21% of the operation energy-saving, depending on the passive house performance and material alternatives. A judicious selection of construction materials may decrease non-operational primary energy by up to 40%, especially when wood is used [11]. The paper described the major energy implications of a multi-story residential structure with various building technologies during its life cycle. The buildings' principal structural elements are precast concrete, cross-laminated timber (CLT), and prefabricated. The study includes energy and material fluxes from several life cycle phases of the building variants, which are meant to fulfill the energy performance requirements of the Swedish building code (BBR) and passive home criteria. CLT and modular structures were shown to use less primary energy and produce more biomass leftovers than concrete buildings. The heating value of the recoverable biomass leftovers from the CLT building's production phase is substantially more than the primary energy required for its creation. Primary energy usage for production and construction accounts for 20–30% and 36–47% of total primary energy usage for production, respectively, BBR and passive building construction, space heating, ventilation, and deconstruction. Space heating using combined heat and power (CHP) and ventilation electricity for the BBR and passive building variants account for 70–79% and 52–63% of total primary energy usage for production, respectively, while construction, space heating, ventilation, and deconstruction for an 80-year lifespan When space heating is provided by CHP, CLT and modular structures use 20–37% and 9–17% less total life cycle primary energy, respectively, than the concrete equivalent [12]. The study demonstrates how material selection may impact both embodied energy and recycling potential in one

of Sweden's most energy-efficient apartment-type housing developments (estimated energy for operation is 45

2 Methodology

2.1 Building Design

Proper designing of the building is the most crucial part which can affect energy consumption because the factors which influence the energy consumption of a building mostly depend on the design. A standard residential building of G + 2 floors was designed using Autodesk REVIT software to obtain a 3D model of the building as mentioned in [1]. The orientation and ventilation of the building were provided in such a way that it can maximize the usage of thermal energy obtained from solar radiation and minimize the need for artificial energy. The orientation-related research of the building where there is maximum thermal comfort is mentioned in [2]. The selection of material is another major design criteria that affect the thermal energy requirement of a building. For this all the suitable materials were allotted to the building in REVIT Structure. A further material study to improve the building's energy efficiency is done in [13].

2.2 Building Description

The model created is rectangular-shaped with a front width of 7.62 mMm and a height of 10.27 mMm, which consists of a total of three levels each of height 3.42 mMm. Basic wall of 200 mm thickness was provided for the building. Internal dimensions of all the partitions are given in Figs. 1 and 2. Single flush doors were provided in the model and windows were provided with sash as frame material and glass as pane material. The isometric view of the building is shown in Fig. 3, and the elevation of the building is shown in Fig. 4.

2.3 Climatic Data

All the climatic data which are required to perform analysis such as average temperature, external temperature, and wind intensities are automatically taken from the nearest weather station of the selected location to perform analysis. The latitudinal position helps in determining the amount of solar radiation for that particular location.

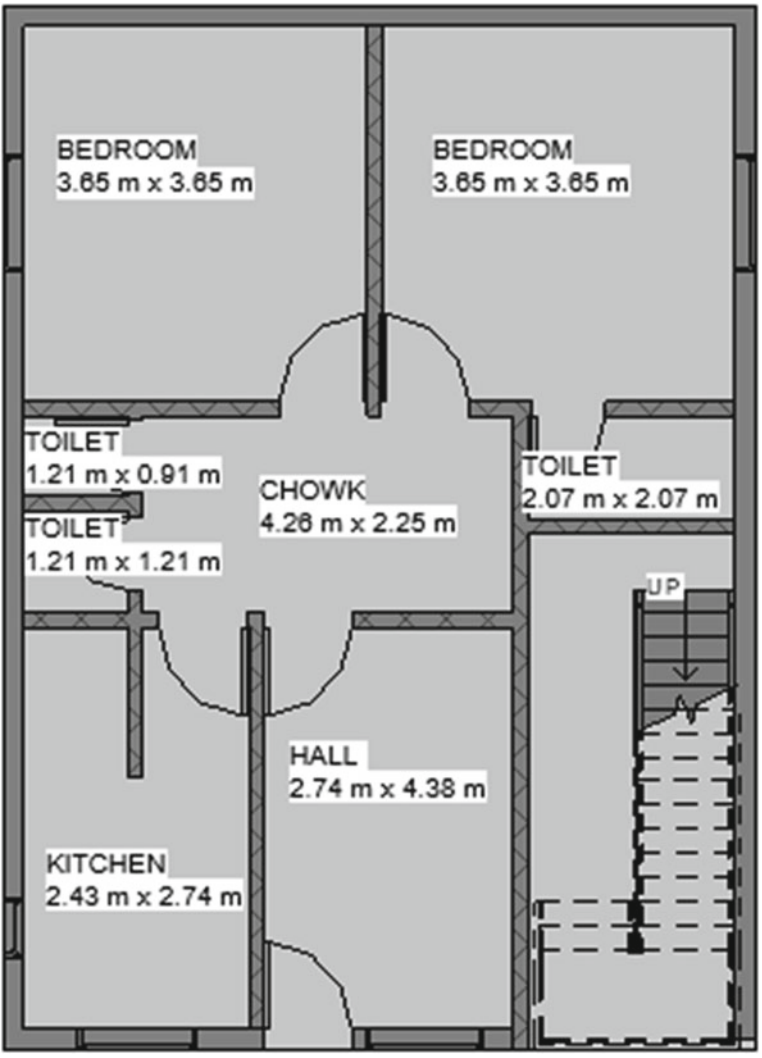

Fig. 1 2D plan of ground floor

2.4 Selection of Materials Using Nanotechnology Testing

The selection of the new material for the wall infill is one of the major factors in optimizing the structure and making it as economic as possible. So, to make the wall infill economic, we started to test the materials by recycling the waste material [12]. Finally, sludge, industrial waste, fly ash, and basalt fiber are taken as the experimental infill materials. These materials are easily available and are very economical in nature. So now the extensive testing has to be done to check if they can meet the strength and other standards.

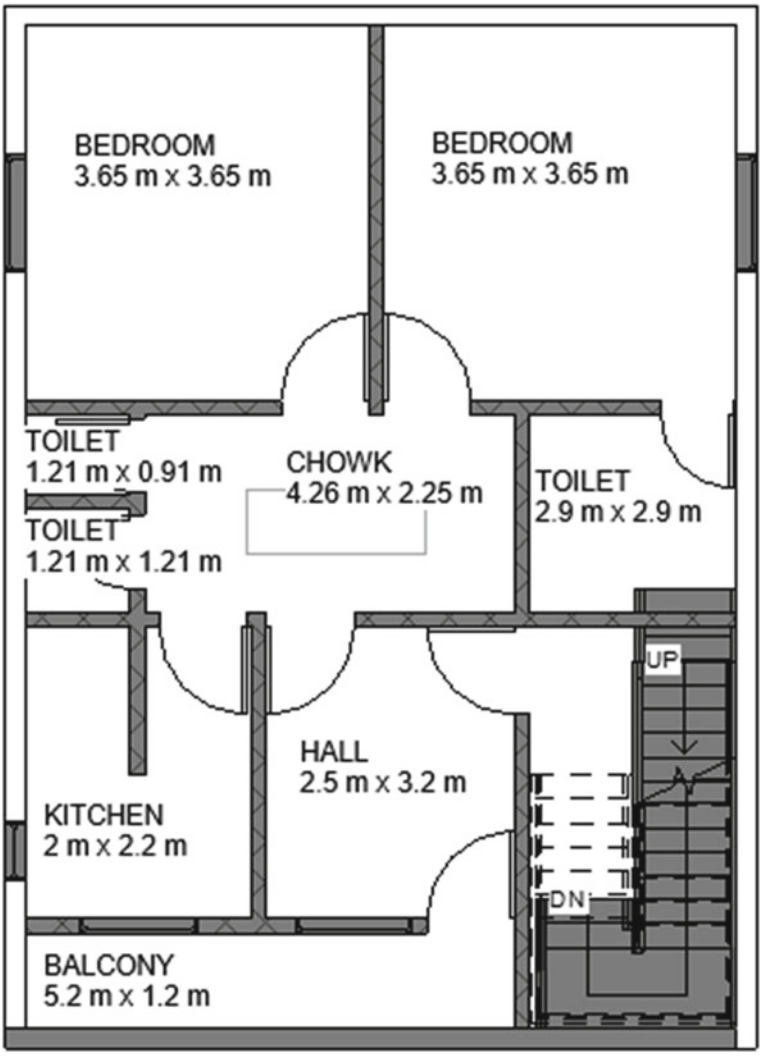

Fig. 2 2D plan of I and II floors

2.4.1 FTIR Analysis

For the detailed composition of these materials, we have done FTIR and SEM analysis in the nanotech laboratory. The FTIR spectroscopy uses mid-infrared rays to extract information about the functional groups in the substance [14]. The sample absorbs the infrared rays and emitted spectrum, and the position and magnitude of this spectrum is the fingerprint of the molecule. This method is faster and the results are acquired in a fraction of seconds. This test helped to know the major chemical groups in the

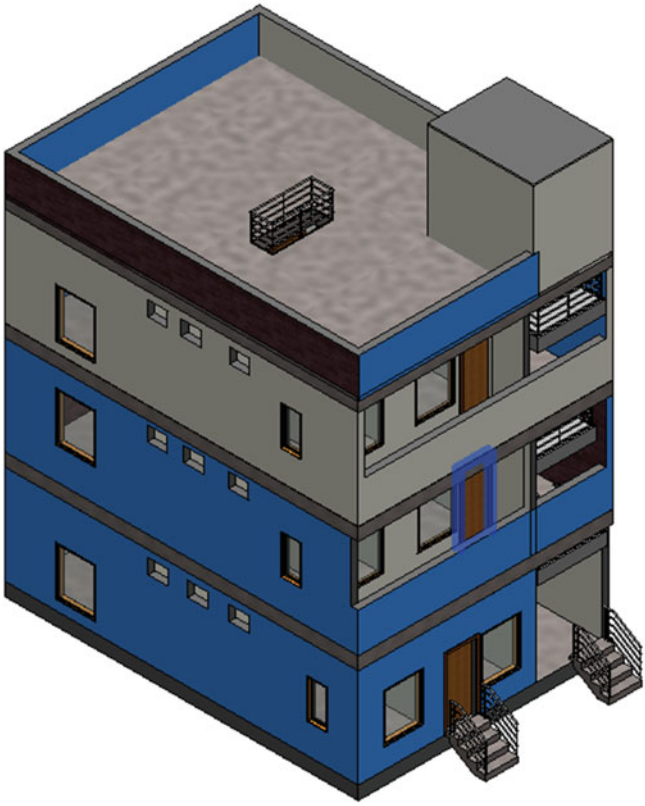

Fig. 3 Isometric view

material which will help us to know the reactions which can happen. This helped to know the durability and life of the material used and these results are compared with the standard compounds such as cement as this material is replacing the cement. The test results which are shown in Table 1 helped us to consider the industrial waste as it has similar results compared to the calcined clay, which is used previously in the industry.

2.4.2 SEM Analysis

It is done using the electron beam to magnify the image. This helped us to texture and magnify the images of the compounds. This also helped to know about the elemental composition of the samples. These results as shown in Tables 2, 3 and 4, where when compared with the composition of the cement and other standard material we can get the basic characteristics of the samples.

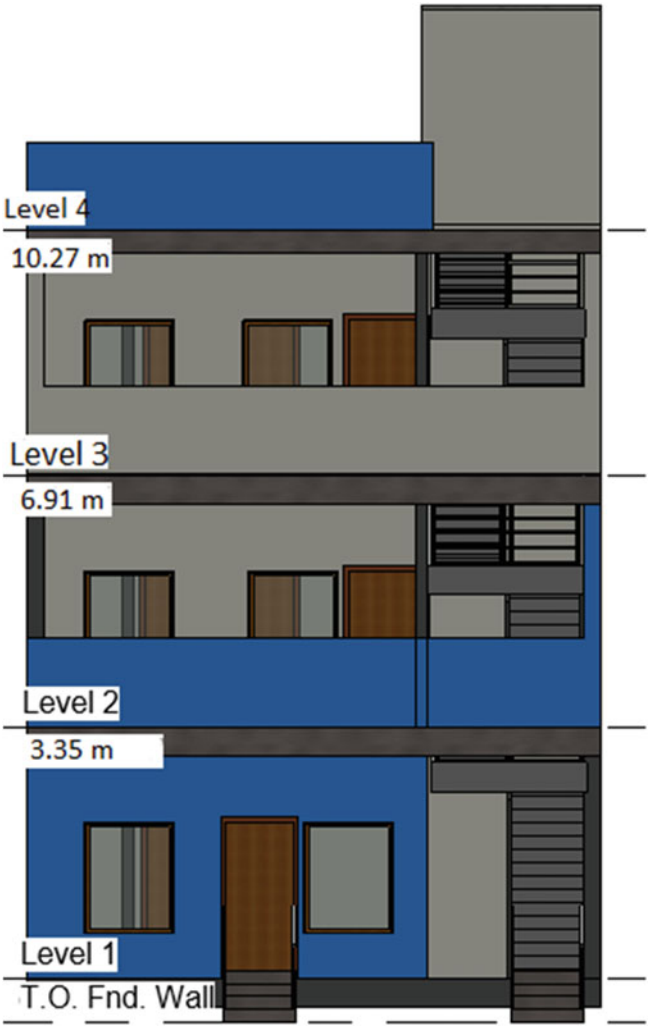

Fig. 4 Elevation

Table 1 The result of FTIR analysis

Sample	Absorption (cm^{-1})	Appearance	Group	Compound class
Sludge	561.29	Strong	C–I stretching	Halo compound
	3278.99	Strong, sharp	C–H stretching	Alkyne
Industrial waste	416.62	Strong	C–I stretching	Halo compound
	3500.80	Medium	N–H stretching	Primary amine
Sisal fibre	1024.20	Strong	C = C bending	Alkene
	1595.13	Strong	N–O stretching	Nitro compound

Table 2 SEM analysis results for sisal fibre

Element	At. No	Mass [%]	Mass Norm. [%]	Atom [%]
C	6	51.47	51.47	60.25
O	8	42.23	42.23	37.12
Ca	20	1.92	1.92	0.67
K	19	1.35	1.35	0.49

Table 3 SEM analysis results for industrial waste

Element	At. No	Mass [%]	Mass Norm. [%]	Atom [%]
O	8	60.79	55.12	73.55
Ca	20	28.20	25.57	13.62
S	16	21.06	19.10	12.72
Fe	26	0.15	0.14	0.05

Table 4 SEM analysis results for sludge

Element	At. No	Mass [%]	Mass Norm. [%]	Atom [%]
O	8	35.66	52.19	68.06
Ca	20	9.80	14.35	7.47
Si	14	8.97	13.13	9.76
Mg	12	4.97	7.27	6.24

These materials are then cast for physical testing, which will help us in comparing the compressive strength, thermal conductivity, and various other properties. The mix ratio which has the optimum values will be considered. These properties are then compared with the standards so that the results satisfy the required strength and help in optimizing the energy consumption.

3 Results and Discussion

This section explains how the heating and cooling load values change on introducing a new infill material and the differences in the load values between the results obtained by analyzing using conventional materials and infill material. These values indicate the amount of heat that is to be added or to be removed from the rooms to maintain a comfortable room temperature and to reduce the usage of electrical appliances. These heating and cooling load values can be used to optimize the building design which tells us about the number of ventilations and open spaces that should be provided in the building. The three locations for which the analysis is performed are mentioned below along with the load values, model history, and benchmark comparison obtained.

Table 5 The building summary (Agar)

Inputs	Conventional material	Infill material
Area (m^2)	54.56	54.56
Volume (m^3)	444.58	444.58
Results of calculation		
Total load peak cooling (W)	11,220.47	9786.53
Month and hour for peak cooling	5/21 17:00	5/21 17:00
Sensible load peak cooling (W)	11,003.17	9598.33
Maximum cooling latent load (W)	217.29	188.20
Maximum heating load (W)	2263.39	2841.44
Checksums		
Cooling load density (W/m^2)	205.65	205.65
Heating load density (W/m^2)	41.48	41.48

3.1 Agar

The building summary has been obtained after analyzing the building for the energy analysis. Table 5 explains the calculations of different load values such as peak heating load, peak cooling load, sensible load, and latent load for the Agar city. In this table, the outputs are obtained for the conventional material which is simple cement mortar and the infill material which is a mortar mixture of fly ash and calcined clay.

Figs. 5 and 6 show the benchmark comparison of the building in Agar city for different materials in the building. From these figures, it is seen that a benchmark comparison for power consumption is given for a year. In Agar location, the benchmark comparison for conventional material is 981 kWh/m^2/year, and for the infill material is 756 kWh/m^2/year. Here, for the building in which the infill material is used, the power consumption per year is comparatively less than the building in which conventional material is used.

3.2 Delhi

The building summary has been obtained after analyzing the building for the energy analysis. Table 6 explains the calculations of different load values such as peak heating load, peak cooling load, sensible load, latent load for Delhi city. In this table, the outputs are obtained for the conventional material which is simple cement mortar, and the infill material which is a mortar mixture of fly ash and calcined clay.

Figs. 7 and 8 show the benchmark comparison of the building in Delhi city for different materials in the building. From these figures, it is seen that a benchmark comparison for power consumption is given for a year. In the Delhi location, the

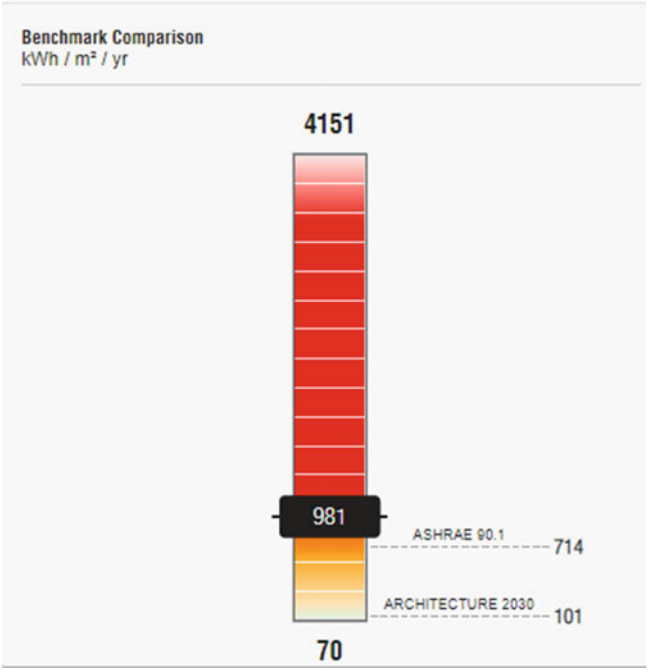

Fig. 5 Benchmark comparison for conventional material (Agar)

benchmark comparison for conventional material is 1025 kWh/m^2/year, and for the infill material is 750 kWh/m^2/year. Here, for the building in which the infill material is used, the power consumption per year is comparatively less than the building in which conventional material is used.

3.3 Chennai

The building summary has been obtained after analyzing the building for the energy analysis. Table 7 explains the calculations of different load values such as peak heating load, peak cooling load, sensible load, and latent load for Chennai city. In this table, the outputs are obtained for the conventional material which is simple cement mortar, and the infill material is a mortar mixture of fly ash and calcined clay.

Figs. 9 and 10 show the benchmark comparison of the building in Chennai city for different materials in the building. From these figures, it is seen that a benchmark comparison for power consumption is given for a year. In Chennai location, the benchmark comparison for conventional material is 978 kWh/m^2/year, and for the infill material is 601 kWh/m^2/year. Here, for the building in which the infill material

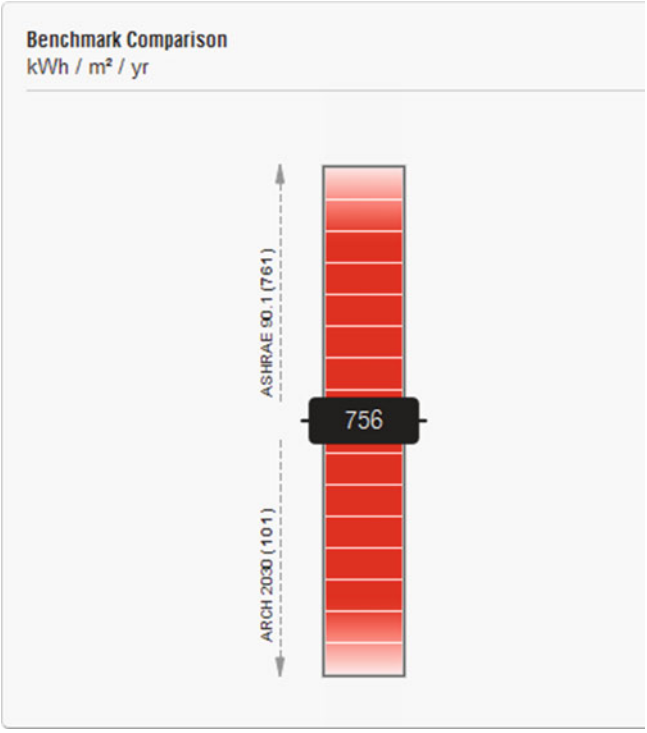

Fig. 6 Benchmark comparison for infill material (Agar)

is used, the power consumption per year is comparatively less than the building in which conventional material is used. As the same materials have been checked for three different locations, it is feasible to use infill material in place of conventional material in construction so as to decrease the power consumption of the building. Table 8 compares the various load parameters like peak cooling load, peak heating load, sensible load, and latent load among Agar, Delhi, and Chennai city. In this table, the comparison of the important results has been done for the conventional material and infill material.

From the values obtained from the analysis performed, a trend can be observed from load values obtained. Due to the introduction of new infill material, the cooling loads demand of the building are decreased while the heating loads demand has increased. From the test conducted for thermal conductivity of the new infill material, it was observed that there was an increase in thermal conductivity which concludes that more heat can be transmitted in the spaces inside the building which therefore decreases the energy demand for the building; therefore, the cooling load demand for the building also decreases for all the three locations. From the above table, it can also be observed that the heating load demand for the building has increased due to the introduction of new infill material; therefore, that indicates there is a need

Table 6 The building summary (Delhi)

Inputs	Conventional material	Infill material
Area (m^2)	54.56	54.56
Volume (m^3)	444.58	444.58
Results of calculation		
Total load peak cooling (W)	37,473.00	33,430.00
Month and hour for peak cooling	5/21 17:00	5/21 17:00
Sensible load peak cooling (W)	38,400.00	32,903.00
Maximum cooling latent load (W)	927.00	527.00
Maximum heating load (W)	19,853.00	23,874.00
Checksums		
Cooling load density (W/m^2)	299.94	299.94
Heating load density (W/m^2)	158.91	158.91

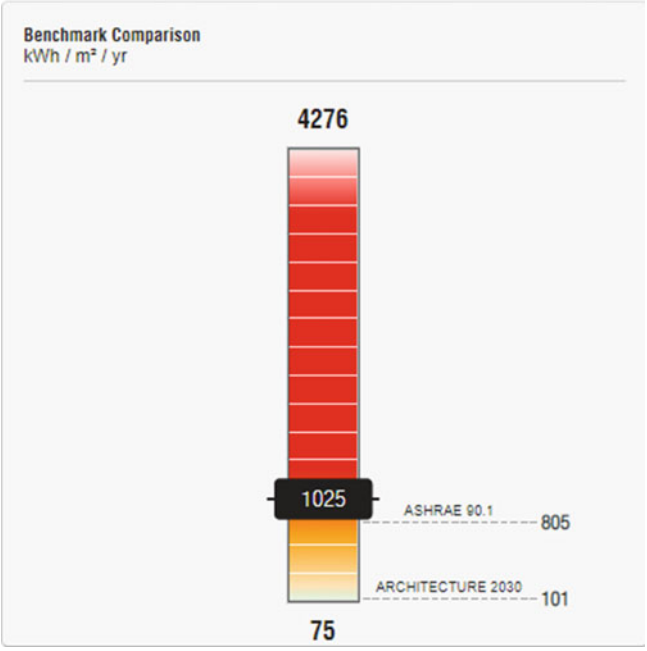

Fig. 7 Benchmark comparison for conventional material (Delhi)

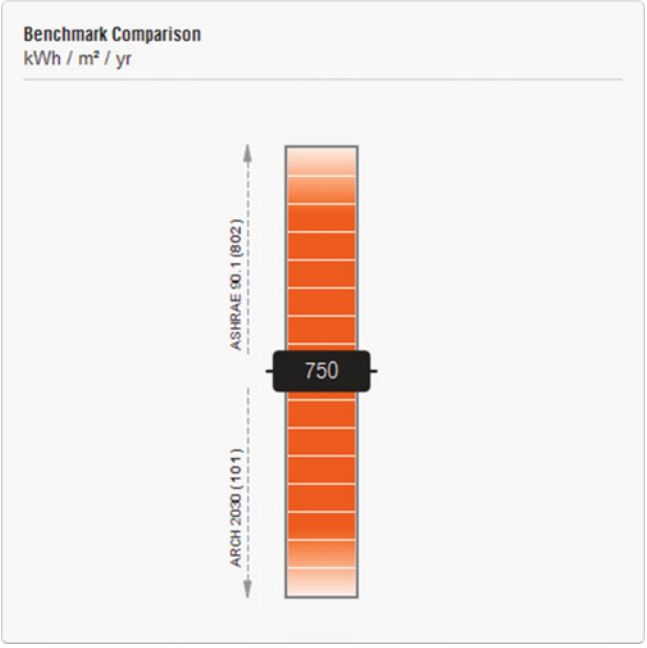

Fig. 8 Benchmark comparison for infill material (Delhi)

Table 7 The building summary (Chennai)

Inputs	Conventional material	Infill material
Area (m^2)	54.56	54.56
Volume (m^3)	444.58	444.58
Results of calculation		
Total load peak cooling (W)	32,879.00	28,051.00
Month and hour for peak cooling	5/21 17:00	5/21 17:00
Sensible load peak cooling (W)	30,363.00	26,067.00
Maximum cooling latent load (W)	2515.00	527.00
Maximum heating load (W)	673.00	1165.00
Checksums		
Cooling load density (W/m^2)	263.17	263.17
Heating load density (W/m^2)	5.39	5.39

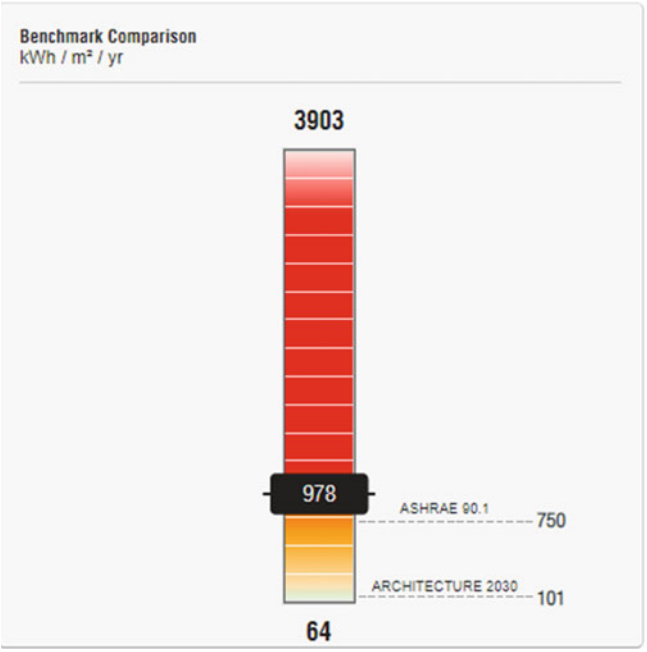

Fig. 9 Benchmark comparison for conventional material (Chennai)

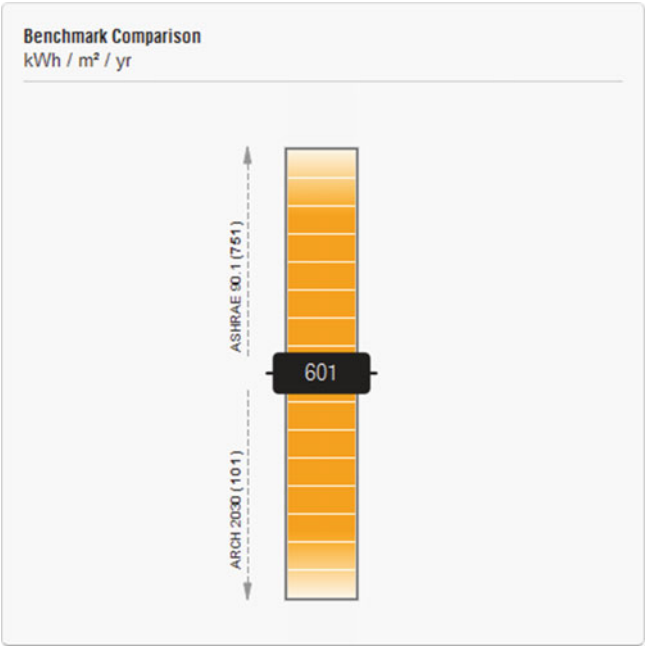

Fig. 10 Benchmark comparison for infill material (Chennai)

Table 8 The comparison of results

I. Parameters	II. Agar		III. Delhi		IV. Chennai	
	V. Conventional material	VI. Infill material	VII. Conventional material	VIII. Infill material	IX. Conventional material	X. Infill material
XI. Maximum cooling XII. Total load (W)	11,220.47	9786.53	37,473.00	33,430.00	32,879.00	28,051.00
XIII. Sensible load peak cooling (W)	11,003.17	9598.33	38,400.00	32,903.00	30,363.00	26,067.00
XIV. Maximum cooling latent load (W)	217.29	188.20	927.00	527.00	2515.00	1984.00
XV. Maximum cooling latent load (W)	2263.39	2841.44	19,853.00	23,874.00	673.00	1165.00

to provide wider window openings and ventilation for the heat to pass through the building. This increase in the peak heating load and decrease in the peak cooling load for the new infill material makes the material feasible and helpful to be used in the construction of the building to optimize it.

4 Conclusion

In this research, an investigation is done to find out the variations in the energy consumptions and energy requirements on the basis of the factors such as ventilation, openings, wall materials, thermal properties, etc. for three different locations. The analysis is done using Autodesk INSIGHT and the values obtained from the analysis show that there is significant potential for reducing the building's energy usage model. The orientation of the building also played a major role in determining the energy requirement of a particular section of a building. Before reaching a conclusion, it is also necessary to determine the usage or the purpose for which the building is being designed. When the building usage is such that it needs continuous thermal energy then it might be suitable to provide more thermal energy for the building. On the other hand, a building that does not require continuous thermal energy, a

continuous supply of thermal energy might not be suitable. In the end the impact of thermal ability of the walls are taken into consideration because its impact is more in warm climatic conditions where the radiations coming from Sun are stored in the wall materials and is transmitted inside when necessary.

References

1. Venkataraman A, Ramesh Kannan M (2015) Whole building energy analysis using BIM. ResearchGate. https://www.researchgate.net/publication/281965883. January 2013
2. Pathirana S, Rodrigo A, Halwatura R (2019) Effect of building shape, orientation, window to wall ratios and zones on energy efficiency and thermal comfort of naturally ventilated houses in tropical climate. Int J Energy Environ Eng 10(1):107–120. https://doi.org/10.1007/s40095-018-0295-3
3. Khaddaj M, Srour I (2016) Using BIM to retrofit existing buildings. Procedia Eng. 145:1526–1533. https://doi.org/10.1016/j.proeng.2016.04.192
4. Bencheikh D, Bederina M (2020) Assessing the duality of thermal performance and energy efficiency of residential buildings in hot arid climate of Laghouat, Algeria. Int J Energy Environ Eng 11(1):143–162. https://doi.org/10.1007/s40095-019-00318-z
5. Bianco V, De Rosa M, Scarpa F, Tagliafico LA (2014) Analysis of energy demand in residential buildings for different climates by means of dynamic simulation. Int J Ambient Energy 37–41. https://doi.org/10.1080/01430750.2014.907207
6. Analysis E, Wall OF, Building U, Modeling I, Countries C (2016) Energy analysis of wall materials using building information modeling (BIM) of public buildings in the tropical. Jurnal Teknologi 10:35–41
7. Elnemr A (2019) Open Access Role of water/binder ratio on strength development of cement mortar, no 1, pp 172–183
8. Kraus M, Kubečková D (2017) Analysis of the building materials in the energy efficient buildings, no. March 2016. https://doi.org/10.4028/www.scientific.net/AMR.1041.3
9. Huberman N, Pearlmutter D (2008) A life-cycle energy analysis of building materials in the Negev desert. Energy Build. 40(5):837–848. https://doi.org/10.1016/j.enbuild.2007.06.002
10. Piccardo C, Dodoo A, Gustavsson L, Tettey UYA (2019) Retrofitting with different building materials: life-cycle primary energy implications. Energy. https://doi.org/10.1016/j.energy.2019.116648
11. Tettey UYA, Dodoo A, Gustavsson L (2019) Effect of different frame materials on the primary energy use of a multi storey residential building in a life cycle perspective. Energy Build 185:259–271. https://doi.org/10.1016/j.enbuild.2018.12.017
12. Thormark C (2006) The effect of material choice on the total energy need and recycling potential of a building. Build Environ 41(8):1019–1026. https://doi.org/10.1016/j.buildenv.2005.04.026
13. Xiao L, Liu Y, Du Z, Yang Z, Xu K (2019) Model analysis and optimization of BIM technology in high-rise shear wall residential structure. In: MATEC Web Conferences, vol 267, p. 02001. https://doi.org/10.1051/matecconf/201926702001
14. Medhat A, Ali M (2015) Analytical investigation on a coptic Wooden icon from the 18th century using sem-EDX microscopy and ftir spectroscopy, vol 15, pp 151–161

Design and Energy Analysis of Green Villa Compared with Conventional Villa Using Virtual Design Modelling

Atul Kumar Singh, L. Krishnaraj, and V. R. Prasath Kumar

1 Introduction

BIM stands for building information modelling which is an upcoming concept for information handling in large projects. It involves a simultaneous design process across all involved disciplines, thereby removing the possibility of conflicts, as well as any ambiguity in the execution phase. Large building projects such as multipurpose dams and planned cities always generate a massive amount of data in the form of plans, contracts, documentation, etc. They also involve multiple disciplines aside from civil engineering such as mechanical, electrical, environmental engineering, etc. The centralized handling of this data, from the planning stage to the execution stage is one of the main concepts of BIM [1–4].

Green buildings are defined as projects which give high priority to environment conservation, control of pollution, and energy saving during construction as well as during service life. Green buildings are certified and recognized by Indian Green Building Council (IGBC) nationally and by Leadership in Energy and Environmental Design (LEED) internationally [5, 6]. Energy analysis of buildings is carried out using certain software (such as Autodesk Revit, Energy +) to find the energy consumption of the building and the effects of the materials used on the same. With this analysis, we can get energy efficiency solutions to minimize energy consumption as well as the use of materials that cause environmental damage [7].

The application of green building concepts in small residential buildings such as villas on a larger scale will have a positive effect on the national and global energy consumption and help to alleviate the pressures of energy crises. Since the green building concepts encourage the use of natural energy sources like solar power and

A. K. Singh · L. Krishnaraj (✉) · V. R. P. Kumar
Department of Civil Engineering, SRM Institute of Science and Technology, Tamil Nadu, Kattankulathur 603 203, India

A. K. Singh
e-mail: as7689@srmist.edu.in

K. S. Satyanarayanan et al. (eds.), *Sustainable Construction Materials*, Lecture Notes in Civil Engineering 194, https://doi.org/10.1007/978-981-16-6403-8_21

wind, it not only reduces the load on commercial grids but also reduces pollution since the energy is produced cleanly. Another significant advantage of villas made using green building concepts is the reduction of pollution and the reduction of usage of harmful materials in construction. Retention and recovery of green cover, as defined by IGBC guidelines, improve the aesthetic quality of the neighbourhood, and heightens the ecological value as well [8, 9].

The use of BIM in small-scale projects such as villas not only helps in the more effective application of the aforementioned green building concepts but also minimizes delays, ambiguities in the interpretation of plans and design mistakes, and also reduces construction time and cost. With the help of this tool, the engineers can easily identify mistakes, while a layman can visualize the progress of construction [6, 7, 10–13].

2 Analytical Programme

2.1 Project Methodology

Autodesk AutoCAD is used for the creation of the plan drawings as well as the detailed diagrams of the structural elements. Bentley Engineering STAAD.Pro is used for structural analysis and load simulation. Autodesk Revit software is used for building modelling and energy analysis. For this study, BIM model creation and the energy simulations for the building are carried out using Autodesk Revit.

- Study on building information modelling and its applications
- Collection of data for conventional building:
- Structural analysis and design of the conventional building
- Modelling of conventional building
- Energy analysis of the conventional building
- Conversion of conventional to green building
- Modelling of the green building
- Energy analysis of the green building
- Comparative study

2.2 Parameters Studied

The parameters considered for the energy analysis were taken from IGBC Affordable Housing codebook. Samples were taken as per their relevance to the context of the report and applied as per the stipulations of the guidebook [14]. The total credits accredited are taken against the median of the overall credit breakup given in the IGBC Affordable Housing codebook, and the expected level of certification is awarded. The parameters were considered in the evaluation of both villas and are given in Table 1.

Table 1 Major parameters studied for energy analysis

Site selection	Proximity to construction material sources
	Proximity to transportation facilities
	Avoiding ecologically high-value areas
Social infrastructure	Access to basic amenities
	Proximity to the urban environment
On-site green cover	Minimal damage to local ecosystem during construction
	Retain/recover as much green cover as possible
Heat island effect	Reduce damage to the local ecosystem
	Provide shades of paths, roads, etc
	Provide roof garden
Efficient appliances	Use of 5-star-rated appliances
	Strategic installation to maximize efficiency
Efficient lighting	Use of LED lights
	Strategic installation to maximize efficiency
	Reduce the energy bill
Day lighting	Use of large windows
	Lower energy bill
	Maximize the use of natural lighting when available
Efficient materials	Use of thermally efficient materials
Transplanting of trees	Transplanting of valuable trees, if any
HVAC	Controlling interior air quality
	Removal of indoor pollutants
	Cycling of fresh air into the building
Environmental effect	Use of low-VOC (volatile organic compound) materials
	Use of eco-friendly and reusable construction materials

2.3 Data Collection and Analysis

The following data was collected for the purposes of design and analysis of the two villas and is given in Table 2.

The above plan was created for the conventional villa design as per IBC given in (Figs. 1 and 2). It focuses on giving large open spaces and is characterized by the considerably large living room, combined kitchen and dining room, and the patio. The upper floor is focused on residents of the house, for whom several sizable bedrooms are provided. The garage can comfortably accommodate two family sedans with extra storage space to spare.

Table 2 Property details of the site

Description	Details
Area	464.5 m^2
Location	Engineers Park, Phase–III, Kandigai, Chennai South
Groundwater depth	Feasible at 40–50 ft
Social infrastructure	All religious places, departmental stores, banks, restaurants
Floor area	204.4 m^2
No. of floors	2
No. of bedrooms	5
Additional amenities	Open patio, terrace, attic storage space, spacious balconies

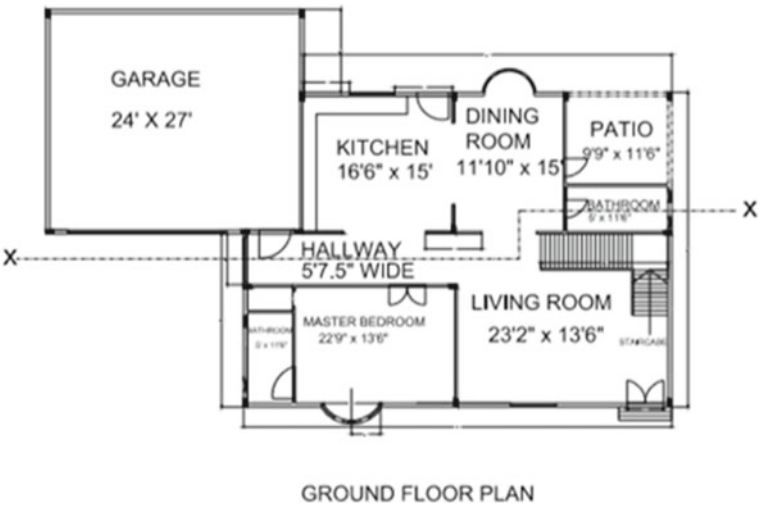

Fig. 1 Plan for conventional villa: Ground floor plan

2.4 Structural Analysis

The structural analysis is done to ensure the serviceability and safety of the design, as stipulated by the Limit State Design Method in IS456. The simulated loads, as taken from IS875, show potential points of failure in the structure, and therefore indicate the structural elements to be designed as shown in Fig. 3.

- The framed structure of the house was analysed using STAAD SPro V8i SS6.
- Using the bending moment, axial force, and shear force analysis results, the structural elements undergoing the highest of these values were selected.
- Manual calculations were performed to obtain dimensions of structural elements.

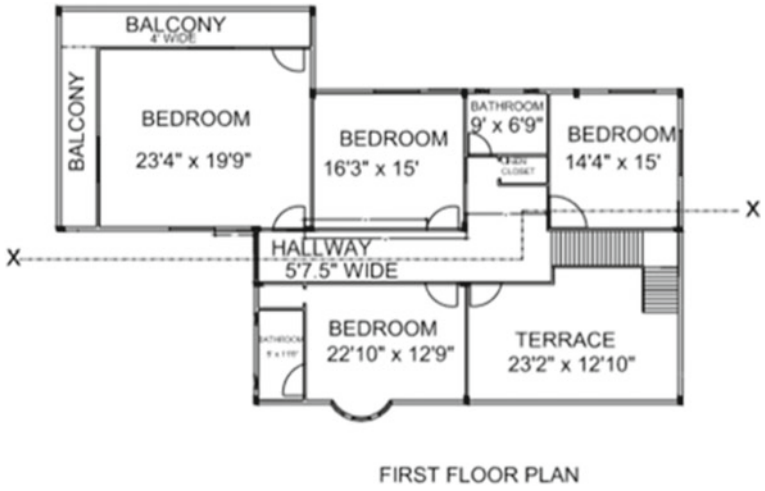

Fig. 2 Plan for conventional villa: First floor plan

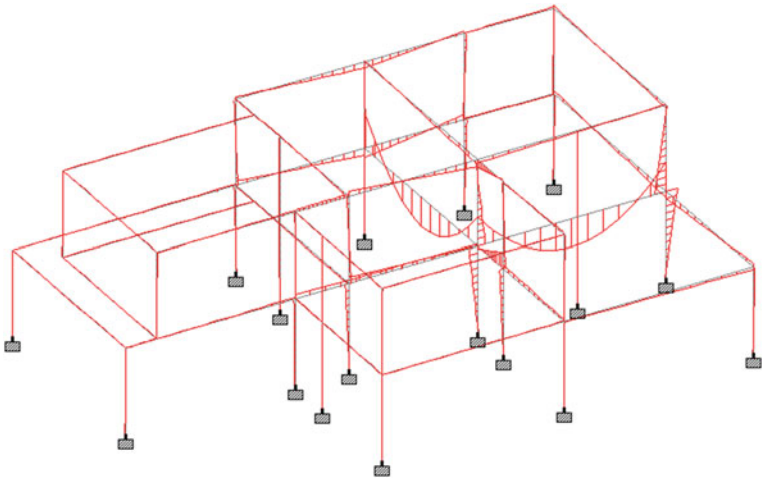

Fig. 3 Bending moment diagram

2.5 Energy Analysis

The model of the villas is created by importing the "cad" files from AutoCAD and given doors and windows. The rooms are designated and the materials are assigned in Revit, after which the energy analysis tools are used to obtain energy consumption results (Figs. 4 and 5).

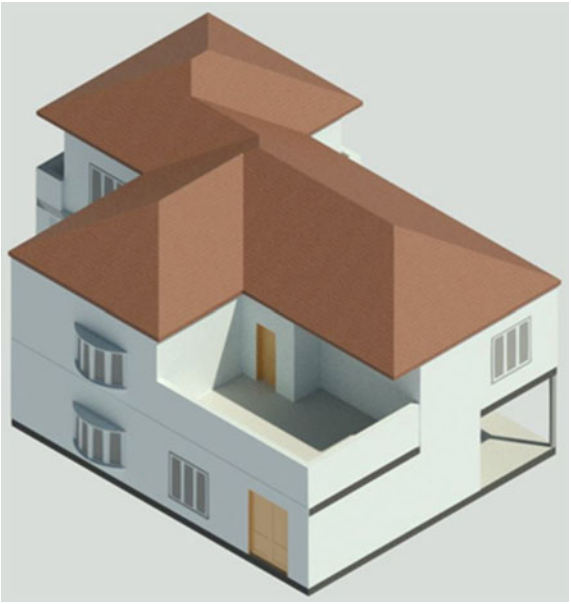

Fig. 4 Model of the conventional villa

Fig. 5 Model of the green villa

- The two villas were analysed using Autodesk Revit 2018.
- The villas were modelled separately in the software, and the inbuilt energy analysis tool was used to determine the energy consumption.
- These results along with several other factors defined by the IGBC Affordable Housing codebook were considered for the total green rating.

3 Results and Discussions

The results obtained in the analyses give crucial information used for the IGBC review criteria (Figs. 6 and 7). The factors relevant to energy analysis are considered

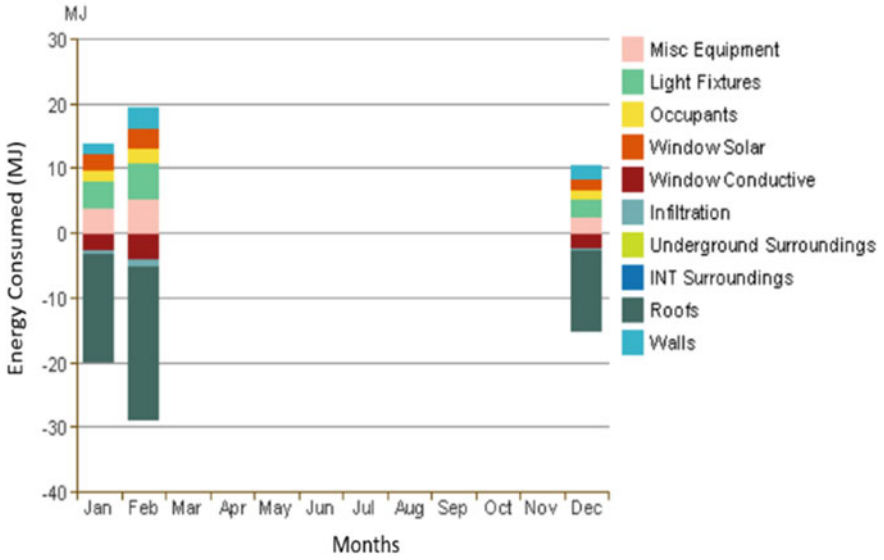

Fig. 6 Heating load of the conventional villa

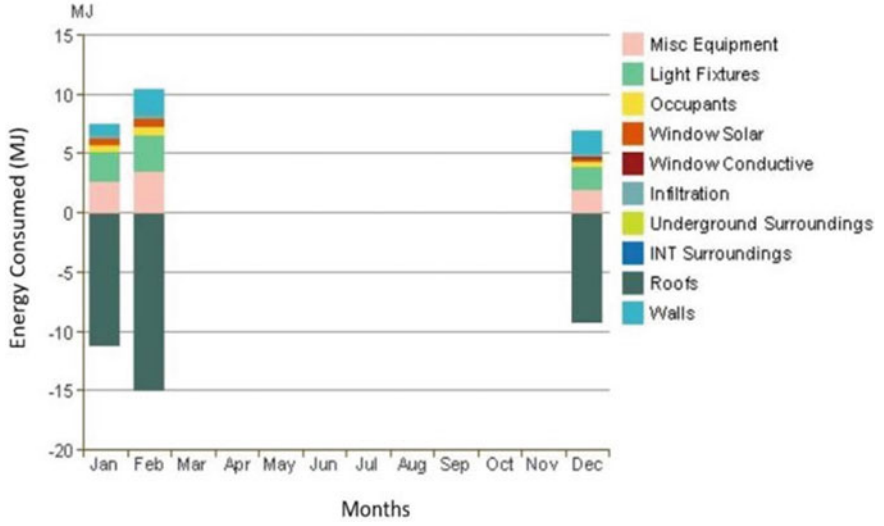

Fig. 7 Heating load of the green villa

for both villas, and the houses are rated accordingly. Several construction techniques used in the construction of green villa also improves its rating [15–19].

Figures 8 and 9 show the reduced heating loads for the winter period for the green villa. This is due to improved heat retention, thermal insulation, and optimized ventilation, designed with the annual local wind patterns. The lower heat loss (represented by the negative side of the chart) and the energy required to bring the interior to a comfortable temperature (represented by the positive side of the chart) is seen to be lesser for green villa [17, 20, 21]. The above charts represent the cooling loads for

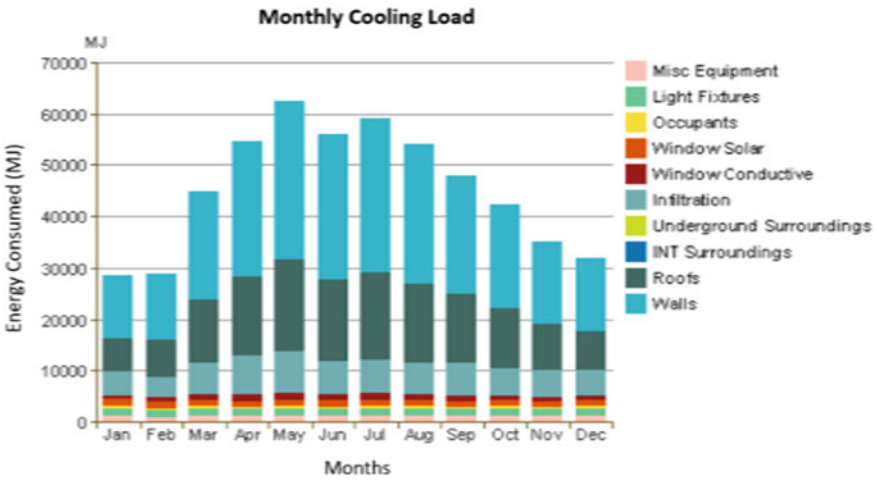

Fig. 8 Cooling load for conventional villa

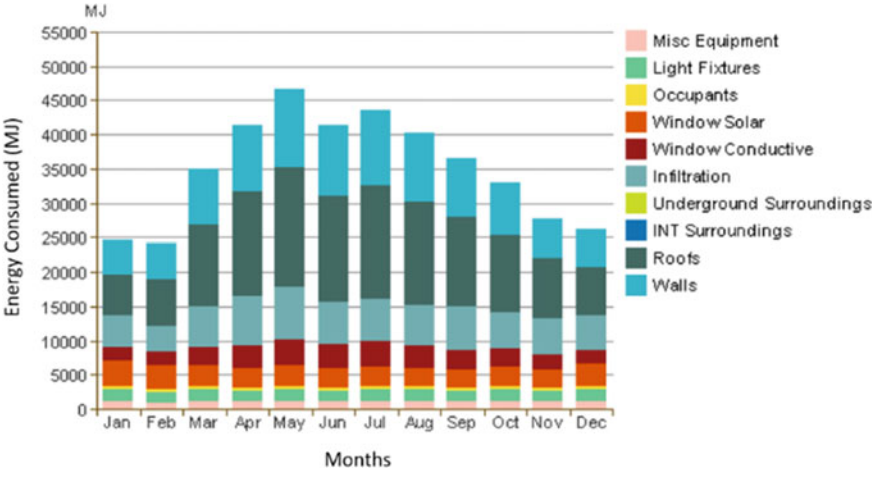

Fig. 9 Cooling load for green villa

the respective villas. It is seen that the improvements made in the green villa reduce the cooling energy requirements [22–24].

Table 3 shows the comparison of the energy analysis outputs for both villas. The green villa shows a marked reduction in energy consumption, due to the aforementioned modifications [21, 24–26].

The complete list of all factors considered for the comparative study and the credits awarded to each villa are shown in Table 4. Green villa consistently shows lower energy consumption and greater environment-friendliness. Besides the changes in design and the inclusion of a skylight and roof garden, these results can be attributed to improved construction materials and the use of optimized ventilation solutions.

Table 3 Comparative results of energy analysis

Inputs	Conventional Villa	Green Villa
Area (m^2)	327	325.57
Volume (m^3)	995.48	793.87
Cooling setpoint	23 °C	23 °C
Heating setpoint	21 °C	21 °C
Supply air temperature	12 °C	12 °C
Number of people	4	4
Air volume calculation type	VAV- Single Duct	VAV- Single Duct
Relative humidity	44.00% (Calculated)	46.00%
Psychrometrics		
Psychrometric message	None	None
Cooling coil entering dry-bulb temperature	28 °C	28 °C
Cooling coil entering wet-bulb temperature	19 °C	20 °C
Cooling coil leaving dry-bulb temperature	12 °C	12 °C
Cooling coil leaving wet-bulb temperature	14 °C	13 °C
Mixed air dry-bulb temperature	28 °C	28 °C
Calculated results		
Peak cooling load (W)	98,595	18,884.8
Peak cooling month and hour	May, 15:00	July, 17:00

(continued)

Table 3 (continued)

Inputs	Conventional Villa	Green Villa
Peak cooling sensible load (W)	96,075	15,983.6
Peak cooling latent load (W)	2520	2901.2
Peak cooling airflow (L/s)	5242.7	826
Peak heating load (W)	3506	34,799.9
Peak heating airflow (L/s)	223.2	1590
CHECKSUMS		
Cooling load density (W/m^2)	301.57	58.01
Cooling flow density ($L/(s\text{-}m^2)$)	16.04	2.54
Cooling flow/load (L/(s-kW))	53.17	43.76
Cooling area/load (m^2/kW)	3.32	652.62
Heating load density (W/m^2)	10.72	106.89
Heating flow density ($L/(s\text{-}m^2)$)	0.68	4.88

4 Conclusion

The following conclusion can be drawn from the analytical work:

- The energy analysis shows the marked reduction in cooling energy requirements of the green villa, as compared to the conventional villa (98 kW for the conventional villa to 18 kW for the green villa).
- The use of environmentally friendly materials and ecologically conscious construction procedures which the green building concepts give high priority to produce far less pollution and harmful effects on the environment.
- The IGBC rating system easily quantifies the ecological value of the two villas, and clearly shows that the green villa is superior (14 out of 40 credits for conventional villa, and 36 credits for green villa).

Table 4 Factors considered for the comparative study

Parameters	Conventional villa	Green villa
Site selection (SM1) Proximity to construction material	Point not awarded	Point awarded
Site selection (SM1) Proximity to social infrastructure	Point awarded	Point awarded
Site selection (SM1) Avoiding high-value areas	Point awarded	Point awarded
On-site green cover (SM2)	2 Credits	4 Credits
Recover green cover (SM2)	0 Credit	4 Credits
Heat island effect (SM4)	2 Credits	6 Credits
Energy-efficient appliances (EC1)	2 Credits	4 Credits
Day lighting (EC3)	2 Credits	6 Credits
Efficient materials (EC4)	1 Credit	2 Credits
HVAC (EC6)	3 Credits	6 Credits
Environmentally friendly materials	1 Credits	4 Credits
Total	14 Credits	36 Credits
IGBC certification level	Certified	National excellence

References

1. Soltani S (2016) The contributions of building information modelling to sustainable construction. World J Eng Technol 4:193–199
2. Manning R, Messner J (2008) Case studies in BIM implementation for programming of healthcare facilities. J Inf Technol Constr 13:246–257
3. Vinoth Kumar J, Mukherjee M (2009) Scope of building information modelling in India. J Eng Sci Technol Rev 2:165–169
4. Robert E et al (2014) Building information modeling adoption: an analysis of barriers to implementation. J Eng Archit 2:77–101
5. Gupta NK (2013) Quantifying embodied energy using green building technologies under affordable housing construction. Open J Energy Effic 2:171–175
6. Hartmann T, Van Meerveld H, Vossebeld N, Adriaanse A (2012) Aligning building information model tools and construction management methods. Autom Constr 22:605–613

7. Odunfa KM et al (2015) Energy efficiency in building: case of buildings at the University of Ibadan, Nigeria. J Build Constr Plan Res 3:18–26
8. Ko YS, No ST (2015) A study on comparison of building energy simulation and measurement results for a city hall. J Build Constr Plan Res 3:1–9
9. Ilhan B et al (2013) Meta-analysis of building information modeling literature in construction. J Eng Innov Technol 3(4):373–379
10. Xia J, Ma Y (2014) Exploring on energy-saving design of building based on BIM technology. J Chem Pharm Res 6(7):2642–2645
11. Moakher PE, Pimplikar SS (2012) Building information modeling (BIM) and sustainability using design technology in energy efficient modeling. IOSR J Mech Civil Eng (IOSRJMCE) 1:10–21. ISSN:2278-1684
12. Marsh R, Larsen VG, Kragh M (2011) Housing and energy in Denmark: past, present, and future challenges. Build Res Inf 38(1):92–106
13. Keeler M, Burke B (2009) Fundamentals of integrated design for sustainable building. Wiley, New York, pp 1–408
14. Affordable Housing Energy Efficiency (AHEE) (2007) Affordable housing energy efficiency handbook, pp 1–106
15. Chani PS et al (2003) Comparative analysis of embodied energy rates for walling elements in India, IE (I). J Archit Eng 84:47–50
16. Eastman C, Teicholz P, Sacks R, Liston K (2008) BIM handbook: a guide to building information modeling for owners, managers, designers, engineers and contractors. Wiley, NJ, pp 1–490
17. Becerik Gerber B, Jazizadeh F, Li N, Calis G (2012) Application areas and data requirements for BIM-enabled facilities management. J Constr Eng Manag (ASCE) 138:431–442
18. Ramesh T et al (2013) Life cycle energy analysis of a multifamily residential house: a case study in Indian context. Open J Energy Effic 2(1):34–41
19. Azhar S, Brown J (2009) BIM for sustainability analyses. Int J Constr Educ Res 5:276–292
20. Hansen HTR, Knudstrup M (2005) The integrated design process (IDP): a more holistic approach to sustainable architecture. In: Murakami S, Yashiro T (eds) Action for sustainability, the world sustainable building conference, Tokyo National Conference Board, pp 894–901
21. Petersen S, Svendsen S (2012) Method for component-based economical optimization for use in design of new low energy buildings. Renew Energy 38(1):173–180
22. Zhou Q, Wang SW, Xu XH, Xiao F (2008) A grey box model of next day building thermal load prediction for energy efficient control. Int J Energy Res 32:1418–1431
23. Kivits RA, Furneaux C (2013) BIM: enabling sustainability and asset management through knowledge management. Sci World J Article ID: 983721
24. European Commission (2003) Directive 2002/91/EC of the European Parliament and of the council on the energy performance of buildings. Off J Eur Commun 1:65–70
25. Ahn D, Cha H (2014) Integration of building maintenance data in application of building information modeling. J Build Constr Plan Res 2:166–172
26. Zhang JP, Hu ZZ (2011) BIM and 4D-based integrated solution of analysis and management for conflicts and structural safety problems during construction vol 20, pp 155–166

Experimental Investigation on Lightweight Concrete with Kegrete Bowling Ball

S. Dheepak, P. Deepak, and S. Pradeep

1 Introduction

The project's aim is to figure out the physical and mechanical properties of concrete mix, medium-weight concrete, and polypropylene fibre concrete [1]. The lightweight concrete has paved its own way in the civil engineering industry. Many lightweight bridges and decks are being created and constructed with lightweight materials [2, 3]. There are many benefits of using low-density concrete. It assists in the reduction of dead load, the acceleration of construction, and the reduction of haulage and handling costs. The low thermal conductivity of lightweight concrete is another significant feature [4, 5]. It contains fibres of equal length which will increase the structural integrity. For a good fibre-reinforced concrete, the shape, dimensions, and texture of the fibre are important [6]. The usage of fibres in the concrete will reduce the plastic shrinkage cracking and dry shrinkage cracking [7]. These fibres make the concrete low permeable and prevent the bleeding of water. Polypropylene fibres have a good impact and durability properties over the concrete [8, 9].

S. Dheepak · P. Deepak (✉) · S. Pradeep
Department of Civil Engineering, SRM Institute of Science and Technology, Kattankulathur, Tamil Nadu 603203, India

S. Pradeep
e-mail: pradeeps@srmist.edu.in

K. S. Satyanarayanan et al. (eds.), *Sustainable Construction Materials*, Lecture Notes in Civil Engineering 194, https://doi.org/10.1007/978-981-16-6403-8_22

2 Material Properties

2.1 Cementitious Material

2.1.1 Cement

Ordinary portland cement is the cement used in general use around the world, used as an essential ingredient of concrete and mortar. When the raw materials' oxides are exposed to high clinkering temperatures, they combine to form four complex compounds.

2.1.2 Fly Ash

Fly ash is a by-product of coal combustion that comes out of the boiler. The constituents of fly vary depending on the coal's composition, including varying concentrations of silicon dioxide, aluminium oxide, and calcium oxide. Nowadays, fly ash is used as a cement replacement in concrete due to its high pozzolanic activity. Since it is a waste from the boilers it can be utilized properly without being polluting the environment by just leaving that as a landfill. It also decreases the amount of cement in the concrete, lowering the amount of carbon dioxide released during cement manufacturing. Fly ash is divided into two classes based on its calcium content: class F and class C.

2.1.3 Silica Fume

Silica fume is produced when high purity quartz is carbothermically reduced with carbonaceous materials such as coal or coke. It is a by-product of silicon and ferrosilicon alloy production. The key production is increased pozzolanic activity in concrete due to the presence of high silica material.

2.1.4 Metakaolin

Thermally activated ordinary clay and kaolinitic clay are natural pozzolans. Metakaolin is a term used to describe these impure materials. Metakaolin has high pozzolanic properties. While it has a lot of pozzolanic properties, it is not very reactive. Different densifications of the cement paste have been observed. This densification provides a boost in strength and a decrease in permeability.

2.2 Aggregate

2.2.1 Cenosphere

Cenospheres are light, inert hollow spheres made primarily of silica and alumina and filled with air or inert gas that are usually created as a by-product of coal combustion at thermal power plants. Thin-walled hollow spheres, or cenospheres, make up a small proportion of the particles of pulverised coal ash. Due to the ultrafine nature of microsphere, this contains low specific gravity. The specific gravity ranges from 0.45 to 0.7. Since they have less specific gravity they can also be replaced as fine aggregate and gives good strength than lightweight materials.

2.3 Admixture

2.3.1 Polycarboxly Ether

High-range water reducers are used as additives in high-strength concrete. Their addition to concrete or mortar allows for a lower water-to-cement ratio without compromising the mixture's workability, allowing for the manufacture of self-consolidating and high-performance concrete. As the water-to-cement ratio decreases, concrete strength decreases.

2.3.2 Air Entraining Agent

This agent is used mainly or added to the structure which has been exposed to potential frost damage. Improves cohesion and workability of concrete mixes. It is used for ready mixed retarded mortar. Improves workability and further enhancing durability. Excellent air bubble stability can be used in a wide range of mixes.

2.3.3 Polypropylene Fibres

Polypropylene fibres were first proposed as a concrete admixture in 1965 by the US Corps of Engineers for the construction of blast-resistant buildings. Since then, the use of these fibres in the construction of buildings has increased dramatically, owing to the fact that the use of these fibres in concrete increases the resilience, flexural strength, tensile strength, and impact strength of concrete, as well as the failure mode of concrete. Cracks play a crucial role because they turn concrete structures into components, exposing them to a high risk of corrosion. The structure would be affected if the crack width widens. As a result, it is critical to reducing the structure's

Table 1 Mix design

Materials	Quantity (kg/m^3)
Cement	300
Cenosphere	385
Silica fume	50
Fly ash	100
Metakaolin	52
Superplasticizer	6
Water	299
Air entrainer	1

crack pattern, which can be accomplished by using polypropylene fibres. The length of the fibres must be determined before they are added to the cement concrete.

3 Mix Design

One of the most critical stages of concrete production is mix design. The mix design provides precise details on the strength and density of the concrete (Table 1). The concepts taught in the concrete laboratory were put into practice. Several trail mixes were made, and the one that produced the best results was chosen for casting the canoe. However, while mixing the chemical admixtures safety precautions were taken, and proper dosage of chemicals as superplasticizer, etc.

4 Mould

As this is a spherical mould, to get better shape and better accuracy, the 3D printing technique was adopted to make the hallow mould. The design of the mould was created in the solid works software. This typically consists of a hallow portion inside the ball and it has an outer portion with a flat strip outside. This flat strip is generally provided to bolt the mould. The mould was designed for two halves, in that one half was containing 100 mm diameter and the other half contained a diameter of 100 mm and these two halves were joined together with M5 bolts and nuts. The modelling and the moulding were carried for one part and it was replicated to the other part. The initial inner to inner diameter was given as 200 mm and clearance was given. The mould was modelled in such a way that to carry a maximum mass of 5.5 kg the accuracy of the mould should also be taken into account to get the exact dimensions of the ball. The thickness of the mould is 3 mm. After the modelling was finalized the solid works file was sliced into different parts so as to determine the number of grams required for printing the mould in the 3D printing machine. After slicing the

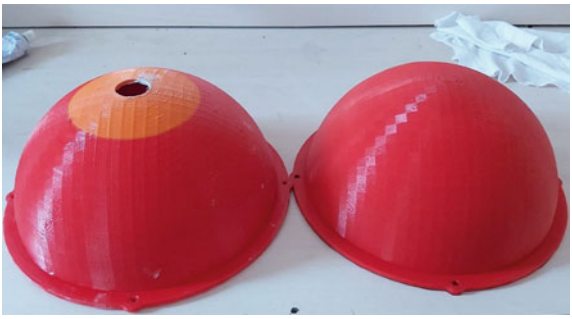

Fig. 1 3D printed mould

model, the 3D printer started to print the mould by heating the polylactic acid which is commonly called PLA (Fig. 1). Once the heating is started the printer automatically prints the mould in the appropriate design which was fended into the printer. After one half was completed another half was started to print.

5 Casting and Demoulding

After printing the mould, the mix was finalized and the bowling ball was ready to get casted. The mould was cleaned properly and with the help of sandpaper the surface was cleaned properly in order to get a smooth finish over the ball. The mix proportions were made already and the mould was applied with shuttering oil in order to get the ball easily out of the mould. The batching was done for the mix proportions (Fig. 2).

The cementitious materials were added first and water was also added to the mix (Fig. 3). The polypropylene fibres were added and after adding water the superplasticizers were added and then the cenosphere was added and the mortar was mixed in the mixer for 2 min. Then it was transferred into the trays and was placed ready to fill up the ball and the cube. The ball and the cube were cast and it was given vibration in order to get even compactness for the materials. Then one rupee coin was embedded on the top of the cube and on the top of the ball. The mould was then bolted tightly

Fig. 2 Batching of materials

Fig. 3 Mixing of materials

in order to make sure that the ball was held in its position firmly. For two days the mortar was allowed to remain in the moulds, then it was demoulded, weighed, and cured for 28 days.

6 Test Results

6.1 Compression Test

The cubes had been cast and cured in water for 28 days. The compression test is performed for 7, 14, and 28 days (Fig. 4). Power was achieved by 60–70% in 7 days and by 95–100% in 28 days as shown in Table 2. After 28 days of curing, the concrete density was 1050 kg/m^3 with a compression strength of 6.3 N/mm^2.

Fig. 4 Compression test

Table 2 Compression test

Material	7 days	14 days	28 days
Mix	4.3 N/mm^2	5.6 N/mm^2	6.3 N/mm^2

Fig. 5 Kegrete bowling ball

7 Conclusion

The fibre-reinforced bowling ball was cast and cured for 28 days and then the weight of the ball was also taken. The fibre-reinforced concrete mixes generally provided an increase in the mechanical properties of the concrete compared to the control mixes. Cylinders were also cast, and they were put through a compression test as well as an impact resistance test. After 28 days of curing, the concrete density was 1050 kg/m^3 with a compression strength of 6.3 N/mm^2. Finally, the specification requirements were applied to the fibre-reinforced kegrete bowling ball (Fig. 5).

References

1. Chandra S, Berntsson L (2002) Lightweight aggregate concrete. Elsevier
2. Thomas M, Bremner T (2012) Performance of lightweight aggregate concrete containing slag after 25 years in a harsh marine environment. Cement Concrete Res 42:358–364
3. Bogas JA, Gomes A, Pereira MF (2012) Self-compacting lightweight concrete produced with expanded clay aggregate. Constr Build Mater 35:1013–1022
4. Sales A, De Souza FR, Dos Santos WN, Zimer AM, Almeida FD (2010) Lightweight composite concrete produced with water treatment sludge and sawdust Thermal properties and potential application. Constr Build Mater 24:2446–2453
5. Li Z (2011) Advanced concrete technology. John Wiley & Sons
6. Kisku N, Joshi H, Ansari M, Panda SK, Nayak S, Dutta SC (2017) A critical review and assessment for usage of recycled aggregate as sustainable construction material. Constr Build Mater 131:721–740
7. Esfandiari J, Loghmani P (2019) Effect of perlite powder and silica fume on the compressive strength and microstructural characterization of self-compacting concrete with lime-cement binder. Measurement 147:106846

8. Fapohunda C, Akinbile B, Shittu A (2017) Structure and properties of mortar and concrete with rice husk ash as partial replacement of ordinary Portland cement–A review. Int J Sustain Built Environ 6:675–692
9. Huang Z, Padmaja K, Li S, Liew JR (2018) Mechanical properties and microstructure of ultra-lightweight cement composites with fly ash cenospheres after exposure to high temperatures. Constr Build Mater 164:760–774

Polymers and Functional Materials

Performance of Jute Fabric-Reinforced Polymer Concrete as Permanent Formwork

Shyue Leong Lee, Mohammad Abdul Mannan, Ivonson Kwee, and Chiang Chong Kian

1 Introduction

The penetration of chloride ions from seawater or deicing salt into the steel-reinforced concrete leads to the formation of rust and causes cracking and spalling of concrete cover [1]. Therefore, in order to protect/delay the penetration of chloride ions to steel reinforcement, more durable and sustainable materials compared to concrete can be investigated. Permanent formwork, also known as a stay-in-place (SIP) system, can be used. It remains permanently compared to conventional wood formwork [2, 3].

Permanent formwork can be categorized into non-participating and participating permanent formwork. Non-participating formwork acts as a protective layer and does not involve in structures load-carrying system. It only involves supporting the weight of concrete during pouring and construction loads [4, 5]. As for participating formwork, it involves in structures load-carrying system with composite action and acts as protective layer [4–7].

In general, permanent formwork can be divided into four major types, known as organic-based permanent formwork—bamboo, semi-organic-based permanent formwork—wood cement composite, polymer-based permanent formwork, and

S. L. Lee (✉) · M. A. Mannan
Department of Civil Engineering, Faculty of Engineering, Universiti Malaysia Sarawak, 94300 Kota Samarahan, Sarawak, Malaysia

M. A. Mannan
e-mail: mannan@unimas.my

I. Kwee · C. C. Kian
SCIB Concrete Manufacturing SDN, BHD. Lot 1258, Jalan Utama, Pending Industrial Estate, 93450 Kuching, Sarawak, Malaysia
e-mail: ikwee@scib.com.my

C. C. Kian
e-mail: kcchong798@scib.com.my

K. S. Satyanarayanan et al. (eds.), *Sustainable Construction Materials*, Lecture Notes in Civil Engineering 194, https://doi.org/10.1007/978-981-16-6403-8_23

cement-based permanent formwork. For organic-based permanent formwork, half-sectioned bamboo as permanent formwork for slab was used by Akmaluddin et al. [8] in their research. For semi-organic-based permanent formwork—wood cement composite—Li et al. [9] used this formwork as permanent formwork for wall panels.

Cement-based permanent formwork can be categorized into fiber-reinforced concrete (FRC), ultra-high-performance concrete (UHPC)/ultra-high-performance fiber-reinforced concrete (UHPFRC), textile-reinforced concrete (TRC)/fabric-reinforced cementitious matrix (FRCM), and engineering cementitious composite (ECC). Researchers such as Bank et al. [4], Tian et al. [7], Kim et al. [10], Leung and Cao [11], Li et al. [12], and Kim et al. [13] investigated the cement-based permanent formwork.

As for polymer-based permanent formwork, there are many types of polymer-based permanent formwork such as pultruded and no pultruded fiber-reinforced polymer (FRP) plate, FRP and glass-fiber-reinforced polymer tubes (GFRP), and polyvinyl chloride (PVC). For example, Amir et al. [14] and Nicoletta et al. [15] tested FRP for composite beam and composite tube. However, Amir and Mark [16], Mark and Amir [17], Patrick et al. [18], and Raouf et al. [19] tested FRP for full-scale bridge deck and scaled-down bridge deck. Noran and Khaled [20] and Scott et al. [21] tested PVC as permanent formwork for the wall.

The aim of this research is therefore to investigate the potential use of jute fabric-reinforced polymer concrete (JFRPC) as a permanent formwork by means of mechanical testing. This is because PCs are well performed in corrosive environments and chemical attacks [22–24]. Thus, JFRPC would be proposed as a protective layer and as a participating permanent formwork on the basis of the tests carried out. The JFRPC will be prepared using quarry dust, fly ash, orthophthalic unsaturated polyester resin, and jute fabric. Because fly ash is a waste product from the power plant, both jute fabric and fly ash are very cheap in cost, and jute fabric is cheaper than polymer-based fiber and geotextile.

2 Research Materials

There were two types of concrete which were Portland cement concrete (PCC) and polymer concrete (PC). Grade 30 (G30) PCC was prepared from coarse aggregate, sand, Portland cement, water, and the water–cement ratio of 0.58. The used coarse aggregate was passing 20 mm sieve and retained on 5 mm sieve and the used sand was passing 600-micron sieve and retained on the pan. The gradings of coarse aggregate and sand were shown in Fig. 1. The PC was made from quarry dust, fly ash, and orthophthalic unsaturated polyester resin. The used quarry dust passed through a 5 mm sieve and was retained on a 1.18 mm sieve and the quarry dust grading was shown in Fig. 1. In addition, jute fabric, as shown in Fig. 2, was used as reinforcement in PC to form jute fabric-reinforced polymer concrete (JFRPC).

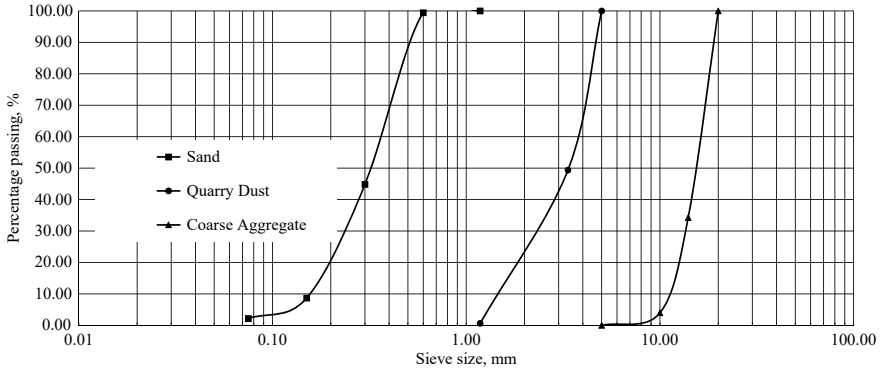

Fig. 1 Aggregate grading of sand, quarry dust, and coarse aggregate

Fig. 2 Jute fabric as reinforcement

3 Result and Analysis

The research objective is to investigate the mechanical performance of jute fabric-reinforced polymer concrete (JFRPC) and its potential as permanent formwork for the construction structure. The steel-reinforced PCC beam is known as a composite beam with the use of JFRPC as permanent formwork. In this research, the composite beam means that the PCC has been cast on top of the JFRPC plate.

Section 3 was divided into three separate sub-section. Sect. 3.1 concerns the mechanical properties of PCC, PC, and JFRPC. After investigation of the mechanical properties of PCC, PC, and JFRPC, the composite beam (JFRPC permanent formwork + PCC) was prepared and tested for performance and is shown in Sect. 3.2. In practice, the composite beam will be larger than the samples prepared in the laboratory. The connection between the permanent formworks is therefore very important and needs to be investigated and is shown in Sect. 3.3.

3.1 Mechanical Properties of PCC, PC, and JFRPC

PCC was tested for compressive and flexural strengths using cube and beam with dimensions of 100 mm and 100 × 100 × 500 mm, respectively. The prepared PCC samples were water cured, tested for compressive strength in accordance with BS EN 12,390–3:2002, and the three points flexural test was conducted using SE 100 Universal Testing Frame, 400 kN, due to the broke down of the flexural machine. The compressive and flexural strengths and deflection of the beam were shown in Table 1.

The PC was tested for compressive and flexural strengths using cube and beam with dimensions of 50 mm and 40 × 160 × 12 mm, respectively. The PC was prepared with 1 part resin, 1 part fly ash, and 2 parts quarry dust by mass of the total materials. The prepared PC was cured at an ambient temperature. BS EN 12,390–3:2002 was used for compressive strength determination. The three points flexural test was conducted using a California bearing ratio (CBR) testing machine with a loading rate of 1 mm/min. This is due to the breaking down of the flexural machine. The compressive and flexural strengths and deflection of the beam were shown in Table 1.

For PC, it took only 4 h to achieve more than 50% of its optimum compressive strength (80.10 MPa) and more than 60% of its flexural strength (16.52 MPa), respectively. The PC achieved its optimum compressive strength and flexural strength on days 7 and 3, respectively. In contrast, PCC required 3 days to achieve more than 60% of its compressive strength of 28 days and more than 70% for its flexural strength. As a result, the strength of PC development was faster than PCC by comparing PCC and PC.

For JFRPC, it was tested for flexural strength using a beam with dimensions of 40 × 160 × 12 mm. The mix proportion was the same as PC. For JFRPC, a thin layer of PC was poured, followed by a layer of fabric and then the remaining PC to form a JFRPC beam with a thickness of 12 mm. The flexural strength of JFRPC was shown in Table 1. With the use of jute fabric as reinforcement in PC, the flexural strength increased by 21.20% compared to PC. This shows that jute fabric has the potential as reinforcement in PC and it is of low cost.

Table 1 Performance of PCC, PC, and JFRPC

Types of concrete	Properties		
	Compressive strength, MPa	Flexural strength, MPa	Deflection, mm
Portland cement concrete	32.96 (28 days)	3.93 (28 days)	0.175
Polymer concrete	80.10 (7 days)	16.52 (7 days)	0.771
Jute fabric-reinforced polymer concrete	–	20.02 (7 days)	0.937

From Table 1, it can be observed that concrete prepared using resin as a binder had a minimum of four times higher deflection compared to concrete prepared using Portland cement as a binder. In addition, PC with jute fabric as reinforcement had a deflection of 1.2 times higher than PC without reinforcement. This shows that the brittleness of the PC was improved with the use of jute fabric as reinforcement.

3.2 Composite Beam

Composite beam means the PCC was cast on top of the JFRPC plate. The JFRPC plates were prepared, and topping aggregate was immediately spread over the top of the plates and at least 7 days of ambient temperature curing. The size of the plates was 100 × 500 × 12 mm. Four types of JFRPC plates had been prepared, as shown in Table 2, and had been assigned four different codes. For example, in Table 2, JF-P20R14-30, JF means jute fabric, P20R14 means aggregate passing 20 mm sieve and retained on 14 mm sieve as topping aggregate, 30 means 30 g of topping aggregate for 100 mm diameter, and F means fully topping on the surface. P14R10 means aggregate passing 14 mm sieve and retained on 10 mm sieve.

The prepared JFRPC plate was placed in a mold of 100 × 100 × 500 mm and the PCC was poured to form a composite beam using JFRPC as permanent formwork. After 24 h, the composite beams were demolded, water cured for 27 days, and only the PCC part was immersed in water, but the composite beam was not fully immersed. The composite beam was tested for three-point flexural strength using SE 100 Universal Testing Frame, 400 kN, and was measured for deflection using a dial gauge at the mid-point of the composite beam.

Table 2 is the flexural strength and deflection of the composite beam determined using different types of JFRPC plates. It can be observed that the composite beam using JFRPC plate with full topping aggregate (JF-P20R14-F, JF-P14R10-F) had higher flexural strength and deflection than the composite beam using JFRPC plate with 30 g of topping aggregate for a diameter of 100 mm (JF-P20R14-30, JF-P14R10-30). In addition, the composite beam using a JFRPC plate with a small aggregate size as topping aggregate (JF-P14R10-30, JF-P14R10-F) had a lower deflection compared to the composite beam using a JFRPC plate with a larger aggregate size as topping

Table 2 Performance of composite beam

Types of concrete	Properties	
	Flexural strength, MPa	Deflection, mm
JF-P20R14-30	5.58	0.415
JF-P20R14-F	6.27	0.470
JF-P14R10-30	5.55	0.300
JF-P14R10-F	6.69	0.385

aggregate (JF-P20R14-30, JF-P20R14-F) but there is an insignificant change in flexural strength. In addition, the composite beam (all types as shown in Table 2) had a minimum flexural strength of 1.40 times higher than the PCC, and the PCC deflection (0.175 mm) was lower than the composite beam.

In accordance with ACI 318, there are four deflection limits as specified, two for live load deflection, span length/180 and span length/360; and two for long-term deflection, span length/240 and span length/480. As for Eurocode 2, the deflection is limited to span length/250. By comparing the obtained deflection as shown in Table 2, the deflections of the composite beam were lower than the deflection limits set by the ACI 318 and Eurocode 2.

3.3 Connection of PC and JFRPC

In actual practice, the size of permanent formwork will be bigger than in Sect. 3.2. The permanent formwork will be placed together and used for a bigger beam and slab. Therefore, the connection between the permanent formworks is very crucial. Thus, this Sect. 3.3 investigates the effect of different connection gaps and connection angles between the permanent formworks.

The prepared samples were PC and JFRPC with the dimension of 40 × 160 × 12 mm and cured for 7 days. Later, the samples were cut into two different angles as shown in Figs. 3 and 4, and drilled to a depth of more than half the thickness of samples. As can be observed in Table 3, there were different codes assigned to PC and JFRPC. PC means polymer concrete, JF means jute fabric, 90° means the connection angle between the samples as shown in Fig. 3, 45° means the connection angle between the samples as shown in Fig. 4, NG means no gap which the cut and drilled samples were placed close with each other and 2G means 2 mm gap which the cut and drilled sample were placed 2 mm apart from each other, as shown in Figs. 3 and 4.

Steel with a diameter of 1 mm and a length of approximately 15 mm was used as reinforcement at connection. After placement of reinforcement at the connection, a PC paste containing a mixture of 1 part resin and 1 part fly ash with a total mass of resin and fly ash was poured at the connection and tested for a three-point flexural test using CBR test machine after 7 days of curing at ambient temperature. The result of flexural strength and deflection for PC and JFRPC with different connection gaps and angles of connection is shown in Table 3.

For PC with connection, the angles of connection affected the flexural strength and deflection as shown in Table 3. PC-45°-NG and PC-45°-2G had higher flexural strength and deflection compared to PC-90°-NG and PC-90°-2G, respectively. The difference in flexural strength is more obvious than deflection. This is because the 90° connection angle was a weak point due to the testing load (three-point flexural test) applied at the middle of the connection. As for the 45° connection angle sample, although the applied testing load was at the middle of the samples it was not as critical as the 90° connection angle sample. In terms of the gap, PC-90°-2G and PC-45°-2G

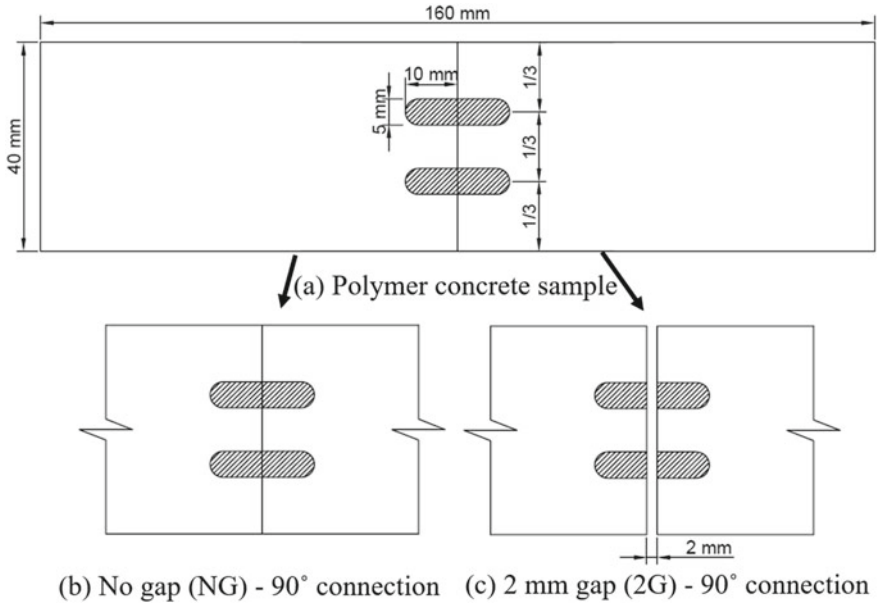

Fig. 3 90° connection of PC

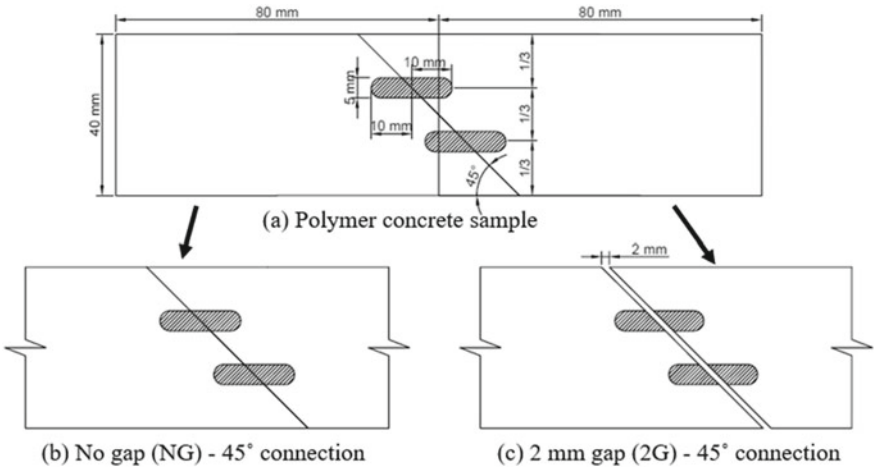

Fig. 4 45° connection of PC

had higher flexural strength and deflection compared to PC-90°-NG and PC-45°-NG. This is because, for no gap sample, the PC paste cannot fully fill the gap between the samples. Although the testing parameter was called no gap, there was still a little gap that was less than 1 mm between the samples. So, the bond strength between the sample was affected compared to the sample with a 2 mm gap.

Table 3 Performance of PC and JFRPC with different types of connection

Types of concrete	Properties	
	Flexural strength, MPa	Deflection, mm
Polymer concrete		
PC-90°-NG	5.60	0.771
PC-45°-NG	17.34	0.942
PC-90°-2G	12.01	0.986
PC-45°-2G	20.53	1.176
Jute fabric-reinforced polymer concrete		
JF-90°-NG	6.27	0.820
JF-45°-NG	18.39	1.134
JF-90°-2G	10.93	1.139
JF-45°-2G	24.20	1.152

For JFRPC, the trends of the results for the effects of gaps and angles are the same as for PC with connections. The reasons for the effect are the same for a PC with a connection for both different connection angles and connection gaps. By comparing the result from Tables 3 to 1 (no connection), it is shown that only PC-45°-NG, PC-45°-2G, and JF-45°-2G had higher flexural strength and deflection compared to PC and JFRPC without connection. Therefore, it can be summarized that the suitable connection angle is 45° with a 2 mm gap.

4 Conclusion

This research was conducted to investigate the potential use of jute fabric-reinforced polymer concrete (JFRPC) as permanent formwork for building a structure by investigating its mechanical performance. The composite structure is the use of JFRPC as a permanent formwork cast with the PCC on top. A comprehensive study was conducted to investigate the properties of Portland cement concrete (PCC), polymer concrete (PC), and JFRPC in terms of compressive strength, flexural strength, and deflection. Moreover, the performance of composite beams was investigated. In addition, the connection between the permanent formworks was conducted. From the results and analysis, it can be concluded that:

- The strength development of compressive strength and flexural strength for PC was 4.00 times and 9.30 times faster than PCC (28 days strengths), respectively.
- Composite beam had higher flexural strength ranging from 41.20 to 70.20% compared to PCC. In addition, the deflection of composite beams still achieved the minimum requirement of deflection limits as stated in ACI 318 and Eurocode 2.
- The connection between the JFRPC permanent formworks was affected by different connection gaps and connection angles. The suitable connection gap

and connection angle are 2 mm and 45°, respectively, between the permanent formworks.

Therefore, from the results and analysis, JFRPC plates have the potential to be used as permanent formwork for building a structure.

Funding This work was supported by Universiti Malaysia Sarawak (UNIMAS) Research Grand [grant number F02/InRG/1927/2019].

References

1. Jin Q, Leung CK, Yu C (2013) Effective joining method for pseudo-ductile permanent formwork. Mater Struct 46:345–360
2. Gai X et al (2013) Experimental investigation into a ductile FRP stay-in-place formwork system for concrete slabs. Constr Build Mater 49:1013–1023
3. Hasselhoff J, Cheng L, Waimer F, Gabler M, Knippers J (2015) Design, manufacturing and testing of shear-cone connectors between CFRP stay-in-place formwork and concrete. Compos Struct 129:47–54
4. Bank LC, Malla AP, Oliva MG, Russell JS, Bentur A, Shapira A (2009) A model specification for fiber reinforced non-participating permanent formwork panels for concrete bridge deck construction. Constr Build Mater 23(7):2664–2677
5. Kim H, Lee CJ, Shon CS, Moon H, Chung CW (2020) Mechanical performance and chloride ion penetration of polyolefin fiber reinforced concrete designed for shotcreting at marine environment. J Struct Integr Maint 5(1):8–17
6. Huang BT, Li QH, Xu SL, Li CF (2017) Development of reinforced ultra-high toughness cementitious composite permanent formwork: experimental study and digital image correlation analysis. Compos Struct 180(15):892–903
7. Tian H, Zhou Z, Zhang Y, Wei Y (2020) Axial behavior of reinforced concrete column with ultra-high performance concrete stay-in-place formwork. Eng Struct 210
8. Gazalba Z (2015) Flexural behavior of steel reinforced lightweight concrete slab with bamboo permanent formworks. Proc Eng 125:865–872
9. Li M et al (2018) Structural response of cement-bonded wood composite panels as permanent formwork. Compos Struct 209:13–22
10. Kim GB et al (2008) Development of thin FRP reinforced GFRC permanent formwork systems. Constr Build Mater 22(11):2250–2259
11. Leung CK, Cao Q (2010) Development of pseudo-ductile permanent formwork for durable concrete structures. Mater Struct 43:993–1007
12. Li QH, Huang BT, Xu SL (2016) Development of assembled permanent formwork using ultra high toughness cementitious composites. Adv Struct Eng 19(7):1142–1152
13. Kim HY, Koh KT, You YJ, Ryu GS, Seo DW, Jin SS, Nam JH, et al. (2020b) Load-deflection behaviour of concrete slab-type elements casted on stay-inplace TRC formwork. Compos Struct 244
14. Fam A, Cole B, Mandal S (2007) Composite tubes as an alternative to steel spirals for concrete members in bending and shear. Constr Build Mater 21(2):347–355
15. Nicoletta B, Woods J, Gales J, Fam A (2019) Postfire performance of GFRP stay-in-place formwork for concrete bridge decks. J Compos Constr 23(3):1–15
16. Amir F, Nelson M (2012) New bridge deck cast onto corrugated GFRP stay-in-place structural forms with interlocking connections. J Compos Constr 16(1):110–117
17. Mark N, Fam A (2014) Full bridge testing at scale constructed with novel FRP stay-in-place structural forms for concrete deck. Constr Build Mater 50(15):368–376

18. Richardson P, Nelson M, Fam A (2014) Fatigue behavior of concrete bridge decks cast on GFRP stay-in-place structural forms. J Compos Constr 18(3)
19. Boles R, Nelson M, Fam A (2015) Durability of bridge deck with FRP stay-in-place structural forms under freeze-thaw cycles. J Compos Constr 19(4)
20. Noran W, Soudki KA (2013) Flexural behavior of PVC stay-in-place formed RC walls. Constr Build Mater 48:830–839
21. Scott B, Wahab N, Al- A, Soudki KA (2016) Effect of stay-in-place PVC formwork panel geometry on flexural behavior of reinforced concrete walls. Structures 5:123–130
22. Yeon KS et al (2015) Comparative study on the elastic modulus of polymer concrete. Adv Mater Res 1129:145–150
23. Sousa SPB et al (2017) Mechanical behaviour analysis of polyester polymer mortars reinforced with tire rubber fibres. Ciência Tecnol Dos Mater 29(1):162–166
24. Hashemi MJ et al (2018) Investigating fracture mechanics and flexural properties of unsaturated polyester polymer concrete (UP-PC). Constr Build Mater 163:767–775

Microstructural Properties of Polymer-Modified Self-Healing Concrete Using Scanning Electron Microscopy and X-ray Diffraction

C. Manoj Kumaar and M. Mageswari

1 Introduction

Concrete's adaptability, sustainability, and economy have made the world's most extensively used composite material in construction. It is the product of the reaction of hydraulic cement with water. It is generally preferred for desired compressive strength and excellent durability during the service life of the structures. The properties of concrete are influenced by the properties of both constituent phases and the existence of their interfaces. Unfortunately, concrete is susceptible to many sources of cracking. Cracking is a common cause of grievances in the concrete industry. Cracks can form at any stage of its life. The presence of cracks may reduce the durability and affect the aesthetics of concrete structures. Apart from cracks, the porous matrix of concrete can also be a point of concern. If the pores are connected in the form of a network, the detrimental matter may permeate the concrete and may chemically or physically destruct the concrete as well as the reinforced steel.

Self-healing concrete is the ability of concrete to heal its microcracks autonomously like any living organism [1]. Repairing cracks in concrete structure is vital for its durability and structural safety. Types of self-healing concrete can be carried out by several processes and are identified in past research works for the design of self-healing concrete. The main three categories are (1) natural self-healing, (2) biological self-healing and (3) chemical self-healing [2].

C. Manoj Kumaar (✉)
Department of Civil Engineering, Sathyabama Institute of Science and Technology, Chennai, India

M. Mageswari
Department of Civil Engineering, Panimalar Engineering College, Chennai, India
e-mail: mag_rajabishek@rediff.com

K. S. Satyanarayanan et al. (eds.), *Sustainable Construction Materials*, Lecture Notes in Civil Engineering 194, https://doi.org/10.1007/978-981-16-6403-8_24

1.1 Super-Absorbent Polymer

The super-absorbent polymers act as hydrogels and absorb water through hydrogen bonding with hydrogen molecules as they are cross-linked [3]. A SAP has the ability to absorb water up to 300 times by its weight. It is a network of polymeric chains in parallel and regularly linked to each other by cross-linking the agents [4]. When SAP is in contact with water, it draws and stores the water molecules into the core of its polymeric network.

1.2 Microstructural Study

At the microscopic level, the behaviour of every material can be understood in terms of discontinuities among the interfacial zones, pores, cracks and the relationship between its structure and properties.

At the microstructural level, the concrete is exceptionally a complex matrix of solid phases, pores and water, with a poor degree of homogeneity. There are two broad categories of microstructural study, namely indirect or bulk techniques and direct techniques. Indirect techniques include thermogravimetry (TG), X-ray diffraction and mercury intrusion porosimetry (MIP) [5]. The direct techniques which provide information about the way in which the component phases are arranged in the microstructure are scanning electron microscope and backscattered electron images [5]. SEM can observe large cross-sectional areas. However, they do not show good secondary electron contrast. Using a pair of backscattered electron detectors, images can be produced in which the intensity is dependent on the average atomic number of the scanned area. Thus, in polished unetched sections, the anhydrous gel, enormous calcium hydroxide, other hydrates, porosity and aggregate particles can be distinguished from one another.

1.3 Scanning Electron Microscopy Test

The scanning electron microscope test was conducted using a high-resolution field emission electron microscope with an EDS instrument to reveal the information about the hydrated cement paste including its external morphology, chemical composition and crystalline structure [6]. The magnifications adopted in the test were 5000 $\times$ and 20,000 $\times$.

1.4 X-ray Diffraction Test

X-ray powder diffraction is used for phase identification of the crystalline hydrants in the cement paste [7]. The hardened cement paste is finely ground, homogenized and used for the test.

2 Methods

2.1 Control Concrete (CC)

Control concrete of M40 grade was designed to achieve a 28-day compressive strength of 40 MPa at a water–cement ratio of 0.43. The CC mix included 400 kg/m^3 of cement, 735 kg/m^3 of river sand and total water content of 172 kg/m^3. The coarse aggregate of size varying from 20 to 12 mm was used and the total content of coarse aggregate used was 1136 kg/m^3.

2.2 Polymer-Modified Concrete (PMC)

The same mix design was followed for PMC with an addition of 1% of PVA as a super-absorbent polymer in the form of an aqueous solution. Since PVA was added in the form of an aqueous solution, the water content was reduced according to the concentration of PVA, till a true slump was obtained from the slump test. An equal water–cement ratio of 0.43 is maintained in both samples.

2.3 Preparation of Samples

A total of 24 samples were prepared out of which 12 samples belonged to the control concrete and the other 12 belonged to the polymer-modified concrete. The sample was cast in the standard mould of 150 × 150 × 150 mm cube. The casted control concrete cubes were placed under the water for curing and PMC was air-cured.

2.4 Testing

The samples are tested on the 7th, 21st and 28th day for compressive strength. The three cubes from each batch were given pre-cracks that are visible by naked eyes under a range of load varying from 17 to 25 MPa. The pre-cracked cubes were

exposed to open air for a self-healing process for a period of 28 days from the day the crack was given. The samples which were subjected to complete failure on the 56th day were collected to study the microstructural effect of the addition of SAP. The samples were collected on its 28th day for the microstructural study using SEM and XRD. The samples kept for self-healing were again taken after 28 days and the healed cracks were observed in both samples [8]. The conventional concrete showed partial healing, whereas the PMC resulted in complete healing of the crack. The samples again were taken and tested for compressive strength and the obtained result was compared and studied.

3 Test Result and Discussion

3.1 Compression Test

This test was conducted to determine the compressive strength of concrete at its various ages. The cubical moulds of size 150 mm × 150 mm × 150 mm are adopted for casting the samples. From the values obtained in Table 1, it can be observed that 95%, 96.3% and 98.6% strength of CC is achieved by the PMC on 7th, 21st and 28th day, respectively. The marginal decrease in strength of PMC in the initial stage is due to the slow hydration process due to the presence of PVA. This can be due to the entrapment of the cement particles by the super-absorbent polymer in the PMC. As the SAP was added in the PMC the hypothetical delay in the hydration process can be attributed to the polymer film that is formed around the cement particles [9]. Thus as these cement particles are arrested within the SAP all the cement particles could not actively participate in the hydration, thus giving a minor reduction in the compressive strength. After a healing period of 28 days, the PMC achieved the same strength as that of CC. The addition of SAP has increased the viscosity by forming air encapsulation in the mixing stage of concrete and hence it is the cause of reduction in compressive strength [10].

The compressive strength after the 28 days of self-healing showed that the PMC had better hydration during the self-healing phase and the main reason for this could be that the arrested cement particles within the PMC would have reacted rapidly as

Table 1 Compressive test result

Stress	Age (days)	CC (MPa)	Polymer-modified concrete (MPa)
Ultimate	7	27.19	21.46
Ultimate	21	37.63	35.92
Ultimate	28	41.44	39.93
Pre-cracking stress	28	37.3	37
After healing	56	40.73	42.5

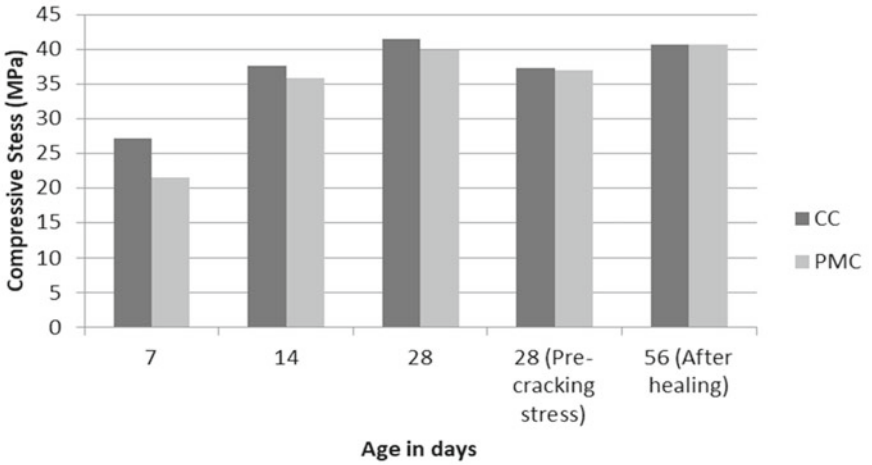

Fig. 1 The comparison of the average values of compressive strength of CC and PMC

soon as the cracks provided allowed the atmospheric moisture and gases to enter the concrete allowing it to react with the unhydrated cement particles and helping for self-healing (Fig. 1). The products of hydration filled the gaps and self-healed the PMC concrete in an exceptional way. However, the control concrete, on the other hand, showed a minute self-healing effect and this is because the hydration was rapid on the initial phase of curing and almost all the cement particles were already hydrated, hence when the cracks were developed there remained very few cement particle to take part in hydration for self-healing.

3.2 Self-Healing Efficiency

The self-healing efficiency is the parameter to measure the closure of cracks in terms of recovery of mechanical property in terms of compressive strength after the healing process [11].

Self-healing efficiency is given by Eq. (1):

$$\eta^{\infty} = \frac{(\text{Strength of healed specimen} - \text{Pre - cracking stress})}{(\text{Strength of Virgin specimen} - \text{Pre - cracking stress})} \times 100\,\% \qquad (1)$$

The self-healing efficiency of PMC and CC are 122% and 83%, respectively. This is because enormous unhydrated cement particles were present in PMC unlike in CC which could re-hydrate during the self-healing period.

3.3 Formation and Healing of Microcracks

Normally, a large number of microcracks of range 0.1 mm in length and macrocracks are observed in the cement matrix before loading. Under stress, these microcracks disseminate to develop major cracks and subsequently causes damage to structure [12]. The samples of both mixes developed minor cracks at the same pre-cracking stress as mentioned in Table 1. The cracks before and after the healing period are shown in Figs. 2, 3, 4, 5 and 6.

Fig. 2 The initial crack stage in CC

Fig. 3 The self-healed image of CC

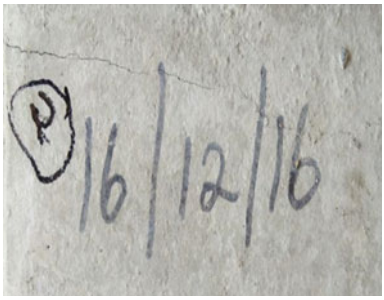

Fig. 4 The initial crack of PMC

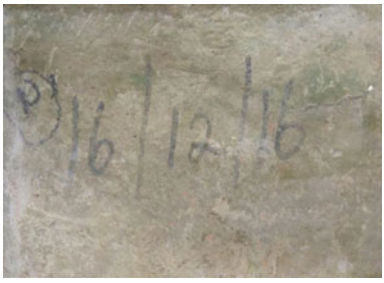

Fig. 5 The self-healed image of PMC

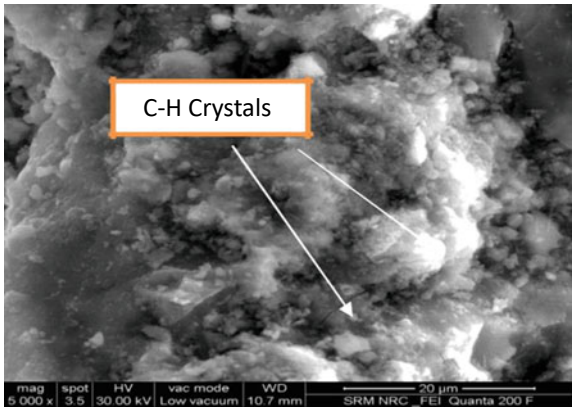

Fig. 6 The SEM image of CC under a magnification of 5000 ×

The number, size and propagation of microcracks traced in the interfacial zones (ITZ) of concrete can affect its strength, ductility and durability [12].

3.4 SEM Analysis

The magnification of 5000 × revealed a very homogeneous plain concrete (Fig. 6), while a large fluffy shape occurred in PMC (Fig. 7). Under the magnification of 20,000 x, the CC has shown denser matrix (Fig. 8) while the PMC has exhibited quite fluffy hydrates (Fig. 9) [13]. In fact, in the samples without PVA (Figs. 6 and 8), the dense matrix representing the characteristics of crystalline formations, interlocked by fibrous structures has been observed. From the microstructure of the CC obtained by SEM images, the cementitious compounds in the form of hydrated crystals were observed. The crystalline calcium hydroxide gel and calcium silicate hydrate are the products formed out of a reaction between calcium silicates and water, due to which the whole microstructure of the control specimen is found to be dense with a few pores. The precipitated C-S–H slows down the rate of reaction. The SEM micrographs of concrete containing super-absorbent polymer are shown in Figs. 7

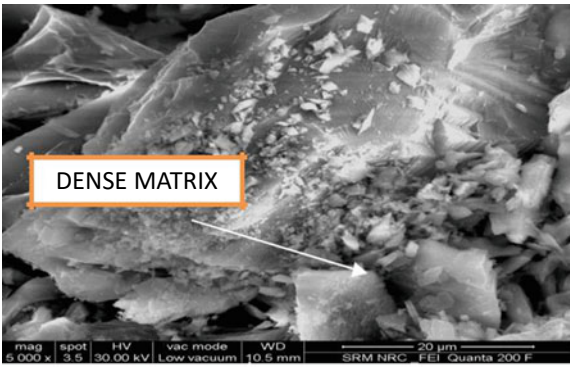

Fig. 7 The SEM image of PMC under a magnification of 5000 ×

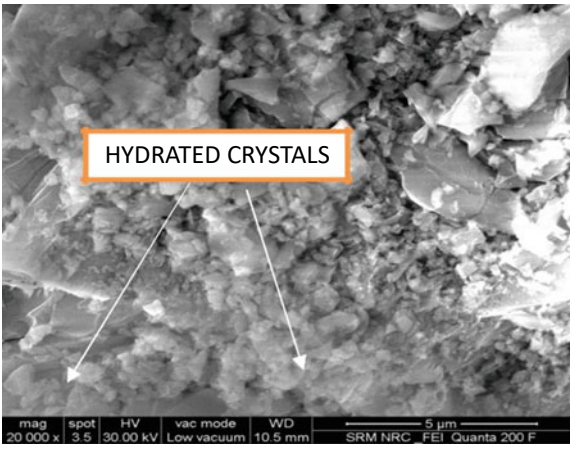

Fig. 8 The SEM image of CC under a magnification of 20,000 ×

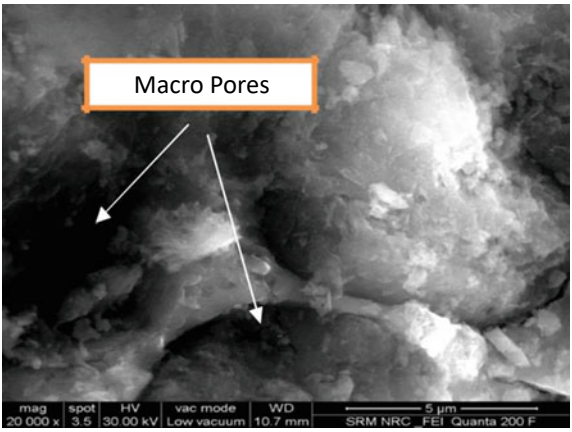

Fig. 9 The SEM image of PMC under a magnification of 20,000 ×

and 9. Hence the presence of unhydrated cement particles proves that it will help in the self-healing at the later stage when cracks are formed.

SEM analysis of the control concrete and polymer-modified concrete showed a varying morphology under various magnification. The control concrete showed a compact homogeneous crystalline structure interlaced with gel structure composition. Magnification of higher resolution of PMC revealed the unhydrated cement mass in the pores of ITZ giving a fluffy colloidal nature rather than a crystalline nature, where the CC showed a sharp structure with the product of hydration which can be attributed to the hydration products of calcium silicate [11].

The presence of the unhydrated cement particle proves that this trapped cement particle would enhance the self-healing procedure because once the crack is given the atmospheric moisture is going to enter the cracks and this unhydrated cement particle trapped within the PMC will break and react with moisture content helping to seal the cracks with their reacted products. The modifications in the internal structure of the hydrated crystals of the sample containing SAP can be easily observed in the SEM micrographs. The SEM analysis of the control concrete and polymer-modified concrete showed a varying morphology under various magnification. The control concrete showed a compact homogeneous crystalline structure interlaced with gel structure composition.

Magnification of higher resolution of PMC revealed the unhydrated cement mass in ITZ before the self-healing period, giving a large fluffy [14] colloidal nature rather than a crystalline nature. However, the CC showed a sharp structure with the product of hydration which can be attributed to the hydration products of calcium silicate before self-healing. This unhydrated cement particle trapped within the PMC will get exposed and react with moisture content when the crack occurs, helping to seal the cracks with their reacted products.

3.5 X-ray Diffraction

The XRD is a technique used to determine the crystalline growth of calcium hydroxide (portlandite) and ettringite in concrete [15]. This technique is also being extended to determine the early hydration process of cement, for example in the synthesis of ettringite [16]. However, the identification of cement phases present in concrete is more complex because hydration phases of concrete have weak diffraction peaks as they are mostly amorphous.

From the XRD analysis of diffractograms of CC (Fig. 10), it is visible that a higher number of peaks have resulted. The control concrete sample was analysed and from the graph we can infer that the maximum intensity count goes up to 11,000 and the highest peak touches an intensity count of 10,393. The diffraction angle of the highest peak corresponds to 26.5° 2ɵ. The second highest peak ranges between an angle of 24.3° 2ɵ. The third highest peak ranges from 28.5° 2ɵ. Other minor peaks are visible in ranges of 37.5°, 35.5°, 21.5°, 49.5°, 51.5°.

From the diffractograms of PMC (Fig. 11), the maximum intensity count goes up to 15,000 and the highest peak touches an intensity count of 14,418. The diffraction angle of the highest peak corresponds to 27.5° 2ɵ. The second highest peak ranges between an angle of 28.5° 2ɵ. Weak peaks were visible at a diffraction angle of 67.8° to 69° and very weak and minute peaks were also noted at a range of 21.5° and 55.5°.

The intensity of the X-ray diffraction line depends on the elemental composition of the sample and its preparation conditions. Samples may have a preferred direction (preferred orientation) for their growth. The crystallization and the more orderly arrangement of crystals are achieved as it shows a sharp peak with high intensity. The variation in the diffractogram can be there due to the more arranged crystalline nature of CC than that of the PMC. The XRD analysis was carried out on the 28th day before the self-healing phase started; hence because of this the peaks in CC correspond to the hydration products such as C-S–H, C-A-S–H, $Ca(OH)_2$ etc., whereas the PMC-modified concrete sample did not show variation as the SAP provided within the PMC arrested a large amount of water preventing it from reacting and forming various components.

XRD diffractograms of the CC gave a higher number of peaks than that of the PMC. From this, it is understood that the CC on the 28th day had a better crystalline structure than that of the PMC because the hydration during the initial stage of curing was higher in CC than in that of PMC because super-absorbent polymer absorbs a relatively larger quantity of water and transform it into gel rather than allowing the cement components to form crystalline structures initially. Due to the entrapped cement particle in PMC which was evident from the SEM analysis, it is confirmed that the crystalline structure formation in the PMC was low before the self-healing process because most of the cement particles could not involve in the hydration process. Thus from this, we can understand that the unhydrated cement will enhance the self-healing process during crack curing time, giving a more prominent crystalline nature to the PMC.

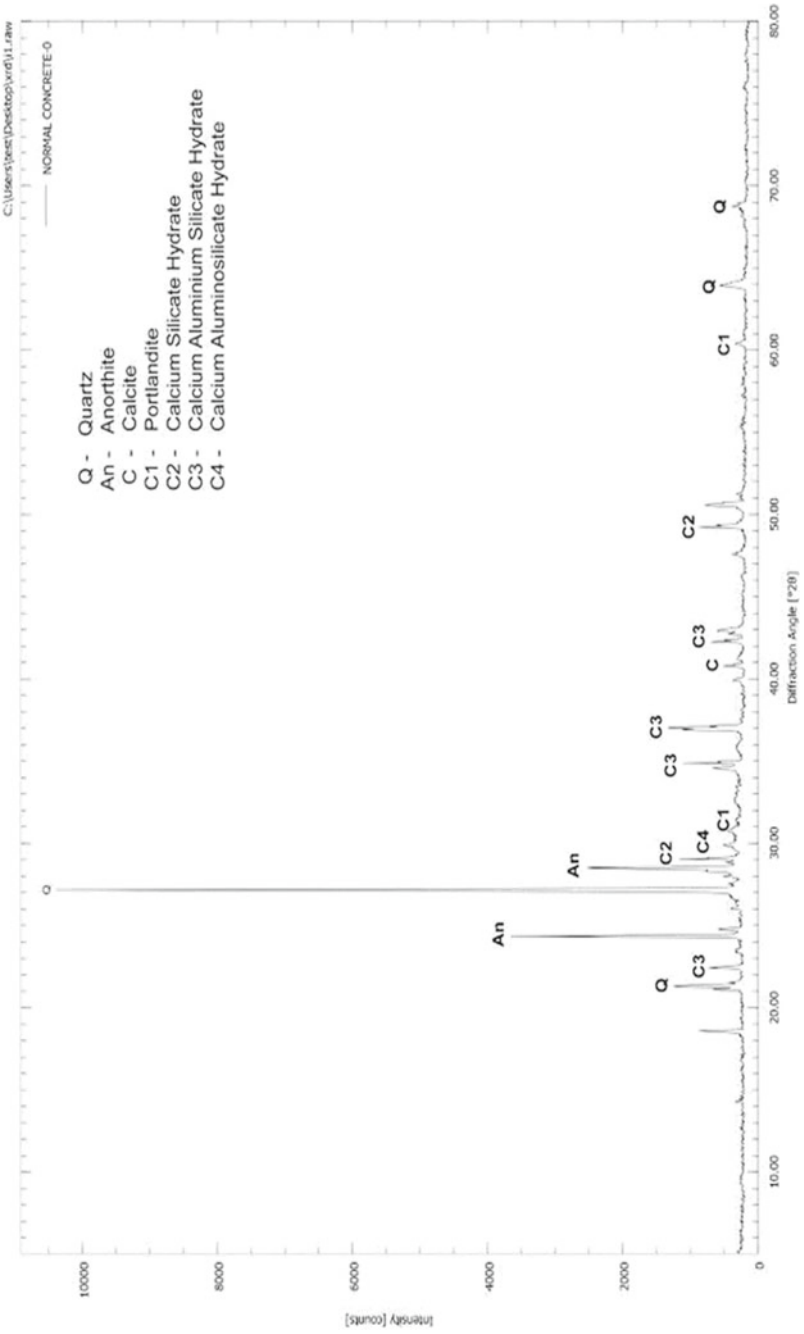

Fig. 10 Diffractograms resulted from the CC on the 28th day

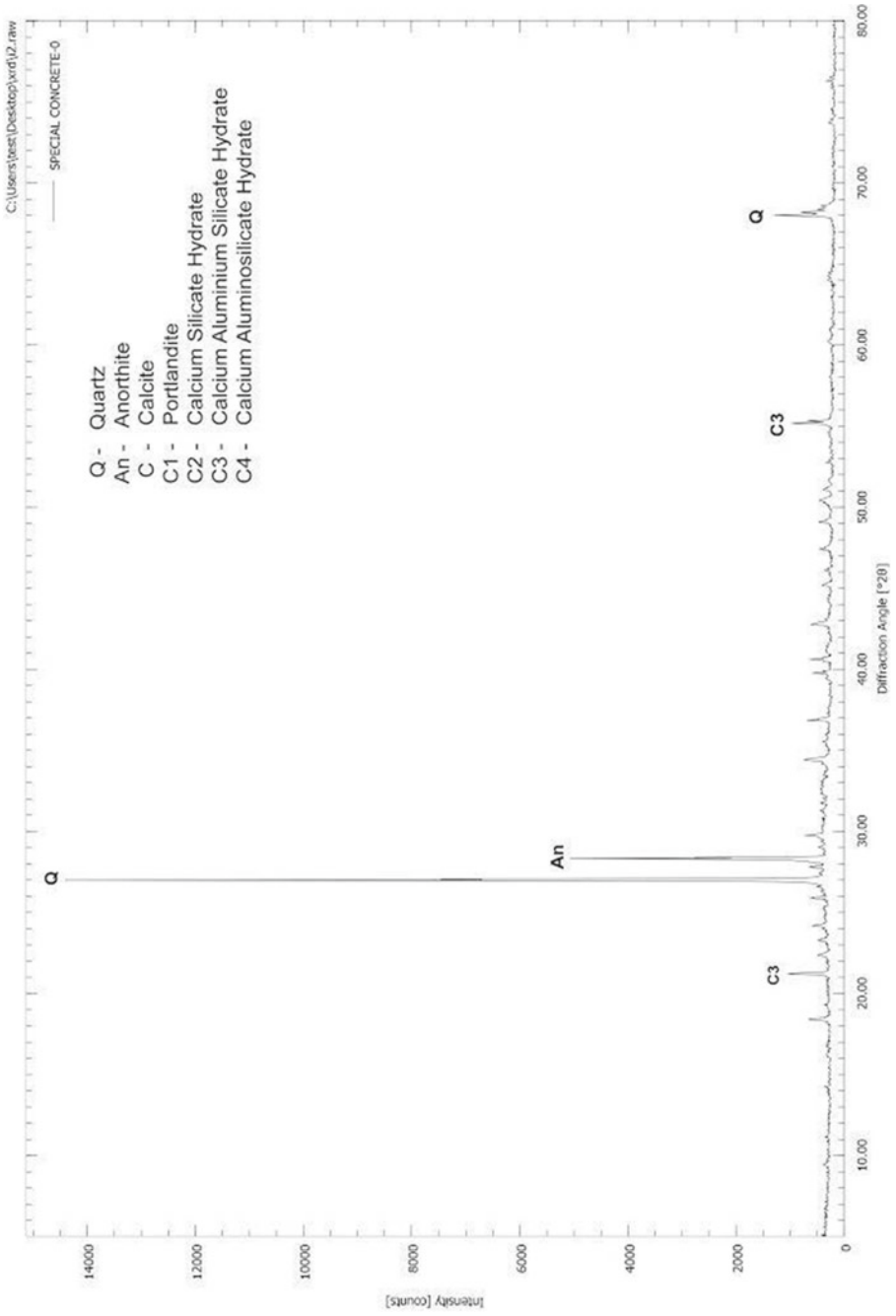

Fig. 11 Diffractograms resulted from the PMC on the 28th day

4 Conclusion

The performance behaviour of both fresh concrete and hardened concrete has been improved upon the addition of super-absorbent polymer in terms of workability and internal curing ability. It also helped in distributing the pores uniformly throughout the matrix. The comparative lower mechanical strength on the addition of the SAP effect is more noticeable at early ages due to the higher amount of total porosity. This total porosity reduces when the internal curing is carried out by the SAP. This leads to slow and prolonged hydration and thus the effect of SAP on gaining strength is achieved at later ages.

Acknowledgements The authors would like to thank Sathyabama Institute of Science and Technology for providing facilities to carry out the casting, curing and performing compression tests. The authors would also like to thank the Department of Chemistry, Indian Institute of Technology, Madras for helping to carry out the XRD analysis and Nanotechnology Research Centre, SRM Institute of Science and Technology, for carrying out the SEM analysis.

References

1. Manoj Kumaar C, Mageswari M (2021) Incorporation of nanocatalyst and its behaviour in green concrete structures: mechanical and microstructural study. Appl Nanosci (Switzerland), no. 0123456789
2. de Rooij M, Schlangen E, De Belie N, Van Tittelboom K (2013) Self-healing phenomena in cement-based materials, vol. 11. Springer
3. Kumaar MC, Mageswari M (2019) Recovery of mechanical properties of self healing concrete using super absorbent polymer (SAP). Int J Civil Eng Technol 10(2):202–210
4. Iffat S, Manzur T, Noor MA (2015) Super absorbent polymer in concrete as internal curing material. In: UKIERI concrete congress—concrete research driving profit and sustainability, no. November, pp 1632–1643
5. Ho H-L, Huang R, Lin W-T, Cheng A (Jan. 2018) Pore-structures and durability of concrete containing pre-coated fine recycled mixed aggregates using pozzolan and polyvinyl alcohol materials. Constr Build Mater 160:278–292
6. Qureshi T, Kanellopoulos A, Al-Tabbaa A (Dec. 2018) Autogenous self-healing of cement with expansive minerals-I: Impact in early age crack healing. Constr Build Mater 192:768–784
7. Qureshi T, Kanellopoulos A, Al-Tabbaa A (Jan. 2019) Autogenous self-healing of cement with expansive minerals-II: Impact of age and the role of optimised expansive minerals in healing performance. Constr Build Mater 194:266–275
8. Manoj Kumaar C, Mageswari M (2021) Thermal analysis on self-healing concrete using polyvinyl alcohol. Int J Ambient Energy 42(2):220–226
9. Wang Z, Yu J, Li G, Zhang M, Leung CKY (Jul. 2019) Corrosion behavior of steel rebar embedded in hybrid CNTs-OH/polyvinyl alcohol modified concrete under accelerated chloride attack. Cement Concr Compos 100:120–129
10. Paiva H, Silva AS, Velosa A, Cachim P, Ferreira VM (2017) Microstructure and hardened state properties on pozzolan-containing concrete. Constr Build Mater 140:374–384
11. Chindasiriphan P, Yokota H, Pimpakan P (2020) Effect of fly ash and superabsorbent polymer on concrete self-healing ability. Constr Build Mater 233:116975
12. Zhou J, Ye G, Van Breugel K (2016) Cement hydration and microstructure in concrete repairs with cementitious repair materials. Constr Build Mater 112:765–772

13. Blaiszik B (2010) Self-healing polymers and composites. Annual Rev Mater Res, no. October 2015, pp 179–211
14. Sclofani DAS, Contrafatto L (2013) Experimental behaviour of polyvinyl-alcohol modified concrete. Adv Mater Res 687(July):155–160
15. Li G, Huang X, Lin J, Jiang X, Zhang X (2019) Activated chemicals of cementitious capillary crystalline waterproofing materials and their self-healing behaviour. Constr Build Mater 200:36–45
16. Sidiq A, Gravina RJ, Setunge S, Giustozzi F (2019) Microstructural analysis of healing efficiency in highly durable concrete. Constr Build Mater 215:969–983

Post-buckling Analysis of Plate Girder with Web Opening

K. M. Akash Nithish, R. Nirmala, and S. T. Dhaarini

1 Introduction

Plate girders are currently made by welding three plates together: two flange plates and an I-section to a web fit. Blade curter is a cost-effective solution for broad span beams (over 20 m). The flexural strength of a plate is highest along its circumference. Welded plate girders, the most common form of plate girders, are structural steel members that consist of flange plates welded to a web plate with fillet welds. They are used to support loads at long intervals and to support structural loads that are too large to be supported by rolled steel forms. They are used as transfer ropes in building structures to support columns above areas where there is no large column. Plate ropes can be used to rehabilitate existing building structures that require non-columns and existing columns must be cut below a certain ground level or removed. Plate girders are used as crane support girders in heavy industrial structures with long gaps. The web plates or edge plates are connected as an assembly by appropriate angles. Also, since the plate circumference is expected to carry large loads, horizontal and vertical stiffeners are used in places where concentrated loads are operated to avoid excessive buckling [1]. To increase the moment of resistance, flange plates can be inserted at the flange angles. The bending moment to be resisted is reduced and the plates can be lowered where the plates are not needed [5].

Over the past decades, a majority of researchers have been openly studying steel plate blocks. The strength behaviour of trapezoidal curved corrugated beams with different radii of curvature, web thickness and edge thickness were examined. The result is reduced beam weight without compromising on strength, which can reduce costs by up to 30%. The use of corrugated nets in bridge construction will minimise the need for intermediate diaphragms for cross-load movement [10]. The dynamics of plate cutting buckling are studied using an experimentally validated finite element

K. M. Akash Nithish · R. Nirmala (✉) · S. T. Dhaarini
Department of Civil Engineering, Sathyabama Institute of Science and Technology, Chennai, India
e-mail: nirmala.civil@sathyabama.ac.in

K. S. Satyanarayanan et al. (eds.), *Sustainable Construction Materials*, Lecture Notes in Civil Engineering 194, https://doi.org/10.1007/978-981-16-6403-8_25

model. The findings of this analysis suggest that an abbreviated approach to calculating plate post-bucking shear performance is well reflected by an honest representation of shear bucking dynamics and detailed test data, where advanced associations with stress field action formulas are found in many situations [2, 4]. Thin-plate rope web panels are often exposed to a combination of bending, cutting and localised compression edge or patch loading [3]. While contact formulas for the final resistance to the combination of the two in the three types of loading have been suggested and tested by test results, it does not appear that any contact formula has been proposed for the three types of loading relation. Test results for integrated curvature, cut and connection loading are used to validate an integrated formula for the final resistance of thin-plate perimeter web panels [8]. The shear resistance of the transversely stiffened steel I-girders was evaluated and implemented in the bridge design specification [5, 6].

2 Test Specimens

The test specimens consist of two plate ropes 1.5 m long. Although two-blade curters were tested in each series, the girder measures 120 mm wide for both the sections and 500 and 400 mm depth for plate girders 1 and 2, respectively, as shown in Fig. 1 and Table 1. Four-blade curter were discovered and checked for inspection. The aperture

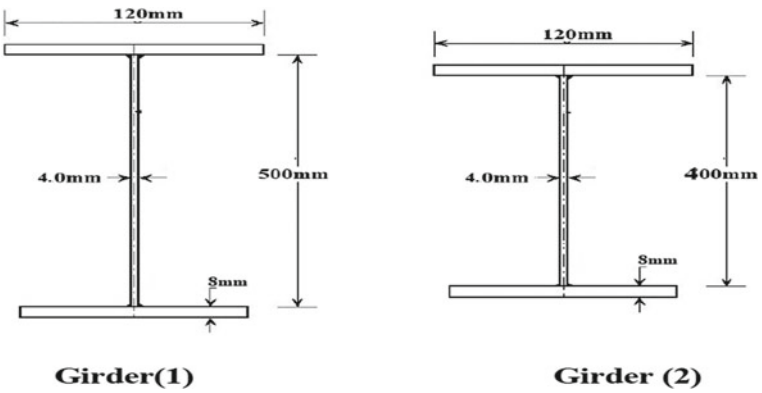

Fig. 1 Details of the specimen's configuration

Table 1 Details of the specimens tested

Specimen name	Web height (mm)	Web thickness (mm)	Flange width (mm)	Flange thickness (mm)
PG1	500	4	120	8
PG2	400	4	120	8

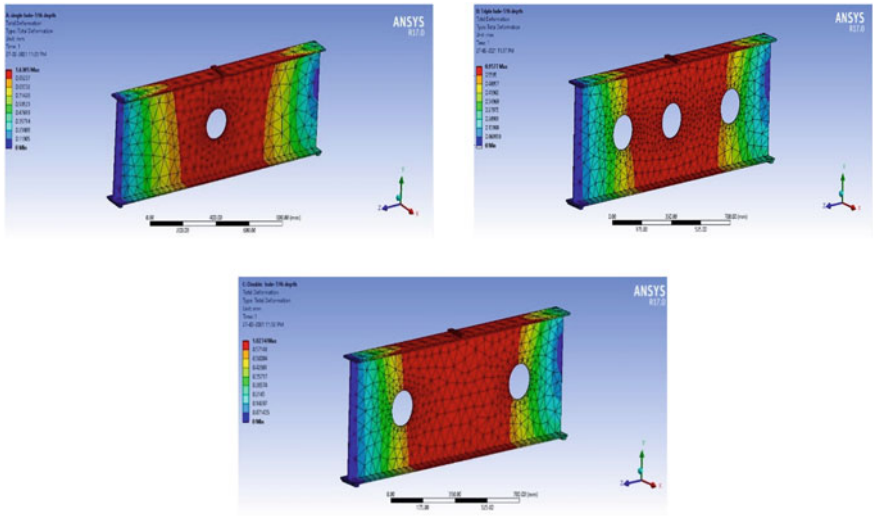

Fig. 2 Total deformation for plate girder 1

of the first model is 150 mm and the second model is 75 mm. The steel used has a yield strength of 250 N/mm. The web depth is the only distinction between the two girders. By welding the vertical mesh layer to the horizontal edge plates, each enclosure made of three plates functions as a unit (one upper and one lower edge).

3 Analytical Procedure

The finite element analysis is done using ANSYS software. All the beams were modelled and material specification as per IS516 was assigned. Fine meshing was applied to all the beams in order to avail the accuracy in the result. The beams are simply supported with one end pinned and another end roller. All beams are loaded with a uniformly distributed load. The load is applied gradually, and corresponding stress, strain and total deformation are analysed. The total deformation for the beam is given in Figs. 2 and 3.

4 Experimental Investigation

The investigation was performed in a loading frame of capacity 1500 kN and the plate girder was subjected to flexural test by one point load for a single hole and is presented in Fig. 4. The ends of plate girders are of simply supported conditions and loaded at mid-span. The application of loading was shown in the proving ring and the

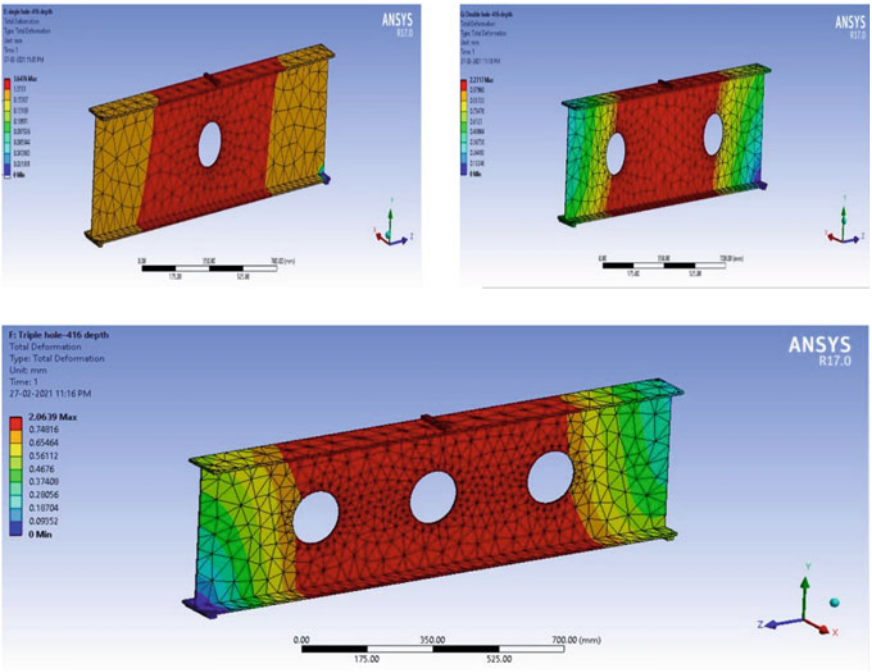

Fig. 3 Total deformation for plate girder 2

Fig. 4 Testing specimen of plate girders 1 and 2 for single hole

girder deformations were displayed with the help of dial gauges positioned below the mid-span of the girder. At each 2 kN/min load rise, the deviation was measured. The test was called off as the ropes began to sag and a significant deformation occurred, and there was no way to raise the load on the web panel and edges. The load was withdrawn after the girders collapsed.

5 Discussion on Results

The nonlinearity of the material was analysed using the von-Mises yield criteria theory. The outcomes exhibited that the peak load of the plate girder 1 are 379.45, 217.8 and 195.69 kN, while for plate girder 2 is 170.94, 101.55 and 88.029 kN for single-hole, double-hole and triple-hole, respectively, which are shown in Figs. 5 and 6. For investigational outcomes, the plate girders with single hole were studied by applying load progressively till the attainment of fracture. The peak load of plate girder 1 is 204 kN and for the plate girder 2 is 152.5 kN. The provision of increase in the number of web openings in the web portion of the plate girder decreases the peak load capacity [7]. Moreover, the provision of web opening fails the plate girder in the shear buckling of the web [9].

For performing experimental results from six ANSYS results, two best specimen results are taken and proceeded for experimental work, i.e., single hole with 500 × 120 mm and 400 × 120 mm are taken. From the comparison of ANSYS and experimental test values shown in Fig. 7, plate girder 1 bears the peak load capacity influenced by dimensions of the web of girder and the span/depth ratio.

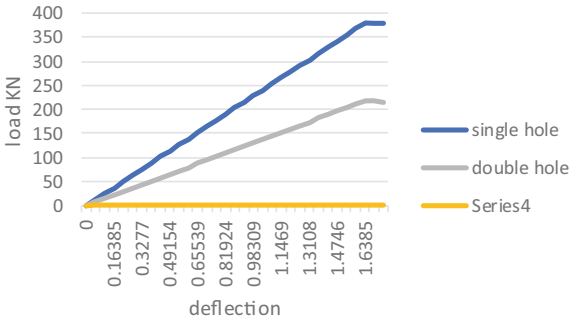

Fig. 5 Load versus deflection characteristics of plate girder 1 (single hole)

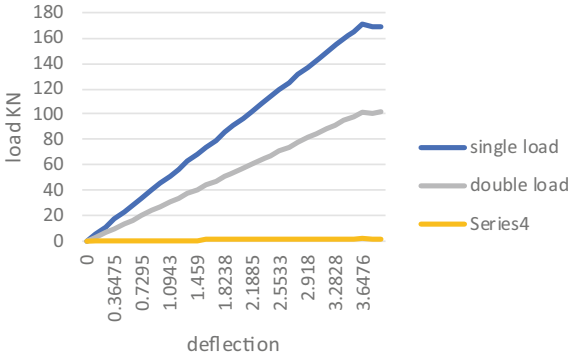

Fig. 6 Load versus deflection characteristics of plate girder 2 (single hole)

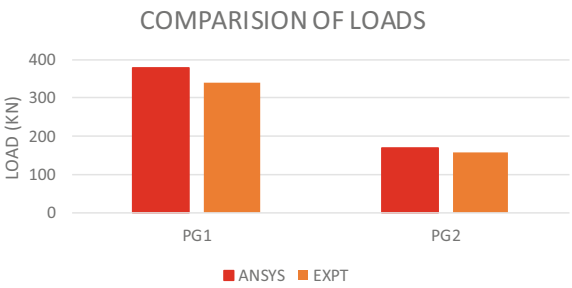

Fig. 7 Comparison of load–deflection observations using ANSYS and investigational approach (single hole)

6 Conclusion

The resulting inferences made from the analytical and experimental work conducted on the structural behaviour of plate girders with opening are:

- Owing to the consequence of shear and bending for perusing the performance of the shear strength and buckling, the plate girders were tested till failure.
- The outcomes exposed that the peak shear strength of the web panel can be exaggerated significantly by the web dimensions and the span/depth ratio.
- By pretending the behaviour of the web panel, there is an acceptable and good pact between the outcomes attained from the experimental and numerical study.
- The provision of openings in the web and its size leads to decreasing peak load capacity.
- As the web slenderness and flange stiffness ratios increase, the peak load decreases.
- The plate girders with opening failed by shear buckling of the web.
- The failure has arisen due to local flange buckling first for the 500 mm depth of plate girder.
- The validation of the investigational approach and ANSYS analysis were found to differ among 5 and 9%. This variance to some extent encompasses the let-downs of the experimental beams before comprehensive breakdown.

References

1. Lee SC, Yoo CH (1998) Strength of plate girder web panels under pure shear. J Struct Eng 124:184–194
2. Elgaaly M, Hamilton RW, Seshadri A (1996) Shear strength of beams with corrugated webs. J Struct Eng 122(4):390–398
3. Jiang J, Zhu Qi, Li G-Q (2015) Local bucking of compression flanges of H-beam with corrugated webs. J Constr Res 112:69–79
4. Glassman JD, Garlock MEM (2016) A compression model for ultimate post buckling shear strength. Thin—Wall Struct 102:258–272

5. Kim YD, White DW (2014) Transverse stiffener requirements to develop shear-buckling and post buckling resistance of steel-girders. J Struct Eng 140:198–208
6. Chacon R (2014) Mechanical behavior of the shear-patch loading interaction on transversally stiffened steel plate girders. Latin Am J Solids Struct 39:1721–1743
7. Morkhade SG, Lokhande RS, Gund UD, Divate AB, Deosarkar SS, Chavan MU (2020) Structural behaviour of castellated steel beams with reinforced web openings. Asian J Civil Eng
8. Ishac I, Hosseiny OE, Matar E, Mandour S (2014) Behaviour analysis of stiffened slender plate girders. Glob Think Struct Eng 3:1644–1648
9. Shahabian F, Roberts TM (2008) Behaviour of plate girders subjected to combined bending and shear loading. Sci Iran 15:16–20
10. Sruthi VV, Aathira BK, Sruthi D (2019) Finite element investigation on buckling behaviour of corrugated web beams-ansys workbench. Int Res J Eng Technol 6(5):6599–6604

Textile Fibre-Wrapping Techniques Used for Textile-Reinforced Concrete

A. Mohan and T. Ch Madhavi

1 Introduction

In the last 100 years, steel has been widely used as reinforcement in concrete along with superior properties such as strength, stiffness and very heavyweight. Steel reinforcement is limited to the size and shape of the concrete specimens. Due to corrosion of steel reinforcement, it loses most of the properties and also affects the properties of concrete. To increase the strength of reinforced concrete structures various strengthening methods are followed for decades.

Fibre-reinforced polymer (FRP) is found promising material in the field of strengthening due to its properties such as high strength and non-corrosive nature. FRPs strengthening materials are in the form of fabrics and laminates bonded to strengthen specimens with chemical-based epoxy resins [1]. Even though the usage of epoxy resins results in good bonding and high strength, it possesses some negative drawbacks that it cannot withstand high temperature, risk in human life, difficulties in bonding under wet conditions, poor fire resistances, non-reversible and low permeability.

One possible way to overcome these drawbacks is by replacing epoxy resins (organic materials) with cementitious binder matrix (inorganic binders) [2] with the development of new technology, namely known as textile-reinforced concrete or textile-reinforced mortar or fabric-reinforced concrete. The use of cementitious binder possesses some advantages which are not present in FRP, especially when used as reinforcement in old buildings as the matrix (inorganic binder). They are highly compatible and vapour permeable [3].

The textile-reinforced concrete strengthening technique may be considered as an alternative strengthening technique for fibre-reinforced polymer (FRP), which has been already laid its way into the field of strengthening. With the aim of

A. Mohan (✉) · T. Ch Madhavi
Department of Civil Engineering, SRM Institute of Science and Technology, Ramapuram, Chennai 600089, India

K. S. Satyanarayanan et al. (eds.), *Sustainable Construction Materials*, Lecture Notes in Civil Engineering 194, https://doi.org/10.1007/978-981-16-6403-8_26

overcoming specified problems raised with the use of organic resins used in fibre-reinforced polymer strengthening system, textile-reinforced concrete strengthening system comprised open long fibres or fabric roving in bi-direction and tri-direction along with inorganic mortar matrix is been applied. The TRC system can be applied similarly to that of the FRP system to any reinforced concrete or unreinforced concrete structure, i.e., masonry structure.

The main objective of the textile-reinforced concrete (TRC) strengthening system is to increase the strength of the existing structure (reinforced and unreinforced) as well as to increase the overall capacity of the strengthening structure.

For over the last two years textile fabric has been used for strengthening old reinforced and unreinforced structures. TRC was found to be a useful strengthening material alternative to FRP due to its advantages when combined with an inorganic binder such as good bonding behaviour under high temperature, high permeability, reversibility and good fire resistance.

Due to its high strength textile reinforcement is widely used in the field of construction works. Textile-reinforced concrete is mainly made of textile fibres or fabrics. These textile fibres or fabric are roved, yarn and wrapped as reinforcement mesh for strengthening structures. When the roving of yarn is bi-directional that is parallel and perpendicular to each other then they are known as 2D mesh (Fig. 1). Similarly, when the direction of textile fibre roved in a transverse direction they are known as tri-directional or 3D mesh (Fig. 2).

The properties, amount and arrangement of textile fibre materials have a great influence on the characteristics of composite TRC. Therefore, hence fibre material and fibres are made to meet the demands. In total, four types of textile fibre mesh reinforcement are available. All the meshes are made up of roving textiles filaments

Fig. 1 2D mesh

Fig. 2 3D mesh

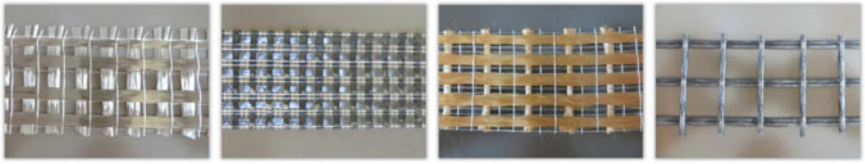

Fig. 3 Types of textile reinforcement concrete [14]

in two or more directions. High tensile materials, with negligible properties, are reinforced with fabrics. Different types of textile fibre available are (Fig. 3):

- Carbon textile reinforcement concrete [4]
- Glass/AR-glass textile reinforcement concrete [5]
- Basalt textile reinforcement concrete [6]
- Polyphenylene benzobisoxazole textile reinforcement concrete [7]

The experimental results of beams strengthened using carbon-FRCM (carbon-fibre-reinforced cementitious matrix) subjected to four-point loading concluded that beam strengthening achieves higher flexural capacity [8]. According to [9] based on confinement of cylinder and rectangular column (short) strengthening using textile mortar jacketing results in a sustainable increase in compressive strength and deformation, and gain in strength is achieved when the number of layers is increased. The application of PBO-FRCMb (polyparaphenylene benzobisoxazole fibre-reinforced cementitious matrix) mesh as shear strengthening improves the shear capacity of the bending structure [10]. Both axial load capacity and serviceability of reinforced columns are improved when strengthened using AR-glass textile-reinforced concrete [11]. The flexural behaviour of basalt textile-reinforced concrete plates, when tested under a four-point bending test, show an improvement in flexural capacity and toughness of the BTRC plates [12]. The axial loading capacity of a cylindrical element increases with an increase in the number of layer mesh [13].

In the present paper, various wrapping techniques adopted for strengthening reinforced or unreinforced structures are studied.

2 Wrapping Techniques

TRC is applied in the form of external jackets to any structure and should be located in the primary area where the load is acting. A critical evaluation and proper selection of the system should be made concerning standards for preservation. A building is made of different structural elements or components such as beams, columns and slabs. For strengthening these elements, different types of wrapping techniques are used such as

- Intrados or external wrapping
- U-wrapping
- Fully wrapping
- Partial wrapping
- Extrados or internal wrapping

Depending upon the structural performance and size of the section, the wrapping techniques are adopted. The application of textile-reinforced concrete can be employed for the following conditions of concrete structure:

- For increasing flexural and shear capacity of the structure to resist tensile stresses within the structure or in between joints.
- Crack with limitations
- Stiffen the structure
- For enhancing the axial capacity of the capacity.

2.1 Intrados or Externally Wrapping

Intrados strengthening or external wrapping strengthening system is mainly used for strengthening beams and slabs. Externally wrapping are done on the outer or exterior part of the strengthening specimen. This type of strengthening technique improves the flexural capacity of structural specimens.

Strengthening of beam or slab in flexural is obtained by bonding textile-reinforced concrete layer to tensile face or bottom surface of the structure, which is typically soffit or weak (Fig. 4). Textile-reinforced concrete is placed at the region or area where additional moment-carrying capacity needs to be increased. The anchorage length of textile reinforcement is provided to the full length of strengthening specimens.

Strengthening of beams or slabs significantly depends upon various parameters such as.

i. Number of layers of textile reinforcement used
ii. Reinforced concrete member detailing
iii. The inorganic cementitious binder used
iv. Material properties

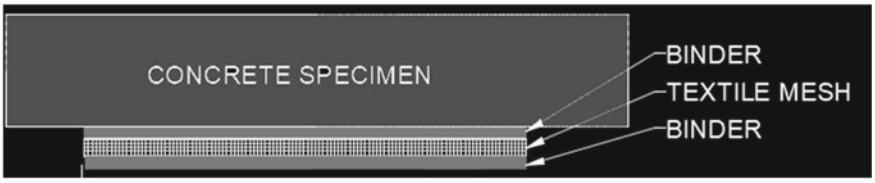

Fig. 4 Intrados wrapping

2.2 U Wrapping

U type wrapping is mostly done for strengthening beams under shear behaviour. Shear strengthening is one of the most common requirements when assessing the strength of the reinforced concrete structure. Shear strengthening is done when.

- Structure weak in shear reinforcement
- Improper shear reinforcement
- Corroding of shear reinforcement
- Low load-carrying capacity

Hence to increase the shear capacity of the reinforced concrete structure, U wrapping of textile reinforcement is applied at the critical section of the specimen (Fig. 5). As explained in Sect. 2.1 (external wrapping), U wrapping also depends upon parameters. Since the reinforced concrete specimen is strengthened using U-type wrapping in shear reinforcement, the shear strength is increased with a reduction in diagonal cracks width.

For strengthening reinforced or unreinforced structures using textile-reinforced concrete to increase both shear and flexural capacity, RC structures are strengthened using both U wrapping and external wrapping (Fig. 6).

Fig. 5 Shear strengthening U wrapping

Fig. 6 Combined wrapping

2.3 Fully Wrapping and Partial Wrapping

Fully wrapping and partial wrapping techniques of strengthening are mainly done for structures carrying an axial load (column (short and long column)). If the full length of the structural element is wrapped then it's known as full wrapping. Similarly, if wrapping techniques are adopted to the effective length of any structural element then it's known as partial wrapping.

To increase the compressive strength and deformation capacity, any structural component is subjected to axial force or axial load. A column with low axial capacity and poor detailing needs extra confinements with textile-reinforced concrete. Wrapping with textile reinforcement also increases seismic retrofitting or behaviour of the column. Similar to fibre-reinforced polymer, textile-reinforced concrete also can be wrapped easily in circular, rectangular or square columns. All sides of the column are fully or partially wrapped.

2.4 Extrados Wrapping

Structural elements with single curvature like arches, barrel vaults or double curvature like domes, due to the formation of hinges results in failure leads to the collapse of the partial or whole structure. Hinges result in zero tensile strength.

After the formation of hinges on the curved structure lead to collapse and failure of the curve structure. Failure mechanisms are related to hinge formation and can be meshed by bonding TRC to top reinforcement or bottom reinforcement (intrados or extrados strengthening) of the structural arch (Fig. 7). Generally, TRC layers can be applied on both sides of elements. By strengthening with textile-reinforced concrete mesh, the load-carrying capacity and structural performance of the arch or curved section are improved.

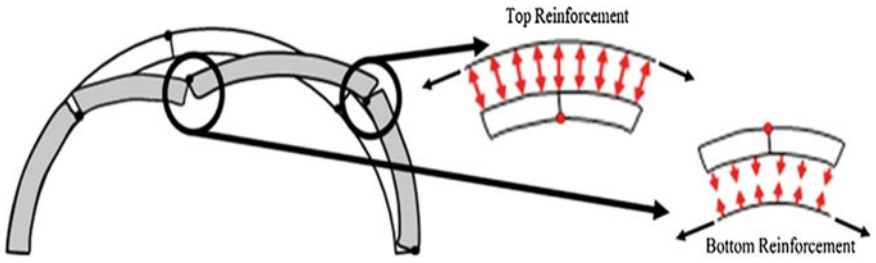

Fig. 7 Intrados and extrados strengthening [15]

3 Conclusion

This paper aims to study the various methods of wrapping techniques adopted for bonding textile-reinforced concrete with reinforced or unreinforced structures. Hence textile-reinforced concrete is a promising material in the field of strengthening and an alternative to the fibre-reinforced polymer strengthening technique.

References

1. Ombres L (2011) Flexural analysis of reinforced concrete beams strengthened with a cement based high strength composite material. Compos Struct 94:143–155. https://doi.org/10.1016/j.compstruct.2011.07.008
2. Loreto G, Leardini L, Arboleda D, Nanni A (2013) Performance of RC slab-type elements strengthened with fabric-reinforced cementitious-matrix composites. J Compos Constr 18:A4013003. https://doi.org/10.1061/(asce)cc.1943-5614.0000415
3. Arboleda D, Carozzi FG, Nanni A, Poggi C (2015) Testing procedures for the uniaxial tensile characterization of fabric-reinforced cementitious matrix composites. J Compos Constr 20:04015063. https://doi.org/10.1061/(asce)cc.1943-5614.0000626
4. Carozzi FG, Bellini A, D'Antino T, de Felice G, Focacci F, Hojdys Ł, Laghi L, Lanoye E, Micelli F, Panizza M, Poggi C (2017) Experimental investigation of tensile and bond properties of Carbon-FRCM composites for strengthening masonry elements. Compos Part B Eng 128:100–119. https://doi.org/10.1016/j.compositesb.2017.06.018
5. Gopinath S, Prakash A, Ahmed AKF (2020) Synergy of hybrid textile reinforced concrete under impact loading. Sadhana–Acad Proc Eng Sci 45. https://doi.org/10.1007/s12046-020-1312-9
6. Du Y, Zhang M, Zhou F, Zhu D (2017) Experimental study on basalt textile reinforced concrete under uniaxial tensile loading. Constr Build Mater 138:88–100. https://doi.org/10.1016/j.conbuildmat.2017.01.083
7. Zhang M, Zhou F, Zhu D (2017) Experimental study on basalt textile reinforced concrete under uniaxial tensile loading. Constr Build Mater 138:88–100. https://doi.org/10.1016/j.conbuildmat.2017.01.083
8. D'Ambrisi A, Feo L, Focacci F (2013) Experimental analysis on bond between PBO-FRCM strengthening materials and concrete. Compos Part B Eng 44:524–532. https://doi.org/10.1016/j.compositesb.2012.03.011
9. D'Ambrisi A, Focacci F (2011) Flexural strengthening of RC beams with cement-based composites. J Compos Constr 15:707–720. https://doi.org/10.1061/(asce)cc.1943-5614.0000218
10. Triantafillou TC, Papanicolaou CG, Zissimopoulos P, Laourdekis T (2006) Concrete confinement with textile-reinforced mortar jackets. ACI Struct J 103:28–37 https://doi.org/10.14359/15083
11. Trapko T, Urbańska D, Kamiński M (2015) Shear strengthening of reinforced concrete beams with PBO-FRCM composites. Compos Part B Eng 80:63–72. https://doi.org/10.1016/j.compositesb.2015.05.024
12. Ortlepp R, Ortlepp S (2017) Textile reinforced concrete for strengthening of RC columns: a contribution to resource conservation through the preservation of structures. Constr Build Mater 132:150–160. https://doi.org/10.1016/j.conbuildmat.2016.11.133
13. Du Y, Zhang X, Zhou F, Zhu D, Zhang M, Pan W (2018) Flexural behavior of basalt textile-reinforced concrete. Constr Build Mater 183:7–21. https://doi.org/10.1016/j.conbuildmat.2018.06.165

14. Al-Gemeel AN, Zhuge Y (2019) Using textile reinforced engineered cementitious composite for concrete columns confinement. Compos Struct 210:695–706. https://doi.org/10.1016/j.compstruct.2018.11.093
15. Escrig C, Gil L, Bernat-Maso E, Puigvert F (2015) Experimental and analytical study of reinforced concrete beams shear strengthened with different types of textile-reinforced mortar. Constr Build Mater 83:248–260. https://doi.org/10.1016/j.conbuildmat.2015.03.013

Experimental Study on a Concrete Member in Rectangular Cross-Section Using Wrapping of Sisal Fibre-Reinforced Concrete

M. Balasubramanian, K. Omraj, P. Mukilan, and S. Aishwarya

1 Introduction

In the following applications, natural fibre-reinforced polymer composites were replaced by plastic composites. Audi A3 side panel replaced by hemp fibre epoxy resins were composited with acrylonitrile–butadiene–styrene. The properties of natural fibre composites are determined by the fibres, matrix, and interactions between them. The majority of car panels are made from fibre. In recent years, natural fibres such as sisal, jute, pineapple, hemp, coconut coir, palm, cotton, bamboo, and wood have been used as reinforcement in polymer composite materials [1]. The mechanical properties of wood and glass of polypropylene composites are sufficient. The wire basket which is made from wood fibre and furniture pieces were often favoured in rural areas. Natural fibres have proved to be superior to synthetic fibres in the automotive, railways, coaches, aero-space, military, residential, structural, and construction industries for making ceiling panels and partition boards. Natural fibres are derived from seeds, fish, fruits, or some other mineral source; these natural fibres have a marginal length in contrast to agglomerations of cells that have a length, such as cotton, wood, leather, and plastic, etc. (Fig. 1). According to the report, in order to face these challenges, our country needs innovative, energy-efficient building materials for efficiency and good structure in a fast method of contracting construction at a fair cost. According to the research, fibre-reinforced concrete is a common form of concrete [2]. Fibre-reinforced cement concrete (FRCC) which contains synthetic materials will improve the fundamental trustworthiness and strength of the structure. Fibres are often used in concrete to control cracking due to both plastic and drying shrinkage. They also reduce the permeability of concrete, which can reduce water seepage. Sisal fibre is derived from the sisal, which is a solid leaf that resembles an overgrown pineapple plant and can be used to make brouds [3].

M. Balasubramanian (✉) · K. Omraj · P. Mukilan · S. Aishwarya
Department of Civil Engineering, SRM Institute of Science and Technology, Kattankulathur, Chengalpattu District, Tamil Nadu, India

K. S. Satyanarayanan et al. (eds.), *Sustainable Construction Materials*, Lecture Notes in Civil Engineering 194, https://doi.org/10.1007/978-981-16-6403-8_27

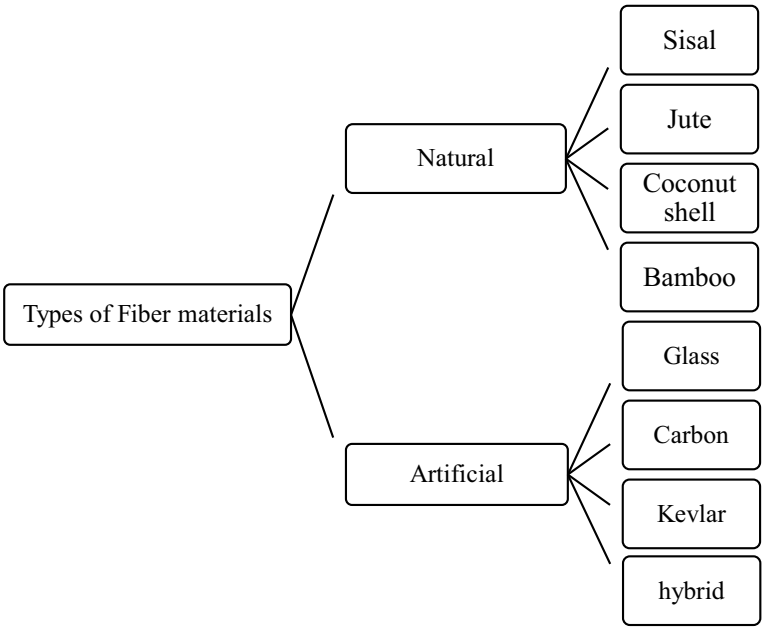

Fig. 1 Types of fibre materials

Agave sisalana is its botanical name, derived from the genus Agava, and sisal refers to fibre. The wire basket is made from wood fibre, and furniture pieces are often favoured in rural areas. The fibres are used as a traditional rope and twine as well as paper, linen, footwear, bags, carpets, caps, and so on. The plant has sword-shaped leaves that are about 2 m long at their height and have few teeth along the edges that fall down as the plant matures. Wrapping the surfaces of the beams will increase the flexure in the concrete action of the beams. Fibres are lightweight that can be extended more than 500% from their original size, while stress is relaxed or increased to its limit. These fibres are present naturally in plants and artificially derived from other materials that have fibre properties. Until wrapping sisal fibre, all faces should be clean, and the specimen should be cleaned. All holes in honeycombs should be filled with white putty. Then, in RCC beam faces, add a double coat of primer to cure for at least one day. A roller is used to add the output to the concrete floor, and it can cure in 7 days. RCC beams have characteristics such as being simple to plan and having a low corrosion rate in steel. It is suitable for use in thin items such as wooden door panels, patricians, and so on. The world suffers as a result of the consumption of these materials [4].

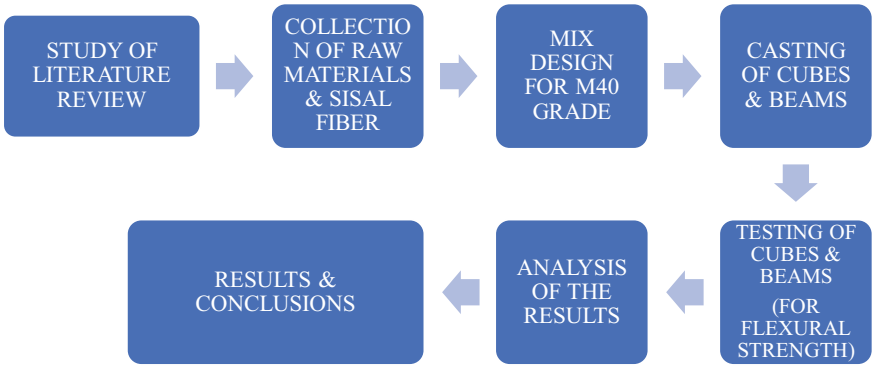

Fig. 2 Flowchart for methodology

2 Methodology

The methodology for this study is provided in Fig. 2.

3 Materials

3.1 Sisal Fiber

Fibre is a material that is introduced to protect materials from their hazardous. For example, earlier people used fibres as a covering material which helps them to protect from various hazardous activities like climate, heat, cold, etc., and these fibres are long strands that have a liner string-like structure. Sisal fibre obtained from the sisal is a strong leaf that looks like an overgrown pineapple plant which may be like brouds. It has a botanical name of Agave sisalana which derives from the species Agava in which the name sisal refers to the fibres [5]. Majorly sisal fibres are used as traditional rope and twine as well as paper, cloth, footwear, bags, carpets hats, etc., the plant has sword-shaped leaves around 2 m length maximum in which the young plant has few teeth along the margins and fall down after they mature shown in Figs. 3 and 4 [6]. Sisal plant has a 7–10 years life span which grows under 25 °C and sunshine which considered to be a plant of the tropics and subbing tropics. Sisal fibre is the only fibre that has higher tensile properties than that any other natural fibre available commercially [7]. From the available literature, polypropylene is used as a chemical admixture in order to create a very good bond strength between the fibre and the concrete [8]. Here to get a good value of flexural strength for concrete. The mechanical properties of sisal fibre are listed [9]. The detail form as given in Tables 1 and 2 show the chemical composition of sisal fibre.

Fig. 3 The henequen agave plants

Fig. 4 Sisal fibres

Table 1 Mechanical properties of sisal fibre

S. no	Type	Tensile strength (MPa)	Young's modulus (GPa)	Poisson ratio	Density kg/m^3	Length (cm)	Diameter mm
1	Natural	68	3.77	0.2–0.25	1450	12.5	50–200

Table 2 Chemical composition of sisal fibre

S. no	Composition	Percentage %
1	Cellulose	68
2	Hemi cellulose	15
3	Liginin	9.8
4	Waxe	1.9

4 Results and Discussion

4.1 Compressive Strength Test

In the compressive test, the cubes are placed in the compression testing machine with their faces at right angles to that as cast in the machine. According to the indicated standard specifications, the load on the cube was applied on the cube in a uniform manner till the cracks appeared in the cubes and finally the ultimate load is noted [10]. Table 3 contains the value for the cubes on different days.

Figures 5 and 6 describe the compressive strength test carried out for conventional concrete cubes.

4.1.1 Flexural Strength Testing

Three beams are used for the test where two beams are normal conventional concrete beams (B1, B2) and the remaining one used wrapping of sisal fibre (B3). The loading is provided generally as 20, 40, 60 KN, and so on till the ultimate load is obtained [11].

The flexural strength has been found out based on the results obtained and the results are provided in the form of a table below for better understanding [12]. Figures 7 and 8 show the testing of wrapping of sisal fibre RCC beam testing.

Table 3 Compressive strength of concrete cube

S. no	Grade of concrete	Compressive strength 7 days	Compressive strength 28 days
1	M40	29.50	41.58
2	M40	28.30	43.80
3	M40	28.70	40.39

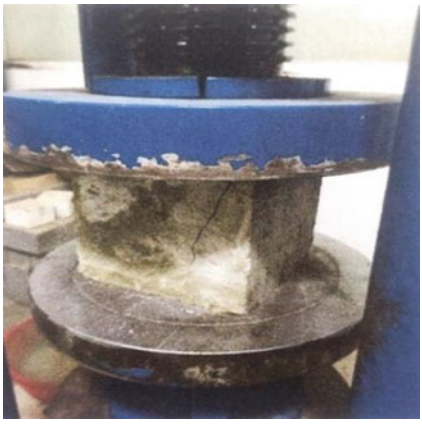

Fig. 5 Compressive strength test

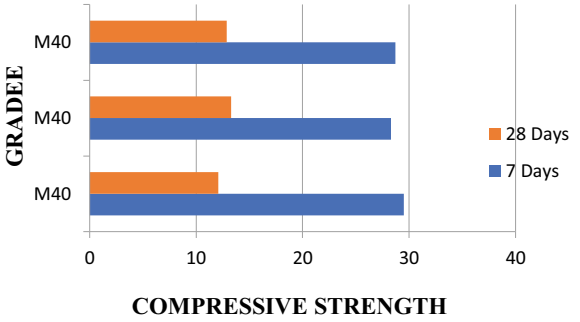

Fig. 6 Compressive strength test value

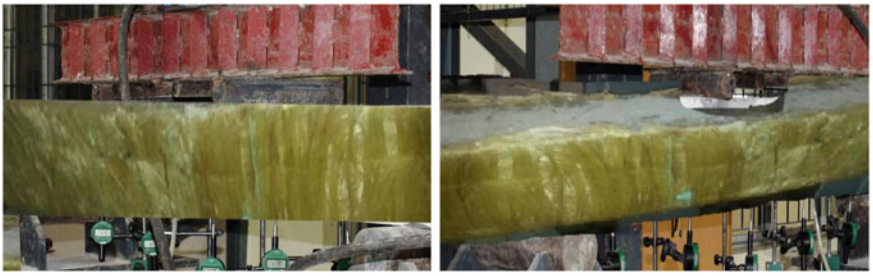

Fig. 7 Testing of wrapping of sisal fibre RCC beam

Fig. 8 Typical view of testing of wrapping of sisal fibre RCC beam

It is shown in Table 3 that the percentage values in the deflection of the beam sample of wrapping of SISAL fibre may be reduced by 40%. The load–deformation characteristic is developed to a big extend in the case of wrapping specimens over the normal conventional concrete [12].

5 Calculation

The full load and deflections are required for further measurements shall be obtained from the digital data stored from the test. The first peak load (*P*max) is obtained as the load at the point where the slope of the load bending curve value is zero [13]. Table 4 shows the flexural strength of different RCC beams.

The flexural strength is obtained for the first peak load (Eq. 1), P_{max}, as

$$f_{ct} = (P_{max} xL)/bd^2 \quad (1)$$

It should be noted that the value obtained may be significantly different from that obtained in a conventional test carried out under load control, where the specimen fails at the peak load. The load–deflection curve for the normal and wrapping of sisal fibre RCC concrete is shown in Fig. 9.

5.1 Flexural Testing Values

Figure 5.1 shows the load–deflection curves for normal conventional and wrapping of sisal fibre RCC beams, where B1, B2, and B3 were tested. B1 and B2 show the deflection increments with a normally expand load at 101 KN. The little crack was shown in the flexure in the beam. After the cracking load further increments in the applied load, deflection values are getting increased, and the maximum deflection of the reference beams was 8.15 mm. It uncovers that the reinforcing procedure has fundamentally expanded the most extreme burden in the arrangements B1, B2, and B3. The maximum load in curve B1 was 101 KN and the deflection is 8.15 mm. The

Table 4 Flexural strength of different RCC beams

S. no	Type of beam	Maximum load (KN)	Maximum deflection (mm)	Flexural strength (MPa)
1	Conventional concrete beam B1	101	8.15	35.56
2	Conventional concrete beam B2	110	6.58	38.77
3	Wrapping of sisal fibre B3	141	4.37	49.53

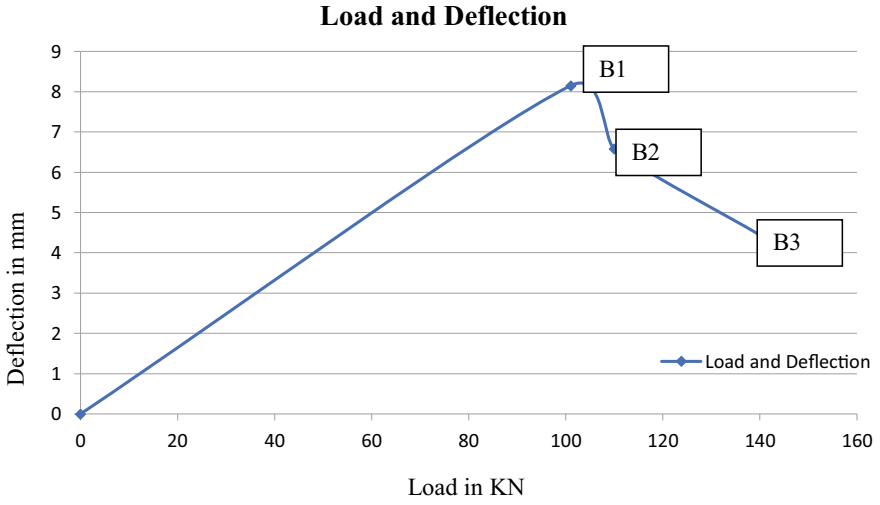

Fig. 9 Load deflection curve for the normal and wrapping of sisal fibre RCC concrete

maximum load for the beam B2 was 110 KN and the deflection is 6.58 mm. For B3 the maximum load was 141 KN and the deflection is 4.37 mm. The greatest load was 141 KN which is related to 39.9% increments in most extreme loads. Beams with the wrapping of sisal fibre have fewer deflection values. The bend of the beam was decreased and the normal bend of the B3 beams was 3.78 mm. There was improved torsional strength of reinforced components in different percentages and perspective proportion of fibres by utilizing wrapping of sisal fibres [14].

6 Result

The analysis of the calculations is mainly performed from the results of the experimental work carried out with the cubes and RCC beams (Table 5) [15]. The results are obtained from the compression test and the flexural strength test [15]. The following are the points that are the results of the analysis obtained from various experiments.

- From the compression test details the conventional type cubes have a maximum of 43.80 N/mm^2.

Table 5 Percentage of reduction in deflection in conventional and wrapping of sisal

S. no	Type of beam	Deflection in mm	Percentage reduction in deflection
1	Conventional concrete beam B1	8.15	–
2	Conventional concrete beam B2	6.58	25.4%
3	Wrapping of sisal fibre B3	4.37	39.8%

- From the flexural test details, the deformation of the conventional type beams is undergoing more amount of deformation than that of the wrapping of sisal fibre-reinforced beams [16].
- The crack width that is obtained from the flexural test indicates the amount of bending and the capacity of the beam to expand or bend [17].

7 Conclusion

- The compressive strength of the fibre included cubes that were slightly lower than the conventional type cubes. This was mainly due to the undulating arrangement of fibres. But the compressive strength was reduced slightly; this is due to the sternness capacity of the fibres during the bending.
- The bending cracks were greatly reduced in the fibre-reinforced concrete beam specimens.
- The crack width results mainly indicate that the deflection and the tendency to crack were greatly reduced upon the addition of wrapping of sisal fibre.
- The reinforced beam higher than the conventional type samples is used in the flexural test that was carried out.
- The strength of the beam also improves the torsion to the wrapping of the sisal fibre surface of the RCC beam.

References

1. de Andrade Silva F, Toledo Filho RD, de Almeida Melo Filho J, Fairbairn EDMR (2010) Physical and mechanical properties of durable sisal fiber-cement composites. Constr Build Mater 24(5):777–785
2. El-awady E, Husain M, Mandour S (2013) FRP-reinforced concrete beams under combined torsion and flexure. 2(1):384–393
3. Herrera-Franco PJ, Valadez-González A (2005) A study of the mechanical properties of short natural-fiber reinforced composites. Compos B Eng 36(8):597–608. https://doi.org/10.1016/j.compositesb.2005.04.001
4. Zhong JB, Lv J, Wei C (2007) Mechanical properties of sisal fibre reinforced ureaformaldehyde resin composites. Express Polym Lett 1(10):681–687. https://doi.org/10.3144/expresspolymlett.2007.93
5. Joseph K, Tolêdo RD, James B, Thomas S, Carvalho LHD (1999) A review on sisal fiber reinforced polymer composites. Rev Bras Eng Agrícola E Ambient 3(3):367–379. https://doi.org/10.1590/1807-1929/agriambi.v3n3p367-379
6. Nwankwo PO, Achuenu E (2014) Compressive behaviour of sisal fibre reinforced ternary concrete at elevated temperatures. Int J Adv Res Technol 3(8):123–131
7. Received 24 July 2005 Accepted 27 June 2006, no. July 2005
8. Naidu VNP, Kumar MA, Reddy GR, Khanam PN, Reddy MM, Chakradhar K (2011) Tensile & flexural properties of sisal/glass fiber reinforced hybrid. https://www.researchgate.net/publication/285770135_Tensile_flexural_properties_of_sisalglass_fiber_reinforced_hybrid_composites Accessed 09 April 2021

9. de Andrade Silva F, Toledo Filho RD, de Almeida Melo Filho J, Fairbairn EDMR (2010) Physical and mechanical properties of durable sisal fiber-cement composites. Constr Build Mater 24(5):777–785. doi: https://doi.org/10.1016/j.conbuildmat.2009.10.030
10. Li Y, Mai YW, Ye L (2000) Sisal fibre and its composites: a review of recent developments. Compos Sci Technol 60(11):2037–2055. https://doi.org/10.1016/S0266-3538(00)00101-9
11. Xin X, Xu CG, Qing LF (2007) Friction properties of sisal fibre reinforced resin brake composites. Wear 262(5–6):736–741. https://doi.org/10.1016/j.wear.2006.08.010
12. Joseph PV, Joseph K, Thomas S (1999) Effect of processing variables on the mechanical properties of sisal-fiber-reinforced polypropylene composites. Comp Sci Technol 59(11):1625–1640. https://doi.org/10.1016/S0266-3538(99)00024-X
13. Almusallam TH, Al-Salloum YA (2007) Seismic response of interior RC beam-column joints upgraded with FRP sheets. II: analysis and parametric study. J Compos Constr 11(6):590–600. https://doi.org/10.1061/(asce)1090-0268(2007)11:6(590)
14. Sharmila P, Dhinakaran G (2016) Compressive strength, porosity and sorptivity of ultra fine slag based high strength concrete. Constr Build Mater 120:48–53. https://doi.org/10.1016/j.conbuildmat.2016.05.090
15. Standard ASTM C150 (2020) Standard specification for portland cement. ASTM International, pp 1–9. https://www.astm.org/Standards/C150. Accessed 09 April 2021
16. Wu Y, Li Y, Niu B (2014) Assessment of the mechanical properties of sisal fiber-reinforced silty clay using triaxial shear tests. Sci World J 2014. https://doi.org/10.1155/2014/436231
17. Ramaswamy HS, Ahuja BM, Krishnamoorthy S (1983) Behaviour of concrete reinforced with jute, coir and bamboo fibres. Int J Cem Compos Lightweight Concrete 5(1):3–13. https://doi.org/10.1016/0262-5075(83)90044-1

Multi-disciplinary Materials and Composites

Investigation of Physical and Mechanical Properties of Locally Available Aggregates with Different Combinations for Pavement

Ron Aldrino Chan, Ron Buking, Mahathir Mohd Noor, Ervin Rangga Edwin, and Wan Hashim Wan Ibrahim

1 Introduction

The growing shortage of quality quarried materials and natural gravel for road construction and maintenance is a major challenge facing road agencies. These are finite resources, and the current resources are being exhausted. Gravel quarry products are transported over longer distances, resulting in increased costs for road construction and maintenance. This problem has been exacerbated by the trend towards stricter environmental legislation, legislation on the operation of quarries and requirements for land access, which add to the cost and limit the opportunity to initiate new quarries and to open new gravel pits.

The aggregates are an important structural component of the pavement, and their properties govern the performance and serviceability of the pavement over its service life. As a result, many researchers have stressed the significant impact of Unbound Granular Materials (UGMs) on the engineering performance of pavements [3, 4, 6, 7, 11, 18, 20]. The use of long-lasting, tough, and durable aggregates is, therefore, a primary goal in the development of long-lasting pavements [2, 5, 8, 13]. There are several types of aggregate that can be used for road construction in Malaysia such as granite, sandstone, microtonolite, basalt and limestone. The most common type of aggregate used in Malaysia for road construction is granite. In Sarawak, owing to the increasing road construction projects, the need for quality aggregate for pavement wearing courses has increased drastically. However, due to the geological structure of Sarawak, the production of granite aggregates is low due to the limited resources.

R. A. Chan · R. Buking (✉) · M. M. Noor · E. R. Edwin · W. H. W. Ibrahim
Faculty of Engineering, Department of Civil Engineering, Universiti Malaysia Sarawak, 94300 Kota Samarahan, Sarawak, Malaysia

R. A. Chan
e-mail: acron@unimas.my

W. H. W. Ibrahim
e-mail: wiwhashim@unimas.my

K. S. Satyanarayanan et al. (eds.), *Sustainable Construction Materials*, Lecture Notes in Civil Engineering 194, https://doi.org/10.1007/978-981-16-6403-8_28

Standard practice for road construction in Malaysia is Standard Specification for Road Work (SSRW) Sect. 4: Flexible Pavement [12] provided by Public Work Department, Malaysia. According to this standard, aggregates for asphalt concrete must be a mixture of coarse and fine aggregates as well as a mineral filler such as cement. This aggregate must also comply with the physical and mechanical quality requirements of the Public Work Department standard specification. The limestone aggregate, on the other hand, is not permitted to be used as a wearing course in accordance with this specification's requirements. Tan [19] mentioned that due to its low polished stone coefficient, limestone aggregate is not recommended for wearing courses since it is well known that many skidding incidents have occurred on polished limestone road surfaces.

Aggregates used in road construction can be divided into two categories, that is, standard and non-standard. A non-standard aggregate is described as any aggregate, that is, usually unusable due to a lack of conformity with the current specification [1]. According to Toole et al. [21], natural gravel and weathered rocks are marginal and non-standard road building materials. Even though they do not meet the required standards; however, for some roads, these materials are known to perform well as granular base and sub-base materials. Compared to the original materials, the non-standard aggregates are likely to be susceptible to faults because they are weak and unable to withstand the current specified capacity [22].

Besides that, the amount of aggregate required for a mega road project is enormous, and aggregates are often left unprotected from harsh weather, leaving aggregate quality unobserved. Furthermore, some of the aggregates are not protected because the contractor does not have sufficient covered storage, leaving the aggregates exposed to the weathering process on sunny and rainy days. As such, the quality of the aggregate can be significantly affected by the weathering process. In general, both wear resistance (degradation of particles as crushing loads) and decay resistance (i.e. weather resistance under the complex environmental conditions encountered by UGMs) affect the durability characteristics of the materials [5, 10, 16, 18]. The purpose of this research is to examine the effect of wetting and drying cycles, the mechanical properties of aggregates on the various aggregate combinations of granite, limestone, and microtonalite in order to evaluate the potential use of these materials for road construction in Sarawak, particularly locally available non-standard materials.

2 Aggregates in Sarawak

Malaysia's quarrying industry has consistently contributed to the country's economic development. According to Kei [14], more than 80 million tonnes of construction aggregate are produced in Malaysia with the quarrying industry contributed RM 7,119.6 million to the Malaysian economy in 2015 [15]. This emphasises how important it is for Malaysia's construction industry to obtain high-quality aggregate. Peninsular Malaysia (also known as West Malaysia) is situated in the southern part

Table 1 Location and classification of aggregates found in Sarawak

Site	Group classification of aggregates
Bau, Kuching Division	Limestone
Bau/Lundu, Kuching Division	Sandstone
Sebuyau, Samarahan Division	Granite
Santubong, Kuching Division	Granite
Muara Tuang, Samarahan Division	Microtonalite
Batu Kawa, Kuching Division	Microtonalite
Kakad Quarry, Mile 16, Kuching Division	Microtonalite
Ex. Pendu Quarry, Mile 29, Kuching Division	Limestone
Mile 22, Btu/Miri Road, Bintulu Division (Ex. JKR Quarry)	Sandstone
Mile 21, Kuching Division	Limestone
Mile 7, Kuching Division	Microtonalite
Mile 9, Kuching	Microtonalite
Sebuyau/Simunjan Division	Granite

(Source JKR Sarawak, Central Material Lab)

of Asia, while the Eastern part of Malaysia (Sabah and Sarawak) is located on the Island of Borneo. The rocks from Peninsular Malaysia were known to be much older as compared to the rocks in Sabah and Sarawak and have been exposed for a long time to tropical tropic conditions and the earth's atmosphere, which may lead to the formation of deep weathering profiles and laterite over various types of bedrock [9]. In Sarawak's construction industries, aggregates such as microtonalite, limestone, granite, quartz, sandstone, slag, dolomite, and others are commonly available and used, particularly for road construction. Additionally, granite, limestone, and microtonalite are the three types of coarse aggregates widely used in Sarawak for road construction. The location and classification of local aggregates found in Sarawak are shown in (Table 1 and Fig. 4). Locally available aggregates such as sandstone, granite, limestone and microtonalite as shown in (Figs. 1, 2 and 3) are generally quarried and utilised in Sarawak.

3 Materials and Methodology

Three (3) different types of aggregate known as granite aggregate (GA), limestone aggregate (LA) and microtonalite aggregate (MA) were used in this research. Granite aggregate is used as a standard aggregate, while limestone and microtonalite aggregates are known as a low-quality/non-standard aggregate. Non-standard aggregate

Fig. 1 Limestone

Fig. 2 Sandstone

is classified as any aggregate that is not commonly used because it lacks the specifications' requirements nonetheless may possibly be successfully used by modifying standards for construction procedures and pavement design [1]. The general definition of non-standard or substandard aggregate is "any aggregate that is not normally used because it does not have the characteristics required by the specification but could be used successfully by modifying normal pavement design and construction procedures". The methodology used are in accordance with standard practice for road construction in Malaysia as specified in Standard Specification for Road

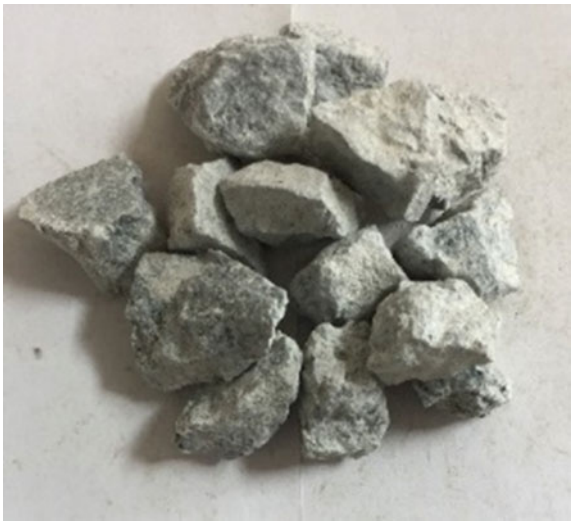

Fig. 3 Granite

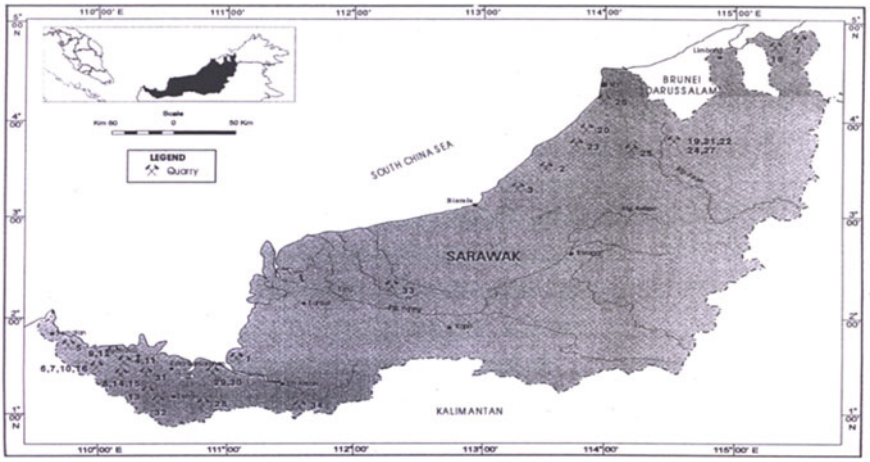

Fig. 4 Quarries locations in Sarawak. *(Source Industrial Mineral Production Statistic & Directory of Producers in Malaysia 2002)*

Work (SSRW) Sect. 4: Flexible Pavement [12] provided by Public Work Department, Malaysia. For the purpose of this research, three types of aggregates were selected namely granite as standard aggregate, while limestone and microtonalite areconsider as non-standard aggregate. These materials are sourced locally from nearby quarries by sampling method as specified in ASTM D75.

Table 2 Standard specification for physical and mechanical properties

Property	Test	Standard specification
Physical	Specific gravity	ASTM C127-07
	Water absorption	
	Flakiness Index	BS 812-105.1:1989
	Elongation Index	BS 812-105.2:1990
Mechanical	Aggregate Crushing Value (ACV)	BS 812-110:1990
	Aggregate Impact Value (AIV)	BS 812-112:1990
	Los Angeles Abrasion (LAA)	ASTM C 131-06

Table 3 Aggregate combination percentage

Testing	Aggregate	Percentage of combination (%)
1. Aggregate Crushing Value 2. Aggregate Impact Value 3. Los Angeles Abrasion	GA	100
	LA	100
	MA	100
	GA: MA	50–50
	GA: LA	50–50
	GA: MA	75–25
	GA: LA	75–25

The physical and mechanical standard specifications used for testing of aggregates are shown in Table 2. All the used aggregates were tested for physical properties and followed by mechanical properties. Different combination ratios of granite, limestone and microtonalite aggregates for mechanical tests are described in Table 3. For ACV and AIV, the size for the used aggregate passed the 5 mm sieve and was retained on the 3.35 mm sieve. The aggregate size for LAA passed the 5 mm sieve and was retained on 2.36 mm. There were two testing conditions to test the mechanical properties of aggregates known as controlled condition and wetting and drying condition. The purpose of performing wetting and drying is to investigate how well the aggregate can resist the weathering effect since, in most construction projects, the aggregate stockpiles are not fully protected and are exposed. Controlled condition means the mechanical tests were conducted in accordance with the referred standard specifications using aggregate from Table 2. Wetting and drying condition means the aggregates went through 5 cycles of wetting and drying before being tested for mechanical properties using aggregates from Table 3. For each application, the aggregate is exposed to a different set of physical and chemical degrading forces. Some of the forces that an aggregate may be exposed throughout its service life are abrasive, tensile, shear, and compressive forces, sulphate exposure, wetting and drying cycles, and freezing and thawing cycles [17]. One (1) wetting and drying cycle

means 1 day of full water immersion and 1-day of ambient temperature air drying. After 5 cycles of wetting and drying, the aggregates were oven-dried for 1 day before being used for mechanical tests. After the tests, the results were compared to standard specifications. The aim of combining various types of aggregate is to determine the mechanical properties of the two aggregates when they are combined. As a result, the potential use of limestone and microtonalite in pavement wearing courses can be explored.

4 Result and Discussion

4.1 Physical Properties of Aggregate

The physical properties of granite, limestone and microtonalite aggregates used in this research are shown in Table 4.

4.2 Aggregate Under Controlled Condition

The mechanical performance of different types of aggregate and different combination ratios of aggregates is shown in Table 5. It was observed that MA 100% had better performance than GA 100% and LA 100%. From the result, ACV, AIV and LAA for GA 100%, LA 100% and MA 100%, only LAA for GA 100% did not achieve the requirement. For different combination ratios, the combination ratio consisted of MA had better performance than other types of combination. For example, the ACV, AIV and LAA of GA 50%: MA 50% were better than GA 50%: LA 50%. In addition, the ACV, AIV and LAA of GA 75%: MA 25% were better than GA 75%: LA 25%. Only GA 50%: LA 50%, GA 75%: LA 25% and GA 50%: MA 50% did not achieve the requirement for LAA. Overall, controlled conditions for different combination ratios, GA 50%: MA 50% and GA 75%: MA 25% can be selected.

Table 4 Physical properties of aggregates

Tests	Experimental value			Public work department standard specification (1988)
	GA	LA	MA	
Specific Gravity	2.44	2.45	2.52	–
Water Absorption, %	0.74–9.04	0.48–8.11	0.58–14.36	<2%
Flakiness Index, %	10.86	20.13	10.20	<25%
Elongation Index, %	29.31	40.06	16.51	–

Table 5 Controlled and wetting and drying conditions—mechanical properties of aggregate

Condition	Test	Experimental value							Public work department standard specification	BS 812-112
		GA 100%	LA 100%	MA 100%	GA: LA 50%: 50%	GA: MA 50%: 50%	GA: LA 75%: 25%	GA: MA 75%: 25%		
Controlled	ACV	17.38	14.96	11.54	16.36	14.56	15.25	14.74	<30% Note 1	
	AIV	8.64	6.42	5.56	7.29	5.87	7.66	6.84		<30%
	LAA	30.96	19.17	21.49	26.22	25.69	29.41	24.86	<25% Note 2	
Wetting and drying	ACV	16.71	12.44	10.77	14.77	13.46	15.41	15.03	<30% Note 1	
	AIV	13.02	9.77	5.23	10.00	6.56	11.78	8.23		<30%
	LAA	36.10	25.70	19.71	27.45	24.03	27.71	26.85	<25% Note 2	

Note 1 Public Work Department, 2008
Note 2 Pubic Work Department, 1988

4.3 Aggregate Under Wetting and Drying Condition

For aggregate that went through 5 cycles of wetting and drying before being tested for mechanical performance, the result is shown in Table 5. From Table 5, for ACV, AIV and LAA, it can be observed that only GA 100% did not achieve the LAA requirement compared to LA 100% and MA 100%. MA 100% had the highest performance than LA 100% and MA 100%.

For different combination ratios, same as controlled conditions, combination ratios consisted of MA had better performance than other types of combination. For example, GA 50%: MA 50% had better performance in terms of ACV, AIV and LAA than GA 50%: LA 50%. Same as GA 75%: MA 25% were better than GA 75%: LA 25%. Only GA 75%: MA 25%, GA 50%: LA 50% and GA 75%: LA 25% did not achieve the requirement for LAA. Overall, wetting and drying conditions for different combination ratios, GA 50%: MA 50% and GA 75%: MA 25% can be selected. By comparing the result of controlled conditions and wetting and drying conditions, wetting and drying cycles do have an effect on the mechanical properties of aggregate.

For AIV, wetting and drying show a higher value compared to the controlled samples. This shows that aggregates that have been exposed to wetting and drying conditions may reduce the impact value of aggregates. For the Aggregate Crushing Value, the sample shows a higher value for the 100% aggregate sample which varies from 11.54 to 17.38 for the controlled sample while for the wetting and drying sample it varies from 10.77 to 16.71 which is slightly lower compared to the controlled sample. However, the 50%: 50% result combination samples shows a lower value compared to 75%: 25% combination aggregates with a higher value. The Granite and Limestone combination on 75% and 50% shows that there is no significant difference in the result. Conversely, the result of Granite and Microtonalite with a 50% and 75% Granite combination showed wide gap result for both controlled, wetting and drying effects. The difference in value between the 50-percent and the 75-percent mix is roughly 50-percent different. While for the Los Angeles Abrasion, the wetting and drying samples for the 100% aggregates show a higher value for both Limestone and Microtonalite except for Granite with values varies from 30.96 to 36.10 which are the above-average result. For the 50%: 50% and 75%: 25% aggregates combination, Microtonalite shows a higher value compared to Limestone with different of ± 1 in 50%: 50% combination whereas 75 per cent: 25% combination shows the highest value of 24.86 for controlled samples. The significant different findings obtained from the results are highly due to the wetting and drying effect which made the aggregate less durable mainly in the Aggregate Impact Value testing.

5 Conclusion

From the overall test result and significant findings, it was observed that the aggregates tested for AIV and LAA are highly affected due to wetting and drying conditions, making the value for AIV and LAA higher but still meeting the standard requirement. However, the wetting and drying effect does not show any effect under the compressive condition as shown in the ACV result which still meets the standard requirement of less than <25%. According to the results of the laboratory work, the following conclusions can be drawn:

- The different combination ratio of different types of aggregates has the potential to be used as alternative materials for road construction.
- The different combination ratios can have the potential of cost saving for road construction.
- Further research needs to be carried out such as polishing stone value to evaluate the polishing resistance of the aggregate.

References

1. Ahlrich RC, Rollings RS (1994) Marginal aggregates in flexible pavements: background survey and experimental plan. Atlantic City: U.S. Department of Transportation. Retrieved from http://www.tc.faa.gov/its/worldpac/techrpt/ct94-58.pdf
2. Chang K, Kang Y, Ge L, Cheng M (2015) Mechanical properties of gravel deposits evaluated by nonconventional methods. J Mater Civ Eng 27(0401503211)
3. Chen DH (2009) Investigation of a pavement premature failure on a weak and moisture susceptible base. J Perform Constr Facilit 23:309–313
4. Chen DH, Sun R, Yao Z (2013) Impacts of aggregate base on roadway pavement performances. Constr Build Mater 48:1017–1026
5. Collis L, Smith M (2001) Aggregates: sand, gravel and crushed rock aggregates for construction purposes. Geolog Soc
6. Fookes P, Gourley C, Ohikere C (1988) Rock weathering in engineering time. Quart J Eng Geol Hydrogeol 21:33–57
7. Gandara JA, Kancherla A, Alvarado G, Nazarian S, Scullion T (2005) Impact of aggregate gradation on base material performance. University of Texas, El Paso Center for Transportation Infrastructure Systems
8. Gondal MMI, Ahsan N, Javid AZ (2008) Evaluation of Shaki Sarwar and Rajan Pur aggregates for construction in southern Punjab province, Pakistan. Geol Bull Punjab Univ 43:101–107
9. Haile NS (1969) Geosynclinal theory and the organizational pattern of the NW borneo geosyncline. J Geol Soc Lond 124:171–194
10. Hussain J (2012) Performance of unbound granular basecourse materials under varying moisture conditions. A thesis for the degree of doctor of philosophy in engineering, The University of Auckland
11. Hussain J, Wilson DJ, Black PM (2014) The effect of moisture and relative proportions of clay minerals (smectite, chlorite and illite) on the performance of unbound granular base course (UGM). Quart J Eng Geol Hydrogeol 47:169–176
12. Jabatan KR (2008) Standard specification for road work (SSRW) section 4: flexible pavement. Public Work Department, Kuala Lumpur

13. Kleyn E, Bergh A, Botha P (2009) Practical implications of the relation between the clay mineral content and the Plasticity Index of dolerite road construction material. J South African Inst Civil Eng 51:2–5
14. Kei HM (2017) Economic census 2016- mining and quarrying. economic census. Kuala Lumpur: Department of Statistics Malaysia, 2017. Retrieved from https://www.dosm.gov.my/v1/index.php?r=column/pdfPrev&id=dVE3UXhFcVkzTFVPVXVWNkt6NDlpUT09
15. Murlidhar BR, Mohamad ET, Asmawisham MN, Armaghani DJ (2016) Geological study and mining plan importance for mitigating alkali silica reaction in aggregate quarry operation. Jurnal Teknologi 78:71–79. https://doi.org/10.11113/jt.v78.9486
16. Meininger RC (2003) Rock products: aggregates provide pavement friction. United State. PRIMEDIA Business Magazine & Media Inc
17. Richard EW, Gregory SW (2005) Testing method to determine long term durability of Wisconsin aggregate resources. Wisconsin Highway Research Program
18. Sangsefidi E, Wilson DJ, Larkin TJ, Black PM (2017) australasian transport research forum 2017 Proceedings 27–29 November 2017, Auckland, New Zealand
19. Tan, Denis NK. Potential and properties of some rock aggregates in Sarawak (1983)
20. Tao MJ, Abu-Farsakh M, Zhang Z-J (2008) Characterization of unbound aggregates revealed through laboratory tests. Int J Pavement Res Technol 1:72–75
21. Toole T et al (2018) Appropriate use of marginal and non-standard materials in road construction and maintenance. No. AP-T335-18
22. TRL (2002) A framework for the appropriate use of marginal materials. world road association (PIARC)-technical committee C12 seminar in Mongolia, June 2002

Experimental Study of the Addition of Aquatic Calcium Carbonate Composites in Cement Mortar

R. Monisha and M. Balasubramanian

1 Introduction

Solid waste management from industries, the public, and several sectors causes major concern for the environment. There are several considerable methods to reduce waste production [1]. Aquaculture is the fastest growing area compared to other sectors. The worldwide production of waste in aquaculture is about 14.6 million tonnes in 2010 [2]. Seashell waste causes major problems in some countries [3]. The formation and conversion of aquatic $CaCO_3$ are shown in Fig. 1. In recent years, researchers have taken numerous innovation initiatives to reduce the carbon footprint in cement production. This innovation involves incorporating wastes and reuse the waste materials as a binder in a mortar mixture [4]. Having undergone the concept of green environmental development and low zero carbon materials, there are few methods like traditional casting, ready-mix casting prefabricated concrete, and considerable interest has been shown about the usage of aquatic waste material in the construction industry. When the cement mortar is formed by mixing two or more ingredients, it is termed as mixture components. The mixture component such as cement, sand, supplementary cementitious materials, and water develops a new way of optimizing these raw materials. Remunerative scares material into economical and eco-friendly natural waste materials are utilized. The main aim is to find out the substitution ratio and optimum dosage to increase the strength and durability of cement mortar [5, 6]. Also to find out the optimum dosage with the best proportions of each specimen and best compressive strength of each specimen are experimented with simultaneously. Seashell waste causes major problems in some countries. The feasibility of using shell waste as the partial or total replacement of construction materials has been studied [7]. As a supplementary cementitious material in cement mortar, aquatic waste may reduce the CO_2 emission from cement manufacturing.

R. Monisha · M. Balasubramanian (✉)
Department of Civil Engineering, SRM Institute of Science and Technology, Chengalpattu District, Kattankulathur 603203, Tamil Nadu, India

K. S. Satyanarayanan et al. (eds.), *Sustainable Construction Materials*, Lecture Notes in Civil Engineering 194, https://doi.org/10.1007/978-981-16-6403-8_29

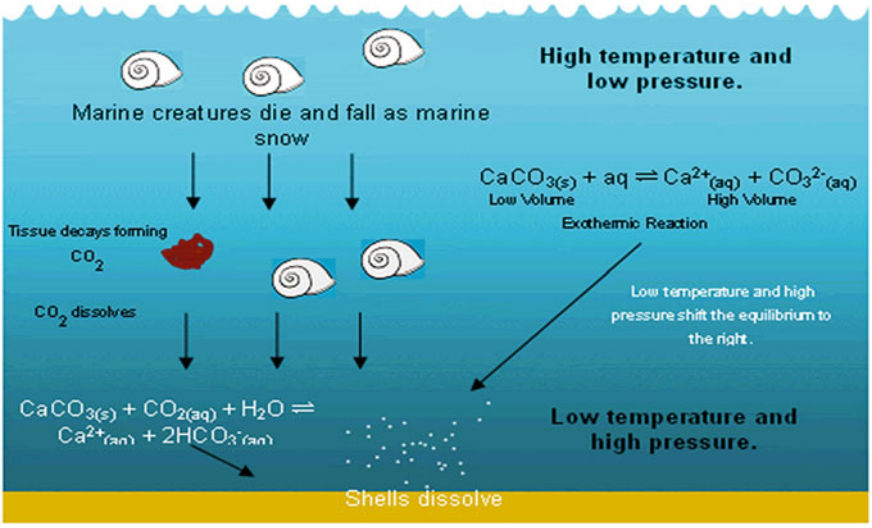

Fig. 1 The formation and conversion of aquatic $CaCO_3$ [8]

2 Materials and Methods

2.1 Preparation of Supplementary Material

The preliminary treatments are followed to make supplementary cementitious material as an aquatic $CaCO_3$ [9]. The aquatic shells are scrubbed with a brush and submerged in water for about 7 days to remove all the impurities [6] By manual grinding process, the shell wastes are sieved under 150 μm sieve and the fineness of the material experimented by BET was 1.932 m^2/g. Using a thermal process to remove the impurities, the shell must be washed and dried at 120 ± 5 °C for 24 h. After drying for 24 h, the shell is a ground and sieved up to granular size. Reducing the toxicity in shells needs thermal treatment at 130–140 °C for 35 min. This thermal treatment effectively removes the bacteria and other impurities in shells. Continuously, the heat treatment is followed two to three times. The cleaning process procedure is carried out using bleaching and abrasive agents, then boiled in water and dried to remove all the organic matters as per the ASTM C989 [6]. The density and specific gravity of supplementary material are tested. The surface area of A $CaCO_3$ is 2.90 g/cm^3 and 4220 cm^2/g, respectively.

Table 1 Summary of the chemical composition report in SEM analysis

Chemical components	Conventional cement (%)	Aquatic waste (%)
$CaCO_3$	67	96.9
SiO_2	23	3.1
Al_2O_3	5.4	0.5
MgO	4.3	0.65
SO_3	2.7	0.79

2.2 Properties of Aquatic Shell Waste

The percentage of $CaCO_3$ calcium carbonate with a percentage that exceeds 90% is similar to the conventional at limestone is summarized. The XRD analysis proves that the aquatic wastes are made of a few amounts of aragonite and calcite. The results show that 93% of $CaCO_3$ content with an average range of particle size is drawn on a graph. SEM analysis's results compared with chemical components present in aquatic waste and the conventional limestone cement, respectively, are summarized in Table 1. In cement mortar mix design, the aquatic $CaCO_3$ is used as a substitution material for cement with sieving in 850 μ m. The exact process was followed by other researchers [10]. The average particle size ranges from 0.5 to 40 μm. When the powered sample is used in the replacement mixture, the water absorption rate is higher than that of the conventional mixture. Due to the higher initial pores in the material, the absorption rate increases. The aquatic waste shell's specific gravity is between 2.6 and 3.0 that is not equipment to the specific gravity of cement. Hence, the specific gravity of a material is efficient to influence the density of the mortars.

2.3 Microstructure Study

Scanning electron microscopy (SEM) and X-ray diffraction (XRD) tests are conducted to determine the chemical composition of the material. SEM and XRD are well-established methods to investigate the internal and the surface structure of the material and identified by this equipment [10]. The XRD patterns and SEM analysis of aquatic $CaCO_3$ are shown in Figs. 2 and 3. From the figures, the shape and crystallization patterns of the material are identified. Based on the results, the element study of the material is analysed in detail. The aquatic $CaCO_3$ is in angular shape due to the crushing, grinding, and sieving process in their manufacturing [11]. The XRD analysis concentrates only on the total carbon concentration in the graph. It results in peak integration for accurate analysis of $CaCO_3$ in the aquatic material. The ideal average particle size is similar to the binder particle in cement mortar. The X-ray scans on two different concentrations of $CaCO_3$ before and after heated at 1200 °C

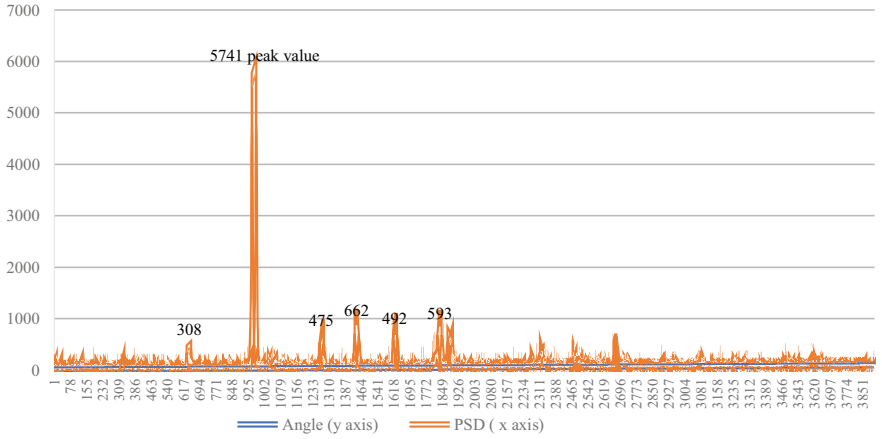

Fig. 2 The XRD analysis of peak intensity value of $CaCo_3$ in aquatic calcium carbonate

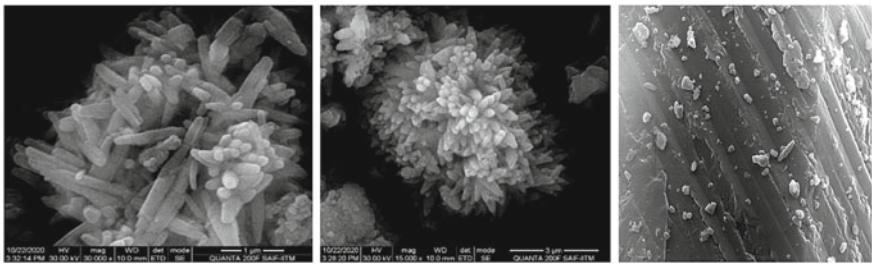

Fig. 3 The crystallization study of material in SEM analysis

temperature. Mapping of calcium carbonate, calcium silicate and oxygen analysis by EDS. The material's hydration value can be easily identified by the volume of the material and the percentage of internal hydration density. The mapping study provides a reliable measure to identify the different CSH phases that were not in composition only with densities quality of different components dented in different colours [12].

The peak value with 2θ angle and particle size distribution, which remains as the pure relative intensity of the material is shown in Fig. 2 and the crystalline nature of the oyster shells in different magnifications, and the irregular shape of the fine material is visible in the given image (Fig. 3).

3 Result and Discussion

3.1 Fresh Concrete Tests

3.1.1 Workability

The workability of mortar and concrete is a great attribute that affects the mechanical properties of the cement. Workability affects the material properties mixing and the water absorption coefficient, etc. [12]. The aquatic calcium carbonate acts as the substitutional material in mortar improves workability. The larger pores in the hydration process of mortar mixing cause an increase in the fresh mortar mix's water absorption coefficient. According to the SEM analysis, the material's internal structure is studied as the shells are granular and irregular in shape. It leads to increase in water absorption in fresh mortar results in reducing the slump and consistency value.

3.1.2 Density

The cement mortar density is defined by the ratio of the volume of sand, cement, admixtures and water in it [13]. The nominal density of cement mortar ranges from 2200 to 3200 kg/m^3. From the microstructure analysis and workability test, the characteristic nature of the material is identified. A large number of porous in mortar led to reducing the density. The observed density of aquatic calcium carbonate mortar is 2100–2800 kg/m^3, and there is a slight decrease in density compared to the conventional cement mortar. The sample observation of density value in the weighing machine is shown in Fig. 4.

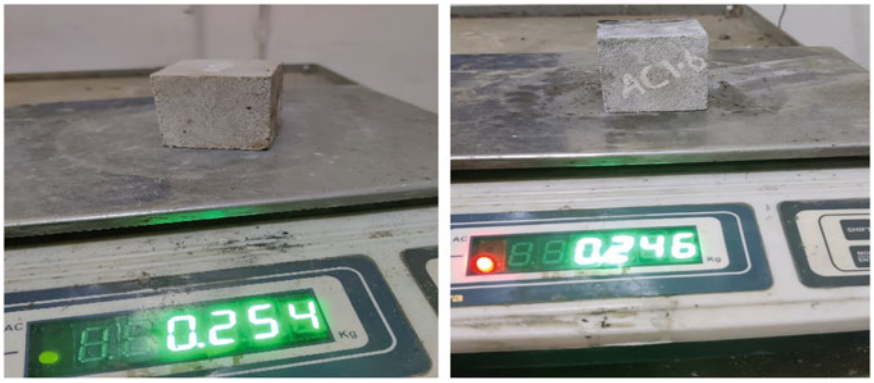

Fig. 4 The sample density observation value of aquatic $CaCo_3$ mortar

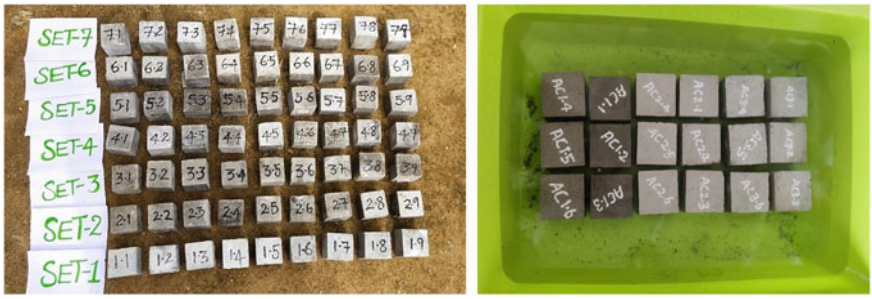

Fig. 5 The different proportions of specimen cast and curing

3.1.3 Water Absorption

Due to the aquatic waste material used in mortar, they observe a little higher volume of water in mortar mixing. It shows the irregular shape and porous in the raw material. The 50 mm cube mortar is cast and demoulding for curing [14]. In the curing process, the specimens absorbed water up to the period of 28 days. From the moulding to the curing period, the density of the mortar specimen varies based on the range. The water absorption increases gradually until the period of curing. The different proportions of specimen cast and curing are shown in Fig. 5. Different proportions of specimens have differed in water absorption value. Among all proportions of mortar specimens, 30% replacement of cement substitution mortar attains a similar absorption value as conventional mortar. When the dosage of substitution material is increased, it changes in water absorption of mortar directly.

3.2 Mechanical Properties of Mortar

3.2.1 Compressive Strength

The compressive strength of the mortar cube containing aquatic waste calcium carbonate is shown in Fig. 6. The experimental result shows the significance of compressive strength for 10, 20 and 30% of mortar cubes from 7th day to 28th day. The development of compressive strength for the 1:4, 1:5 and 1:6 ratio of mortar a static strength is obtained compared to conventional cement mortar [15]. The compressive strength of conventional cement mortar and aquatic waste mortar was compared with the various aspect ratio discussed earlier [16]. The results for 7, 14 and 28 days are shown in Fig. 6. From the graphical representation, the compressive strength of AWCM is gradually increasing the strength at the 28th day is not satisfying the strength compared to the conventional mortar. In a previous study, the recommended substitution ratio is not greater than 30%. The dosage of aquatic

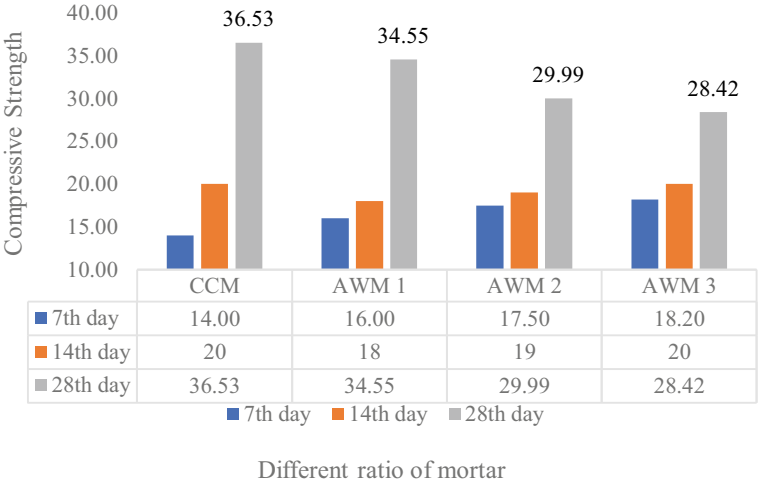

Fig. 6 The graphical representation of compressive strength of conventional and aquatic mortar

waste calcium carbonate increases in mortar mix. It results in decreases in compressive strength. In aquatic calcium carbonate, there is a huge amount of organic matter content and in an irregular shape, the pores in the mortar mix are higher. It causes the water absorption rate to increase and decreases the mechanical property. The aquatic calcium carbonate also has a negative impact on reducing the bonding in cement paste and sand.

3.2.2 Split Tensile Strength

Tensile strength is the essential property in concrete and cement mortar. The conventional mortar has low tensile strength because the cement mortar does not have elasticity in nature [13]. The split tensile strength reaches 7–10% of its compressive strength. The aquatic waste calcium carbonate has comparatively low mechanical property compared to conventional. It does not have elasticity in nature; hence, the split tensile also slightly reduce compared to conventional cement mortar. But in the different proportions, there are gradual increases in the mechanical property of mortar. The largest calcium content in aquatic $CaCO_3$ causes slow improvement in mechanical properties up to 90 days of curing. The graphical representation of split tensile of conventional and aquatic mortar is shown in (Fig. 7). The optimum dosage of 30% of substitution material attains similar mechanical strength to conventional mortar.

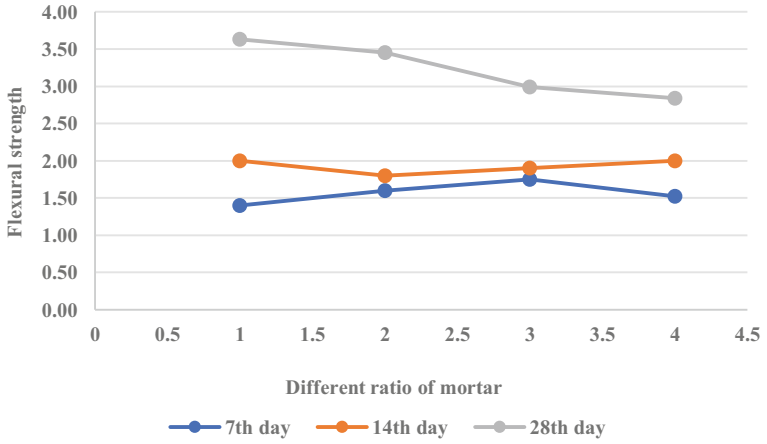

Fig. 7 The graphical representation of split tensile of conventional and aquatic mortar

3.2.3 Flexural Strength

Flexural strength and tensile strength are related to the elasticity formation in concrete and cement [4]. Elastic properties decide the flexural strength values. In this study, no additive material comprises the tensile properties in a mortar. Therefore, there is not much deviation in flexural strength when comparing the conventional with aquatic mortar. The graphical representation of flexural strength is shown in Fig. 8.

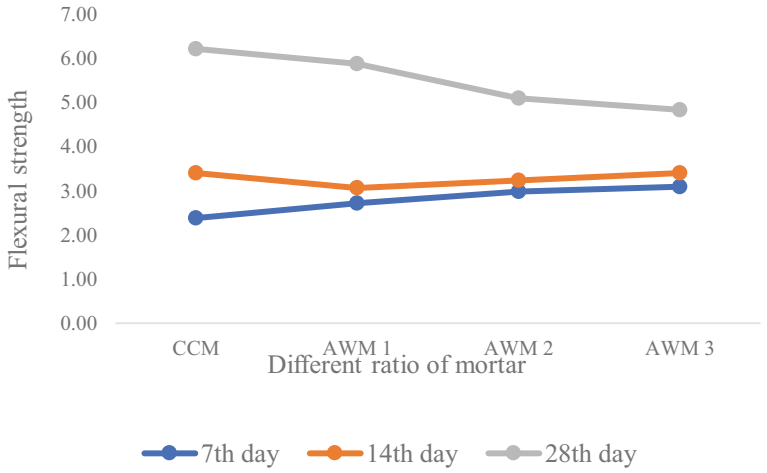

Fig. 8 The graphical representation of flexural strength

Fig. 9 The moisture content in mortar

3.2.4 Thermal Behaviour

The incorporation of calcium carbonate additives in cement-based materials leads to thermal insulation behaviour despite the mechanical properties [17]. Previous tests examine that aquatic raw material contains organic substances, high porous and low density in nature. The moisture content in mortar conducts low thermal conductivity compared to conventional mortar. If the substitutional rate increases in mortar specimen it improves the thermal insulation. Compared to other substitution materials in cement and concrete, aquatic wastes have remain excellent thermal resistivity and CO_2 emission in building material. The moisture content in mortar is shown in Fig. 9. The results conclude that aquatic waste $CaCO_3$ material is energy efficient and natural thermal constraints in raw construction material.

4 Conclusion

This study concluded that the feasibility of utilizing aquatic calcium carbonate as a supplementary material in cement replacement. According to the characterization study and experimental results, the chemical, physical and mechanical properties are analysed. The optimum dosage of material is 20% in replacement of cement attains better performance similar to conventional cement mortar. Our environmental concerns, energy consumption, and CO_2 emission are mainly concentrated in the upcoming research. The aquatic waste materials have low thermal conductivity. It reduces the heating at room temperature and improves the air conditioning in the building. The use of waste materials as raw materials in cement system improves the sustainable developments and green concept in construction. Further work is recommended to analyse the energy audit in the building by using this material and simulating in updated software.

References

1. El Biriane M, Barbachi M (2021) State-of-the-art review on recycled mussel shell waste in concrete and mortar. Innov Infrastruct Solut 6(1):1–10. https://doi.org/10.1007/s41062-020-00394-9
2. Ubachukwu OA, Okafor FO (2020) Formulation of predictive model for the compressive strength of oyster shell powdercement concrete using Scheffe's simplex lattice theory. Epa - J Silic Based Compos Mater 72(6):210–218. https://doi.org/10.14382/epitoanyag-jsbcm.2020.34
3. Abousnina RM, Manalo A, Lokuge W (2016) Physical and mechanical properties of cement mortar containing fine sand contaminated with light crude oil. Procedia Eng 145:250–258. https://doi.org/10.1016/j.proeng.2016.04.071
4. Bheel N, Ibrahim MHW, Adesina A, Kennedy C, Shar IA (2021) Mechanical performance of concrete incorporating wheat straw ash as partial replacement of cement. J Build Pathol Rehabil 6(1):1–7. https://doi.org/10.1007/s41024-020-00099-7
5. Nasr MS, Shubbar AA, Abed ZAAR, Ibrahim MS (2020) Properties of eco-friendly cement mortar contained recycled materials from different sources. J Build Eng 31:101444. https://doi.org/10.1016/j.jobe.2020.101444
6. Naqi A, Siddique S, Kim HK, Jang JG (2020) Examining the potential of calcined oyster shell waste as additive in high volume slag cement. Constr Build Mater 230:116973. https://doi.org/10.1016/j.conbuildmat.2019.116973
7. Barnaby C (2004) An investigation into the reuse of organic waste produced by the New Zealand Mussel Industry
8. Al-shalchi W, Expert G (2008) Storing carbon dioxide gas. Carbon NY 2(l):3–6
9. Chen Z, Tang Y, Mai C, Shi J, Xie Y, Hu H (2020) Experimental study on the shear performance of brick masonry strengthened with modified oyster shell ash mortar. Case Stud Constr Mater 13:e00469. https://doi.org/10.1016/j.cscm.2020.e00469
10. Igarashi S, Kawamura M, Watanabe A (2004) Analysis of cement pastes and mortars by a combination of backscatter-based SEM image analysis and calculations based on the Powers model. Cem Concr Compos 26(8):977–985. https://doi.org/10.1016/j.cemconcomp.2004.02.031
11. Çomak B, Bideci A, Salli Bideci Ö (2018) Effects of hemp fibers on characteristics of cement based mortar. Constr Build Mater 169:794–799. https://doi.org/10.1016/j.conbuildmat.2018.03.029
12. Yang J et al. (2021) Effect of steam curing on compressive strength and microstructure of high volume ultrafine fly ash cement mortar. Constr Build Mater 266:120894. https://doi.org/10.1016/j.conbuildmat.2020.120894
13. Shubbar AA, Jafer H, Dulaimi A, Hashim K, Atherton W, Sadique M (2018) The development of a low carbon binder produced from the ternary blending of cement, ground granulated blast furnace slag and high calcium fly ash: An experimental and statistical approach. Constr Build Mater 187:1051–1060. https://doi.org/10.1016/j.conbuildmat.2018.08.021
14. Jung CT, Siang TC, Kwong TH, Boon K (2019) Compressive strength and water absorption of mortar incorporating silica fume. Int J Civ Eng 6(8):39–43. https://doi.org/10.14445/23488352/ijce-v6i8p106
15. Madurwar MV, Mandavgane SA, Ralegaonkar RV (2014) Use of sugarcane bagasse ash as brick material. Curr Sci 107(6):1044–1051. https://doi.org/10.18520/cs/v107/i6/1044-1051
16. Sharma P, Sharma N, Singh P, Verma M, Parihar HS (2020) Examine the effect of setting time and compressive strength of cement mortar paste using iminodiacetic acid. Mater Today Proc 32:878–881. https://doi.org/10.1016/j.matpr.2020.04.336
17. Liu HY, Wu HS, Chou CP (2020) Study on engineering and thermal properties of environment-friendly lightweight brick made from Kinmen oyster shells & sorghum waste. Constr Build Mater 246:118367. https://doi.org/10.1016/j.conbuildmat.2020.118367

Study on the Influence of Manufactured Sand on Deflection Characteristics of Coconut Shell Concrete Slab

R. Ramasubramani and K. Gunasekaran

1 Introduction

Concrete is the most commonly used material, due to its strong and versatile nature. It is a composite material, made of cement, aggregates and water. Sometimes admixtures and many other ingredients are added to improve its properties. Hence concrete is considered as the major base material for construction. Coarse aggregates are used in the concrete, which provides strength to the material. Generally, crushed stones, gravel and recycled aggregates are used as a coarse aggregate. The use of these aggregates reduces the natural resources, thereby damaging the environment, which in turn leads to ecological imbalance. Therefore, many alternate approaches have been put forward, like using industrial wastes, domestic wastes, and recycled materials. Likewise, agricultural wastes can also be used as an alternate material. In countries like India, where agriculture is the major work, a large amount of solid wastes is discharged from agriculture. One such agricultural waste is coconut shell (CS). This shall be used as a replacement material for conventional coarse aggregate [1–7], since it is one of the most propitious agro wastes.

Fine aggregates are used in the concrete, which provides workability to the material. Natural river sand (R-sand) was used initially, but in recent times due to the continuous extraction of R-sand, manufactured sand (M-sand) is used as an alternate material [8–12]. This M-sand is manufactured by pulverizing the granite stone and it is graded well in the desired proportion. It is also found to be cost-effective, has lesser impurities and good working properties than R-sand. The utilization of M-sand

R. Ramasubramani · K. Gunasekaran (✉)
Department of Civil Engineering, College of Engineering and Technology, SRM Institute of Science and Technology, Chengalpattu District, Kattankulathur 603203, Tamil Nadu, India
e-mail: gunasekk@srmist.edu.in

R. Ramasubramani
e-mail: ramasubr@srmist.edu.in

K. S. Satyanarayanan et al. (eds.), *Sustainable Construction Materials*, Lecture Notes in Civil Engineering 194, https://doi.org/10.1007/978-981-16-6403-8_30

Fig. 1 **a** Coconut shell crusher, **b** Crushed coconut shells

is said to be eco-friendly since it prevents the dredging of riverbeds. Hence, in this study, it is proposed to use M-sand as fine aggregate and CS as coarse aggregate in the production of concrete.

1.1 Coconut Shell Aggregate

Coconut shell (CS) is very durable, possesses high resistance to abrasion, and does not degenerate easily. Traditionally, it has been used to make ornaments, fancy items, and household utensils and also made into activated carbon. Large percentages of CS are discarded daily as solid waste. Therefore, it is an effective means of disposing of this abundant waste and to keep a cleaner environment. CS is used as coarse aggregate in the production of lightweight concrete (LWC) because of the lower density compared to the density of conventional crushed stone aggregate (CSA) [1, 2]. For this study, raw CS was collected and crushed using a crusher. The size of the CS is confined to a maximum size of 12.5 mm because of its low strength and stiffness compared to CSA. The appearance of the CS is impartially smoothened on one side and rugged on the other side [5]. The pounded boundaries are uneven and sharp. The crusher used to crush the CS is shown in Fig. 1a and the crushed CS is shown in Fig. 1b.

1.2 Manufacture Sand (M-Sand)

Manufactured sand (M-sand) was obtained by the crushing rock deposition to produce a fine aggregate of superior quality that conforms to IS standard. It also develops high concrete strength compared to R-sand used concrete [8–12].

Table 1 Details of mix ratios adopted

Mix	R-sand (%) & M-sand (%)	Mix ratio Cement: River sand: M-Sand: CSA: w/c
Conventional concrete (CC)—Cement content used: 320 kg/m^3		
CCM1	100 & 00	1: 2.22: 0.00: 3.66: 0.55
CCM2	75 & 25	1: 1.66: 0.60: 3.66: 0.56
CCM3	50 & 50	1: 1.11: 1.21: 3.66: 0.58
CCM4	25 & 75	1: 0.55: 1.81: 3.66: 0.59
CCM5	00 & 100	1: 0.00: 2.42: 3.66: 0.60
Coconut shell concrete (CSC)—Cement content used: 510 kg/m^3		
CSCM1	100 & 00	1: 1.47: 0.00: 0.65: 0.42
CSCM2	75 & 25	1: 1.10: 0.40: 0.65: 0.42
CSCM3	50 & 50	1: 0.73: 0. 80: 0.65: 0.42
CSCM4	25 & 75	1: 0.37: 1.21: 0.65: 0.42
CSCM5	00 & 100	1: 0.00: 1.61: 0.65: 0.42

2 Materials and Mix Proportions

In this experimental work, the binder used was 53 grade ordinary Portland cement (OPC) conforming to IS 12269: 2013 [13]. CSA and CS as coarse aggregates and R-sand and M-sand as fine aggregates in concrete production. Potable water that is free from contamination was utilized for the whole process of producing concrete. The mix proportions for CC and CSC with varying proportions of R-sand and M-sand in which 100% R-sand used mixes (ref Table 1) were selected from the earlier studies [1, 2].

In each mix, the M-sand and R-sand are increased and decreased, respectively, in the percentage of 0, 25, 50, 75 and 100%. Since many studies have been carried with R-sand, holding it as a reference, M-sand was added partially as per the percentage given above to the mix proportions. Whereas the CSA was completely substituted by CS in the concrete. Different water-cement (w/c) ratios were adopted for varying proportions accordingly.

3 Experimental Study

In this experimental study, concrete cubes and slabs were cast and examined to find the compressive strength, density and deflection characteristics. The specimens were made in both the types of CCM and CSCM concretes. These two sets of concretes were made with varying percentages of R-sand and M-sand and a comparative study was made. A total of ninety cubes 100 × 100 × 100 mm size were cast as per IS

516: 2018 [14], and ten slabs 533 × 838 × 40 mm (selected from the literature) [15, 16] were cast and examined to find the compressive strength, density, and deflection of the both CC and CSC.

3.1 Specimen Test

The concrete constituents were mixed with respect to the mixed proportions in a concrete mixture machine and then put in frames in three layers, tamping each layer using a tamping rod, till the frame is filled completely. The purpose of tamping is to remove the excess air and lower the void content. Aluminum handheld floating was done to ensure that the holes were completely filled. This process was adopted over the top surface of the slabs after following the evaporation of excess water. To produce a smooth and dense surface of the slabs, troweling was done using a steel trowel after the aluminum handheld floating. After casting, the specimen was kept in an undisturbed manner for 24 h, then the specimen was taken out from the frame and placed in a curing tank, where the water level was maintained at a minimum of 50 mm above the top surface of the slab specimen. The curing period was 28 days to attain the targeted strength.

After 28 days, slabs were left for surface drying and whitewashed before testing. Also, before testing, required markings were plotted on the specimen and then placed in the loading frame of capacity 40 T. The edges of the slab were provided as simply supported. Alignment of the slab was tested and leveling was checked using the plumb bob for making concurrent of both slab center and loading from the center [15, 16]. A steel ball was exactly placed at the middle of the slab using plaster of Paris. The digital dial gauge was fixed at the bottom of the slab and was set to zero before loading. Then the load was persistently applied on the steel ball using a hydraulic jack and the slab was gradually subjected to an increase in loading till the slab fails. The readings from the dial gauge were also noted. The samples of cast cube and slab specimens are shown in Fig. 2. The cast slabs before testing are indicated in Fig. 3, the schematic diagram of deflection testing is shown in Fig. 4, and the slab testing arrangement for the deflection study is shown in Fig. 5. All tested specimens are shown in Fig. 6.

4 Results and Discussion

The CC and CSC with various proportions of R-sand and M-sand fine aggregates were compared. The use of M-sand in its place of R-sand exhibited better results in both CC and CSC. Since this study focused mainly on deflection characteristics slabs, it is found that the CS plays an important role in this property. In this study,

Fig. 2 Sample of cast specimens **a** cube **b** slab

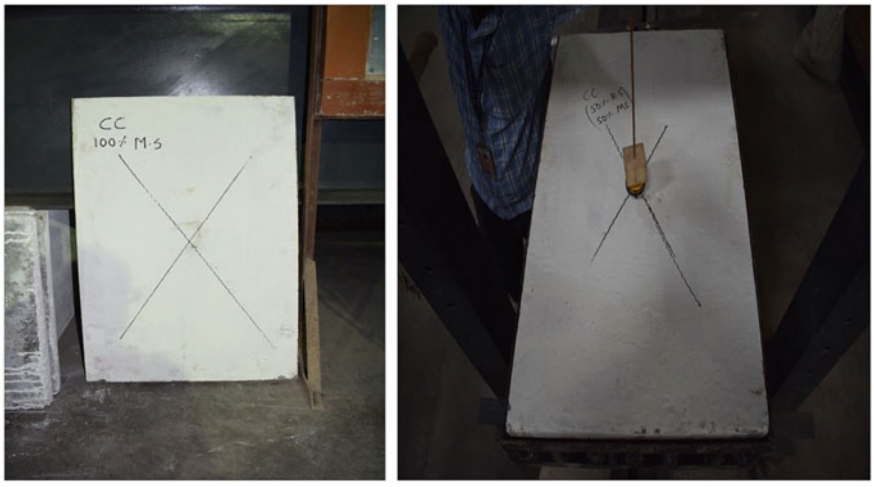

Fig. 3 Cast slabs before test

no reinforcements were used in order to avoid its effects in the concrete, since this experimental study mainly focuses on the cracking and deflection behavior of the plain concrete slabs. Test results are discussed in this section.

4.1 Compressive Strength

For all the mixes CCM1 to CCM5 and CSCM1 to CSCM5, compressive strength and density were found at 3, 7 and 28 days as per IS 516: 2018 [14]. Fresh and hardened concrete properties of both CC and CSC in different mixes are presented in Table 2.

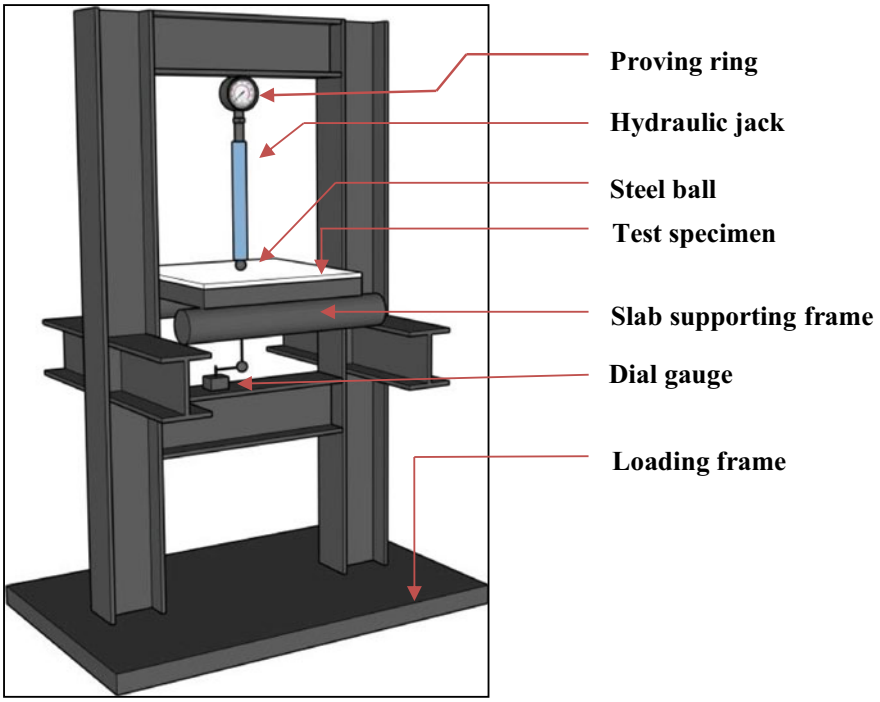

Fig. 4 Schematic diagram of deflection test

Fig. 5 Slabs under deflection load

4.2 Slabs Deflection

Load versus deflection curve is plotted as a graphical representation for CCM1-CCM5 as shown in Fig. 7 and CSCM1-CSCM5 is shown in Fig. 8. From the graph, it could be noticed that the CSC shows more deflection than the CC. But as a whole, the CSCM took less load than the CCM. Load taken by CCM5 is greater than CCM1

Fig. 6 Tested slab specimens

Table 2 Fresh and hardened concrete properties

Mix types	Fresh concrete density (kg/m^3)	3 days		7 days		28 days	
		Density (kg/m^3)	Strength (N/mm^2)	Density (kg/m^3)	Strength (N/mm^2)	Density (kg/m^3)	Strength (N/mm^2)
Conventional concrete (CC)							
CCM1	2480	2450	17.30	2460	22.70	2465	29.00
CCM2	2515	2485	18.60	2495	23.68	2505	29.98
CCM3	2545	2520	20.50	2535	24.65	2545	30.97
CCM4	2580	2550	22.60	2560	25.62	2570	31.96
CCM5	2605	2585	23.10	2600	26.60	2610	32.95
Coconut shell concrete (CSC)							
CSCM1	2035	1935	16.80	1950	19.20	1980	26.85
CSCM2	2065	1970	17.10	1980	19.70	2025	27.20
CSCM3	2100	2010	17.85	2025	20.40	2065	27.85
CSCM4	2135	2045	18.90	2065	22.10	2110	28.30
CSCM5	2165	2080	20.80	2100	23.30	2150	29.10

and CSCM5 is greater than CSCM1. Hence, it can be stated that when the percentage of M-sand is increased the strength in both CC and CSC increases. The same trend was reported in the literature on deflection characteristic study on CSC with QD [16] also stated that the use of QD in CSC also contributed to reducing the deflection characteristics on the slab in addition to CS role [15, 16]. Also, CSC warns against failure as compared with CC. This suggests that CS plays a crucial role in the concrete ductility property. The load versus deflection of CCM and CSCM mixes used slabs are shown in Tables 3 and 4.

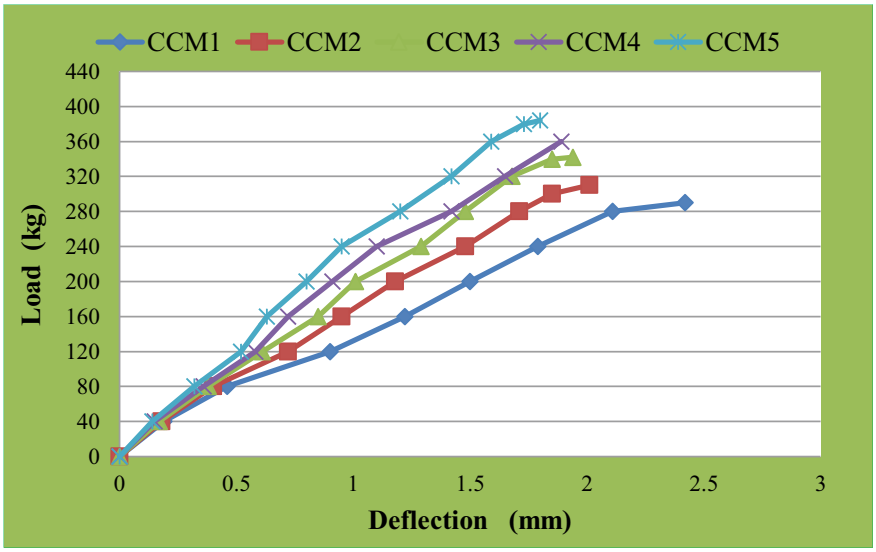

Fig. 7 Load versus deflection for CCM1 to CCM5

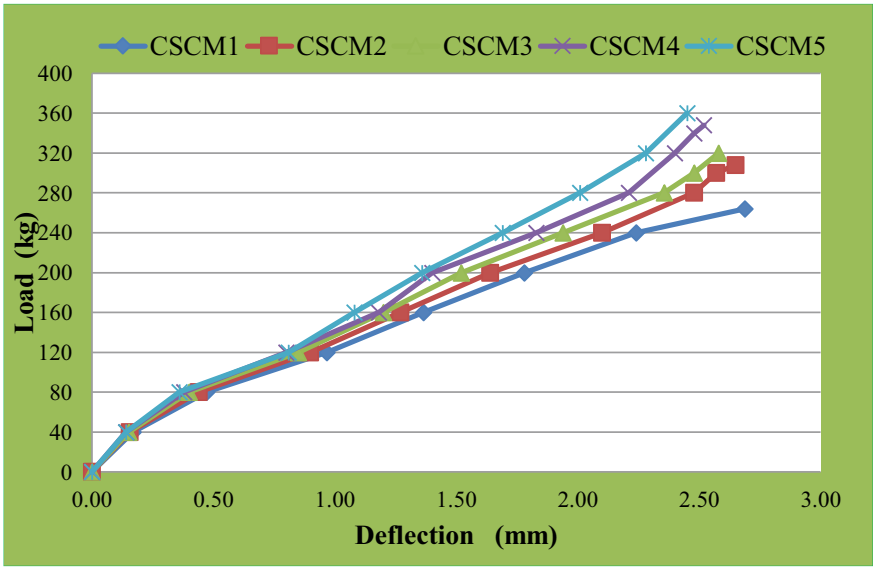

Fig. 8 Load versus deflection for CSCM1 to CSCM5

Table 3 Load versus deflection on CCM mixes slabs

Load in kg	Deflection in (mm)				
	CCM1	CCM2	CCM3	CCM4	CCM5
0	0	0	0	0	0
40	0.19	0.18	0.17	0.15	0.14
80	0.46	0.4	0.38	0.36	0.32
120	0.9	0.72	0.61	0.58	0.52
160	1.22	0.95	0.85	0.72	0.63
200	1.5	1.18	1.01	0.91	0.8
240	1.79	1.48	1.29	1.1	0.95
280	2.11	1.71	1.48	1.42	1.2
290	**2.42**	–	–	–	–
310	–	**2.01**	–	–	–
320	–	–	1.68	1.65	1.42
342	–	–	**1.94**	–	–
360	–	–	–	**1.89**	1.59
384	–	–	–	–	**1.80**

Table 4 Load versus deflection on CSCM mixes slabs

Load in kg	Deflection in (mm)				
	CSCM1	CSCM2	CSCM3	CSCM4	CSCM5
0	0	0	0	0	0
40	0.17	0.16	0.15	0.14	0.14
80	0.47	0.44	0.40	0.38	0.36
120	0.97	0.90	0.85	0.8	0.81
160	1.37	1.27	1.20	1.18	1.08
200	1.78	1.64	1.52	1.4	1.36
240	2.24	2.10	1.94	1.83	1.69
264	**2.69**	–	–	–	–
280	–	2.48	2.36	2.21	2.01
308	–	**2.65**	–	–	–
320	–	–	**2.58**	2.40	2.28
348	–	–	**–**	**2.52**	–
360	–	–	**–**	**–**	**2.45**

4.3 Comparison with IS Code

Span to effective depth ratio of the tested slabs is 13.34 (L/d = 533/40) [17]. Maximum deflection from the results of the deflection test for different percentages of substitutes of M-sand used CC is 1.80 mm and CSC is 2.45 mm which is less than the 13.34 mm.

5 Conclusion

The characteristics of CC and CSC were compared with varying proportions of R-sand and M-sand. From the observations, it was noted that the concrete with 100% M-sand gives better results. The compressive strength of CC is higher and deflection is lower than CSC. When the percentage of M-sand increases, concrete density and compressive strength increase and vice versa. Results of the deflection show that if percentages of M-sand increase the central deflection of the slab decreases. It was found that CSCM mixes exhibit greater deflection compared to CCM mixes. Also, CSCM warns against failure compared with CCM. This indicates that CS plays an important role in concrete ductility property. CSC is also suitable in accordance with IS 456: 2000 code criteria of span to effective depth ratio. It should, however, further works are to be carried out before it can be used along with reinforcement.

References

1. Gunasekaran K, Kumar PS et al (2011) Mechanical and bond properties of coconut shell concrete. Constr Build Mater 25(1):92–98
2. Gunasekaran K, Kumar PS et al (2011) Study on properties of coconut shell as an aggregate for concrete. Indian J Indian Concrete Inst 12(2):27–33
3. Gunasekaran K, Praksah Chandar S et al (2017) Augmentation of mechanical and bond strength of coconut shell concrete using quarry dust. Europ J Environ Civil Eng 21(5):629–640. https://doi.org/10.1080/19648189.2016.1144540
4. Prakash Chandar S, Gunasekaran K et al (2018) Study on some durability properties of coconut shell concrete with quarry dust. Europ J Environ Civil Eng 24(6):709–723. https://doi.org/10.1080/19648189.2017.1418435
5. Kalyana Chakravarthy P, Janani et al (2017) Properties of Concrete partially replaced with coconut shell as coarse aggregate and steel fibres in addition to its concrete volume. IOP Conf Ser Mater Sci Eng 183:012028. https://doi.org/10.1088/1757-899x/183/1/012028
6. Anandh S, Gunasekaran K (2018) Optimization of coconut fiber in coconut shell concrete and its mechanical and bond properties. Materials 11:1726. https://doi.org/10.3390/ma11091726
7. Kumar VRP, Gunasekaran K et al (2019) Characterization study on coconut shell concrete with partial replacement of cement by GGBS. J Build Eng 26:100830
8. Wani FA, Ramasubramani R (2019) All-in-one about a momentous review study on manufactured-sand as fine aggregate in concretes. Int J Innov Technol Exploring Eng (IJITEE) 18(7):1946–1952
9. Rao SK, Sravana P et al (2016) Investigating the effect of M-sand on abrasion resistance of roller compacted concrete containing GGBS. Constr Build Mater 122:191–201

10. Saravanan S, Nagajothi S et al (2019) Investigation on compressive strength development of geopolymer concrete using manufactured sand. Mater Today Proc 18:114–124
11. Ramkumar S, Dineshkumar R (2020) Experimental study on impact on fineness of sand and M- sand in M20 grade of concrete. Mater Today Proc 21:36–40
12. Vijaya B, Selvan SS (2015) Comparative study on the strength and durability properties of concrete with manufactured sand. Indian J Sci Technol 8(36):1–7
13. IS 12269:2013, Indian Standard, Ordinary Portland cement 53 Grade—Specification, Bureau of Indian Standard, March 2013, New Delhi, 110002
14. IS 516 (Part 4): 2018. Indian Standard, Hardened concrete- methods of test. Bureau of Indian Standard, December 2018, New Delhi, 110002
15. Gunasekaran K, Annadurai R et al (2013) Plastic shrinkage and deflection characteristics of coconut shell concrete slab. Constr Build Mater 43(1):203–207
16. Prakash Chandar S, Gunasekaran K (2019) Study on the effect of quarry dust on deflection characteristics of coconut shell concrete slab. Rasayan J Chem 12(3):1038–1048
17. IS 456: 2000, Indian Standards, plain and reinforced concrete—code of practice, Bureau of Indian Standard, New Delhi; 2000

Reduction of Pores and Water Absorption of Coconut Shell Aggregate on Treatments

T. Thilagashanthi, K. Gunasekaran, and K. S. Satyanarayanan

1 Introduction

In the production of lightweight concrete (LWC), coconut shell (CS) is used as coarse aggregate [1–7]. An agricultural solid waste, in the presence of certain moisture and air content CS is a non-biodegradable material. Decorative and domestic materials are produced using CS [8]. Durability properties of CS used concrete are not similar to conventional aggregate used concrete, particularly water absorption, permeability, and resistance to temperature [7]. Compared to normal weight concrete (NWC), LWC has some differences in properties. However, there should not be any compromise on durability aspects between NWC and LWC. In view of this, it is necessary to improve the CS quality so that the quality of CS used concrete could be enhanced. The objective of this study is to treat the CS through different methods and selecting suitable treatment methods for CS, so as to produce in future durable and sustainable CS aggregate concrete.

T. Thilagashanthi · K. Gunasekaran (✉) · K. S. Satyanarayanan
Department of Civil Engineering, SRM Institute of Science and Technology, Kattankulathur 603203, Tamil Nadu, India
e-mail: gunasekk@srmist.edu.in

T. Thilagashanthi
e-mail: thilagat@srmist.edu.in

K. S. Satyanarayanan
e-mail: satyanak@srmist.edu.in

K. S. Satyanarayanan et al. (eds.), *Sustainable Construction Materials*, Lecture Notes in Civil Engineering 194, https://doi.org/10.1007/978-981-16-6403-8_31

2 Treatment Procedures

There are some references to treating the wood-based materials. Oil palm shell (OPS) aggregate is treated through slaked lime (SL), it modifies the surface of wood-based materials [9, 10]. Sago flour (SF) is used as adhesive in CS charcoal powder [11, 12]. In reference to the literature, the details of treatments selected for CS are listed in Table 1.

Crushed raw CS (RCS), and oven-dried CS (ODCS) are considered at first. RCS is placed in the oven for a duration of 24 h at 100 ± 5 °C to obtain ODCS. Based on the literature study, the maximum size of CS aggregate selected is 12.5 mm and used for treatments. The SL solution was prepared using 20 g of SL added with 500 ml potable water [9, 10]. Likewise, the SF solution was prepared using 20 g of SF (150 microns) with 250 ml potable water [11, 12]. To start with, RCS and ODCS are immersed in water for 24 h. RCS (T1) and RCS (T2)) and ODCS (T1) and ODCS (T2)) were soaked in SL and SF and obtained the quantum of absorption of SL and SF. The results are shown in Table 2.

The samples of CS aggregate treated with SL and SF are shown in Fig. 1. The details of water absorption of CS aggregate in various treatments are presented in Table 3.

Table 1 Classification of treatments on CS aggregate

Designation used	Classification of treatments on CS aggregate
RCS(W)	Raw coconut shell immersed in water
ODCS(W)	Oven-dried coconut shell immersed in water
RCS(T1)	Raw coconut shell immersed in SL mixture
ODCS(T1)	Oven-dried coconut shell immersed in SL mixture
RCS(T1W)	Raw coconut shell immersed in SL mixture and subsequently in water
ODCS(T1W)	Oven-dried coconut shell immersed in SL mixture and subsequently in water
RCS(T2)	Raw coconut shell immersed in SF mixture
ODCS(T2)	Oven-dried coconut shell immersed in SF mixture
RCS(T2W)	Raw coconut shell immersed in SF & subsequently in water
ODCS(T2W)	Oven-dried coconut shell immersed in SF mixture & subsequently in water

Table 2 Quantum of SL and SF absorbed by CS aggregate

Designation used	Quantum of absorption (%)
RCS (T1)	14.00
ODCS (T1)	25.14
RCS (T2)	13.00
ODCS (T2)	21.57

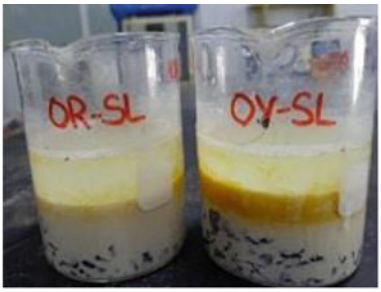

(a) RCS and ODCS in SL

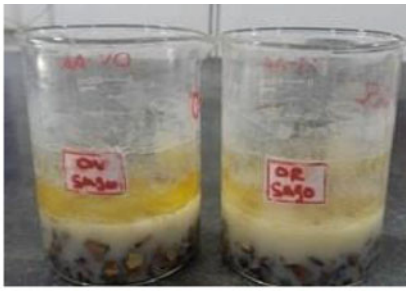

(b) RCS and ODCS in SF

(c) After RCS (T1) & ODCS (T1)

(d) After RCS (T2) & ODCS (T2)

(e) Water absorption test: RCS(T1W) & ODCS(T1W)

(f) Water absorption test: RCS(T2W) & ODCS(T2W)

Fig. 1 Various treatments processed

Table 3 Water absorption details of CS in treatments

Notations used	Water (%)
RCS(W)	16.25
ODCS(W)	22.38
RCS(T1W)	1.19
ODCS(T1W)	0.56
RCS(T2W)	0.00
ODCS(T2W)	1.00

3 Quality Improvement of CS

The literature stated that the water absorption % of CS varies between 20 and 25% [1–7]. In this study, methods of treatment employed particularly such as RCS (T1W), ODCS (T1W), RCS (T2W), and ODCS (T2W) were enhanced a lot and decreased the water-absorbing capacity considerably. Thus, if CS aggregate is treated, its water absorption ability also decreased. Pores present in the interior microstructure of CS are filled up by SL and SF treatments, and therefore decrease the water absorption. Scanning electron microscope (SEM) images are obtained. SEM images of RCS (T1W) and ODCS (T1W) are shown in Fig. 2.

SEM images of RCS (T1W) and ODCS (T1W) show few pores present even after the SL treatment. (Figure 2a) RCS (T1W) indicates few pores present due to the presence of some moisture content. The ODCS (T1W) image shows the pores formed due to oven-drying are almost completely filled up by SL (Fig. 2b). This shows that the SL solution is completely filled the pores and mild coated the CS aggregates. Therefore, compared to RCS (T1W), ODCS (T1W) treatment show fewer pores and hence less absorption of water 0.56% in ODCS (T1W) compared to 1.19% in RCS (T1W). SEM images of RCS (T2W) and ODCS (T2W) are shown in Fig. 3a, b.

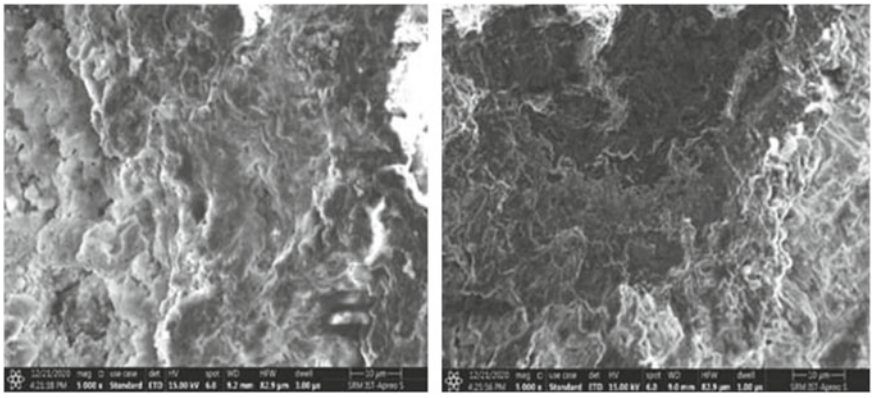

(a) (b)

Fig. 2 SEM Images of **a** RCS(T1W) **b** ODCS(T1W) treated CS

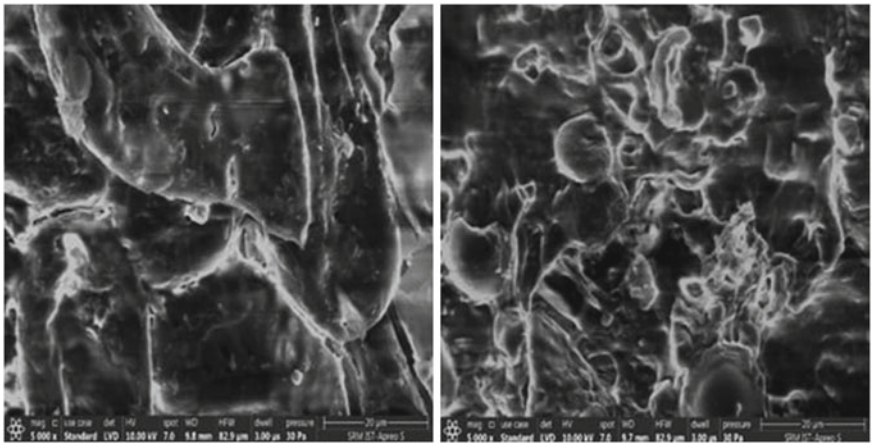

(a) (b)

Fig. 3 SEM Images of **a** RCS(T2W) **b** ODCS(T2W) treated CS

SEM image of RCS (T2W) and ODCS (T2W) shows few pores are present even after the SF treatment. (Figure 3a) RCS (T2W) indicates pores are present due to the presence of some moisture content almost filled up by SF. The ODCS (T2W) image shows the few pores formed due to oven drying are not completely filled up by SF (Fig. 3b). This could be the reason why the water absorption is 0% in case of RCS (T2W) compared to 1% of water absorption in case of ODCS (T2W). Compared to the treatments RCS (T1W), ODCS (T1W), and ODCS (T2W), RCS (T2W) method of treatment shows 0% water absorption. In particular using SF, the RCS (T2W) method of treatment is best compared to ODCS (T2W). Since this RCS (T2W) method of treatment gives 0% water absorption compared to 20 to 25% water absorption of untreated CS. Also, compared to SL, the cost of SF is only about 50 to 60% cost of SL.

4 ImageJ Analysis on SEM

Images obtained from SEM are analysed through ImageJ software in two ways: (even though many ways are available) 8 bits and RGB colors (R-Red, G-Green and B-Blue). These two ways are employed on SEM images to obtain the location, number, maximum area, minimum area and mean area of pores. These values determined using ImageJ software are presented in Table 4. For a typical example, ImageJ software analysed images for RCS (T1W) and RCS (T2W) are shown in Fig. 4a, b. The image extracted from ImageJ software for these treatments is shown in Fig. 5a, b, in that pores are represented in yellow colour. The model data of RCS (T2W) and ODCS (T2W) determined from ImageJ software is shown in Table 5.

Table 4 Area of pore in SL and SF treatments

Designation used	Maximum area (μm^2)		Minimum area (μm^2)		Mean area (μm^2)	
	8 bits	RGB	8 bits	RGB	8bits	RGB
RCS	17.044	16.847	2.004	2.001	4.835	4.979
ODCS	34.591	34.792	2.087	2.001	7.770	7.757
RCS(W)	20.123	20.632	2.171	2.052	6.385	5.346
ODCS(W)	14.643	14.643	2.302	2.302	6.005	6.005
RCS(T1)	4.655	4.572	2.165	2.126	2.898	2.846
ODCS(T1)	49.808	50.167	2.060	2.074	7.939	7.996
RCS(T1W)	18.964	18.828	2.020	2.006	6.764	6.715
ODCS(T1W)	15.644	15.672	2.026	2.030	6.056	6.066
RCS(T2)	6.998	6.935	2.632	2.609	4.798	4.755
ODCS(T2)	10.995	10.995	2.115	2.115	4.791	4.791
RCS(T2W)	12.505	12.079	2.297	2.274	6.342	6.149
ODCS(T2W)	32.814	32.932	2.347	2.355	10.583	10.621

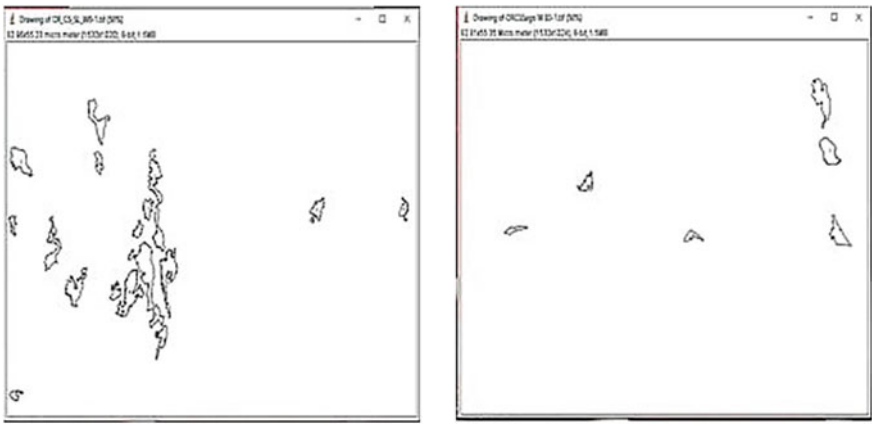

(a) (b)

Fig. 4 Pores presented in **a** RCS (T1W) **b** RCS (T2W)

Maximum pore areas of 18.964 and 18.828 μm^2 obtained for the treatment RCS (T1W) from 8 bits and RGB analysis is more compared to maximum pore areas of 17.044 and 16.847 μm^2 obtained for the treatment RCS, respectively. But maximum pore areas of 15.644 and 15.672 μm^2 obtained for the treatment ODCS (T1W) from 8 bits and RGB analysis are less compared to maximum pore areas of 34.591 and 34.792 μm^2 obtained for the treatment ODCS. Compared to maximum pore areas of 17.044 and 16.847 μm^2 obtained for the RCS from 8 bits and RGB analysis, the respective maximum pore areas of 4.655 and 4.572 μm^2 obtained for RCS (T1) are

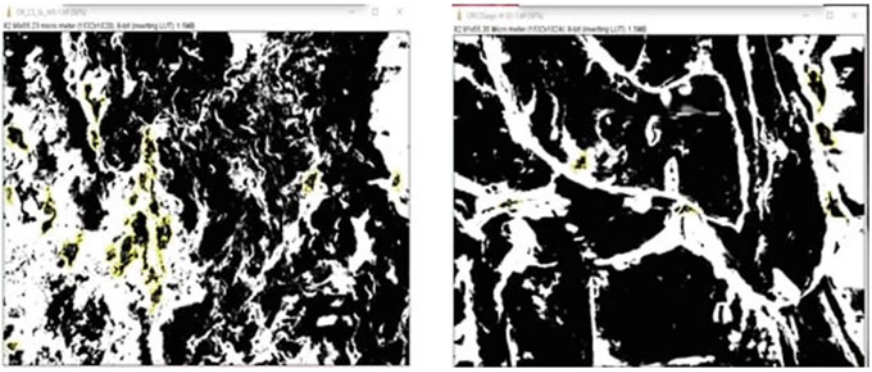

(a) (b)

Fig. 5 Images of pores in **a** RCS (T1W) **b** RCS (T2W)

reduced considerably. Similarly, compared to maximum pore areas of 32.814 and 32.932 μm^2 obtained for ODCS (T2W) from 8 bits and RGB analysis, respective maximum pore areas of 12.505 and 12.079 μm^2 obtained for RCS (T2W) are reduced considerably. Likewise, compared to maximum pore areas of 6.998 and 6.935 μm^2 obtained for RCS (T2) from 8 bits and RGB analysis, the respective maximum pore areas of 17.044 and 16.847 μm^2 obtained for RCS are more. Similarly, compared to the maximum pore areas of 10.995 μm^2 obtained for ODCS (T2) from both 8 bits and RGB analysis, the respective maximum pore areas of 34.591 and 34.792 μm^2 obtained for ODCS are more. As far as the number of pores present is concerned, treatment types RCS (T2) and RCS (T2W) show fewer number of pores. The number of pores in CS aggregate treated using SL and SF and CS aggregate immersed in water, respectively are shown in Tables 6 and 7. From all these types of treatments, raw CS treated using SF is the best method for treating CS compared to treating using SL as per this study.

5 Results and Discussion

Slaked lime (SL) absorption in ODCS (T1) is 79.57% higher than the SL absorption in RCS (T1). Likewise, SF absorption in ODCS (T2) is 65.92% higher than the SF absorption in RCS (T2), as shown in Table 2. The moisture content present in the interior structure of RCS evacuates due to oven drying for 24 h. Therefore, it creates more pores in RCS. Through treatments, the quality of absorption of water by CS is considerably reduced. In case of RCS (T1W), the capacity of water absorption is 1.19%. Water absorption of RCS (T1W) is much less (92.67%) compared to RCS (W) (16.25%). Similarly, in the case of ODCS (T1W) capacity of water absorption is 0.56%. Water absorption of ODCS (T1W) is also much less (97.49%) compared to ODCS (W) (22.38%). In the type of treatment RCS (T2W), capacity of water

Table 5 Model data of ImageJ software

	RCS(T2W)				ODCS(T2W)			
	Area	Mean	Threshold limit		Area	Mean	Threshold limit	
			Min	Max			Min	Max
–	–	–	0	255	17.366	253.889	–	–
–	–	–			9.884	248.916	–	–
–	–	–			9.127	254.837	–	–
–	–	–			2.486	255	–	–
–	–	–			25.838	253.075	–	–
–	–	–			4.026	252.787	–	–
–	–	–			2.347	255	–	–
–	–	–			32.814	252.670	–	–
–	–	–			3.645	254.593	–	–
–	–	–			12.970	254.943	–	–
–	–	–			2.536	254.414	–	–
–	–	–			3.412	253.477	–	–
–	–	–			7.773	253.185	–	–
–	–	–			6.079	244.009	–	–
–	12.505	254.225			18.341	249.455	0	255
–	9.572	252.976			14.501	253.362		
–	3.757	246.870			8.425	252.268		
–	7.354	255			9.476	254.922		
–	2.297	255			14.283	251.310		
–	2.568	255			6.323	245.960		
Mean	6.342	253.179			10.583	252.404		
SD	4.165	3.19	0		8.154	3.084	0	
Min	2.297	246.870	0	255	2.347	244.009	0	255
Max	12.505	255			32.814	255		

Table 6 Number of pores in the treated CS

Notation	Pore sizes (μm^2)	Number of Pores	
		8 bits	RGB
RCS	2 μm^2—infinity	15	14
ODCS		22	22
RCS(T1)		8	8
ODCS(T1)		21	21
RCS(T2)		3	3
ODCS(T2)		8	8

Table 7 Pores in treated CS aggregate immersed in water

Notation	Pore sizes (μm^2)	Number of Pores	
		8 bits	RGB
RCS(W)	2 μm^2—infinity	10	12
ODCS(W)		6	6
RCS(T1W)		19	19
ODCS(T1W)		18	18
RCS(T2W)		6	6
ODCS(T2W)		20	20

absorption is 0%. Water absorption of RCS (T2W) is 100% less compared with RCS (W). Similarly, in ODCS (T2W) capacity of water absorption is decreased to 1%. Water absorption of ODCS (T2W) is 95.53% less compared to ODCS (W). In the ODCS (T1), the absorption of SL is 25.14%. This is 79.57% higher than RCS (T1), which absorbs SL by 14%. In the ODCS (T1W) type of treatment, the water absorption is 0.56%. This is 52.94% less compared with RCS (T1W) (1.19%). In RCS (T1), the maximum pore area is 4.655 μm^2. This pore area is approximately 90.65% less when compared with ODCS (T1) (49.808 μm^2). Likewise, in the ODCS (T2) the absorption of SF is 21.57%. This is 65.92% higher than RCS (T2) which absorbs SF by 13%. In the RCS (T2W) type of treatment, the water absorption is 0%. This is 100% less compared to ODCS (T2W) (1%). In ODCS (T2), the maximum pore area is 10.995 μm^2. This pore area is approximately 57.11% higher when compared with RCS (T2) (6.998 μm^2).

6 Conclusion

In order to enhance CS aggregate quality, treatments using SL and SF were carried out, and suitable types of treatment were selected. From this study, a significant conclusion is furnished below:

- The SL solution forms a thin layer of coating on the CS and hence reduces the absorption of water by the CS aggregate.
- The SF solution forms a thin layer of resin on the CS aggregate and hence prevents the entry of water into the CS aggregate.
- ODCS (T1) shows 79.57% more absorption of SL than the absorption of SL by RCS (T1). Likewise, ODCS (T2) absorbs 65.92% SF than that of RCS (T2).
- In the treatment type RCS (T1W), water absorption ability is reduced to 1.19% which is 92.67% less in comparison to RCS (W) (16.25%). Similarly, water absorption ability in the treatment type ODCS (T1W) was reduced to 0.56% which is about 97.49% less than that of ODCS (W) (22.38%).

- In the treatment-type RCS (T2W), water absorption ability is 0% which is 100% less compared to RCS (W). Likewise, water absorption ability in the treatment type ODCS (T2W) reduced to 1% which is about 95.53% less than that of ODCS (W).
- Coconut shells treated with SF and SL show improvement in quality. Particularly, treating the RCS with SF shows improvement in quality compared with ODCS and without treatment.
- The results of image analysis support the results obtained through treatment methods.
- It is certain that the water absorption ability of CS aggregate can be reduced if the CS aggregate is treated.
- As regards the cost effect, the cost of SF is about 50 to 60% of the SL, and therefore SF can be effectively used to treat the CS aggregates than using SL.
- More research works are necessary on CS aggregates treated with SL and SF for the purpose of obtaining durable CS aggregate concrete.

Acknowledgements The authors desire to acknowledge SRM Institute of Science and Technology's Management for their sustenance to complete this research. Also, thanks to those who directly or indirectly assisted in this research study.

References

1. Gunasekaran K, Kumar PS, Lakshmipathy M (2010) Compatibility studies on the coconut shell cements composites. Indian J Indian Concrete Inst 11(1):27–31
2. Gunasekaran K, Kumar PS, Lakshmipathy M (2011) Study on properties of coconut shell as an aggregate for concrete. Indian J Indian Concrete Inst 12(2):27–33
3. Gunasekaran K, Kumar PS, Lakshmipathy M (2011) Mechanical and bond properties of coconut shell concrete. Constr Build Mater 25(1):92–98
4. Gunasekaran K, Annadurai R, Kumar PS (2013) Study on reinforced lightweight coconut shell concrete beam behavior under flexure. Mater Design 46:157–167
5. Gunasekaran K, Annadurai R, Kumar PS (2013) Plastic shrinkage and deflection characteristics of coconut shell concrete slab. Constr Build Mater 43:203–207
6. Gunasekaran K, Ramasubramani R, Annadurai R, Prakash Chandar S (2014) Study on reinforced lightweight coconut shell concrete beam behavior under torsion. Mater Design 57:374–382
7. Gunasekaran K, Annadurai R, Kumar PS (2015) A study on some durability properties of coconut shell aggregate concrete. Mater Struct 48:1253–1264
8. https://www.google.com/search?q=coconut+shell+products&oq=coconut+shell+&aqs=chrome.4.69i57j0l7.6698j0j8&sourceid=chrome&ie=UTF-8. Retrieved on 01.07.2020 at 09.00 am
9. Mannan MA, Alexander J, Ganapathy C, Teo DCL (2006) Quality improvement of oil palm shell (OPS) as coarse aggregate in lightweight concrete. Build Environ 41:1239–1242
10. Traore YB, Messan A, Hannawi K, Gerard J, Prince W, Tsobnang F (2018) Effect of oil palm shell treatment on the physical and mechanical properties of lightweight concrete. Constr Build Mater 161:452–460

11. Maryono, Sudding and Rahmawati (2013) Preparation and quality analysis of coconut shell charcoal briquette observed by starch concentration. J Chemica 14:74–83
12. Sudding and Jamaluddin (2016) The processing of produce Reneweable energy sources. ICMSTEA 2016: international conference on mathematics, science, technology, education and their applications, Makassar, Indonesia, 3–4 October 2016

Analysis of RCC Beam with Varying Stirrups Pattern Subjected to Two-Point Loading by Using ABAQUS

M. Ananth, R. Sivasankar, G. Selvaganapathy, and T. Sevakapandian

1 Introduction

1.1 General

Beams and columns are the structural components used to move load charges from the superstructure to the substructure. The concrete is compressive solid but stresses more when it is subjected to bending [1]. Reinforcements were implemented to rectify the deficiencies in concrete. Reinforcements are positioned in the region where the tensile forces act [2–5]. In beams, reinforcements were provided for holding the flexural loads, while in the shear case, stirrups were added as shear reinforcement. If the loads exceed the beam's load-carrying capacity, cracks in beams may occur. The excessive shear force results in shear splits. Various possibilities were introduced to improve the shear potential of the beam and to reduce the crack formations in the beam, such as increasing the number of shear reinforcements, spacing the stirrups. For this analysis, stirrups were given as shear strengthening by varying the stirrup patterns along with the reinforcement. Using the program ABAQUS/CAE, the beams with varying shear reinforcements were prepared and analyzed [6–10].

M. Ananth · R. Sivasankar (✉) · G. Selvaganapathy · T. Sevakapandian
National Engineering College, KR Nagar, Kovilpatti, Tamilnadu, India
e-mail: rsscivil@nec.edu.in

M. Ananth
e-mail: am1981@srmist.edu.in

G. Selvaganapathy
e-mail: 1616043@nec.edu.in

T. Sevakapandian
e-mail: 1616044@nec.edu.in

K. S. Satyanarayanan et al. (eds.), *Sustainable Construction Materials*, Lecture Notes in Civil Engineering 194, https://doi.org/10.1007/978-981-16-6403-8_32

1.2 Literature Review

Work was revealed on shear monitoring of concrete beams with a non-stop circular rectangular spiral reinforcement [11]. The action of concrete shear beams with an oblong cross-section and continuous oblong spiral reinforcement is experimentally investigated as being obliquely reinforced under monotonous pressure. Additionally, a dynamic rectangular circular reinforcement is added and tested as shear-reinforcing with shear-favourably inclined vertical links. The Research System requires eight beams. Test findings suggest that the activity of oblong spiral reinforcement inside the examined beams provided improved bearing efficiency and improved shear recital. Beams with a spiral reinforcement length of 120 mm and 80 mm demonstrated 14.9% and 14.7% increased shear performance with respect to the corresponding stirrup beams [12–15]. In comparison, beams with advanced spirals with a spacing of 120 mm and 80 mm reported 17 and 21.7% higher shear efficiency for the corresponding stirrup beams. In addition, the beams with advanced spirals displayed ductility values of deformation 2.10 and 2.60, respectively, showing this pattern increased ductility after peak deformation relative to the beams with the same quantity of widely used stirrups [21, 22]. They had discussed the 3D nonlinear FE model to know about the behaviour of RC beams under flexure. The same model was done in ABAQUS/CAE. Lubliner and collaborators developed the damaged plasticity model for concrete and variation in steel reinforcements. The crack model was obtained and the stress–strain values were also investigated. In accordance with the results, the mesh values were changed and defined. By giving the CDP values the crack patterns were also obtained are not accurate as the real model was not developed to interpret them.

The efficiency of basalt fibre reinforced polymer-reinforced concrete short beams, they dealt with various effects of deep RC beams without network reinforcement 10 numbers were studied [6]. From the number of beams, two 10 m long and 140 mm wide rectangular beam with variable depth were tested under a loading condition of four stages. They are fully reinforced with steel bars. To withstand the BFRP to opposite beams, effective depth, reinforcement ratio, and span width ratio (a/d) were analysed. ABAQUS was used to develop the final element model. The BFRP RC beams showed less rigidity hence they can be used in short components.

The publication of a study of the impact of the stirrup and inclined bar rust on the shear actions of RC beams were described [16–19]. The experimental work is introduced on the shear actions of rusted reinforced concrete beams with stirrups and inclined bars. The proposed research intends to monitor corrosion properties on the deterioration of shear strength of RC beams with a short shear period to successful depth ratios in the two forms of shear reinforcement. The improved corrosion regulation is used in stem cells and inclined bars in 14 beams to obtain various degrees of corrosion. Functionally the concrete cracking induced by erosion and portion degradation was addressed. It displayed shear behaviour including reaction to load-deformation, residual shear power, diagonal cracking and failure mode. A revised

ACI system measured the shear strength of the beams given the lack of shear reinforcement corrosion and the harm to concrete portions. The depletion of corrosion in stirrups and inclined bars is observed to be less than 10 per cent because it has little impact on the weakening of the shear motion. Serious rust of stirrups and inclined plates, and exposure to the concrete section of the convoy significantly reduces shear strength and durability. Rust of the stirrup and the bent bars do not change the shape of the compression arm shear. High corrosion raises the amount of cracks in the beams and causes the shear reinforcing to split early.

The shear variations of RC beams with the grids being welded with the reinforcement were discussed [12]. The grids were made to cut as shear reinforcements. Cyclic loads were applied to test the shear variations. Bended stirrups were also used to increase the shear capacity of the beam. Under cyclic loads, the smooth rebar got affected by the concrete. To beat the deficiency, the effectiveness was experimentally tested. It was designed in a way that pre-weld failure should not occur. A quantified prediction model has not been developed by them as they got only a limited number of test results.

The effectiveness of spirally formed stirrups on concrete beams. Shear reinforcement usually consists of conventional stirrups in concrete beams by positioning them individually and engaged to the most bars were studied [17]. The use of spiral shear reinforcement was explored during this analysis by evaluating 24 concrete beams in an extremely static four-point bending test. Crack evolution was tracked during the experiments, thus studying and comparing the fracture mechanisms of the beams. The findings suggest that shear reinforcement, spirally formed, may be a viable alternative that would be used in international codes [20]. A sequence of 24 beams undergoes a flexure test to determine the effectiveness of spirally formed stirrup arrangements. The findings suggest that a spiral stirrup configuration works equally well in the conventional cases as compared with straight stirrups. Also, with current codes, a spiral structure can be constructed safely. The spiral model shows an increase in the intensity of about 18.7 per cent compared to the normal one.

The materials used in civil engineering structures have typically low tensile properties compared to reinforced concrete, as stated [22]. Here we will test the behaviours of the reinforced concrete using hoops to achieve high strength and properties. Experimental investigation regarding the circular RC columns was taken down. Thirty 150 mm diameter and 300 mm high units of longitudinal and lateral steel were casted with varying numbers such axial load acting on it loading to the failure according to the speed of the loading. The interpretation of works was done and it shows the importance of the speed of loading. Hence, slow loading of the specimen under controlled test machines was conducted. More practical features were considered for the seismic loading conditions.

Table 1 Tensile test results of steel bars

Description	TMT bar
Yield stress	354.226 N/mm^2
Load at yield	28.380 kN
Load at break	36.28 kN
Tensile strength	478.542 N/mm^2
Load at peak	38.34 kN

Table 2 Test results of cubes and cylinders sample

Average axial compression of the cylinder	2.136×10^4 N/mm^2
Young's modulus	22,360.679 N/mm^2
Average density	2389.62 kg/ m^3
Average compressive strength	20.22 N/mm^2

2 Material Study

2.1 Tensile Test in TMT Bars

The tensile test was carried out in a 10 mm diameter main bar with a different welded reinforcement spacing of approximately 150 mm and 300 mm to know the behaviour of steel under welded conditions (Table 1).

2.2 Testing of Cylinders and Cubes

To find out the physical properties of concrete and mechanical properties of concrete, the characteristic compressive strength of the cubes of size 150 mm × 150 mm × 150 mm and the axial compression test of cylinders of size 150 mm × 300 mm were performed and the results obtained were tabulated below (Table 2) (Fig. 1).

3 Abaqus/Cae

3.1 Analysis

In this study, two types of beams were analysed, at first the beam of size 150 mm x 150 mm x 700 mm was taken into account to decide if the method is right, because the results showed no significant improvement in both ABAQUS/CAE [6] and the beam of size 150 mm x 230 mm x 1200 mm was adopted in an experimental manner

Fig. 1 Compression test for cubes and cylinders sample

to determine the actual beam behaviour in both bending and shear. The model has been optimized for the traditional 300 mm spacing stirrup design derived from IS 456:2000 for the conformation of the method, the concrete damaged plasticity model has been developed and evaluated and the different parameters have been taken into account. Compression behaviour and tension values are tabulated below (Table 3).

3.2 Beams with Truss Models

A total of seven different models of shear reinforcements were analysed by varying the shape of the stirrup placement using the ABAQUS/CAE, the dimensions are of 150 mm x 230 mm x 1200 mm, all of them were tested in the same way of flexure testing machine (Fig. 2).

3.2.1 Result and Discussion for Truss Models

ABAQUS results with truss models are shown in (Table 4) (Fig. 3).

3.3 Beams with Angular Changed Models

The second type of model was prepared by varying the inclination of stirrups [3] from 45^0 to 135^0 and the models were analysed using the ABAQUS (Fig. 4). The

Table 3 Input datum in ABAQUS

Module parameter	Values
Part	Beam, 8 mm diameter longitudinal bar, Stirrups (8 mm)
Property	Mechanical - Elastic
Young's modulus for concrete	22,360.679 N/mm^2
Young's modulus for steel	200,000 N/mm^2
Poisson's ratio for concrete	0.2
Poisson's ratio for steel	0.3
Load	25 kN
Boundary condition	Pinned, Fixed
Mesh size	15
Concrete damaged plasticity values	
Dilation angle	30^0
Eccentricity	0.1
fb0/fc0	1.16
K	0.67
Viscosity parameter	0
Compressive behaviour	
Yield stress	2.51
Inelastic strain	0
Tensile behaviour	
Yield stress	0.9387
Cracking strain	0

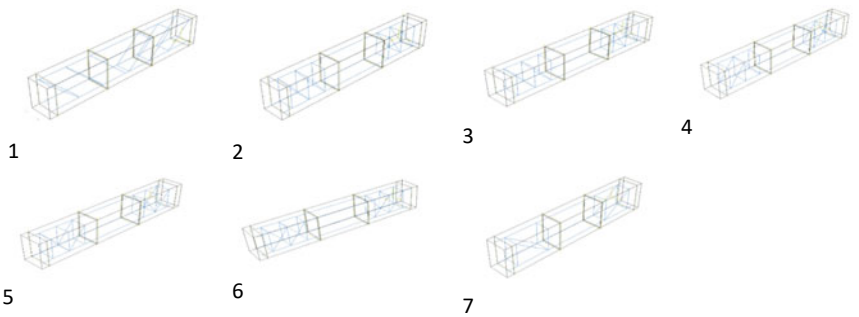

Fig. 2 Beams with truss model stirrups

Table 4 ABAQUS result with truss models

Truss Model	Load (kN)
1	89.23
2	76.5
3	76.28
4	76.32
5	74.34
6	76.25
7	76.27

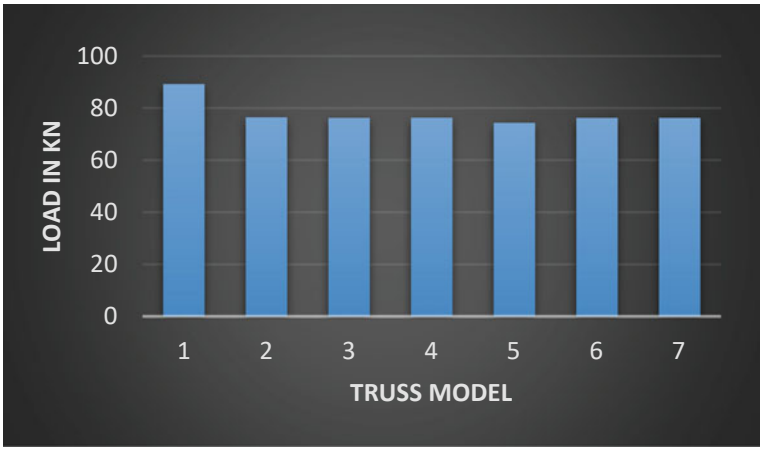

Fig. 3 Result for truss model beams

results obtained for the various angles of inclination of stirrups were tabulated below (Table 5) (Fig. 5). The width adopted for stirrups was 100 mm, with a 125 mm cover.

4 Result Interpretation

The 150 mm × 230 mm × 1200 mm stirrup beams were analysed using ABAQUS/CAE. The stirrups mounted in it are roughly perpendicular to the main reinforcement which are usually found in traditional beams, whereas the beams in truss and angular models show a steady increase in the load while analysing. Therefore, the truss model 1 and angle in 135^0 shows the optimal load.

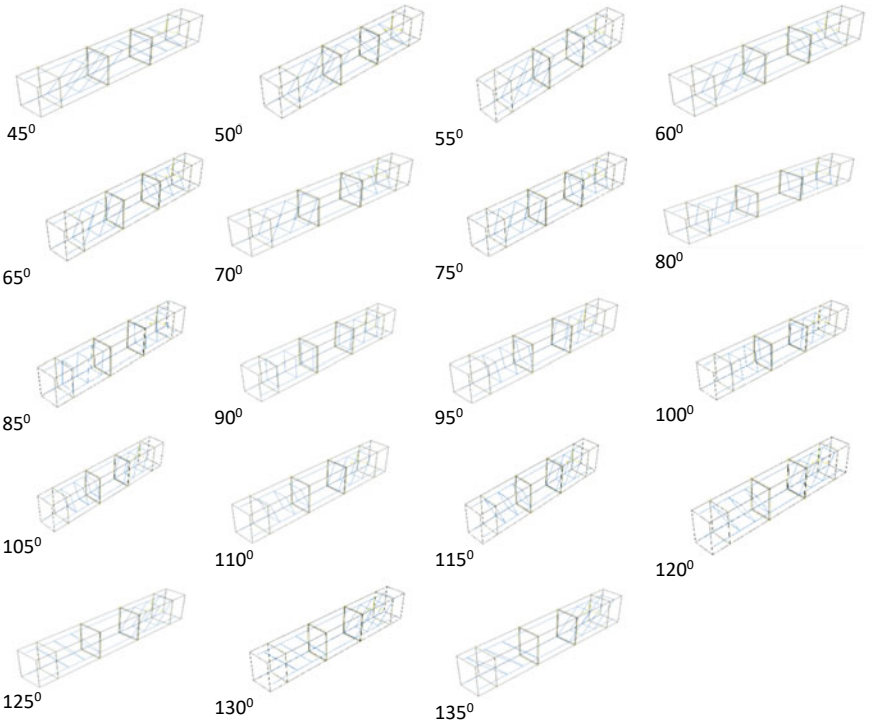

Fig. 4 Beams with truss model stirrups

5 Conclusion

The ABAQUS/CAE model for a beam of size 1200 mm x 150 mm x 230 mm was adopted for knowing the exact behaviour of bending and shear force acting on the beam. Various models were analysed to find the pattern of stirrups that can carry the maximum load with minimum deflection. The stirrups of angles that are perpendicular to the shear force acting direction show a greater response than that of parallel one. The model of 135^0 shows the maximum response of the force and gives the optimum value. The truss model 1 also gives maximum response the force and gives the optimum value, but special considerations are to be done with the stirrups to make those truss models.

Table 5 ABAQUS result with various angles models

Angle	Load (kN)
45^0	80.9
50^0	53.65
55^0	60.14
60^0	47.58
65^0	46.28
70^0	62.97
75^0	80.03
80^0	92.08
85^0	92.77
90^0	79.61
95^0	92.44
100^0	92.39
105^0	94.96
110^0	96.75
115^0	94.65
120^0	93.91
125^0	94.42
130^0	94.28
135^0	98.79

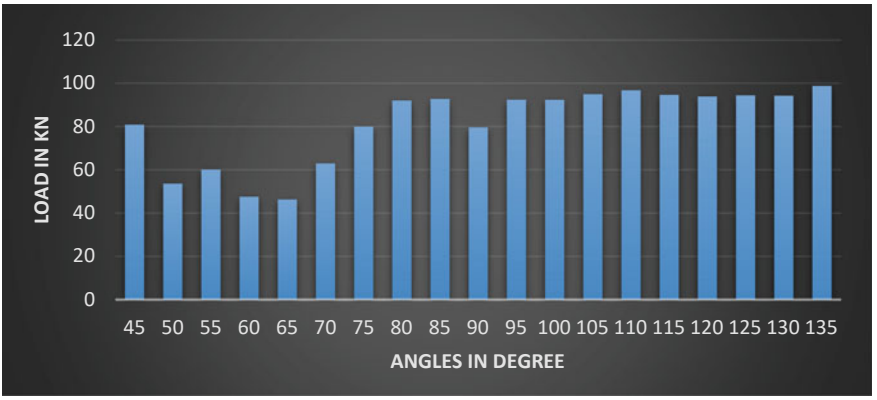

Fig. 5 Result for various angles model beams

References

1. Abaqus Analysis User Manual – Abaqus Version 6.8. (2008). Retrieved November 5, 2010
2. El-Sayed AK (2017) Shear capacity assessment of reinforced concrete beams with corroded stirrups. Construct Building Mater 134, 176–184
3. Karayannis CG et al (2013) Shear tests of reinforced concrete beams with continuous rectangular spiral reinforcement. Construct Build Mater 46:86–97
4. Dassault Systèmes Simulia Corp (2008). Abaqus v. 6.8 [Software]. Providence, RI: Dassault Sys/tèmes Simulia Corp
5. Doo-Yeol Yoo et al (2017) Feasibility of replacing minimum shear reinforcement with steel fibers for sustainable high-strength concrete beams. Eng Struct 147:207–222
6. Abeda F et al (2019) Experimental and finite element investigation of the shear performance of BFRP-RC short beams. Structures 20:689–701
7. Jumaa GB (2019) Size effect on the shear failure of high-strength concrete beams reinforced with basalt FRP bars and stirrups. Construct Build Mater 209:77–94
8. Joergensen HB et al (2018) Experimental investigation on the shear capacity of RC beams with curtailed reinforcement. Eng Struct 169:81–93
9. Fisker J (2016) Mechanical model for the shear capacity of R/C beams without stirrups: A proposal based on limit analysis. Eng Struct 115:220–231
10. Bantilas KE (2017) Shear strength of reinforced concrete beam-column joints with crossed inclined bars. Eng Struct 140:241–255
11. Wang L et al (2015) Effects of stirrup and inclined bar corrosion on shear behaviour of RC beams. Construct Build Mater 98:537–546
12. Cui M et al (2019) Experimental study on the shear performance of RC beams reinforced with welded reinforcement grids. Construct Build Mater 203:377–391
13. Colajanni P (2014) Shear capacity in concrete beams reinforced by stirrups with two different inclinations. Eng Struct 81:444–453
14. Wakjira TG et al, FRCM/internal transverse shear reinforcement interaction in shear strengthened RC beams. Composite Struct 201:326–339
15. Ebead U (2019) Experimental and analytical study on strengthening of reinforced concrete T-beams in shear using steel reinforced grout (SRG). Composites Part B 177:107368
16. Visintin P (2017) Shear behaviour of Geo-polymer concrete beams without stirrups. Construct Build Mater 148:10–21
17. de Corte W et al, Effectiveness of spirally shaped stirrups in reinforced concrete beams. Eng Struct 52:667–675
18. IS 456:2000 Indian standard plain and reinforced concrete - code of practice (fourth revision)
19. IS: 2386 (part iii) (1963) Methods of test for aggregates for concrete
20. IS :4031 (part 4) (1988) Methods of physical tests for hydraulic cement part 4 determination of consistency of standard cement paste
21. Earij A et al (2017) Nonlinear three–dimensional finite–element modelling of reinforced–concrete beams: computational challenges and experimental validation. Eng Failure Anal 82:92–115
22. Rajasekhar K et al (2017) Stress-strain behaviour of confined normal grade concrete. Int J Prof Eng Stud viii(3)

Comparative Study on Seismic Performance of Steel Diagrid Structures with and Without Dampers

M. Vishali, S. Pradeep, and K. S. Satyanarayanan

1 Introduction

Tall buildings are fundamentally a reaction to the extreme weight on the accessibility of land. Advances in analytical technique, material, structural system for analysis, construction technology and design quickened the advancement of tall structures. The sidelong loads because of quakes and wind are the central point that causes the structure of tall business structures. The lateral loads resisting systems used widely are mainly Braced Tube System, Tubular System, Shear Wall-Frame, Outrigger System, Rigid Frame, and Diagrid Systems. Of late, the Diagrid Structural System is ending up generally famous and featuring solution in the plan of tall structures because of its Esthetically Dominant and Inherent Structural. The Diagrid is a diagonally intersecting framework of a metal, concrete or timber beams that are used for the construction of buildings and roofs. They carry both Gravity loads and Lateral loads. Because of their triangulated design, inward hub powers emerge in the part and the structure are much more effective in minimizing shear deforming [1–3]. Most diagrid structural systems are fabricated from steel and few of them are only constructed with concrete. The main principle is to eliminate the vertical segments present at the border of the building. The corner to corner converging structure goes about as both slanted segments and as propping components [4].

An early case of the diagrid structure is the IBM building (Fig. 1a) in Pittsburgh work in the mid-1960s, which has 13 storeys. The Central China Television (CCTV) (Fig. 1b) in Beijing built in 2004, it is a 51-storey skyscraper. The Swiss Re in London (Fig. 1c) is another famous example of diagrid structures all around the world, it was

M. Vishali (✉) · S. Pradeep · K. S. Satyanarayanan
Department of Civil Engineering, College of Engineering and Technology, SRM Institute of Science and Technology, SRM Nagar, Kattankulathur 603 203, Tamilnadu, India
e-mail: vm4814@srmist.edu.in

S. Pradeep
e-mail: pradeep.s@ktr.srmuniv.ac.in

K. S. Satyanarayanan et al. (eds.), *Sustainable Construction Materials*, Lecture Notes in Civil Engineering 194, https://doi.org/10.1007/978-981-16-6403-8_33

(a) (b) (c) (d) (e)

Fig. 1 **a** IBM building **b** CCTV **c** Swiss Re **d** Hearst Tower **e** Cyclone Tower

constructed in 2003 which has a 41-storey 180-m building height. Hearst tower in New York (Fig. 1d) which was constructed in 2003, has a 60 storeys and 182 m of building height. The cyclone tower in Asan, South Korea (Fig. 1e), which has 55 storeys, 284 m in height.

The major difference between a diagrid structure and a braced tube structure is that the diagrid structures carry both gravity loads as well as lateral loads and there are no vertical segments present in the border of the structure though in supported cylinder structure they convey just horizontal burdens and vertical segments are available in the edge of the structure [5]. Diagrid system can be of crystalline, planar or take on multiple curvatures and these save approximately 20% of structural steel weight when compared to conventional frame structures [6].

2 Analytical Work

2.1 Descriptions of Model and Material Properties

The modeling of the conventional structural system has been stimulated as shown in (Fig. 2a and c). The system consists of 50 storeys with a plan dimension of 40 m × 20 m as per aspect ratio (H/L) is 4.5. The system consists of an inner core and an outer perimeter column. The outer perimeter consists of a closely spaced column at 4 m to the center that forms a tube. The inner core consists of closely spaced columns. The inner core resists gravity loading while the outer perimeter column resists lateral loading. The columns are fixed at the base.

The modeling of diagrid steel structures has been stimulated as shown in Fig. 2b and d. The system consists of 50 storeys with a plan dimension of 40 m × 20 m as per aspect ratio (H/L) is 4.5. The system consists of an inner core and outer diagonal elements. The outer perimeter consists of diagrid element of angle 62° at 8 m spacing along the perimeter for the entire structure. The inner core consists of closely spaced columns. The inner core resists the gravity loading while the outer diagrid resists the lateral loading. The columns and diagrid are fixed at the base.

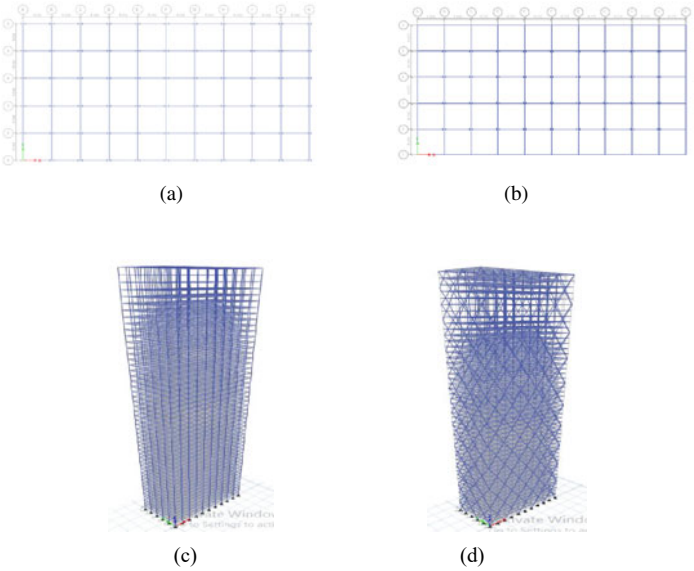

Fig. 2 **a** Plan of the conventional steel system **b** Plan of the diagrid steel system. **c** Model of the conventional steel system **d** Model of the diagrid steel system

The structural element such as beams, diagrids and columns that has the basic steel properties while the chunks are considered of RCC. In diagrid structures, there are two different behavioral characteristics that are observed as Model-A (Diagrid structures with corner columns) as shown in (Fig. 3a and c) and Model-B (Diagrid structures without corner columns) as shown in (Fig. 3b and d) [7]. Comparisons between these two models are also compared and results are analyzed based on effective structures for tall buildings and more interesting in aesthetic choice.

The modeling of diagrid steel structures with dampers has been stimulated as shown in Fig. 4a and b. The system consists of 50 storeys with a plan dimension of 40 m $\times$ 20 m as per aspect ratio (H/L) is 4.5. The system consists of an inner core and outer diagonal elements. The outer perimeter consists of the diagrid element of angle 62° at 8 m spacing along the perimeter for the entire structure. The inner core consists of closely spaced columns. The inner core resists the gravity loading while the outer diagrid resists the lateral loading. The columns and diagrid are fixed at the base. The friction dampers are introduced in the diagrid intersecting points. In damper, data properties are the total mass of the damper which is 44 kg and the weight of the damper is 250 kN.

Dampers are defined as essentialness setback in the response over the interval of time. Vitality dispersal includes factors, for example, materials, radiation of soil, and so forth. A clear comprehension of damping is required for consolidating its impact on the structure. The state of reaction bend doesn't change by damping; however, the extents are diminished. The significance of damping is the point at which the structure has much retaining limit than the seismic vitality then it can withstand the

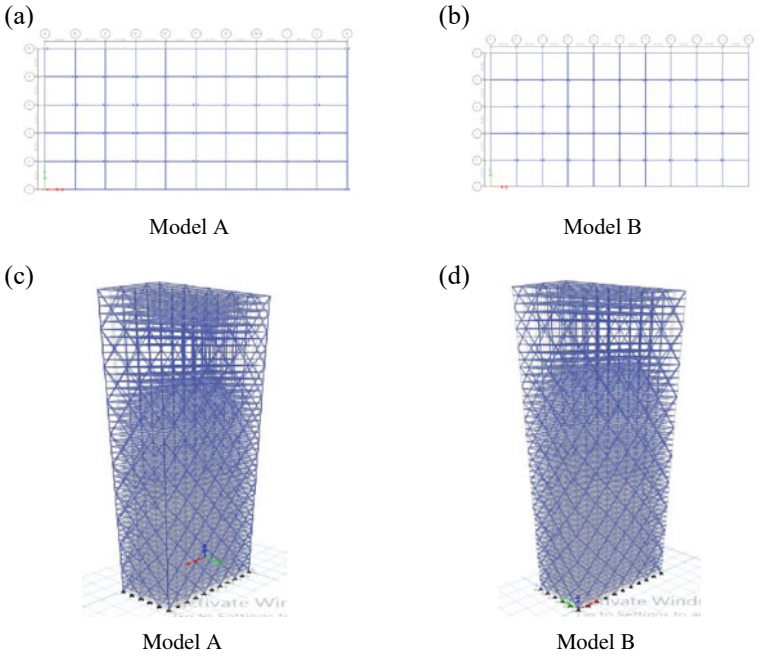

Fig. 3 **a** Plan of the diagrid structure with corner columns **b** Plan of the diagrid structures without corner columns **c** Plan of the diagrid structure with corner columns **d** Plan of the diagrid structures without corner columns

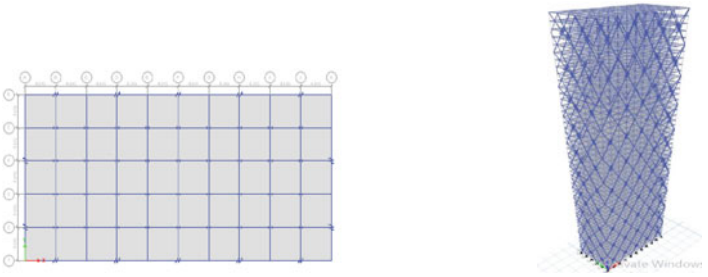

Fig. 4 **a** Plan of the diagrid steel system with damper. **b** Plan of the diagrid steel system with damper

Fig. 5 Elecentro function graph

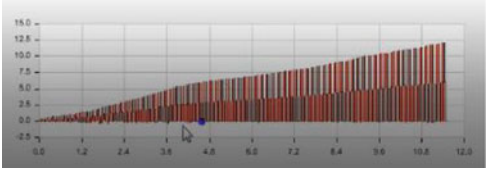

Table 1 The physical premises and information of the model

Description	Values
Storey height	3 m
Structural type	Steel frame
Types of dampers	Friction damper
Steel section	Fe250
Concrete section	M25
Column section	ISHB 450
Beam section	ISMB 400
Diagrid section	ISMB 250
Dead load	3 KN/m^2
Live load	4 KN/m^2
Floor slab	250 mm
Steel design code	IS 800:2007

auxiliary harm. Relatively soft type of damping can be utilized as a plausible method for diminishing the basic harm. Friction dampers are a kind of damper. Among others, highlights of these dampers can be delegated maintaining a strategic distance from exhaustion in served burdens and their execution free to stacking speed and surrounding temperature. These dampers are introduced in parallel to supporting. Because of direct lead and easy to present and make this sort of damper is changed over to a champion among the most sorts of crushing dampers.

The modeling and analysis are done using ETABS software. The dead loads and live loads are taken as per IS875:1987(Part1) and IS875:1987(Part 2) [8, 9]. The wind load is taken as per IS875:1978(Part 3) [10]. Response spectrum analysis has been done for two models.

The input values and earthquake load are in accordance with the Indian standard IS1893 (part 1)-2002 [11]. The structure is considered to be in Zone III with a zone factor of 0.16. Importance factor I is 1.5. Response reduction factor R is 5 as specified for special moment-resisting frames. Type 2 medium soil is selected. When the structure vibrates the amplitude decreases due to internal friction and absorbed energy. This damping is taken as 5% for steel structures. The square root of sum of squares (SRSS) method of modal combination is chosen. The physical premises and information of the model for the present study has been shown in (Table 1).

2.2 Analysis

2.2.1 Time History Analysis

In time history investigations, the auxiliary reaction is processed at various consequent time moments. To perform such an examination, an agent seismic tremor time

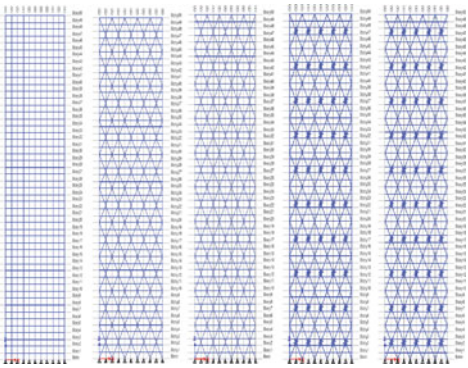

Fig. 6 Typical elevation for model 1, 2, 3, 4, 5

history is required for a structure being assessed. In this function, Elecentro is being used, because it is the most dangerous and disastrous earthquake. The values at equal intervals are 0.02. The Elecentro function for time history analysis is shown in Fig. 4.

In load case data, the initial condition should be zero. The load applied in the direction should be acceleration whereas the function is Elecentro and the scale factor has been calculated (Eq. 1).

$$\text{The scale factor} = (\mathbf{Ig/R}) * (\mathbf{0.85} * \mathbf{Static\ bases\ hear/Response} - \mathbf{spectrum\ base\ shear}) \quad (1)$$

In the number of output time steps when there are a greater number of steps, the accurate values can be determined. The model damping has a constant value of 0.05 (Fig. 5).

The comparison of seismic analysis using time history analysis is going to be done between these models followed below and the typical elevation of the below models are shown in (Fig. 6).

Model 1-Conventional structure.
Model 2-Diagrid structure with corner columns.
Model 3-Diagrid structure without corner columns.
Model 4-Diagrid structure with corner columns using dampers.
Model 5-Diagrid structure without corner columns using dampers.

3 Results Comparison and Discussion

3.1 Maximum Storey Displacement

In storey displacement, it represents the correlation of the most extreme storey removals for every structure. It is observed that the general relocation esteems are very higher for traditional structures that have appeared in Fig. 7. Along these lines,

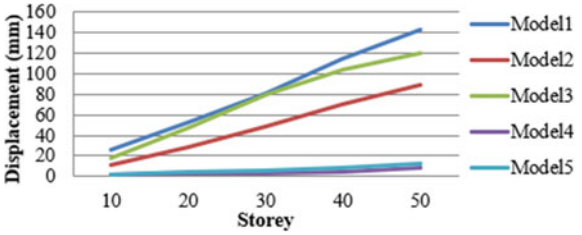

Fig. 7 Maximum storey displacement

it demonstrates the viability of diagrid structures, whereas the displacement values for the structure using dampers are lesser compared to all the structures. Hence, it is proved that the effectiveness of diagrid structures using dampers is more, which is 83% higher when compared to conventional structures.

3.2 Maximum Storey Drifts

The storey drifts of 50-storey diagrid structures with and without dampers and conventional structures are compared. It is observed that the inter-storey drifts of diagrid structures using dampers are less compared to conventional structures that has been stimulated as shown in (Fig. 8). The maximum storey drifts for conventional structures have occurred between storey 15 and 20. The maximum storey drifts for conventional systems are 0.000923. The maximum drifts for diagrid structures using dampers have occurred between storey 15 and 20. The maximum storey drifts for diagrid structures using dampers are 0.000654, which is 29% lesser than the conventional structure.

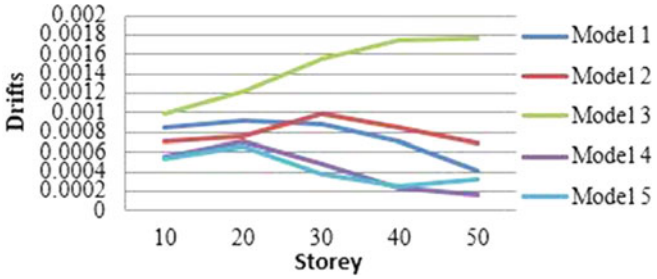

Fig. 8 Maximum storey drifts

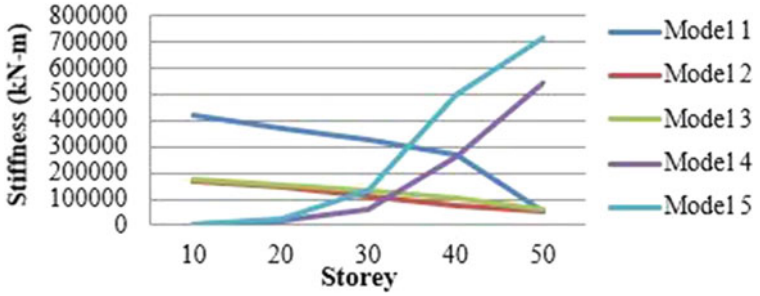

Fig. 9 Storey stiffness

3.3 Storey Stiffness

The comparison of the storey stiffness for the conventional structures and diagrid structures using with and without dampers is being observed. The stiffness of diagrid structures with dampers is gradually increased when compared to the other structures, which is 92% higher than the conventional structures. Whereas the remaining structures expect diagrid structures with dampers are gradually decreased as shown in (Fig. 9).

3.4 Storey Shear

The comparison of the storey shear for all the models have been compared. It is observed that each storey shear is taken from the bottom of the storey. The base shear is 64% more for conventional structures when compared with diagrid structures; whereas it is 93% less when compared with diagrid structures using dampers has been stimulated as shown in Fig. 10.

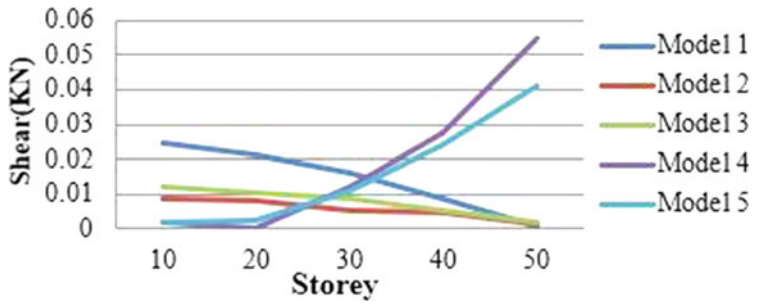

Fig. 10 Storey shear

4 Conclusion

The seismic analysis of 50-storey conventional steel structures and diagrid steel structures with and without dampers has been completed. From this result, it is clear that diagrid structure with dampers has maximum strength and lateral load resistance than a conventional structure. The stiffness of the diagrid structure with a damper is 13 times higher than the conventional structure. Diagrid structures with dampers have the minimum storey displacement and storey drift compared to the conventional structure. Thus, the seismic execution of the structure is enhanced and the basic effectiveness is expanded.

References

1. Revankar RK, Talasadar RG (2014) Analysis of diagrid structure. Int J Eng Innovat Technol 04:168–174
2. Panchal NB, Patel VR, Pandya II (2014) Optimum angle of diagrid structural system. Int J Eng Tech Res 02:150–157
3. Montuori GM, Mele E, Brandonisio G, De Luca A (2014) Secondary bracing systems for diagrid structures in tall buildings. Eng Struct 75:477–488
4. Jerome J (2007) Connor et al, Diagrid structural system for tall buildings: characteristic and methodology for preliminary design. The structural design of tall and special buildings, Wiley Interscience 16:205–230
5. Kyoung Sun Moon (2011) Diagrid structures for complex-shaped tall buildings. ScienceDirect, procedia engineering, the twelfth east Asia-Pacific conference on structural engineering and construction Elsevier Ltd 14:1343–1350
6. Jani K, Patel PV (2014) Analysis and design of diagrid structural system for high rise steel buildings. In: Sciverse scienedirect, procedia engineering, chemical, civil and mechanical engineering tracks of 3rd Nirma university international conference on engineering (NUiCONE-2012), vol 04. Elsevier Ltd, pp1147–1165
7. Moon KS (2007) Diagrid structural systems for tall buildings: characteristics and methodology for preliminary design. In: the structural design of tall and special buildings, vol 16. Wiley Interscience, pp 205–230
8. Bureau of Indian Standards (BIS) (1987) IS 875 (Part 1): code of practice for design loads (other than earthquake) for buildings and structures. part 1: dead loads—unit weights of building materials and stored materials (second revision)
9. IS 875–2: code of practice for design loads (Ot...” [Online]. https://archive.org/stream/gov.in.is.875.2.1987#page/n3/mode/2up. Accessed: 13 Jul 2017
10. “IS 875–3: Code of practice for wind loads (Ot...” [Online]. Kisan M, Sangathan S, Nehru J, Pitroda SG (1987) म ा नक
11. IS 1893–1: Criteria for earthquake resistant design of structures, part 1: general provisions and buildings : bureau of Indian standards : free download and streaming : internet archive. https://archive.Org/details/gov.in.is.1893.1. 2002. Accessed: 13 Jul 2017

Feasibility Study of Tannery Waste as an Alternative for Fine Aggregate in Concrete

N. Sunmathi, R. Padmapriya, and J. S. Sudarsan

1 Introduction

Concrete is a more promising and evergreen required material in the construction field from older days to now. Concrete can resist all types of loadings. It is brittle in nature with a high impact resistance capacity. Due to the increase in high-rise buildings and technology on the construction of buildings, the requirement of additives is needed to increase the strength of concrete. Increasing work of construction increases the demand for the material. Fine aggregate is a material that contributes to the main role in concrete and at the same time cost of river sand increasing day by day. So, people are moving on to the new economical material without reducing the strength of concrete. The growth and development lead to an increase in technologies and many industries. This development can give a prosperous lifestyle to people. The growth of industries becoming advanced with the growth of environmental impact. Tannery industries are one of the leading industries in India, which generates higher income for a country. The waste generated from the industry is also higher and creates many impacts on soil, water and human health [1–4]. Waste can be defined as the thing that cannot be used for anything. As implementing waste is a cost consuming concept, a study on partial replacement of tannery industry waste for fine aggregate in concrete with different percentages was done.

Hassan S [5] framed the main objective to measure the possibility of reduction of chemical compositions in waste from tannery industry and to calculate the serviceability of the waste with concrete. During the study, 0, 1, 5, 10, 15, and 20% of sludge were used for the replacement of fine aggregate by mass of certain cement percentage.

N. Sunmathi · R. Padmapriya (✉)
Department of Civil Engineering, Sathyabama Institute of Science and Technology, Jeppiar Nagar, Chennai 600119, Tamil Nadu, India

J. S. Sudarsan
National Institute of Construction Management and Research (NICMAR), Balewdi, Pune 411045, India

K. S. Satyanarayanan et al. (eds.), *Sustainable Construction Materials*, Lecture Notes in Civil Engineering 194, https://doi.org/10.1007/978-981-16-6403-8_34

Tests were conducted for six trial mixes. By repeatability test and analyzing the result, a suitable sludge/cement ratio was selected.

Sathish Kumar and Vijayaravind [6] studied the partial replacement of tannery shredded waste for fine aggregate and compute the concrete properties. The concrete made with replacement has a reduction in weight and gives better strength than conventional concrete. Replacement of 0, 5, 15, 20% was made. On replacement of 15% of tannery waste, the compressive strength increases by 24% and tensile strength increases by 88%.

Muniraj K et al. [7] deals with a study to find the practicability of using sludge as fine aggregates in M25 grade of concrete. Specimens of concrete were cast with various proportions of sludge that is 0, 5, 15 and 20% for sand in concretes. By this alternative, solid waste could be disposed of in a healthier way without affecting the atmosphere. CS of concrete was found at the stage of 7th and 28th day. The optimum percentage of sludge in concrete by test result is 5%.

Vasudevan and Raj (2016), [8] **s**tudied the outcome of the addition of textile and tannery sludge for replacement of sand in the concrete. Textile and tannery sludge manufacturing wastes utilized in this development comprises some heavy metals which are adverse in nature. The experimental study was done at the stage of 7th and 28th day with M15 grade concrete. The best result obtained for the replacement of both tannery and textile sludge is 15 and 20% for the replacement of textile waste alone.

Based on the revisions made on tannery industry and their waste, many types of research were done on their characteristics, effects/impacts, treatment, and all. But the study on tannery waste on concrete replacement is minimum. To fulfill this research gap and to use waste material as useful material, this feasibility study of tannery waste on concrete for replacement of fine aggregate was studied. The objectives of the study are as follows:

- To determine the chemical properties of tannery waste.
- To determine material properties of waste.
- To determine the mechanical property of concrete for replacement of fine aggregate by waste.
- To determine the durability of concrete for replacement of fine aggregate by waste.

2 Materials and Methods

2.1 Materials

The basic materials required during the study were procured and the basic properties were also studied as represented in Tables 1, 2, 3, 4 and 5 [9].

Table 1 Characteristics of cement

S. no	Test	Result	Permissible limit	IS specification
1	Consistency	25%	26–33%	IS 4031:1988, Part 4
2	Initial setting time	31 min	30 (min)	IS 4031:1988, Part 5
3	Fineness	8.5%	10 (max)	IS 4031:1996, Part 1
4	Specific gravity	3.15	3.1–3.16 g/cc	IS 2720, Part 3

Table 2 Characteristics of fine aggregate

S.no	Test	Result	Permissible limit	IS specification
1	Specific gravity	2.62	2.50–3.0	IS 2386:1963, Part 3
2	Fineness modulus	2.60	2.0–2.4	IS 2386:1963, Part 1& BS 812 Part 2
3	Water absorption	2.12%	3% (max)	IS 2386:1963, Part 3

Table 3 Physical characteristics of sludge

S.no	Test	Result
1	Appearance	Fine powder
2	Colour	Grey
3	Odour	Yes
4	Fineness modulus	6.25%
5	Water absorption	1.25%
6	Specific gravity	1.70

Table 4 Chemical characteristics of sludge

S.no	Test	Result (%)
1	Silica dioxide	6.1
2	Aluminium oxide	66.12
3	Chloride content	1.43
4	Chromium oxide	0.85
5	Phosphorous pent oxide	0.06
6	Sodium oxide	0.18
7	Calcium oxide	23.52
8	Potassium oxide	0.07
9	Ferric oxide	0.47
10	Volatile organic matter	2

Table 5 Characteristics of coarse aggregate

S.no	Test	Result	Permissible limit	IS specifiation
1	Specific gravity	2.56	2.5–3.0	IS 2386:1963, Part 3
2	Water absorption	0.74 %	2% (max)	IS 2386:1963, Part 3
3	Impact value	10.87%	45% (max)	IS 2386: 1963, Part 4

2.1.1 Cement

OPC grade 43 cement was used in experimental works. The properties of cement were tested as per IS specifications [10–13] and values are as follows.

2.1.2 Fine Aggregate

M - sand is used as a FA in concrete for the experimental work. The properties of fine aggregate were tested as per IS specifications (IS 2386- Part III) (IS2386 - Part I) [15–16] and values are as follows.

2.1.3 Tannery Sludge

Tannery waste used for this study was collected from Pallavaram, Chennai. Tannery sludge is replaced for fine aggregate. Tannery sludge properties and their chemical removal or reduction techniques were studied [17–20]. Physical properties and chemical properties of sludge were found and the test values are as follows.

2.1.4 Coarse Aggregate

The locally accessible CA of maximum size 20 mm is used in this study. The properties of CA were studied as per IS specification [14] (IS 2386- Part IV) and the values are as follows.

2.2 Methodology

Based on the initial study carried out, the following methodology was derived and executed. The flowchart for methodology is mentioned in Fig. 1.

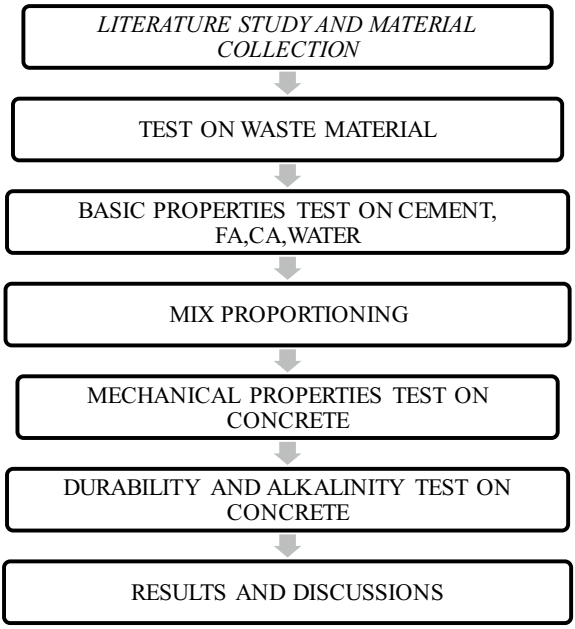

Fig. 1 Methodology flowchart

3 Mix Design and Proportion

According to IS 10262:2009, the M20 mix design was adopted and tabulated in Table 6 [22].

The workability of fresh concrete can be calculated by various methods. The slump cone test is to evaluate the consistency of concrete. Based on the study, the

Table 6 Mix ratio and proportion

Grade of concrete: M20						
Cement: 1 FA: 1.5 CA: 3 W/C Ratio: 0.5						
Mix	Materials					
	Cement (kg)	Fine aggregate			Coarse aggregate (kg)	Water
		Tannery waste (%)	Tannery waste (kg)	Fine aggregate (kg)		
Nominal mix	16.5	0	0	27	53.5	8.25
Mix 1	16.5	10%	2.7	24.3	53.5	8.25
Mix 2	16.5	20%	5.4	21.6	53.5	8.25
Mix 3	16.5	30%	8.1	18.9	53.5	8.25
Total	66		16.2	91.2	214	33 litres

Table 7 Test on fresh concrete

S.no	Mix	Slump	Compaction factor	Workability
1	Nominal mix	63	0.90	Medium
2	Mix 1	60	0.89	Medium
3	Mix 2	61	0.91	Medium
4	Mix 3	55	0.86	Medium

workability of concrete found on both slump and compaction factor tests is medium as mentioned in Table 7.

4 Results and Discussion

Specimens of cube, cylinder and prism were cast to find the feasible use of tannery waste in concrete for fine aggregate. Basic test for the strength of concrete was done and the test results were discussed further [21, 23].

4.1 Compressive Strength Test

Concrete is applied in structural elements to resist compressive stress and compressive strength is one of the notable properties in concrete. To find the capability of concrete to counterattack crushing force, a compression strength test was carried out for casted cube specimens. The test specimen cube of size 150 mm × 150 mm × 150 mm is cast at curing 7th, 14th, 28th day. CS of cast concrete gets increasing in all percentages compared to IS456:2000 as mentioned in Fig. 2. But on comparing with nominal mix concrete the test values vary with varying percentage and varying curing period.

Fig. 2 Compressive strength for different proportions

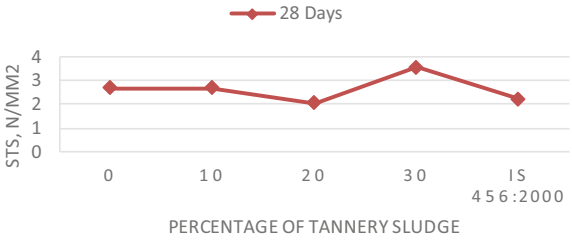

Fig. 3 Split tensile strength for different proportions

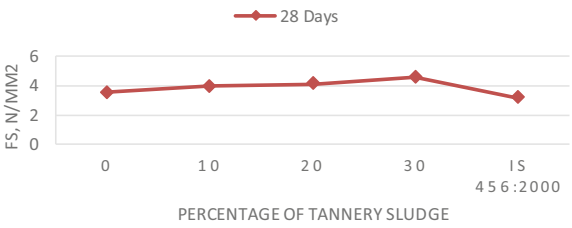

Fig. 4 Flexural strength for different proportions

4.2 Split Tensile Strength Test

The split tensile strength of concrete is the basic property of concrete to find its tensile force indirectly. The test was carried out on a specimen cylinder of 150 mmϕ and 300 mm height are cast at curing on the 28th day. STS of concrete gets increased in all percentages when compared to IS456: 2000 guidelines as mentioned in Fig. 3. On comparing with nominal mix concrete, the test values vary with varying percentage.

4.3 Flexural Strength Test

The flexural strength of concrete was tested to find the capability of concrete to counterattack the breaking force. The test was carried out on specimen prism of size 100 mm $\times$ 100 mm $\times$ 500 mm are cast at curing 28 days. Flexural strength test by three-point loading method is adopted. Flexural strength of concrete gets increased in all percentages on comparing to IS 456:2000 and also increase in the addition of waste is mentioned in Fig. 4.

4.4 Durability of Concrete Test

The durability of concrete is about the lifetime of concrete to withstand different circumstances. Tests such as water absorption, alkali attack and acid attack were carried out and the test results procured are mentioned in Table 8.

Table 8 Durability of concrete test

S.no	Mix	Water absorption (%)	Alkali attack (%)	Acid attack (%)
1	Nominal Mix	1.32	2.62	4.78
2	Mix 1	1.58	2.60	4.64
3	Mix 2	1.63	2.54	4.06
4	Mix 3	1.92	2.52	3.88

5 Conclusion

Experimental investigations were done to determine the effect and characteristics of concrete with the replacement of FA by tannery waste. Conclusions derived from the test results are as follows:

1. CS of concrete at 10% replacement increases and gives better results than nominal concrete at 7th, 14th and 28th day after curing.
2. STS of concrete decreases at 20% and increases at 10% and 30% of replacement on comparing to nominal concrete at 28th day after curing.
3. FS of concrete constantly gets increased on every percentage of replacement of sludge in concrete.
4. Durability of concrete is acceptable on all percentages of tannery waste replacement.

On comparing the above results, an optimum percentage of 10% replacement of sludge for M20 concrete is recommended. This study was made with the conventional M20 grade concrete replacement itself, and in the future it can be extended for a higher grade of concrete and can be recommend to remove heavy metals from sludge before replacement.

References

1. Geethakarthi A, Nivedha T, Preethi S, Priyanka S, Sneha M, Yuvaraja G (2017) Environmentally sound disposal of tannery sludge. Int J Civ Eng Technol 8(9):371–375
2. Hasnat A, Rahman I, Pasha M (2013) Assessment of environmental impact for tannery industries in Bangladesh. Int J Environ Sci Dev 4(2):217–220
3. Wahid Murad ABM, Mia A. Md, Rahman MA (2018) Studies on the waste management system of a tannery: an overview. Int J Sci Eng Technol Res 7(4):253–267
4. Vamshi P, Dharmapuri AK, Pajuri S, Deepthi KM, Sudarsan JS (2020) Utilization of foundry slag as a partial replacement for fine aggregate to attain sustainability in construction. vol 7, no 15, 1219–1223
5. Hassan S (2014) Effect of using tannery sludge in concrete, pp 1–89
6. Sathish Kumar and Vijayaravind (2015) Utilization of tannery shredded waste as fine aggregate in concrete. Int J Eng Res 4(04):484–486
7. Muniraj K, Asha B, Raja Ramachandran P (2019) Application of fine aggregate by replacement of tannery dry sludge in concrete. Int J Appl Environ Sci 9:2805–2815

8. Raj M, Vasudevan N (2016) Reuse of textile and tannery sludge in concrete fine aggregates. Int J Sci Res Dev 4(07):217–220
9. TamilThendral TBV, Sachin Anand K, Shandra Banu K (2018) Experimental investigation on tannery waste with partial replacement of coarse aggregate in concrete. Int Res J Eng Technol 5(9):7039–7041
10. IS 4031- Part V (1988) Methods of physical tests for hydraulic cement. Part V- determination of initial and final setting times. Bur Indian Stand. New Delhi, p. Reaffirmed in 2005
11. IS 4031- Part IV (1988) Methods of physical tests for hydraulic cement. Part IV- Determination of consistency of standard cement paste. Bur Indian Stand. New Delhi, p. Reaffirmed in 2005
12. IS 4031- Part I, "Method of physical tests for hydraulic cement: Determination of fineness by dry sieving," *Bur. Indian Stand. New Delhi*, p. Reaffirmed in 2005, 1996.
13. IS 2720-Part III (1980) Determination of specific gravity. J AOAC Int. https://doi.org/10.1093/jaoac/20.3.535
14. IS 2386- Part III (1963) Method of Test for aggregate for concrete. Part III- Specific gravity, density, voids, absorption and bulking. Bur. Indian Stand. New Delhi, p (Reaffirmed 2002)
15. P. 1 IS2386 (1963) IS : 2386 (Part I)-1963- Indian method of test for aggregate for concrete. Part I - Particle size and shape. Indian Stand. p (Reaffirmed 2002)
16. BS 812–2 (1995) BS 812–2 Method of determination of density. Br. Stand., no. March, pp 1–22
17. Haroun M, Idris A, Syed Omar SR (2007) Characterisation and composting of tannery sludge. Malaysian Soc Soil Sci Malaysian J Soil Sci 11:71–80
18. Chuan MC, Liu JC (1996) Release behavior of chromium from tannery sludge. Water Res 30(4):932–938
19. Pinto CA, Hamassaki LT, Valenzuela-Diaz FR, Dweck J, Büchler PM (2004) Tannery waste solidification and stabilization: thermal and mechanical characterization. J Therm Anal Calorim 77(3):777–787
20. Vasek V, Kolomaznik K, Janacova D, Thang PM (2005) Control system for chromium recycling technology from tannery waste. IFAC Proc Vol 16(c):139–142
21. IS 2386 -Part IV (2002) IS : 2366 (Part IV)-1963-Methods of test for aggregates for concrete, part 4 : mechanical properties. Indian Stand, pp 1–37
22. BIS:10262 (2009) Indian standard guidelines for concrete mix design proportioning," Bur. Indian Stand. New Delhi, p New Delhi, India
23. IS 456 (2000) Concrete, plain and reinforced. Bur Indian Stand. Dehli, pp 1–114

Hydraulic Engineering and Amorphous Materials

Adsorption of Cadmium Heavy Metal in Water by Using Orange Peel

B. Priyadharshini and Marykutty Abraham

1 Introduction

The polluted water from industries and water from industrial waste are released with different metals, i.e. heavy metals reaches the sustenance shackle of aquatic life [1, 2]. Industrial wastewater discharges constitute the foremost accumulation of metal pollution in water [3]. Cadmium, Zinc, Chromium, Lead, and Copper were some of the metals that are produced from the industries such as nickel batteries industry, tanneries, dyes, paint manufacturing industry and as additives of alloys, and also from municipal waste, dumping waste [3, 4]. The deadliness and healthiness risks of these pollutants were analysed, and their occurrence in consumption liquid above a convinced limit can pose dangers to the people [5, 6]. Metal removal from wastewater or contaminated groundwater was the greatest challenge to the environment. The effects of metals like cadmium and lead on human being wellness were being investigated extensively [7]. The probable indications of these include high hypertension, stress disorders, depression, augmented allergy reactions, vascular occlusion, and memory loss [8, 9].

An important parameter in heavy metal concentration is cadmium (Cd). This metal was largely used in plastic and metal industries and the wastewater from these was discharged into the environment by which the water gets contaminated [10]. Cadmium heavy metal will often be present in various concentrations in contaminated water, which may affect human health and lead to the risk of human health. This metal is considered as one of the major pollutants to be concentrated which will be deposited in the kidney, affect the lungs, and lead to lung cancer [9, 11, 12]. The allowable limit of cadmium in water is 0.05 mg/l by the WHO.

B. Priyadharshini (✉)
Department of Civil Engineering, Satyabhama Institute of Science and Technology, Chennai, India

M. Abraham
Centre for Remote Sensing, Satyabhama Institute of Science and Technology, Chennai, India

K. S. Satyanarayanan et al. (eds.), *Sustainable Construction Materials*, Lecture Notes in Civil Engineering 194, https://doi.org/10.1007/978-981-16-6403-8_35

To remove this cadmium from the aquatic environment, some of the techniques have been applied for this purpose such as coagulation, flotation, ion exchange method, membrane method, adsorption, electrochemical treatment, bioremediation, and chemical precipitation [10, 13]. These studies exposed that adsorption process would be the very active method for the removal of heavy metals [8, 12].

2 Material and Methods

2.1 Study Area

Samples were collected from different places of Chrompet industrial area randomly from open wells. So many industrial activities like leather factories, electroplating industries were present in the study area. Due to the discharge of this industrial wastewater, the water gets contaminated. Therefore, the collected samples have been analysed for the concentration of Lead and Cadmium heavy metals. From the test reports, it was analysed that the concentration of Cadmium is more when compared with Lead which is shown in (Fig. 1). Therefore, the experiment was performed to reduce the concentration of Cadmium heavy metal.

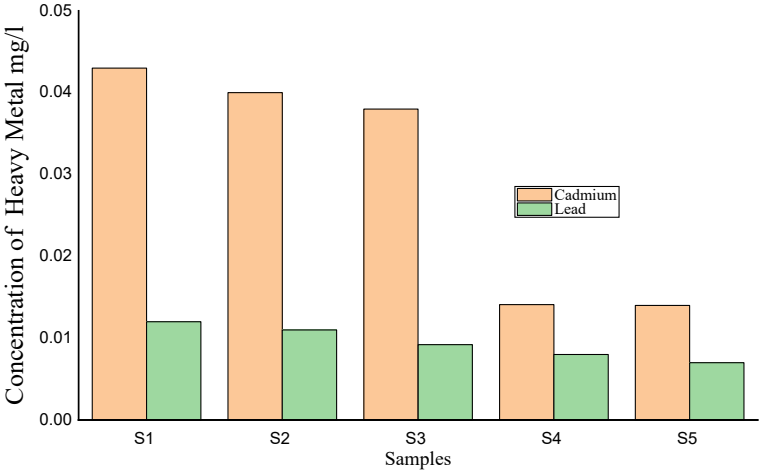

Fig. 1 Concentration of heavy metal in samples

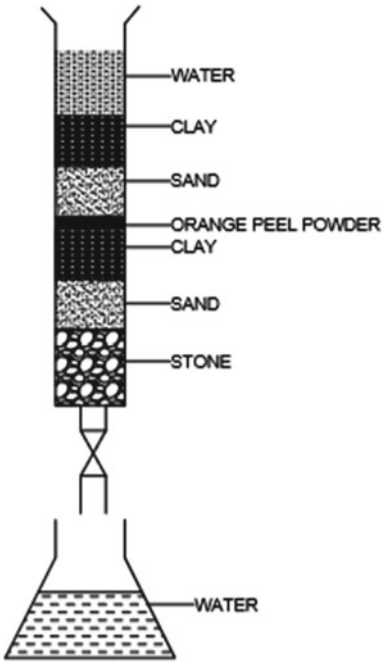

Fig. 2 Column setup

2.2 Column Setup

To analyse the performance of the peel adsorbent on metal under different states under laboratory scale and to study the cadmium adsorption by the peel, the column was packed with some adsorbents. The column setup was prepared using filter paper, pebbles or small stones, sand, clay, and orange-peel powder as adsorbents. The area of the column was 78 cm^2 and the height was 40 cm. The column setup is shown in (Fig. 2).

2.3 Preparation of Orange Peel

The orange peel was collected and initially cleaned with water and then dried out in an oven at 50 °C for a total of 3 days. After drying, the peels were crushed into powder form which passes through a 0.1 mm sieve. This powder was then synthesized by the co-precipitation technique. This was performed by utilizing manganese salts of two unique anions which are manganese (II) sulphate and manganese oxalate. The two salts of equivalent focus, i.e. 0.2 M are blended in with persistent mixing at a consistent temperature of 60 °C. The pH of the reaction medium was adjusted. The mixture was stimulated at a temperature of 80 °C for 30 min and then allowed to cool to room temperature. Then, the black precipitate was formed and it was collected by

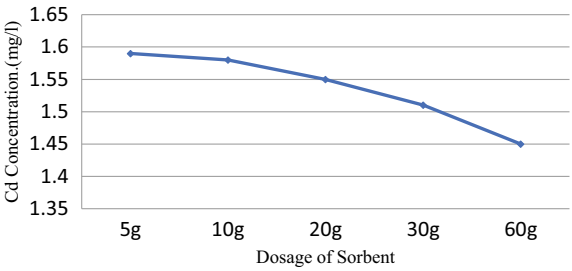

Fig. 3 Cadmium concentration for different dosages

filtering, washed, and allowed to dry out at 50 °C for 24 hours and stored for further use.

2.4 Stock Solution Preparation

A stock solution of cadmium heavy metal is prepared by adding 0.5 g of Cadmium chloride ($CaCl_2H_2O$) in 1 lit of distilled water and given for test for initial concentration. By the test analysis, the concentration of Cadmium heavy metal is 1.6 mg/l.

2.5 Experimental Investigation

The prepared stock solution is allowed to pass through the filter bed setup which was designed for the adsorption process. Columns are designed for different number of dosages 60, 30, 20, 10, and 5 g of adsorbent.

The stock solution prepared is allowed to pass through the column setup. The passed samples through various dosages were collected and analysed for the cadmium heavy metal concentration. The concentration is shown in (Fig. 3).

3 Result and Discussion

3.1 Isotherm Study

Isotherms elaborate the detailed relation of the metal ions adsorption with the solution concentration at a continuous temperature [16]. The effectiveness of the orange peel adsorbent on cadmium metal was evaluated based on the below (Eq. 1) [1, 14].

$$q = ((C_i - C_e) \times V)/M \tag{1}$$

where initial concentration is C_o(mg/l) and the final concentration is C_e (mg/l) and the capacity of the adsorption was determined using (Eq. 2).

$$R\% = \frac{C_i - C_e}{C_i} \times 100 \tag{2}$$

To evaluate the liquid phase adsorption equilibria data, there are numerous models developed and researched. In these, very commonly used isotherm models were Langmuir and Freundlich. Langmuir isotherm was founded on assuming standardized surface and energy on the adsorbent surface, while Freundlich was an empirical model applied for varied systems. Based on these, huge number of analyses had been done as the equations were modest and also fit with the derived data.

$$\text{Langmuir adsorption isotherm } \frac{C_e}{q_m} = \frac{1}{q_m K_L} + \frac{1}{q_m} C_e$$

$$\text{Freundlich isotherm equation } \log q_e = \log K_f + \frac{1}{n} \log C_e$$

where the amount of adsorption was q_e (mg/g), initial concentration is C_o(mg/l), the final concentration is C_e (mg/l), and m was mass of adsorbent (g). Where the Langmuir constant (q_m) and K_L give the capacity of adsorbent and other constant K_F called Freundlich constant and n is the dimensionless unit indicates the uniformity of the surface. The greater value of 'n' represents a different surface system [15, 16]. The numerical value of n represents the range of deviation from the standard line. The values of n and K_f were evaluated from slope and intercept of ln qe vs ln Ce plots metal adsorption the n value gives the information about the shape of the curve [17].

The derived data were fitted to the isotherm equations and the results are shown in (Figs. 4, 5, 6, 7, 8 and 9). Freundlich model isotherm fit the graph which was plotted using the isotherm equation data. From Freundlich isotherm models, the correlation coefficient factors were around 0.95–0.97, which shows that the data fit well into the model.

Gardiner (1974) followed the Freundlich isotherm on the study of metal adsorption against orange peel at the same time as, earlier Salim and Cooksey (1980) showed that the adsorption of Pb^{2+} up to 1.8 g litre fitted to Freundlich equation. Our results show

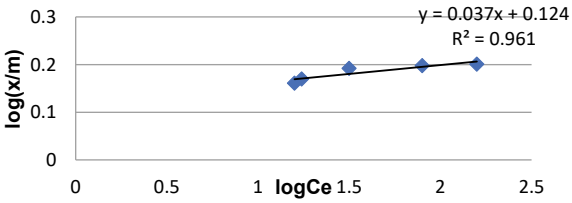

Fig. 4 Cadmium concentration for different dosages

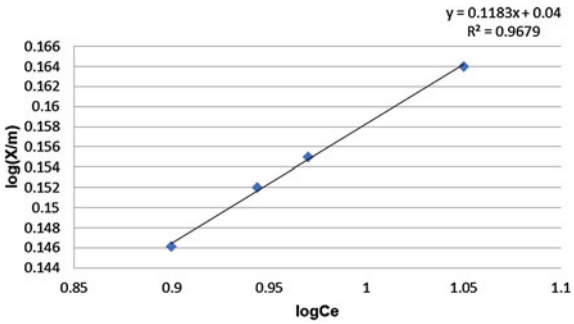

Fig. 5 Isotherm graph for 60 g dosage

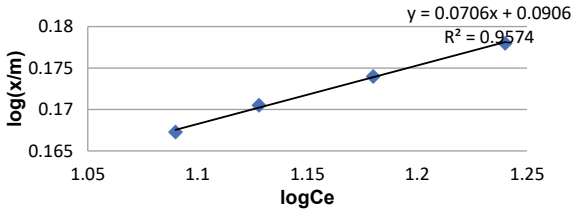

Fig. 6 Isotherm graph for 30 g dosage

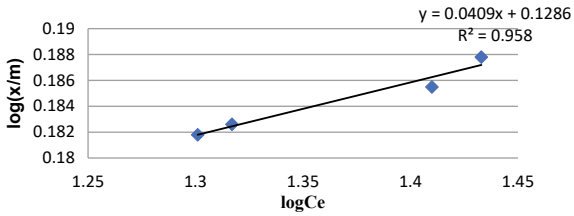

Fig. 7 Isotherm graph for 20 g dosage

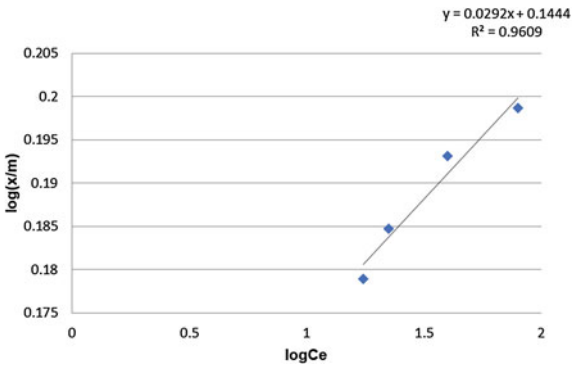

Fig. 8 Isotherm graph for 10 g dosage

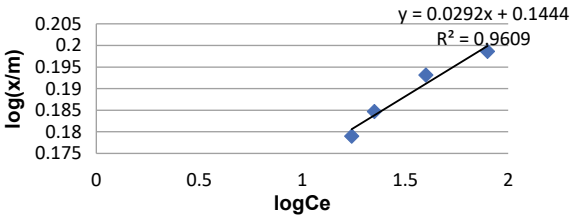

Fig. 9 Isotherm graph for 5 g dosage

that the isotherm values were from 0.95 to 0.97, which was fitted to the isotherm graph for different dosages concentration. The results of the adsorption of the heavy metal were fitted to the isotherm. The charcoal is used as a good adsorbent for removing the heavy metal pollutants in water [18]. The effect of adsorbent was studied by varying the contact time, pH, and dosage of adsorbent. The characterization of the adsorbent was done through SEM analysis [19, 20].

3.2 Scanning Electron Microscope

The SEM analysis of orange peel before and after treatment is shown in (Fig. 10). The SEM image shows that the pores of the orange adsorbent had been reduced after the treatment. (Fig. 10a and c) shows the structure of original peels before treatment has a highly porous structure. (Fig. 10b and d) shows the peels had a surface that

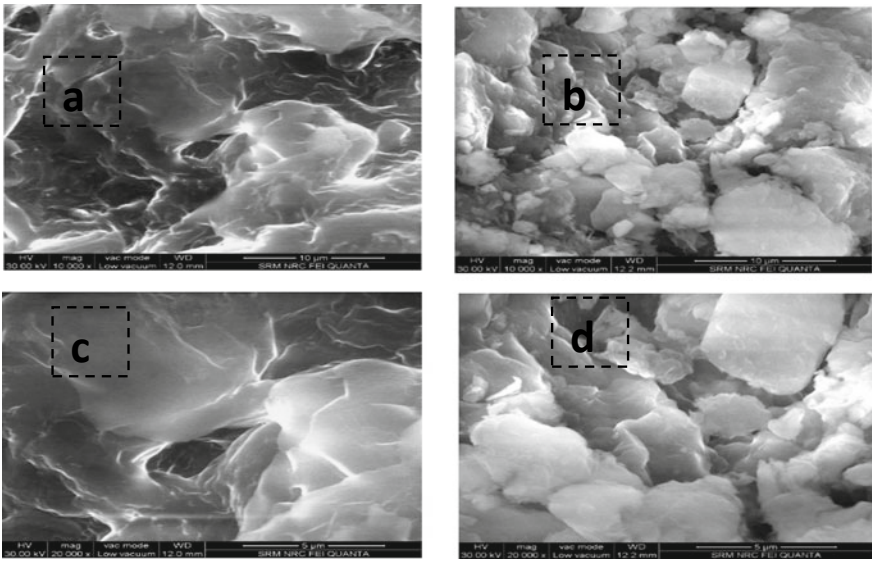

Fig. 10 SEM analysis before and after adsorption

was partially covered by heavy metals. It shows the dispersion of cadmium metal modified the peel samples and the structure was modified after adsorption [20]. However, the surface of the adsorbent was held moderately closed and tight in a joined mode consisting of a composite structure. Also, the surface has many pores and a coarsened outlying, which may have occurred by the presence of alkali ions in heavy metal during the adsorption treatment.

4 Conclusion

A natural adsorbent orange peel was prepared and explored to eliminate the toxic metal cadmium from the prepared aqueous solution using a small-scale column study. The adsorption dosage was varied and passed through the small column and fitted to an isotherm curve. The results show that the isotherm values were from 0.95 to 0.97, which was well fitted to the isotherm graph. The results revealed that the adsorption of cadmium from the aqueous solution by the low-cost adsorbent was far more efficient. This type of adsorbent can also be applied for the removal of other heavy metals.

References

1. Wang X, Cui Y, Peng Q, Fan C, Zhang Z, Xingchang (2020) Removal of Cd(II) and Cu(II) from aqueous solution by Na+-Modified Pisha Sandstone. J Chem 1:1–13
2. Visa A, Maranescu B, Lupa L, Crisan L, Borota A (2020) New efficient adsorbent materials for the removal of Cd(II) from aqueous solutions. Nanomaterials 10, 899
3. Laxen DPH∗ (1984) Adsorption of Cd, Pb and Cu during the precipitation of hydrous ferric oxide in a natural water. Chem Geol 47(3–4):321–332
4. Florence TM (1982) The speciation of trace element in water. Talanta 29:345–364
5. Kadirvelu K, Thamaraiselvi K, Namasivayam C (2001) Removal of heavy metal from industrial wastewaters by adsorption onto activated carbon prepared from an agricultural solid waste. Biores Technol 76:63–65
6. Low KS, Lee CK, Leo AC (1995) Removal of metals from electroplating wastes using banana pith. Bioresource Technol 51(2–3):227–231
7. Sajid M, Nazala MK, Ihsanullah NB, Osman AAM (2018) Removal of heavy metals and organic pollutants from water using dendritic polymers based adsorbents: a critical review. Separation Purifi Technol 191:400–423
8. Qu X, Alvarez PJ, Li Q (2013) Applications of nanotechnology in water and wastewater treatment. Water Res 47(12):3931–3946
9. Al-Khaldi FA, Abusharkh B, Khaled M, Atieh MA, Nasser MS, Laoui T, Agarwal S, Tyagi I, Gupta VK (2015) Adsorptive removal of cadmium(II)ions from liquid phase using acid modified carbon-based adsorbents. J Mol Liq 204:255–263
10. Li Q, Wu S, Liu G, Liao X, Deng X, Sun D, Hu Y, Huang Y (2004) Simultaneous biosorption of cadmium(II) and lead(II) ions by pretreated biomass of Phanerochaete chrysosporium. Sep Purif Technol 34:135–142
11. Ragan HA (1983) The bioavailability of iron, lead, and cadmium via gastrointestinal adsorption: a review. Sci Total Environ 28:317

12. Jusoha A, Shiungb LS, Alia N, Noorc MJMM (2007) A simulation study of the removal efficiency of granular activated carbon on cadmium and lead. Desalination , vol 206, pp 9–16
13. Rodriguez-Narvaez OM, Peralta-Hernandez JM, Goonetilleke A, Bandala ER (2017) Treatment technologies for emerging contaminants in water: a review, vol 323, pp 361–380
14. Shah LA, Khan M, Javed R, Sayed M, Khan MS, Khan A, Ullah M (2018) Superabsorbent polymer hydrogels with good thermal and mechanical properties for removal of selected heavy metal ions. J Cleaner Prod 201:78–87
15. Huang Z, Wu Q, Liu S, Liu T, Zhang B (2013) A novel biodegradable β-cyclodextrin-based hydrogel for the removal of heavy metal ions. Carbohydr Polym 97:496–501
16. Liu P, Jiang L, Zhu L, Wang A (2014) Novel approach for attapulgite/poly (acrylic acid) (ATP/PAA) nanocomposite microgels as selective adsorbent for Pb (II) ion. React Funct Polymer 74:72–80
17. Priyadharshini B, Abraham M, Parvathy (2020) Treatment of contaminated water using eco friendly material IOP Conference Series: materials science and engineering, 993(1), 012168
18. Priyadharshini B, Abraham M, Varshaa Laxmi P, Kavisri M (2020) Experimental investigation on removal of chromium metal using coconut shell. Int J Adv Sci Technol 29(6):103–109
19. Eshanthini P, Mary C, Kalaivani P (2017) Assessment of groundwater quality and mapping using GIS- A Case study. Pollution Res 36(2):253–259
20. Atta AM, Al-Lohedan HA, Othman ZAL, Abdel-Khalek AA, Tawfeek AM (2015) Characterization of reactive amphiphilic montmorillonite nanogels and its application for removal of toxic cationic dye and heavy metals water pollutants. J Ind Eng Chem 31:374–384

An Experimental Study on Quarry Dust as Fine Aggregate in M50 Grade Concrete

S. Prakash Chandar and S. Loganathan

1 Introduction

Concrete is a substance made up of coarse and fine aggregates that are bound together with cement and water [1]. Concrete is efficient to cast some structural elements like beam and column in a high-rise building. So in the field of construction, there is an increasing need for concrete. The physical and chemical properties of fine aggregate affect the consistency, workability, and strength of concrete, so it's an important part of concrete [2–4]. As there is a high demand for river sand, an alternative material can be replaced without disturbing the strength of the concrete. By replacing RS with QD, the waste produced in the quarry is reduced and the consumption of river sand in the concrete is also decreased. Quarrying operations include crushing rock into different sizes; the dust produced during this process is known as quarry dust, and it is disposed of as waste [5]. Rock quarrying industries contain large amounts of quarry dust, which is harmful to the atmosphere. Adding GGBS and micro silica will increase the performance as well as durability of concrete. This paper explains about the replacement of natural river sand by quarry dust in M50 grade mix concrete. In this paper, the M50 grade mix concrete made with quarry dust is used to partially replace sand in concrete in various percentages (25, 50, 75, and 100%), as well as superplasticizer is also used. The expanding substance of superplasticizer extends the workability [6, 7].

S. P. Chandar (✉) · S. Loganathan
Department of Civil Engineering, SRM Institute of Science and Technology, Kattankulathur, Tamil Nadu 603203, India
e-mail: prakashs2@srmist.edu.in

S. Loganathan
e-mail: ls9208@srmist.edu.in

K. S. Satyanarayanan et al. (eds.), *Sustainable Construction Materials*, Lecture Notes in Civil Engineering 194, https://doi.org/10.1007/978-981-16-6403-8_36

2 Materials

The essential components in concrete used for this research work are cement, coarse aggregate, fine aggregate, water, micro silica, GGBS, and chemical admixture.

2.1 Cement

Cement is a crucial substance which helps to bind coarse and fine aggregates in the production of concrete. According to OPC 53 grade as per IS 12269:2013 all concrete specimens were cast. On the construction field the most used cement is OPC.

2.2 Fine Aggregate

The fine aggregate fills the space between the coarse aggregate and river sand which passes through a 4.75 mm sieve taken. The code used for natural river sand to cast concrete specimens was IS 383:2016 [8].

2.3 Quarry Dust

The quarry dust is a waste product formed after crushing the granite stones. It has been proposed as an alternative material for the natural river sand. The code used for quarry dust to cast the concrete specimens was IS 383:2016 [9].

2.4 Coarse Aggregate

The maximum quantity of concrete is occupied by coarse aggregate which provides additional solidity to the concrete and 20 mm size of coarse aggregate is used as per IS 383:2016 [10].

2.5 Micro Silica

Micro silica, is one kind of fly ash that is collected from the ferrosilicon plant dust. It is also known as silica fume, is an extremely-fine chemical dust collected as an outgrowth of the ferrosilicon and silicon alloy making; its average particle diameter

is around 150 mm. By adding active micro silica in concrete will improve concrete performance and improve the concrete quality. To improve concrete performance, micro silica is used as per IS 15388:2003 [11].

2.6 GGBS

GGBS is a chemical component used primarily in the manufacture for concrete as per IS12089:1987. It is widely used in the manufacture of RMC (Ready Mix Concrete), and it is used to improve the concrete's durability [12].

2.7 Admixture

Aura mix 300 is the superplasticizer used to enhance the workability, reduce the initial setting time, and also the quick gain of strength.

3 Experimental Program

The properties of hardened concrete were tested and results are discussed in Table 1.

3.1 Compressive Strength Test

The most standard concrete test is the cube compression test; it should be conducted at a specific time, from the particular time of casting the concrete cubes as per IS 516:1959 [13]. The mix proportion of concrete is adopted for M50 grade concrete. The average strength of the 3rd day, 7th day, and 28th day of concrete replaced quarry dust in a range of 0–100% shown in Table 2. Collection of materials, casting

Table 1 Mix ratio

Replacement in %	Mix ratio by weight cement: GGBS: MS: RS: QD: CA: Water
100% River Sand	1: 0.2: 0.12: 1.25: 0.00: 1.83: 0.37
25% Quarry dust and 75% River Sand	1: 0.2: 0.12: 0.93: 0.32: 1.83: 0.37
50% Quarry dust and 50% River Sand	1: 0.2: 0.12: 0.62: 0.65: 1.83: 0.37
75% Quarry dust and 25% River Sand	1: 0.2: 0.12: 0.31: 0.97: 1.83: 0.37
100% Quarry dust	1: 0.2: 0.12: 0.00: 1.30: 1.83: 0.37

Table 2 Compression strength test

Replacement in %	Density (kg/m^3)	Compressive strength (N/mm^2)		
	28th day	3rd day	7th day	28th day
100% River Sand	2420	19.77	31.91	53.2
25% Quarry dust and 75% River Sand	2424	19.95	31.37	53.9
50% Quarry dust and 50% River Sand	2430	20.31	32.08	54.64
75% Quarry dust and 25% River Sand	2430	19.42	30.53	55.31
100% Quarry dust	2432	19.02	31.6	57.2

of specimen, and demolded specimens are shown in Figs. 1, 2, and 3. The specimen is placed for testing as shown in Fig. 4. The graphical view of compressive strength on cube specimens is shown in Fig. 5.

Fig. 1 Material collection

Fig. 2 Cube casting

Fig. 3 Demolded specimen

Fig. 4 Compressive strength test

3.2 Split Tensile Strength Test

The splitting characteristics of cylinders are calculated by performing a tensile strength test as per ASTM C496/C496M [14]. The average strength of the 3rd day, 7th day, and 28th day concrete replaced quarry dust in a range of 0–100% shown in Table 3. The specimen is placed for testing as shown in Fig. 6. The graphical view of split tensile strength on concrete specimens is shown in Fig. 7.

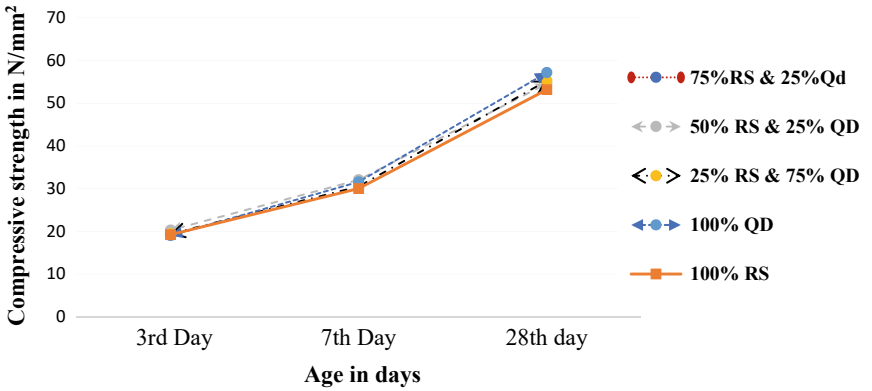

Fig. 5 Compressive strength is represented graphically

Table 3 Split tensile test on cylinder specimens

Replacement in %	Split tensile strength (N/mm^2)		
	3rd day	7th day	28th day
100% River Sand	2.84	3.93	6.086
25% Quarry dust and 75% River Sand	3.029	3.72	5.93
50% Quarry dust and 50% River Sand	3.007	4.03	6.12
75% Quarry dust and 25% River Sand	2.74	3.73	5.95
100% Quarry dust	2.84	3.765	5.916

Fig. 6 Split tensile strength test on cylinder

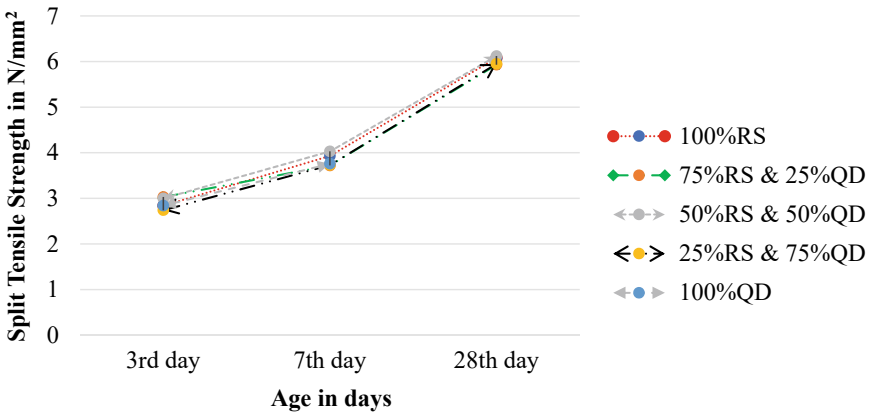

Fig. 7 Split tensile strength is represented graphically

3.3 Flexural Strength Test

The bending characteristics of the beam are calculated by performing a flexural strength test as per ASTM C78-84 [15]. Maximum amount of strain and stress are calculated on the additional load applied. The average strength of the 3rd day, 7th day, and 28th day of concrete replaced quarry dust in a range of 0–100% is shown in Table 4. The specimen is placed for testing as shown in Fig. 8. The graphical view of flexural strength on concrete specimens is shown in Fig. 9.

4 Micro Structural Analysis

Microstructural research may be used to analyze and improve materials in a variety of fields, including failure mechanisms. In production, microstructural analysis is generally used to examine materials.

Table 4 Flexural strength of beam

Replacement in %	Flexural strength (N/mm^2)		
	3rd day	7th day	28th day
100% RS	3.2	4.0	5.6
25% Quarry dust and 75% River Sand	2.4	4.0	5.2
50% Quarry dust and 50% River Sand	3.2	4.4	6.0
75% Quarry dust and 25% River Sand	2.8	3.6	5.2
100% Quarry dust	2.8	3.6	5.6

Fig. 8 Flexural strength test on beam

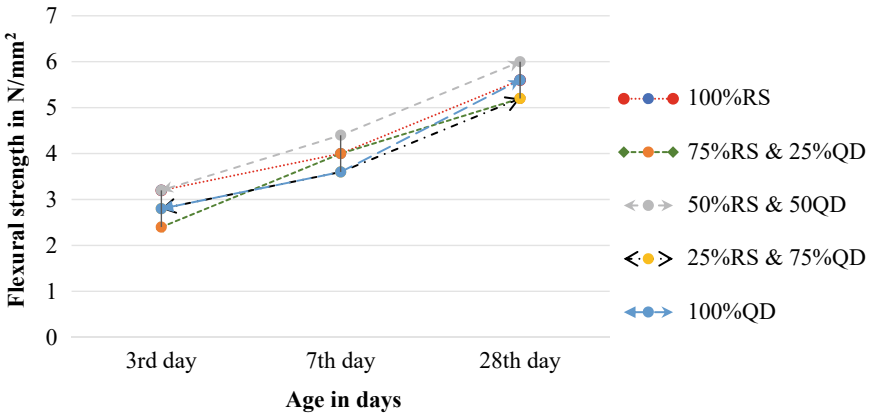

Fig. 9 Flexural strength is represented graphically

4.1 SEM Analysis

Electron Microscopy (SEM) is a test methodology that examines an example to make an amplified picture for examination utilizing an electron bar. The strategy is otherwise called SEM investigation and SEM microscopy and it is utilized productively in strong inorganic materials microanalysis and disappointment examination. The SEM analysis graphs represent the different replacement of concretes, 100% river sand is shown in Fig. 10, 25% quarry dust and 75% river sand shown in Fig. 11, 50% quarry dust and 50% river sand is shown in Fig. 12, 75% quarry dust and 25% river sand is shown in Fig. 13, and 100% quarry dust is shown in Fig. 14.

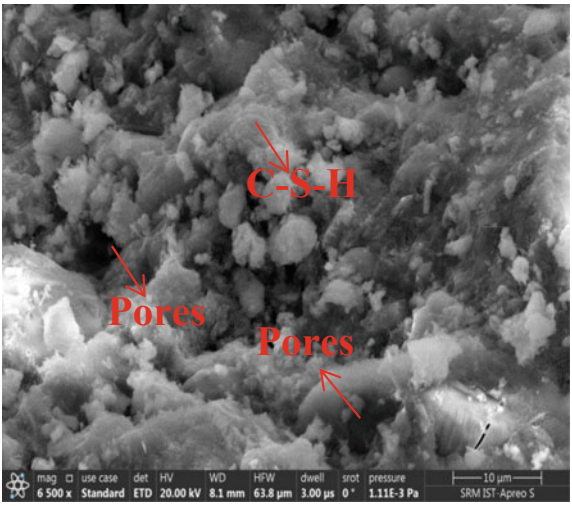

Fig. 10 100% RS

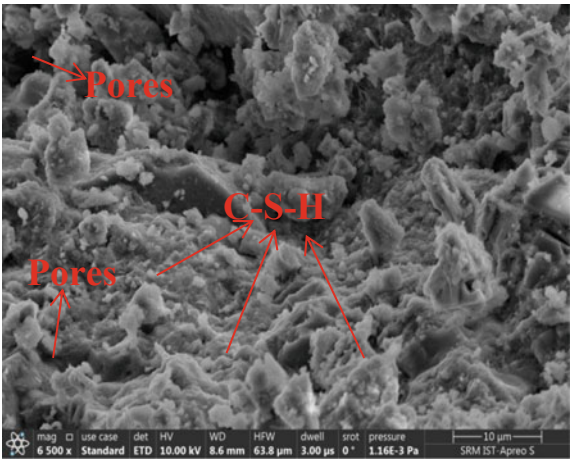

Fig. 11 75% RS and 25% QD

4.2 XRD (X-ray Diffraction)

Decide the direction of a solitary precious stone or grain. Discover the gem design of an unknown substance. Measure the size, structure, and interior strain of little translucent districts. Measure the normal dividing of layers or columns of particles.

The electrons pummel into a metal level headed, X-radiations are mold. A hot W fiber supply of electrons, a high, quickening voltage between the cathode (W) and anode Copper, Aluminum, Molybdenum, Magnesium. The anode is a Copper block that is water-cooled and incorporates the ideal objective metal. The XRD analysis graphs representing the different chemical components present in the replacement of QD are shown in Figs. 15, 16, 17, 18, and 19.

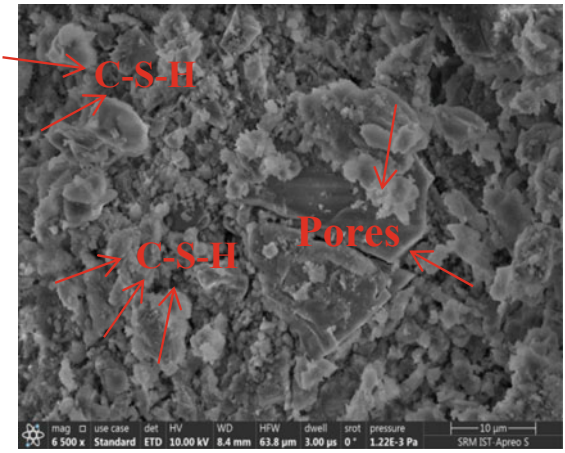

Fig. 12 50% RS and 50% QD

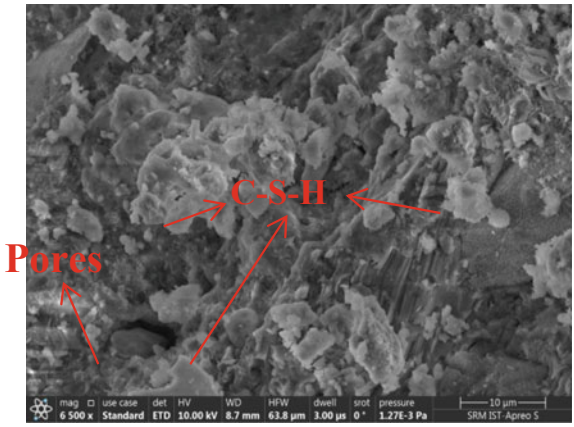

Fig. 13 25% RS and 75% QD

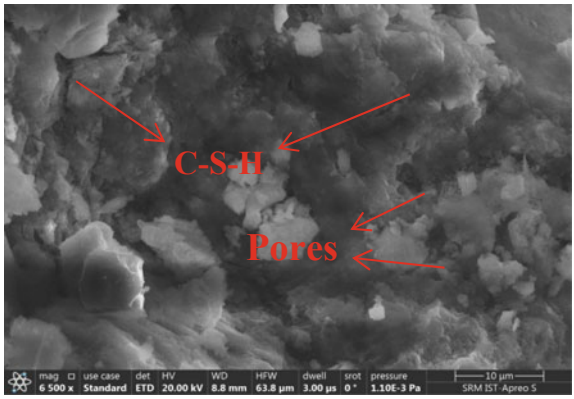

Fig. 14 100% QD

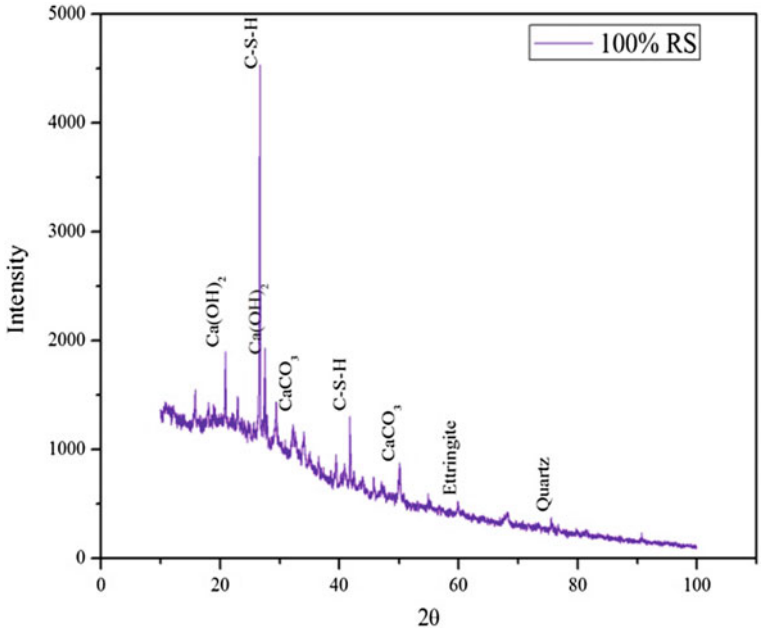

Fig. 15 100% RS

Fig. 16 25% RS and 75% QD

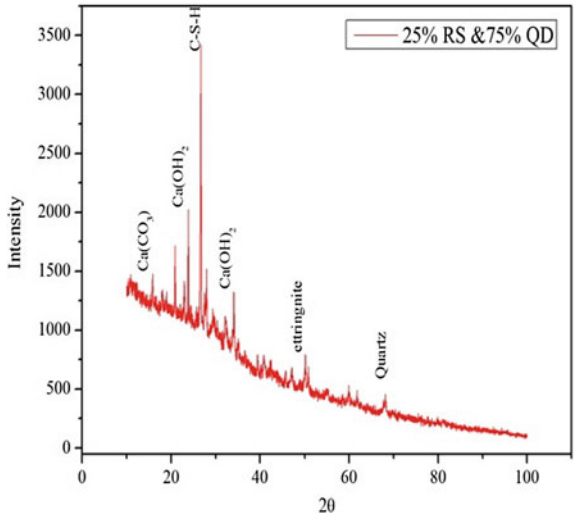

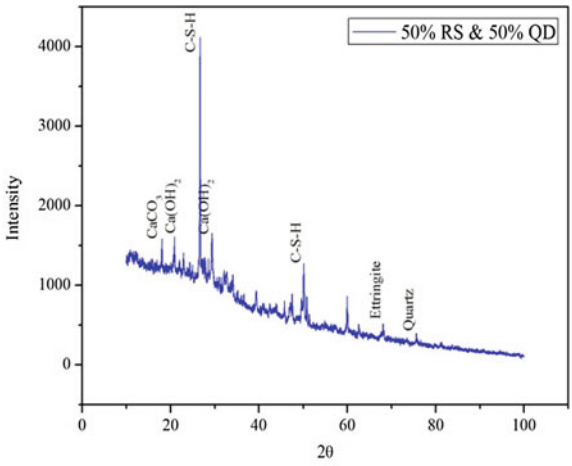

Fig. 17 50% RS and 50% QD

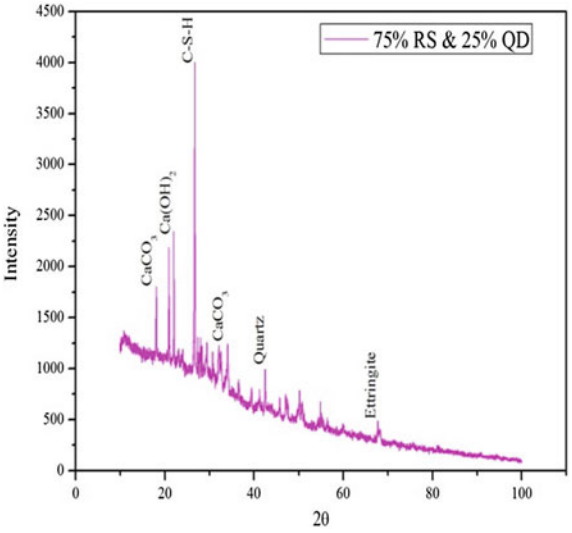

Fig. 18 75% RS and 25% QD

5 Conclusion

- The compressive strength of 100% replaced quarry dust concrete has greater compressive strength than the normal concrete.
- It can be finalized from the test results that utilizing quarry dust as fine aggregate with the addition of GGBS and Micro silica gives a greater performance compared to normal concrete.

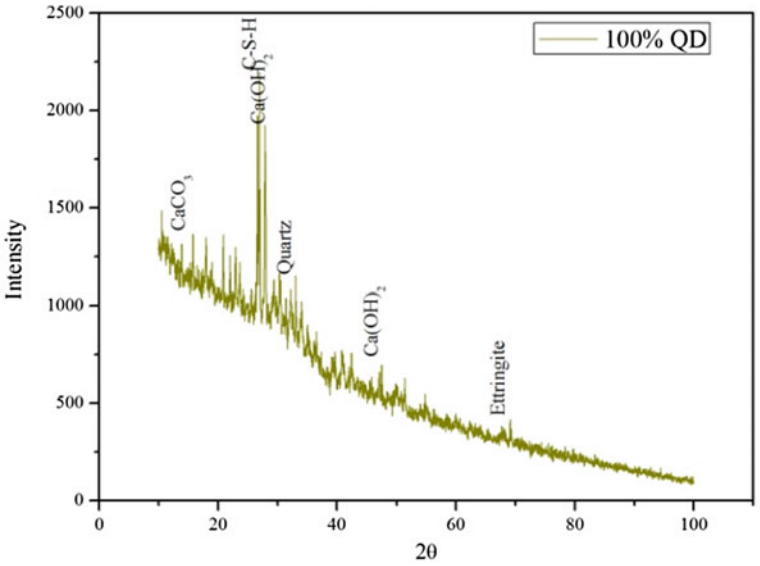

Fig. 19 100% QD

- The splitting strength results gives the greater tensile characteristics in the replacement of river sand by quarry dust with the addition of GGBS and micro silica.
- Flexural strength test results of beams built with quarry dust as a fine aggregate shows that they have greater flexural strength than ordinary concrete.
- Quarry dust replacement helps to reduce the utilization of river sand in the production of concrete.
- The microstructure analysis on M50 grade quarry dust concrete has greater compressive strength and shows the maximum silicon dioxide presence when compared to other samples. Calcium aluminum silicate hydrate maximizes the binding process and forms a compact matrix which will be increasing the concrete strength.
- According to SEM analysis, the rise in compressive strength of concrete is caused by the density of the microstructure.

References

1. Prakash CS, Gunasekaran K et al (2018) Study on some durability properties of coconut shell concrete with quarry dust. Eur J Environ Civ Eng 24(6):709–723
2. Panchal S, Mathew M (2015) Quarry dust as partial replacement material for sand in concrete. Int J Sci Eng Res 6(12):164–168

3. Kanan CK, Meisuh BK (2017) Stress strain characteristics of concrete containing quarry rock dust as partial replacement of sand. Case Studies Constr Mater 7:67–72
4. Srivastava M, Srivastava H et al (2017) Behaviour of concrete on the use of quarry dust and superplasticizer to replace sand. IOSR J Mech Civil Eng 14:06–11
5. Prakash KS, Hanumantha Rao C (2016) Study on Compressive strength of quarry dust as fine aggregate in concrete, ID 1742769. Hindawi Publishing Corporation Advances in Civil Engineering
6. Divya bhavana T (2015) Strength and workability properties of concrete replaced by quarry dust and GGBS. Int J Eng Res Technol 5(3):23–27
7. Venkata KB, Sudha Mani J (2017) Behavior of concrete on replacement of sand with quarry stone dust as fine aggregate. Int J Technol Res Eng 5(4):3036–3043
8. Jagadeesh P, Sundara KP et al (2017) Influence of quarry dust on compressive strength of concrete. Indian J Sci Technol 9(22):1–6
9. Prakash KS, Hanumantha Rao C (2017) Strength characteristics of quarry dust in replacement of sand. IOP Conf Ser Mater Sci Eng 225:012074
10. Nayana AM, Rakesh P (2018) Strength and durability study on cement mortar with ceramic waste and micro-silica. Mater Today Proc 5:24780–24791
11. Sivakumar A, Prakash M (2011) Characteristic studies on the mechanical properties of quarry dust addition in conventional concrete. J Civil Eng Construct Technol 2(10):218–235
12. Hmaid Mir A (2015) Improved concrete properties using quarry dust as replacement for natural sand. Int J Eng Res Dev 11(3):46–52
13. Ukpata JO, Ephraim ME (2012) Flexural and tensile strength properties of concrete using lateristic sand and quarry dust. ARPN J Eng Appl Sci 7:324–331
14. Ilangovana R, Mahendrana N, Nagamanib K (2008) Strength and durability properties of concrete containing quarry rock dust as fine aggregate. ARPN J Eng Appl Sci 3(5):20–26
15. Sakthivel PB, Ramya C, Raja M (2013) An innovative method of replacing river sand by quarry dust waste in concrete for sustainability. Int J Sci Eng Res 4(5)

Effect of Curing Conditions on Properties of Slag Cement Concrete Partially Replaced with Recycled Aggregates

Sujatha Takkellapati, K. Prudvi, and Chava Srinivas

1 Introduction

Security of assets is consistently the need of society. *At* the beginning of human progress, the *assets were* utilized; however, after beginning, once again it was misused. These resulted in the shortage of assets. Later on, the assets need to be monitored. Thus, people have concluded that utilization of assets has to be done effectively and shrewdly. This marvel is examined by utilizing the rule of 3R, for example, lessen, reuse, and recycle. This study primarily focuses on these "3R." Concrete is an inevitable material utilized in all designing works in the foundation advancement at all stages. In construction sector, it has proved that its ingredients are broadly accessible in the essential world. Because of far reaching utilization and quick foundation improvement everywhere in the world, there is a lack of regular and quality aggregates. Concrete can be cast to any form and shape at the required sites very easily. So, everyday millions of cubic meters of concrete are being made and used all over the world. The making of concrete is a one-way process, i.e., once it is made it is difficult to get the previous form back. Due to this, disposal of the demolished construction waste creates several environmental problems. So, demolished construction wastes can be recycled and utilized as recycled coarse aggregates generally termed as R.C.A, which replaces the ordinary coarse aggregate. Concrete made with 100% NCA has higher density than RCA. RCA has low thermal conductivity and increases the specific heat capacity. Peng et al. [1] investigated on the mechanical behavior of recycled aggregate concrete by using heating treatment with

S. Takkellapati (✉) · C. Srinivas
Department of Civil Engineering, V R Siddhartha Engineering College, Vijayawada, India
e-mail: sujathace@vrsiddhartha.ac.in

C. Srinivas
e-mail: hodce@vrsiddhartha.ac.in

K. Prudvi
Department of Civil Engineering, Andhra Univerity, Vishakapatnam, India

K. S. Satyanarayanan et al. (eds.), *Sustainable Construction Materials*, Lecture Notes in Civil Engineering 194, https://doi.org/10.1007/978-981-16-6403-8_37

low and high water binder ratios; because of heating the mechanical properties of RAC was reduced with low W/B ratios and the properties were improved with higher W/B ratios; and also the fracture energy was reduced with low W/B ratios than higher W/B ratios. Damdelen [2] carried out research work on replacement of 30% RCA with NA by adding admixtures to identify thermal effect on concrete mixes. The primary point is to expand the use of RCA in inventive development for limiting the construction waste and limiting the harm of the climate. It proved that there is no substantial difference in thermal decrement factor of the concrete mixes and RCA has higher insulation effect than conventional concrete. Bhusan Mukarjee et al. [3] studied the effect of Nano-silica on properties of recycled aggregate concrete. It shows that 3% Nano-silica in RCA has the similar compressive strength to that of conventional concrete. Hydration of cement is accelerated by adding NS, the stiffness of paste is enhanced by the pozzolanic reaction. Abdel-Hay [4] studied the effect of curing on concrete under varied conditions (air, water, paint) at different ages; compressive strength of concrete was enhanced with age. In all cases at all ages, curing with paint improved material strength than air and water curing. Whereas in water curing, mechanical properties of RCA were improved. Internal curing can provide additional moisture distributed throughout the concrete volume for added efficient hydration of cement and reduced self-desiccation. Han et al. [5] claimed that traditional curing preserves water shortages on the outside of cement, whereas inner relieving makes interior water fulfil hydration requirements throughout the solid's body, and thus expected to have superior presentation Jau [6]. Mohamed [7] studied the influence of Nano materials like NS, NC together with different percentages to evaluate the flexural behavior and compressive strength of concrete. Based on findings it was concluded that 3% of Nano particles have of 25% Nano- silica and 75% Nano clay provides higher mechanical properties among other percentages [8–11].

2 Methodology of Investigation

Most research on recycled concrete was carried out using ordinary Portland cement replaced with various mineral admixtures including Nano-silica but have not studied the usage of slag cement. Slag-based cements are eco-friendly since they reduce the effect of CO_2 on the environment [12–14]. This paper presents the impact on properties of RAC with OPC and PSC. In the first phase of the study, the effect of RCA on RAC using OPC and PSC was studied. In the second phase, the effect of Nano-silica (1.5% weight of cement) on OPC and PSC was studied. Finally in the third phase, the effect of curing conditions on RAC using OPC and PSC, with and without Nano-silica was studied. The samples experienced two types of curing conditions: water curing (WC); and curing compound introduced at 1% by weight of cement (CC). In order to find out the effect of different curing conditions on the mechanical performance of RAC, four grades of concrete made with a replacement ratio of NCA by 30% RCA were subjected to different curing conditions, ranging from water curing to curing compound. Comparisons between the performance variations

measured within each grade were made, as well as the analysis of the effect of curing conditions was performed [15–17].

3 Experiment Program

Four grades of concrete were selected to study the effect of RCA on RAC with OPC and PSC with and without Nano-silica. Cubes of dimensions 150 × 150 x 150 mm, Cylinders of dimensions 150 × 300 mm, and prisms 100 × 100x500mm of concrete M20, M25, M30, M35 grades were casted to test compressive, tensile, and flexural strength correspondingly. The casted specimens were water cured and curing compound cured tested after 7 and 28 days (ref Table 1).

3.1 Materials and Mix Design

Ordinary Portland cement: Compressive strength of cement at 28 days is 45.5 MPa. (Grade of cement is 43) Portland slag cement: Compressive strength of slag cement at 28 days is 47.5 MPa (ref Table 2).

Fine aggregate: FA was collected locally, conforming to Zone II as per IS383; Specific gravity of 2.95; Recycled aggregate concrete: The crushed waste concrete was collected from 15-year-old building. The recycled concrete aggregate was obtained by crushing in laboratory with a jaw crusher. Gradation was done as per IS383. Nominal maximum size of 20 mm aggregates was taken. Specific gravity of RCA: 2.65; water absorption: 1.75%; Crushed aggregate: Nominal maximum size of

Table 1 Casting program

Type of specimens	Water curing (WC)	Curing compound (CC)
Cubes	48	48
Cylinders	48	48
Prisms	48	48

Table 2 Properties of cement

Parameter		OPC	PSC
Specific gravity		2.90	3.10
Initial setting time		58 min	55 min
Consistency		29%	31%
Compressive strength	7 days	34 N/mm^2	33 N/mm^2
	28 days	45.5 N/mm^2	45.5 N/mm^2

Table 3 Mix proportion of natural coarse aggregate concrete (NCA)

Grade	OPC (kg/m^3)	Slag Cement (kg/m^3)	Fine aggregate (kg/m^3)	Natural Coarse aggregate (NCA) (kg/m^3)	Water (lt)	Nano silica (ml)
M20	320	320	692	1240	179	4.8
M25	330	330	689	1235	179	4.95
M30	382	382	650	1225	178	5.73
M35	412	412	625	1215	178	6.18

Table 4 Mix proportion of recycled aggregate concrete (RAC)

Grade	OPC (kg/m^3)	Slag Cement (kg/m^3)	Fine aggregate (kg/m^3)	Natural Coarse aggregate(NCA) (kg/m^3)	Recycled aggregate(RAC) (kg/m^3)	Water (lt)	Nano Silica (NS) (ml)
M20	300	300	726	782	500	183	4.5
M25	326	326	710	778	489	182	4.89
M30	365	365	695	752	480	181	5.47
M35	400	400	688	734	475	181	6.0

20 mm and minimum size of 10 mm; Specific gravity of NCA: 2.75; water absorption: 0.5%; Nano-silica: Nano-SiO2 is a white fleecy powder made out of high virtue shapeless silica powder. As a result of its little molecule size, nano-SiO2 had the upsides of enormous explicit surface region, solid surface adsorption, huge surface energy, high compound virtue, and great scattering. Specific gravity:1.-1.1 and PH of Nano-silica range from 9.3–9.6. The improvement of compressive and tensile and flexural strength of concrete was improved by addition of Nano-silica as nano particles of silica fill the void in recycled aggregate and make concrete stronger and denser (ref. Tables 3 and 4).

3.2 Workability

It has been discovered that functionality of cement with regular and recycled coarse aggregate is nearly the equal if saturated surface dry recycled coarse aggregate is used. Likewise, whenever dried up recycled coarse aggregate is utilized, it requires extra water during blending, a similar functionality can be accomplished after a recommended time. Addition of NS at a 1.5%, the workability of concrete was reduced (Figs. 1 and 2) due to entrapped air entering into concrete while manufacturing of concrete [18].

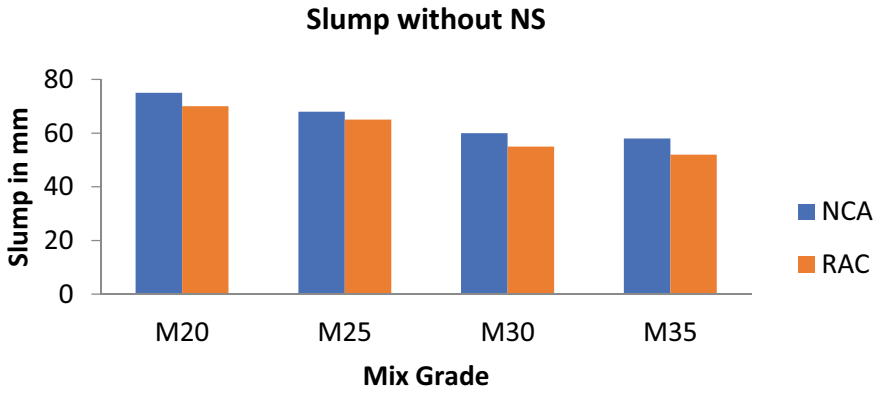

Fig. 1 Slump without NS

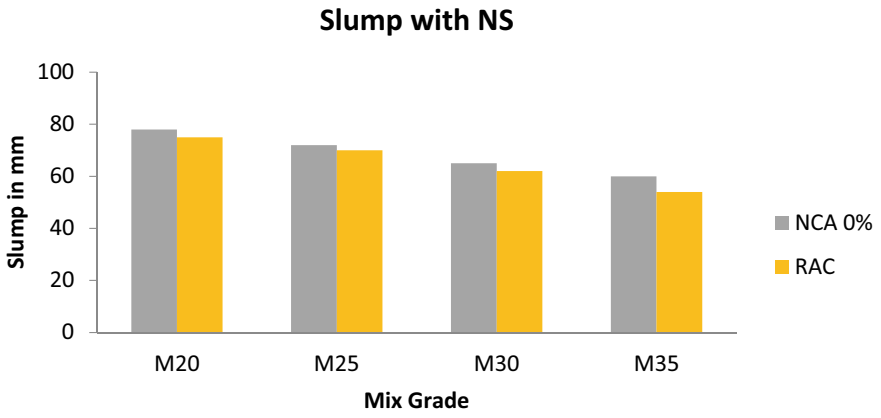

Fig. 2 Slump with NS

Higher grades were acquiring lower slump in both conditions and similar trend was followed with Nano-silica.

3.3 Curing Conditions

The specimens were immersed in water for 7 and 28 days strengths. Similarly, specimens were casted by incorporating of curing compound ***(PEG 400)***. Then, the results were compared. ***Polyethylene Glycol (PEG 400)***: It has low-atomic weight evaluation of polyethylene glycol. PEG 400 is dissolvable in water, alcohols, benzene, glycerin, glycols, and fragrant hydrocarbons, and is somewhat solvent in aliphatic hydrocarbons (ref Table 5).

Table 5 Properties of PEG400 form manufacture

Properties	
MF	HO(C2H4o)/nH
Molar mass	380–420 g/mol
Density	1.126–1.128 g/cm^3
Hydroxyl number	267–295
Viscosity	85-105cS

4 Experimental Results

The Cubes (150 × 150 x 150 mm) were casted and tested under compressive testing machine with and without NS for OPC and slag cements at 7 and 28 days for both curing conditions. Likewise, cylinders and prisms were casted and tested at 7 and 28 days with and without NS for both curing conditions (ref Fig. 3).

4.1 Compressive Strength

From the table, the compressive strength of RAC Portland slag cement gained 10% more than ordinary Portland cement. Cube strength of concrete with NS has been improved 5–8% than without NS. Concrete strength was reduced about 6% due to incorporation of curing compound in concrete. Natural coarse aggregate partially replaced with 30% recycled coarse aggregate was not affected on strength parameters (ref. Tables 6 and 7).

Casting of Specimens

Testing of prisms

Fig. 3 Casting and testing of specimens

Table 6 Compressive strength of concrete at 28 days with water curing

Grade	Compressive strength N/mm^2 (7 days, 28 days) OPC without NS		Compressive strength N/mm^2 (7 days, 28 days) PSC without NS		Compressive strength N/mm^2 (7 days, 28 days) OPC with NS		Compressive strength N/mm^2 (7 days, 28 days) PSC with NS	
	7 days	28 days	7 days	28 days	7 days	28 days	7 days	28 days
M20NCA	18	29.5	15	31.5	18.50	33.5	16.5	34
M20(30%)RAC	16.5	29.0	15	30.5	17	31.0	16	32
M25NCA	20	32.0	17	34.6	22	36.0	18.5	36.5
M25(30%)RAC	18	30.20	15.8	31.9	19.5	32.5	17	33.25
M30NCA	22	36.5	18.5	38.9	24	38.5	20.5	39.5
M30(30%)RAC	21.5	35.9	18.0	36.2	23.5	36	20	36.5
M35NCA	24.6	38.9	22	39.5	26	40	24	42
M35(30%)RAC	20.9	36.20	20.5	36.4	23	38	22	39

Table 7 Compressive strength of concrete at 28 days with curing compound

Grade	Compressive strength N/mm^2 (7 and 28 days) OPC without NS		Compressive strength N/mm^2 (7 and 28 days) PSC without NS		Compressive strength N/mm^2 (7 and 28 days) OPC with NS		Compressive strength N/mm^2(7 and 28 days) PSC with NS	
	7 days	28 days	7 days	28 days	7 days	28 days	7 days	28 days
M20NCA	17	29.0	14	30	17.50	32.5	16.5	32
M20(30%)RAC	16	27.5	13.5	28.25	16.0	30.90	16	30.9
M25NCA	18	30.0	15.9	32.5	20	33.0	18.5	34.5
M25(30%)RAC	16	28.50	14.5	27.9	18	30.0	17	32
M30NCA	19	34.5	14.5	36.5	22	36.5	20.5	39.0
M30(30%)RAC	20	35.0	18.0	34.75	20.5	34.5	20	35.5
M35NCA	22.5	34.5	20	36	24	38.5	24	40
M35(30%)RAC	18.5	34	18	33.5	20	36.9	22	37.25

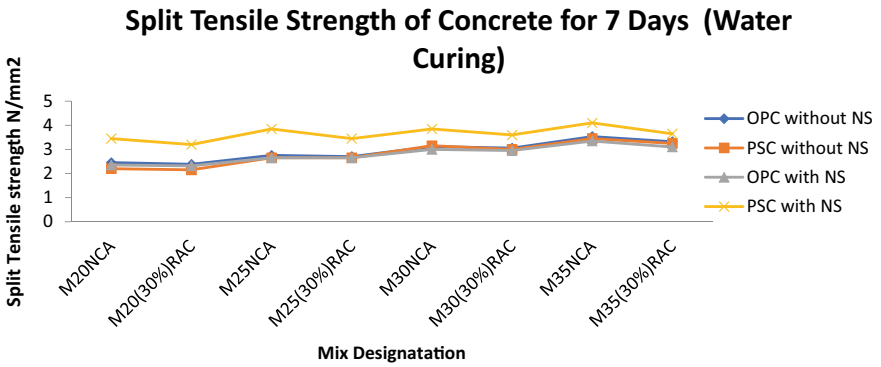

Fig. 4 Split tensile strength of concrete at 7 days with water curing

4.2 Split Tensile Strength

From the above graphs, split tensile strength of slag-based concrete with water curing gives higher strength than concrete cured with compound (Figs. 4, 5, 6, and 7).

4.3 Flexural Strength

From the above graph, flexural strength of slag-based concrete with NS has shown higher strength than concrete using OPC (ref Figs. 8 and 9).

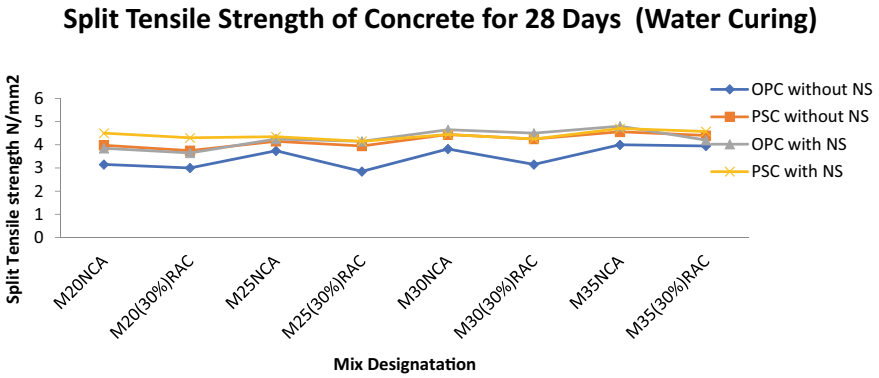

Fig. 5 Split tensile strength of concrete at 28 days with water curing

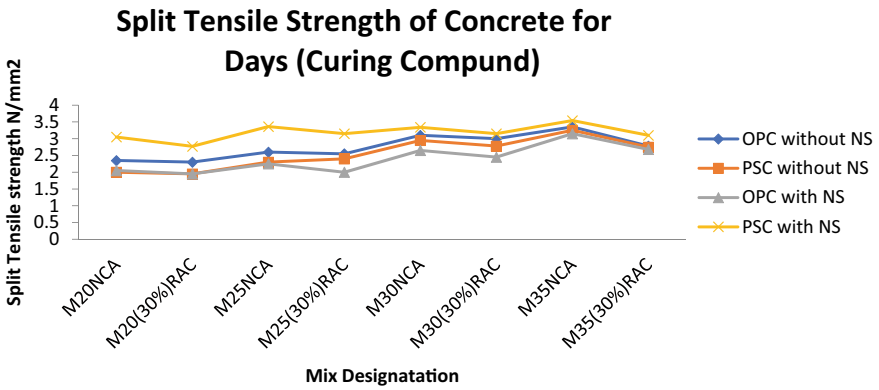

Fig. 6 Split tensile strength of concrete at 7 days with curing compound

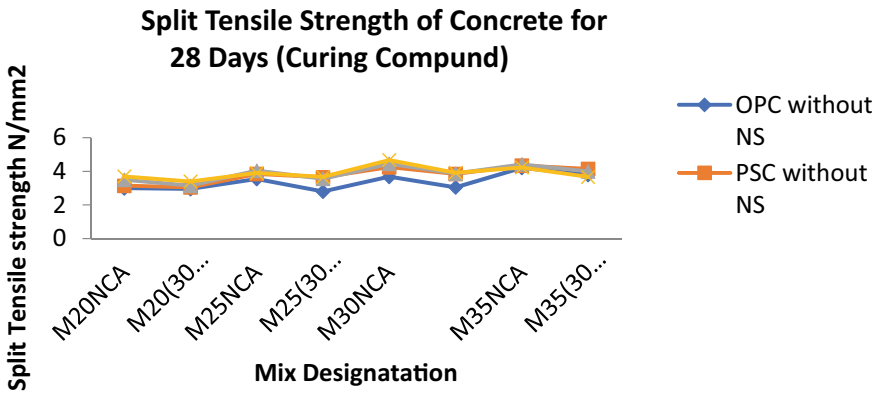

Fig. 7 Split tensile strength of concrete at 28 days with curing compound

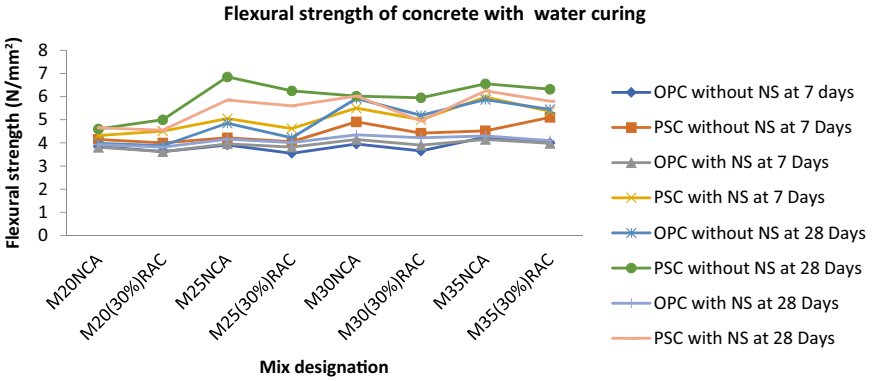

Fig. 8 Flexural strength of concrete with water curing

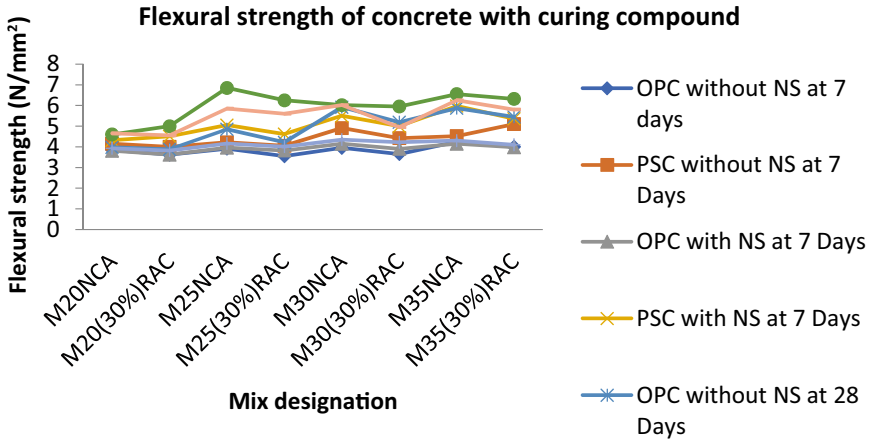

Fig. 9 Flexural strength of concrete with curing compound

5 Conclusion

- Natural resources are not infinite. A comparative analysis is made on test results of the properties of concrete with coarse aggregate replaced by 30% recycled coarse aggregate and also effects of Nano-silica on cement and curing conditions recycled aggregate concrete is studied. M20, M25, M30, and M35 mixes of recycled aggregate concrete 28 days strength was achieved. Mechanical properties of Recycled aggregate concrete were not effected with 30% replacement of RAC with natural aggregate.
- This investigation carried out on recycled aggregate concrete with slag cement in the presence of Nano-silica showed that mechanical properties of RAC were improved. The workability of concrete was reduced without Nano-silica.

- By incorporating curing compound (PEG 400), the strength of concrete was not affected in the presence of Nano-silica. Water curing is more effective than curing compound. However, the concrete cured by curing compound met the minimum required strength at 28-day curing period. This is attributed to the sufficient moisture available for good cement hydration reaction resulting in improvement of the concrete pore structure.
- It is observed that there is a decrease in water content for higher grades. The effects on concrete are trivial due to replacement of natural coarse aggregates by recycled coarse aggregates up to 30%, Portland slag cement was used which reduces the load on the environment.

References

1. Peng G-F, Huang Y-Z, Wang H-S, Zhang J-F, Liu Q-B (2013) Mechanical properties of recycled aggregate concrete at low and high water/binder ratios. Adv Mater Sci Eng 2013, ArticleID 842929, 6 pp. https://doi.org/10.1155/2013/842929
2. Damdelen O (2018) Investigation of 30% recycled coarse aggregate content in sustainable concrete mixes950–0618/Ó2018. Published by Elsevier Ltd https://doi.org/10.1016/j.conbuildmat.2018.06.149
3. Gowda R, Narendra H, Nagabushan BM, Rangappa D, Prabhakara R (2017) Investigation of nano-alumina on the effect of durability and micro-structural properties of the cement mortar. Proc Mater Today 4(11)Part 3:12191–12197, ISSN 2214–7853. https://doi.org/10.1016/j.matpr.2017.09.149
4. Abdel-Hay AS Properties of recycled concrete aggregate under different curing conditions. https://doi.org/10.1016/j.hbrcj.2015.07.001
5. Han B, Zhang L, Ou J (2017) Self-curing concrete. Smart and multifunctional concrete toward sustainable infrastructures. Springer, Singapore, pp 55–66
6. Jau W-C (2011) Self-curing concrete. U.S. Patent No. 8,016,939
7. Mohamed AM Influence of nano materials on flexural behavior and compressive strength of concrete. https://doi.org/10.1016/j.hbrcj.2014.11.006
8. Sandeep MV, Ravi Kiran K, Anukesh CH (2018) Study on effect of curing compounds on recycled aggregate concrete on strength and other properties. Ind J Sci Res 17(2):528–535. ISSN: 0976–2876 (Print) ISSN: 2250–0138(Online)
9. Fonseca N, de Brito J, Evangelista L (2011) The influence of curing conditions on the mechanical performance of concrete made with recycled concrete waste. Cement Concr Compos. https://doi.org/10.1016/j.cemconcomp.2011.04.002
10. Bitra HCR, Prasad BBVSV (2014) Dielectric of nano structured BaTi1-xSnxO3 solid solutions. Int Lett Chem Phys Astron 13(2):191–201. ISSN 2299–3843. https://www.publication/280776822_Dielectric_of_nano_structured_BaTi_1-x_Sn_x_O_3_solid_solutions [accessed Dec 31 2020].
11. Gopinadhan V, Sivabala P, Ravikumar M (2018) An experimental study on properties of m50 concrete cured using PEG 400. Int J Civil Eng Technol 9:725–732
12. Prasad D, Pandey A, Kumar B (2021) Sustainable production of recycled concrete aggregates by lime treatment and mechanical abrasion for M40 grade concrete. Constr Build Mater 268. https://doi.org/10.1016/j.conbuildmat.2020.121119

13. Siva Rama Krishna S, Sowjanya Vani V, Vali Baba SK (2018) Studies on mechanical properties of ternary blended self compacting concrete using different percentages of recycled aggregate. Int J Civil Eng Technol (Ijciet) 9(11):1672–1680. Article Id: Ijciet_09_11_163 Available online at http://www.iaeme.com/ijciet/issues.asp?ISSN Print: 0976–6308 and ISSN Online: 0976–6316
14. Bureau of Indian Standards IS 383 (1970) Methods of tests for strength of concrete
15. Bureau of Indian Standards IS 516 (1959) Methods of tests for strength of concrete
16. Bureau of Indian Standards IS 456 (2000) Code of practice for plain and reinforced concrete
17. Bureau of Indian Standards IS 10262 (2009) Recommended guidelines for concrete mix design
18. Yu R, Spiesz P, Brouwers HJH (2014) Effect of nano-silica on the hydration and microstructure development of Ultra-High-Performance Concrete (UHPC) with a low binder amount. Constr Build Mater 65:140–150

Behaviour of Double-Skin Tubular Concrete Column with Stiffened Plate

C. Pavithra, J. Revathy, P. Gajalakshmi, and V. Kamalesh

1 Introduction

A composite material is composed of at least two materials to give properties better than that of conventional concrete. The use of composite members in the construction creates a stiffer, lightweight, less expensive structure, easy to erect, and speedy construction than the traditional construction. The advantage of using composite members in the construction site is to facilitate the ease of work and the shuttering can be minimized. The main objective of the composite structure is to effectively use the properties of concrete and steel. One such construction is the concrete-filled pipe, where the concrete is poured into the steel tube. This type of construction further proposed leaving the steel tuber hollow and changing the void ratios, increasing the thickness of the steel tube, or with different shapes other than circular like square, rectangular, hexagon, etc., in order to resist the load. Due to the composite structure, it has a high strength-to-weight ratio. It was widely used in most buildings in the past. Since concrete has good compressive strength and steel has good tensile strength, the combination of these two materials will produce an efficient and lightweight design. FRP (fibre-reinforced polymer) offers a new hybrid member by combining with concrete or steel or timber. Using of FRP in the structural member gives excellent

C. Pavithra (✉) · J. Revathy · P. Gajalakshmi
School of Infrastructure, B. S. Abdur Rahman Crescent Institute of Science and Technology, Chennai,
Tamil Nadu, India

J. Revathy
e-mail: revathyj@crescent.education

P. Gajalakshmi
e-mail: gajalakshmi@crescent.education

V. Kamalesh
Department of Civil Engineering, SRM Institute of Science and Technology, Chennai, Tamil Nadu, India

K. S. Satyanarayanan et al. (eds.), *Sustainable Construction Materials*, Lecture Notes in Civil Engineering 194, https://doi.org/10.1007/978-981-16-6403-8_38

ductility, good corrosion resistance, additional load-carrying capacity to the member [1, 2]. FRP with different orientation angles has been wrapped around concrete columns to find the strength, ductility, and failure modes. When the FRP is oriented at an angle between the hoop direction and the axial direction, the strength of the column may vary. A new form of hybrid member was prepared by Teng [3], Hybrid FRP double-skin tubular concrete columns, in which, the FRP is placed at the outer side of the column and the steel is placed on the inner side and the concrete is poured in between these two tubes. Placing the strain gauge is at a certain height outside the steel pipe to evaluate the deformation value of the steel pipe. By keeping the inner steel tube hollow, the cylindrical member plays a lightening role, and because the concrete is constrained by the two tubes, local buckling in the column can be delayed or suppressed [4–6]. According to the above in the article, some local buckling deformations were found in the internal steel tubes in the upper and lower areas. Therefore, reinforcing plates were introduced to further delay the buckling process in the column. This paper, therefore, represents the comparison between the behaviour of DSTC columns with and without stiffened plates at critical points with different orientation angles and Column loading capacity with different void fractions [7].

2 Experimental Study

2.1 Specimen Details

A total of six DSTC samples were prepared and tested. All samples are cast in one batch. The total diameter of all specimens is 150 mm and the height is 300 mm. The common thickness of all FRP pipes and steel pipes is 2 mm. The strain gauge was placed vertically at the average height of each sample outside the steel pipe and FRP pipe to evaluate the strain value. Steel tubes with different void ratios have been used in the DSTC column (Fig. 1). The steel tubes of 76, 89, and 100 mm Ø have been used in the DSTC specimens. Larger void ratios lead to reduction in the amount of concrete needed for the column. The stiffened plate with a dimension of

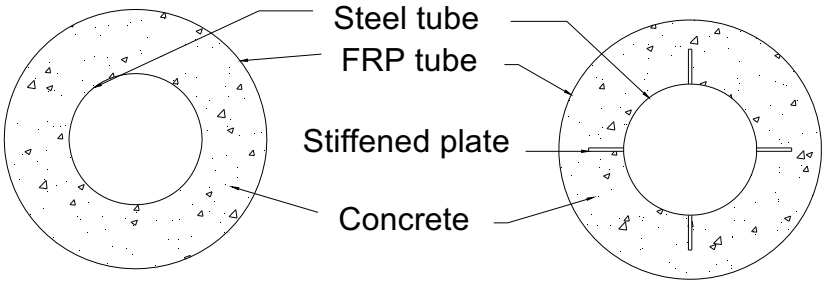

Fig. 1 Layout of columns

Table 1 Sample details

Specimen details	Sample size			Steel tube		FRP		
	D(mm)	H(mm)	φ	Type	$D_s(t_s)$ (mm)	Type	Thickness (mm)	Orientation
C30S76F0	150	300	0.5	WSF	76(2)	GFRP	2.2	0
C30S88F0	150	300	0.58	WSF	89(2)	GFRP	2.2	0
C30S100F0	150	300	0.66	WSF	100(2)	GFRP	2.2	0
C30S76F0-SP	150	300	0.5	SF	76(2)	GFRP	2.2	0
C30S88F0-SP	150	300	0.58	SF	89(2)	GFRP	2.2	0
C30S100F0-SP	150	300	0.66	SF	100(2)	GFRP	2.2	0

30 mm length and 20 mm wide with a thickness of 2 mm are placed axially in the steel tubes. A total of four plates were placed at a region of 100 mm from the top in the hoop direction and another four plates were placed at 100 mm from the bottom. The stiffened plates are placed outside the steel tube at particular loacations based on the damages in the steel tubes without stiffened plate. M30 grade concrete is used for the confinement between the two tubes. Table 1 lists the detailed information of the sample. Specimens are labeled as two categories, CSF and CSF-SP, that is, steel tube without and with stiffened plate, respectively. The letter C represents a concrete and followed by a number that indicates the grade of the concrete followed by the letter s that represents the steel pipe, and the number next to the letter s represents the diameter of the steel pipe and followed by a letter F which indicates the FRP and followed by a number that indicates the orientation of fibre. The term SP indicates the use of the stiffened plate. For example, C30S76F0-SP represents concrete compressive strength of grade 30 N/mm^2, steel tube of diameter 76 mm, and followed by FRP of zero degrees orientation. SP indicates with the stiffened plate.

3 Material Used and Its Properties

3.1 Concrete Properties

All column samples use M30 grade concrete. This M30 grade concrete was prepared by the ordinary Portland cement, GGBS, M-sand, coarse aggregate of size 10 mm, and superplasticizers. Concrete cubes and cylinders were made in each concrete batching to determine the concrete properties which are tested on the 28th day. Some basic tests were made to find the properties of ordinary portland cement 53 grade as fineness—4.6%, consistency—31%, initial cement setting time—34 min, final setting time—560 min, specific gravity—3.12. The physical properties of the fine aggregate near the II zone are specific gravity 2.69, bulk density—1525 kg/m3, and water absorption rate 0.64%. The size of the coarse aggregate is 10 mm and is

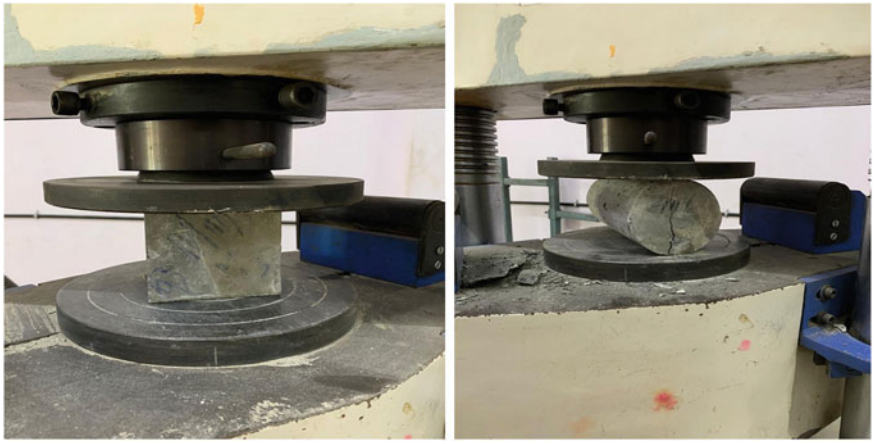

(a) Compression test **(b)** Split tensile test

Fig. 2 Tests on concrete

Table 2 Concrete properties

Concrete grade	f_{co}(MPa)	E_c (GPa)	ε_{co}(%)
M30	38.2	30.2	0.273

affected by the measured values of physical properties (such as specific gravity—2.7, bulk density—1575 kg/m3, and water absorption—0.3%). The concrete after casting concrete cubes and cylinders was tested to find the concrete strength using compression tests and split tensile tests (Fig. 2). The average compressive strength f'co of the concrete and its corresponding deformation εco are 38.2 MPa and 0.273% (Tables 2, 3 and 4). For concrete mix proportion (ref. Table 5).

3.2 FRP Tube

According to ASTM D3039 [1], the FRP coupon was cut in the longitudinal direction of length 250 mm, width 25 mm, and thickness 2 mm. The average tensile strength and elastic modulus of the FRP with 0° fibre orientation is represented in Table 3. The common diameter of the FRP tube is 150 mm, the height is 300 mm, and the

Table 3 FRP properties

Orientation Angle	Thickness of FRP (mm)	Tensile strength f_f (MPa)	Ultimate tensile strain ε_{frp} (%)	Young's modulus E_{frp} (MPa)
0°	2	2465	0.67	3916.1

fibre direction is the same at 0°. Though the dimensions of the FRP tubes are the same, it is expected that all the FRP tubes have the same longitudinal compression material property. Fibre orientation controls the strength, ductility, and failure mode of FRP-wrapped column pieces.

3.3 Steel Tube

Standard steel coupons were cut lengthwise for tensile tests according to ASTM A1067. Table 4 shows the ultimate stress and Young's modulus of steel pipe. The steel tubes used in the specimens have differed concerning their diameter. All the steel tubes have the same height as that of the FRP tubes. In a total of six steel tubes, three are made with the stiffened plate after computing the results from tubes without stiffened plates. All the steel tubes have a common thickness of 2 mm (Table 5).

4 Specimen Preparation

All steel pipes of the same type are cut with the same steel plate, folded to the desired diameter, and welded. When a column without a reinforced plate is tested, the reinforced plate is placed at the essential critical point of the steel pipe. The axial deformation value of the steel pipe is evaluated by placing an axial strain gauge at an intermediate height outside the steel pipe. The FRP tube is also cut to the designed length and processed. Steel pipes and FRP tubes are all placed concentrically on wooden boards using nails to resist movement during concrete placement. Before pouring the concrete, it is necessary to take the wire of the strain gauge out of the hole previously drilled in the surface of the FRP tube. Tamping of concrete is done using a shaking table. It is compacted into three layers of concrete poured between two tubes (ref. Figs. 3 and 4).

Table 4 Properties of steel

Thickness (mm)	Elastic modulus E_s(GPa)	Yield stress F_y(MPa)	Ultimate stress f_u(MPa)
2	210	74.53	314.5

Table 5 Concrete mix proportions

Specimen Batch	Cement (kg/m^3)	GGBS (kg/m^3)	Fine Aggregate (kg/m^3)	Coarse Aggregate (kg/m^3)	Superplasticizer (kg/m^3)	Water (kg/m^3)	Water Cement Ratio
1	230	120	857	1080	2.1	155	0.5

Fig. 3 Columns without stiffened plates

Fig. 4 Columns with stiffened plates

5 Test Setup

DSTC specimens were tested on a 2000 kN load capacity compression tester. A strain gauge is placed axially at the outer mid-height of the steel pipe to measure the axial strain. Before pouring the concrete between the two tubes, the wire from the strain gauge is taken out through the predrilled holes in the FRP tubes [8]. Likewise, two strain gauges are placed in the outside of the FRP tube column to obtain the axial strain. Four number of LVDTs (Linear Variable Displacement Transducer) have been fixed in the DSTC column specimens at a mid-height of 75 mm, while testing in both horizontal and vertical directions which will calculate the axial and lateral displacement when the load is applied. A rectangular plate was placed on top of the pillar to ensure a uniform load distribution. A load of 2 KN per second was applied in the early stages of the elastic behaviour of the column. Two L-shaped steel plates were stuck at the mid-height in both the directions so that vertical LVDTs can be fixed. The setup of the instrumentations is shown in (Fig. 5).

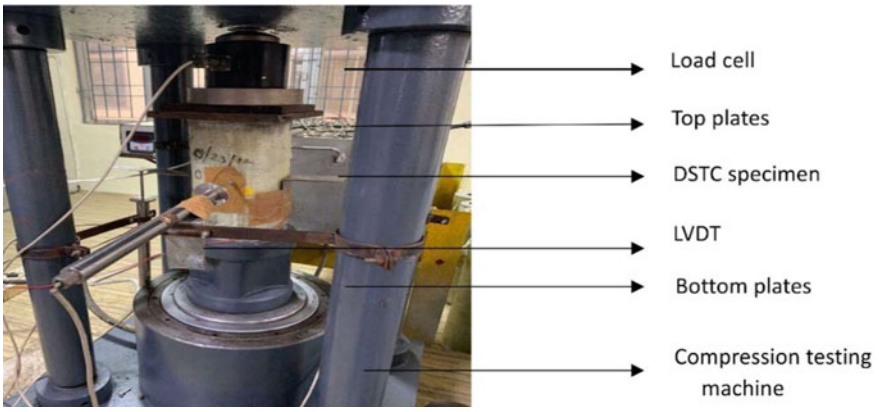

Fig. 5 Instrumentation setup

6 Result and Discussions

6.1 Failure Modes in Columns

All columns without stiffened plates mostly failed due to FRP rupture mostly near to the centre from the top and bottom. The column specimens with 0° fibre orientations failed due to hoop rupture and failed from the top to the mid-regions in the columns till its ultimate load. But, all the columns with stiffened plates with the same fibre orientations failed only up to the stiffened plates placed at the top after attaining the ultimate load. Beyond the stiffened plates placed at the top region, the column remains safe without any failures occurring. As a result of failure from all the columns, it is observed that the columns without stiffened plates failed with respect to the orientation of fibre in the column as in the hoop direction, and also the stiffened columns further resist the failure in the columns when compared to the columns without stiffened plates. (Figs. 7 and 8) show the failure modes of each column and also failures in the inner steel tubes. The failures that occur in the steel tubes are pointed by marking it. The tests of these columns presented that the failures are similar for both the inner side of steel tubes and the outer side of the FRP tubes.

6.2 Failure Modes in the Steel Tubes

In consideration of three steel tubes with a diameter of 76, 89, and 100 mm, the steel tubes with 89 mm Φ and 100 mm Φ failed mostly from top to bottom when compared to the steel tube with 76 mm diameter. The steel tube in 0° fibre failed due to inward buckling at the mid-region and some local buckling failure at the top and the bottom of the tubes. Since the steel tubes are constrained by the concrete,

Table 6 Test results

Specimen	P_t (kN)	P_s (kN)	P_{co} (kN)	$P_t/(P_s + P_{co})$	Void ratio
C30S76F0	900	310	410	1.25	0.5
C30S89F0	800	365	375	1.08	0.59
C30S100F0	750	385	340	1.03	0.66
C30S76F0- SP	1624	310	410	2.25	0.5
C30S89F0- SP	1350	365	375	1.82	0.59
C30S100F0- SP	850	385	340	1.17	0.66

the failure more likely occurs in the inward positions. On the other hand, all the steel tubes in the columns with stiffened plates failed only up to the stiffened plate at the top regions. Some inward local buckling occurs at the steel tubes at the top of the column which further resists the failure in the steel tubes and the stiffened plates. From the tests of the columns with and without stiffeners, it is observed that the specimens C30S76F0, C30S88F0, C30S100F0 have failures in different regions like the steel tube of specimen C30S76F0 shows the local inward buckling takes place near the centre from the top at one side alone. Specimen C30S88F0 shows that the steel tube failed close to the centre from the bottom, and specimen C30S100F0 shows that the inward buckling takes place the most nearly to the centre from the top of the column in a circular manner. Whereas all the columns with stiffeners show the local buckling occurs at the top regions alone and further resists the buckling.

6.3 Axial Load-Bearing Force of the Column

The DSTC column specimens tested under axial loads have the DSTC column (Pt) shown in Table 6, the ultimate load transfer capability of steel pipes (Ps), and unconstrained concrete strength (Pco). Pt / (Ps + Pco) represents the ratio between the final load of the DSTC column and the strength of the combination of the final load of steel and concrete strength [9]. As a result, it is observed that the load-bearing capacity of DSTC is higher than the load-bearing capacity of the adhesive strength between the steel pipe and concrete, except for the test piece C30S76F0, which has a void ratio of 0.5.

6.4 Influence of Void Ratio

The vacuum rate of the column can be checked by the ratio of the inside diameter to the outside diameter of the concrete [10]. It is observed that the column with a large vacuum index exhibits low stress values. The void percentages of all test samples are

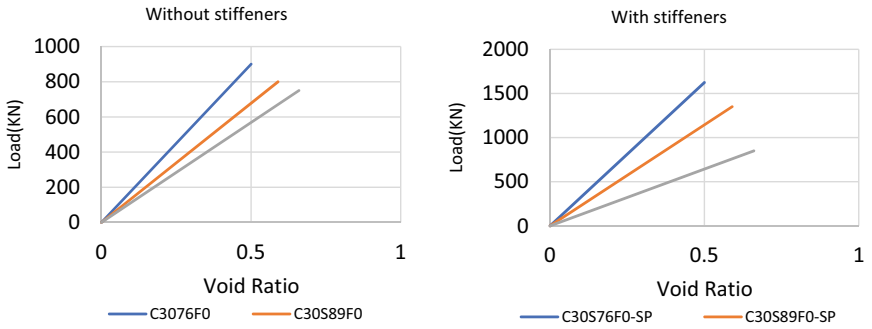

Fig. 6 Load corresponding to void ratio curves

listed in Table 6. Based on experimental observations, the decrease in stress–strain values of columns with smaller voids is not significant compared to columns with a greater void rate. Therefore, it is shown that the void rate plays an important role in the load capacity of the column as increasing the void rate will lead to a decrease in the load capacity of the column. Increasing the vacuum ratio leads to a decrease in the cross-section of the concrete, which also leads to breakage of the inner steel tubes of the 100 mm columns. The effect of the load on the columns corresponding to the void ratio is shown in Fig. 6.

6.5 Axial Stress–strain Characteristics of DSTC Column

The axial stress–strain curve of the steel pipe in the 0° fibre oriented column shown in Fig. 9 indicates that the column with a smaller porosity tends to produce higher stress and strain values. The axial load on the concrete is divided by the cross-section of the concrete to obtain the concrete stress (Pco) [11, 12]. It can be seen from (Fig. 9) that compared to the other three reinforced columns, the axial stress–strain value of the column without reinforcing plate drops suddenly due to the fracture of the FRP. As a result of all the columns without stiffened plates, the axial stress–strain value is lower for all the specimens without stiffeners due to column having a higher void ratio and FRP rupture. When these columns are compared to columns with stiffeners, it shows higher stress–strain values, where the stiffeners resist the loads. As the concrete is well confined by the two tubes, all the column specimens perform higher stress–strain values.

(a) 76mm without stiffeners

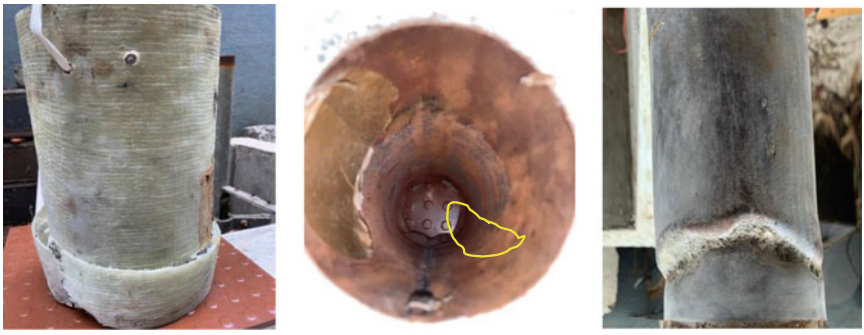

(b) 89mm without stiffeners

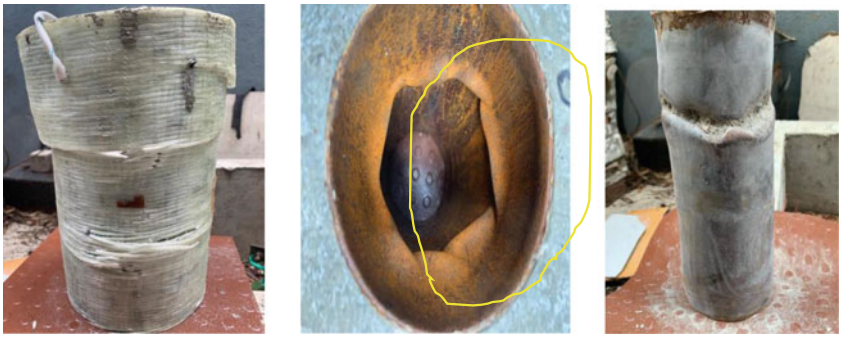

(c) 100mm without stiffeners

Fig. 7 Failure modes of DSTC specimens without stiffeners

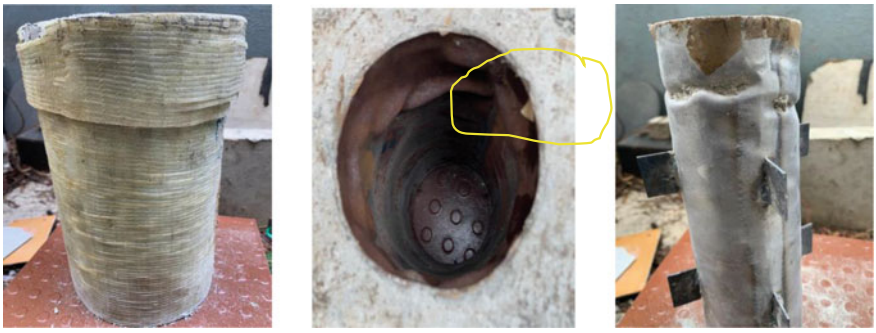

(a) 76mm with stiffeners

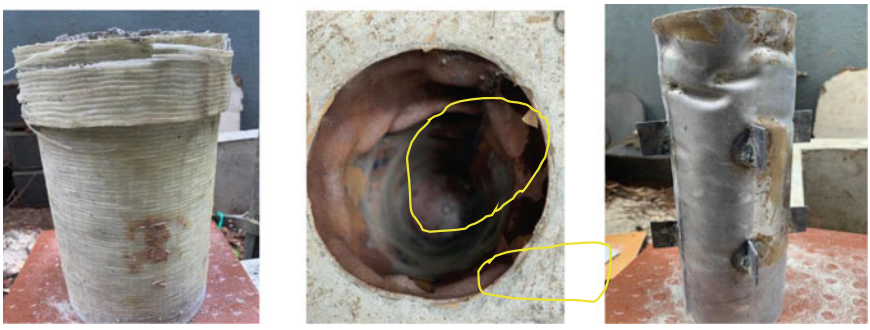

(b) 89mm with stiffeners

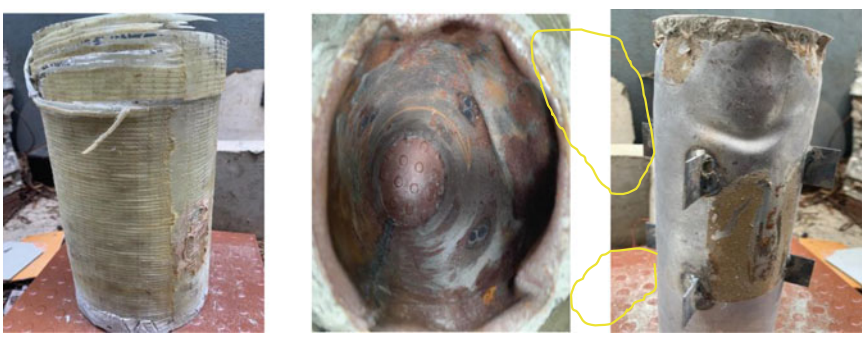

(c) 100mm with stiffeners

Fig. 8 Failure modes of DSTC specimens with stiffeners

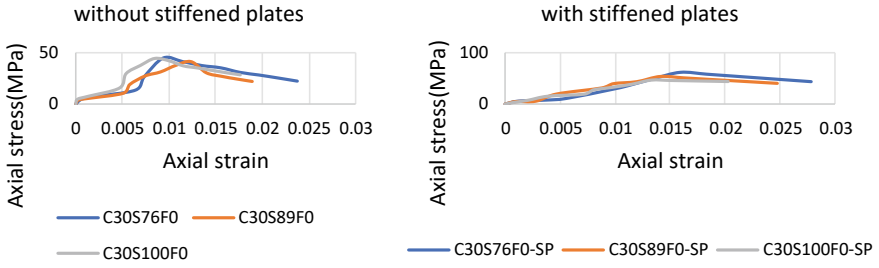

Fig. 9 The axial deformation behaviour of the column

6.6 Load Deformation Curves

The ultimate loads attained by all the six DSTC columns are shown in (Table 6). The column specimens without stiffened plates show low load-carrying capacity when compared to the columns with stiffened plates. The deflections are observed in mid-regions of every column by means of LVDTs. As a result of load and deformation curve shown in Fig. 10, it is observed that comparison between the columns with and without stiffened plates can be classified by three ways (1) The modes of failures

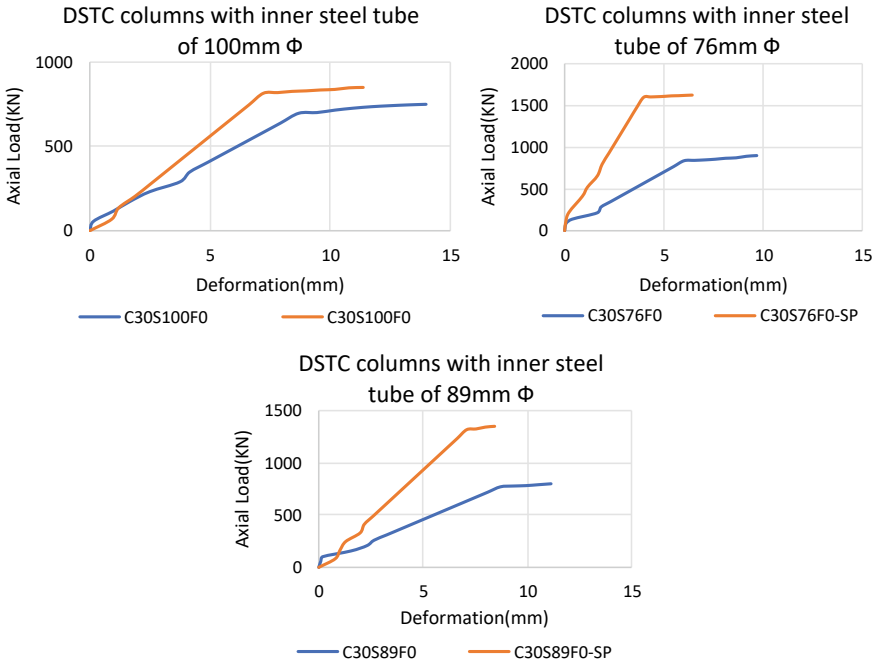

Fig. 10 Load vs Deformation curves

in the DSTC columns; (2) Failure corresponding to the void ratio; (3) Initial failure at elastic behaviour of columns. All columns without stiffeners indicate that the steel tubes inside the columns were randomly damaged, but most of the upper and lower areas were damaged. Column deformation increases as the voids of the column increases. On increasing the void ratio, the steel tubes more likely failed more from the top to the bottom. The specimen C30S76F0 shows some small cracks that occurs in the FRP at the top region, later the column failed at the middle region due to the hoop rupture of the FRP. The specimen C30S89F0 with 89 mm inner steel tube diameter shows that the column failed only at the bottom regions, also the inner steel tube failed in the bottom region due to inward buckling. The specimen C30S100F0 with 100 mm inner steel tube diameter failed only at the top regions but the inner steel tube failed randomly staring from the top to the bottom. All the column specimens with stiffened plates show a unique difference when compared to the columns without stiffeners.

The stiffened test specimens represent all the columns that failed only at the top region which includes the inner steel tube, FRP tubes, and confined concrete. Further failures are constrained by the stiffeners.

6.7 Effect of Stiffened Plates Between the Tubes

The advantage of using the stiffeners in the columns is observed by comparing the columns with load-deformation curves and the stress–strain curves. From Table 6, it shows increasing steel diameter will certainly reduce load-carrying capacity on both concrete (P_{co}) and steel (Ps), whereas the ratio of load of DSTC specimen to the combined load of steel and concrete is decreasing. Instead of placing stiffener plates longitudinally in the column, plates in the critical points provide excellent load-carrying capacity to resist further buckling in the column as compared with the column specimens without stiffeners. As a result, it was observed that the inner steel tubes of the column were damaged only by inward buckling due to the confinement of the concrete and the stiffer plates in the column. The stiffened plates in the columns allow only the tubes to fail further no failures in the stiffeners. The stiffeners remain same without any deformations.

7 Conclusion

In this work, the performance of a double-layer tubular concrete column with stiffening plates is proposed. Experimental results includes a total of six columns in which three were with stiffened plates and the other three were without stiffened plates. All the DSTC columns were designed and studied for the behaviour of concrete in the columns, stress–strain relation, load deformations of the columns, the effect of void

ratio corresponding to the load-carrying capacities, and the effect of stiffened plates. As a result of all the above parameters, it is concluded as following:

(1) The stiffened plates in the critical points of the column, reducing the void ratio all lead to increasing the load-carrying capacity of the columns, increases the stress–strain values, and further reduces the buckling in the columns.
(2) The experimental results show that the FRP DSTC mixed column has excellent ductility and can be predicted due to the inward buckling failure of the steel pipe.
(3) The experimental behaviour of the DSTC column and the inner steel shows the same failure, which indicates that the failure that occurs in the external FRP tube is the same as the failure that occurs in the internal steel pipe.
(4) It can be predicted that the column tends to fail only in the upper region above the stiffeners in both FRP and steel pipes in columns without stiffeners.
(5) As the column fails in different areas, but due to the direction of the optical fibre and the initial break of the FRP, the failure occurs along the ring direction.

References

1. ASTM (2014) Astm D3039/D3039M. https://doi.org/10.1520/D3039
2. Fanggi BAL, Ozbakkaloglu T (2013) Compressive behavior of aramid FRP-HSC-steel double-skin tubular columns. Constr Build Mater 48:554–565. https://doi.org/10.1016/j.conbuildmat.2013.07.029
3. Teng JG, Yu T, Wong YL, Dong SL (2007) Hybrid FRP-concrete-steel tubular columns: Concept and behavior. Constr Build Mater 21(4):846–854. https://doi.org/10.1016/j.conbuildmat.2006.06.017
4. Xiong Z, Deng J, Liu F, Li L, Feng W (2018) Experimental investigation on the behavior of GFRP-RAC-steel double-skin tubular columns under axial compression. Thin Walled Struct 132(May):350–361. https://doi.org/10.1016/j.tws.2018.08.026
5. Yu T, Teng JG, Wong YL (2010) Stress-strain behavior of concrete in hybrid frp-concrete-steel double-skin tubular columns. J Struct Eng 136(4):379–389. https://doi.org/10.1061/(ASCE)ST.1943-541X.0000121
6. B Zhang, J G Teng, and T Yu. 2015. Experimental behavior of hybrid FRP – concrete – steel double-skin tubular columns under combined axial compression and cyclic lateral loading. 99: 214–231. https://doi.org/10.1016/j.engstruct.2015.05.002
7. Zhou Y, Liu X, Xing F, Li D, Wang Y, Sui L (2017) Behavior and modeling of FRP-concrete-steel double-skin tubular columns made of full lightweight aggregate concrete. Constr Build Mater 139:52–63. https://doi.org/10.1016/j.conbuildmat.2016.12.154
8. Ozbakkaloglu T (2015) Thin-walled structures a novel FRP – dual-grade concrete – steel composite column system. Thin Walled Struct 96:295–306. https://doi.org/10.1016/j.tws.2015.08.016
9. Deng J, Zheng Y, Wang Y, Liu T, Li H (2017) Study on axial compressive capacity of FRP-confined concrete-filled steel tubes and its comparisons with other composite structural systems. Int J Polym Sci
10. Zhang B, Teng JG, Yu T (2017) Compressive behavior of double-skin tubular columns with high-strength concrete and a filament-wound FRP tube. J Compos Constr 21. https://doi.org/10.1061/(ASCE)CC.1943-5614.0000800

11. Louk Fanggi BA, Ozbakkaloglu T (2015) Square FRP-HSC-steel composite columns: Behavior under axial compression. Eng Struct 92:156–171. https://doi.org/10.1016/j.engstruct.2015.03.005
12. Yu T, Zhang B, Cao YB, Teng JG (2012) Thin-walled structures behavior of hybrid FRP-concrete-steel double-skin tubular columns subjected to cyclic axial compression. Thin Walled Struct 61:196–203. https://doi.org/10.1016/j.tws.2012.06.003

Numerical Optimization of Mix Proportioning of Self-Compacting Concrete with Silica Fume—A Machine Learning Perspective

D. Annlin Jebitha and M. Ramesh Kannan

1 Introduction

Self-Compacting Concrete (SCC) is one of the significant special concretes which possess remarkable functional characteristics in terms of workability and flowability properties. SCC has a huge advantage over conventional concrete regarding the inherent passing-ability and filling-ability in a confined and also in the congested environment. To be more particular, SCC is generally used in the confined and thin concrete column formwork system and in the casting of the structural member with highly congested reinforcement where the flow of concrete gets adversely affected despite the use of formwork or external vibrators and internal vibrators. SCC is more or less a highly viscous fluid and has the natural tendency to flow itself due to the application of chemical admixtures, such as Superplasticizers (SP), Viscosity Modifying Agent (VMA), and Air Entraining Agent (AEA). However, the proportioning of SCC with an optimal percentage of SP, VMA, and AEA is highly indispensable. Saranya and Kannan have investigated the optimal percentage of VMA and AEA for SCC based on segregation resistance and workability characteristics [1]. Additionally, SCC is also prepared with mineral admixtures, namely, Fly Ash (FA), Silica Fume (SF), Metakaolin (M), and Rice Husk Ash (RHA), and so on, in addition to the aforementioned chemical admixtures. However, the application of these mineral admixtures in SCC tends to alter the workability and flowability properties. Saranya and Kannan reported that with the addition of mineral admixtures in SCC, the workability gets reduced despite the presence of chemical admixtures, thus the resulting

D. Annlin Jebitha · M. Ramesh Kannan (✉)
School of Civil Engineering, Vellore Institute of Technology Chennai, Chennai, Tamil Nadu 600127, India
e-mail: rameshkannan.m@vit.ac.in

D. Annlin Jebitha
e-mail: annlinjebitha.d2020@vitstudent.ac.in

K. S. Satyanarayanan et al. (eds.), *Sustainable Construction Materials*, Lecture Notes in Civil Engineering 194, https://doi.org/10.1007/978-981-16-6403-8_39

mixture requires additional chemical admixtures but not proportionate to the additional quantity of mineral admixtures [1]. Thus, a thorough introspective assessment on the proportioning of SCC with mineral admixtures in addition to the chemical admixtures concerning the workability characteristics is necessitated.

2 Review of Literature

Alsanusi stated that the mineral admixture silica fume is a viable subordinate material, which cannot be replaced by more than 6% by mass [2]. The substitution of cement with 5% SF in SCC revealed significant compressive strength and split tensile strength. The increase in the SF range of 2.5–15% at an interval of 2.5% decreases the flowability of concrete as determined by Gowda et al. [3]. The SCC mixes with 15% replacement of cement by SF can attain maximum compressive strength, as investigated by Mohamed [4]. Ofuyatan et al. have testified that the highest compressive strength is attained at 5% substitution of cement with silica fume and when the percentage is increased, the compressive strength gets decreased [5]. At 7 and 28 days, Janagan et al. have investigated the significant compressive strength and is achieved for M30 SCC mix with 5–15% replacement of cement by SF in the interval of 5% [6]. The improvement in compressive strength is obtained by 5% substitution of cement with SF at 7 and 14 days with a w/cp ratio of 0.8 as reported by Vivek and Dhinakaran [7]. Iyappan investigated that the compressive strength of SCC with 2.5 and 5% substitution of cement by SF has increased when related to control specimens but the concrete flow has reduced [8]. Above 30% substitution of cement with silica fume in SCC decreases the strength values [9]. The substitution of cement by 10% of silica fume in SCC gives increment in compressive strength. As the replacement level increases, the workability of concrete gets diminished. Besides, the decrease in the strength of concrete is due to a rise in the w/c ratio as determined by Kankariya et al. [10]. Admixture plays a prominent role in SCC in the size of air pores [11]. The addition of SF in SCC improves the long-term performance of concrete and the durability of concrete [12]. The addition of mineral admixture in optimal quantity in SCC helps to improve the workability of concrete [13]. Saranya and Kannan investigated the optimal percentage of chemical admixture for SCC [1].

An increase in the percentage of mineral admixture in SCC decreases the strength of concrete [14]. Investigation on the effect of Metakaolin, FA, and SF in M30 and M40 grade SCC was carried out by Seelapureddy et al. [15], and from their experimental results, it is inferred that 10% replacement of cement with SF increases the compressive strength by 24.5% in 7 days and 38.9% in 28 days for M30 grade, and for M40 grade, 10% replacement of cement with SF increases the compressive strength by 33.4% in 7 days and 48.5% in 28 days. Okamura and Ouchi concluded that when SCC is used widely it can be regarded as ‘standard concrete’ rather than ‘special concrete’ [16]. The SF content is fixed as 15% in replacement of cement and that provides a significant increase in compressive strength, which is greater than 25 MPa when compared to normal concrete [17]. The SCC with 10% SF, 40% PC,

and 50% FA that gives maximum compressive strength at 28 days is investigated by Mustapha et al. [18]. The performance of SCC in a hardened state with SF shows better result as reported by Benaicha et al. [19]. The permeation coefficient of SCC is determined by Lu et al. [20] and reported that the permeability of the SCC reaches the peak value when cement with the percentage of replacement of SF superseded 4%. Dybel and Furtak deduced that the incorporation of SF could both increase and decrease the quality of bond conditions, and the bond failure depends on the concrete cover thickness [21]. The influence of SF with 10% and 20% made a significant rise in compressive strength to 75.5 and 79.5 MPa at 28 days [22]. Dinesh et al. determine the compressive strength values of SCC and the compressive strength value is increasing by 3.95, 5.9, 7.56, 9.15, and 14.05% when cement is superseded with 2.5, 5, 7.5, 10, and 12.5% SF respectively [23]. The properties of SCC depend on the dosage and type of chemical admixture used [24]. Ramanathan et al. reported that the performance of mechanical properties of SCC with SF has shown better results [25]. The percentage of SF is inversely proportional to the compressive strength. Therefore, the optimal percentage of replacement of cement with SF is considered as 30%. Chavan and Kannan used Response Surface Methodology (RSM) [26] and Jiji et al. used heuristic search for optimizing the mix proportioning of SCC [27].

3 Mix Proportioning of SCC

The different SCC mix proportions (M40 grade) augmenting this research are delineated in Table 1.

Table 1 Mix proportioning of special concrete (SCC)

Mix no.	CC (kg/m^3)	% SF	CA (kg/m^3)	FA (kg/m^3)	W (kg)	% SP	% VMA	% AEA	W/C_P
1	485	0	977	561	267	1.14	0.63	0	0.55
2	475	2	977	561	261	1.33	0.75	0.15	0.55
3	466	4	977	561	256	1.53	0.88	0.30	0.55
4	456	6	977	561	251	1.72	1.00	0.45	0.55
5	446	8	977	561	245	1.92	1.13	0.60	0.55
6	437	10	977	561	240	2.11	1.25	0.75	0.55
7	427	12	977	561	235	2.30	1.38	0.90	0.55
8	417	14	977	561	229	2.50	1.5	1.00	0.55

Table 2 Test results for eight mixes of SCC

Mix no.	Flow table (mm)	V-funnel (s)	V-funnel (5 min)	U-box (mm)	J-ring (mm)	L-box	Compressive strength (N/mm^2)
1	660	10.00	2.50	30	3.00	0.78	48.10
2	645	8.20	2.49	27	4.50	0.79	49.38
3	642	7.50	2.43	24	5.90	0.80	47.44
4	640	9.80	2.42	23	7.80	0.80	45.21
5	636	7.90	2.40	20	8.60	0.82	39.92
6	634	7.36	2.38	18	9.20	0.83	38.13
7	632	5.70	2.34	17	9.60	0.84	37.05
8	630	5.60	2.30	15	9.64	0.86	36.66

4 Experimental Investigation

The prepared SCC mixes are investigated for filling ability, passing ability, and segregation resistance based on corresponding testing procedures as recommended by European Federation of National Associations Representing for Concrete (EFNARC) [12]. The results are displayed in Table 2.

The standard values for different test methodologies for SCC as per EFNARC [12] are as follows: for flow table, the limited value ranges from 650 to 800 mm; for V-funnel (s), the value ranges from 6 to 12s; for V-funnel (5 min), the value ranges from 0 to 3s; for U-box, ranges from 0 to 30 mm; for J-ring ranges from 0 to 10 mm; and for L-box, value ranges from 0.8 to 1.0. From Table 2, it is inferred that the test outcomes are within the allowable constraint (or limit) as per EFNARC [12] recommendations. These crisp values are converted into their equivalent fuzzy number (0–1) for incorporating into Machine Learning (ML) paradigm as discussed in the following section.

5 Results and Discussion

A thorough introspective examination of the test results is highly significant to interpret the optimal mix proportioning. An innovative hybrid ML methodology known as Adaptive Neuro-Fuzzy Inference System or Adaptive Network-based Fuzzy Inference System (ANFIS) is considered for optimizing mix proportioning of SCC as shown in Fig. 1.

The input parameters, and the target parameter i.e., the compressive strength (CS) are depicted in Fig. 1. A trapezoidal fuzzy membership function with five-point linguistic variables (‘very high’, ‘high’, ‘neutral’, ‘low’, and ‘very low’) is considered for all the input parameters and a constant fuzzy membership function is taken

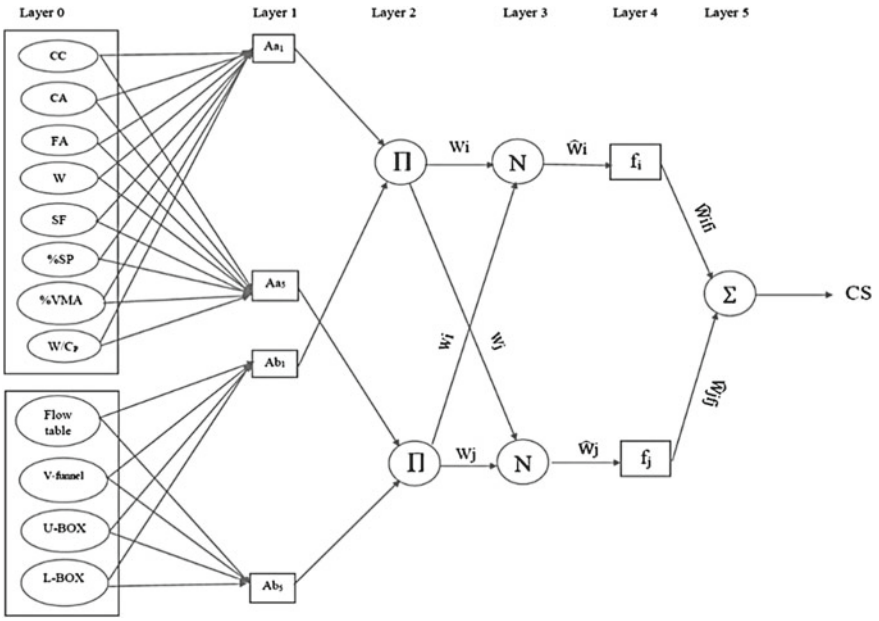

Fig. 1 ANFIS architecture for optimization of mix proportioning of SCC

for the target parameter. ANFIS consists of a 'two-pass computational procedure', i.e., the forward pass learning and backward pass learning. The premise parameters are identified by the 'least square method' [28–30] and 'Levenberg–Marquardt backpropagation algorithm' [31] in the forward pass and backward pass learning, respectively.

Initially, the crisp dataset of the experimental values gets converted to its equivalent fuzzy numbers and using that, the fuzzy membership systems (i.e., system of fuzzy membership function) is formulated. The formulated system of fuzzy membership function of each variable gets incorporated into the ANFIS framework. The weights of each layer of ANFIS and the learning rules gets generated in the forward pass, and using the standard gradient-descent learning technique known as 'Levenberg–Marquardt backpropagation algorithm' in the backward pass, the parameters are fine-tuned to optimize the output parameter after the epoch (iteration) reaching the stopping criterion. From ANFIS, the optimal mix proportion for the special concrete (SCC with SF, SP, VMA, and AEA) is CC—460 kg/m^3, SF—20 kg/m^3, CA—925 kg/m^3, FA—532 kg/m^3, W—138 kg, SP—1.27%, VMA—0.78%, AEA—0.3%, and the compressive strength using this optimized mix proportioning is 49.41 MPa (with coefficient of determination value, R^2 of 0.9782), well above the theoretical target compressive strength, i.e., 48.25 MPa (with 5.0 Standard Deviation). Additionally, thirty concrete cubes of SCC are prepared with the optimal mix proportioning and are tested at 28 days after ambient curing, the average value of the compressive

strength of the SCC samples obtained is 48.47 MPa, with approximately only 2% variations, which is negligible.

6 Conclusion

This research provides a comprehensive framework analogy on optimizing mix proportioning of SCC with percentage of Silica Fume (SF) as a significant mineral admixture, and also with commonly used chemical admixtures such as Superplasticizers (SP), Viscosity Modifying Agent (VMA), and Air Entraining Agent (AEA) using an intriguing hybrid Machine Learning approach known as ANFIS. This comprehensive framework can be further extended to predict compressive strength for other blended and special concretes with additional input parameters such as water absorption, sorptivity, permeability, and so on, as well. Notwithstanding that this neoteric framework can be used to predict other mechanical properties of concrete such as flexural strength, split tensile strength, creep, and so on, by providing appropriate input parameters. This framework holds good for mix proportioning of any type of concrete, as well as any concrete construction works ranging from regular minor plain cement concrete work PCC to speciality concrete construction works such as bridges, silos, and so on. Withal, external parameters like temperature, humidity, and other fuzzy parameters can be incorporated into this framework. Ultimately, the outcome of ANFIS for various special concrete can be collated for creating nomograms for the ease of the end-users.

References

1. Paranji S, Kannan R (2015) Numerical optimization of mix proportioning of self-compacting concrete. Int J Eng Res Technol 4(4):1393–1397. https://www.ijert.org/research/numerical-optimization-of-mix-propotioning-of-self-compacting-concrete-IJERTV4IS041500.pdf
2. Alsanusi S (2013) Influence of silica fume on the properties of self compacting concrete. Int J Civil Environ Eng 7(5):348–352. https://www.doi.org/10.5281/zenodo.1070295
3. Gowda MR et al (2016) Development of self compacting concrete using silica fume. Int J Sci Res Dev 4(11):36–38. http://www.ijsrd.com/articles/IJSRDV4I110075.pdf
4. Mohamed HA (2011) Effect of fly ash and silica fume on compressive strength of self-compacting concrete under different curing conditions. Ain Shams Eng J 2:79–86. https://doi.org/10.1016/j.asej.2011.06.001
5. Ofuyatan OM et al (2019) Incorporation of silica fume and metakaolin on self compacting concrete. J Phys: Conf Ser 1378(4):1–12. https://doi.org/10.1088/1742-6596/1378/4/042089
6. Janagan SS et al (2019) An experimental study on self-compacting concrete by using silica fume as partial replacement of cement. Int J Curr Eng Sci Res 6(3):110–115. http://troindia.in/journal/ijcesr/vol6iss3/110-115.pdf
7. Vivek SS, Dhinakaran G (2015) Effect of silica fume in flow properties and compressive strength of self compacting concrete. Int J ChemTech Res 8(5):1–5. http://www.sphinxsai.com/2015/ch_vol8_no1/1/(01-05)%20V8N1.pdf
8. Iyappan G et al (2017) Experimental investigation of SCC using silica fume. Int J Innov Res Sci Eng Technol 6(4):6080–6089. https://doi.org/10.15680/IJIRSET.2017.0604250

9. Rathod RM, Vyawahare MR (2015) To study the effect of varying proportion of fly ash and silica fume on fresh and mechanical properties of high strength self compacting concrete. Int J Innov Sci Eng Technol 2(7):64–68. https://www.ijeit.com/Vol%205/Issue%201/IJEIT1412201507_13.pdf
10. Kankariya CS et al (2017) Review article: study and optimization of silica fume in concrete. Int J Recent Trends Eng Res 3(5):562–565. https://doi.org/10.23883/IJRTER.2017.3271.ATW1L
11. Okamura H (1997) Self-compacting high-performance concrete. Concrete Int, ACI 50–54
12. EFNARC (2005) The European guidelines for self-compacting concrete: specification, production and use. The European Federation of Specialist Construction Chemicals and Concrete Systems, UK
13. Sahmaran M et al (2006) The effect of chemical admixtures and mineral additives on the properties of self-compacting mortars. Cement Concrete Comp 28(5):432–440. https://doi.org/10.1016/j.cemconcomp.2005.12.003
14. Uysal M, Yilmaz K (2011) Effect of mineral admixtures on properties of self-compacting concrete. Cement Concr Compos 33(7):771–776. https://doi.org/10.1016/j.cemconcomp.2011.04.005
15. Seelapureddy J et al (2011) Effect of metakaolin and micro silica on strength characteristics of standard grades of self-compacting concrete. Mater Today: Proc (In press). https://doi.org/10.1016/j.matpr.2020.02.936
16. Okamura H, Ouchi M (2003) Self-compacting concrete. J Adv Concrete Technol 1(1):5–15. http://www.j-act.org/headers/1_5.pdf
17. Salim K et al (2013) Formulation and characterization of self-compacting concrete with silica fume. J Eng Technol Res 5(5):160–169. https://doi.org/10.5897/JETR2013.0306
18. Mustapha FA et al (2021) The effect of fly ash and silica fume on self-compacting high performance concrete. Mater Today: Proc 39(2):965–969. https://doi.org/10.1016/j.matpr.2020.04.493
19. Benaicha M et al (2015) Influence of silica fume and viscosity modifying agent on the mechanical and rheological behavior of self-compacting concrete. Constr Build Mat 84:103–110. https://doi.org/10.1016/j.conbuildmat.2015.03.061
20. Lu C et al (2015) Relationship between slump flow and rheological properties of self-compacting concrete with silica fume and its permeability. Constr Build Mater 75:157–162. https://doi.org/10.1016/j.conbuildmat.2014.08.038
21. Dybel P, Furtak K (2017) Influence of silica fume content on the quality of bond conditions in high-performance concrete specimens. Arch Civil Mech Eng 17(4):795–805. https://doi.org/10.1016/j.acme.2017.02.007
22. Sabet FA et al (2013) Mechanical and durability properties of self-consolidating high performance concrete incorporating natural zeolite, silica fume and fly ash. Constr Build Mater 44:175–184. https://doi.org/10.1016/j.conbuildmat.2013.02.069
23. Dinesh A et al (2017) Experimental study on self-compacting concrete. Int J Eng Sci Res Technol 6:42–50. https://doi.org/10.5281/zenodo.345692
24. Ahmad S (2013) Evaluation of effect of superplasticizer on performance of self-compacting concrete. J Test Eval ASTM 41(5):754–760. https://doi.org/10.1520/JTE20120208
25. Ramanathan P et al (2013) Performance of self-compacting concrete containing different mineral admixtures. KSCE J Civ Eng 17(2):465–472. https://doi.org/10.1007/s12205-013-1882-8
26. Chavan R, Kannan R (2016) Numerical optimization of mix proportioning of self compacting concrete by response surface methodology. In: Proceedings of the 2016 national conference on science, engineering and technology. Vellore Institute of Technology Chennai, Chennai, Tamil Nadu, India (Electronic)
27. Jiji A et al (2019) Optimisation of mix proportioning of self-compacting concrete using heuristic search. Int J Recent Technol Eng 8(9):5339–5346. https://www.ijrte.org/wp-content/uploads/papers/v8i4/D7560118419.pdf
28. Jang J-SR (1993) ANFIS: adaptive-network-based fuzzy inference system. IEEE Trans Syst Man Cybern 23(3):665–685. https://doi.org/10.1109/21.256541

29. Jang J-S et al (1997) Neuro-fuzzy and soft computing: a computational approach in learning and machine intelligence. Prentice-Hall
30. Kannan MR (2019) Constructability analysis of concrete formwork system. Ph.D. dissertation, Vellore Institute of Technology Chennai, India
31. Rumelhart DE et al (1986) Learning representations, by backpropagation errors. Nature 323:533–536. https://doi.org/10.1038/323533a0

A Cost Analysis of Selected Building Materials on South Zone Market in India: 2016–2020

S. Prakash Chandar and S. Prasanth

1 Introduction

Costs of construction and development resources are pivotal in deciding the expense of lodging in each nation. It is irrefutable that covering payment will increment when components include the costs of building materials increment. The enormous extent of resources in development projects is a huge aspect that immensely affects the development project's total expense [1]. Costs of building and development materials are generally influenced by monetary variables, including market interest of the resources or their crude resources. The prices of imported structure and development materials like concrete, support bars, and clean product vacillate mostly because of the impact of expansion and conversion scale [2]. Huan and Jianhua [3] the impact factors about building materials are the estimation of cost reqiured, market interest and extensive public scale strategy. Akanni et al. [4] demonstrated an extraordinary ascent of the expense of construction and development resources in the Nigerian market, which inclines to influence the presentation of the building business in the nation. The costs of assembling resources have gotten additional costly in the Republic of Kenya due to the materials' import and transport [5]. Construction resources and hardware are two driving components to expand Malaysia's development costs [6]. The constant ascent in the expense of construction and development resources is liable for the increment price of lodging completed somewhere in the range of 1988 and 2008 in Cyprus [7, 8]. Danso et al. [9] recognized the components that impact the estimating choices for deciding the expense of construction and development resources in the south market, and vital between them are market-correlated variables. Barely any investigations have examined the cost pattern of building materials, despite being a typical event in many nations. Prasanna et al. [10] examined the structural materials value pattern between 2009 and 2013 in Malaysia. Prakash Chandar and Gunasekaran [11]

S. Prakash Chandar (✉) · S. Prasanth
Department of Civil Engineering, SRM Institute of Science and Technology, Kattankulathur, Tamil Nadu 603203, India

K. S. Satyanarayanan et al. (eds.), *Sustainable Construction Materials*, Lecture Notes in Civil Engineering 194, https://doi.org/10.1007/978-981-16-6403-8_41

explored the structural materials cost design in South Africa. There is the necessity additionally to examine the cost pattern of building and development resources in different nations. In this way, the current examination explores the cost pattern of some who chose regular structure and development on India's development market. Average yearly costs of construction materials from 2016 to 2020 were gathered from the market and utilized to assure India's building and development materials cost pattern. In previous research, all the authors have measured the cost comparison for outside India and also the research has been made previously in 2018 only for river sand and quarry dust. But this research is made in recent 2020 rates of river sand and quarry dust.

2 Literature Review

The cost of construction resources is a significant cause of the expense of gaining the right household. Development of lodging with easy construction and development resources gives moderate housing and expands the admittance to the dwelling by individuals in the low-level pay [9]. The present-day development industry lays a lot of accentuation on modern development procedures and strategies and utilizes traditional structure materials, price, and liveliness concentrated [12]. The spate of expanded lodging costs is a worry to managements internationally, especially in the short-pay nations [13]. The reasons for lodging prices is raises because the development and construction resources as the more prominent extent of to increase the price of lodging. Jagboro and Owoeye [14] The cost of using various construction resources, like concrete, ordinary Portland cement, oil palm shell in solid, rice husk ash, and mortar. In construction project the concrete accoupied 41% in building cost. Danso and Manu [15] investigated the primary driver of building material costs in the south India market and discovered that the significant price of resources assembly is a significant funder to the country's spending. The issue of rising construction and development materials costs could be qualified to factors such as a shortage and high price of introduced construction and development resources [16]. A mutual tendency shows a dangerous rise in the costs of construction and development resources such as concrete, steel, and totals everywhere in the world, and in Nepal, one significant explanation for the cost rise is the absence of energy, which has made precious the price of manufacturing these resources [17]. The alternative causal issue in Nepal, according to the creator, is the consistent lack of petroleum and diesel, which sources a massive rise in transport prices, disturbing interest and availability of structure resources accordingly, resulting in quickly rising costs. Gunasekaran et al. [18] acknowledged eight factors available of 29 as the primary issues that limit the cost increment in construction and building materials in the south India market development sector. High crude material prices, unrefined petroleum costs, electricity costs, fuel costs and force supply, high job costs, and high transportation costs are all variables in proposals and high running expenses. They also established a

multi-collinearity relationship between the factors responsible for price increases in construction and production materials.

3 Research Method

For the studies, the researchers chose basic structure and construction materials from the Indian development industry. They chose coarse aggregate, standard Portland concrete, river sand, Quarry dust as their materials. These materials were selected since they are promptly accessible and plentifully available, and both development experts and non-experts can identify with them without much of a stretch. By and large, the costs of the structure materials on the Indian market are not equivalent all through the country. There are contrasts in the prices because of various topographical areas. Supplementary information was attained in the Indian market for this study. The costs cited by the market were anticipated costs organized to counter the country's routine expenditure of construction and development materials. The available knowledge was from 2016 to 2020. The data were entered into Microsoft Office Professional Plus Excel 2016 for visualization.

4 Results

Cost analysis of river sand, quarry dust, coarse aggregate, cement, and the values are compared for the years between 2016 and 2020. The trend analysis has been plotted as linear difference and forecasted for 2 years for river sand, coarse aggregate, quarry dust, and cement.

4.1 River Sand

Costs of sand acquired were utilized to consider the pattern structure from the year 2016 to the year 2020. The cost of the river sand was decreased in the years between 2016 to 2020 and the cost slitly increased after 2020 because of non availibility of river sand in market. For unpleasant powder and laterite satisfying, the charges expanded from the year 2017 to 2020 and diminished in 2014, after which the costs grew again till 2016. There was, by and large, a fluctuating pattern in prices for every one of the four kinds of good totals. In any case, there was a general cost increment in the fair calculations over the time frame under investigation. There were 16, 40, 4, and 14% increments and laterite filling, separately, between 2016 and 2020 as shown in Table 1 and Fig. 1.

Table 1 Price of river sand

River sand	Year	Price
	2016	8000
	2017	12,000
	2018	15,000
	2019	18,000
	2020	12,000

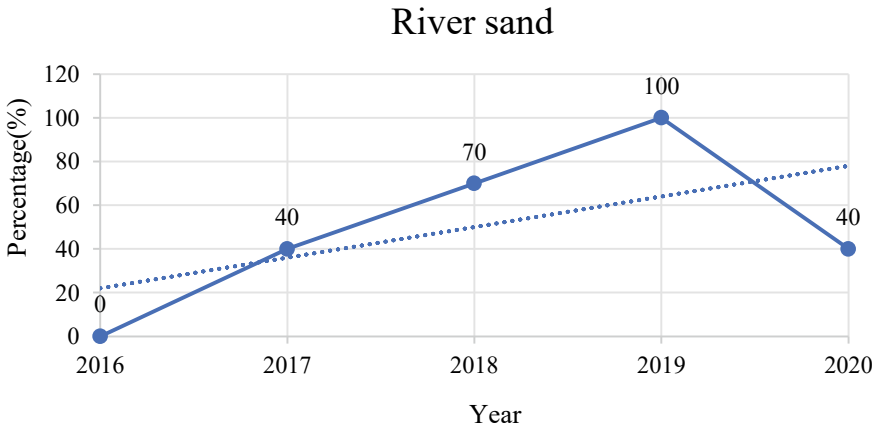

Fig. 1 Graphical representation on river sand

4.2 Quarry Dust

With the right quality materials, the right dose of superplasticizer, adequate mixing techniques, and proper curing, concrete containing quarry dust as fine aggregate can be successfully used in the building industry, ensuring sustainable growth against environmental contamination. The cost of quarry dust is a concentrated consequence of the overwhelming process that can be used as aggregates in concrete, especially fine aggregates. The rock has been creased into several dimensions during mining activities; during the dust generated—price pattern of quarry dust is shown in Fig. 2 and Table 2.

4.3 Coarse Aggregate

On the production market, the coarse aggregate is accessible in two structures: apparatus slammed and needle-sphe the coarse aggregate sizes are 10 to 20 mm and 20 to 40 mm. In Fig. 3 and Table 3, the costs of these dimensions of needle-cracked totals are analyzed and introduced.

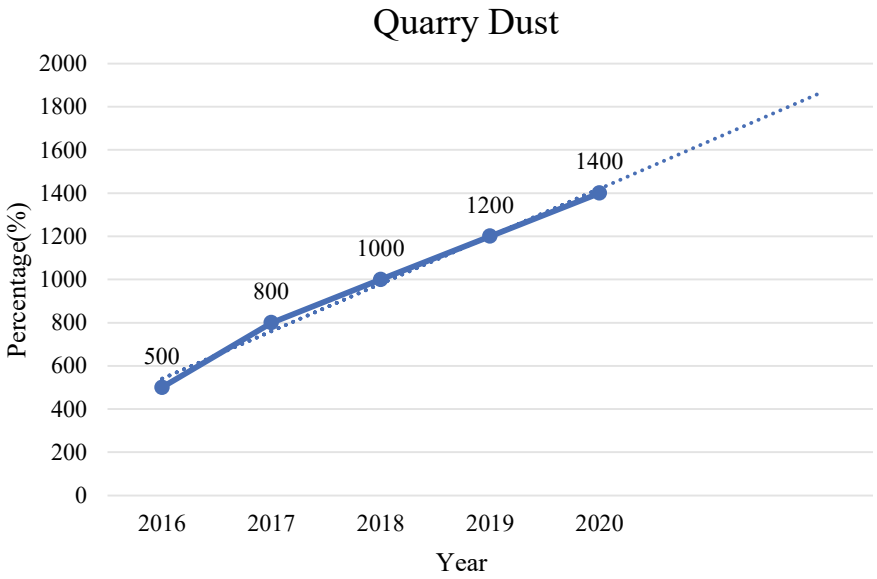

Fig. 2 Graphical representation on quarry dust

Table 2 Price on quarry dust

Quarry dust	Year	Price
	2016	500
	2017	800
	2018	1000
	2019	1200
	2020	1400

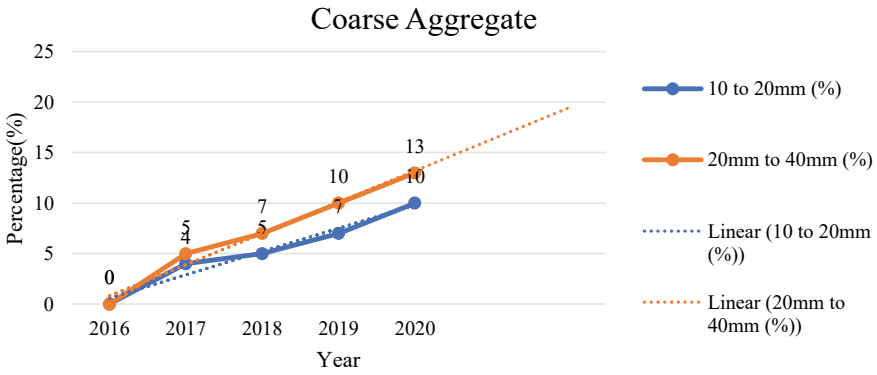

Fig. 3 Graphical representation on coarse aggregate

Table 3 Price on coarse aggregate

Coarse aggregate	Price		
	Year	10–20 (in mm)	20–40 (in mm)
	2016	2500	2000
	2017	2900	2500
	2018	3000	2700
	2019	3200	3000
	2020	3500	3300

The rate of change in value for needle-cracked coarse aggregate accessible on the Indian production market is depicted in Fig. 3. Costs for both 10–20 and 20–40 mm sizes continued to fluctuate between 2016 and 2020. Throughout the long term, the costs continued to rise without a single decline. Costs have risen steadily over the years under consideration, with increases of 100 and 71.45% for 10–20 and 20–40 mm sizes, respectively, from 2016 to 2020.

4.4 Cement

Conventional Portland concrete and PPC 50 kg is the most famous concrete in the Indian development market. Costs acquired were utilized at the cost pattern investigation showed in Fig. 4 and Table 4. There was a predictable expansion in costs with no abatement over the years under examination. Notwithstanding, prices stayed unaltered between the years 2014 and 2015 and afterward kept on expanding till

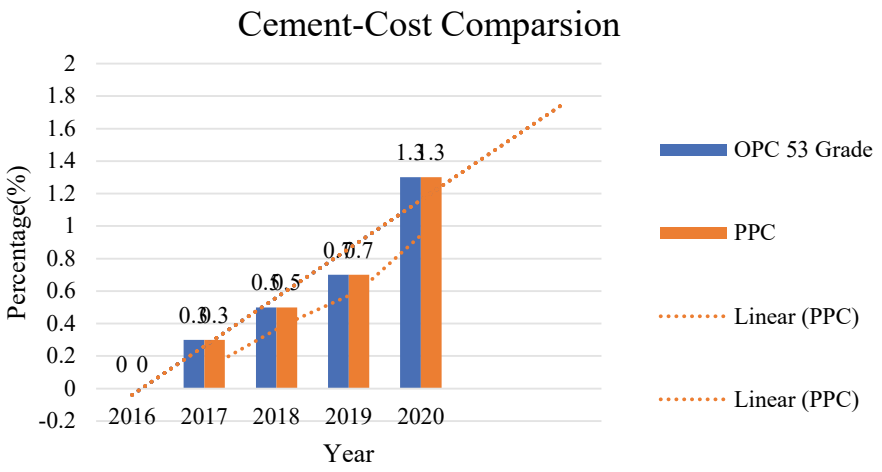

Fig. 4 Graphical representation on cement

Table 4 Price on cement

Cement	Price		
	Year	OPC 53 grade	PPC
	2016	300	290
	2017	330	320
	2018	350	340
	2019	370	360
	2020	430	420

2021. The concrete recorded an overall increment of 63% in costs from the year 2016 to the year 2020.

5 Discussion

A cautious examination of the findings reveals a rise in the financial rate or expense of these selected construction products during the investigation. The few fabrics has undulating design, cost increased, and while in the case of other resources there was a changing in cost and the examination historical. The cost of conventional Portland concrete, which is factory-made in the southerly part of the nation, is a model. Shifting it to the north part of the nation, however, necessitates higher transportation costs, resulting in a higher cost of concrete in the northern region than in the southern region. Exorbitant material fees, unrefined petroleum costs, price of electricity, fuel price and force source, high work price, high transport price, and high successive expense were discovered as the primary factors contributing to the rise in the cost of construction resources in India's south region. These elements should be kept under control to avoid more rises in the structure's and building resources costs. As a result, the government, legislative bodies, and various stakeholders in the construction sector market must confirm that this tendency does not continue.

6 Suggestions in the Study

This investigation adds to the overall group of knowledge development materials, explicitly in valuing building and development materials. It recognized the value pattern of some who chose standard structure and development materials on India's development market. The reasons for examining the expanded costs of building and development materials is to consider the partners (like Research and development experts and Government) on heightening expense of building materials to find a way to check its impact on lodging cost. The examination discoveries are expected to help specialists and professionals of the development business concentrate on the

most proficient method to research the possible utilization of appropriate structure materials to guarantee economic development.

The Indian Government may use this investigation's findings to support current policies aimed at reducing the increasing price of construction and production resources, which tends to raise the overall price of structures. It is evident from the consequences that the estimated construction and development materials' fees will continue to grow for an indefinite period. The Government is expected to develop arrangements to manage the causal elements of cost rises in construction and development resources.

7 Conclusion

The results from the research pointed towards the pattern in the costs of some chosen basic structure and development materials in south India's development market from the year 2016–2020. This sets the new paradigm in the construction sector to pertain to materials.

- The analysis gives different gazes of the materials examined, recorded the cost increases eventually. Accordingly, the study concludes that in the south Indian construction industry, there is a reliable and changing increment cost tendency of the chosen construction and development materials.
- The variations will reflect well in an escalation of materials and also will affect the construction cost.
- This study is expected to aid development experts in better understanding the issue of rising building, building resources costs in the development sector and taking the essential steps to mitigate their effect on lodging costs.
- Besides, it is proposed that additional studies be conducted to forecast the potential tendency of construction and building material costs in the Indian development sector if current conditions remain unchanged.
- The future work can be done for adding some other superplasticizer and also checking the intermediate proportions made in this study wisely.

References

1. Windapo A, Cattell K (2012) Examining the trends in building material prices-built environment stakeholders' perspectives. Manage Constr Res Pract 1:187–201
2. Oladipo FO, Oni OJ (2012) A review of selected macro-economic factors impacting building material prices in developing countries—a case of Nigeria. Ethiopian J Environ Stud Manage. 5(2):131–137
3. Huan Z, Jianhua Z (2013) Analysis of factors to cause the price change of building materials. Adv Mater Res 683:668–671

4. Akanni P, Oke A, Omotilewa O (2014) Implications of rising cost of building materials in Lagos State Nigeria. SAGE Open, pp 1–7, October–December 2014
5. Wagura TJ (2013) Determinants of housing supply in Kenya [Post Graduate Diploma Thesis]. School of Built Environment, University of Nairobi, Kenya
6. Mansur SA, Abdul Hamid AR (2016) Rising trend in construction cost and housing price. J Adv Res Bus Manage Stud. 3(1):94–104
7. Pashardesa P, Savva CS (2009) Factors affecting house prices in Cyprus: 1988–2008. Rev 3(1):3–25
8. Schildkamp M (2009) Suitability of local soil for cost saving construction techniques. Smart Shelter Foundation
9. Danso H, Obeng-Ahenkora NK (2018) Major determinants of prices increase of building materials on Ghanaian construction market. OJCE 8(2):142–154
10. Prasanna K, Lakshminarayanan B, Anandh KS (2017) Study on strength of concrete by partial replacement of river sand with sawdust and robosand. ARPN J Eng Appl Sci 12(8):2423–2427
11. Prakash Chandar S, Gunasekaran K (2018) Study on some durability properties of coconut shell concrete with quarry dust. Eur J Environ Civil Eng 24(6):709–723
12. Jalam UA, Jalam AA, Sale IM (2016) Cost evaluation of utilising building materials derived from agricultural waste as sustainable materials for lightweight construction. Econ Environ Stud 16(4):673–685
13. Ihuah PW (2015) Building materials cost increases and sustainability in real estate development in Nigeria. AJESD 4(3):218–233
14. Jagboro GO, Owoeye CO (2004) A model for predicting the prices of building materials using the exchange rate in Nigeria. Malaysian Surveyor 5(6):9–14
15. Danso H, Manu D (2013) High cost of materials and land acquisition problems in the construction industry in Ghana. Int J Res Eng Appl Sci 3(3):18–33
16. Aliyu AA, Kasim R, Martin D (2011) Factors affecting housing development in Makama Jahun Area of Bauchi Metropolis Nigeria. IJTEF 2(4):263–268
17. Prasanna K, Anandh KS, Kiruthiga K (2017) Study on high-performance concrete with the replacement of fine aggregate by manufactured sand. Int J Civil Eng Technol 8(8):1502–1514
18. Gunasekaran K, Chandar P, Annadurai S, Satyanarayanan RKS (2017) Augmentation of mechanical and bond strength of coconut shell concrete using quarry dust. Eur J Environ Civil Eng 27:629–640